

RAYMOND L. BERNOR, HEINZ TOBIEN, LEE-ANN C. HAYEK & HANS-WALTER MITTMANN

Hippotherium primigenium (Equidae, Mammalia) from the late Miocene of Höwenegg (Hegau, Germany)

Abstract

We report here on the hipparion skeletal sample from Höwenegg (Hegau) Germany. Höwenegg is a 10.3 m.y. locality which preserves several partial-to-complete skeletons of late Miocene rhinoceros, deer, tragulid, bovid and the tridactyl horse *Hippotherium primigenium*. This sample was excavated by JÖRG and TOBIEN in the 1950's and 1960's, and represents a remarkable paleontological sample. We employ anatomical description and measurements of continuous variables for the complete skeleton, along with documentation of 49 discrete multistate characters of the skull and dentition, to characterize the skeletal biology of the Höwenegg hipparion population. We find, for the most part, that the Höwenegg hipparion population exhibits a low range of statistical variability for most continuous variables except some dental and postcranial parameters. Character state distributions range from 100% incidence for a given state to modest variability of character state distribution due largely to ontogenetic factors. When accounted for by stage-of-wear, most dental characters are seen as being reasonably stable for characterizing a single species of hipparion.

Our analysis reveals that the Höwenegg horse is not only one of the chronologically oldest European hipparions, but also morphologically archaic and phylogenetically near the base of the entire Old World hipparion radiation. The dentition was low crowned, heavily plicated and exhibits strong mediolateral grooving indicative of a substantial browse component to its diet. The locomotor system shows adaptations of the spine as well as the feet to springing and quick mediolateral movement suitable for its life in the non-seasonal warm temperate/subtropical mesophytic forests of the Middle European Vallesian and early Turolian.

Kurzfassung

Hippotherium primigenium (Equidae, Mammalia) aus dem späten Miozän Höweneggs (Hegau, Südwestdeutschland)

In dieser Arbeit beschreiben wir die Skelette und Skelettelemente der Hipparien, die von JÖRG und TOBIEN zwischen 1950 und 1968 in Höwenegg bei Grabungen geborgen worden sind. Diese Fundstelle ist ca. 10,3 Millionen Jahre alt und in ihr sind mehrere fragmentarische aber eben auch vollständige Skelette von Rhinocerotiden, Cerviden, Traguliden, Boviden und insbesondere dem dreizehigen Urpferd *Hippotherium primigenium* überliefert.

Die Beschreibung dieser vollständigen Skelette basiert zunächst auf einer anatomischen Analyse der einzelnen Skelettelemente. Dann werden die Meßwerte der kontinuierlichen Variablen dieser Elemente für die gesamte Höwenegg Population statistisch untersucht, und schließlich die Variabilität der Ausprägung von 49 Schädel- und Zahnmerkmalen innerhalb dieser Population analysiert.

Die Analysen der kontinuierlichen Variablen zeigen im allgemeinen nur eine geringe Streubreite, einige Parameter an den Schneidezähnen und an postcranialen Elementen ausgenommen. Die Verteilung der Merkmalsausprägungen innerhalb des untersuchten Materials zeigt eine weitestgehende Konstanz der Merkmale; geringe Variabilitäten können durch ontogenetische Faktoren erklärt werden. Berücksichtigt man z. B. den Abnutzungsgrad der Kauflächen der Zähne zeigen sich auch schon die meisten Zahnmerkmale allein hinreichend konstant, festzustellen, daß an dieser Fundstelle nur eine einzige *Hipparion*-Art festgestellt werden kann.

Unsere Untersuchungen zeigen, daß das Höwenegg-Pferd nicht nur eines der ältesten Vertreter der Gruppe der Hipparien in Europa war, sondern zudem morphologisch noch äußerst urtümlich ist und stammesgeschichtlich nahe der Basis der Radiation der Hipparien in der Alten Welt steht. Seine Zähne sind noch relativ flachkronig, auf der Oberfläche stark gefaltet und durch tiefe mediolaterale Furchen gekennzeichnet. Dies deutet auf einen nur geringen Gras- und vermehrten Blattanteil in der aufgenommenen Nahrung hin. Der Bewegungsapparat zeigt Anpassungen im Bereich der Wirbelsäule sowie der Extremitäten an Sprung- und schnelle Seitwärtsbewegungen. Beides sind notwendige Anpassungen für ein Tier dieser Größe, um in den warm-gemäßigten bis subtropischen mesophytischen Wäldern des mitteleuropäischen Vallesiums und frühen Turoliums überleben zu können.

Résumé

Hippotherium primigenium (Equidae, Mammalia) du jeune miocène de Höwenegg (Hegau, Allemagne)

Dans ce travail sont décrits les restes de squelettes d'hipparion provenant de Höwenegg (Hegau) en Allemagne. Ce gisement, daté de 10,3 Ma, a livré des squelettes partiels ou complets de rhinocerotidé, cervidé, tragulidé, bovidé et équidé tridactyle *Hippotherium primigenium*, le tout exceptionnellement bien préservé et d'un intérêt paléontologique considérable. Le matériel a été récolté par JÖRG et TOBIEN dans les années 1950 jusqu'à 1968.

Ce travail donne la description anatomique et la biométrie des variables continues de tous les éléments du squelette, en plus d'une documentation sur 49 caractères multi-états du crâne et de la dentition, afin de mettre en évidence la biologie squelettique de la population d'hipparion à Höwenegg. Il apparaît que pour la plupart des variables continues, la population d'hipparion de Höwenegg montre une faible variabilité statistique, sauf peut-être pour quelques paramètres dentaires et post-craniens. La distribution de l'état des caractères peut varier d'un état consistant à 100 % pour un caractère donné à un état de variation relativement modeste pour d'autres, due essentiellement à des facteurs ontogénétiques. Lorsqu'on prend en compte l'état d'usure, la plupart des caractères dentaires apparaissent comme

étant raisonnablement stables, en démontrant ainsi qu'il n'y a qu'une seule espèce d'hipparion à Höwenegg.

Nos analyses ont mis en évidence que l'hipparion de Höwenegg n'est pas seulement l'un des plus anciens représentants du groupe en Europe, mais aussi il possède des caractères archaïques qui le placent proche du début de la radiation des hipparions dans tout l'Ancien Monde. Ses dents à couronne basse sont très plissées et montrent des fortes rainures

médio-latérales (transversales) qui indiquent une alimentation partiellement de type brouteur de feuillages. Le système locomoteur montre des adaptations de la colonne vertébrale et des pattes au saut et à des mouvements rapides médio-latéraux, nécessaires pour vivre dans les environnements forestiers mésophytiques à climat à saison unique de type tempéré chaud ou sub-tropical du Vallésien et du Turolien inférieur en Europe centrale.

Contents

1.	Introduction	8
2.	Materials and Methods	12
3.	Systematics	16
3.1	Systematic Perspective	16
3.2	Taxonomy	17
4.	Skull, Mandible and Hyoid (the neurocranium and viscerocranium)	17
4.1	Description and Variability of the Skull and Maxillary Dentition	17
4.1.1	Definition of the <i>Hippotherium primigenium</i> Skull by Discrete Characters	17
4.1.2	Description of the Höwenegg skulls	17
4.1.3	Summary of Character State Distribution	27
4.1.4	Statistical Characteristics of Skull Measurements	29
4.1.5	Statistical Characteristics of the Maxillary Dentition	29
4.2	Description and Variability of the Mandible and Dentition	37
4.2.1	Definition of the <i>Hippotherium primigenium</i> Mandible by Discrete Characters.	37
4.2.2	Description of the Höwenegg Mandibles	37
4.2.3	Summary of Character State Distribution	40
4.2.4	Statistical Characteristics of Mandibular Measurements.	40
4.2.5	Statistical Characteristics of the Mandibular Dentition.	41
4.3	Hyoideum.	42
5.	Axial Skeleton	48
5.1	Anatomy of the Vertebral Classes	49
5.1.1	Cervical Vertebrae	49
5.1.2	Thoracic Vertebrae	54
5.1.3	Lumbar Vertebrae	62
5.1.4	Sacrum	65
5.1.5	Caudal Vertebrae	66
5.1.6	Costae	71
5.1.7	Sternum	74
5.1.8	Summary – The Spine as a Functional Unit.	74
6.	The Thoracic Limb – Anatomy and Statistics of the Osteological Elements	75
6.1	Scapula	75
6.2	Humerus	76
6.3	Radius	80
6.4	Ulna	86

6.5	Scaphoideum	87
6.6	Lunatum	90
6.7	Pyramidale	92
6.8	Pisiforme	94
6.9	Trapezium	95
6.10	Trapezoideum	96
6.11	Magnum	98
6.12	Unciforme.	100
6.13	Summary of the Carpalia as a Functional Unit	101
6.14	Metacarpale III	101
6.15	Sesamoidea of the Distal Metacarpale III	105
6.15.1	Medial Sesamoid.	105
6.15.2	Lateral Sesamoid.	106
6.16	Metacarpale II	107
6.17	Sesamoidea of Distal Metacarpale II	109
6.18	Metacarpale IV	110
6.19	Sesamoidea of the Distal Metacarpale IV	111
6.20	Proximal Sesamoid Bones of Metacarpale II and IV	113
6.21	Metacarpale V	113
6.22	Anterior 1st Phalanx III.	114
6.23	Anterior 2nd Phalanx III	117
6.24	Anterior 3rd Phalanx III	119
6.25	Distal Sesamoidea of Anterior Phalanx III.	122
6.26	Anterior 1st Phalanx II	124
6.27	Anterior 2nd Phalanx II.	125
6.28	Anterior 3rd Phalanx II	127
6.29	Anterior 1st Phalanx IV	129
6.30	Anterior 2nd Phalanx IV	130
6.31	Anterior 3rd Phalanx IV	132
6.32	Summary of the Osteological Contrasts between Phalanges 1, 2 and 3 of Digits II and IV.	133
7.	The Pelvic Limb – Anatomy and Statistics of the Osteological Elements	138
7.1	Pelvic Girdle	138
7.2	Femur.	138
7.3	Patella	144
7.4	Tibia	145
7.5	Fibula	151
7.6	Astragalus	152
7.7	Calcaneum	155
7.8	Naviculare	157
7.9	Cuneiforme 1+2	159
7.10	Cuneiforme 3.	160
7.11	Cuboideum	162
7.12	Metatarsale III	164
7.13	Sesamoidea of Distal Metatarsale III	168
7.14	Metatarsale II.	171
7.15	Sesamoidea of the Distal Metatarsale II.	173
7.16	Metatarsale IV	173
7.17	Sesamoidea of Distal Metatarsale IV	176

7.18	Posterior 1st Phalanx III	176
7.19	Posterior 2nd Phalanx III	178
7.20	Posterior 3rd Phalanx III	180
7.21	Distal Sesamoidea of Posterior Phalanx III	183
7.22	Posterior 1st Phalanx II	184
7.23	Posterior 2nd Phalanx II	185
7.24	Posterior 3rd Phalanx II	186
7.25	Posterior 1st Phalanx IV	188
7.26	Posterior 2nd Phalanx IV	189
7.27	Posterior 3rd Phalanx IV	190
7.28	Summary of the Osteological Characteristics of the Abaxial and Adaxial Phalanges of the Hind Foot	191
8.	Discussion	194
9.	Summary	195
10.	Literature Cited	196
Appendix: Legends for those figures which indicate morphological features		200

1. Introduction

The late Miocene locality of Höwenegg, Hegau south Germany (Fig. 2.1), is well known for its preservation of complete mammalian skeletons and associated invertebrate and plant fossils. The first fossil found in the Höwenegg district was reported by DEEKE (1917). In 1936, a local pharmacist A. FUNK, discovered the actual site of Höwenegg. WITTMANN (1937) followed with an initial description of the site's geology. Later, TOBIEN (1932) described some teeth of "*Hipparion*" from the locality, citing the importance of the site. Further investigation of the site was interrupted at the onset of World War II.

A period of carefully organized and intensive excavation activity ensued between 1950 and 1963. Excavations were initiated by M. PFANNENSTIEL and F. KIRCHHEIMER, and financially supported by the PRINZ MAX ZU FÜRSTENBERG. H. TOBIEN and E. JÖRG were designated scientific leaders of the excavations, and produced the first detailed descriptions of the work from 1951 to 1965 (JÖRG 1951, 1954, 1956, 1957, 1965; JÖRG, REST & TOBIEN 1955; TOBIEN 1951, 1952, 1954, 1956, 1957 a, b, 1958, 1959 a, b, 1962, 1970, 1982; TOBIEN & JÖRG 1959). Other reports relevant to the Höwenegg site included: RUTTE (1962), LUTZ (1965), BERG (1970), WOODBURN & BERNOR (1980), BERNOR, WOODBURN & VAN COUVERING (1980), BERNOR, TOBIEN & WOODBURN (1989), HÜNERMANN (1982) and FORSTÉN (1985). TOBIEN (1986) gave a detailed summary of this work in German, which we largely follow here.

Independent geological investigations at Höwenegg have been pursued locally by SCHREINER and MÄUSNEST & SCHREINER (1963), as well as regionally MÄUSNEST & SCHREINER (1966, 1970, 1976), while radioisotopic dating was done and discussed widely by LIPPOLT, GENTNER & WIMMENAUER (1963), WEISKIRCHNER (1975), WAGNER, DELALOYE & KEDLEY (1975), BARANYI, LIPPOLT & TODT (1976) and BECKER-PLÄTEN ET AL. (1977).

A new period of investigation on the Höwenegg site was initiated by S. RIETSCHEL and H. TOBIEN in 1985 to ensure publication of incompleting monographic work on the fauna and geology and to give a basis for future work at the site. DE BEAUMONT (1986) described the carnivores, SCHLEICH (1986) the turtle fauna, HÜNERMANN (1989) the skeletons of the rhinoceros *Aceratherium*, ZAPPE (1989) the chalicothere *Chalicotherium grande*, and finally JÖRG & ROTHHAUSEN (1991) published all the geological profiles from the various excavation campaigns (1956 – 1963) and discussed the sedimentary environments recorded at the site.

Since WITTMANN'S (1937) early description of Höwenegg's sediments as a sequence of thinly stratified fresh water limestone and brownish hornblende tuff, there has been considerable uncertainty about the site's physical stratigraphy and sedimentary origin. JÖRG (1951) initially characterized the Höwenegg deposits as being "Upper Miocene" and similar in age to the nearby site of Öhningen. However, the discovery of in-situ "*Hipparion*" remains made it evident that Höwenegg was younger than the late middle Miocene locality of Öhningen (TOBIEN,

1951; JÖRG, 1954). Recent European Mammal Neogene (MN) correlations have agreed that the "Höwenegg-Schichten" are referable to the early Vallesian = MN 9 (BERNOR, WOODBURNE & VAN COUVERING 1980; TOBIEN 1986; BERGGREN & VAN COUVERING 1972; VAN COUVERING & BERGGREN 1972; BERNOR et al. 1988; BERNOR, TOBIEN & WOODBURNE 1989; STEININGER et al. 1989; MEIN, 1989). Radioisotopic dating by LIPPOLT et al. (1963) gave an age of 7-6 Ma for the basalts, and 12,4 +/- 1 Ma for a hornblende tuff from within the Höwenegg section. WEISKIRCHNER (1975) dated an olivine-nephelinit basalt (olivine-nephelinit) as being 11,8 +/- 0,6 Ma, and the Hornblende Tuff as being 9,4 +/- 0,5 Ma. Regionally, SCHREINER (1976) has argued that the "Höwenegg-Schichten" might have accumulated in a crater produced by the eruption of the hornblende ash which had penetrated an older basalt 800 m SE of the site. Lake deposits are believed to have filled this depression, and included a sequence of carbonatic sediments mixed with tuffaceous sediments. Section profiles of the "Höwenegg-Schichten" have been published by JÖRG & ROTHAUSEN (1991). The plant remains are relatively abundant by volume, but few in species diversity (GREGOR 1987). GREGOR has argued that the existing plant species are similar to other middle Miocene Central European taxa. BERNOR et al. (1988) have shown that these floras constituted a warm mesophytic forest with nominal seasonality. TOBIEN's (1986) interpretation of the paleoecology based on Höwenegg's mammal assemblage is concordant with GREGOR's (1987) and BERNOR et al.'s (1988). The invertebrate faunas include principally gastropods and ostracods, and are in need of a major revision (LUTZ 1965: 18; TOBIEN 1986). There is a common occurrence of the whitefish *Leuciscus*, also known from older occurrences in southern Germany. The fish *Tinca furcata* has been found at the late middle Miocene southern German locality of Öhningen. The tortoise *Cheirogaster* is known most usually from Paleogene levels of Europe (SCHLEICH 1986). The mammalian fauna includes a mixture of middle Miocene autochthonous forms and earliest late Miocene immigrants (TOBIEN 1986; BERNOR et al. 1988). TOBIEN (1986) has argued that the mammalian assemblage was transported and subsequently deposited in the Höwenegg lake by very low velocity riverine currents (Fig. 2.3). The turtle, catfish and ostracod fauna indicate shallow water conditions with stable, warm temperatures, while molluscan species indicate that the water was stagnant and oxygen deficient. The latest phase of field investigation was undertaken during the Summers of 1991 and 1992, and organized jointly by S. RIETSCHEL and R.L. BERNOR. The project's goals included: reidentify JÖRG and TOBIEN's stratigraphic section, determine how much of the site had been excavated and what remains, determine if there are any further fossil-bearing horizons, evaluate the sedimentologic and paleoenvironmental contexts of the site, and reassess the radioisotopic age of the locality.

WOODBURNE et al. (1996) have forwarded the recent geological results. The Höwenegg beds represent a lake deposit with periodic episodes of mudflow. The Höwenegg lake sequence originally had 12+ meters thickness, with only the lower 4+ meters remaining. Neither our excavations, nor JÖRG and TOBIEN's ever established the actual basal contact of the lacustrine and underlying "Älterer" tuff deposits within the quarry, and it is possible that they are locally thicker than elsewhere in the section. The excavation of a geological trench did lead to the identification of JÖRG & ROTHAUSEN's (1991) stratigraphic levels 25-44, and the collection of a complete skull and some postcrania of a bovid, *Miotragocerus pannoniae*, from level 43. This find is important because it reveals that fairly complete vertebrate fossil material occurs lower in the section, and suggests that the Höwenegg beds have the potential for yielding further important fossil finds. The results of THEOBALD's sedimentological investigations (in WOODBURNE et al., 1996) largely confirm TOBIEN's (1986) conclusions that fossils were accumulated in a shallow lake, with low velocity currents and under anaerobic bottom conditions, except for the occurrence of episodic mudflows or lahars. There is the further indication that the lake deposits accumulated over a relatively short geochronologic interval. SWISHER (1996) has given an extensive age evaluation of the Höwenegg beds using single crystal argon and paleomagnetic methodologies. He has dated the underlying, and interfingering "Älterer" Hornblende Tuff, hornblende "tuffites" from within the Höwenegg fossil-bearing lacustrine horizons and an intrusive phlogopite-bearing igneous plug from an adjacent rock quarry which tilted the Höwenegg lake beds and caused cessation of their deposition. The "Älterer" Hornblende Tuff yielded an age of 10.36 +/- 0.19 Ma., while the basalt plug yielded a date of 9.82 +/- 0.20 Ma. Three laser incremental-heating analyses of hornblende from level 33-2 resulted in plateau ages ranging from 10.86-10.23 Ma, while a hornblende from level 33-10 yielded a plateau age of 10.29 +/- 0.07 Ma. All of these analyses of materials from within the lake bed sequence indicate variable disturbance in the lower temperature steps and the loss of excess argon which leads SWISHER to conclude that the youngest date is the most precise. While the hornblende from within the Höwenegg fossil-bearing horizons is fresh, SWISHER argues that the 10,29 +/- 0.07 Ma should be considered a maximum age, but one that is likely close to the actual age of the Höwenegg beds. Paleomagnetic samples were collected from three distinct levels within the Höwenegg fossil quarry, the lowest being below the dated horizon. All samples indicated a normal polarity magnetization consistent with a correlation within the long Chron C5n.2n normal interval (10.95-9.92 Ma; re: BERGGREEN et al., 1995 and STEININGER et al., 1996). As can be seen by the reconstruction of the Hö A skeleton (Fig. 1.1 & 1.2), fossil preservation is remarkable,

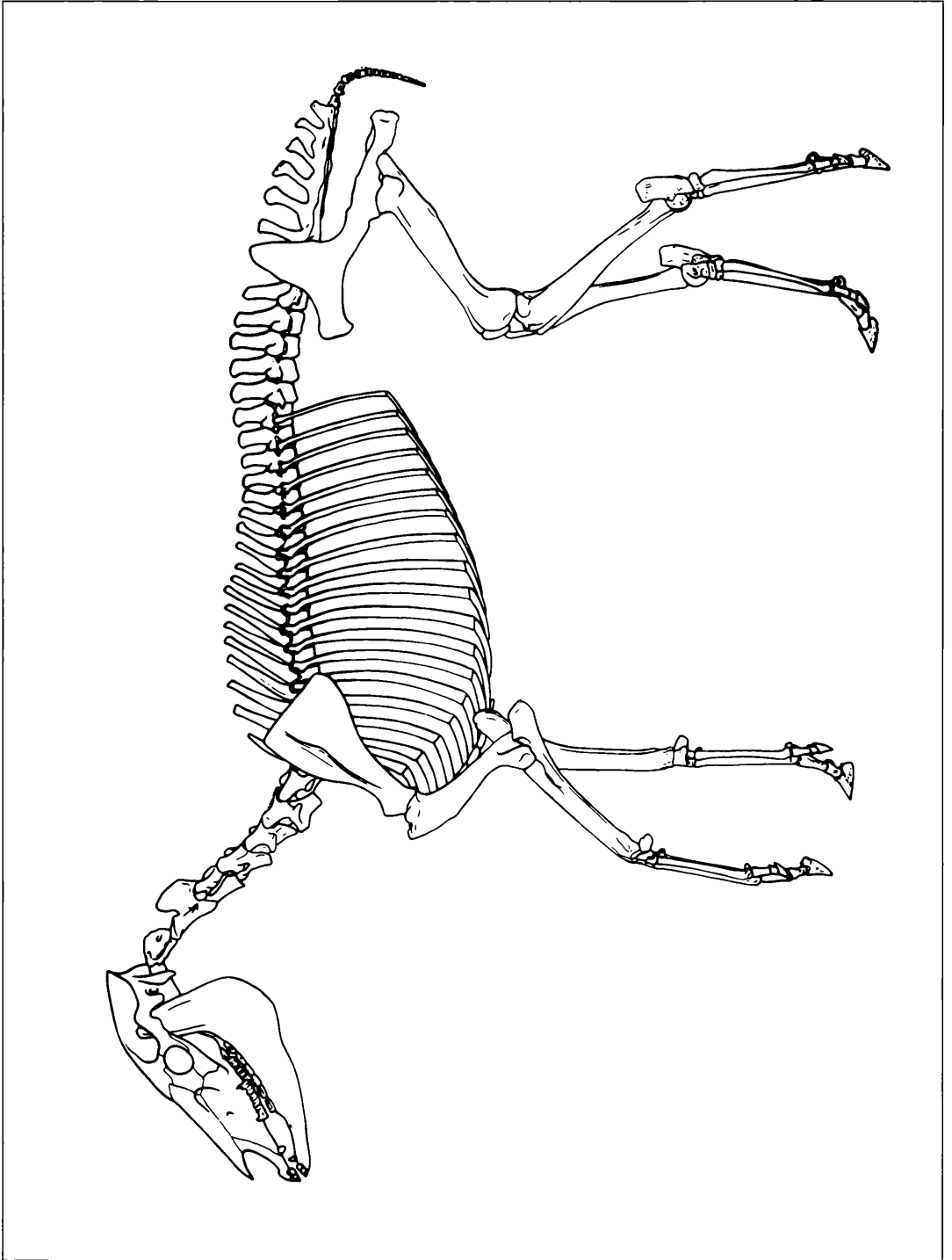


Figure 1.1. GARRAUX'S Reconstruction of the Hö A Skeleton (x 0,075).

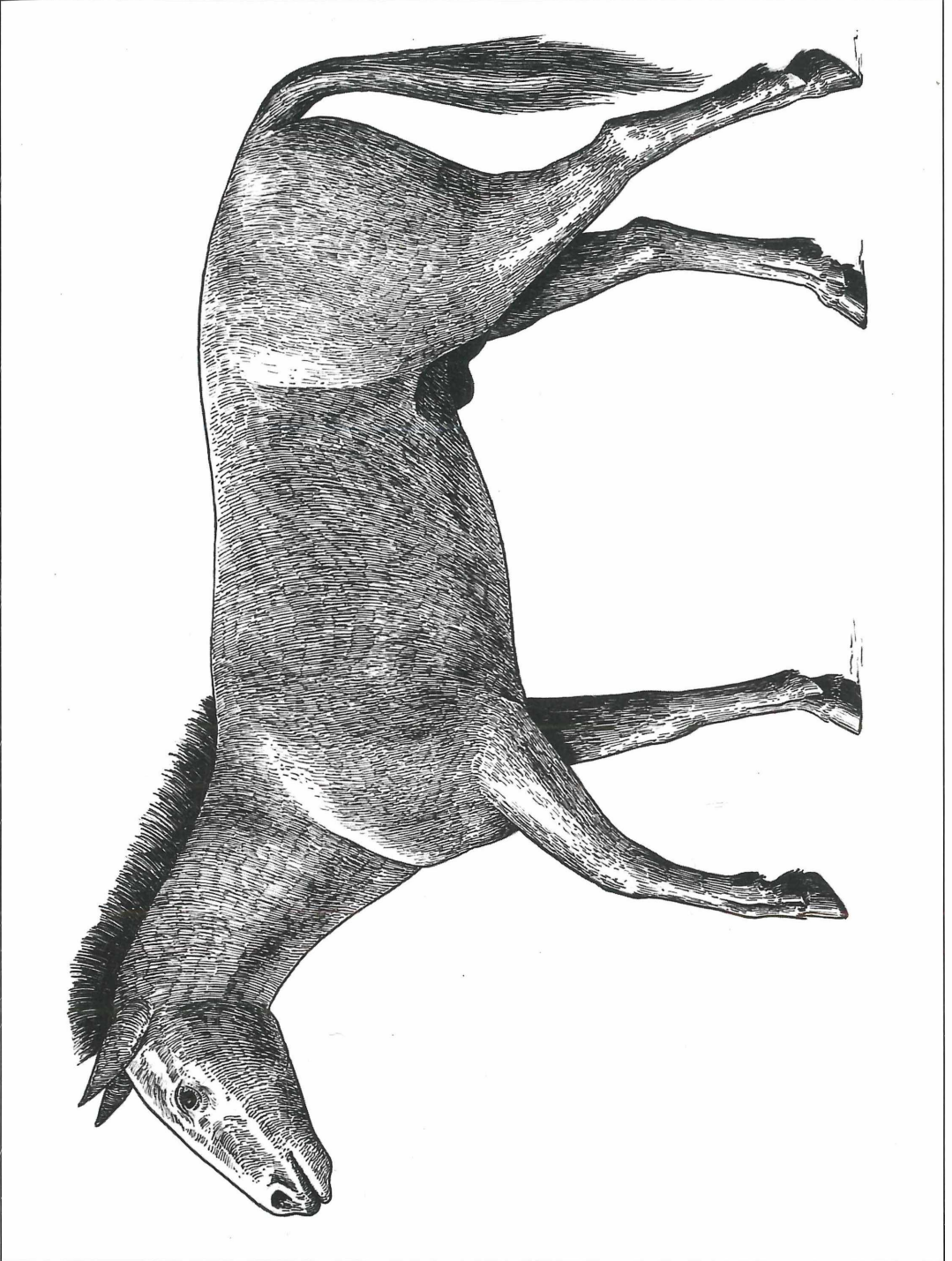


Figure 1.2. GARRAUX's Reconstruction of the Höwenegg horse, *Hippotherium primigenium* (0,075 x).

and is the principal reason for their paleobiological value, particularly with regard to the so-called "Hipparion" Datum controversy. BERNOR in WOODBURNE, BERNOR & SWISHER (1996) has determined that while the Höwenegg horse, *Hippotherium primigenium* is primitive in nearly every regard, there are some noticeable advances in the dentition which suggest that it is younger than the earliest occurring Old World hipparions. This observation is in accord with recent radioisotopic and magnetostratigraphic evaluations of the "Hipparion Datum" in the Siwaliks (10.7 Ma; PILBEAM et al., 1996); Turkey (10.3 Ma, KAPPELMAN et al., 1996; also see SEN, 1996) Central Europe (11.2 Ma; RÖGL and DAXNER-HÖCK, 1996) and relevant peri-Mediterranean and East African late Miocene sections (STEININGER et al., 1996; SWISHER, 1996). Moreover, analyses of Central European populations of *Hippotherium primigenium* have served to reinforce the phylogenetic position of the Höwenegg hipparion (BERNOR, MITTMANN & RÖGL, 1993; BERNOR et al., 1993; RÖGL et al., 1993 and BERNOR & LIPSCOMB, 1995). This monograph does not attempt to analyse or review all aspects of the Höwenegg hipparion's biology and evolution. It is rather a text which principally focuses upon a description of the horse's osteology from both an anatomical and morphometric perspective with the aim to establish the variability in all relevant morphological characters, whether they be discontinuous or continuous variables. Other relevant work such as the taphonomic context, paleodietary reconstructions and close comparison with other hipparion species are ongoing and will be published in the future. We begin by identifying our materials and methods (Chapter 2) and systematic perspective (Chapter 3). Thereafter we follow with an anatomical and morphometric description of the skulls, mandibles and hyoid bone (neuro- and viscerocranium, Chapter 4), axial skeleton other than the skull (Chapter 5), bones of the thoracic limb (Chapter 6) and pelvic limb (Chapter 7). We complete our presentation with a discussion of the broader evolutionary significance of the Höwenegg hipparions (Chapter 8).

2. Materials and Methods

Following the 1981 American Museum of Natural History Workshop on hipparion research, EISENMANN et al. (1988) illustrated standard measurements proposed at that workshop for most bones. These measurements have been adopted by BERNOR (1985) on the Maragheh hipparionines, QIU, HUANG & GUO (1988) and BERNOR, QIU & HAYEK (1990) on suites of Chinese hipparionines, BERNOR, MITTMANN & RÖGL (1993; Austria), BERNOR et al. (1993; Hungary) and BERNOR & FRANZEN (in press; Germany) on Central European populations of *Hippotherium primigenium*, BERNOR & ARMOUR-CHELU (in press a, b) for African hipparions and BERNOR, TOBIEN & WOODBURNE (1989) in a review of the evolutionary history of Old World hipparions.

We use here 49 morphological character states of the skull, mandible and dentition, which have been progressively refined

through many of the studies cited above, and by BERNOR & LIPSCOMB (1991, 1995) as well as those used for analysis of North American hipparion evolution, including: MACFADDEN (1977), WOODBURNE & BERNOR (1980), WOODBURNE, MACFADDEN & SKINNER (1981), MACFADDEN (1984), WEBB & HULBERT (1986), HULBERT (1988), HULBERT & MACFADDEN (1991) and WOODBURNE (1996a, b). Utilization of postcranial character states awaits further comparative study.

The Höwenegg hipparions are unique in that they represent the only collection of articulated hipparion skeletons from a stratigraphically and temporally restricted locality (Fig. 2.1). With the Höwenegg horses we can say with a good degree of certainty what a single hipparion "population's" range of statistical variability is for every skeletal measurement. This allows future investigators with a direct comparison to other hipparion assemblages to determine whether a single, or multiple species are present, or more directly how they compare to a population of *Hippotherium primigenium* (re: methodology of BERNOR, TOBIEN & WOODBURNE, 1989; BERNOR, MITTMANN & RÖGL, 1993; BERNOR et al., 1993; BERNOR & ARMOUR-CHELU, in press a, b; BERNOR & FRANZEN, 1997). Raw measurements are available on a 3.5" disk in ASCII and dBase IV format on request.

In this manuscript, we describe the skeletal anatomy of the Höwenegg horse based principally on the Hö A skeleton (Fig. 1.1) and compare various morphological features with homologous structures in extant *Equus* (when of course they occur; re: distolateral and distomedial appendages not included). In cases where the Hö A skeleton is damaged, or elements are missing, we use other skeletal material from the population and cite it accordingly. We use the entire sample of hipparion bones to statistically characterize the population. The completeness and preservation state of the Hö skeletons varies from being virtually pristine (e.g. T-skeleton) to rather crushed and fragmentary. Occasional poor preservation is due to the "marly" matrix within which all the bones were embedded, and later compacted (TOBIEN, 1986: Tab. 2). Besides the fragile vertebrae, crushing affected mainly scapulae, pelvis, stylopodia and zeugopodia, the last because of their large in vivo marrow cavities. The limb distal extremities including the basipodia, metapodia and acropodia are more resistant to breakage by compaction; they have thicker compacta and spongiosa, and are also smaller and less linear in their dimensions. Figures 6.3.1.1 and 6.3.1.2 provide an example of the magnitude of crushing on the Hö A-54 radius-ulna, and the degree of reconstruction which was necessary to restore these bones.

We follow the nomenclature used in the English translation of "The Anatomy of the Domestic Animals, Volume I. The Locomotor System of the Domestic Mammals" by NICKEL et al. (1968). We also refer in some circumstances to ELLENBERGER-BAUM (1977), GETTY (1975) and BARONE (1966). We follow NICKEL et al. (1968) and EISENMANN et al. (1988) in figuring only left side bony elements (except when they are unpaired). The osteological nomenclature and technical terms used in NICKEL et al. (1968) were adopted as far as possible in this text.

Silicone casts of the Hö A skeleton were made by the Karlsruhe preparation staff for comparison with skeletal material in other institutions. Moreover, the Hö A skeleton was drawn by OTTO GARRAUX (1904 – 1989; re: Fig. 1.1), renowned scientific illustrator and artist, who by his outstanding illustrations made highly significant contributions to mammalian vertebrate paleontology and paleoanthropology. The Hö A skeleton is the best preserved of the Höwenegg horses (TOBIEN & JÖRG, 1959: pl. 10), and is presently on exhibit in Staatliches Museum für Naturkunde at Karlsruhe (RIETSCHEL, TRUNKO & WEISSBROD, 1985: fig. 47) as a taphonomic model, and the Staatliche Museum für Naturkunde,

Stuttgart (since 1987) as a free-standing mount (Fig. 5.2). Figure 2.2 presents the in situ Hö E skeleton with its fetus. Measurements, osteological comparisons, and studies of statistical variation have included all of the Höweneegg skeletal material (as far as possible). Besides the Hö A skeleton these include: Hö B-54, Hö C-54, Hö E, Hö G, Hö J-54, Hö M-55, Hö N-55 (mostly destroyed), Hö T-56, Hö V-58, Hö Y-58, Hö I-53, Hö II-53, Hö III-53, Hö 15/58 and Hö 25. (TOBIEN, 1986: 29). In some limited cases, poorly preserved elements of the Hö A skeleton were supplied or replaced by corresponding bones from other skeletons; we document these cases accordingly in the following text. Besides the articulated skeletal material, we include isolated Höweneegg bones in all our statistical analyses (see raw measurement tables).

Every skeletal element is usually figured in six anatomical views: cranial, caudal, lateral, medial, proximal and distal, except for the foot elements where we use dorsal and palmar in lieu of cranial and caudal. Moreover, every element is figured at least two times: the first are text-figures; the second are reduced for reference to various anatomical structures indicated in the text by numbers and/or subnumbers (e.g. 2, 2', 3", 4''' etc.). When we define new measurements for those bones not included in EISENMANN et al. (1988), we render these as a third figure. Measurements were taken in millimeters to the nearest tenth using Helios digital calipers following, as far as possible and with only a few exceptions, EISENMANN et al. (1988). Measurements were entered into dBase IV, then checked for any outliers. Outliers were remeasured and if greatly different from

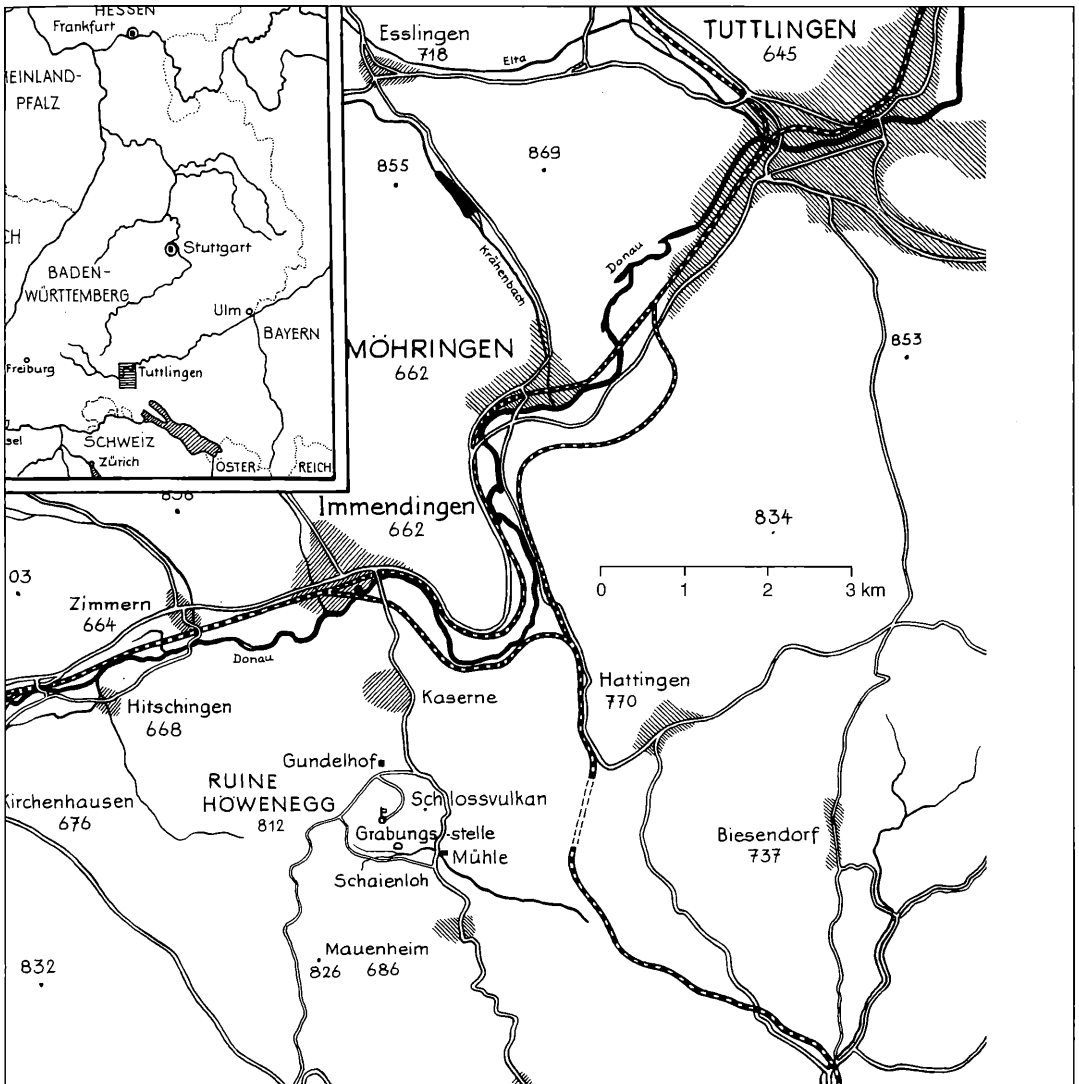


Figure 2.1. Map of Höweneegg's Geographic Location.



Figure 2.2. Höwenegg E Skeleton: Female with Fetus.

the original measurements, corrected; otherwise no change was made.

Because the fossil bones are often crushed, incomplete or missing, there exists a sizable number of missing observations for any given specimen. Because side differences were negligible, right and left side observations over but not within individuals were combined in order to increase sample size for statistical tests. In particular, a combined file was formed according to a set of rules: 1) if a given specimen had both right and left sides complete, left was selected; 2) for any specimen with only a right or only a left side, all of its data was included in the combined file; 3) in no case did we select variables from one side and include them with the opposite side; 4) selection was for specimen, not for variable; 5) fragments were not included in the side files but were incorporated into the combined files. Descriptive statistics and confidence intervals about the mean and the coefficient of variation were then calculated on these combined data files and correlation coefficients were determined for any samples with sizes greater than or equal to three. Our following discussions of significant correlations always refer to calculations on the combined bone file.

Basic descriptive statistics were calculated for the Höweneqq quarry sample on each individual measurement for each body part file (Appendix 1). Calculations were made separately on right and left sides for all files except those of the skull, mandible and cheek teeth, where only one side was measured. The statistical computer package employed was determined by the size of the selected data file. All calculations were made using SYSTAT 5.01, initially on a Compaq 386/20 and later on an AST Pentium 100.

After basic statistics were reviewed, outliers detected and checked, and programs rerun where necessary, inferential statistics were determined. Both homoscedasticity and equality of means were tested for each measurement on each major body part where side had been recorded in the data file. The F-test for variance was performed whenever we had a sample size of at least 5 for each group. A STUDENT t-test was performed whenever the equality of variance hypothesis was accepted and for the few cases for which this was not the case, a WELSH t-test was employed to test side equality. No significant differences between right and left sides were detected for any measurement. Tables for each body part and measurement contain confidence intervals about both the mean and the coefficient of variation (CV). The formula used for the standard error of the CV was the approximation $CV/\sqrt{Q^2(2n)}$ (SOKAL & ROLF 1969).

Abbreviations and Conventions

SMNK – Staatliches Museum für Naturkunde, Karlsruhe

HLMD – Hessisches Landesmuseum, Darmstadt

The taxon *Hipparion* has been used in a variety of ways by different authors. We utilize the following definitions in this work: hipparonine or hipparion: horses with an isolated protocone on maxillary premolar and molar teeth and, as far as known, tridactyl feet, including species of the following genera: *Cormohipparion*, *Neohipparion*, *Nannippus*, *Pseudhipparion*, *Hippohipparion*, *Cremohipparion*, *Hipparion*, "*Sivalhippus*", *Eurygnathohippus* (= senior synonym of "*Stylohipparion*") *Proboscoidipparion*, "*Plesiohipparion*" Characterizations of these taxa can be found in MACFADDEN (1984), BERNOR & HUSSAIN (1985), WEBB & HULBERT (1986), HULBERT (1987), QIU et al. (1988), BERNOR et al. (1988), BERNOR, TOBIEN & WOODBURN (1989), WOODBURN (1989) and HULBERT & MACFADDEN (1991).

Hipparion s.s.: The name is restricted to a specific lineage of horses with the facial fossa positioned high on the face

(MACFADDEN, 1980, 1984; WOODBURN & BERNOR, 1980; WOODBURN et al., 1981; MACFADDEN & WOODBURN, 1982; BERNOR & HUSSAIN, 1985; BERNOR, 1985; BERNOR et al., 1987 and Fig. 4; BERNOR, TOBIEN & WOODBURN 1989; WOODBURN, 1989). The posterior pocket becomes reduced and eventually lost, and confluent with the adjacent facial surface (includes Group 3 of WOODBURN & BERNOR, 1980). BERNOR's definition departs from some investigators in not recognizing North American species of *Hipparion* s.s. BERNOR (1985) and BERNOR (in BERNOR et al., 1989) does not recognize any North American taxon as belonging to *Hipparion* s.s.; any morphologic similarity between them is argued by him to be homoplasious.

"*Hipparion*": several distinct and separate lineages of Old World hipparonine horses once considered to be referable to the genus *Hipparion* (WOODBURN & BERNOR, 1980; BERNOR, WOODBURN & VAN COUVERING, 1980; MACFADDEN & WOODBURN, 1982; BERNOR & HUSSAIN, 1985; BERNOR, 1985; BERNOR et al., 1988; BERNOR, TOBIEN & WOODBURN 1989).

Measurements: mm – millimeters (all measurements as defined by EISENMANN et al., 1988 and rounded to 0.1 mm). Note that all statistical and measurement data tables presented here we round numbers to the second decimal point (0.00), and therefore cumulative percentages for characters may accordingly slightly exceed 100 %.

Skeletal Designations in Appendix: ast = astragalus; calc = calcaneum; cub1 = cuboid; humer = humerus; mpiii = metapodial III; mciii = metacarpal III; mtiii – metatarsal III; p1ph2: here, either anterior or posterior 1st phalanx II (it is virtually impossible to distinguish anterior from posterior elements in disarticulated specimens); p1ph3: again, either anterior or posterior 1st phalanx III; p2ph3: again, either anterior or posterior 2nd phalanx III; radii = radius; scap = scapula; tibia = tibia; txP2, txP3, txP4, txM1, txM2 and txM3 = tooth maxillary P2, P3...etc; tmP2, tmP3, tmP4, tmM1, tmM2 and tmM3 = tooth mandibular P2, P3...etc. Tx or tm P34 is used when it is unclear whether the tooth is a P3 or P4.

M1-M39: indicate measurement numbers as published by EISENMANN et al. (1988) and by BERNOR & ARMOUR-CHELU (in press a, b). The definitions of measurements made for maxillary and mandibular cheek teeth are included as table legends below. Anatomical Descriptions – The osteological nomenclature, the enumeration and/or lettering of the figures have been adapted from NICKEL et al. (1986). GETTY (1982) was also consulted for morphological identification and comparison. *Hipparion* monographs by GROMOVA (1952) and GABUNJA (1961) were cited after the French translations.

We use a paired nomenclature for the orientation of single bones and/or parts of the skeleton:

cranial – caudal (sometimes identical with anterior and posterior)

dorsal – ventral

medial – lateral

proximal – distal

adaxial – abaxial (respectively, near to or distant from the long axis of the skeleton or of a bone).

The terms superior and inferior are avoided.

We implement the nomenclature for the podalia suggested by EISENMANN et al. (1988: 44, fig. 58) and give the corresponding names of human, zoological and comparative anatomy in brackets below (after NICKEL et al., 1986: 60, 88; PETERS, 1987).

We further use the following specific names for given carpalia and tarsalia elements: First row of carpals:

Scaphoideum (= os scaphoideum, os carpi radiale, os naviculare manus, navicular, radiale)

Lunatum (= os carpi intermedium, os lunatum, lunar, lunate, semilunar, intermedium)

Pyramidale (= os triquetrum (used by NICKEL et al., 1986), os carpi ulnare, os triquetrum, os cuneiforme, cuneiform, cubital, pyramidal)

Pisiforme (= os carpi accessorium, os pisiforme, pisiform)

Second row of carpals:

Trapezium (= os trapezium, os carpale primum, os carpale 1, distal carpal 1, multangulum majus)

Trapezoideum (= os trapezoideum, trapezoid, os carpale secundum, os carpale 2, distal carpal 2, multangulum minus)

Magnum (= os carpale tertium, os carpale 3, capitatum, distal carpal 3)

Unciforme (= unciform, os carpale quartum, os carpale 4, os hamatum, hamate, distal carpal 4)

Tarsalia:

Astragalus (= os tarsi tibiale, talus tibiale)

Calcaneum (= os tarsi fibulare, os calcis)

Naviculare (= os tarsi centrale, os naviculare pedis, navicular, scaphoideum, centrale)

Cuneiform 1+2 (= small cuneiforme, os tarsale primum & secundum, os tarsale 1 & 2, os cuneiforme mediale & intermedium, entocuneiforme & mesocuneiforme)

Cuneiform 3 (= large cuneiforme, os tarsale tertium, os tarsale 3, os cuneiforme laterale, os cuneiforme tertium, ectocuneiforme)

Cuboideum (os tarsale quartum, os tarsale 4, os cuboideum)

Acknowledgements

This work was initiated by PROF. DR. HEINZ TOBIEN as a student in the 1930's. It continued over several years as an excavation campaign jointly organized by JÖRG (Karlsruhe) and TOBIEN (then Darmstadt). As a result of this fruitful and personally warm friendship we all benefit from an extraordinary collection of early late Miocene Höwenegg mammals. It is most unfortunate that PROF. TOBIEN passed away during the last phases of this project. We dedicate this work to his memory.

The current collaborative work began in the mid-1980's when TOBIEN invited BERNOR to participate in the research and monographic publication of the Höwenegg horse sample. It was determined early on that developing a statistical protocol for characterizing this sample was essential to our work and Dr. LEE-ANN HAYEK graciously agreed to provide her assistance to this problem. DR. HANS-WALTER MITTMANN joined this effort somewhat later providing continuity between the statistics, morphology and coordination of the publication effort.

We wish to thank the ALEXANDER VON HUMBOLDT STIFTUNG for supporting two 1 year fellowships to BERNOR principally for this work. BERNOR also thanks HOWARD UNIVERSITY'S COLLEGE OF MEDICINE, and particularly Dean CHARLES H. EPPS and Dean FLOYD MALVEAUX for providing liberal leave time to study this and comparative collections in the United States and Europe. The NATIONAL SCIENCE FOUNDATION, the SMITHSONIAN INSTITUTION'S INTERNATIONAL PROGRAMS, the NATIONAL GEOGRAPHIC SOCIETY, the L.S.B. LEAKEY FOUNDATION, the ANN and GORDON GETTY FOUNDATION, NATO and DFG all contributed funds to this project. We give special thanks to PROF. DR. SIEGFRIED RIETSCHEL for providing us full access to all of the facilities at the STAATLICHES MUSEUM FÜR NATURKUNDE KARLSRUHE for undertaking this study. We thank RENE KASTNER, WOLFGANG MUNK and ROLF SCHUPPISER for their continuous technical support. We further thank Dr. FRIEDEMANN SCHRENK of the Hessisches Landesmuseum Darmstadt for his assistance with those collections. There are many European and American colleagues who have directly and indirectly contributed to the development of this monograph over the last 12 years. We especially thank PROF. DR. MICHAEL O. WOODBURNE for his support and critical evaluation of this work over its duration. We thank Dr. MIRANDA ARMOUR-CHELU for reviewing this text and

Dr. SEVKET SEN for the French translation of the abstract. We also thank PROF. DR. NOEL T. BOAZ, PROF. DR. BERNARD CAMPBELL, PROF. DR. DARYL DOMNING, DR. ROBERT EMMY, PROF. DR. VOLKER FAHLBUSCH, PROF. DR. MIKAEL FORTELIUS, DR. JENS FRANZEN, DR. EBERHARD FREY, DR. KURT HEISSIG, DR. ELMAR HEIZMANN, PROF. DR. RICHARD HULBERT, PROF. DR. TASEER HUSSAIN, DIPL.-GEOL. HEINZ KÖNIG, PROF. DR. LASZLO KOROS, DR. JOHANNA KOVAR-EDER, PROF. DR. DIANA LIPSCOMB, DR. FRED RÖGL, PROF. DR. NIKOS SOLOUNIAS, PROF. DR. FRITZ STEININGER, PROF. DR. JEAN-PIERRE SUC, DR. CARL SWISHER, PROF. DR. RICHARD TEDFORD AND PROF. DR. LASZLO TRUNKO for supporting various aspects of this research over the course of this study.

3. Systematics

3.1 Systematic Perspective

Hipparionine horses have long been recognized as valuable index fossils for late Neogene Old World continental deposits. Recently there has been a renewed interest in this group and several approaches to their study have been advanced. In 1981, the AMERICAN MUSEUM OF NATURAL HISTORY hosted, with support from the NATIONAL SCIENCE FOUNDATION, a symposium dedicated to discussing these various approaches and standardizing measurements on hipparionine skeletal elements. While GROMOVA (1952) emphasized the use of both qualitative and quantitative characters of skulls, lower jaws, teeth and postcranial skeletons, subsequent workers have seemingly polarized themselves into two schools of either morphologic and phylogenetic systematics or statistical phenetic systematics. Some investigators have insisted on using only statistics in their discrimination of species, often with little regard for the morphologic, stratigraphic and geographic homogeneity of their sample. Other investigators have taken yet another extreme position of relying on the analysis of only a very few "highly diagnostic" morphologic characters. A review of the previous literature supporting the history of these different approaches has been recently given by BERNOR & HUSSAIN (1985). BERNOR & HUSSAIN (1985), BERNOR (1985), QIU, WEILONG & ZHIHUI (1988) BERNOR et al. (1988), BERNOR, TOBIEN & WOODBURNE (1989) and BERNOR, QIU & HAYEK (1990) have endeavored to bridge the obvious hiatus between these two schools of thought by combining studies of cranial and postcranial morphology with an extensive suite of measurements in a systematic, evolutionary and biogeographic analysis of Old World hipparionine species. Theirs, and other recent analyses of cranial and dental morphology of Old and New World hipparionines (WOODBURNE & BERNOR 1980; BERNOR, WOODBURNE & VAN COUVERING 1980; MACFADDEN & WOODBURNE, 1982), have demonstrated that taxonomic groups of specific and superspecific rank can be recognized and used for a variety of geological and paleobiological studies. BERNOR, TOBIEN & WOODBURNE (1989) have given the most recent accounting of these evolutionary relationships.

The Höwenegg hipparion skeletons are of paramount value for demonstrating the expected range of morphological and statistical variation for a single hipparionine species. These features, coupled with their primitive morphology and relative geological antiquity, make them pivotal for understanding the evolutionary relationships between North American and all Old World hipparions (BERNOR et al., 1988; BERNOR, TOBIEN & WOODBURNE, 1989; BERNOR & LIPSCOMB, 1991, 1995). Following previous observations, we concur that the Höwenegg species is one of the most primitive Old World hipparions, and therefore of considerable importance for phylogenetic studies. The scope of this paper, as defined in Section I, is meant to set the groundwork for subsequent studies on this assemblage and standardize the expected range of variability in all skeletal elements of a single hipparionine species.

3.2 Taxonomy

Order Perissodactyla OWEN 1848

Suborder Hippomorpha WOOD 1937

Superfamily Equoidea HAY 1902

Family Equidae GRAY 1821

Subfamily Equinae STEINMANN AND DODERLEIN 1890

Hippotherium primigenium VON MEYER 1829

Lectotype: Right fragmentary mandible (SENK M1421) from Eppelsheim, Rheinhessen, Germany (as designated by BERNOR in WOODBURNE, BERNOR & SWISHER, 1996). This specimen is preserved in the Senckenberg Museum, Frankfurt, West Germany (contra FORSTEN, 1968). It is referred to in VON MEYER 1833: tabs. XXX-XXXI, Figs. 17, 18, 19.

Type Locality: Eppelsheim, Germany

Age: Vallesian (Late Miocene)

Diagnosis (after BERNOR et al., 1988):

Large hipparionine horse with moderate length snout; preorbital bar long (46–57 mm), with anterior extent of lacrimal placed more than one-half the distance from the anterior orbital rim to the posterior rim of the fossa; preorbital fossa subtriangular-shaped and anteroventrally oriented, deeply pocketed posteriorly, with great medial depth, medial wall lacking internal pits, peripheral border outline strong with a prominent anterior rim; nasal notch well anterior to P², cheek teeth relatively low crowned, in middle stage-of-wear adults, P² – M³ length dimension usually between 155 mm and 165 mm, fossette ornamentation complex, pli caballins bifid or complex, hypoglyphs deeply incised, protocones usually lingually flattened and labially rounded and P² anterostyle elongate; middle wear adult mandibular cheek teeth usually with well developed protostylids and complexly plicated enamel margins; metapodials generally short and rather robust, metacarpals with flattened distal sagittal crests, facet for the hamate/magnum articulation rather low (120–130 mm). A more expanded characterization of *Hippotherium primigenium* is given in chapters 4–6 here.

4. Skull, Mandible and Hyoid Bone

4.1 Description and Variability of the Skull and Maxillary Dentition

4.1.1 Characterization of the *Hippotherium primigenium* Skull by Discrete Characters

BERNOR et al., (1988), BERNOR, TOBIEN & WOODBURNE (1989) and BERNOR & LIPSCOMB (1991, 1995) have formulated a characterization of *Hippotherium primigenium* s.s. as a larger hipparionine species with the following characters: preorbital bar (POB) long with anteriormost lacrimal placed more than half the distance from the anterior orbital rim to the posterior rim of the fossa (Table 4.1, character 1C); nasomaxillary fossa absent, leaving only the nasolacrimal portion (when POF is present; 2C) remaining; orbital surface of the lacrimal bone lacking or having a highly reduced foramen (3B); preorbital fossa subtriangular shaped and anteroventrally oriented (4D), deeply pocketed posteriorly (5A), with great medial depth (6A), medial wall lacking internal pits (7A), with a strongly delineated peripheral border outline (8A) and a distinctly defined anterior rim present (9A); infraorbital foramen placed inferior to, or encroaching upon, the anteroventral border of the preorbital fossa (10B); buccinator and canine fossae distinct (11B); buccinator fossa not posteriorly pocketed (12A); caninus fossa depression lacking (13A); malar fossa lacking (14A); nasal notch shallowly retracted, being approximately half the distance between the canine and P² (15B); dP¹ believed present and/or reduced in juveniles (16Ua/b) and absent in adults (16UC); maxillary cheek teeth moderately curved (17B); unworn cheek teeth with maximum crown height between 40 and 50 mm (18C); except P² which is circa 30 mm in height, unworn); pre- and postfossette enamel plications complex with thickly banded, deeply incised plis (19A); posterior wall of the postfossette distinct (20B); pli caballins mostly double (21A); hypoglyph deeply incised well beyond middle stage-of-wear (22B); protocone lingually flattened and labially rounded (23E) and clearly isolated from the protoloph until very late stage-of-wear (24B); protocone spur very rare to absent (25C); protocone more lingually placed than hypocone in both the premolar (26B) and molar (27B) teeth; P²/P₂ anterostyle/paraconid elongate (28UA/28LA; re: Figs. 4.1.1.1 & 4.1.1.2).

4.1.2 Description of the Höwenegg Skulls

The Höwenegg hipparionine sample preserves nine adult skulls, as well as a single fetal and a single foal's skull. In general the skull material is mediolaterally crushed disallowing measurement of those dimensions. Otherwise the state of preservation is good, usually permitting reasonably accurate length dimensions of the bony portions and excellent measurement and study of the cheek teeth.



Figure 4.1.1.1. Original Höwenegg A Skull and Mandible, Lateral View (x 0,36).

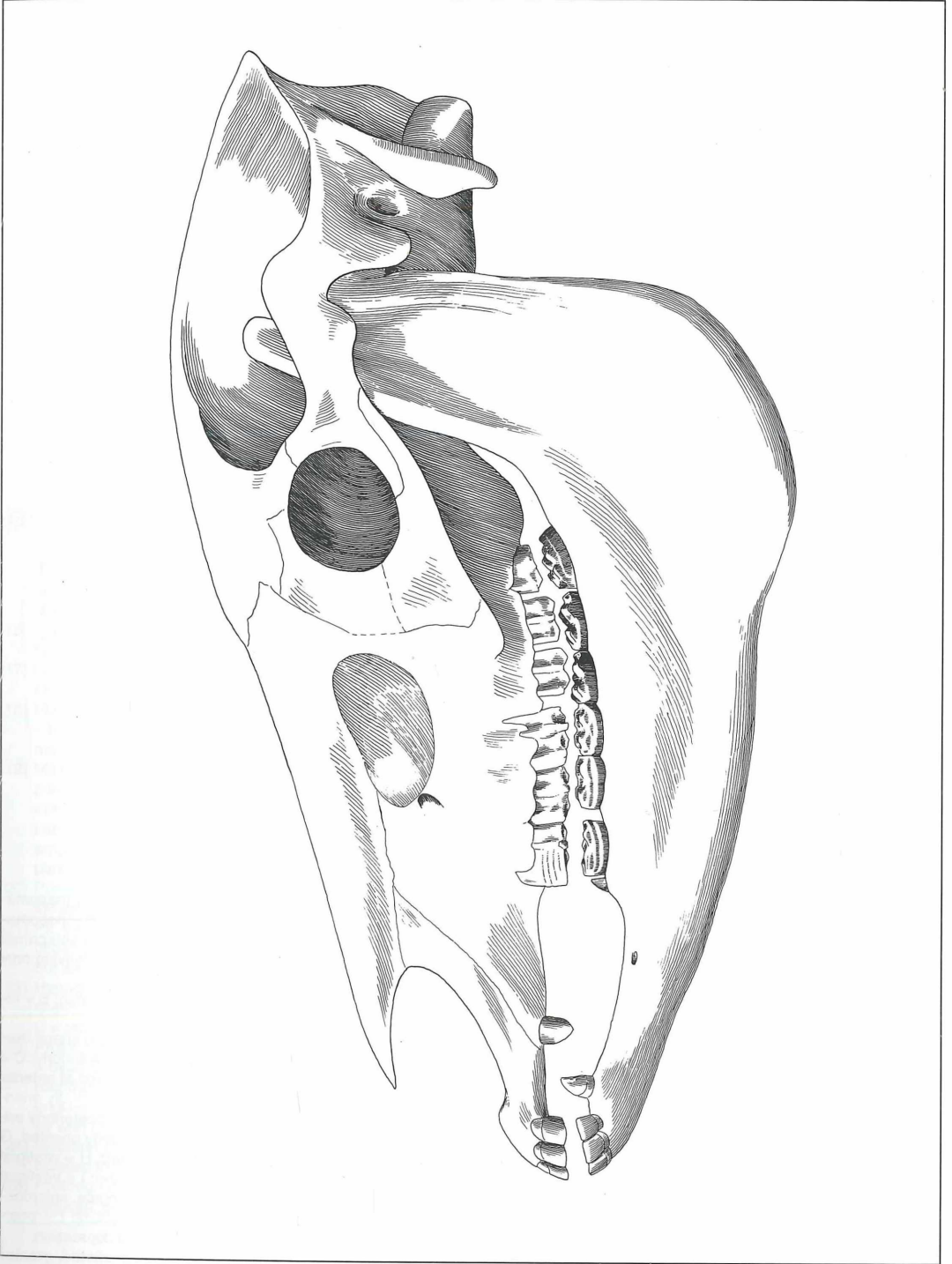


Figure 4.1.1.2. Reconstructed Höwenegg A Skull and Mandible, Lateral View (x 0,36).

Table 4.1. Character State Distribution of the Höwenegg *Hippotherium primigenium* Skulls, Maxillary and Mandibular Dentitions

	I	1	I	2	I	3	I	4	I	5
Hpri s.s.	C C B D A A A A A B B A A A B C B C A B A B E B C B B A A A A A A A A B A B a A C B A B B B A A									
SMNK Hö A	C C B D A A A A A B B A A A B c B C A B a B E B C B B A A A A A A e a a B A B B B B A c B b B A A									
SMNK Hö I	C C B D A A A A A B B A A A B C B C A B C B D B C B B A A A A A A A B A B A B c a c B A B B B A A									
SMNK Hö B	C C B D A A A A A B B A A A B a B C c a A a e B c B B A A A A A A A A B B b B B A c B B A A									
SMNK Hö C	C C B D A ? ? A A ? B ? A A b C B C A B a b e B C B B A A A A A A E A E B B b B B B A B B b A A									
HLMD Hö V	C C B D A A A A A B B A A A b C B C A B C B E B C B A A A A A A A e B E B B C a C B B C A A A A									
HLMD Hö M			C B C A B			A A A A A A	A	A B B a D B A C B B A A		
HLMD Hö G			B C B C			A A A A				A
HLMD Hö III	C C D A A A A B B A A A B a B C A B a B					A A A A			B	A
HLMD Hö E			a B C A B A B E B C B B			A A A A A A A A A	A A B C a	B a C		A A
Hö 25			C			A A A A a a E e	A b a B	B A B B B A A		
HLMD Hö 15/85						A A A A A A E E	E A B b a	B a B		

Note that lower case letters refer to semi-derived characters which are accounted for in the summaries, below.

Summary

Skulls and Maxillary Dentitions

- 1-6C
- 2-6C
- 3-5B
- 4-6D
- 5-6A
- 6-6A
- 7-5A
- 8-5A
- 9-6A
- 10-5B
- 11-6B
- 12-5A
- 13-6A
- 14-6A
- 15-5B, 2b/c, 1C
- 16U-3A, 6C
- 17-9B
- 18-9C
- 19-7A, 1c/a
- 20-1a/b, 7B
- 21-2A, 2a/c, 2C
- 22-2a/b, 5B
- 23-3E, 1c/d, 1e/c
- 24-6B
- 25-1a/c, 5C
- 26-6B
- 27-5B
- 28-11A

Mandibles and Mandibular Dentitions

- 16L-1B, 10C
- 29-11A
- 30-11A
- 31-11A
- 32-8A, 1a/e
- 33-8A, 1a/e
- 34-4A, 1a/e, 3E
- 35-3A, 2B, 1a/b
- 36-3A, 2a/e/b, 3E
- 37-4B, 1A
- 38-6A, 2B
- 39-8B, 1b/c
- 40-2B, 2C, 2a/c, 3b/c
- 41-4B, 5a/b
- 42-1C, 1D, 1c/d
- 43-10B
- 44-6A, 2a/b, 1B
- 45-4B, 2b/c, 3C
- 46-1A, 6B
- 47-5B, 2a/b
- 48-9A
- 49-11A

Hipparionine Character States (following BERNOR et al., 1989 and BERNOR & LIPSCOMB 1991, 1995; BERNOR & ARMOUR-CHÉLU, in press)

- 1) Relationship of lacrimal to the preorbital fossa: A = lacrimal large, rectangularly shaped, invades medial wall and posterior aspect of preorbital fossa; B = lacrimal reduced in size, slightly invades or touches posterior border of preorbital fossa; C = preorbital bar (POB) long with the anterior edge of the lacrimal placed more than half the distance from the anterior orbital rim to the posterior rim of the fossa; D = POB reduced slightly in length but with the anterior edge of the lacrimal placed still more than 1/2 the distance from the anterior orbital rim to the posterior rim of the fossa; E = POB vestigial, but lacrimal as in D; F = P.O.B. absent; G = POB very long with anterior edge of lacrimal placed less than 1/2 the distance from the anterior orbital rim to the posterior rim of the fossa; H = POB absent.
- 2) Nasolacrimal fossa: A = POF large, ovoid shape and separated by a distinct medially placed, dorsoventrally

oriented ridge, dividing POF into equal anterior (nasomaxillary) and posterior (nasolacrimal) fossae; B = nasomaxillary fossa sharply reduced compared to nasolacrimal fossa; C = nasomaxillary fossa absent (lost), leaving only nasolacrimal portion (when a POF is present).

- 3) Orbital surface of lacrimal bone: A = with foramen; B = reduced or lacking foramen.
- 4) Preorbital fossa morphology: A = large, ovoid shape, anteroposteriorly oriented; B = POF truncated anteriorly; C = POF further truncated, dorsoventrally restricted at anterior limit; D = subtriangular shaped and anteroventrally oriented; E = subtriangularly shaped and anteroposteriorly oriented; F = egg-shaped and antero- posteriorly oriented; G = C-shaped and anteroposteriorly oriented; H = vestigial but with a C-shaped or egg-shaped outline; I = vestigial without C-shape outline, or absent; J = elongate, anteroposteriorly oriented; K = small, rounded structure; L = posterior rim straight, with non-oriented medial depression.
- 5) Fossa posterior pocketing: A = deeply pocketed, greater than 15 mm in deepest place; B = pocketing reduced,

- moderate to slight depth, less than 15 mm; C = not pocketed but with a posterior rim; D = absent, no rim but a remnant depression; E = absent.
- 6) Fossa medial depth: A = deep, greater than 15 mm. in deepest place; B = moderate depth, 10 - 15 mm in deepest place; C = shallow depth, less than 10 mm in deepest place; D = absent.
 - 7) Preorbital fossa medial wall morphology: A = without internal pits; B = with internal pits.
 - 8) Fossa peripheral border outline: A = strong, strongly delineated around entire periphery; B = moderately delineated around periphery; C = weakly defined around periphery; D = absent with a remnant depression; E = absent, no remnant depression.
 - 9) Anterior rim morphology: A = present; B = absent.
 - 10) Placement of infraorbital foramen: A = placed distinctly ventral to approximately 1/2 the distance between the preorbital fossa's anteriormost and posteriormost extent; B = inferior to, or encroaching upon anteroventral border of the preorbital fossa.
 - 11) Confluence of buccinator and canine fossae: A = present; B = absent, buccinator fossa is distinctly delimited.
 - 12) Buccinator fossa: A = not pocketed posteriorly; B = pocketed posteriorly.
 - 13) Caninus (= intermediate) fossa: A = absent; B = present.
 - 14) Malar fossa: A = absent; B = present.
 - 15) Nasal notch position: A = at posterior border of canine or slightly posterior to canine border; B = approximately half the distance between canine and P²; C = at or near the anterior border of P²; D = above P²; E = above P³; F = above P⁴; G = above M1; H = posterior to M1.
 - 16) Presence of dP¹ (16U) or dP₁ (16U): A = persistent and functional; B = reduced and non-functional; C = absent.
 - 17) Curvature of maxillary cheek teeth: A = very curved; B = moderately curved; C = straight.
 - 18) Maximum cheek tooth crown height: A = < 30 mm; B = 30 - 40 mm; C = 40 - 60 mm; D = 60 - 75 mm; E = 75+ maximum crown height.
 - 19) Maxillary cheek tooth fossette ornamentation: A = complex, with several deeply amplified plications; B = moderately complex with fewer, more shortly amplified, thinly banded plications; C = simple complexity with few, shortly amplified plications; D = generally no plis; E = very complex.
 - 20) Posterior wall of postfossette: A = may not be distinct; B = always distinct.
 - 21) Pli caballin morphology: A = double; B = single or occasionally poorly defined double; C = complex; D = plis not well formed.
 - 22) Hypoglyph: A = hypocone frequently encircled by hypoglyph; B = deeply incised, infrequently encircled hypocone; C = moderately deeply incised; D = shallowly incised.
 - 23) Protocone shape: A = round q-shape; B = oval q-shape; C = oval; D = elongate-oval; E = lingually flattened-labially rounded; F = compressed or ovate; G = rounded; H = triangular; I = triangular-elongate; J = lenticular; K = triangular with rounded corners.
 - 24) Isolation of protocone: A = connected to protoloph; B = isolated from protoloph.
 - 25) Protoconal spur: A = elongate, strongly present; B = reduced, but usually present; C = very rare to absent.
 - 26) Premolar protocone/hypocone alignment: A = antero-posteriorly aligned; B = protocone more lingually placed.
 - 27) Molar protocone/hypocone alignment: A = anteroposteriorly aligned; B = protocone more lingually placed.
 - 28) P2 anterostyle (28U) / paraconid (28L): A = elongate; B = short and rounded.
 - 29) Mandibular incisor morphology: A = not grooved; B = grooved.
 - 30) Mandibular incisor curvature: A = curved; B = straight.
 - 31) I₃ lateral aspect: A = elongate, not labiolingually constricted; B = very elongate, labiolingually constricted distally; C = atrophied.
 - 32) Premolar metaconid: A = rounded; B = elongated; C = angular on distal surface; D = irregular shaped; E = square shaped; F = pointed.
 - 33) Molar metaconid: A = rounded; B = elongated; C = angular on distal surface; D = irregular shaped; E = square shaped; F = pointed.
 - 34) Premolar metastylid: A = rounded; B = elongate; C = angular on proximal surface; D = irregular shaped; E = square shaped; F = pointed.
 - 35) Premolar metastylid spur: A = present; B = absent
 - 36) Molar metastylid: A = rounded; B = elongate; C = angular on proximal surface; D = irregular shaped; E = square shaped; F = pointed.
 - 37) Molar metastylid spur: A = present; B = absent
 - 38) Premolar ectoflexid: A = does not separate metaconid and metastylid; B = separates metaconid and metastylid.
 - 39) Molar ectoflexid: A = does not separate metaconid and metastylid; B = separates metaconid and metastylid; C = converges with preflexid and postflexid to abutt against metaconid and metastylid.
 - 40) Pli caballinid: A = complex; B = rudimentary or single; C = absent.
 - 41) Protostylid: A = present on occlusal surface often as an enclosed enamel ring; B = absent on occlusal surface, but may be on side of crown buried in cement; C = strong, columnar; D = a loop; E = a small, poorly developed loop; F = a small, pointed projection continuous with the buccal cingulum.
 - 42) Protostylid orientation: A = courses obliquely to anterior surface of tooth; B = less oblique coursing, placed on anterior surface of tooth; C = vertically placed, lies flush with protoconid enamel band; D = vertically placed, lying lateral to protoconid band; E = open loop extending posterolabially.
 - 43) Ectostylids: A = present; B = absent.
 - 44) Premolar linguaflexid: A = shallow; B = deeper, V-shaped; C = shallow U-shaped; D = deep, broad U-shape; E = very broad and deep.
 - 45) Molar linguaflexid: A = shallow; B = V-shaped; C = shallow U-shaped; D = deep, broad U-shape; E = very broad and deep.
 - 46) Preflexid morphology: A = simple margins; B = complex margins; C = very complex.
 - 47) Postflexid morphology: A = simple margins; B = complex margins; C = very complex.
 - 48) Postflexid invades metaconid/metastylid junction by anteriormost portion bending sharply lingually: A = no; B = yes.
 - 49) Protoconid enamel band morphology: A = rounded; B = flattened.

	16U	17	18	19	20	21	22	23	24	25	26	27	28U
HLMD Hö G													
dP1	C												
P2		B											A
P3		B											
P4		B											
M1		B											
M2		B											
M3		B											
HLMD Hö III													
dP1	A												
P2		B		A	B								A
P3		B		A	B								
P4		B		A	B	A	B						
M1		B		A	B	C	B						
M2		B		A	B		B						
M3		B		A	B	A	B						
HLMD Hö E													
dP1	A												
P2		B		B	B	B	B	E	A	C	B		A
P3		B		A	B	A	B	E	B	C	B		
P4		B		A	B	A	B	E	B	C	B		
M1		B		A	B	A	B	E	B	C		B	
M2		B		A	B	A	B	E	B	C		B	
M3		B		A	B	A	A	E	B	C		B	

* = wear related morphological feature

Legend
as for Table 4.1

SMNK Hö A is a very well preserved adult male skull including most of the bony and all of the dental elements (Fig. 4.1.1.1). The medial walls of the orbit and a majority of the cranium have been lost, as well as the medial walls of the preorbital and buccinator fossae. The preorbital bar and lacrimal are as described above (character 1C), except that the orbital surface of the lacrimal is not clearly preserved, making presence/absence of the lacrimal foramen uncertain (3? B). Facial morphology is virtually identical to the description given above (4D), although it is somewhat obscured by mediolateral crushing. Preorbital fossa medial depth is not well preserved, but the distinctiveness of the peripheral border and anterior rim suggests that this aspect of the fossa was deep (6A). The buccinator fossa is not preserved (although clearly there was no posterior pocketing; 12A), and there was no caninus fossa (13A). Nasal notch morphology is similar to the generalized description given above in that it is incised only half the distance between canine and P² (23 mm

anterior to P²; 15B). The incisors are large, well preserved, and each have large, elongate, single infundibula (fig. 4.1.2). The canines are very large, indicating that this individual was a male. Labially, the canines have a smooth, convex contour, while lingually they have a medially positioned, vertically oriented, pyramidal-shaped pillar with the apex directed ventrally; both anteriorly and posteriorly this apical structure is bounded by distinctly concave recesses. The dP¹ is absent (16UC). The premolar and molar teeth (fig. 4.1.3) are large and conform closely to the generalized description given above, except that the pli caballins may be either double (21A) or complex (21C); hypoglyphs are always deeply incised (22B) except on M³ where the incision completely isolates the hypocone, due to its very early stage-of-wear and buccolingual compression of the tooth (22A); protocones are mostly lingually flattened (23E), but show some buccolingual flattening (23ec on M¹) due to their relatively early stage-of-wear. Isolation of the protocone, protoconal spur, premolar

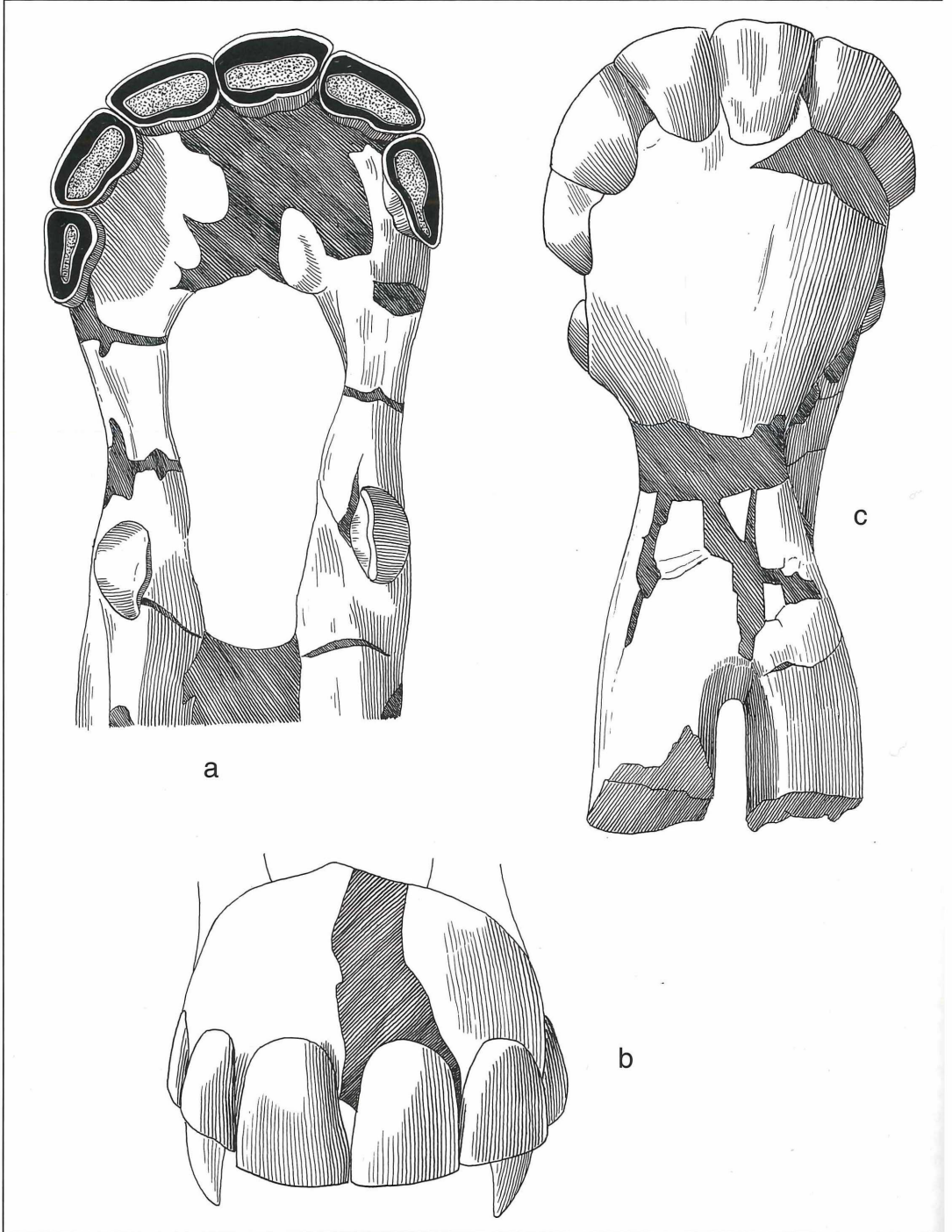


Figure 4.1.2. Höwenegg A maxillary and mandibular anterior dental arcades. Maxillary: a. occlusal view, b. buccal view; mandibular: c. ventral view, d. occlusal view, e. oblique occlusal view (x 1,0).

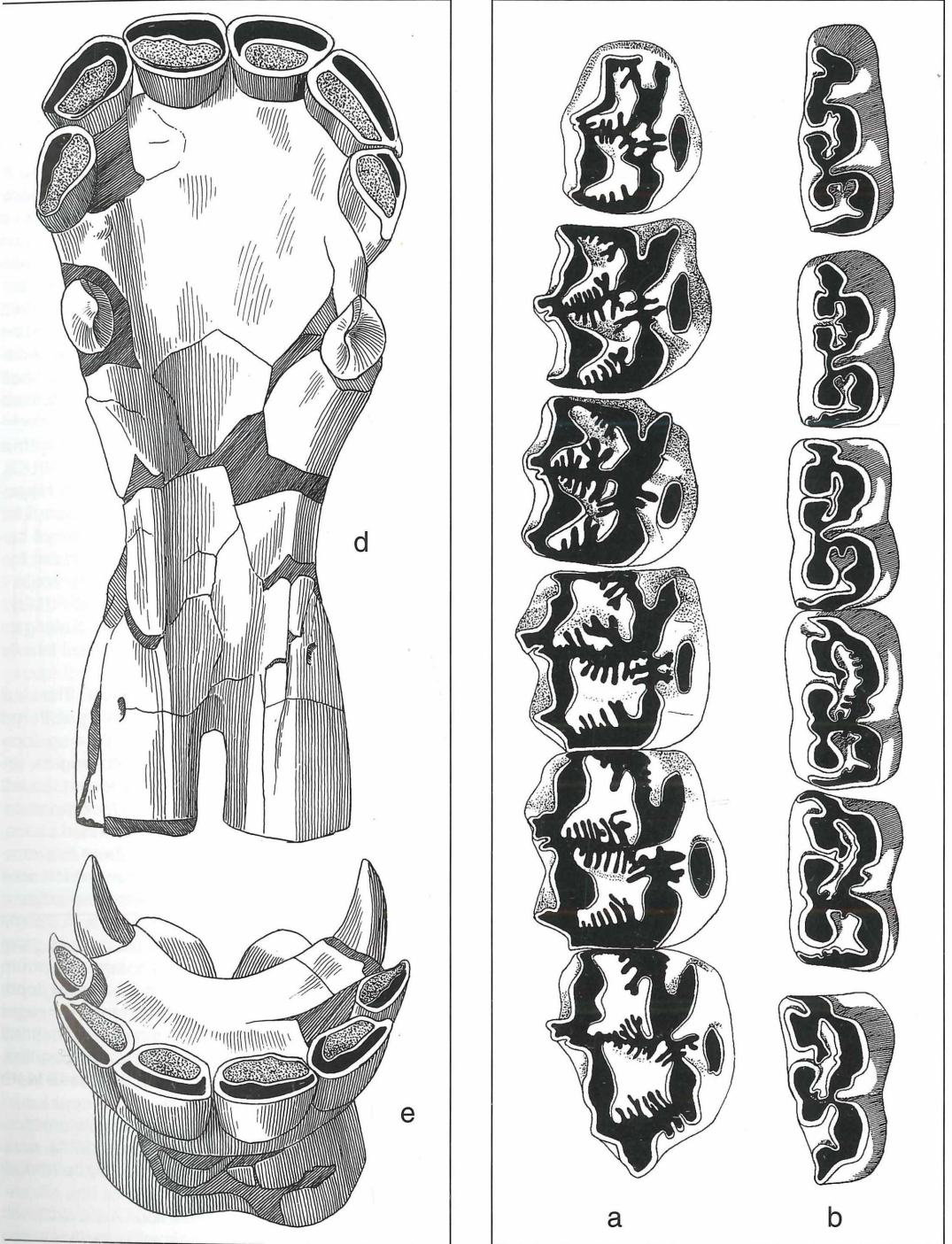


Figure 4.1.3. Höwenegg A left cheek tooth series, occlusal view: a. maxillary; b. mandibular (x 1,0).

protocone-hypocone alignment, molar protocone-hypocone alignment and P² anterostyle are as for *Hippotherium primigenium*'s characterization.

SMNK Hö I is an adult female specimen which is less well preserved than SMNK Hö A, showing multiple small fractures resulting from severe mediolateral crushing. Most of the snout is present but has minimal original contact with the maxillary region preserved. The area of the nasal notch is barely preserved on the right side, and is as in SMNK Hö A (15B). The intervening area including posterior nasals, maxilla, preorbital fossa, lacrimals and the anterior 2/3rds of the left orbital rim is preserved; the posterior 1/3rd of the left orbit, the entire right orbit and cranium are missing. The preorbital bar is as in SMNK Hö A, but neither the lacrimal suture nor the orbital surface of the lacrimal bone are preserved. The facial morphology is as in the generalized characterization given above. The incisors are all preserved and reveal a morphology identical to SMNK Hö A. The right canine alveolus and root are present and reveal a small, peg-shaped structure, and indicate that this individual was female. There is no dP¹ preserved (16UC). P² – M³ depart from *Hippotherium primigenium* s.s. in some details; all have complex pli caballins (21C); again only M³ has the hypocone encircled by the hypoglyph (22A; ontogenetically dependant); protocones are mostly somewhat elongate oval-shaped (23c/d) with only M¹ showing some degree of flattening (23E). In comparison to *Cormohipparion occidentale* (23D), protocones are somewhat restricted in the buccolingual width of their anteriormost and posteriormost limits (BERNOR et al., 1988), and do not have distinctly developed lingual flattening and labial rounding (23E) as is found in the Vienna Basin populations of *Hippotherium primigenium* s.s. (BERNOR et al., 1988). Other maxillary cheek tooth characters are as in *Hippotherium primigenium*. SMNK Hö B is a sub-adult male skull, severely crushed mediolaterally, but otherwise complete. The preorbital bar is long and has a broad, vertically oriented crack running through it, giving longer than actual dimensions. Facial morphology is virtually identical to the generalized description given above (29.7 mm anterior to P²; 15B). DP¹ departs from the specific characterization of *Hippotherium primigenium* in that it is large and still functional (16UA). P²⁻⁴ and M³ are in an early stage-of-wear, and as a result exhibit simple fossette plication amplitudes (19C); M¹⁻² are as for *Hippotherium primigenium*. P²⁻⁴ have the posterior wall of their post-fossettes ill-defined (20A), whereas M¹⁻³ are as in *Hippotherium primigenium*. Only P³ and M¹⁻² have pli caballins expressed, and they are double (20A). The hypoglyph completely encloses the hypocone on the premolars and M³ only (22A) and a small protoconal spur can be seen on right P² (25B). P² has the protocone anteroposteriorly aligned (26A – a primitive condition expressed due to the early stage-of-wear in this

tooth), whereas P³⁻⁴ have the protocone more lingually placed (26B).

SMNK Hö C is a moderately well preserved young adult female skull nearly complete except for restored portions of the premaxilla, maxilla, preorbital fossa, orbit and basicranium. The skull shows strong mediolateral compression. The preorbital bar is best preserved on the left side and the lacrimal bone's morphology would appear to be as in the above described specimens. Although damaged, the preorbital fossa has a subtriangular shape and an anteroventral orientation (4D). Preserved portions of the medial wall and posterior rim suggest that this individual had a POF morphology essentially identical to the above described specimens. The buccinator fossa is not preserved on either side. The nasal bones are preserved and incised well anterior to P², but somewhat more than half the distance from canine to P² (15b/c). The incisors are all preserved, with I³ just beginning to fully occlude. The canine is a small peg-shaped structure with a morphology typical of females. DP¹ is absent (16UC). The maxillary cheek teeth conform closely with *Hippotherium primigenium* s.s.'s characterization except for some following departures: P² has a complex pli caballin (21C); hypoglyph completely surrounds the hypocone on P³⁻⁴ (ontogenetic variation; 22A), while it conforms to the characterization in P² and M¹⁻² (22B); protocone is semi-elongate on M¹⁻² (23ec) and elongate on M³ (23c), being more lingually flattened and labially rounded on the premolars (23E).

HLMD Hö V is an old adult female individual. The skull is the best preserved of the sample having suffered relatively little mediolateral crushing and being complete except for portions of the buccinator region, orbits and cranium. All teeth are present except the left canine. Facial morphology is as defined for *Hippotherium primigenium* s.s. and specimens described above, except for the notable exception that there is a remnant lacrimal foramen distinguishable in the left orbit (3B). This foramen is not clearly present, but rather a rim can be distinguished surrounding matrix in a slight recess. The preorbital fossa clearly preserves its great posterior pocketing (more than 15 mm maximum depth) and medial depth (maximum measured depth is 35 mm). The premaxilla shows relatively slight mediolateral crushing. The incisors have well defined infundibula and the right canine is small and peg-like. The dP¹ is absent (16UC). Likewise, the cheek teeth show an advanced stage-of-wear, and except for pli caballin complexity (21C) and the remarkable anterior-posterior alignment of molar protocones (27A), conform closely to the characterization for *Hippotherium primigenium* s.s.

Hö M is a poorly preserved partial adult male skull with associated lower jaw. The specimen is badly eroded and cracked, with the right side exposed, and includes the premaxilla and the lower one-half of the maxillary

region. The superior one-half of the maxilla, nasals, orbits and cranium are absent. The teeth reveal a middle stage-of wear adult. The incisors have well developed, elongate-shaped infundibula. The right canine is broken, but its base and root reveal its robust build. DP¹ is absent (16UC). When not obscured by rock matrix, the premolars and molars conform very closely with the characteristics for *Hippotherium primigenium* s.s. HLMD Hö G is a complete, although badly crushed skull and mandible of a middle stage-of-wear adult male. The skull and mandible have been left in occlusion, making morphological observations and measurements on cheek tooth features virtually impossible. The preorbital bar is so damaged that its accurate measurement is not possible; however, it is clear that it had a comparable length to other, better preserved specimens. The preorbital fossa is also too poorly preserved to characterize, and the area of the buccinator fossa is not preserved. The nasal notch is preserved, and placed distinctly anterior to P² (15B). I¹⁻² and C are preserved and have an identical morphology to other adult males. The dP¹ is absent (16UC). The premolar and molar teeth are preserved, but their occlusal faces remain unprepared. P² anterostyle (28UA) and incisor morphology can be observed to be as in *Hippotherium primigenium* s.s.

HLMD Hö III is a severely crushed older adult skull with associated lower jaw, of unknown sex. The right side of the specimen is exposed and is mostly complete except for the anterior premaxillary region, incisor and canine teeth. Upper and lower cheek tooth morphology remains largely obscured by matrix and close occlusion of the jaws. The preorbital bar is too crushed for accurate measurement, but would appear to have had a comparable length to other specimens. The facial morphology conforms with *Hippotherium primigenium* s.s. and the specimens described above. The nasal notch would appear to be incised only half the distance from the canine to the P² (15B). DP¹ is moderately large and was functional (16UA; note below that the dP₁ was absent). The upper cheek teeth have the protocone obscured by matrix, disallowing their study. While this specimen agrees well with *Hippotherium primigenium* s.s. in fossate plication amplitude (19A), morphology of the posterior wall of the postfossette (20B) and hypoglyph (22B) morphology, pli caballins are variably double or complex (21a/c).

HLMD Hö E is an older adult female skull fragment with associated lower jaw. This individual had preserved a directly associated fetus in utero. The adult specimen is fragmentary and includes a detached premaxilla with all incisors and the left canine tooth intact; the maxilla and all cheek teeth including dP¹ are preserved as is the inferior border of the preorbital fossa and facial maxillary crest. The nasals, most of the preorbital fossa, preorbital bar, orbits and cranium are entirely lacking, disallowing their characterization. All of the incisor

teeth, except left I³ reveal large, elongate, well developed infundibula; left I³ on the other hand is anomalous, having a medial and a lateral dentine lake engulfed within very fine enamel bands. The maxillary cheek teeth conform to the characterization of *Hippotherium primigenium* s.s. except: dP¹ is large and functional (16UA), even in this late stage-of-wear (note however that mandibular dP₁ was absent [16C]); hypoglyphs are deeply incised, but only enclose hypocone in M³ (22A).

4.1.3 Summary of Character State Distribution

Tables 4.1 and 4.2 give the character state distribution of skulls and maxillary dentitions described above, or characters 1–28U, as well as a summary of their frequency distribution. Of these characters the following are stable in 100 % of the cases studied: 1–14 (facial morphology), 17 and 18 (maxillary cheek tooth curvature and maximum crown height [estimated], respectively), 24 (isolation of protocone), 26 (premolar protocone-hypocone alignment) and 28UL (P² anterostyle). Three characters were less stable, being present in 75 % or more of the cases: 19 (maxillary cheek tooth ornamentation); 20 (posterior wall of postfossette) and 27 (molar protocone-hypocone alignment). In addition, there were a number of characters that were less stable, including (in descending % of stability): 15 (nasal notch incision; 71 % B, 29 % bc); 23 (protocone shape = 60 % E, 20 % cd, 20 % ec). Some variability is of particular interest.

Character 16U, dP¹ morphology showed an interesting variability. Whereas dP₁ (16L) was only found in one adult mandible (Hö A), and was strictly vestigial, dP¹ was found to be large, persistent and functional in Hö B (young adult male), Hö III (old adult, no sex known) and Hö E (old adult female). The presence of a functional dP¹ is a primitive character for hipparionines, and its presence in both males and females precludes it from being a sexually dimorphic character. In the Höweneegg foal, SMNK Hö Y, the maxilla and mandible are naturally cemented in place by rock matrix. One can clearly see here that dP¹ fully occludes with the paraconid of dP₂, and would have functioned as such in juvenile and young adult (at least) individuals.

Character 21, pli caballin morphology, was found to be variably bifid or complex in approximately middle stage-of-wear adult dentitions, whereas in earlier and later stages-of-wear they were simply bifid. The presence of some variable pli caballin complexity in the Höweneegg hipparion is a semi-derived character for Old World hipparions (BERNOR, TOBIEN & WOODBURN, 1989). Character 22, hypoglyph incision, was found to be very deep in middle stage-of-wear individuals. Younger individuals expressed the primitive condition of isolating the hypocone, while older individuals reduced hypoglyph incision to a slight degree. Character 23, protocone morphology, likewise showed some

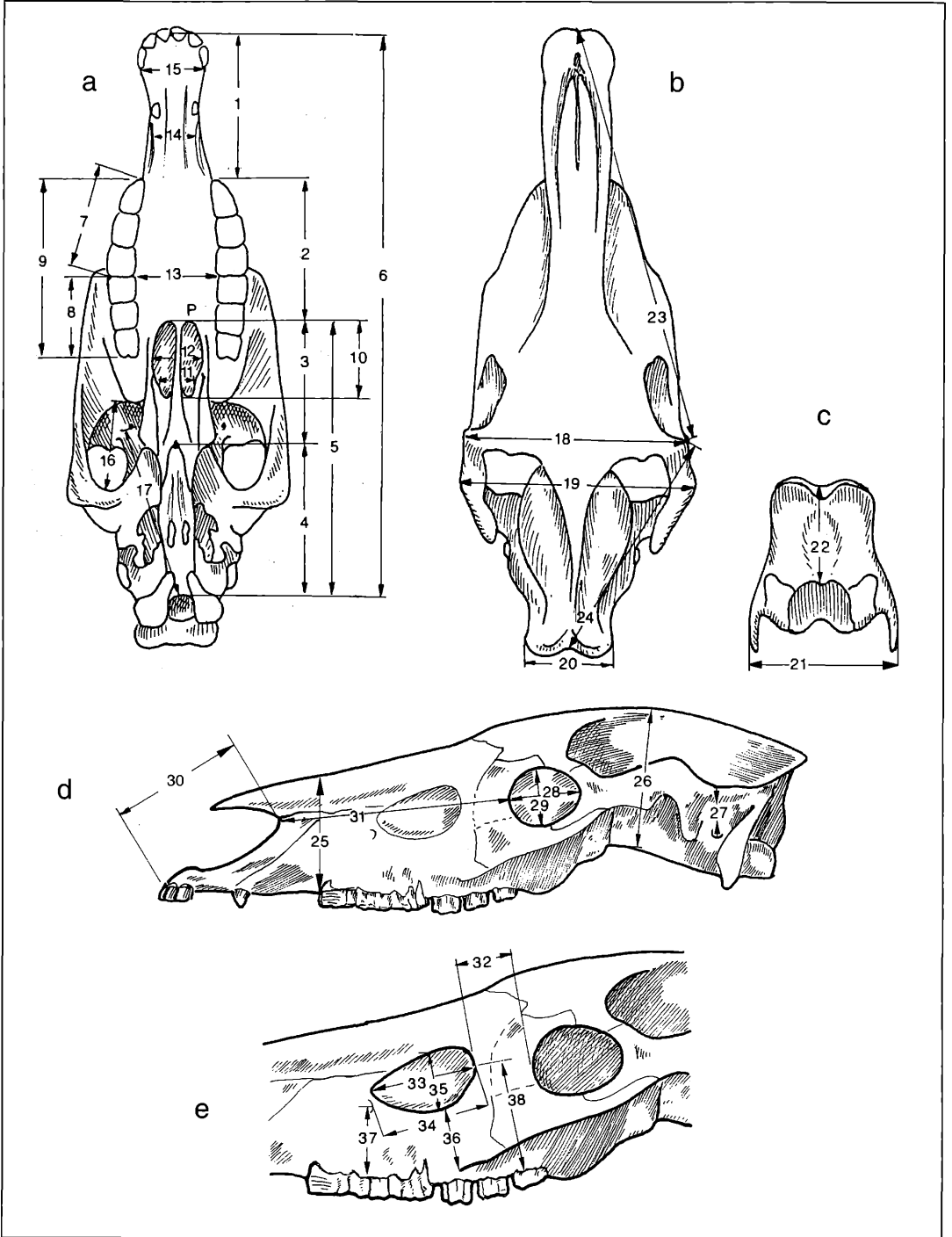


Figure 4.2. Measurements on Skulls: a. ventral aspect; b. dorsal aspect; c. occipital aspect; d. lateral aspect; e. close-up lateral aspect of measurements taken on the preorbital fossa.

ontogenetic variability: young adults tended to have a more oval-shaped morphology; middle stage-of-wear adults predominately had the lingual surfaces flattened; old individuals had more rounded protocones. The middle stage-of-wear adults would therefore best be scored as having lingually flattened, labially rounded protocones.

The Höweneegg hipparion varies slightly from BERNOR, TOBIEN & WOODBURNE'S (1989) characterization of *Hippotherium primigenium* s.s. (Table 4.1) in the following ways: dP¹ (but not dP₁) may remain functional in some (16UA), but not all (16C), adult individuals; pli cabalians may be variably double (21A) or complex (21C). Characters 15 b/c (nasal notch incision) and 16U a/c (presence and function of dP¹) are plesiomorphous and further suggest close affinities between the Höweneegg horse to North American *Cormohipparion* sister taxa; 21 a/c is apparently a synapomorphy shared with more advanced members of the Central European *Hippotherium primigenium* s.s. lineage (re: BERNOR et al., 1993a; BERNOR, MITTMANN & RÖGL, 1993b; WOODBURNE, BERNOR & SWISHER, 1996).

4.1.4 Statistical Characteristics of Skull Measurements

The first 38 of 39 variables were measured on the skull (Fig. 4.2). Our skull data base had many missing cases due to frequent severe mediolateral crushing, reflected in the high number of measurements with CV's above 10 (m15, m16, m22, m29, m30, m31, m32, m33 m34, m35, m36 and m38). This also directly affected the number of significant correlations (Table 4.3), of which only one (m33-m34) was significant at greater than the 99 % level of significance, and 3 others at the 95 % level. It is not surprising that measurements 33 (maximum length of POF) and 34 (distance between posterior aspect of POF and the posterior edge of the infraorbital foramen) are so highly correlated since neither measurement was affected by crushing and the relevant structures have been demonstrated to be extremely stable morphologically (see BERNOR, TOBIEN & WOODBURNE, 1989 for a recent summary).

Measurement 7 (premolar row length)-m9 (cheek tooth row length) were likewise unaffected by crushing and it was expected that these would be highly correlated; it is somewhat surprising that m8 (molar tooth row length) was not similarly correlated with either m7 or m9, but this may in large part be due to size variation in M³. Measurement 9 was also highly correlated with m29 (orbit height); both of these measurements have been used to reflect the size of the animal (WOODBURNE & BERNOR, 1980). Measurement 1 (muzzle length) was significantly correlated with m23 (anterior ocular line); both measurements reflect length of the skull and were minimally affected by mediolateral crushing.

A similar set of descriptive statistics are currently being applied by us to a number of North American Neogene equid quarry samples and should yield a better appreciation of significant correlations and their biological meaning.

4.1.5 Statistical Characteristics of the Maxillary Dentition

Two measurements were taken on all three incisors, the canine and dP¹ (m1 = length and m3 = width at occlusal level). Eleven measurements were taken on the premolar and molar cheek teeth (other than dP¹; Fig. 4.3): m1 = length at occlusal level; m2 = length 10 mm above the tooth's base (in isolated teeth only); m3 = width at occlusal level, taken across mesostyle-protocone; m4 = width 10 mm above the tooth's base (in isolated teeth only); m5 = crown height measured along the mesostyle; m6 = number of plications on the anterior face of the prefossette; m7 = number of plications on the posterior face of the prefossette; m8 = number of plications on the anterior face of the postfossette; m9 = number of plications on the posterior face of the postfossette; m10 = protocone length; m11 = protocone width. Of the maxillary teeth measured, I¹, C, P², P³, M¹, M² and M³ exhibited significant correlations (Table 4.3).

I1 gave a 0.022 probability for negative correlation of m1 versus m3, whereas the same measurements on the canine gave a positive correlation at the .95-.99 level of significance. In the first case as length decreased, width increased. In the second, length and width covaried directly. Maxillary canine length showed a strong bimodality, with males being consistently larger than females (Fig. 4.4). CV's were below 10 on all incisor measurements except m3 for I³ (CV = 37.19) due largely to the change the distal aspect exhibits as it comes into full occlusion and begins to wear. Both canine measurements had very elevated CV's (m1 CV = 39.48; m3 CV = 40.93) due to the sexual dimorphism shown by this tooth. Bivariate plots of both maxillary and mandibular canine length X width measurements by sex are given in Figure 4.4. The maxillary canines show strong sexual dimorphism while the mandibular canines overlap somewhat in their bivariate dimensions. P² exhibited 10 significant correlations, 7 at or above the .01 significance level. Measurements 6, 7, 8 and 9 constituted 5 correlations at the .01 level of significance (m8-m9, m6-m7, m6-m8, m7-m9) and 1 of the correlations significant at the .05 level amongst themselves; this reveals that despite great individual variability for fossette plication, the number of enamel plications on the pre- and postfossettes vary strongly together with tooth-wear. M7 showed a 0.032 probability level of correlation with m10 (protocone length), suggesting that with wear these variables covary so that with fewer plications one would expect a corresponding shorter protocone length. Measurement 3 (width of crown at occlusal level) correlated both with m1 (occlusal le-

Table 4.3. Summary Statistics on Skull Continuous Variables

Measure- ment	Sample size	Mean	Standard Deviation	Confidence Limits		Coefficient of Variation	Confidence Limits		Minimum	Maximum	Median
m1	5	140,14	5,80	134,79	145,49	4,14	1,43	6,84	133,50	149,30	139,00
m2	1	147,00							147,00	147,00	147,00
m3	1	108,00							108,00	108,00	108,00
m4	1	84,10							84,10	84,10	84,10
m5	0										
m6	2	477,25	24,40			5,11			460,00	494,50	477,25
m7	9	85,00	3,13	82,85	87,15	3,68	1,89	5,47	81,00	89,70	86,00
m8	9	74,53	4,08	71,72	77,34	5,48	2,80	8,15	70,60	82,10	72,90
m9	9	159,21	5,99	155,09	163,34	3,76	1,93	5,60	147,00	167,80	161,00
m10	0										
m11	0										
m12	0										
m13	0										
m14	3	30,90	3,10	27,21	34,59	10,03	1,49	18,57	28,50	34,40	29,80
m15	3	46,93	5,01	40,97	52,90	10,67	1,58	19,76	43,10	52,60	45,10
m16	3	96,63	8,66	86,32	106,95	8,96	1,35	16,57	86,80	103,10	100,00
m17	1	115,40							115,40	115,40	115,40
m18	0										
m19	0										
m20	1	71,60							71,60	71,60	71,60
m21	2	77,90	2,97			3,81			75,80	80,00	77,90
m22	2	70,35	8,98			12,77			64,00	76,70	70,35
m23	4	351,63	24,17	326,68	376,57	6,87	1,83	11,91	334,00	385,50	343,50
m24	2	212,25	1,06			0,50			211,50	213,00	212,25
m25	4	102,75	4,41	98,20	107,30	4,30	1,16	7,44	97,20	107,80	103,00
m26	2	129,75	3,89			3,00			127,00	132,50	129,75
m27	0										
m28	4	66,48	4,33	62,00	70,95	6,52	1,74	11,30	61,20	71,30	66,70
m29	4	50,28	7,67	42,36	58,19	15,25	3,87	26,64	44,80	61,50	47,40
m30	4	136,58	15,67	120,41	152,74	11,47	2,99	19,95	122,40	156,80	133,55
m31	6	206,87	24,96	185,83	227,90	12,07	4,77	19,36	174,30	227,20	219,05
m32	5	48,96	5,85	43,56	54,36	11,94	4,04	19,85	43,00	57,00	46,10
m33	6	80,45	9,60	72,36	88,54	11,93	4,72	19,14	64,50	94,00	80,00
m34	4	85,88	10,39	75,15	96,60	12,10	3,14	21,06	73,20	98,00	86,15
m35	6	51,48	7,74	44,96	58,00	15,03	5,87	24,18	39,10	58,50	54,00
m36	5	26,90	12,64	15,23	38,57	46,98	10,17	83,80	15,50	48,00	24,20
m37	4	47,98	2,82	45,07	50,88	5,88	1,57	10,18	45,10	51,80	47,50
m38	5	76,22	12,04	65,11	87,33	15,79	5,23	26,36	62,00	93,10	74,80
m39	0										

vel length) and m10 (protocone length). The only negative correlation found was between m5 (crown height) and protocone width (m11; $r = -0.996$), revealing that as crown height decreases protocone width increases. This metrically reflects what has been observed morphologically: as the tooth wears, protocone transforms progressively from an elongate to a rounded structure.

P^3 showed 7 significant correlations: 3 above the 99 % level: m7-m8, m6-m11, m6-m7. Again, measurements 6, 7, 8 and 9 figured prominently accounting for three

of the significant correlations amongst themselves (m7-m8, m6-m9 and m6-m9) and another, m6, correlated strongly negatively with protocone width (m11). This last indirectly reflects the morphological observation that as the tooth wears, the number of plications decrease in number while protocone width increases. M11 further correlated positively with m10 (protocone length), and negatively with m1 (crown length; with wear, length of tooth decreasing and protocone width increasing) and height (with wear, crown height decreasing and protocone width increasing).

32 BERNOR, TOBIEN, HAYEK & MITTMANN: *Hippotherium primigenium*, Höweneegg

TxC

Measurement	Sample size	Mean	Standard Deviation	Confidence Limits		Coefficient of Variation	Confidence Limits		Minimum	Maximum	Median
m1	9	10,54	4,16	7,68	13,41	39,48	17,48	61,48	5,50	16,80	11,50
m2	0										
m3	9	7,67	3,14	5,51	9,83	40,93	17,92	63,93	3,80	13,60	7,10
m4	0										
m5	0										
m6	0										
m7	0										
m8	0										
m9	0										
m10	0										
m11	0										

TxP2

Measurement	Sample size	Mean	Standard Deviation	Confidence Limits		Coefficient of Variation	Confidence Limits		Minimum	Maximum	Median
m1	12	31,49	1,48	30,61	32,37	4,69	2,71	6,66	29,40	34,30	31,50
m2	0										
m3	10	24,67	1,57	23,64	25,70	6,38	3,43	9,34	22,00	26,60	25,15
m4	0										
m5	7	22,89	8,32	16,40	29,38	36,35	13,80	58,89	14,70	37,90	20,00
m6	12	3,00	2,89	1,28	4,72	96,40	27,73	165,07	7,00	3,50	
m7	12	3,00	2,86	1,30	4,70	95,35	27,91	162,78	8,00	3,00	
m8	12	2,33	2,53	0,82	3,84	108,63	24,74	192,51	7,00	2,00	
m9	12	0,92	0,90	0,38	1,45	98,22	27,39	169,04	2,00	1,00	
m10	8	6,84	0,91	6,17	7,50	13,31	6,32	20,30	5,00	7,80	7,10
m11	8	4,71	1,19	3,84	5,58	25,32	11,44	39,20	2,60	6,10	4,65

TxP3

Measurement	Sample size	Mean	Standard Deviation	Confidence Limits		Coefficient of Variation	Confidence Limits		Minimum	Maximum	Median
m1	13	26,11	1,88	25,03	27,18	7,20	4,27	10,13	21,60	28,60	26,60
m2	0										
m3	10	26,69	1,65	25,61	27,77	6,19	3,32	9,05	24,40	29,30	26,50
m4	0										
m5	8	28,54	12,80	19,20	37,88	44,86	17,45	72,27	12,70	47,40	28,60
m6	13	2,62	2,60	1,13	4,10	99,39	29,99	168,78	6,00	2,00	
m7	13	3,77	2,83	2,15	5,39	75,16	30,76	119,56	8,00	5,00	
m8	13	2,08	1,89	0,99	3,16	91,06	30,96	151,16	5,00	2,00	
m9	13	0,69	1,03	0,10	1,28	149,00	8,32	289,68	3,00		
m10	9	7,99	0,81	7,43	8,55	10,20	5,18	15,21	6,30	9,10	8,10
m11	9	4,89	1,29	4,00	5,78	26,46	12,72	40,21	3,00	6,90	4,40

TxP4

Measurement	Sample size	Mean	Standard Deviation	Confidence Limits		Coefficient of Variation	Confidence Limits		Minimum	Maximum	Median
m1	14	25,09	1,87	24,06	26,12	7,44	4,52	10,35	21,30	27,20	25,75
m2	0										
m3	10	26,50	1,75	25,35	27,65	6,62	3,55	9,69	23,20	28,70	26,90
m4	0										
m5	8	24,11	11,38	15,81	32,41	47,18	17,91	76,45	12,40	45,50	21,25
m6	14	1,93	2,30	0,66	3,20	119,40	28,00	210,79	6,00	1,00	
m7	14	4,29	3,73	2,23	6,34	87,03	33,20	140,87	10,00	5,00	

Description and Variability of the Skull and Maxillary Dentition

33

TxP4 (continued)

Measure- ment	Sample size	Mean	Standard Deviation	Confidence Limits		Coefficient of Variation	Confidence Limits		Minimum	Maximum	Median
m8	14	3,86	3,76	1,78	5,93	97,46	32,73	162,20	12,00	4,00	
m9	14	1,00	1,24	0,32	1,68	124,03	26,35	221,72	3,00		
m10	10	7,87	0,95	7,25	8,49	12,10	6,43	17,77	5,80	8,80	8,15
m11	9	4,41	1,08	3,67	5,15	24,45	11,87	37,04	3,10	6,60	3,90

TxM1

Measure- ment	Sample size	Mean	Standard Deviation	Confidence Limits		Coefficient of Variation	Confidence Limits		Minimum	Maximum	Median
m1	10	23,64	1,46	22,69	24,59	6,17	3,31	9,03	22,20	25,50	22,95
m2	0										
m3	7	25,11	1,38	24,04	26,19	5,49	2,45	8,52	22,90	26,70	25,20
m4	0										
m5	3	25,77	5,47	19,25	32,29	21,24	2,55	39,92	19,50	29,60	28,20
m6	10	2,70	2,63	0,99	4,41	97,29	20,92	173,66	7,00	3,00	
m7	10	4,30	3,34	2,12	6,48	77,56	24,43	130,69	8,00	5,00	
m8	10	4,50	3,72	2,07	6,93	82,65	23,97	141,33	11,00	4,50	
m9	10	2,30	1,95	1,03	3,57	84,63	23,71	145,55	5,00	2,50	
m10	7	7,74	0,96	6,99	8,49	12,43	5,47	19,39	6,20	8,50	8,40
m11	7	4,50	0,55	4,07	4,93	12,24	5,39	19,09	3,80	5,30	4,50

TxM2

Measure- ment	Sample size	Mean	Standard Deviation	Confidence Limits		Coefficient of Variation	Confidence Limits		Minimum	Maximum	Medi
m1	14	24,40	1,71	23,46	25,34	7,02	4,27	9,77	22,40	27,90	24,40
m2	0										
m3	11	24,65	1,44	23,76	25,55	5,84	3,26	8,41	22,40	27,10	24,40
m4	0										
m5	4	36,08	11,82	23,88	48,27	32,76	6,41	59,12	20,70	45,90	38,85
m6	15	3,07	2,43	1,77	4,36	79,37	34,41	124,32	6,00	3,00	
m7	15	4,73	3,06	3,10	6,36	64,61	31,63	97,59	8,00	6,00	
m8	15	3,00	3,14	1,33	4,67	104,65	34,21	175,10	7,00	2,00	
m9	15	2,20	2,31	0,97	3,43	104,79	34,19	175,38	7,00	2,00	
m10	11	8,01	0,66	7,60	8,42	8,20	4,57	11,83	6,10	8,50	8,10
m11	10	4,31	0,80	3,79	4,83	18,61	9,73	27,49	3,00	6,00	4,15

TxM3

Measure- ment	Sample size	Mean	Standard Deviation	Confidence Limits		Coefficient of Variation	Confidence Limits		Minimum	Maximum	Median
m1	13	26,17	2,78	24,58	27,76	10,64	6,28	14,99	22,30	30,80	26,40
m2	0										
m3	10	22,69	3,25	20,57	24,81	14,31	7,57	21,05	17,10	29,00	23,55
m4	0										
m5	5	25,30	12,29	13,95	36,65	48,58	10,11	87,06	14,20	42,30	19,20
m6	14	1,29	1,64	0,38	2,19	127,36	25,02	229,70	4,00	0,50	
m7	14	4,43	3,37	2,57	6,29	76,04	32,49	119,60	9,00	5,50	
m8	14	2,86	2,68	1,38	4,34	93,97	33,01	154,94	7,00	2,00	
m9	14	0,64	0,84	0,18	1,11	130,96	23,44	238,48	2,00		
m10	10	8,18	1,11	7,46	8,90	13,51	7,16	19,86	6,50	10,10	8,20
m11	10	3,95	1,06	3,26	4,64	26,80	13,57	40,03	2,90	5,50	3,65

Table 4.5. Character State Distribution of the Höwenegg Mandibular Cheek Teeth

	16L	28L	32	33	34	35	36	37	38	39	40	41	42	43	44	45	46	47	48	49
SMNK Hö A																				
dP1	B																			
P2		A	A		A	B			A		B	B		B	A		A*	B	A	A
P3			A		A	A			A		B	B		B	A		B	B	A	A
P4			A		A	A			A		B	B		B	A		B	A*	A	A
M1				A			E	B		B	B	B		B		C	B	B	A	A
M2				A			ae	B		B	B	B		B		C	B	B	A	A
M3				A			ab	B		B	C*	B		B		B	B	A*	A	A
SMNK Hö I																				
dP1	C																			
P2		A	A		A	B			A		C	B		B	A		A*	B	A	A
P3			A		A	B			A		A	A	C	B	A		B	B	A	A
P4			A		A	B			A		A	B		B	A		B	B	A	A
M1				A			A	B		B	C	A	D	B		B	B	B	A	A
M2				A			A	B		B	C	A	D	B		B	B	B	A	A
M3				A			A	B		B	C	B		B		B	B	B	A	A
SMNK Hö B																				
dP1	C																			
P2		A	A		A	A					B	B		B	A		A*	B	A	A
P3			A		A	A					B	B		B	A		B	B	A	A
P4			A		A	A					B	B		B	A		B	B	A	A
M1				A			A	B		B	C	B		B		C	B	B	A	A
M2				A			A	B		B	C	B		B		C	B	B	A	A
M3				A			A	B		B	C	B		B		B	B	B	A	A
SMNK Hö C																				
dP1	C																			
P2		A	A		E	B			B		B	B		B	A		A*	B	A	A
P3			A		E	A			B		B	B		B	A		B	B	A	A
P4			A		E	A			B		B	B		B	A		B	B	A	A
M1				A			E	B		B	C	B		B		B	A	A	A	A
M2				A			E	B		B	C	B		B		B	B	A	A	A
M3				A			E	B		B	C	B		B		B	B	A	A	A
HLMD Hö V																				
dP1	C																			
P2		A	A		A	B			B		C	B		B	B		A	A	A	A
P3			A		E	B			B		C	D	C	B	B		A	A	A	A
P4			A		E	B			B		C	A	C	B	B		A	A	A	A
M1				A			E	B		B	C	A	C	B		C	A	A	A	A
M2				A			E	B		B	C	A	C	B		C	A	A	A	A
M3				A			E	B		B	C	A	C	B		C	A	A	A	A
HLMD Hö M																				
dP1	C																			
P2		A	A		A				A		B	B		B	A		A*	B	A	A
P3			A		A				A			A	D	B			B	B	A	A
P4			A		A							A	D	B			B	B	A	A
M1				A			A	B		B		A	D	B		C	B	B	A	A
M2				A			A	B		B		A	D	B		C	B	B	A	A
M3				A			A	B		B		B		B		C	B	B	A	A

	16L	28L	32	33	34	35	36	37	38	39	40	41	42	43	44	45	46	47	48	49	
HLMD Hö G																					
dP1	C																				
P2		A	A	A	A																A
P3																					
P4																					
M1																					
M2																					
M3																					
HLMD Hö III																					
dP1	C																				
P2		A													B						A
P3															B						A
P4															B						A
M1															B						A
M2															B						A
M3															B						A
HLMD Hö E																					
dP1	C																				
P2		A	A		A				A		C	B		B	A					A	A
P3			A		A				A		C	A		B	B					A	A
P4			A		A				A		C	A		B	B					A	A
M1				A			A			B	C	A		B		C				A	A
M2				A			A			B	C	A		B		C				A	A
M3				A			A			B	C	B		B		C				A	A
Hö 25																					
dP1	C																				
P2			A		E				A		A	B		B	A		B	B	A	A	A
P3			A		E				A		A	B		B	A		B	B	A	A	A
P4			E		E				A		A	B		B	A		B	B	A	A	A
M1				E			E			B	C	A*		B		B	B	B	A	A	A
M2				A			E			B	C	B		B		B	B	B	A	A	A
M3				A			A			C	C	B		B		B	A*	A*	A	A	A
HLMD Hö 15/58																					
dP1	C																				
P2		A	A		E				A		B			B	A					A	A
P3			A		E				A		B	A		B	B					A	A
P4			A		E				A		B	A		B	B					A	A
M1				A			E			B	C	A		B		B				A	A
M2				A			E			B	C	A		B		B				A	A
M3				A			A*			B	B	B		B		B				A	A

* = wear related morphological feature

Legend as for Table 4.1

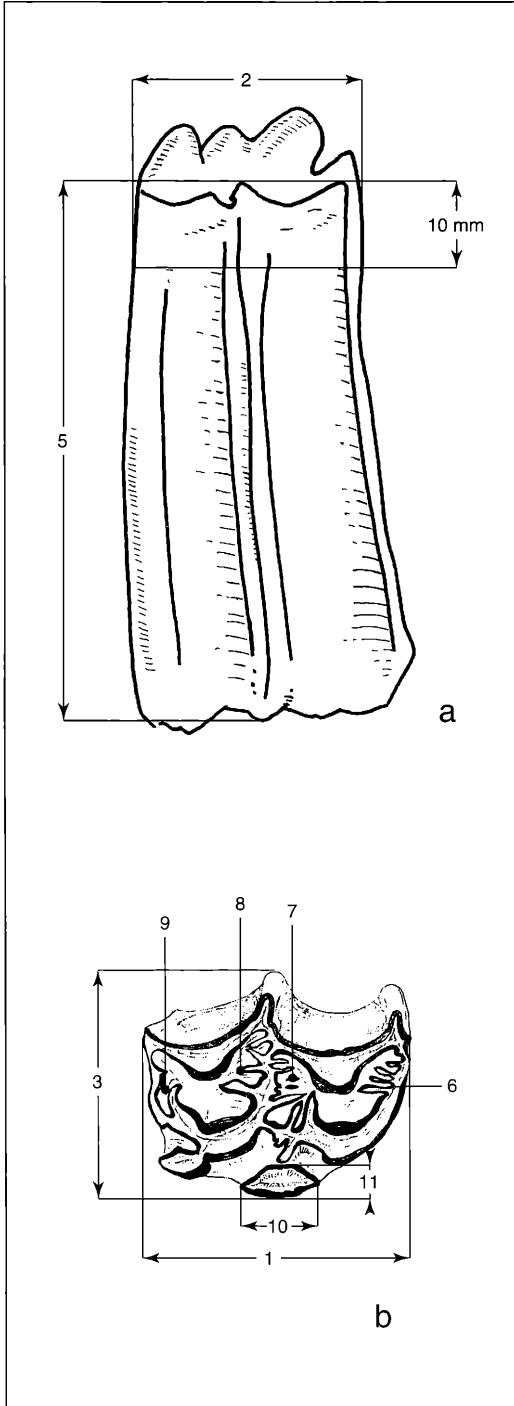


Figure 4.3. Measurements on Maxillary Cheek Teeth: a. buccal aspect; b. occlusal aspect.

P⁴ exhibited 6 significant correlations including 2 at or above the 99 % level (m6-m9 and m7-m8). These 99 % significance correlations reflected the observed pattern of fossette plications covariation: M6 (anterior prefossette plication count) correlated with m9 (posterior postfossette plication count); m7 (posterior prefossette plication count) correlated with anterior prefossette count). Measurement 5 (crown height) correlated with m10 (protocone length) at the 95 % significance level, while m6 correlated with m7 and m8.

M¹ exhibited 8 significant correlations; 5 at or above the 99 % level (m7-m9, m3-m10, m6-m9, m8-m9, m7-m8). Of these eight, m6 (anterior prefossette plication count) and m9 (posterior postfossette plication count) accounted for 4 of the above 99 % and 2 of the 95 %-99 % level of significance. In this tooth, m3 (width of crown at occlusal level) correlated positively with m10 (protocone length); as width of tooth increases so does protocone. Measurement 1 (length at occlusal level) correlated negatively with m11 (protocone width); as length of tooth decreases with wear, protocone becomes wider.

M² showed only 4 significant correlations, divided equally at both test levels. Of these, measurements 6, 7, 8 and 9 accounted for half the correlations. M5 (crown height) was found to be strongly positively correlated with crown length (m1), however, the small frequency (n=3) renders this correlation substantively questionable. Measurement 5 (crown height) was once again strongly negatively correlated with m11 (protocone width), revealing that as crown height diminished, protocone width increased.

M³ exhibited 10 significant correlations, 4 at or above the 99 % significance level (m7-m8, m8-m11, m1-m11 and m3-m5). Of all these correlations, m6, m7, m8 and m9 accounted for three amongst themselves (m7-m8, m7-m9 and m6-m7) and two correlations with other variables: m8-m11 (protocone width) and m7-m11. Protocone width again correlated positively with m1 (occlusal level length) and negatively with m5 (crown height). Measurement 5 also showed a strong negative correlation with m3 (crown width). Occlusal level crown length (m1) correlated with a 0.018 observed probability level. Measurement 3 further correlated with m1 and m10 (protocone length).

Coefficients of variation were generally low for all individual cheek teeth. Except for m3, all other cheek teeth exhibited CV's below 10 (m1 CV = 10.64; m3 CV = 14.31), showing remarkable stability of occlusal level length and breadth measurements. Consistently the greatest CV's were found for pre- and postfossette plication counts of the pre- and postfossettes, these often exceeding 100! We believe that this quarry sample provides direct evidence that enumeration of plication counts has limited value for systematic interpretation: there is simply too much emphasis given to this numerical character.

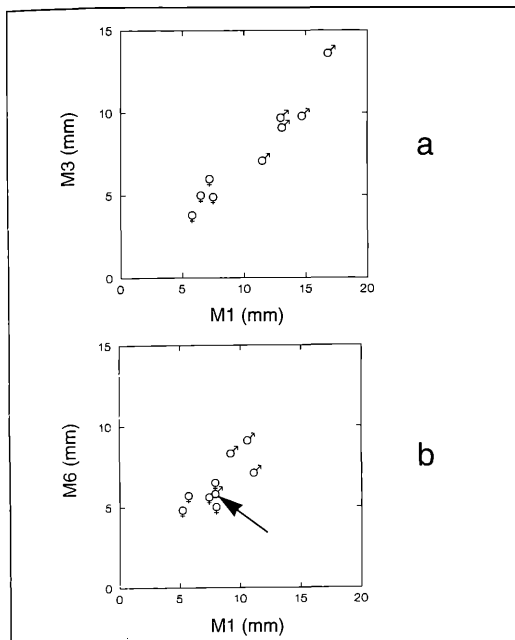


Figure 4.4. Bivariate Plot of Canine L x W Dimensions; a. maxillary canine M1 x M3; b. mandibular canine M1 x M6 (arrow indicates male individual plotted within female grouping).

4.2 Description and Variability of the Mandible and Dentition

4.2.1 Definition of the *Hippotherium primigenium* Mandible by Discrete Characters

In *Hippotherium primigenium* s.s. the mandibular dentition has been characterized by BERNOR, TOBIEN & WOODBURN (1989), and revised by BERNOR & LIPSCOMB (1991, 1995) as having: dP_1 absent in adult individuals (16LC): paraconids elongate (28LA), with mandibular incisors not grooved (29A), curved (30A), and I_3 elongate but not labiolingually constricted (31A); premolars and molars with rounded metaconids and metastylids (32A, 33A, 34A, 36A); premolars variably with metastylid spur (35A), while molars lack them (37B); premolar ectoflexids not separating metaconid and metastylid (38A), while they do so in the molars (39B); lower cheek teeth frequently with complex to single or rudimentary pli caballinids (40a/b); protostylids are commonly present as encircled enamel rings (41A), but never strong and columnar (41C), and are vertically placed, lying flush with the protoconid enamel band (42C); ectostylids absent in adult cheek teeth (43B); linguaflexids usually shallow on the premolars (44A), while being more V-shaped on the molars (45B); preflexids (46B) and postflexids (47B) generally with complex margins, with the latter being more so than the former; the postflexid frequently invades the metaconid/

metastylid junction, but does not bend inward when it does so (48A); protoconid enamel band rounded (49A).

4.2.2 Description of the Höwenegg Mandibles

SMNK Hö A is a complete mandible. It is relatively large for a hipparionine horse and has a typically well developed equid-like curvature of the posteroventral border. The left incisor series is present, while the right side's series has been reconstructed. The incisors lack lingual grooves (29A), are curved (30A) and I_3 is elongate and not labiolingually constricted (31A). The canines are large, laterally convex, and have a broad lingual pillar. On the left side, dP_1 is preserved being quite small and nonfunctional (16LB); $P_2 - M_3$ are preserved on both sides. P_{2-4} are large and rhomboidal shaped, and $M_1 - M_3$ exhibit serial reduction in their length and width dimensions. $P_2 - M_3$ conform to the general characterization for *Hippotherium primigenium* except: a metastylid spur occurs on P_3 and P_4 (35A), but not the P_2 (35B); the molar metastylids vary in their shape from square (36E, M_1) to semi square (36a/e, M_2), to somewhat elongate (36a/b, M_3); pli caballinids are clearly single (40B) except for M_3 where it is absent due to an early wear stage (40C); protostylids are absent on both the PM's and M's (41B) due to relatively early stage-of-wear; M_{1-2} do not have a V-shaped molar linguaflexid as found in the M_3 (45B), but have a shallow U-shaped morphology (45C). Cheek tooth preflexids exhibit complexity on all cheek teeth (46B), except P_2 (due to wear), whereas postflexids are complex only on P_{2-3} and M_{1-2} (47B), most likely due to their relatively early stage-of-wear. Postflexids (48A) and protoconid enamel band (49A) are as in *Hippotherium primigenium* s.s.

SMNK Hö I includes virtually the entire mandible, except for the ascending rami. The symphyseal region preserves all the incisors and canines. DP_1 is absent (16LC). The incisors have large, mediolaterally elongate infundibula exposed by wear. The cheek teeth have the general morphology of *Hippotherium primigenium* s.s. except: pli caballinids are absent on P_2 and M_{1-3} (40C); protostylids are present on P_3 , M_{1-2} (41A), placed vertically flush with the protoconid enamel band in P_3 (42C) and lateral to protoconid enamel band in M_{1-2} (42D); preflexids are complex on all cheek teeth (46B) except P_2 (46A); postflexids are somewhat complex (47B) and invade metaconid/metastylid junction on all cheek teeth.

SMNK Hö B has both mandibles intact, and as with the associated skull, this individual is in an early stage-of-wear. The symphyseal region includes right I_{1-2} , left I_{1-2} and dI_3 . Their morphology is as in SMNK Hö I, except that the enamel lakes are not as well expressed due to the individual's young age. The canine is larger than the former specimen. DP_1 is absent (16LC). The cheek teeth are as described above for *Hippotherium primigenium* s.s. except: premolar pli caballinids are absent on

all molars (40C), but present on all premolars (40B); molar linguaflexids are a shallow U-shape on $M_{1,2}$ (45C), but V-shaped on M_3 (45B); preflexids are simple on P_2 (46A), and complex on the remaining cheek teeth (46B); postflexids are complex on all cheek teeth but invade metaconid/metastylid only on $P_{3,4}$, due to this individual's early stage-of-wear.

SMNK Hö C is a complete mandible except for the left coracoid process and some portions of the corpus and symphysis. All incisors are preserved except for the right I_1 , which has been reconstructed. The I_1 and I_2 show well developed, mediolaterally elongate infundibula; I_3 does not due to its early stage-of-wear; in other regards their morphology is as in *Hippotherium primigenium* s.s. Only the left canine is preserved, it is peg-shaped as in its maxillary homologues, and placed close to I_3 . DP_1 is absent (16LC). The mandibular cheek teeth are as characterized for *Hippotherium primigenium* s.s. except for some notable exceptions: premolar and molar metastylids have a squared aspect (34E and 36E); premolar ectoflexids separate metaconid and metastylid (38B); pli caballinids are single on the premolars (40b), but absent on the molars (40c); no protostylids are expressed occlusally (41b). $P_{3,4}$ and $M_{2,3}$ have complex preflexids (46B), while the absence of complexity on P_2 and M_1 (46A) is most probably due to wear stage.

HLMD Hö V is a complete, well preserved, female mandible. The mandible is typically equine-like in having a prominent, expanded base to the ascending ramus which rises high superiorly to the mandibular condyle and a more highly placed coronoid process. The horizontal ramus shallows anteriorly. $P_2 - I_1$ distance is distinctly less than the $P_2 - M_3$ dimension, revealing a relatively short snout. The mental foramen is placed equidistant from I_3 and P_2 . The lower incisors are as in the other adult individuals, with well developed single dentine lakes, except the right I_3 which has an additional small, laterally placed lake. The canines are very small and peg-like in their morphology, and placed very close to the I_3 's. The dP_1 's are absent (16LC). Mandibular cheek teeth depart in their morphology from *Hippotherium primigenium* s.s. in a number of features including: $P_{3,4}$ and $M_{1,3}$ metastylids have a squared morphology (34E and 36E); no metastylid spurs occur on the premolars (35B); pli caballinids are absent (40C); protostylid is an open loop on P_3 only (41d), while present on the enamel surface as a closed enamel ring on $P_4 - M_3$ (41a); premolar linguaflexids are V-shaped (44B); molar linguaflexids are shallow U-shaped (45C); preflexids (46A) and postflexids (47A) show no complexity due to their late stage-of-wear.

As with the associated skull, the adult mandible HLMD Hö M is badly eroded, cracked, and crushed. The right side of the mandible is exposed, and reveals that the ascending ramus and angle of the mandible are missing. The incisors are still embedded in matrix so that the enamel lakes can not be seen. The canine is ro-

bustly built as is seen in the maxillary canine. The dP_1 is absent (16LC). The cheek teeth are still not completely prepared but some observations are possible and reveal minor differences from the characterization of *Hippotherium primigenium* s.s.: the pli caballinid can be seen on P_2 to be single (40B); protoconids are expressed on $P_{3,4}$, $M_{1,2}$, only and are present as small, encircled rings (41a); all molars have shallow U-shaped linguaflexids (45C). Only P_2 has a simple preflexid (46A); all other cheek tooth preflexids and postflexids are complex (46b and 47B).

HLMD Hö G is a nearly complete, although crushed mandible, exposed on the right side. This specimen is lacking the incisor and most of the canine region except for left I_3 . There is no dP_1 (16LC). The size and proportions of the mandible can be estimated to have been virtually identical to other male individuals in the sample. The cheek teeth do not have their occlusal surfaces free from occlusion with the upper dentition, disallowing study of their morphology (except for P_2 ; re: Table 4.5).

HLMD Hö III is essentially in the same state of preservation as Hö G. Once again, the right side is exposed and the mandible is badly eroded and fragmented, lacking the base of the ascending ramus and symphyseal region. The size and proportions of the mandible would appear to have not significantly differed from other specimens in the sample. Except for the uniform lack of ectostylids (43B) and rounded protoconid band (49A), occlusal morphology of the cheek teeth cannot be observed because of their remaining occlusion with the maxillary cheek teeth.

Specimen HLMD Hö E is a very well preserved and virtually complete adult female mandible; only portions of the ascending rami, the left coronoid process and post-symphysial mandibular ramus are missing. The snout was slightly elongate, with $P_2 - I_1$ dimension greater than $P_2 - M_3$ dimension. The mental foramen is placed intermediate between I_3 and P_2 . The incisors are complete, and reveal expanded dentine lakes; in the I_2 's these invade the lateral margin of the tooth. The canines are small, peg-like, and placed very close to the I_3 's. As cited above, dP_1 is missing (16LC). $P_2 - M_3$ differ from the characterization of *Hippotherium primigenium* s.s. as follows: pli caballinids are absent (40C); whereas $P_3 - M_2$ have protostylids occlusally expressed (41a), P_2 and M_3 do not (41b).

Hö 25 is a virtually complete, young adult female mandible with right $I_{1,3}$, canine (with broken crown), $P_2 - M_3$, left $I_{2,3}$, C, $P_2 - M_3$; left ramus is complete, while the right one is not present. This individual is in an early stage of adult wear and reveals some morphological features which are different from older individuals. The incisors do not have dentine pools restricted to the interior of the crown, but rather they continue close to the mesial and distal borders of I_1 and I_2 , and spill over the lateral border of I_3 . The left canine is small and peg-shaped. DP_1 is absent (16LC). $P_2 - M_3$ depart

Table 4.6. Specimen Character State Comparison Between *Hippotherium primigenium*, the Höweneegg Horses and HULBERT'S 1988 Scored Characters for *Hippotherium primigenium*

	19	23	24	45	46	49	53	57	58	59	60	61	63
<i>Hpri</i>	0	2	0	2	2		1	1	2	1	1		1
Hö A	2	X	0/1	1v	X	X	2	X	X	X	2	2	2
Hö I	2	X	0/1	2	X	X	2	X	X	X	0	2	2
Hö B	0	X	0/1	2	X	X	X	X	X	X	2	0	X
Hö C	2	1	0/1	2	X	X	X	?0	0/1	?1	2	0	0
Hö V	2	X	1	2	X	X	2	0	2	1	0	0	0
Hö M	2	X	X	2	X	X	2	X	X	X	2	X	2
Hö G	2	X	X	2	X	X	X	X	X	X	X	X	X
Hö III	0	X	X	2	X	X	X	X	X	X	X	X	X
Hö E	0	X	1	2	X	X	2	1	0	1	0	0	2
Hö 25	0	X	X	2	X	X	2	0	2	1	2	0	2
Hö 15/58													

Legend (as given by HULBERT 1988)

all X's = state cannot be defined

Characters:

19 = Size of DP1: 0, DP1 large, present in adult dentitions; 1, DP1 small but functional and present in adult dentitions; 2, DP1 vestigial or absent in adult dentitions.

23 = Protocone shape (P3-M2): Based on ratio of protocone length to width (L:W): 0, round (L:W less than 1.2); 1, oval (L:W 1.2-2.0); 2, elongate-oval (L:W 2.0-3.0); 3, elongate (L:W greater than 3.0)

24 = Protocone Lingual Border: 0, protocone lingual border round or convex; 1, lingual border straight; 2, lingual border variably straight or concave.

45 = Retention of dp1: 0, dp1 relatively large, usually retained with permanent dentition; 1, dp1 reduced, variably present with adult dentition; 2, dp1 usually not present with permanent dentition.

46 = Ectostylids on dp2-dp4: 0, absent or rudimentary; 1, moderate (less than 5 mm high); 2, strong.

49 = Depth of Ectoflexid on dp2-dp4. Three states are recognized: 0, ectoflexid deep, completely penetrates isthmus; 1, ectoflexid moderately deep, only partially penetrates isthmus; 2, ectoflexid shallow, does not penetrate isthmus.

53 = Protostylid Attachment: 0, protostylid always connected to protoconid; 1, protostylid initially isolated from protoconid, connects lower on the crown; 2, protostylid persistently isolated from the protoconid.

57 = Development of Pli Entoflexid: 0, pli entoflexid absent or rudimentary; 1, pli entoflexid usually present, at least in early and very early wear-stages.

58 = Development of Isthmus Plications: 0, pli entoflexid absent or rudimentary; 1, pli entoflexid usually present, at least in early and very early wear-stages; 2, isthmus plications frequent and persistent.

59 = Development of Paralophid Plication: 0, paralophid without application into the metaflexid; 1, paralophid frequently applied.

60 = Pli Caballinid on p2-p4: 0, pli caballinid generally absent; 1, pli caballinid small, nonpersistent; 2, pli caballinid large, relatively persistent.

61 = Pli Caballinid on m1-m3: 0, plicaballinid generally absent; 1, pli caballinid small, nonpersistent; 2, pli caballinid moderate, lasts until moderate wear-stages.

63 = Ectoflexid Depth on p3-p4: same states as Character 49

from the generalized description of *Hippotherium primigenium* s.s. in the following characteristics: P₄ and M₁ metaconids are square-shaped (32e and 33e, respectively); premolar (34E) and M₁₋₂ metastylids (36e) are square-shaped; pli caballinids are lacking entirely on the molars (40C); protostylids are only found on M₁ (41a, due to wear). Preflexids and postflexids are complex on all cheek teeth (46B and 47b) except M₃ (47a), due to relatively early stage-of-wear.

SMNK Hö 15/58 is a partial adult mandible with the right corpus and ramus intact, the left side is missing from the symphyseal region, posteriorly. The dentition includes right I₁, roots of I₂₋₃, C, and P₂ - M₃; on the

left side only the roots of I₁₋₃ remain intact. The right I₁ is well worn and reveals an expanded, mediolaterally elongate central dentine lake. The canine is complete, and rather large, indicative of a male individual. DP₁ is absent (16LC). The cheek teeth conform with the characterization of *Hippotherium primigenium* s.s. in all but the following regards: premolar (34E) and molar (36E) metastylids have a squared-shape (except M₃ which is round due to wear); pli caballinids are absent on M₁₋₂ (40c); protostylid is absent on M₃ (41b). Cheek tooth preflexid and postflexid complexity is nominal in this later stage-of-wear individual.

4.2.3 Summary of Character State Distribution

In the mandible characters 29A, 30A, 31A (incisor morphology with regards to grooving, curvature and I_3 lateral aspect), 43B (absence of ectostylids in adult dentitions), 48A postflexid morphology with regards to the invasion of the metaconid/ metastylid junction and 49A, protoconid enamel band morphology were found to be 100 % stable states throughout ontogeny.

Some characters were found to be stable in 75 % of the recorded occurrences: dP_1 was mostly absent (16LC), being present as a highly reduced, nonfunctional structure in Hö A only. Characters 32A and 33A, premolar and molar metaconid morphology, predominately were rounded, but some individuals had a clear square-shaped morphology (32E and 33E), which is autapomorphic for the *Hippotherium primigenium* lineage (BERNOR & LIPSCOMB, 1995; WOODBURN, BERNOR & SWISHER, 1995). Molar metastylid spur was predominately absent (37B). Premolar ectoflexids were usually found not to separate metaconid/metastylid (38A), whereas in the molars they did (39B). It is notable that in two female individuals Hö C (young adult) and Hö V (old adult) the more primitive character of ectoflexid separating premolar metaconid and metastylid was recorded (38B). Finally, preflexid morphology was complex (46B), although not as complex as was found in the postflexids (47B).

A number of mandibular cheek tooth characters were more variable. Premolar (34A) and molar (36A) metastylid morphology were predominately rounded, but some adult individuals showed some form of squaring, and more rarely elongation. Premolar metastylid spurs occurred more frequently (35A) than not (35B). Pli caballinid morphology varied from being complex (40A), to rudimentary or single (40B), to absent (40C); premolars predominately had better developed structures than molars, with the molars *only* exhibiting complete loss of the structure. Protostylids were never present on P_2 (41B), and their presence on $P_3 - M_3$ would appear to be strictly wear-related (41 A or B). In the earlier stages of adult wear, protostylids remain imbedded in the thick cementum surrounding the periphery of the tooth. As the lower cheek tooth wears, the labial aspect of the cementum reduces its thickness considerably, and the protostylid appears as a large, but not columnar shaped structure. Premolar linguaflexids, generally shifted their morphology with wear being shallow (44A) to V-shaped (44B) in adult dentitions. Molar linguaflexids, generally shifted their morphology with wear from V(45B)- to U(45C)-shaped in adult dentitions. Postflexids were most frequently complex (47B), generally showing reduced complexity with wear (47a/b).

HULBERT (1988) has compiled a character state distribution for *Hippotherium primigenium* based on published literature for the purpose of comparison with North American *Cormohipparion*, *Hipparion* and more primi-

tive outgroup taxa. Table 4.6 provides a comparison of the Höwenegg horses' character state distribution, across all relevant specimens, with those given by HULBERT (1988).

- 19 = Size of dP^1 : 0, dP^1 large, present in adult dentitions; 1, dP^1 small but functional and present in adult dentitions; 2, dP^1 vestigial or absent in adult dentitions.
- 23 = Protocone shape ($P^3 - M^2$): ratio, when it can be calculated (due to appropriate wear-stage) varies from being oval to elongate-oval.
- 24 = Protocone lingual border: varies from round or convex to straight.
- 45 = Retention of dp^1 : varies from being present to not present.
- 46 = Ectostylids on $dp^2 - dp^4$: only applies to deciduous dentition, where it is known to be present for *Hippotherium primigenium*.
- 49 = Depth of ectoflexid on $dp^2 - dp^4$: not observable on the Höwenegg hipparion.
- 53 = Protostylid attachment: when known, varies from being initially isolated to persistently isolated from protoconid pl.
- 57 = Development of pli entoflexid: usually present, when observable.
- 58 = Development of isthmus plications: may be absent to frequent.
- 59 = Development of paralophid plication: when present, frequently plicated.
- 60 = Pli caballinid on $p^2 - p^4$: varies from being large and persistent, to small, to absent.
- 61 = Pli caballinid on $m^1 - m^3$: varies from being generally absent, to small and nonpersistent to moderate, lasting to moderate wear-stages.
- 63 = Ectoflexid depth on $p^3 - p^4$: varies from being deep and penetrating isthmus, to moderately deep and only partially penetrating isthmus, to shallow and not penetrating the isthmus.

4.2.4 Statistical Characteristics of the Mandibular Dentition

Fourteen variables were measured on a total of 12 specimens with varying degrees of completeness; measurement 15 of EISENMANN et al. (1988) was deemed unimportant for measurement (Fig. 4.5). Descriptive statistics were calculated on a maximum of ten specimens for any one variable (Table 4.7). The coefficients of variation were elevated above 10 for three variables: m^2 (palatal length; CV = 11.89), m^{11} (height of jaw between P_4 and M_1 ; = 23.50) and m^{14} (CV = 11.00).

There are six significant correlations for mandibles, 2 of which were at or above the 99 % level: m^4 (molar tooth row length)- m^{11} (height of jaw between P_4 and M_1) and m^8 (height of mandible at condyle)- m^9 (height of ascending ramus). Measurement 4- m^{11} was strongly negatively correlated, indicating that as

the tooth row decreased in length m11 remained stable or decreased. The next most significant correlation was between m8 (height of the mandible at the condyle) and m9 (height of the ascending ramus), reflecting more the covariation of these measurements than anything else. Measurement 2 (muzzle length) exhibited positive correlations with m1 (maximum jaw length) and m7 (muzzle breadth), most probably reflecting the stability of these measurements within the Höweneegg population. Measurement 3 (premolar tooth row length) correlated significantly with m5 (cheek tooth row length) and m10 (height of the jaw posterior to M3) correlated with m13 (length of symphysis).

4.2.5 Statistical Characteristics of the Mandibular Dentition

Two measurements were taken on all three incisors, the canine and dP₁ (m1 = length and m3 = width at occlusal level). Ten measurements were taken on the premolar and molar cheek teeth (other than dP₁; Fig. 4.6): m1 = length at occlusal level; m2 = length 10 mm above the tooth's base (in isolated teeth only); m3 = length of metaconid-metastylid (= "double-knot" of EISENMANN et al., 1988); m4 = length of the prefossette; m5 = length of the postfossette; m6 = W1, width of tooth across plane of ectoflexid/linguaflexid; m7 = width 10 mm above base; m8 = W2, width across plane of metaconid and enamel band labial to protoconid; m9 = W3, width across plane of metastylid and enamel band labial to hypoconid; m10 = crown height as measured from base to occlusal level on mesial face of the tooth. Of the mandibular teeth measured, I3, C1 and P2 – M3 exhibited significant correlations (Table 4.8).

I₃ showed a highly significant positive correlation for m1 – m6. In comparison, C showed a somewhat reduced level of correlation between these two variables. Moreover, mandibular canines did not exhibit the clear sexual dimorphism evident in the maxillary canines (Fig. 4.4b). CV's were below 10 for all incisor measurements except m6 for I₂ (CV=11.53) and I₃ (CV=14.59). Canines again exhibited elevated CV's (m1 CV = 27.88; m6 CV = 22.92), due to their sexual dimorphic nature.

P₂ exhibited three significant correlations, one at or above the 99 % level and two at the 95 % level. Measurement 8 (W2) m9 (W3) were the most highly correlated, and reflect the greater stability of these measurements when compared to W1 or WB. Hopefully these measurements will be implemented, and perhaps even replace the standard measurements utilised by equid researchers. Measurements 4 and 5 of preflexid and postflexid length were significantly correlated. Crown length (M1) was negatively correlated with crown width (W1, m6); as length increased, width stayed stable or decreased.

P₃ showed 7 significant correlations: 4 at or above the 99 % level. Again, m8 – m9 and m4 – m5 showed significant correlations. Measurement 4 (preflexid length) and m5 (postflexid length) were significantly *negatively* correlated with m8 (W2) and m9 (W3), reflecting that as the length dimensions decreased the widths remained stable or actually increased. Metaconid-metastylid length (m3) was found to correlate significantly with W2 (m8).

P₄ yielded 5 significant correlations, 4 at or above the 99 % level. Again, m8 – m9 exhibited a highly probable significant correlation. In this tooth, m3 (metaconid-metastylid) was found to correlate very highly with m9 (WB), and somewhat less significantly with m8 (W2), reflecting the stability of these measurements. Likewise, m1 (length at occlusal level) was found to correlate with m5 (postflexid length) and m6 (W1), again reflecting measurement stability.

M₁ exhibited only one significant correlation at the observed probability level of 0.020: m1 (length of crown at occlusal level): m4 (length of preflexid). This reflects the relative stability of these measurements.

M₂ exhibited three correlations, of which one was at or above the 99 % level of significance: m8 (W2) – m9 (W3). Measurement 9 also correlated positively with m3 (metaconid-metastylid length), whereas m8 correlated negatively with m1 (occlusal crown length). The latter of these two cases suggests that as crown length decreases with wear, width remains stable or actually increases.

M₃ exhibited six significant correlations of which only two were at or above the 99 % level. Of these, m9 (W3) exhibited four significant correlations: with m3 (metaconid-metastylid length), the highest correlation on this tooth; with m8 (W2); with m1 (length at occlusal level); and negatively with m4 (preflexid length), suggesting that as m4 decreased, m9 remained stable or increased in dimension. Measurement 4 also correlated negatively with m8 (W2), further reinforcing the interpretation for the m4 – m9 measurement.

Coefficients of variation were not as elevated as those for many of the maxillary cheek tooth measurements. Measurement 10 (crown height) varied consistently above 10 due to the variation in crown height with wear. Measurement 1 (crown occlusal level length) was consistently less than 10. Measurement 3 (metaconid-metastylid length) was below 10 for all teeth except P₄ (CV = 10.63) and m3 (CV = 10.56); these can be viewed as representing relatively small stochastic variability. Measurement 4 (preflexid length) and m5 (postflexid length) showed coefficients of variation, fundamentally hovering around 10 (except P₃: CV = 18.20), which is probably due to some real variability and perhaps some difficulty in striking accurate measurements. The width measurements (m6, m7, m8 and m9) also showed CV's mostly between 6 and 12 due to variability, with M₃ showing even more elevated

Table 4.7. Summary Statistics on Mandible Continuous Variables

Measure-ment	Sample size	Mean	Standard Deviation	Confidence Limits		Coefficient of Variation	Confidence Limits		Minimum	Maximum	Median
m1	6	425,17	30,86	399,17	451,17	7,26	2,91	11,60	374,00	456,00	432,00
m2	7	127,17	15,12	115,38	138,96	11,89	5,24	18,53	109,20	147,00	124,00
m3	11	83,68	5,30	80,38	86,98	6,33	3,53	9,13	76,00	94,30	83,70
m4	10	80,30	7,13	75,65	84,95	8,88	4,75	13,01	75,00	98,70	77,40
m5	10	161,04	5,66	157,34	164,74	3,52	1,89	5,14	153,90	173,00	160,75
m6	8	120,70	10,10	113,33	128,07	8,36	4,02	12,71	106,70	138,00	121,15
m7	6	51,60	4,90	47,47	55,73	9,50	3,79	15,21	47,20	59,70	50,00
m8	8	203,43	16,25	191,57	215,28	7,99	3,84	12,14	171,00	221,80	209,30
m9	7	186,83	16,95	173,61	200,05	9,07	4,03	14,11	153,00	201,30	186,00
m10	9	103,52	9,09	97,27	109,78	8,78	4,48	13,08	91,80	114,30	104,00
m11	10	63,09	14,83	53,41	72,77	23,50	12,07	34,94	22,70	72,80	66,50
m12	10	48,54	4,84	45,38	51,70	9,98	5,33	14,63	42,50	56,70	48,15
m13	7	85,51	7,92	79,34	91,69	9,26	4,11	14,41	78,10	101,50	82,10
m14	6	31,87	3,50	28,91	34,82	11,00	4,37	17,63	27,70	36,90	31,60
m15	0										
m16	0										

CV's for m8 (CV = 13.7) and m9 (= 15.5). For the most part molar cheek tooth measurements exhibited lower CV's than did the maxillary cheek teeth.

4.3 Hyoideum

During the preparation of the Hö V58 skeleton, fragments of a hyoideum were found between the mandibular rami. Figure 4.7 (a-c) depicts the damaged, partial processus lingualis. The body of the basihyoid has a pair of obliquely disposed processes which are thickened at

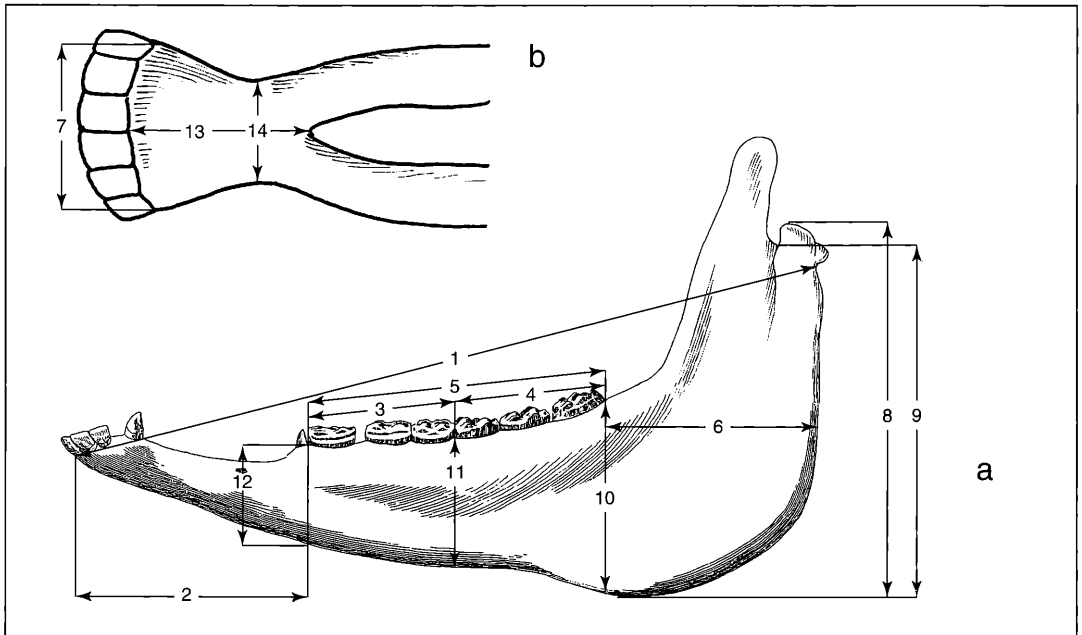


Figure 4.5. Measurements on Mandibles: a. lateral aspect; b. ventral aspect.

TmC											
Measure- ment	Sample size	Mean	Standard Deviation	Confidence Limits		Coefficient of Variation	Confidence Limits		Minimum	Maximum	Median
m1	11	8,62	2,40	7,12	10,11	27,88	14,69	41,07	4,90	11,80	7,90
m2	0										
m3	0										
m4	0										
m5	0										
m6	9	6,43	1,47	5,42	7,45	22,92	11,20	34,65	4,80	9,10	5,80
m7	0										
m8	0										
m9	0										
m10	0										

TmP2											
Measure- ment	Sample size	Mean	Standard Deviation	Confidence Limits		Coefficient of Variation	Confidence Limits		Minimum	Maximum	Median
m1	16	29,06	1,29	28,40	29,73	4,43	2,81	6,05	26,80	31,20	29,00
m2	0										
m3	8	11,36	0,65	10,89	11,83	5,68	2,74	8,62	10,30	12,20	11,50
m4	7	6,16	1,31	5,13	7,18	21,32	9,04	33,60	3,50	7,40	6,60
m5	7	11,43	2,66	9,35	13,50	23,29	9,76	36,81	6,60	13,80	12,20
m6	13	14,76	1,56	13,87	15,66	10,59	6,25	14,92	12,50	17,80	14,70
m7	0										
m8	8	10,55	1,28	9,61	11,49	12,16	5,79	18,53	8,10	12,10	11,00
m9	8	13,13	1,12	12,30	13,95	8,57	4,12	13,02	11,70	15,20	13,10
m10	4	18,60	6,95	11,43	25,77	37,34	6,53	68,16	12,80	27,30	17,15

TmP3											
Measure- ment	Sample size	Mean	Standard Deviation	Confidence Limits		Coefficient of Variation	Confidence Limits		Minimum	Maximum	Medi
m1	17	25,71	1,19	25,11	26,31	4,65	3,00	6,29	23,30	27,20	26,10
m2	0										
m3	8	14,88	1,17	14,02	15,73	7,88	3,79	11,97	12,80	16,40	14,90
m4	8	8,11	0,67	7,62	8,61	8,32	4,00	12,64	7,20	9,10	7,95
m5	8	11,70	2,13	10,15	13,25	18,20	8,50	27,90	8,30	13,70	12,35
m6	12	17,94	1,23	17,21	18,67	6,84	3,95	9,74	16,20	20,10	17,85
m7	0										
m8	7	13,41	1,09	12,56	14,27	8,16	3,63	12,69	11,50	14,50	13,40
m9	7	14,04	0,90	13,34	14,75	6,43	2,87	10,00	12,90	15,20	14,20
m10	2	19,20	13,86			72,18			9,40	29,00	19,20

TmP4											
Measure- ment	Sample size	Mean	Standard Deviation	Confidence Limits		Coefficient of Variation	Confidence Limits		Minimum	Maximum	Median
m1	21	25,86	1,75	25,07	26,64	6,75	4,59	8,91	22,80	30,30	25,90
m2	0										
m3	8	14,21	1,51	13,11	15,32	10,63	5,09	16,18	11,60	16,60	14,15
m4	8	7,75	0,75	7,20	8,30	9,68	4,64	14,72	6,90	8,90	7,45
m5	8	11,65	1,39	10,63	12,67	11,96	5,70	18,23	9,40	13,20	12,00
m6	17	17,31	1,68	16,47	18,15	9,70	6,23	13,16	14,20	19,60	17,60
m7	0										
m8	7	13,53	1,35	12,47	14,58	10,00	4,43	15,57	11,30	15,60	13,20
m9	7	13,43	1,40	12,34	14,52	10,42	4,61	16,23	11,20	14,90	13,20
m10	6	26,58	11,25	17,11	36,06	42,30	12,93	71,67	15,00	42,60	23,55

Description and Variability of the Mandible and Dentition

45

TmM1											
Measurement	Sample size	Mean	Standard Deviation	Confidence Limits		Coefficient of Variation	Confidence Limits		Minimum	Maximum	Median
m1	16	24,03	1,92	23,04	25,02	7,98	5,05	10,91	20,10	27,50	24,05
m2	0										
m3	8	14,28	1,00	13,54	15,01	7,01	3,38	10,65	12,50	16,00	14,30
m4	8	6,99	0,71	6,47	7,51	10,19	4,88	15,50	5,90	7,90	7,00
m5	8	9,75	0,91	9,09	10,41	9,34	4,48	14,20	8,40	11,00	9,70
m6	12	15,13	1,02	14,52	15,73	6,76	3,90	9,61	13,00	16,30	15,50
m7	0										
m8	8	11,80	1,04	11,04	12,56	8,82	4,23	13,40	10,30	13,10	11,90
m9	8	10,68	0,83	10,07	11,28	7,75	3,73	11,78	9,50	12,00	10,60
m10	1	28,30							28,30	28,30	28,30
TmM2											
Measurement	Sample size	Mean	Standard Deviation	Confidence Limits		Coefficient of Variation	Confidence Limits		Minimum	Maximum	Median
m1	18	24,05	1,32	23,41	24,69	5,47	3,58	7,36	20,80	26,70	24,45
m2	0										
m3	8	13,25	0,83	12,64	13,86	6,29	3,03	9,55	12,20	14,50	13,30
m4	8	7,06	0,72	6,54	7,58	10,12	4,85	15,40	6,40	8,40	6,80
m5	8	9,71	1,18	8,85	10,58	12,20	5,81	18,59	7,80	11,50	9,85
m6	14	14,25	1,15	13,62	14,88	8,05	4,89	11,21	11,90	15,80	14,40
m7	0										
m8	8	11,29	1,45	10,23	12,35	12,86	6,12	19,60	9,50	13,00	11,45
m9	8	10,14	1,25	9,22	11,05	12,36	5,89	18,84	8,50	11,80	9,90
m10	4	26,45	7,87	18,33	34,57	29,75	6,20	53,31	15,90	32,90	28,50
TmM3											
Measurement	Sample size	Mean	Standard Deviation	Confidence Limits		Coefficient of Variation	Confidence Limits		Minimum	Maximum	Median
m1	17	28,01	2,50	26,76	29,26	8,92	5,74	12,10	21,30	31,90	28,60
m2	0										
m3	8	11,49	1,21	10,60	12,37	10,56	5,05	16,08	9,60	13,00	11,50
m4	8	6,93	0,80	6,34	7,51	11,57	5,52	17,62	6,00	8,20	6,95
m5	8	8,49	0,87	7,85	9,12	10,22	4,89	15,55	7,00	9,40	8,75
m6	13	12,86	1,06	12,26	13,47	8,21	4,86	11,55	10,50	14,30	13,00
m7	0										
m8	8	9,80	1,34	8,82	10,78	13,70	6,50	20,90	7,80	11,90	9,75
m9	8	8,65	1,34	7,67	9,63	15,50	7,31	23,68	7,00	10,00	9,05
m10	1	18,60							18,60	18,60	18,60

their ends. In the original hyoid, the cornu hyoideum attached to the dorsal surface of these processes. They are absent here. The cornu hyoideum is the attachment site for the stylohyoideum (NICHEL et al. 1986: fig. 252). The ventral wall of the basihyoid (fig. 4.8 a) is flat and smooth, while the dorsal one (fig. 4.8 b) has an uneven contour. The lateral aspect (fig. 4.8 c) presents the bulbous end of the basihyoid, the irregular dorsal wall (at the right side), and the ventral smooth wall (at the left side).

Two larger elongate and thin fragmentary bony plates are parts of the right stylohyoid, and another fragment

(7' in the reconstruction) belongs to the left stylohyoid (both project dorsalward to the larynx). The reconstruction of the whole hyoid apparatus was made based on the structure of the hyoid in extant *Equus*. Shaded portions of Figure 4.8 represent those portions present in the Höwenegg specimen.

Portions of a second hyoid were discovered between the mandibular rami of the B-54 skeleton. Parts of this hyoid include its two bulbous processes and associated thyrohyoids. Two larger thin bony plates belong to the stylohyoids (missing in the V-58 specimen). The basihyoid is very similar to the V-58 specimen, but

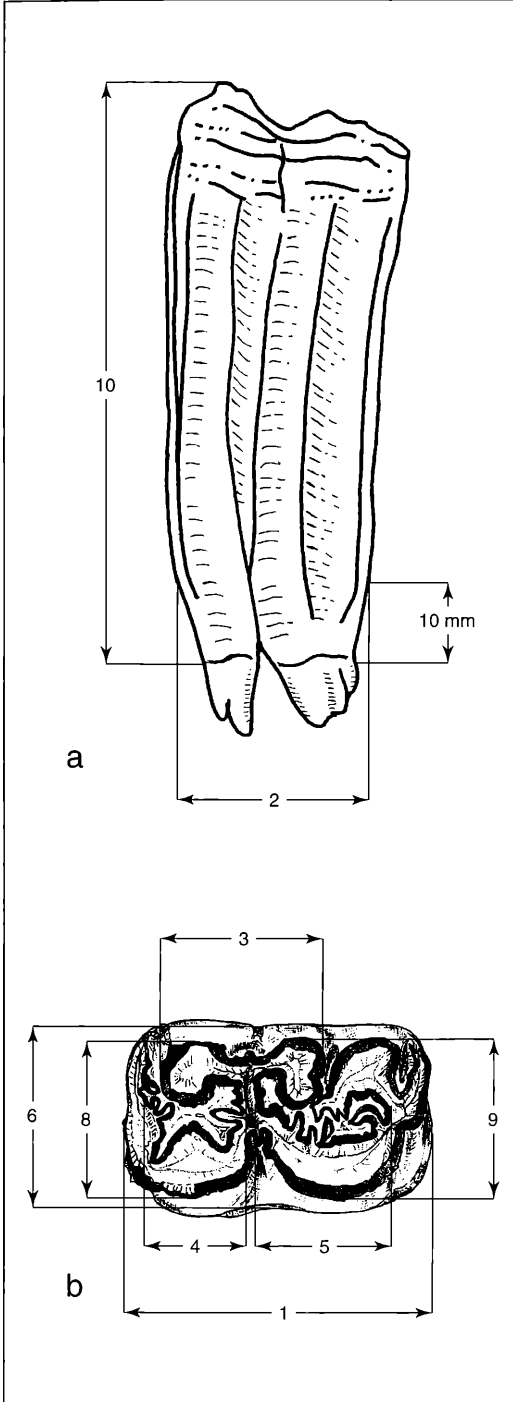


Figure 4.6. Measurements on Mandibular Cheek Teeth: a. buccal aspect; b. occlusal aspect.

rather more gracile. There are no previous reports on hipparionine hyoids. Figure 4.8 illustrates the stylohyoideum while figure 4.9 depicts GARRAUX's reconstruction of the hyoid apparatus.

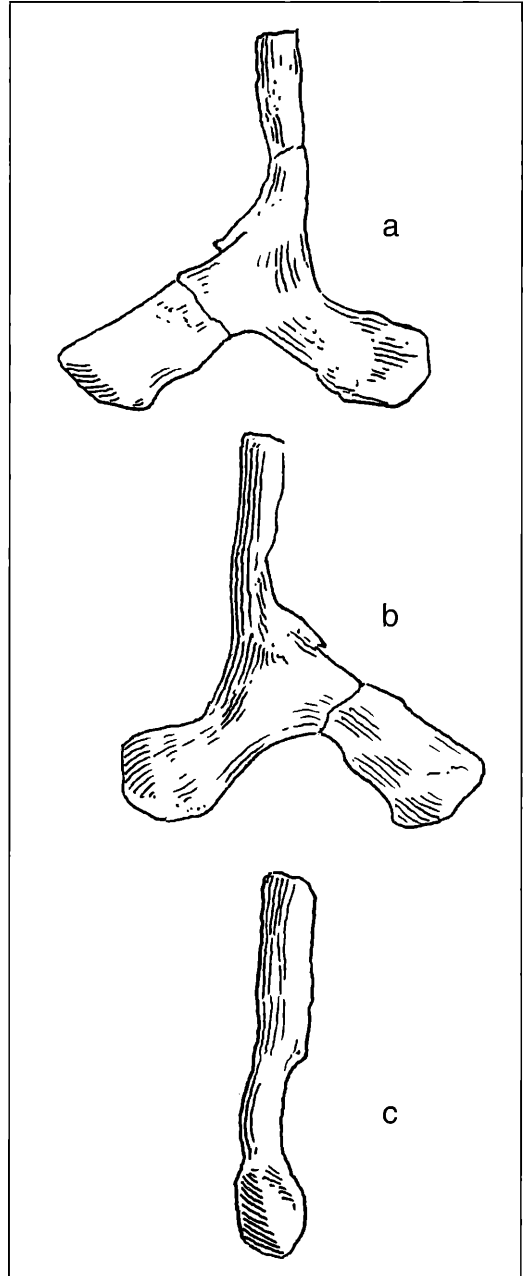


Figure 4.7. Basihyoideum: a. lateral aspect; b. medial aspect; c. dorsal aspect.

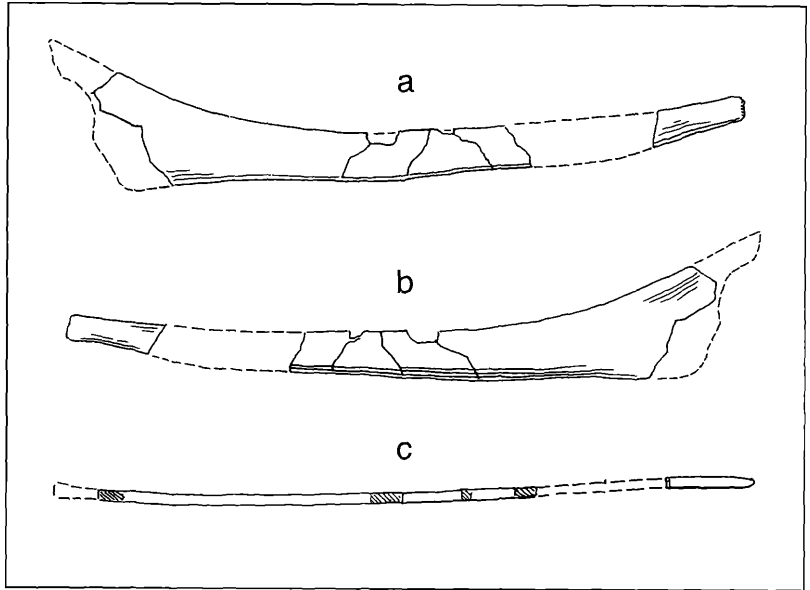


Figure 4.8. Stylohyoideum: a. ventral aspect; b. dorsal aspect; c. lateral aspect (x 0,60).

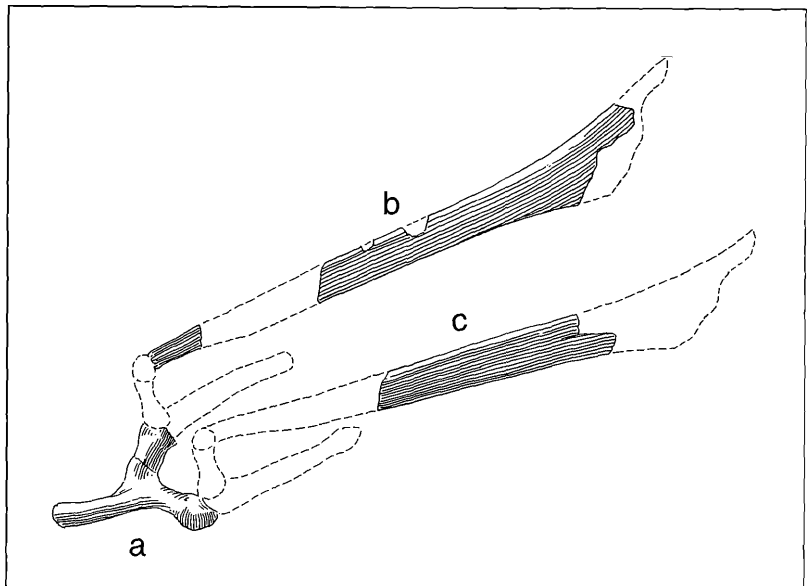


Figure 4.9. Reconstructed Hyoid Apparatus: a. basihyoid-eum; b. right stylohyoideum; c. left stylohyoideum (x 0,50).

5. Axial Skeleton

In the following text we provide a very brief description of the Höwenegg A axial skeleton (other than the skull, mandible and hyoid bone). The Höwenegg hipparion sample is the first from which a complete axial skeleton could be assembled. However, the vertebral column was usually crushed diagenetically causing distortion to most of its elements. GARRAUX was able to provide an accurate depiction as well as a reconstruction of the vertebrae as "Fundzustand" (= state of preservation after excavation) for the Hö A skeleton (fig. 5.1). Of further interest is HEIZMANN's reconstruction of a life-size standing mount of the Hö A skeleton at the Staatliches Museum für Naturkunde, Stuttgart (SMNS; fig. 5.2) which we refer to here. Figure 5.3 is a chart of this reconstruction's standing height measured at the external occipital protuberance and the tips the vertebral spines.

While the Hö A vertebral skeleton was relatively complete, it did suffer some post depositional deformation making it necessary in several cases for GARRAUX to reconstruct their morphology; this is particularly so in the reconstruction of transverse processes of most vertebrae. We do not attempt a detailed morphologic and functional anatomical interpretation of the vertebral skeleton here; this will be undertaken in the future

by R.L. BERNOR and E. HEIZMANN. We do however provide a very basic descriptive comparison to a specimen of Burchell's zebra (*Equus burchelli*, SMNS 6709, female) and when necessary to establish potential biases due to size, to a specimen of domestic African ass (SMNS 7334, female). This comparison in itself provides some key anatomical and functional differences between *Hippotherium primigenium* and extant *Equus*.

As is normal in extant *Equus*, the Hö A skeleton has 7 cervical (hereafter C1 – C7), 18 thoracic (T1 – T18), 6 lumbar (L1 – L6) and 5 sacral (S1 – S5) vertebrae. Whereas the extant horse normally has between 15 and 21 caudal (= coccygeal) vertebrae (NICKEL et al., 1986), the Hö A skeleton has only 11. In figure 5.3 the first measurement is the height of the individual from the top of the external occipital protuberance (EOP) to ground level. Following is the distance from ground level to the tip of the spinous process from the first cervical vertebra to the fifth sacral vertebra. This would give a height at the withers of 1.30 meters in the standing mount. Moreover, the reconstructed mount had a nearly horizontal thoracic through sacral vertebral spine alignment as reconstructed by HEIZMANN based on articulating joint surfaces. Comparison of the Stuttgart mount with the in situ Hö E skeleton (fig. 2.2 here) would suggest a greater in vivo dorsal spinal

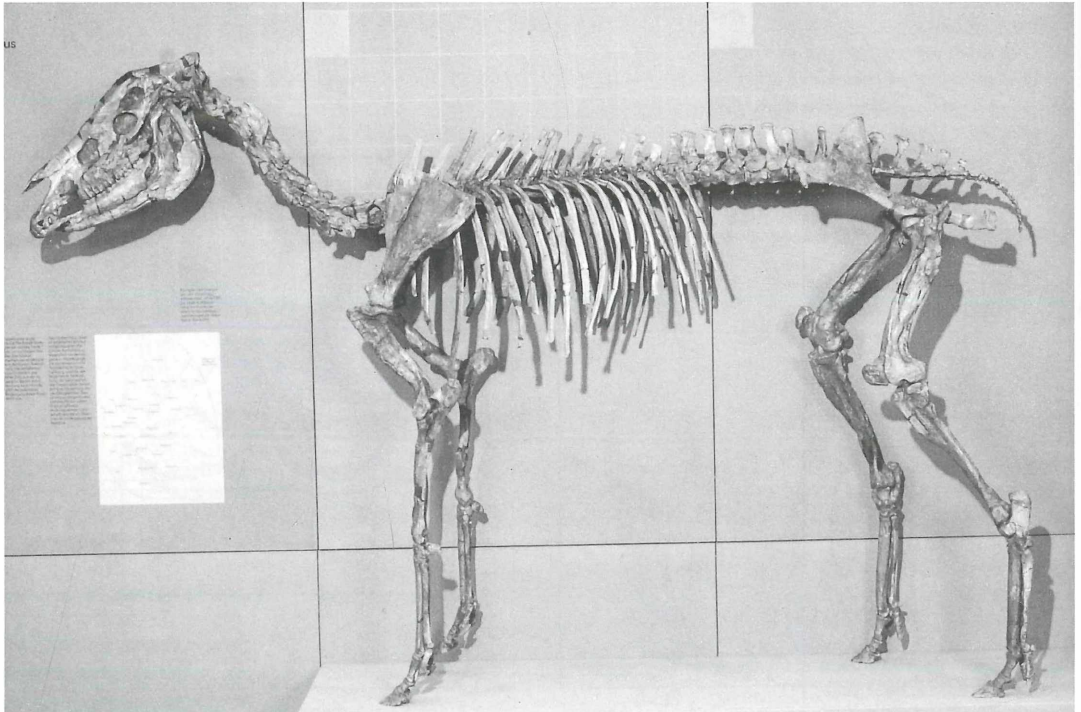
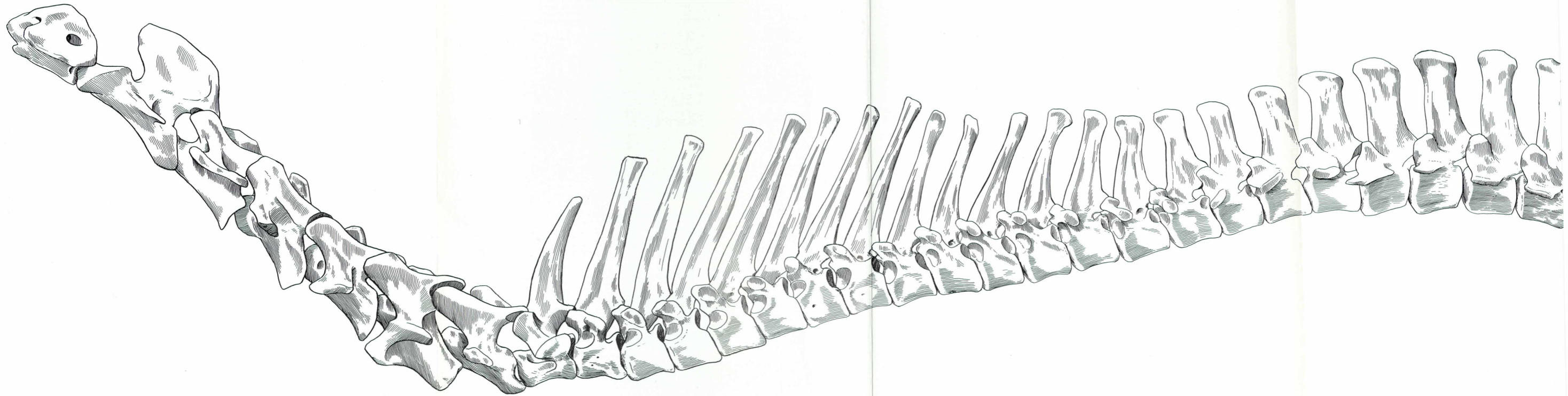


Figure 5.2. Stuttgart Standing Mount of the Höwenegg A skeleton.



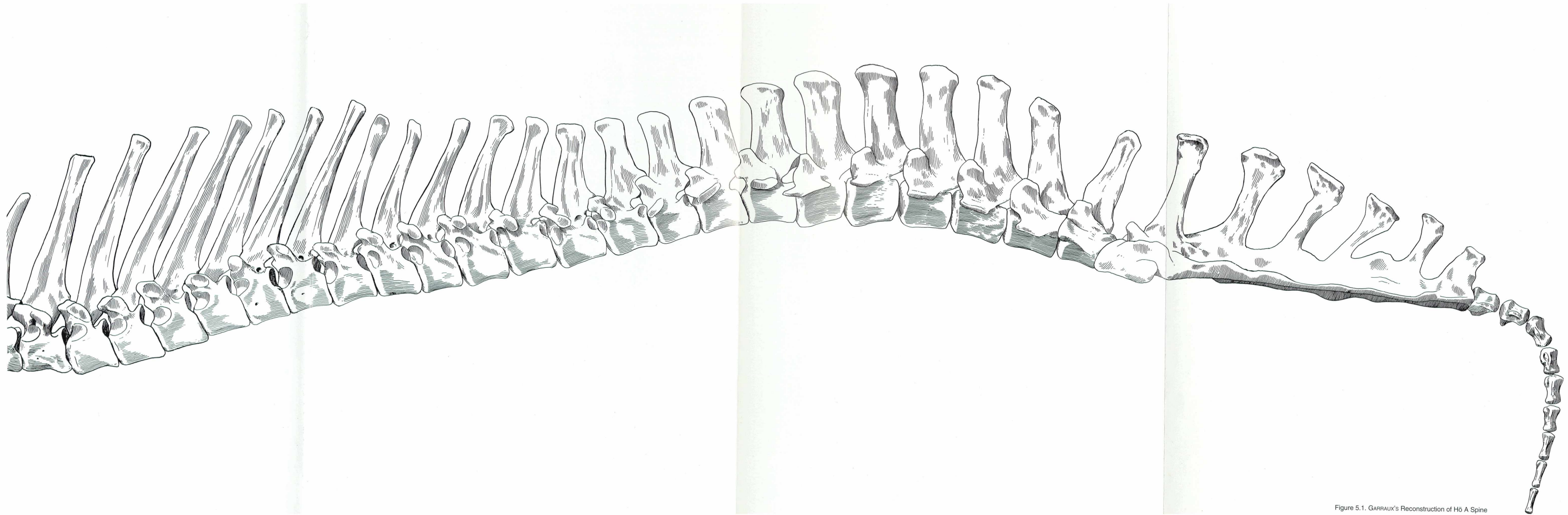


Figure 5.1. GARRAUX'S Reconstruction of H6 A Spine

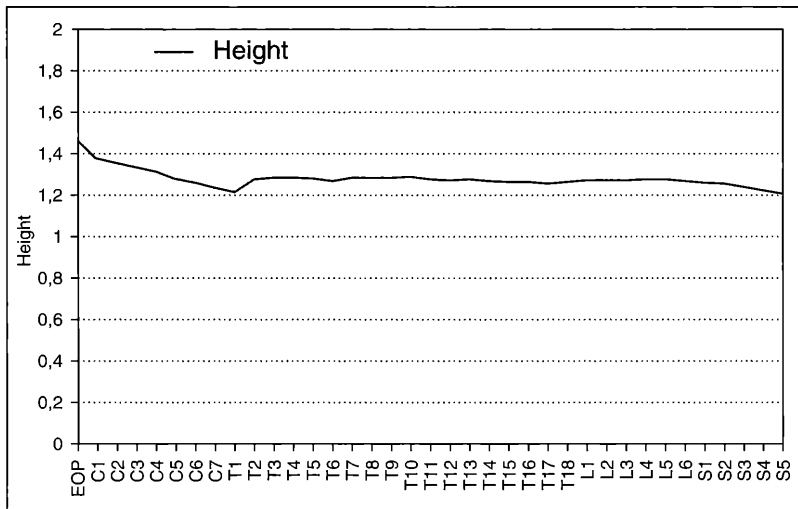


Figure 5.3. Chart of Höwenegg A Stuttgart exhibit measured from ground level to the external occipital protuberance (EOP) and the tip of the processi spinosi C1-S5.

curvature than found in the Stuttgart reconstruction. Yet, as we point out below, there are several important differences between the Höwenegg horse's spine and that of *Equus burchelli*. The height of the Höwenegg A hipparion is remarkable. We estimate with cartilage and soft tissue added, the Höwenegg A hipparion had a standing height at the withers between 1.30 and 1.35 meters clearly falling within the range of a Burchell's Zebra: 1.28–1.40 meters (JARMAN, 1974).

5.1 Anatomy of the Vertebral Classes

5.1.1 Cervical Vertebrae (fig. 5.1.1 – 5.1.7)

As in most mammals, the Hö A skeleton has 7 cervical vertebrae which differ little from living *Equus*. The Hö A C1 is medio-laterally distorted, missing most of the right, and much of the left ala atlantis (fig. 5.1.1.1 here). GARRAUX has reconstructed C1 on an *Equus* model (fig. 5.1.1.2) and neither the original specimen nor the reconstruction figured here differs in any essential details other than size (which is somewhat smaller in the Höwenegg horse) with *Equus burchelli*. The Höwenegg epistropheus (C2; fig. 5.1.2.1 and 5.1.2.2) exhibits some distortion particularly of the tuberculum dorsi which is displaced to the right of the midline and is somewhat compressed vertically. The processus articularis cranialis is much like *Equus*, but appears to be somewhat mediolaterally narrower at its dorso-caudal-most extent. The Hö A C2 differs most significantly from the zebra in the more caudally placed bifurcation of its dorsal margin, giving the effect in lateral view of having a more parallel alignment with the craniocaudal axis of the vertebral body (compare fig. 5.1.2d here with NICKEL et al., 1986: fig. 40). The Höwenegg hipparion also differs markedly from the zebra in its smaller diameter of the caudal articular surface (with C3) than in the zebra. Cervical 3 – C7 (fig. 5.1.3-5.1.7) exhibit some lateral distortion. When placed in articular alignment and directly compared to the zebra, the Hö C3 – C7 would appear to be proportionally longer and narrower. The laterally wider aspect being particularly apparent on the dorsal surface of the processus articularis caudalis. Of further interest is the apparent smaller diameter of the foramen vertebrale (best preserved in the Hö A C7) and the particularly longer dorsal surface of C7's body than seen in the zebra.

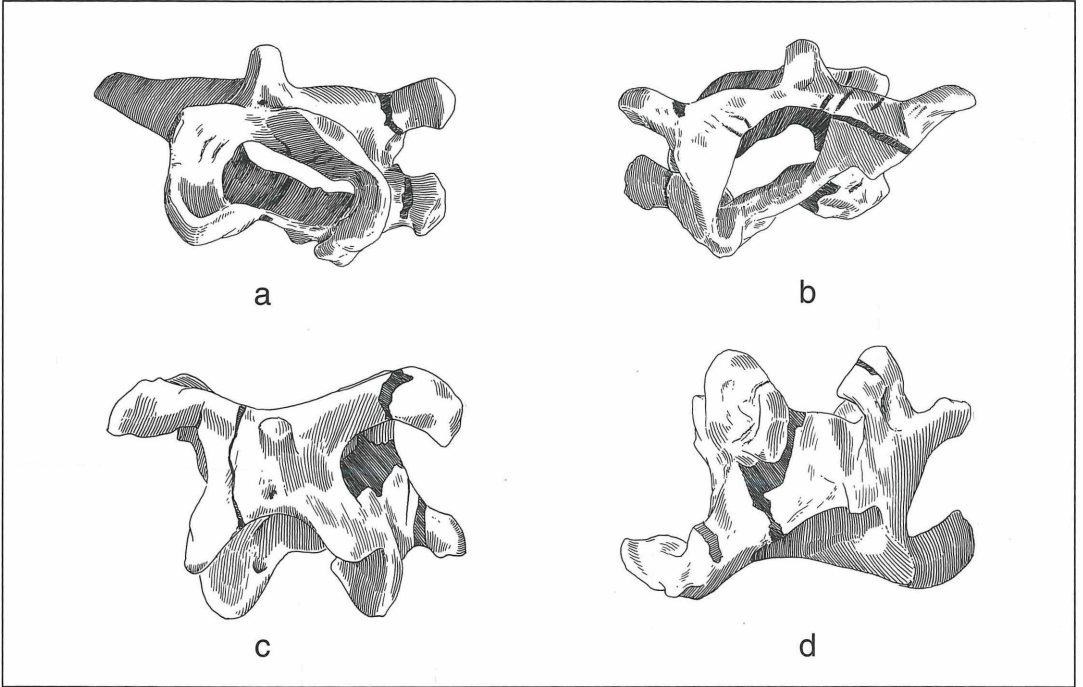


Figure 5.1.1.1. Atlas (unreconstructed): a. cranial aspect; b. caudal aspect; c. dorsal aspect; d. ventral aspect (x 0,40).

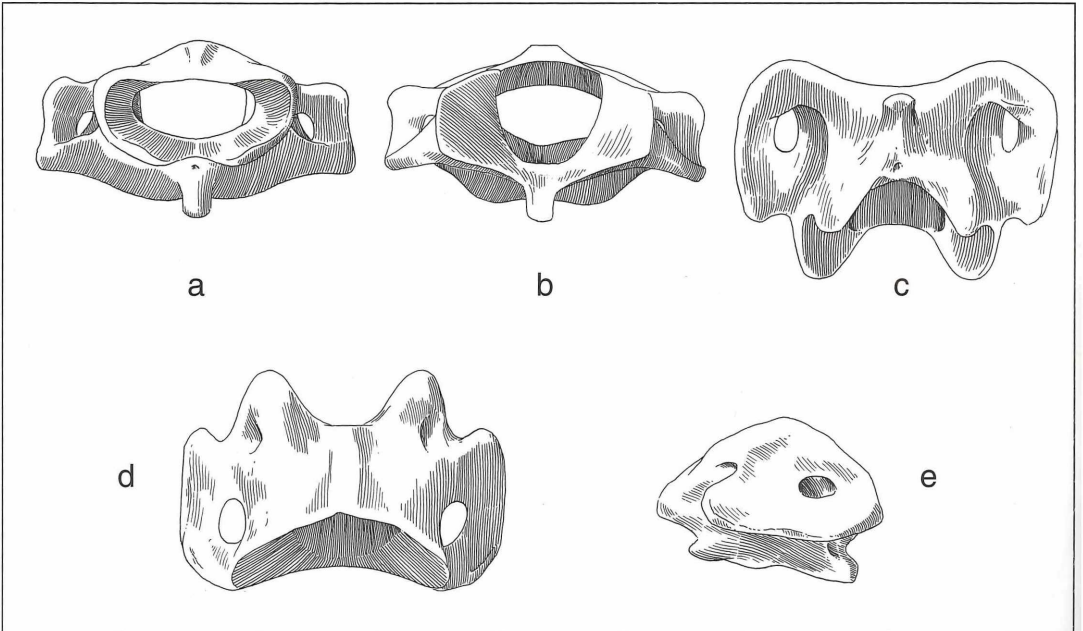


Figure 5.1.1.2. Atlas (reconstructed): a. cranial aspect; b. caudal aspect; c. dorsal aspect; d. ventral aspect; e. lateral aspect (x 0,35).

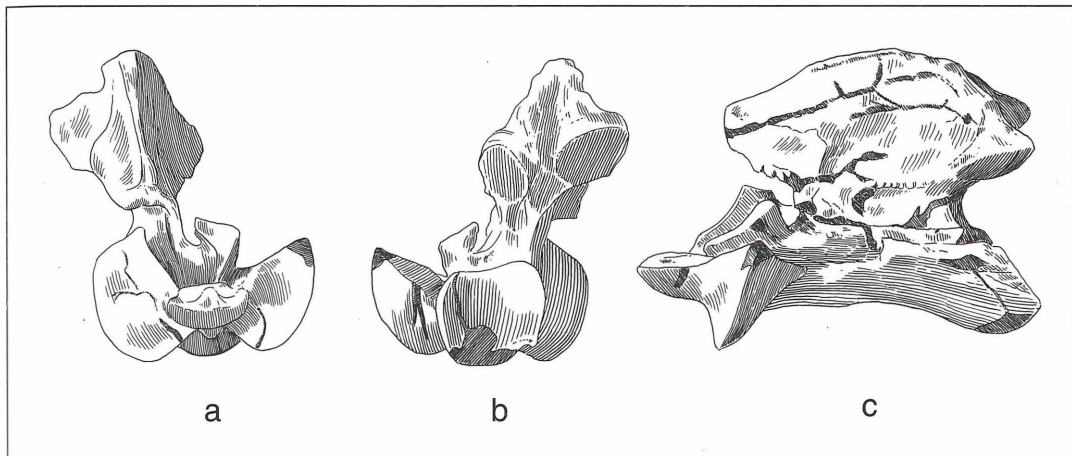


Figure 5.1.2.1. Axis (unreconstructed): a. cranial aspect; b. caudal aspect; c. lateral aspect (x 0,40).

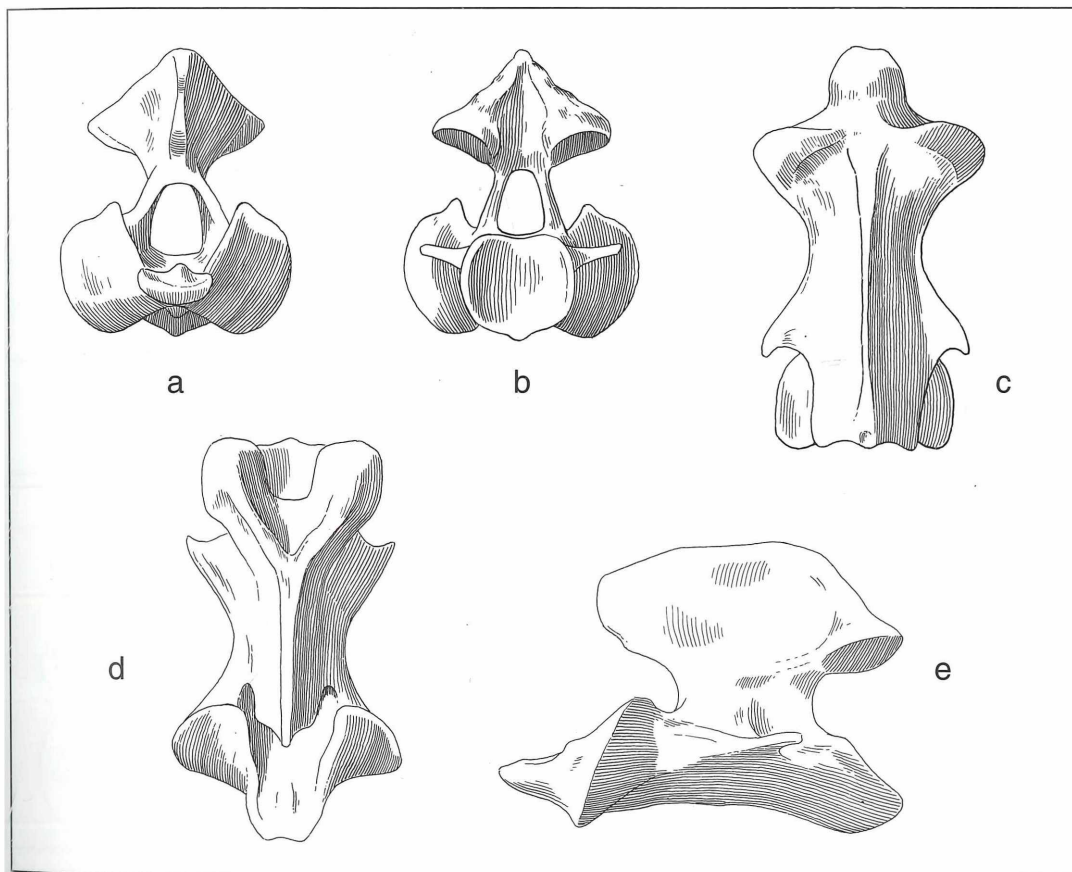


Figure 5.1.2.2. Axis (reconstructed): a. cranial aspect; b. caudal aspect; c. ventral aspect; d. dorsal aspect; e. lateral aspect (x 0,40).

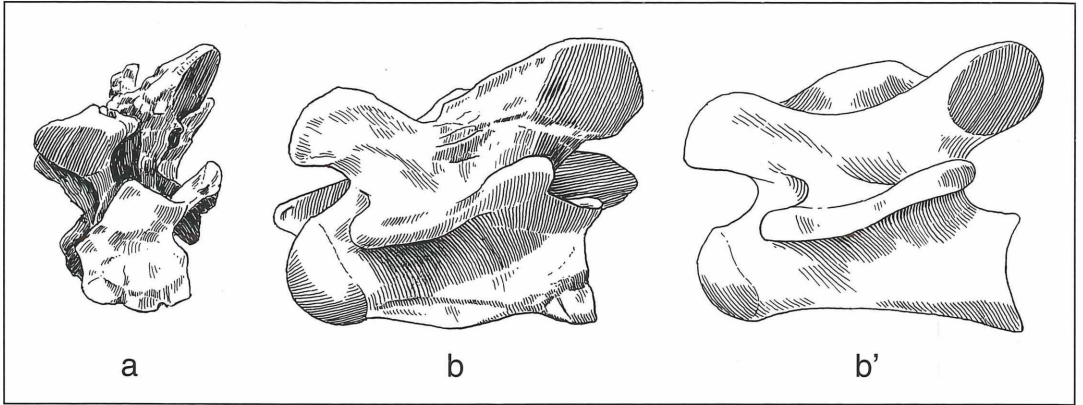


Figure 5.1.3. Cervical 3 Vertebra: a. caudal; b. lateral (a. and b. unreconstructed); b'. lateral (reconstructed) (x 0,50).

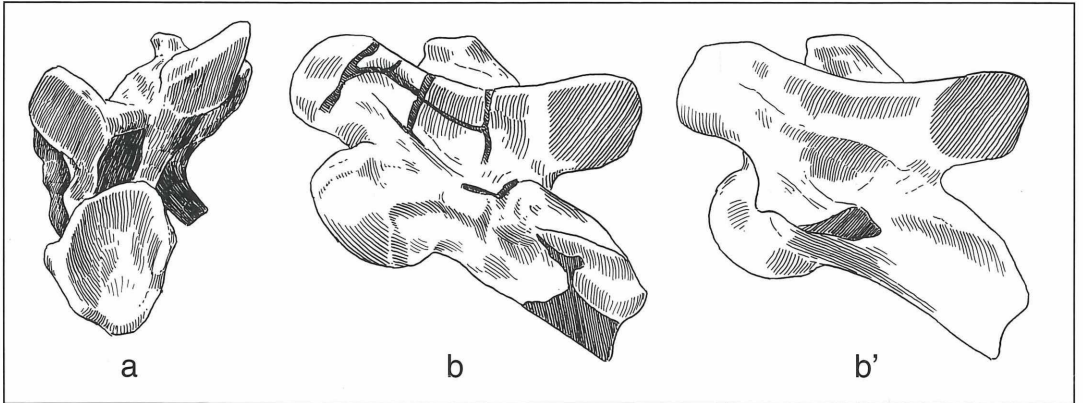


Figure 5.1.4. Cervical 4 Vertebra: a. caudal; b. lateral (a. and b. unreconstructed); b'. lateral (reconstructed) (x 0,50).

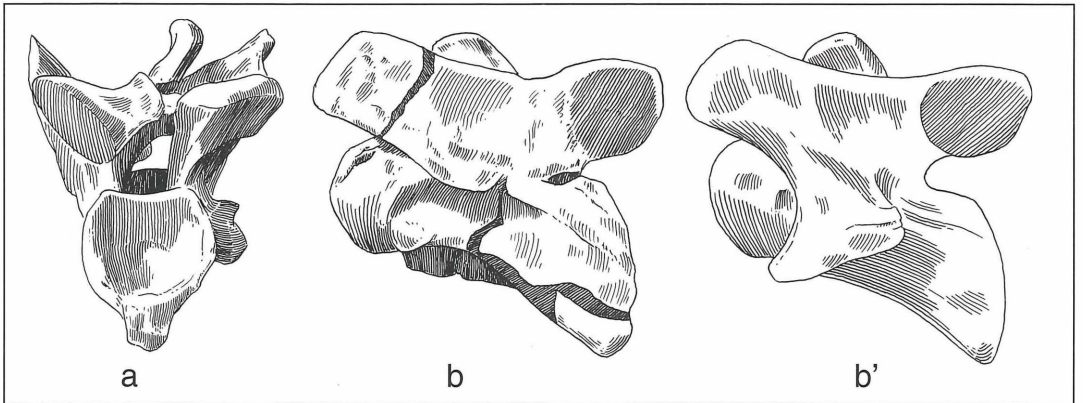


Figure 5.1.5. Cervical 5 Vertebra: a. caudal; b. lateral (a. and b. unreconstructed); b'. lateral (reconstructed) (x 0,50).

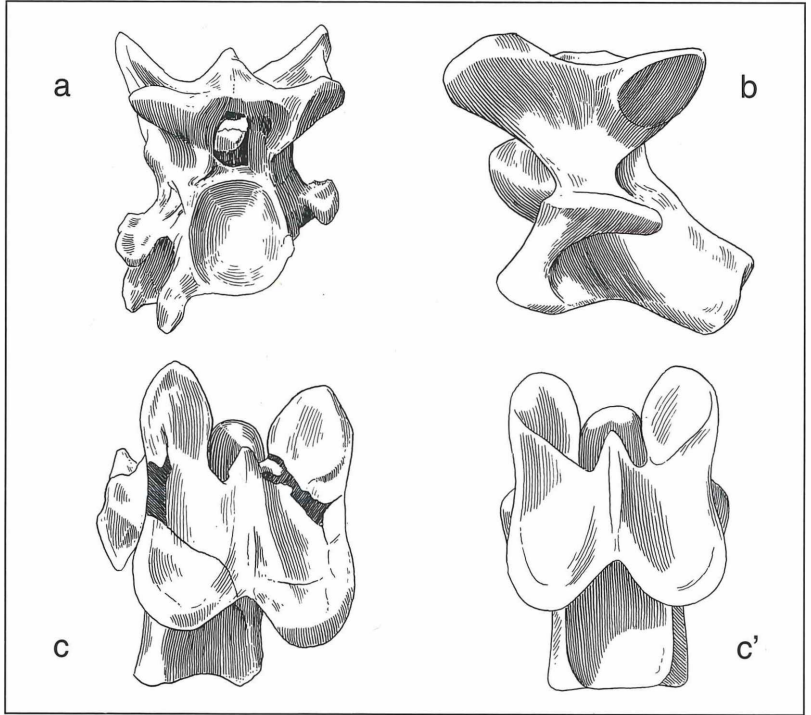


Figure 5.1.6. Cervical 6 Vertebra: a. caudal (unreconstructed); b. lateral (reconstructed); c. dorsal (unreconstructed); c'. dorsal (reconstructed) (x 0,40).

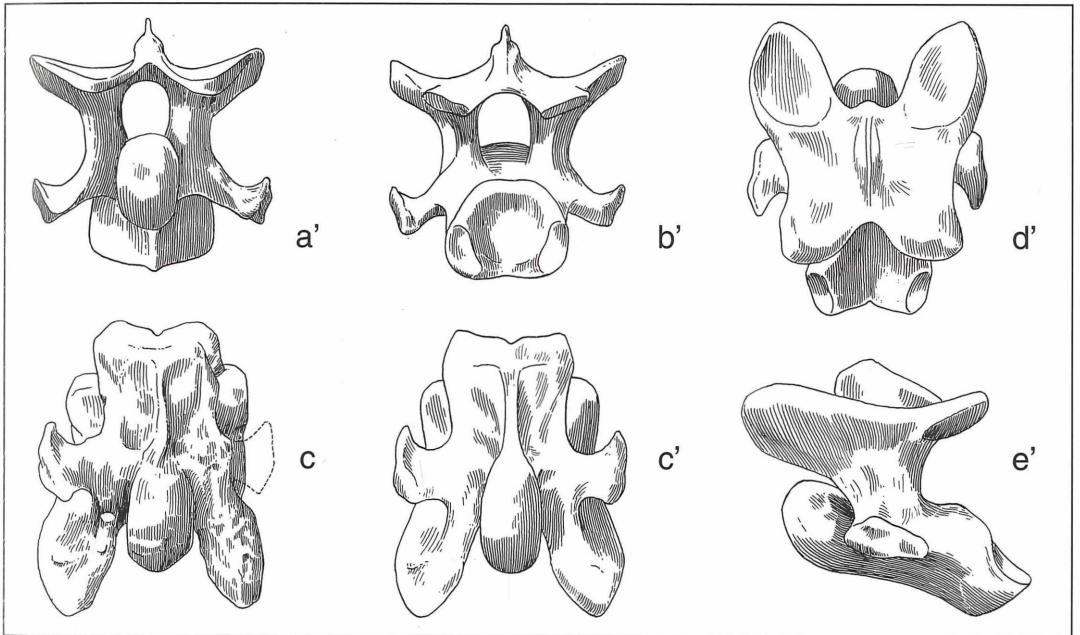


Figure 5.1.7. Cervical 7 Vertebra: a'. cranial; b'. caudal; c. ventral; c'. ventral; d'. dorsal; e'. lateral (only c. is unreconstructed) (x 0,40).

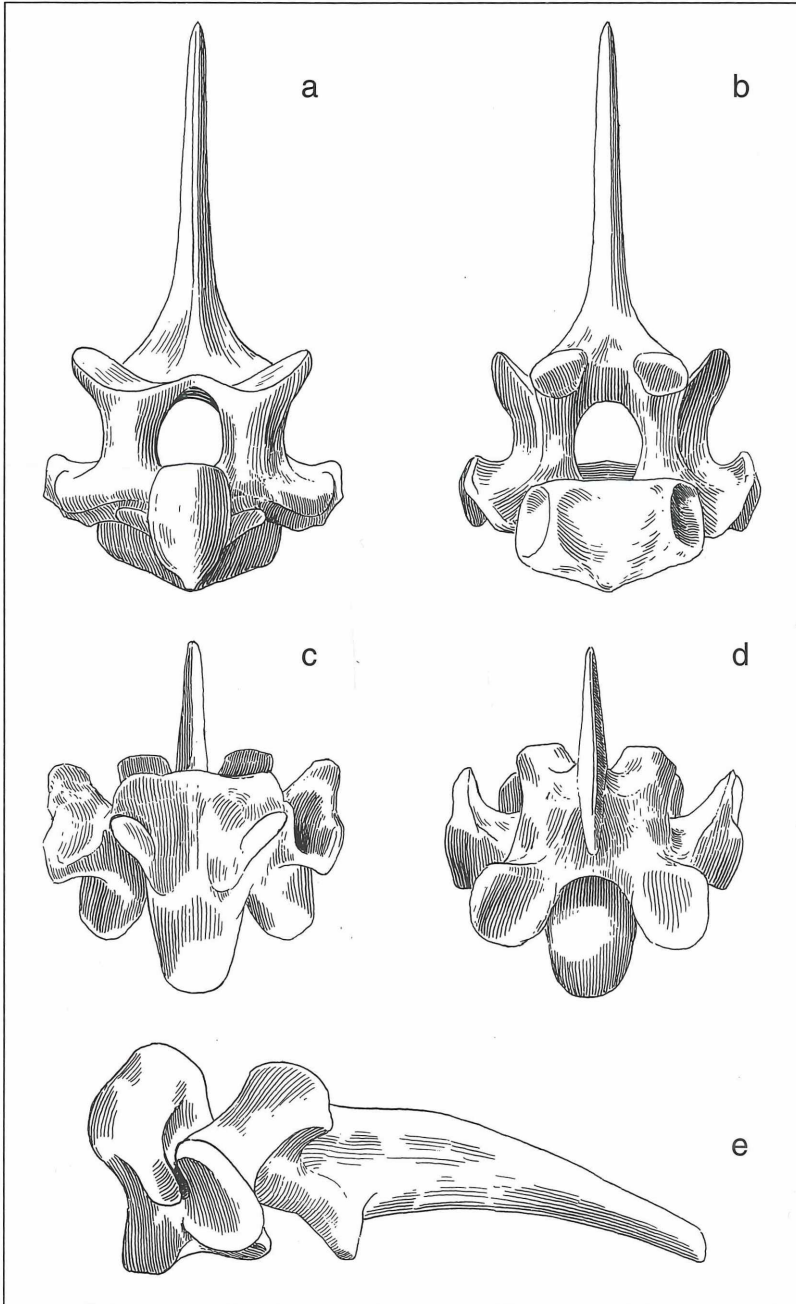


Figure 5.2.1. Thoracic 1 Vertebra: a. cranial aspect; b. caudal aspect; c. ventral aspect; d. dorsal aspect; e. lateral aspect (x 0,50).

5.1.2 Thoracic Vertebrae (fig. 5.2.1 – 5.2.6)

The most immediately recognizable differences between the Hö A thoracic vertebrae and those of the *E. burchelli* vertebral skeleton are in the spinous process-

es. The T1 processus spinosus is remarkably similar in the Hö A skeleton and *E. burchelli*. In contrast, the domestic African ass T1 (SMNS 7334) is relatively

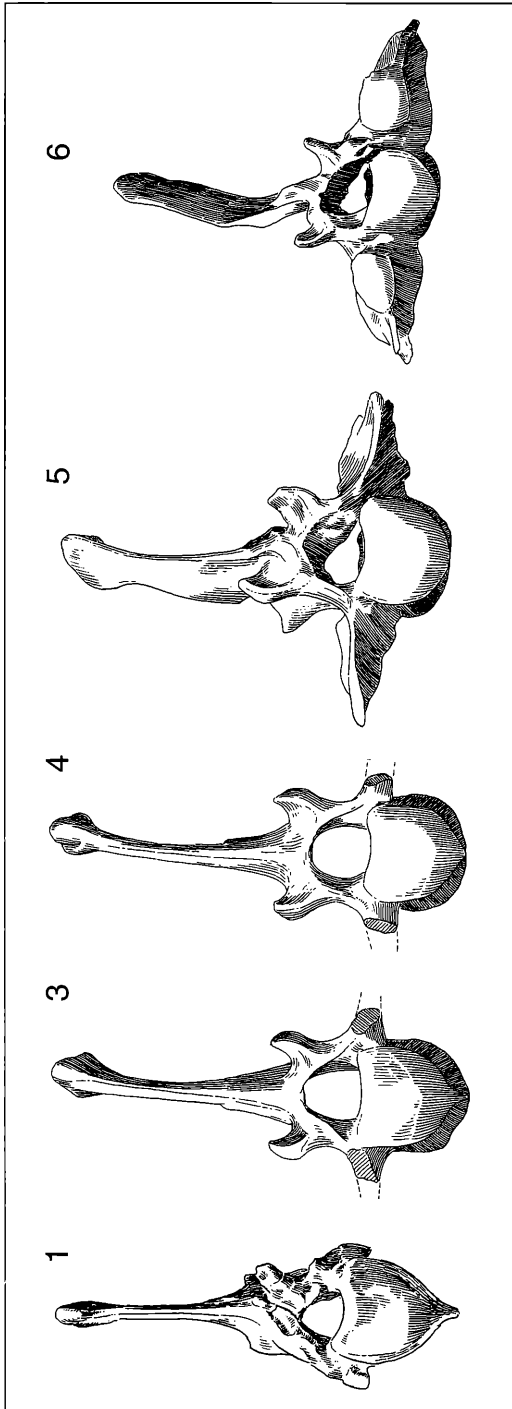


Figure 5.2.2. Thoracic Vertebrae: T1, T3, T4, T5, T6 (all cranial view) (x 0,40).

shorter and more sharply inflected caudalward than in the Hö A and zebra T1 (re: fig. 5.2.1 here).

The processi spinosi of the Hö A T2-T6 (fig. 5.2.2 and 5.2.3) are closely similar in their length and more convex along their cranial edge than in the zebra. Höwenneg A T7 is similar to the zebra, but again as in T2-T6 has a more convex cranialward spine. The Höwenneg T8 processus spinosus is *absolutely* longer than in the zebra, and narrows sharply in its craniocaudal dimension at its dorsalmost extreme. The Höwenneg A T9-T12 contrast further with the zebra in having longer processi spinosi. In the zebra (SMNS 6709), as well as the African domestic ass (SMNS 7334), T11 or T12 is transitional from the typical long thoracic spine to the shorter, more vertically directed lumbarized thoracic spine typical for T13-T18. In the Hö A spine this transition occurs with T14. The distalmost extent of T16's processus spinosus is destroyed, but T17's (fig. 5.2.4) and T18's processus spinosus are directed vertically and are not craniodorsally reflected as in the zebra. The relative lengths and orientation of the spines of the African ass (SMNS 7334) are very similar to the zebra, as well as the higher (T11) transition to lumbarization of the spinous processes.

Figures 5.2.5 and 5.2.6 present the Hö A thoracic vertebrae in both an unreconstructed and reconstructed state. The thoracic vertebrae also exhibit some medio-lateral distortion (fig. 5.2.5), but again it would appear that the foramen vertebrale has a greater diameter in the zebra (and relatively so in the African ass) than in the Hö A thoracic spine. The fovea costalis cranialis and caudalis are more expanded and concave midsagittally in the zebra than the Hö A thoracic vertebrae. Also, in the zebra the processi mamillari project cranialward so as to "interlock" with the preceding vertebral dorsal arcus vertebrae from T3-T18. In T3-T11 the processi mamillari are oriented laterally away from the processi spinosi, but from T12 to T18 they progressively more closely approach the dorsal arcus vertebrae, effectively forming a "locking mechanism" which limits mediolateral rotation of the lower thoracic spine in *Equus*. The mamillary processes are not always preserved in the Hö A horse, but when they are (T3, T4, T5, T8, T11, T12, T13, T14, T15, T17 and T18 usually only one side, and often damaged), they are always less massive, they extend less cranialward and would appear to be less interlocking – especially in the lower thoracic spine.

Compositely then, the Hö A thoracic spine would appear to be adapted to greater rotation along its axis and at the same time was less stable for the strong propulsive forces incurred with sustained high speed running as is seen in the zebra. A premium would be realized however in quick darting and leaping actions which was facilitated by a more flexible spine.

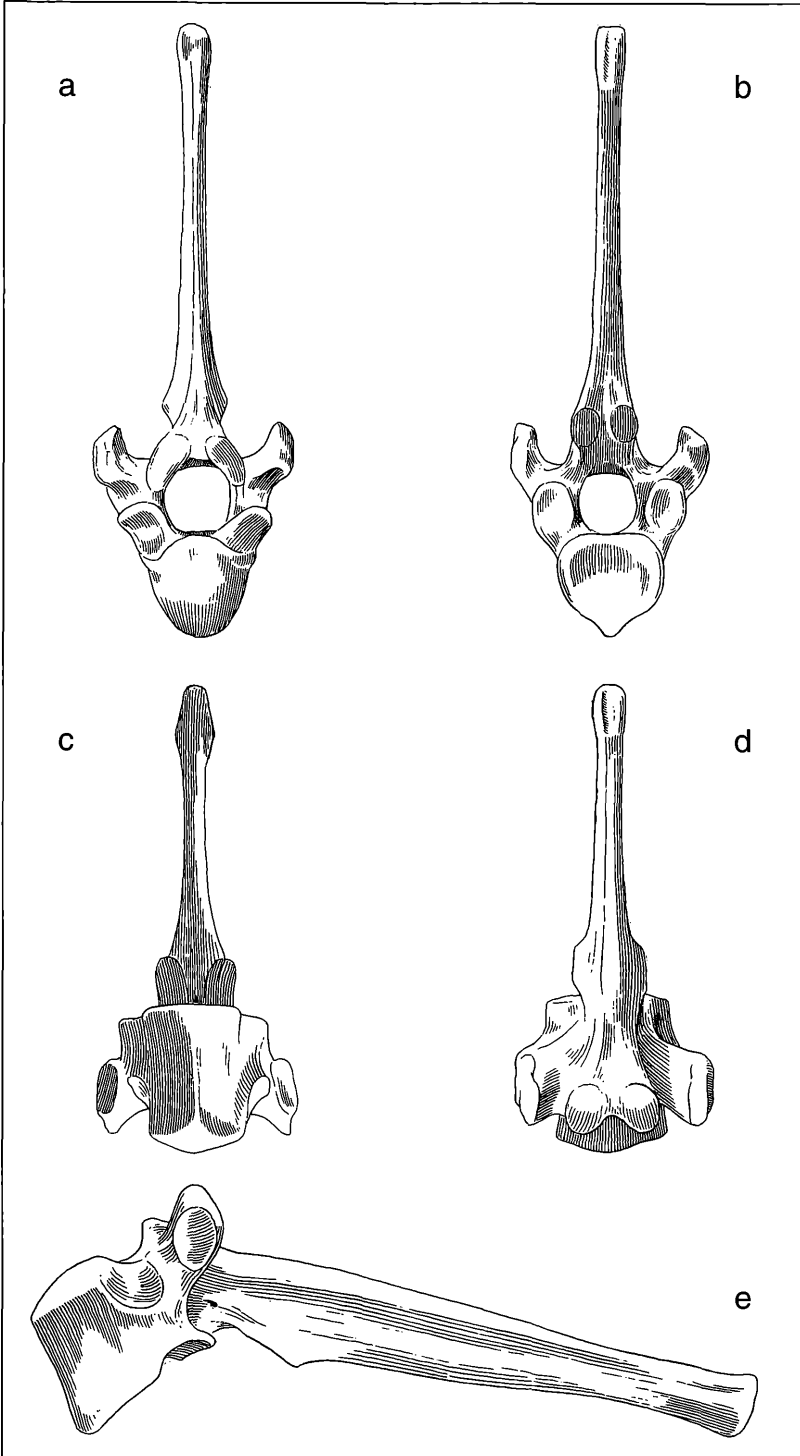


Figure 5.2.3. Thoracic 5 Vertebra: a. cranial; b. caudal; c. ventral; d. dorsal; e. lateral (x 0,45).

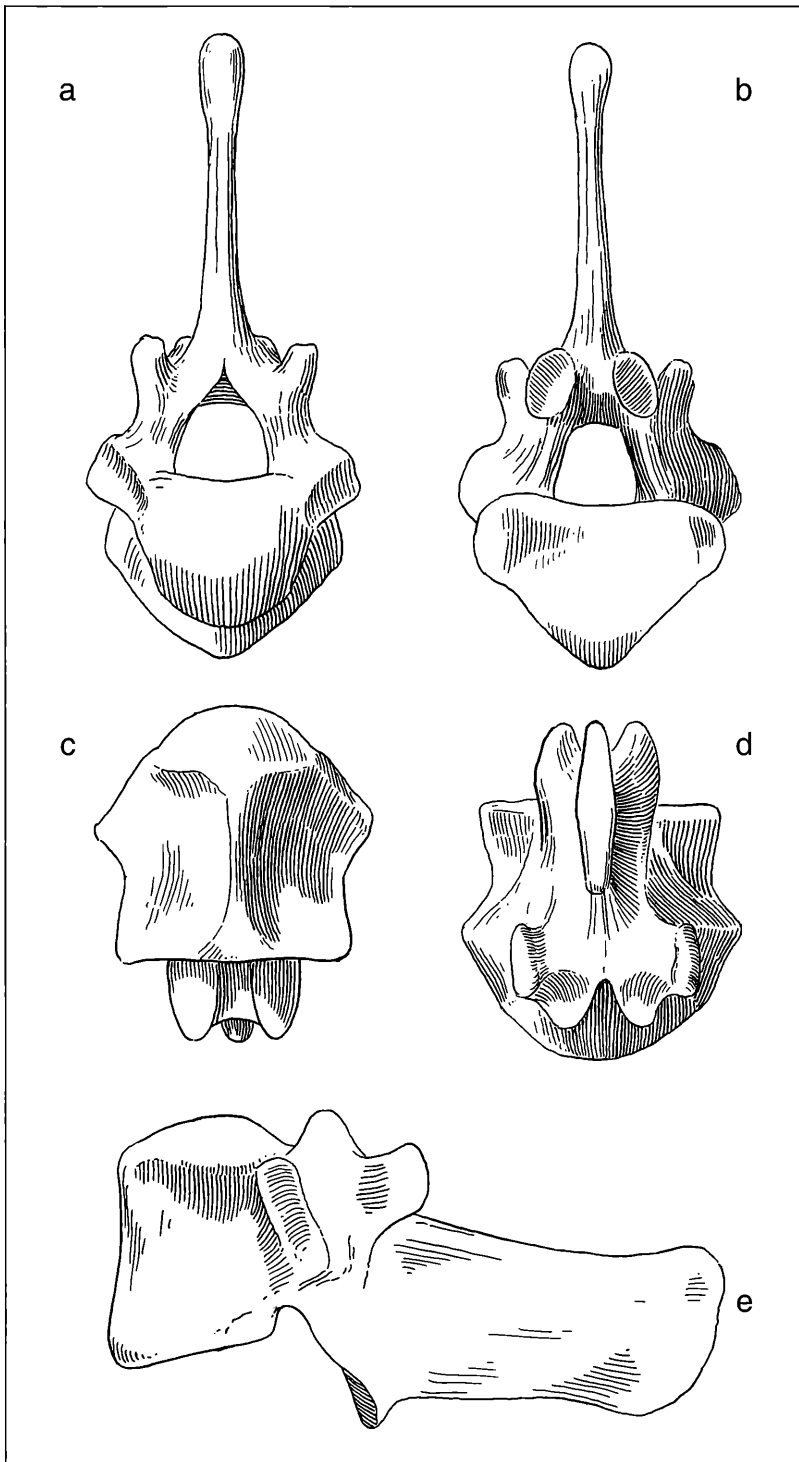


Figure 5.2.4. Thoracic 17 Vertebra: a. cranial; b. caudal; c. ventral; d. dorsal; e. lateral (x 0,50).

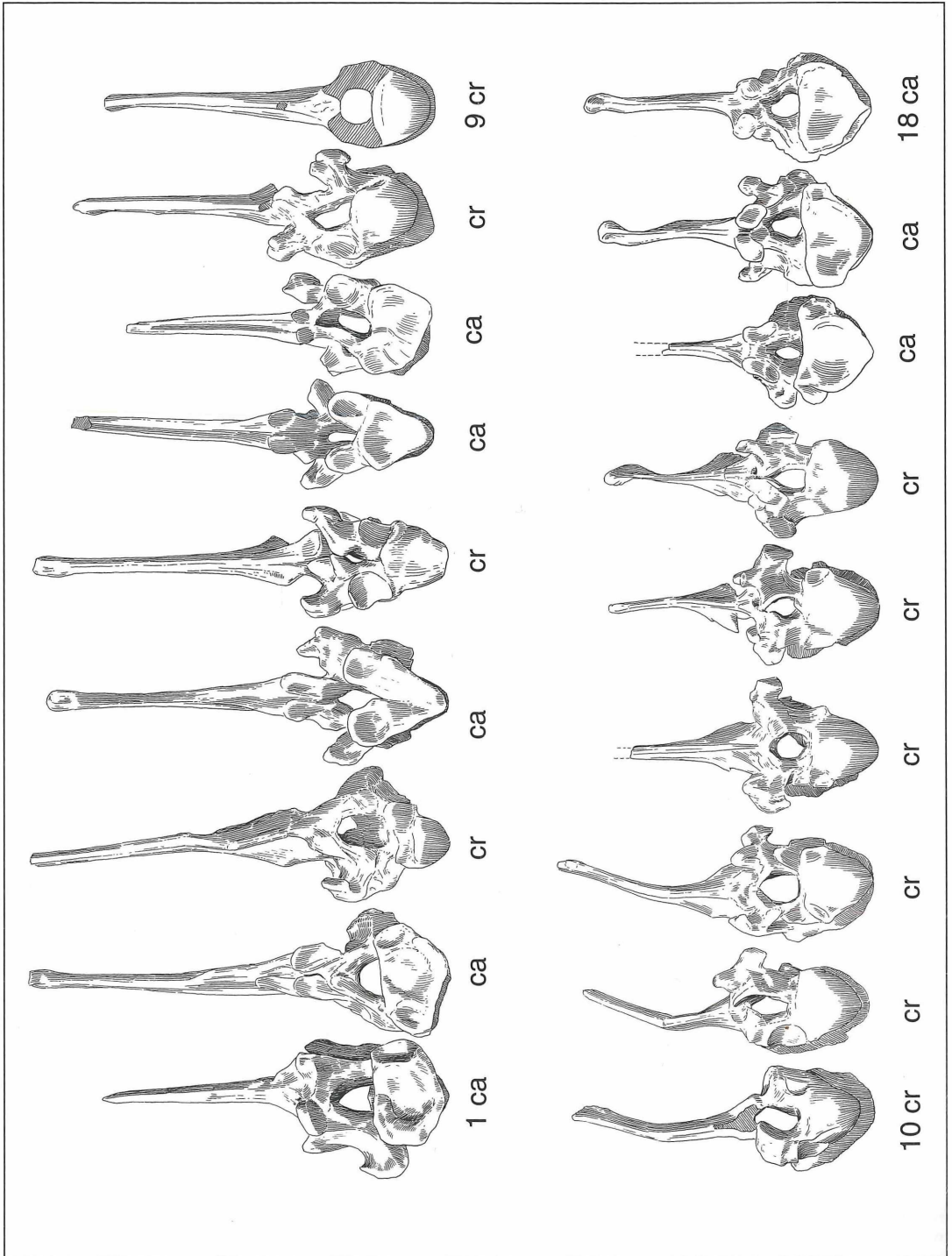


Figure 5.2.5. Thoracic 1-Thoracic 18 Vertebrae: cranial (cr) or caudal (ca) view as indicated (x 0,35).

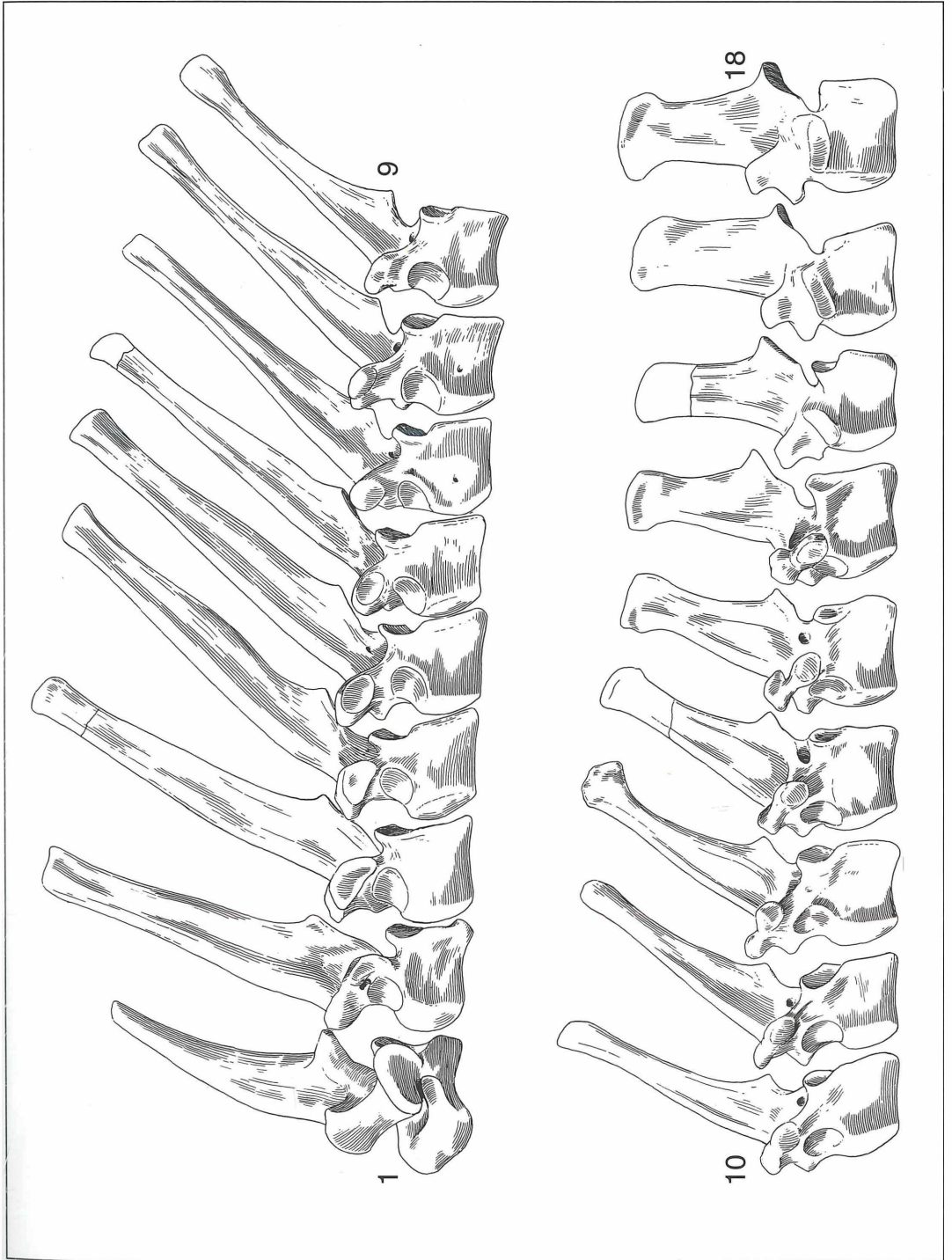


Figure 5.2.6. Thoracic 1-Thoracic 18 Vertebrae: lateral view (x 0,35).

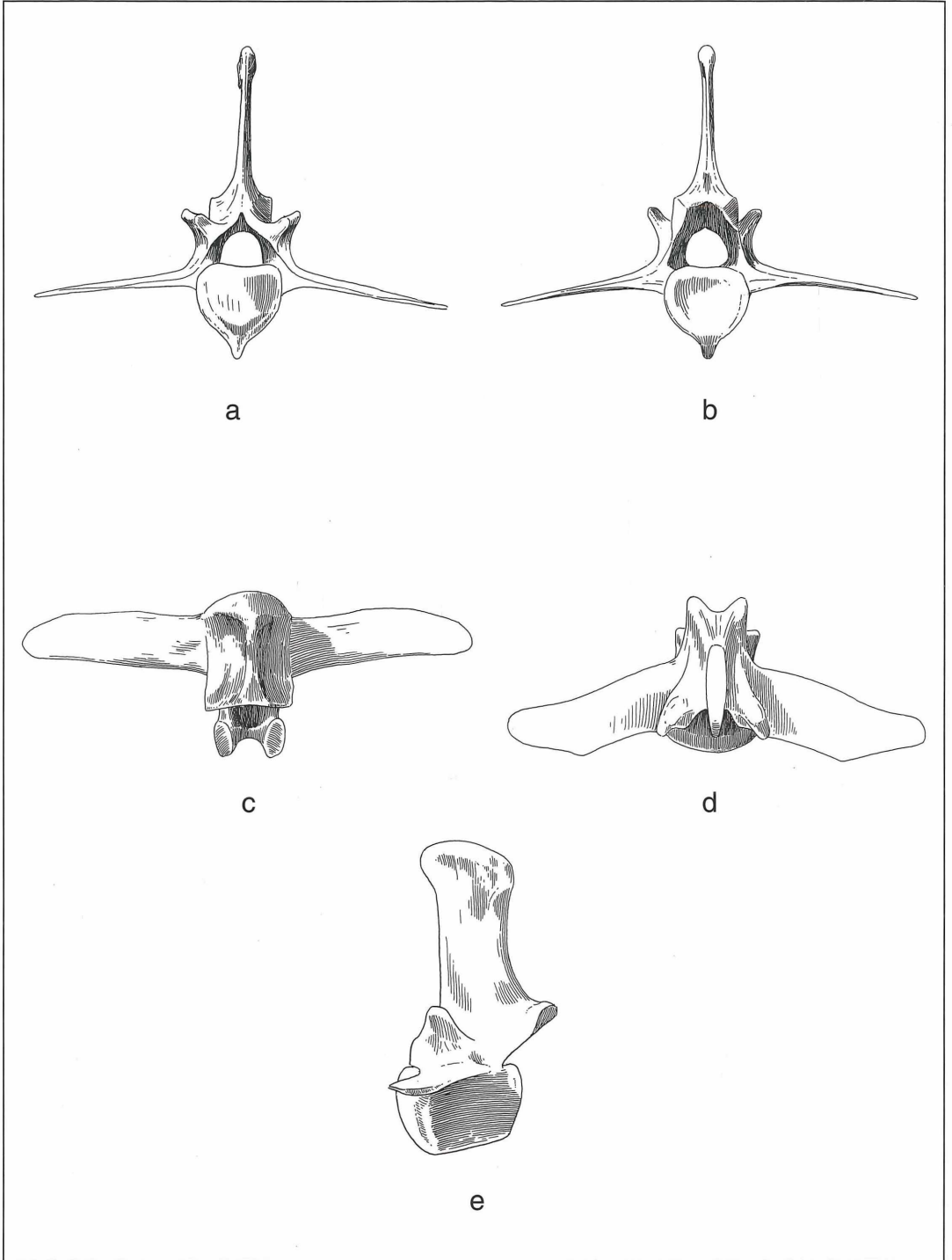


Figure 5.3.1. Lumbar 1 Vertebra: a. cranial aspect; b. caudal aspect; c. ventral aspect; d. dorsal aspect; e. lateral aspect (x 0,35).

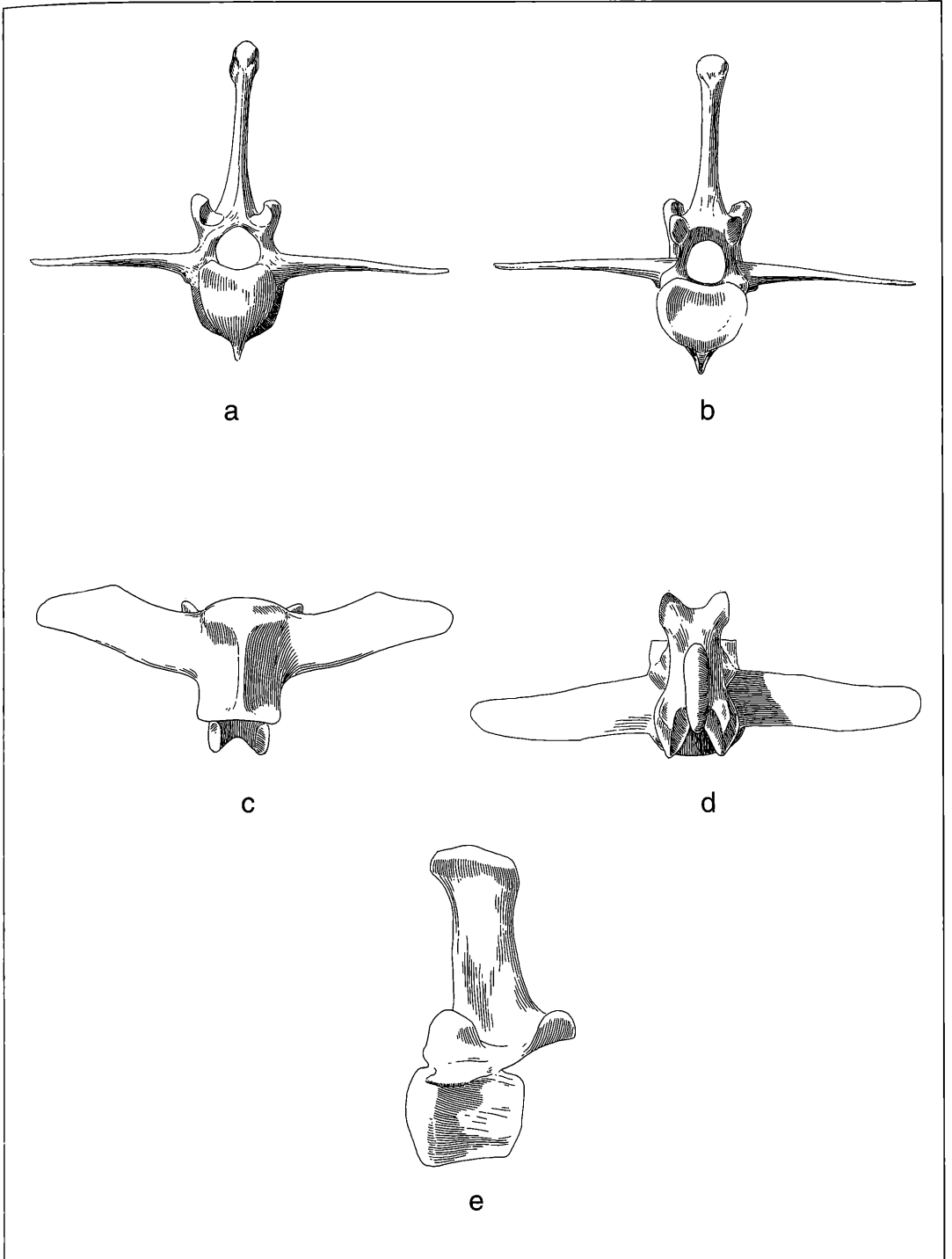


Figure 5.3.2. Lumbar 2 Vertebra: a. cranial; b. caudal; c. ventral; d. dorsal; e. lateral (x 0,35).

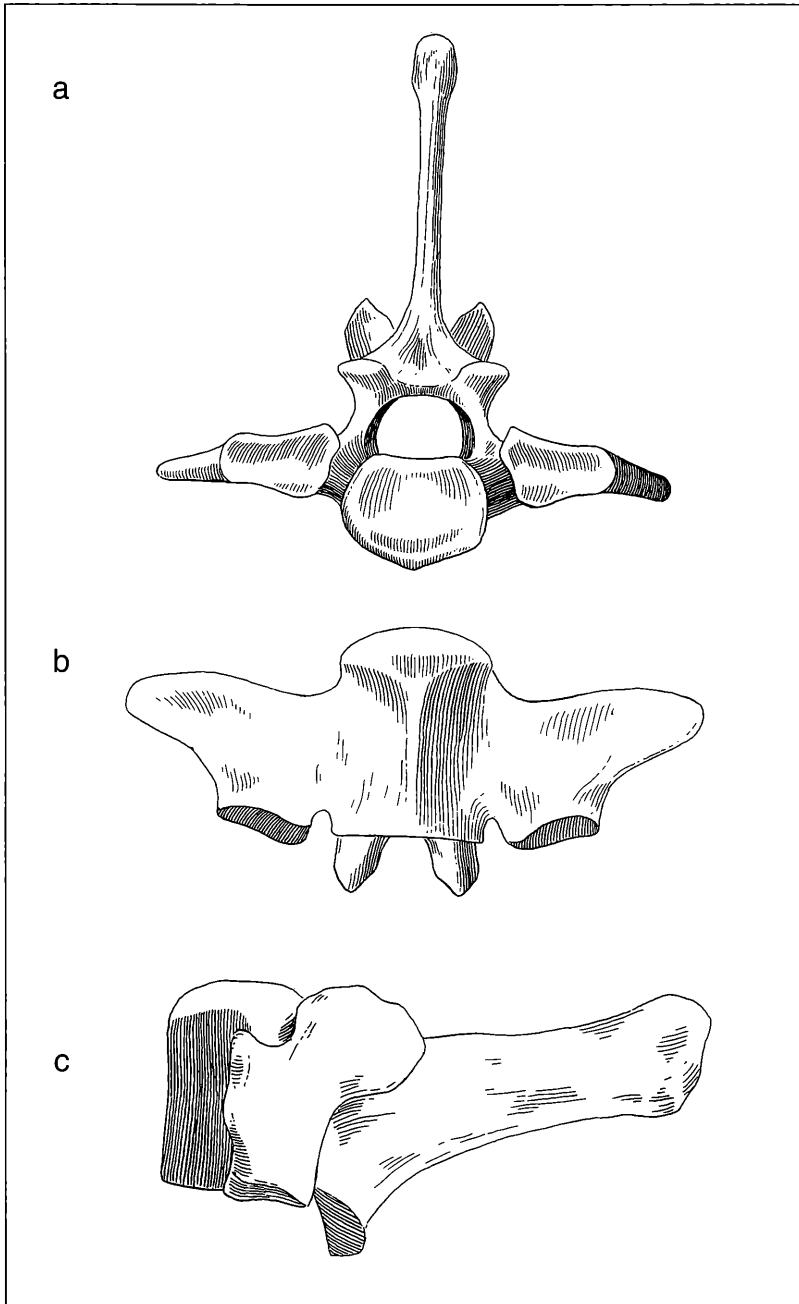


Figure 5.3.3. Lumbar 5 Vertebra (reconstructed): a. caudal; b. ventral; c. lateral (x 0,55).

5.1.3 Lumbar Vertebrae (fig. 5.3.1-5.3.5)

None of the Hö A skeleton's 6 lumbar vertebrae preserve the complete transverse processes. However, L5 does preserve the proximal most portion of both the

right and left transverse spines, and L6's transverse spines are complete except for their distalmost extent. Lumbar vertebra 1 (fig. 5.3.1) has a longer, straighter, dorsally directed spine than is seen in the zebra (which

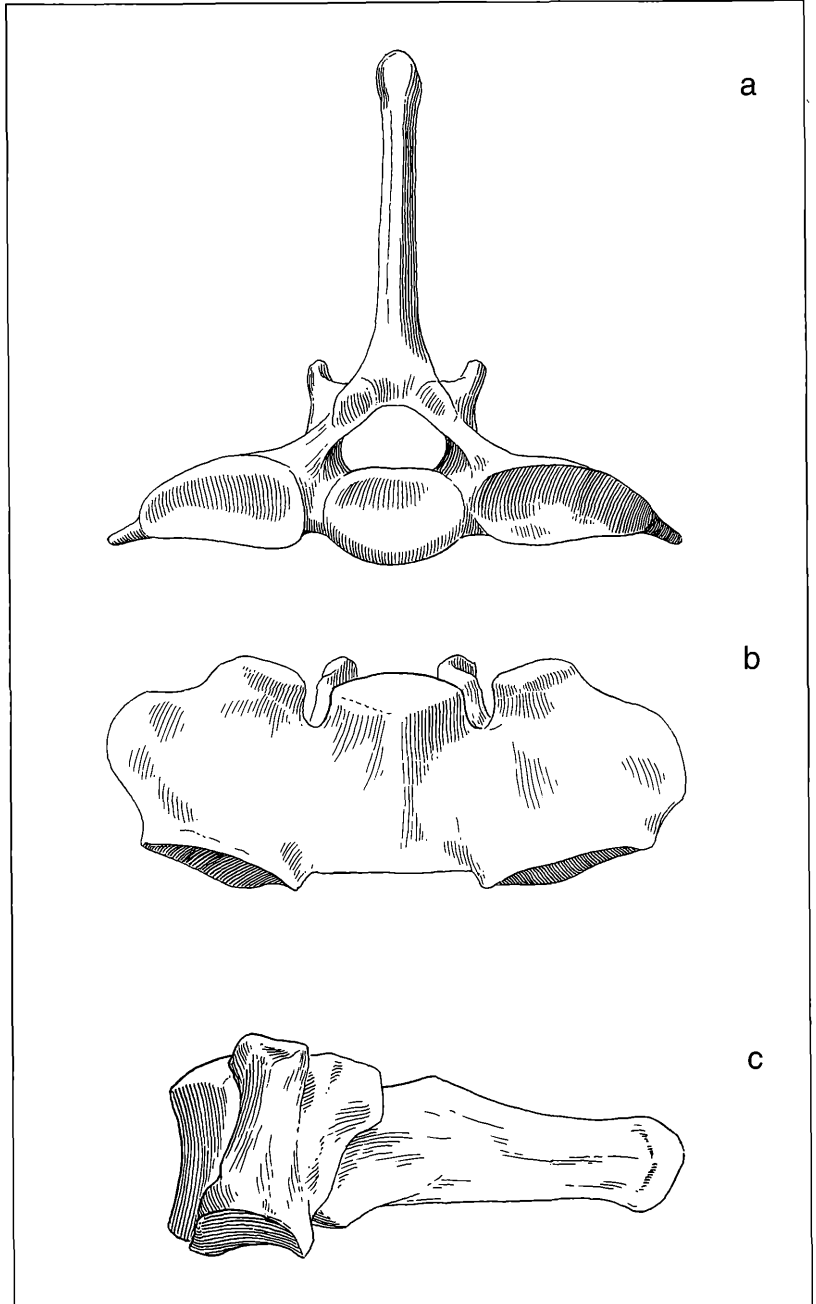


Figure 5.3.4. Lumbar 6 Vertebra (reconstructed): a. caudal; b. ventral; c. lateral (x 0,55).

is reflected cranialward). Likewise, the H_ö A L2 (fig. 5.3.2) and L3 both exhibit longer processi spinosi than that of the zebra, however the H_ö A L3 has a slight cranialward orientation, while in the zebra it is dorsally

directed. In the original H_ö A L5 (fig. 5.3.3) and L6 (fig. 5.3.4) the processi spinosi are distorted; GARRAUX's reconstruction accurately depicts them as being longer and craniocaudally narrower than in the zebra.

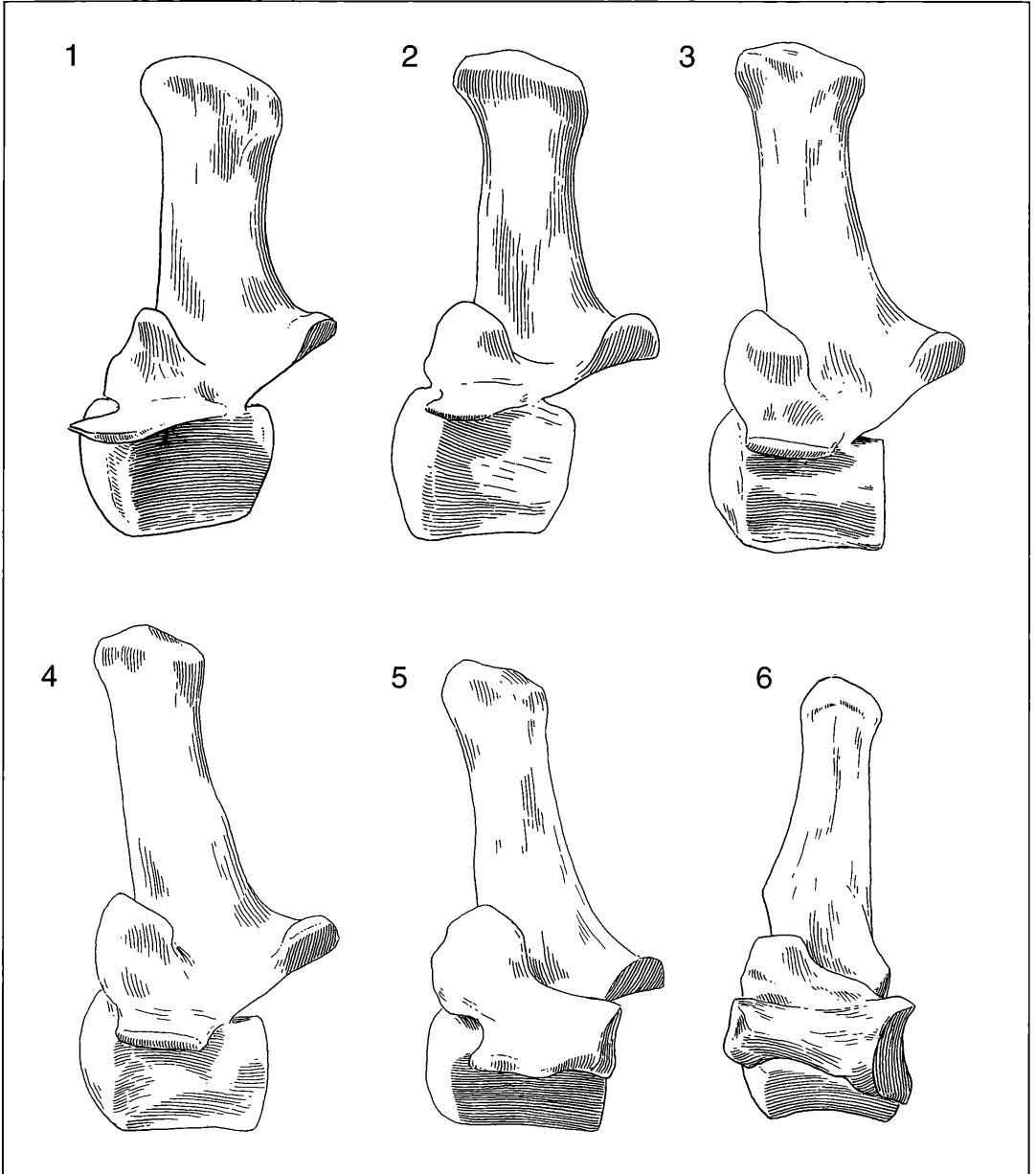


Figure 5.3.5. Lumbar 1-Lumbar 6 Vertebrae (reconstructed), all lateral view (x 0,50).

Figure 5.3.5 exhibits the long and cranio-caudally slender processus spinosii of L1-L6, which contrast so strikingly with the zebra. Also, the Hö A processus cranialis interlock to a lesser extent with the processus caudalis than in the zebra. The Hö A L5 (fig. 5.3.3) and L6 (fig. 5.3.4) transverse processes articular surfaces are

much more expanded than the corresponding structures in the zebra. Compositely then it would again seem that the Hö A skeleton's lumbar spines enjoyed a somewhat greater mediolateral rotation ability than the zebra.

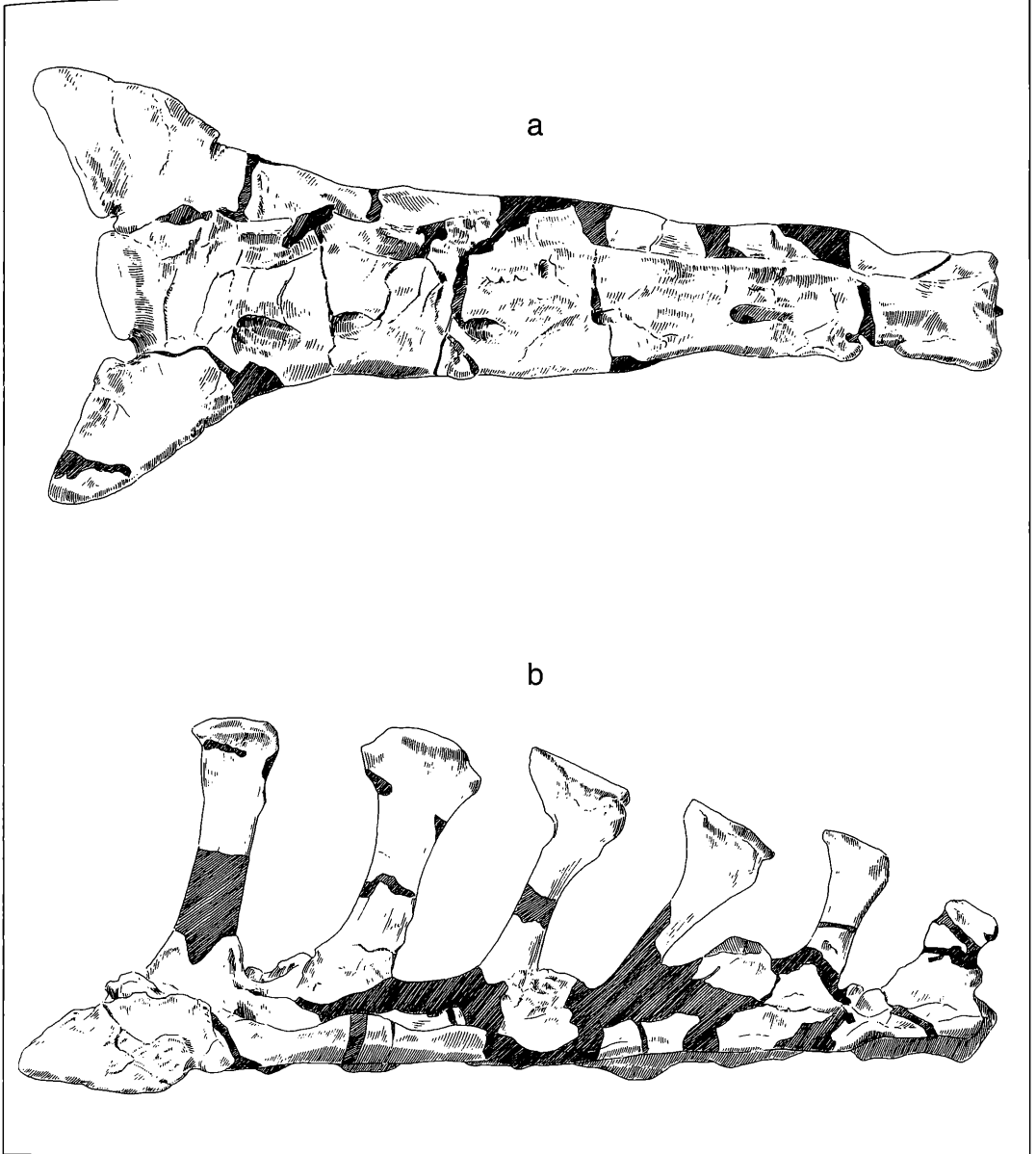


Figure 5.4.1. Sacrum: a. ventral aspect; b. lateral aspect (x 0,40).

5.1.4 Sacrum (fig. 5.4.1-5.4.2)

The Hö A sacrum differs strikingly with *Equus burchelli* in its greater length (distance from body of cranial S1 to body of caudal S5 = 260.1 mm in Hö A versus 177.4 mm in the zebra) and narrower flare of the ala ossis sacrum (maximum width = 150.7 mm in Hö A versus 182.2 mm in the zebra); the length X width ratio in the Hö A sacrum

then is 1.73 and in the SMNS 6709 sacrum it is 0.97. Moreover, all of the Hö A sacral processi spinosi are substantially longer than their counterparts in the zebra. While in the zebra the S1 processus spinosus tapers at its dorsalmost extent, it does not do so in the Hö A S1 spine. All of the Hö A spinous processes have expanded and distantly spaced distal tubercles.

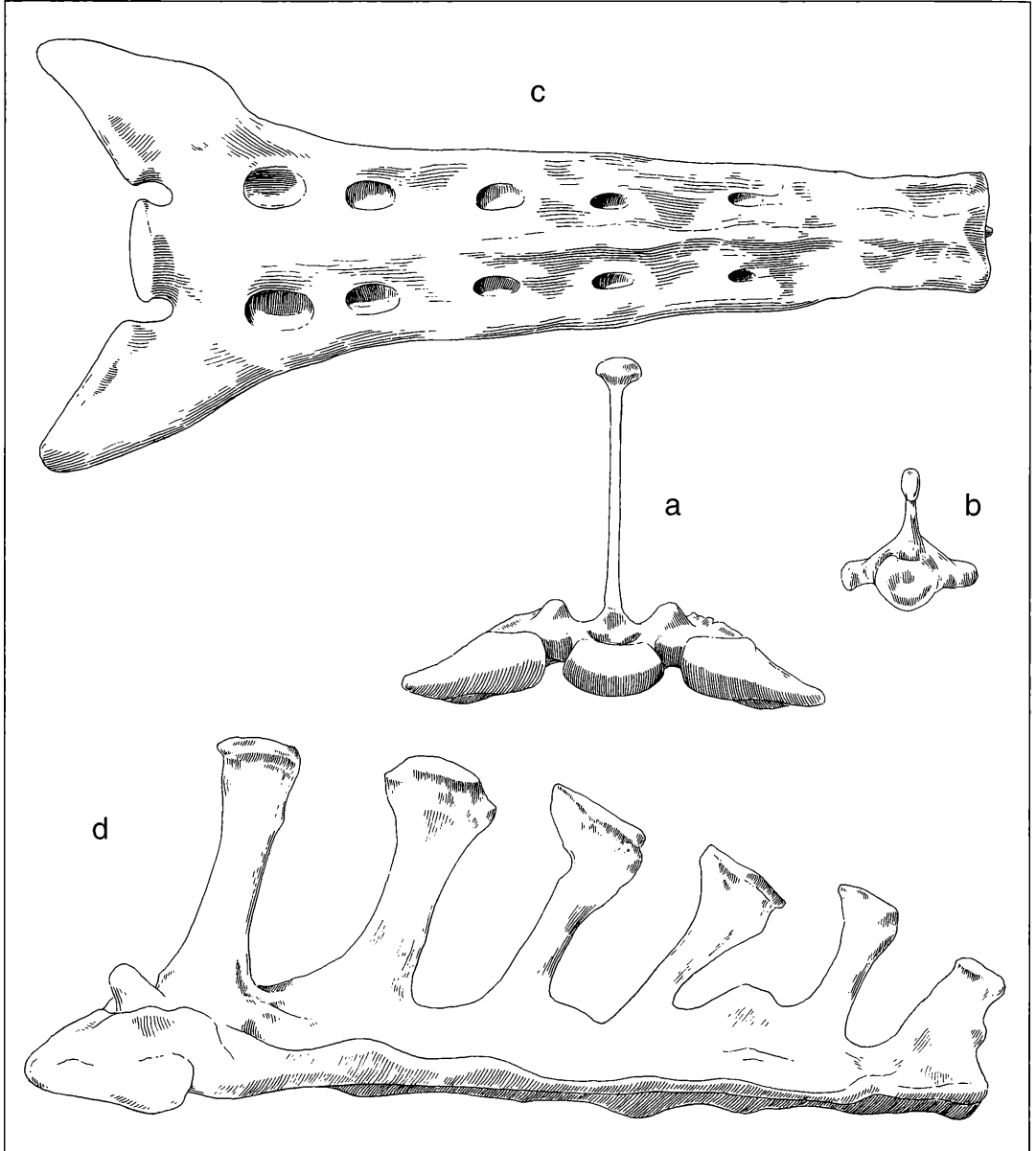


Figure 5.4.2. Sacrum (reconstructed): a. cranial aspect; b. caudal aspect; c. ventral aspect; d. lateral aspect (x 0,40).

5.1.5 Caudal Vertebrae (fig. 5.5.1-5.5.9)

The zebra (SMNS 6709) has 17 caudal vertebrae, 8 less than the maximum reported by NICKEL et al. (1986) for *Equus*. As cited above, the Hö A skeleton has only 11 caudal vertebrae preserved. The caudal vertebrae of each show their most consistent similarity in their convex cranial and caudal articular facies, indi-

cating the presence of thick cartilage between adjacent vertebral bodies (NICKEL et al., 1986).

Both the zebra and the Hö A skeleton have the 1st caudal vertebra fused to the 5th sacral vertebra (Hö A: fig. 5.4.1 a and b and 5.4.2 b and d). The zebra's and Hö A skeleton's 1st caudal vertebra are very similar in their retention of long, caudally reflected processi spi-

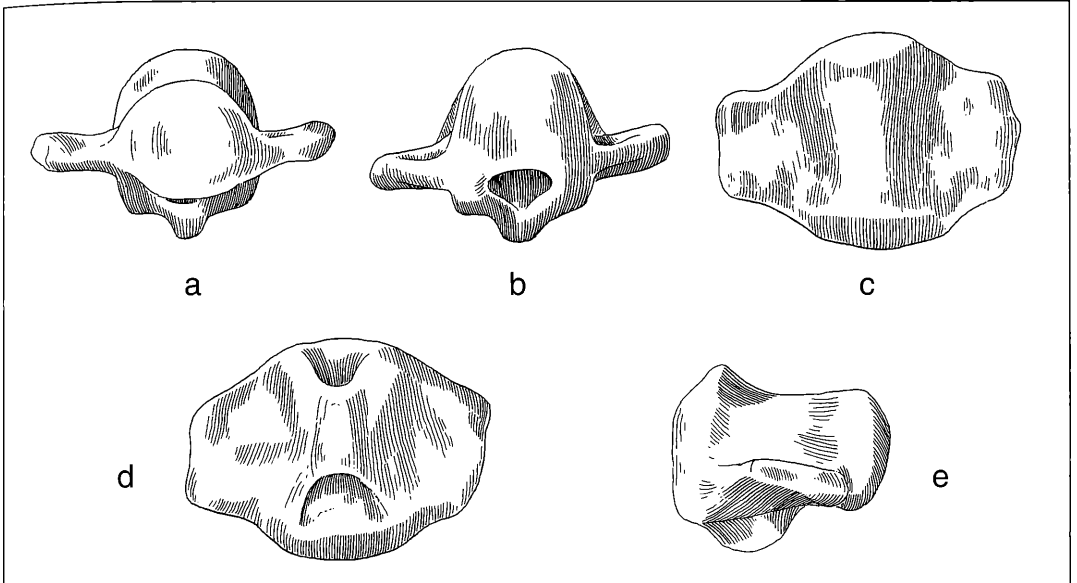


Figure 5.5.1. Caudal 2 Vertebra: a. cranial aspect; b. caudal aspect; c. ventral aspect; d. dorsal aspect; e. lateral aspect (x 1,0).

nosi and short, stout processi transversi. The Hö A 2nd caudal vertebra (fig. 5.5.1) is more reduced in size compared to the zebra and has a shorter processus spinosus and apparently also has a more reduced vertebral foramen than in the zebra (however, note that there is very likely some dorsoventral crushing of the neural arch). The Hö A caudal vertebrae 3 – 7 (figs.

5.5.2-5.5.6) reduce their size serially but retain the same basic square shape and distinct processi transversi characteristic of the 2nd caudal vertebra. However, in the zebra, there is a sharp morphological change with the 4th caudal vertebra which becomes more cylindrically shaped due to the strong atrophy of the processi transversi. In the zebra, both the 3rd and

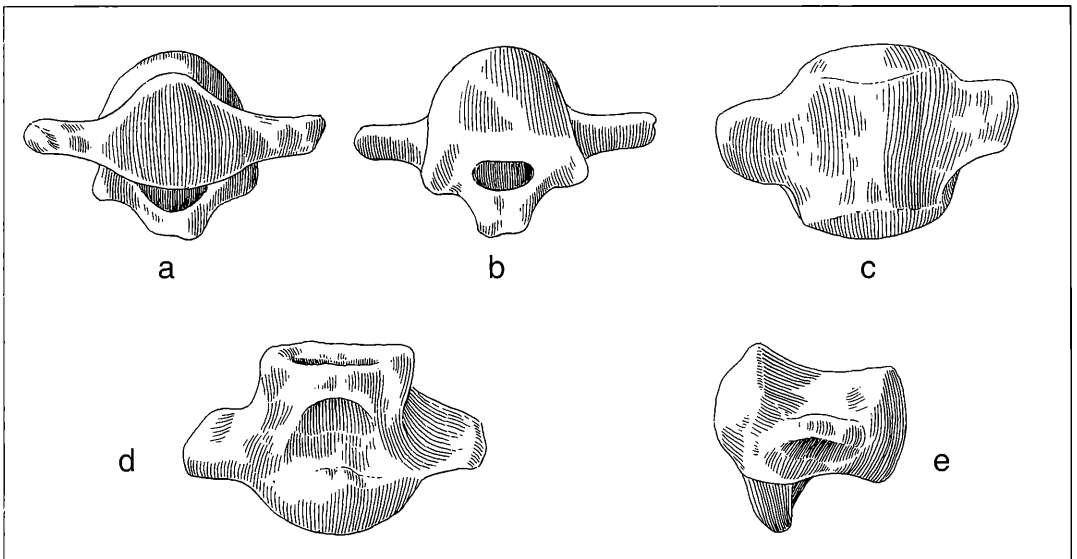


Figure 5.5.2. Caudal 3 Vertebra: a. cranial aspect; b. caudal aspect; c. ventral aspect; d. dorsal aspect; e. lateral aspect (x 1,0).

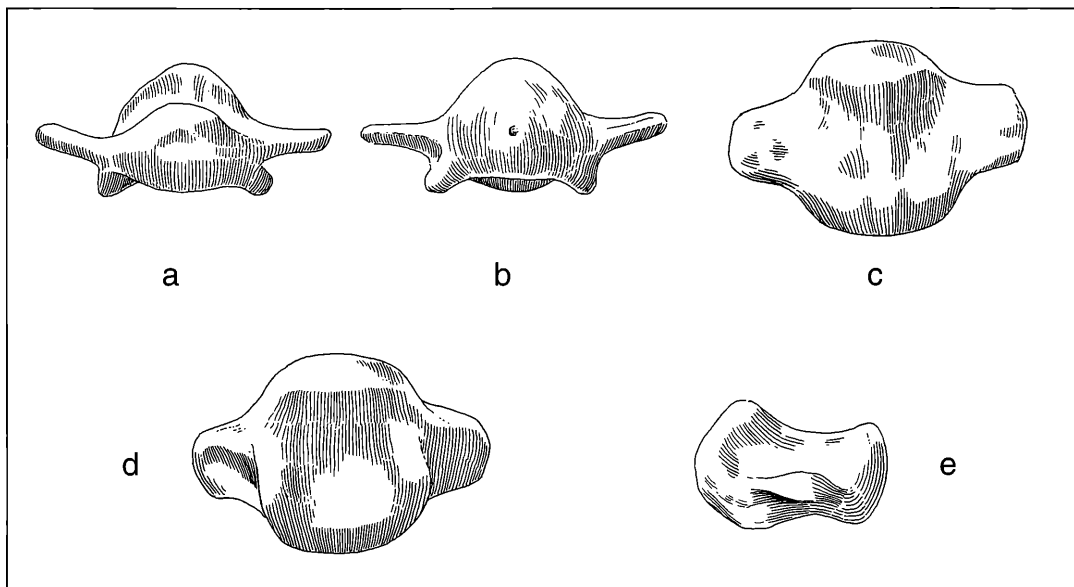


Figure 5.5.3. Caudal 4 Vertebra: a. cranial aspect; b. caudal aspect; c. ventral aspect; d. dorsal aspect; e. lateral aspect (x 1,0).

4th caudal vertebrae have dorsally open vertebral canals due to the failure of the processi spinosi to have formed along the midsagittal axis. In the Hö A skeleton the 3rd caudal vertebral canal is closed dorsally and the processus spinosus is complete and bifid shaped. The Hö A 4th and 5th caudal vertebrae have their processi spinosi laminae badly eroded, but likely also had dorsally open vertebral canals midsagittally. The zebra's 6th and 7th caudal vertebrae are

strikingly dissimilar to the Hö A's equivalent caudal vertebrae in their very long and narrow cylindrical shape. The zebra and Hö A skeletons both have open neural grooves for these vertebrae.

Beginning with the 8th caudal vertebra (fig. 5.5.7), the Hö A skeleton exhibits some lengthening and dorsally, the vertebral canal becomes clearly broadly open. The 9th (fig. 5.5.8) and 10th (fig. 5.5.9) caudal vertebrae are progressively longer and narrower in their propor-

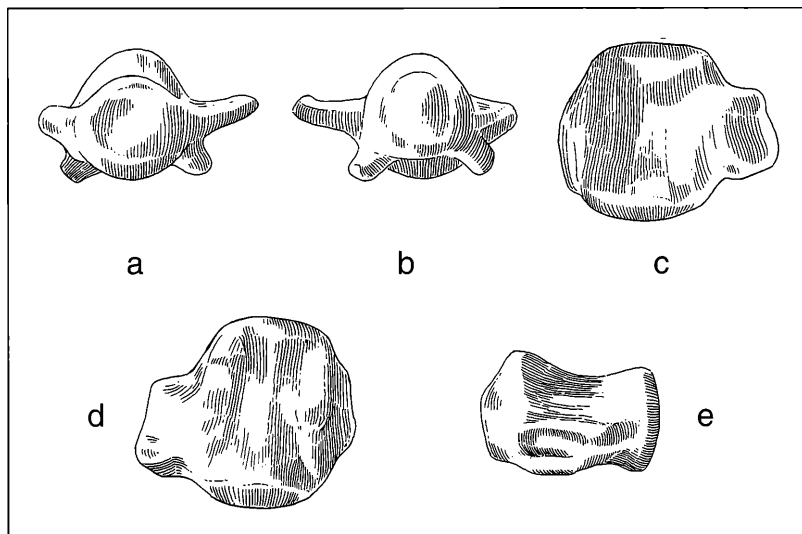


Figure 5.5.4. Caudal 5 Vertebra: a. cranial aspect; b. caudal aspect; c. ventral aspect; d. dorsal aspect; e. lateral aspect (x 1,0).

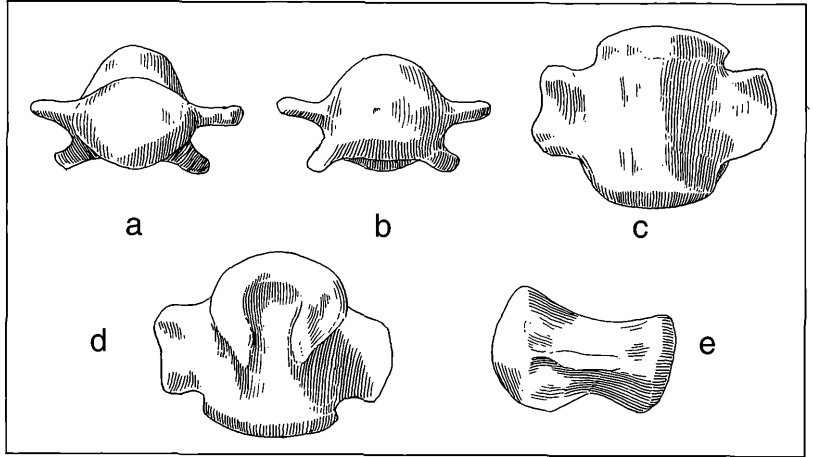


Figure 5.5.5. Caudal 6 Vertebra: a. cranial aspect; b. caudal aspect; c. ventral aspect; d. dorsal aspect; e. lateral aspect (x 1,0).

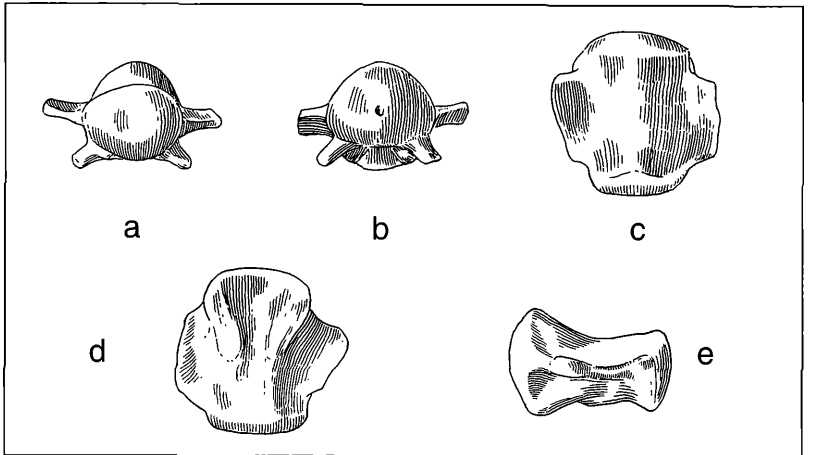


Figure 5.5.6. Caudal 7 Vertebra: a. cranial aspect; b. caudal aspect; c. ventral aspect; d. dorsal aspect; e. lateral aspect (x 1,0).

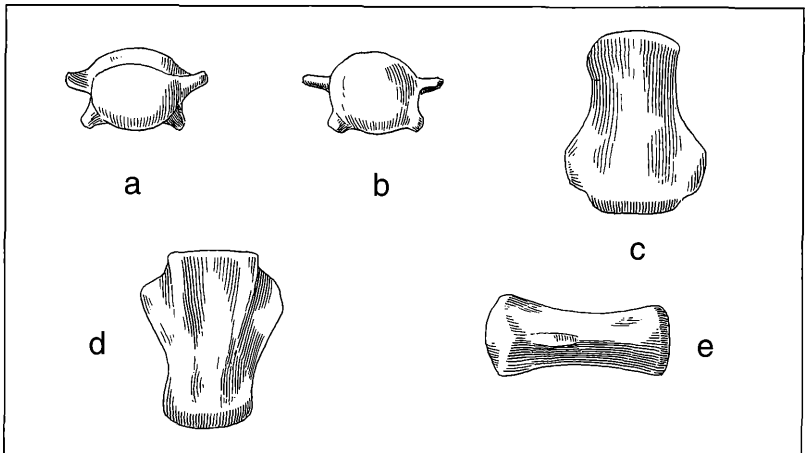


Figure 5.5.7 Caudal 8 Vertebra: a. cranial aspect; b. caudal aspect; c. ventral aspect; d. dorsal aspect; e. lateral aspect (x 1,0).

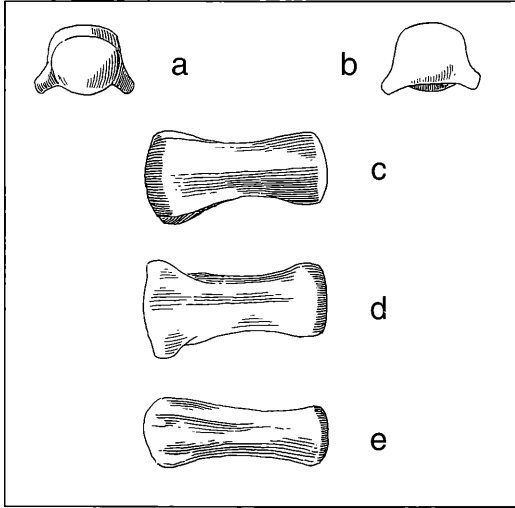


Figure 5.5.8. Caudal 9 Vertebra: a. cranial aspect; b. caudal aspect; c. ventral aspect; d. dorsal aspect; e. lateral aspect (x 1,0).

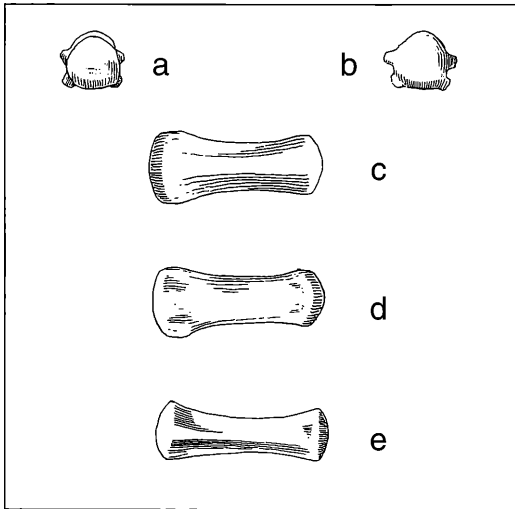


Figure 5.5.9. Caudal 10 Vertebra: a. cranial aspect; b. caudal aspect; c. ventral aspect; d. dorsal aspect; e. lateral aspect (x 1,0).

tions than the preceding vertebrae. The Hö A standing mount (fig. 2.1) has an 11th caudal vertebra which is very small and elongate and not still present in the collection.

Comparing the Hö A and zebra distalmost caudal vertebrae, we have reason to suspect that some vertebrae were lost either prior or subsequent to collection of the skeleton because the size and shape transition is too great after the 7th caudal vertebra.

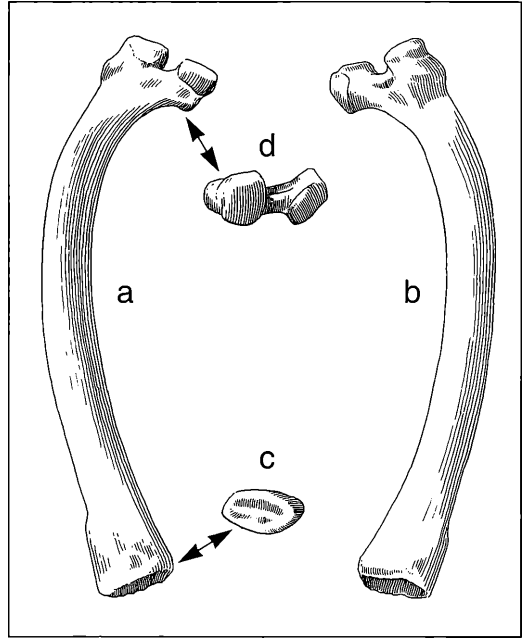


Figure 5.6.1. Rib 1: a. left; b. right; c. ventral; d. dorsal (x 0,40).

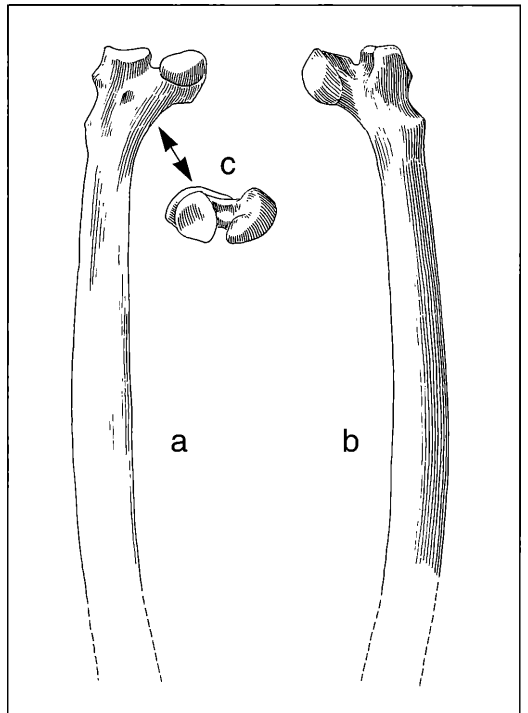


Figure 5.6.2. Rib 2: a. left; b. right; c. dorsal (x 0,40).

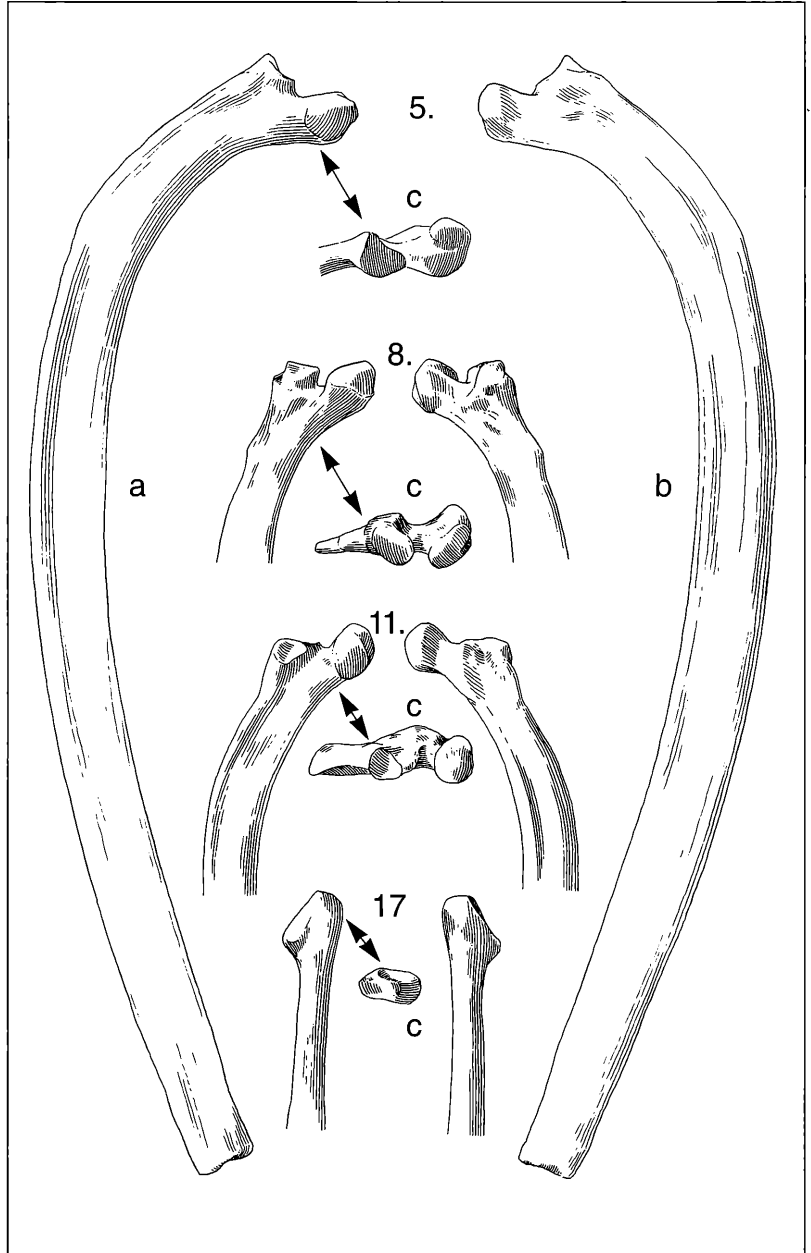


Figure 5.6.3. Ribs 5, 8, 11, 17:
a. left; b. right; c. dorsal (x 0,40).

5.1.6 Costae (fig. 5.6.1-5.6.4)

TOBIEN and GARRAUX elected not to reproduce the entire suite of costae. Instead, they selected a series of characteristic rib pairs for illustration: ribs 1 (fig. 5.6.1), 2 (fig. 5.6.2), 5 and the proximal aspects of 5, 8, 11 and 17 (fig. 5.6.3).

Generally speaking, the ribs of the Burchell's zebra (SMNS 6709) are larger and mostly have proportionally broader mediolateral aspects than seen in the Hö A skeleton. The Hö A 1st rib (fig. 5.6.1) differs from the zebra principally in its longer neck, smaller facies artic-

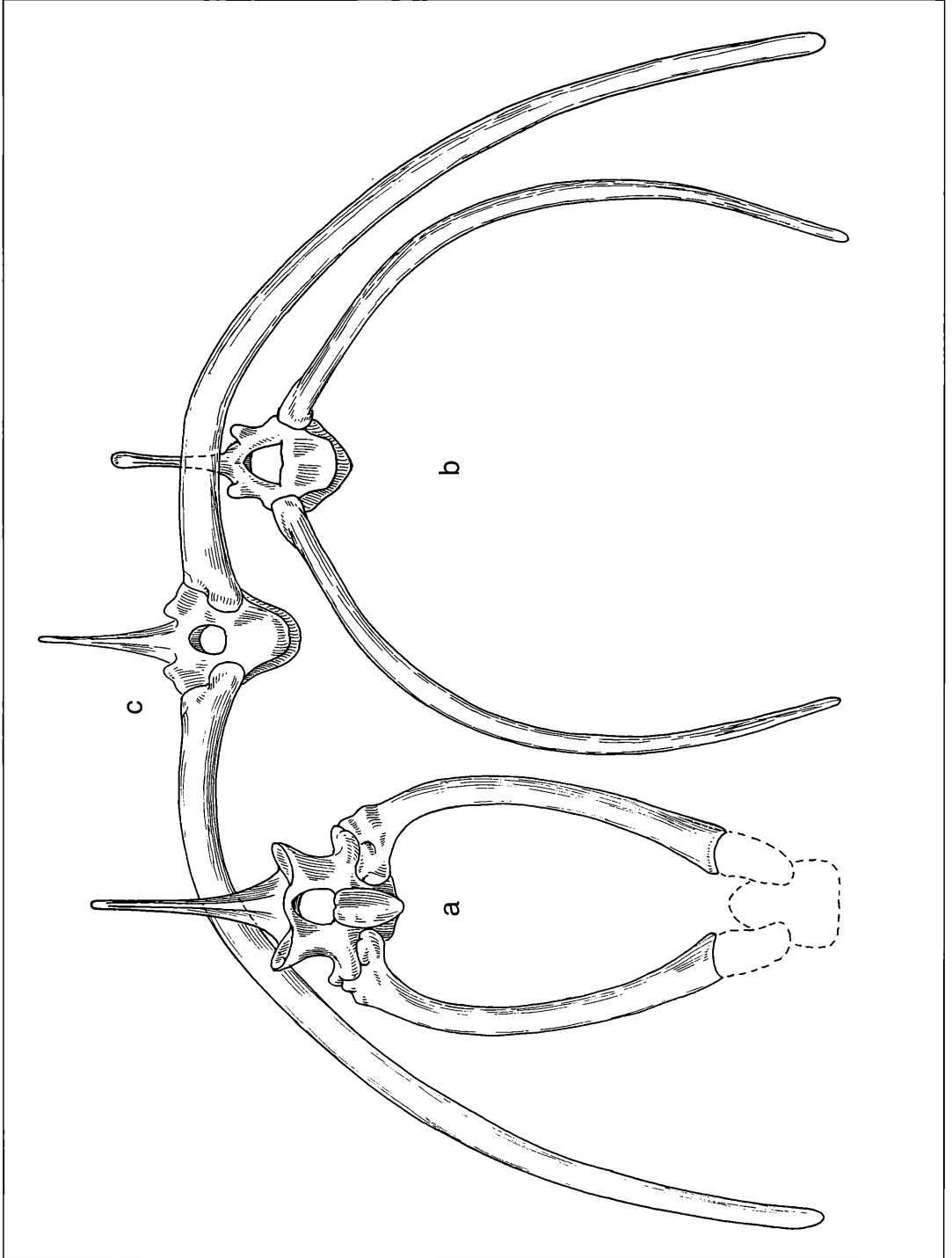


Figure 5.6.4. 3 Pairs of Ribs in Articulation with their Corresponding Vertebrae: a. 1st; b. 13th; c. 17th (x 0,40).

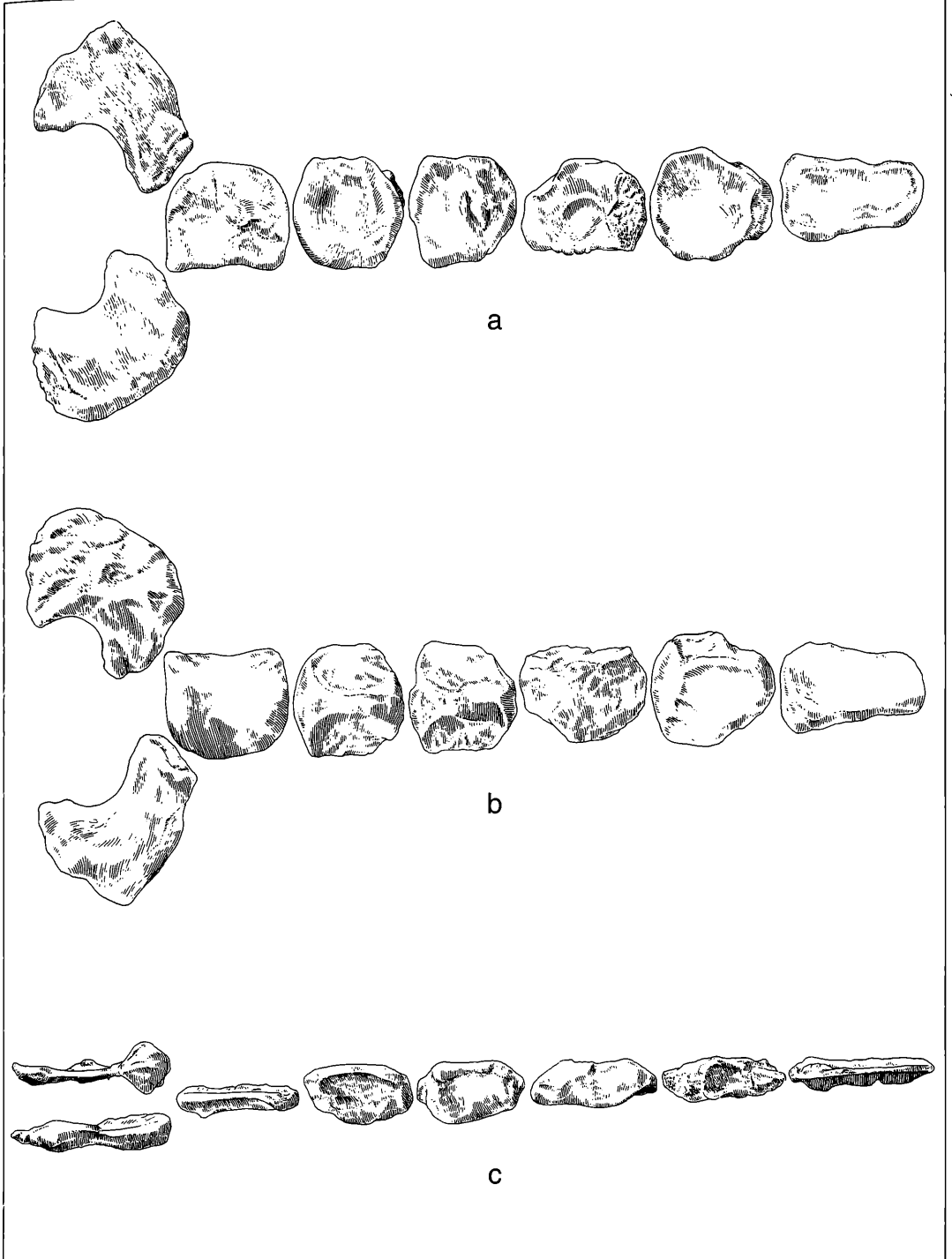


Figure 5.7.1. Sternum: a. dorsal aspect; b. ventral aspect; c. mediolateral aspect (x 0,40).

ularis capitis costae caudalis and cranialis, and the more extensive hiatus between these and the facies articularis tuberculi costae occupied by the sulcus capitis costae. The distal articulation with the sternum is also more restricted than in the zebra.

The Hö A 2nd rib is not as well preserved as the 1st rib, being incomplete at its distalmost extent and not preserving the articular surface with the sternum (fig. 5.6.2). Its proximal articular facies is similar to the Hö A 1st rib, but the sulcus capitis costae is more restricted in large part due to its shorter neck (fig. 5.6.2).

Figure 5.6.3 exhibits the morphologic transition in the proximal aspects of ribs 5, 8, 11 and 17. The Hö A 5th rib is strikingly narrower than the zebra in its mediolateral dimension. The articular facies however are generally similar. Likewise, the rib facies and the mediolateral dimensions are similar between the Hö A skeleton and the zebra for ribs 8, 11 and 17.

Figure 5.6.4 presents the 1st (a), 13th (b) and 17th (c) rib pairs in articulation with their corresponding vertebral bodies, and give an effective estimation of the thoracic region's body cavity volume at these levels.

5.1.7 Sternum (fig. 5.7.1)

In *Equus* the sternum is composed of 6 bones or segments which in young animals are united by sternal synchondroses (NICHEL et al., 1986). Generally speaking, the first three sternal elements of the Höwenegg A sternum are similar to the zebra in their broad, flat plate-like structure; the Hö A 1st sternal element is extraordinarily broad (fig. 5.7.1). However, the zebra's 4th – 6th sternal elements are distinctly more triangular shaped than the equivalent Hö A sternal elements. If the 7th Hö A element is the xiphoid process, it would appear to be clearly ossified and differs with the zebra in this regard. This feature could very well be age related.

5.1.8 Summary – The Spine as a Functional Unit

The Hö A horse had a standing height of 1.30 to 1.35 meters at the withers, and falls well within the range of Burchell's zebra (1.28–1.40 meters high at the withers; JARMAN, 1974). It has a number of anatomical differences when compared with the zebra, most notable being: compared to the zebra, cervical vertebra 2 processus spinosus has its bifurcation more caudally placed giving the effect in lateral view of having a more parallel alignment with the craniocaudal axis of the vertebral body; thoracic processi spinosi are long, craniocaudally thin and most often lack a concave cranial edge; lumbarization of the thoracic processi spinosi occurs at T14 rather than T11 or T12, and the lower thoracic spines are longer than in the zebra; the thoracic processi mamillari are smaller and interlock less with the preceding vertebral bodies allowing more rotation of the spine along the vertebral axis; the lumbar vertebrae have longer and more vertically directed

processi spinosi; the sacrum is relatively long and narrow compared to the zebra (maximum length of sacrum X maximum width of ala = 1.73 in Hö A versus 0.97 in the zebra), and it has longer, thinner spinous processes than the zebra; the tail was apparently shorter with a lower transition to a cylindrical shape (caudal vertebra 8 versus caudal vertebra 4 in the zebra); ribs are mediolaterally thinner; rib 1 has a longer neck and less extensive articular area with the sternum than seen in the zebra; the sternum is flatter than in the zebra and the xiphoid process was evidently fully ossified.

Overall then, the Hö A spine supported a horse that was as tall at the withers as a Burchell's zebra, but more lightly built. The spine was apparently capable of greater rotation along its central axis. This is particularly apparent in the lower part of the thoracic and the lumbar spine. Also, the sacrum was much longer and narrower than the zebra. These lines of evidence, combined with previous observations of the functional tridactyly of this horse, suggest that there was a functional premium placed on springing and quick lateral movement as would be characteristic of an animal running in a closed (wooded) environmental setting, rather than support for sustained cursoriality in an open country setting as is typical for the zebra.

6. The Thoracic Limb: Anatomy and Statistics of the Osteological Elements

In the following text we describe the Höwenegg hipparion thoracic limb. The bony part of the thoracic limb consists of: the scapula and humerus (stylopodium), radius and ulna (zeugopodium), bones of the carpus (basipodium) and the metacarpus (metapodium) and the digits.

6.1. Scapula (fig. 6.1.1)

There are 16 more or less fragmentary scapulae. The bone is not usually well preserved due to its thinness, particularly in the infraspinatous fossa area.

Lateral aspect (fig. 6.1.1 a): The spina scapulae (1) originates about 70 mm distally from the lip of the cavitas glenoidalis (6), rises and is progressively elevated until the tuber spinae scapulae (2), then diminishes in its height until it fades near the bony margo dorsalis (10). There is no rudimentary acromion as is sometimes seen in *Equus*. Halfway along its length, the spina

is enlarged to the tuber spinae scapulae (2) which is rather large and presents a caudal inclination. The dorsally situated fossa suprascapulae (4), with its margo cranialis (11), is rather narrow along its entire length. It is narrowest at the incisura scapulae (11'; = collum scapulae), which continues to the strong tuberculum suprarglenoidale (7). The fossa infraspinata (5) is markedly broader than that of the extant horse, mainly along the bony margo dorsalis (10), between the dorsal-most limit of the spina scapula (1) and the angulus caudalis (14). The margo caudalis (12) of the fossa infraspinata (5) is thickened at its dorsal limit and presents a crest for attachment of the musculus infraspinatus (12') at its dorsocaudal angle. Other lineae musculares (12'') are developed posterior to the ventral aspect of the spina scapula. The cavitas glenoidalis (6) is visible along the thickened ventral aspect of the scapula. There is a strong tuberosity for the origin of the musculus teres minor (13) superior to the caudolateral border of the cavitas glenoidalis (6).

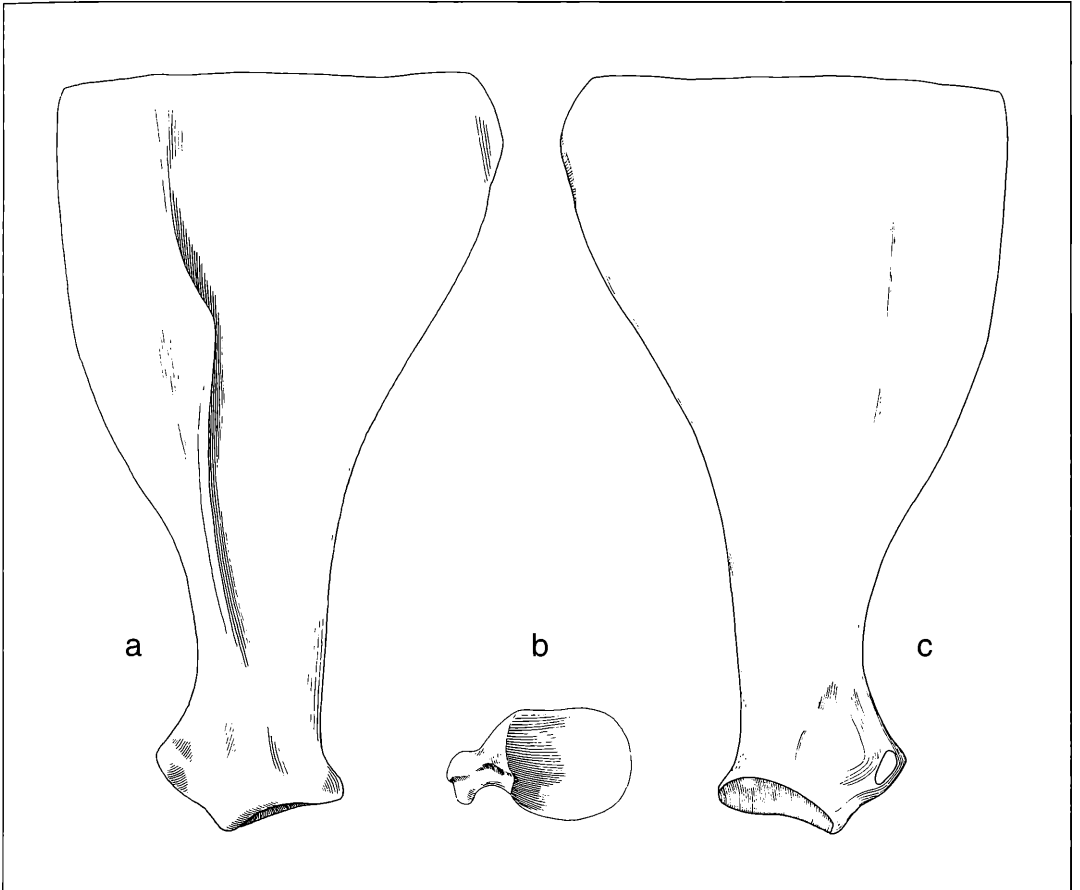


Figure 6.1.1. Scapula: a. lateral aspect; b. ventral aspect; c. medial aspect (glenoid fossa) (x 0,315).

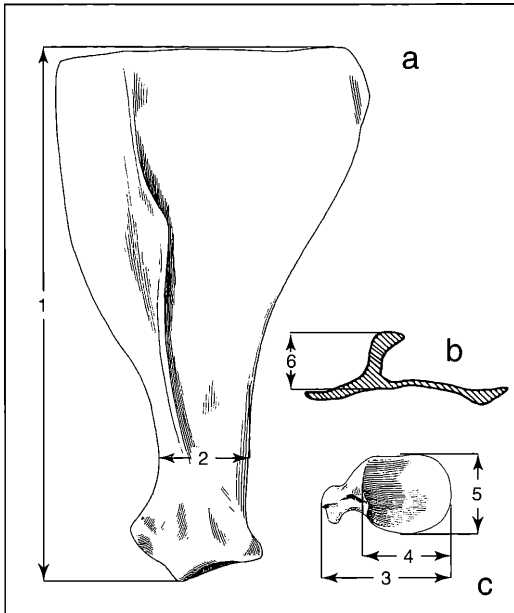


Figure 6.1.2. Measurements on the Scapula: a. lateral aspect; b. cross section through spine; c. view of glenoid fossa.

Ventral aspect (fig. 6.1.1b): The cavitas glenoidalis (6) is nearly circular, being flattened along its lateral border (6'). Its craniomedial portion is interrupted by the incisura glenoidalis (3). The tuberculum supraglenoidale (7) is massive and presents the processus coracoideus (8) along its medial border. Posterior to the processus coracoideus (8) is found a deeply excavated, inversely U-shaped incisura coracoidea (8'), succeeded adjacently by the cranial border of the cavitas glenoidalis (9). In lateral view, the Höwenegg horse's cavitas glenoidalis is nearly horizontally oriented, whereas it is more steeply and cranially inclined in modern *Equus* (re: NICKEL et al., 1986). The angle made between the cavitas glenoidalis (6) and the tuberculum superglenoideum (7) is less in the Hö A skeleton than in modern *Equus*. The incisura glenoidalis (3) is incorporated as a fossa synoviales for articulation with

the humerus. The tuberculum supraglenoidale (7) is stronger, and the incisura coracoidea (8') has a greater angle in *Equus* (GROMOVA, 1955: 79, 80, here "incisura glenoidalis"). The latter may be explained by *Equus*' stronger and somewhat caudally directed processus coracoideus.

Medial aspect (fig. 6.1.1c): The medial border (facies costalis) of most Höwenegg hipparion scapulae are damaged. However, in the Hö I scapulae, and to a more limited extent in the Hö A scapulae, one can discern two subparallel linea serrata (15). These linea are more marginally placed toward the caudal and cranial borders than in *Equus*, and they do not strongly converge as they approach the margo dorsalis (10) as seen in *Equus*. The marginal placement of (15) provides a greater area for the fossa subscapularis (16) than seen in *Equus* (NICKEL et al., 1986:90; e.g.: the central fossa interscapularis, bordered by two proximally converging rims for the musculus serratus ventralis). It should be noted however that the thin bony plates of all Höwenegg hipparion scapulae are usually broken and required extensive restoration.

Statistical Results

Six variables were analysed on a total of 11 (of 15) scapulae. No coefficient of variation was above 10. Only two significant correlations were found: m2 (minimal width at neck): m3 (maximum breadth of the articular process), significant at the 99 % level and m1 (maximum length)-m3 which was significant at the 95 % level. These correlations reflect the stability of these measurements and within hipparions, may represent the only measurements needed.

6.2 Humerus (fig. 6.2.1 a-f):

There are 20 humeri in the assemblage, mostly belonging to articulated skeletons. They vary in their size and state-of-preservation.

Cranial aspect (fig. 6.2.1a): The proximal border presents laterally to medially: the tuberculum majus (2), including the pars cranialis (2'), pars caudalis (2''), and intervening depression (2'''). The sulcus intertuberculus (4) separates the tuberculum majus (2) and the tuberculum minus (3; with its pars cranialis and pars caudalis 3' and 3''); (3) has no intermediate depression. The diaphysis presents a laterally directed tu-

Table 6.1. Summary Statistics on Scapulae

Measure- ment	Sample size	Mean	Standard Deviation	Confidence Limits	Coefficient of Variation	Confidence Limits	Minimum	Maximum	Median
m1	8	320,25	16,66	308,09 332,41	5,20	2,51 7,90	291,10	337,00	326,00
m2	11	53,56	2,21	52,19 54,94	4,12	2,31 5,94	49,40	55,60	54,20
m3	11	79,36	6,29	75,45 83,28	7,93	4,42 11,44	69,10	89,40	81,20
m4	11	55,01	2,96	53,17 56,85	5,38	3,01 7,75	50,80	61,10	54,20
m5	11	45,16	3,42	43,04 47,29	7,56	4,22 10,91	37,00	50,20	45,00
m6	7	37,76	3,49	35,03 40,48	9,26	4,11 14,40	34,00	44,30	37,00

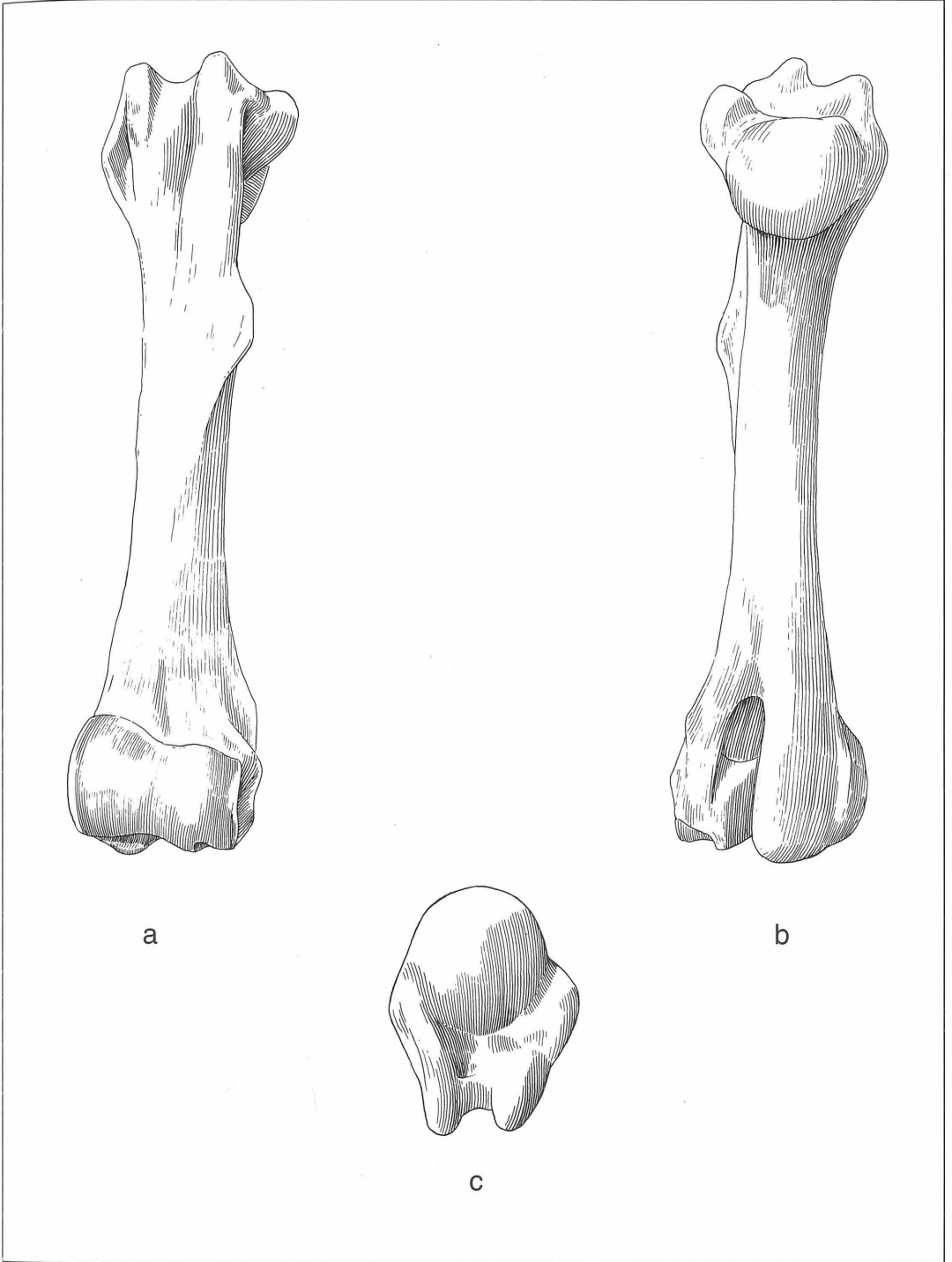


Figure 6.2.1. Humerus: a. cranial aspect; b. caudal aspect; c. proximal aspect; (x 0,40).

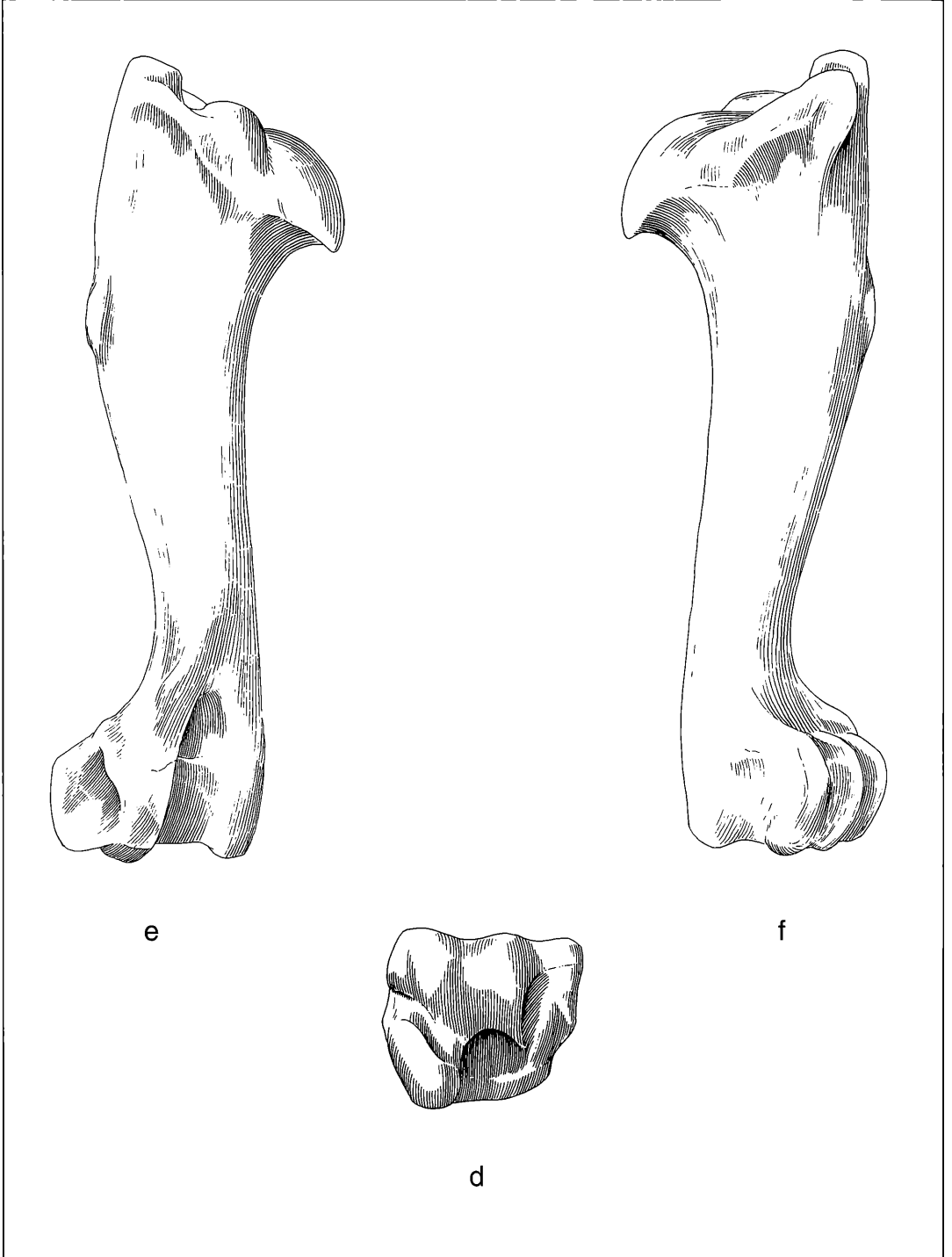


Figure 6.2.1. Humerus: d. distal aspect; e. lateral aspect; f. medial aspect (x 0,40).

berositas deltoidea (10). Arising from (10) is a distomedially coursing crista humeri (9). Distally, there is a distinct sulcus musculus brachialis (11) followed by a crista epicondylus lateralis (12') and the epicondylus lateralis (12). The distal extent includes the medial and lateral condylus humeri (13) with proximal fossa radialis (14) and an accessory fossa for the musculus extensor digitorum (19).

Caudal aspect (fig. 6.2.1b): This aspect presents the caput humeri in the foreground (1), and the tuberculus majus (2'', 2', and intervening depression 2'''), sulcus intertubularis (4) and the tuberculus minus (3, 3', 3'') in the background. The laterally directed tuberositas deltoidea (10) is prominent in this view. Distally is the large, deep, oval-shaped fossa olecrani (18) separating the epicondylus lateralis (12) and medialis (15). The medial distocaudal protuberance (16') and the medial distocaudal depression (17'), both for ligamentous attachments, are found medially.

Proximal aspect (fig. 6.2.1c): The proximal end is dominated by the slightly convex, massive caput humeri (1). It is surrounded laterally by the tuberculum majus (2), including the pars cranialis (2'), pars caudalis (2''), and intervening depression (2'''). The medially situated tuberculum minus (3) is similarly divided into a pars cranialis and pars caudalis (3' and 3''), without, however, a depression between them. Unlike all modern horse species, there is no tuberculum intermedium situated between the greater (2) and lesser (3) proximal tubercles (figured as #5 in NICKEL et al., 1986: fig. 96, 102 and 103; also, ELLENBERGER & BAUM, 1974: fig. 231g). Rather, in the Höwenegg hipparion the sulcus intertubularis (4) separates these two tubercles.

Distal aspect (fig. 6.2.1d): On the distocaudal surface are found mediolaterally: the epicondylus medialis (15), the lateral distocaudal depression for ligamentous attachment (17), and the fossa olecrani (18). Distocranially are the condyli humeri (13).

Lateral aspect (fig. 6.2.1e): Proximally there is a well defined tuberculum majus (2, 2', 2'') and its interve-

ning depression (2'''), as well as the caput humeri (1). Inferior to (2) on the collumm humeri lies the narrow fascies musculus infraspinati (6), and placed adjacently and caudally from this point is located the tuberositas musculus teres minor (7). The thin long ridge of the linea musculus tricipitis (8) is only faintly marked and courses craniodistally to the prominent tuberositas deltoidea (10), which itself continues distally as the crista humeri (9; fig. 6.2.1a). The epicondylus lateralis is located distally (12), and is connected on its proximalateral surface to the crista epicondylus lateralis (12'). The fossa olecrani's (18) great depth is best seen from this aspect. Most distally are found the lateral distocaudal protuberance (16) and a deep lateral distocaudal depression (17).

Medial aspect: (fig. 6.2.1f): This aspect presents in the proximal foreground the tuberculus minus (3'', 3, 3'), intermediately the caput humeri (1), and in the background the tuberculus majus (2'', 2'). On the distal diaphysis there is a faintly developed-to-absent tuberositas teres major (7''); in contrast, this feature is much more strongly developed in extant *Equus* species. The laterally directed tuberositas deltoidea (10) can be faintly seen from this aspect. The medial distocaudal protuberance (16') and a medial distocaudal depression (17') are both prominent in this view. In the background one can discern the outline for the fossa radialis (14).

Characteristic features of the humerus: Compared to extant *Equus* and other reported hipparions, the fossa radialis (14) is found on the cranial surface, proximal to the condylus; the sulcus musculus brachialis (11) is located between the crista humeri (9) and the crista epicondylus lateralis (12'); medial to the epicondylus lateralis (12) is situated a small but deep groove (12 – 14 mm) separated by the lateral surface of the fossa radialis (19). This last feature, the groove separated by (19), is considerably deeper than its homologue in *Equus* (GROMOVA, 1955: 82, pl. 2, fig 14 Aa), and marks the extensive origin attachment of the musculus extensor digitorum communis.

Table 6.2. Summary Statistics on Humeri

Measure- ment	Sample size	Mean	Standard Deviation	Confidence Limits	Coefficient of Variation	Confidence Limits	Minimum	Maximum	Median		
m1	6	277,98	21,14	260,17	295,79	7,60	3,05	12,16	252,20	302,70	281,95
m2	6	261,85	18,55	246,22	277,48	7,08	2,84	11,32	238,40	282,80	261,75
m3	7	32,17	1,02	31,38	32,97	3,17	1,42	4,92	30,90	33,60	32,30
m4	7	41,44	2,24	39,70	43,19	5,41	2,42	8,40	38,30	44,50	41,70
m5	2	75,40	3,39			4,50			73,00	77,80	75,40
m6	5	99,36	10,65	89,53	109,19	10,72	3,64	17,79	83,50	111,90	99,20
m7	13	70,46	2,66	68,94	71,98	3,77	2,24	5,30	65,30	74,10	70,80
m8	10	73,75	3,04	71,76	75,74	4,13	2,22	6,03	67,80	78,00	74,15
m9	12	48,05	2,34	46,66	49,44	4,87	2,81	6,93	44,20	51,30	48,80
m10	13	34,66	2,06	33,48	35,84	5,95	3,53	8,36	31,00	37,50	34,50
m11	13	41,35	2,65	39,83	42,87	6,42	3,81	9,03	37,70	45,70	41,50

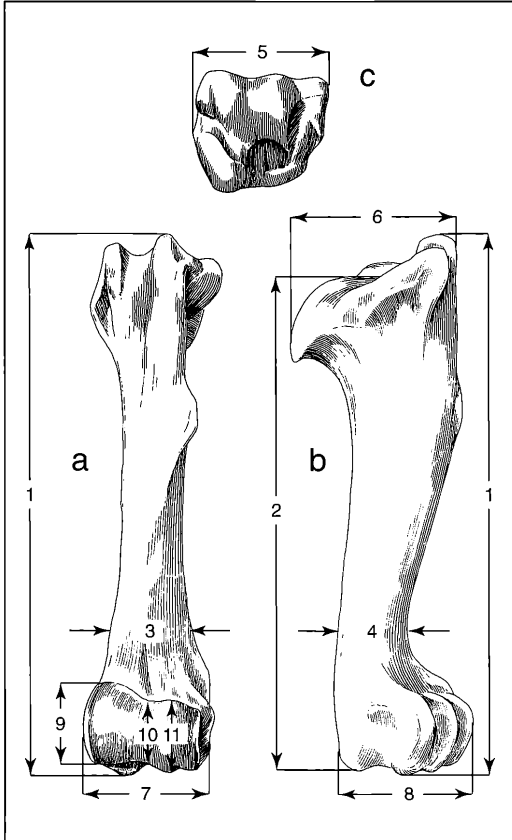


Figure 6.2.2. Measurements on the Humerus: a. cranial aspect; b. medial aspect; c. distal aspect.

Statistical Results

Eleven variables were measured on a total of 19 humeri, of which 13 were included for statistical analysis. The coefficient of variation was above 10 only for m6 (proximal depth at the level of the median tubercle; CV = 10.72). There were 11 significant correlations, 5 of which were at the 99 % level of significance. Measurement 1 (maximum length of the humerus) was correlated with m11 (trochlear height), m2 (maximum length from caput), m10 (minimum trochlear height) and m8 (distal maximum depth), and reflects the stability of this measurement and dependence of a great array of measurements on it. These aspects are further reflected in m2's correlation with m7 (maximum breadth of trochlea), m10 and m11 (both of the trochlea). The final four significant correlations were concerned with humerus distal end measurements: m10-m11, m8-m10, m7-m10 and m7-m8. These reflect the relative size interdependence of these measurements as well as their lack of postdepositional distortion in the Höwenegg sample.

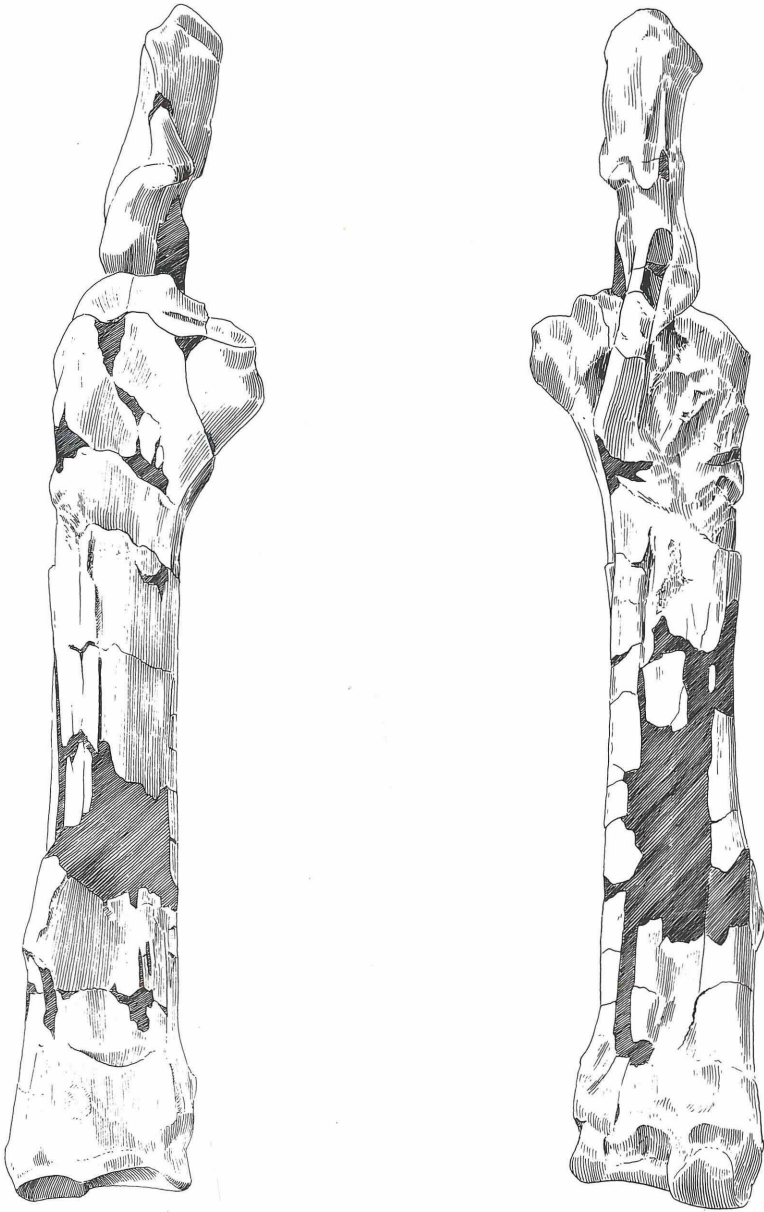
6.3 Radius (fig. 6.3.1.2a-f)

There are 23 more or less complete Hö specimens, most of them belonging to the suite of articulated skeletons. Because of the great degree of reconstruction needed for the Hö A-54 radius-ulna, we refer here to the very well preserved Hö T-56 specimen.

Cranial aspect (fig. 6.3.1.2a): Proximally, the caput radii (2) is broad and contains a flat fovea capitis radii (3), which is divided by two sagittally directed ridges: one medial (3'), and the other lateral (3''). The tuberositas radii and the attachment for the ligamentum collaterales mediale (5) are weakly developed. The extension of (5) below the anteromedial rim is small, and in contrast to extant *Equus*, where the rugose surfaces extend to the middle of the caput cranii. A flat proximal sulcus (5') separates the tuberositas radii from the medial border of the fovea. The protuberance for the ligamentum collaterale laterale (5'') is prominent. The distal end is bounded medially and laterally by the processi styloidei lateralis (8) and medialis (8'), respectively. Whereas the tendinous groove on the processus styloideus ulnae (8) is absent or faint in the Höwenegg radii, it is prominent in extant *Equus* (ELLENBERGER & BAUM, 1977: fig. 270 e'). Centrally there are two distinct grooves which served as guides for tendons of the extensor digitorum communis (12) and the extensor digitorum lateralis (13). These two grooves are more weakly developed in extant *Equus* (GROMOVA, 1955: 84).

Caudal aspect (fig. 6.3.1.2b): The proximal aspect is obscured by the ulna. The caudal (4) facies can be seen to be somewhat concave in this view. The disto-caudal diaphysis (4') has a broadly concave surface, and is bordered medially just proximal to the trochlea carpi (9) by the crista transversa (6). The crista transversa (6) demarks the proximal attachment surface of a strong, plate-like ligamentous layer, the ligamentum carpi volare profundus (ELLENBERGER & BAUM, 1977: 126, 15a); distally this ligament attaches to the metacarpal and carpal bones. This ligamentous layer functions to prevent hyperextension (dorsal flexion) of the carpal joint (NICKEL et al., 1986: 187). The crista transversa (6) is poorly developed in the Höwenegg horse, as is the origin of the reinforcing tendon of the musculus flexor digitorum superficialis, proximal to the crista transversa (ELLENBERGER & BAUM, 1977: fig. 271).

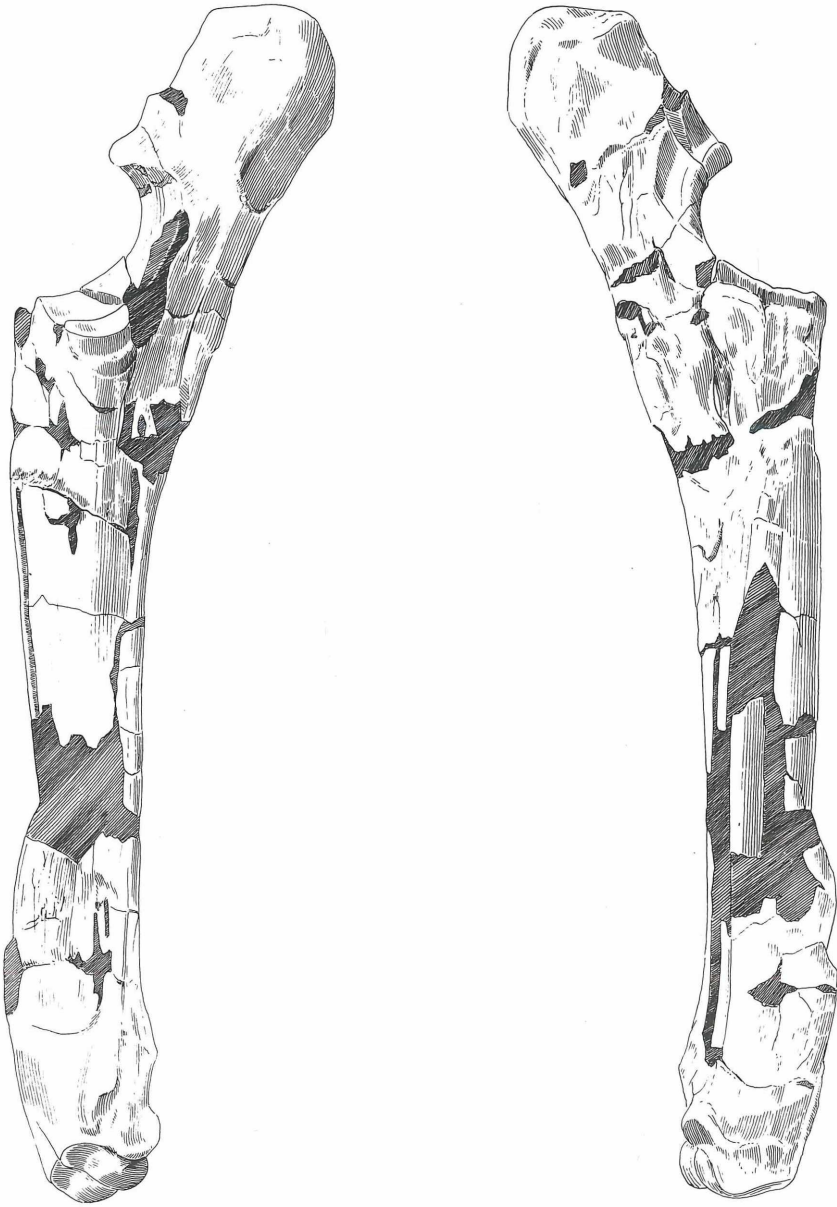
Proximal aspect (fig. 6.3.1.2c): The caput radii (2) has fovea capitis radii (3) subdivided into medial (3') and lateral (3'') ridges. The lateral incisure (3''') is absent in the Höwenegg hipparion, whereas in extant *Equus* it is clearly developed (NICKEL et al., 1986: fig. 134 and TOBIEN's observation in NMB). This incisure reflects a shorter ulnar processus coronoideus lateralis (10) in the Höwenegg hipparion, and its more intimate connection with the radius. GROMOVA (1955: 85) has interpreted this feature as indicating weaker fixation of the radius-ulna articulation. In extant *Equus* there is a



a

b

6.3.1.1. Unreconstructed Radius: a. cranial aspect; b. caudal aspect (x 0,40).



c

d

6.3.1.1. Unreconstructed Radius: c. lateral aspect; d. medial aspect (x 0,40).

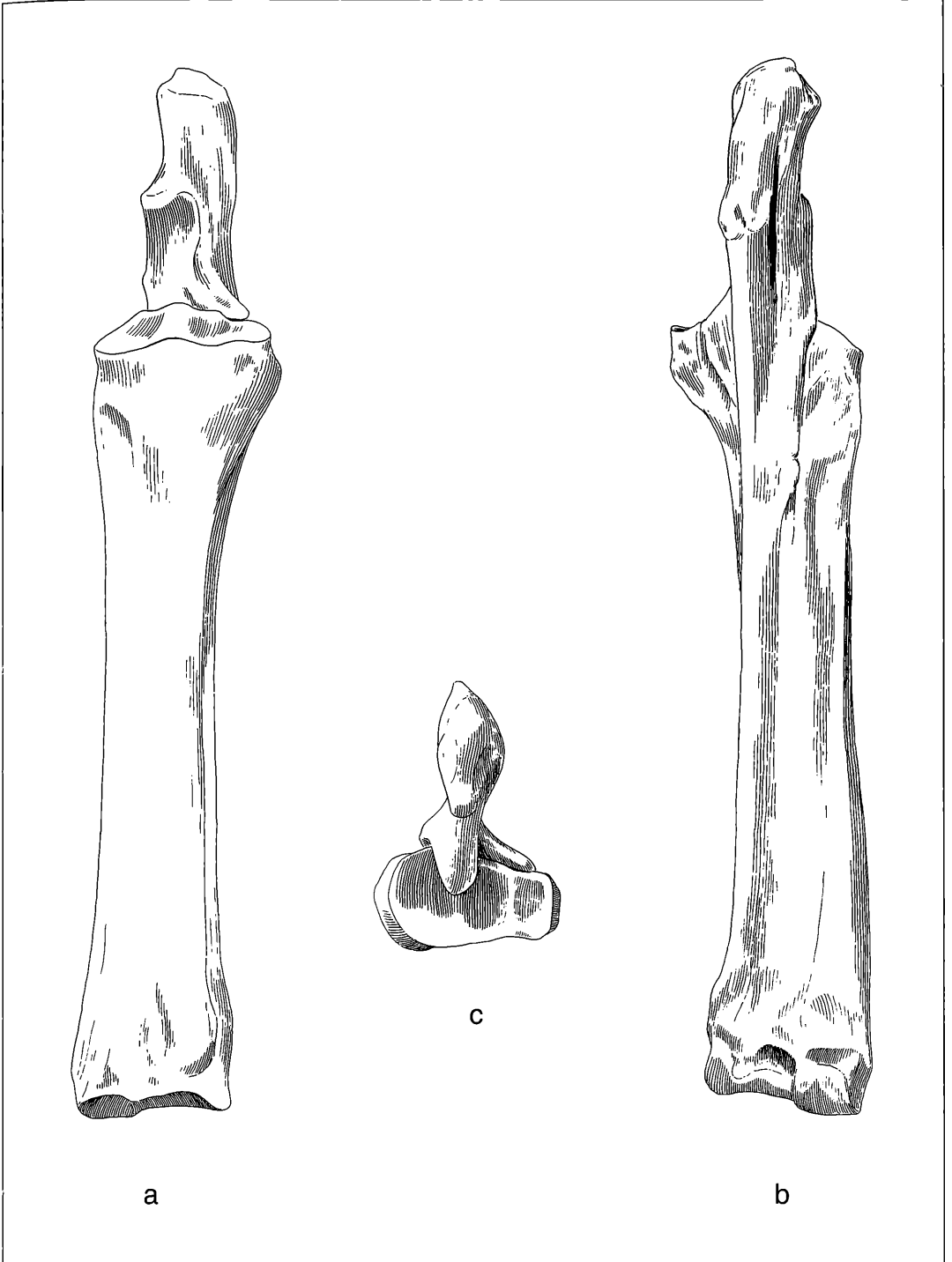


Figure 6.3.1.2. Reconstructed Radius: a. cranial aspect; b. caudal aspect; c. proximal aspect (x 0,40).

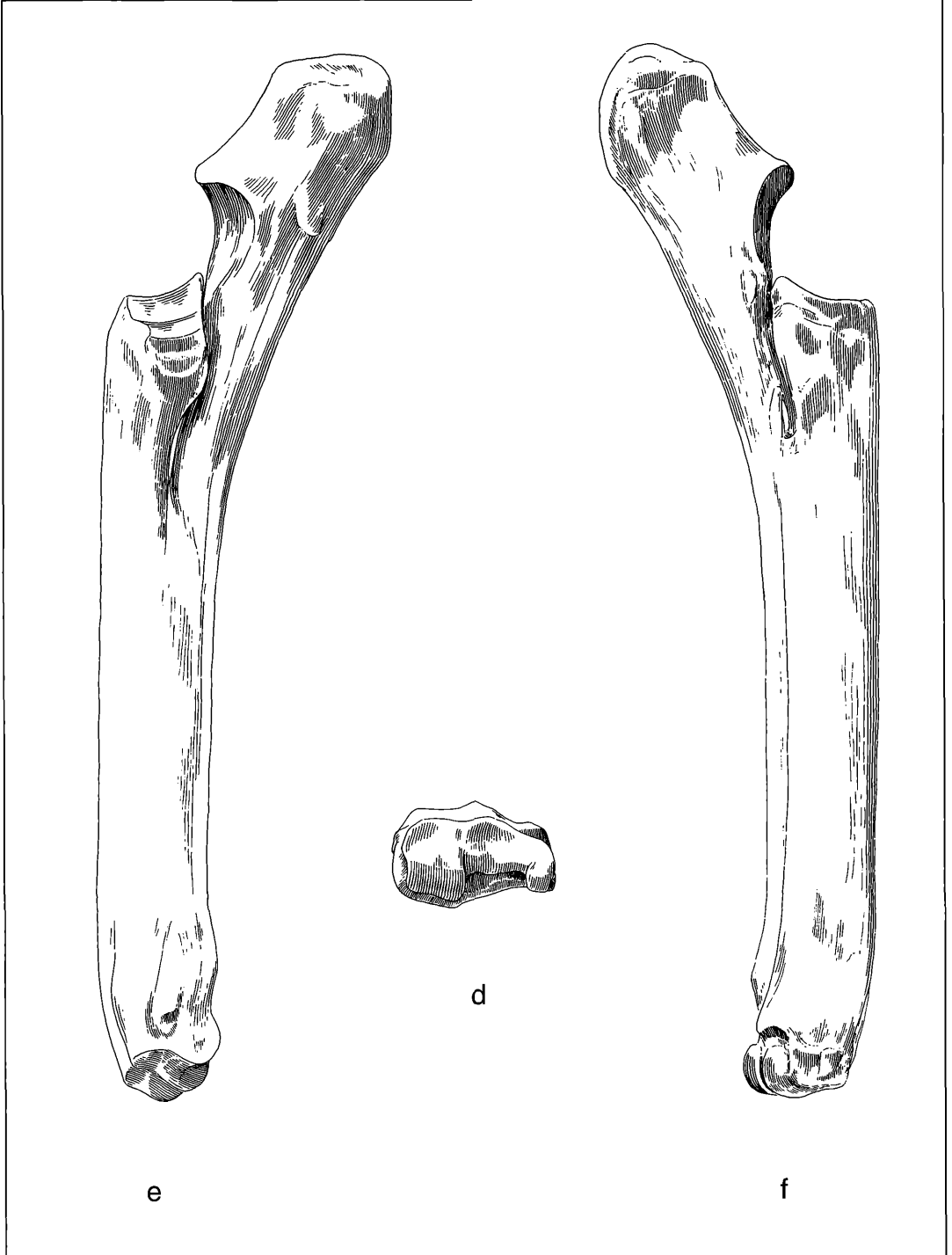


Figure 6.3.1.2. Reconstructed Radius: d. distal aspect; e. lateral aspect; f. medial aspect (x 0,40).

small, oval-shaped fossa synovialis shared by the caudomedial aspect of the fossa capitis radialis and adjacent surface of the ulna intermediate between the processi coronoideus medialis and lateralis (NICKEL et al., 1986, fig. 134: 5 and TOBIEN'S observation in NMB). Only the C-54 fovea presents a fossa synovialis, which extends into the incisura radialis ulnae.

Distal aspect (fig. 6.3.1.2d): The distal articulation of the radius (9) is a tripartite ginglymus (= hinge joint or Wechselgelenk). Its surface includes a medial (9'), intermediate (9'') and lateral (9''') facies articularis carpea articulating with the proximal facets of the scaphoideum, lunatum and pyramidale, respectively (NICKEL et al., 1986: fig. 134: 4,4,4). The radial facet as well as the proximal facet of the scaphoideum are relatively larger in the Höwenegg horse than extant *Equus*. Cranially placed cristae medialis (14'), intermedia (14'') and lateralis (14''') are relatively high areas in this view, whereas the tendonous grooves for the musculus extensor digitorum communis (12) and extensor digitorum lateralis (13) are lower in cross-section.

Lateral aspect (fig. 6.3.1.2e): The lateral border (7) takes its sharp aspect from the vestigial, fused corpus ulnae (8). The distalmost extension of the ulna terminates proximally at the processus styloideus ulnae (8). In contrast to the living horses, and indeed more advanced hipparions (see below under "Ulna"), the Höwenegg radii processus styloideus lateralis (8, fig. 6.1.3 c; caudal view) is not completely coosified with the lateral facia articularis carpea (9''').

Medial aspect (fig. 6.3.1.2f): The medial border is distinct in the central 1/3 of the shaft, becoming flattened proximally and rounded distally. The processus styloideus medialis (8') is distinct in this view. The retention of a sharp medial surface in the Höwenegg hipparion is unlike extant *Equus*.

Characteristic features of the radius: Compared to recent *Equus caballus* and more advanced Old World hipparions, the Höwenegg hipparion has a well devel-

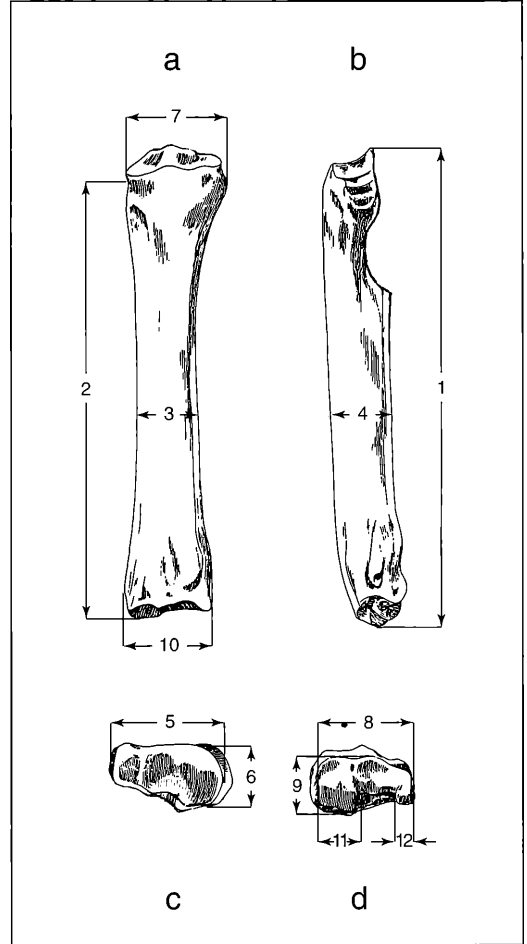


Figure 6.3.2. Measurements on the Radius: a. cranial aspect; b. lateral aspect; c. proximal aspect; d. distal aspect.

Table 6.3. Summary Statistics on Radii

Measure- ment	Sample size	Mean	Standard Deviation	Confidence Limits	Coefficient of Variation	Confidence Limits	Minimum	Maximum	Median
m1	8	282,89	12,03	274,11 291,67	4,25	2,05 6,45	271,10	310,00	281,00
m2	9	269,74	9,18	263,43 276,06	3,40	1,75 5,06	254,00	282,00	271,40
m3	9	43,61	4,04	40,83 46,39	9,26	4,72 13,80	39,50	50,50	41,60
m4	10	28,78	2,36	27,24 30,32	8,19	4,38 11,99	25,00	32,50	28,45
m5	13	64,89	1,82	63,85 65,93	2,81	1,67 3,94	61,70	67,20	65,10
m6	13	36,42	1,51	35,55 37,28	4,15	2,47 5,84	34,10	38,50	36,50
m7	13	69,23	1,77	68,22 70,24	2,55	1,52 3,59	65,80	72,00	69,40
m8	14	56,49	2,49	55,11 57,86	4,41	2,68 6,13	52,10	60,10	55,70
m9	14	34,82	1,24	34,14 35,51	3,56	2,17 4,95	32,50	37,00	35,00
m10	12	64,13	2,04	62,91 65,34	3,19	1,84 4,53	61,50	67,80	63,50
M11	13	21,69	1,49	20,84 22,54	6,85	4,06 9,63	18,50	23,70	22,10
M12	13	12,50	1,43	11,68 13,32	11,44	6,75 16,12	10,20	15,50	12,20

oped lateral ridge and fovea capitis radii (3''); lacks an incisure on the caudal border of the fovea capitis radialis (3'''); lacks a fossa synovialis on most individuals caput radii; has an inclined caput radii (2-2); has poorly developed tuberositas radii and ligamente collaterale medius (5); has a poorly developed processus styloidei ulnae (8) and radii (8'); has a vestigial crista transversa (6); has a poorly developed middle tendon groove for the musculus extensor digitorum communis (12) and lateral tendon groove for the musculus extensor digitorum lateralis (13); has enlarged medial facies trochlea articularis carpi (9'); has an incompletely fused processus styloideus lateralis (8) with the lateral facies trochlea articularis carpi (9''').

Statistical Results

Twelve variables were analysed on a total of 14 (of 21) radii. Only measurement 12 showed a coefficient of variation above 10 (CV = 11.44); this was probably due to the irregular shape of the medial aspect of radial condyle breadth. There were six significant correlations, only one being at or above the 99 % level: m6 (proximal articular depth): m11 (breadth of the radial condyle) probably reflecting the size dependency and measurement consistency of these dimensions. Measurement 5 (proximal articular breadth) showed significant correlations with two other parallel distal articular dimensions (m8 and m9). These same two distal articular dimensions showed significant correlations between one another (m8-m9) because of their parallel (and demonstrably redundant) nature. The two length measurements (m1-m2) and the two distal width measurements (m8-m10) were likewise significantly correlated.

6.4 Ulna (fig. 6.4.1a-e):

The smaller number of ulnae (16), than radii (23), is due mainly to the absence of proximal articular ends in some of the isolated specimens. The ulnae are mostly fused to the radius, and the olecranon is mostly very well preserved.

Cranial aspect (fig. 6.4.1a): The olecranon (5) is concave medially and convex laterally. The bulbous proximal end includes a number of distinguishing features: the laterally located tuber olecrani (5'), the more proximally placed caput laterale of the musculus tricipitis (5''), and the more distolaterally placed attachment scar for the musculus anconeus (5'''). Feature (5''') is more prominent in the Höwenegg horse than in extant *Equus*. These muscles act to fix and extend the elbow joint. The incisura trochlearis (9) is bordered proximally by the processus anconaeus (11) and distally by the processi coronoideus lateralis (10) and medialis (10'). The index of measurements 10 – 10' versus the maximum width of the radius (5 – 5' in radius fig. 10 a) varies between 55 and 64 (mean = 59), giving a mean index of more than half of the maximal width of the radius.

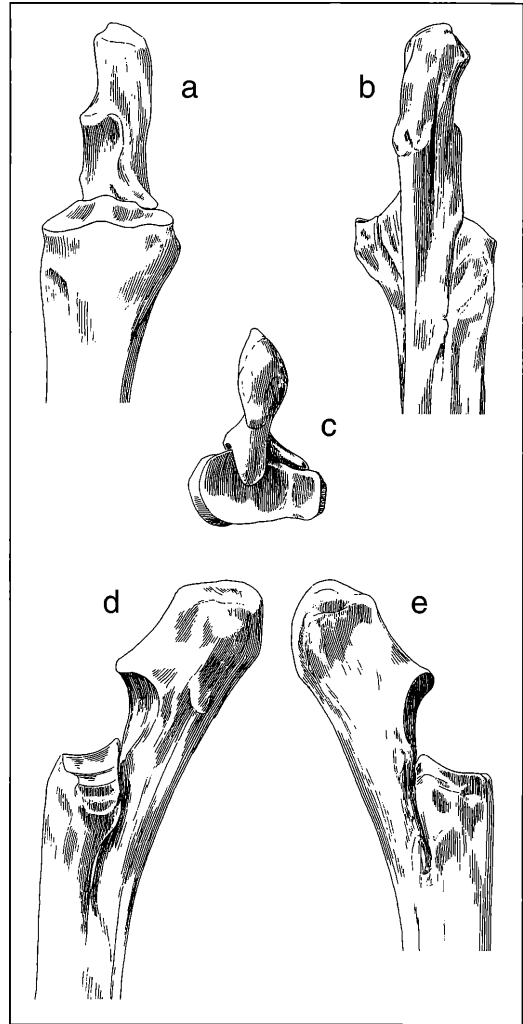


Figure 6.4.1. Ulna: a. cranial aspect; b. caudal aspect; c. proximal aspect; d. lateral aspect; e. medial aspect (x 0,25).

Caudal aspect (fig. 6.4.1b): The tuber olecrani (5') is the most proximal structure in this view. Distally, along the midline, is the attachment scar for the musculus tensor fasciae antebrachii (7), the more prominent tuberosity for the flexor carpi ulnaris (6), and more distally, the attachment site for the musculus flexor digiti profundus (8) (ZHEGALLO, 1978: fig. 20 A, B). Distally, the corpus ulnae (12) is triangular-shaped and more completely developed along its entire length to the processus styloideus lateralis (radius, 6.3.2 a, b, f: 8') than in extant *Equus*, where the distal one-third of the ulnar shaft is completely incorporated into the radial shaft. Although largely fused with the corpus radii distally,

most Höwenegg ulnae have a slender longitudinal sulcus (12'; radius fig. 6.3.1a, b medially of 7) about 4–5 mm distance from the lateral edge of the corpus; this feature marks the co-ossification line of the ulna with the radius.

Lateral aspect (fig. 6.4.1d): This aspect presents features of the olecranon (5, 5', 5''), anconeus muscle scar (5'''), the tuberosity for the musculus flexor carpi ulnaris (6), attachment scar for the musculus tensor fasciae antebrachii (7), incisura trochlearis (9), and processus anconeus (11). The spatium interosseum (13), intervening between the corpus ulnae (12) and the radius, is present in all Höwenegg specimens, with its proximodistal length being variable (36–43 mm), and sometimes obscured by the bony processes of the ulna (13: fig. 6.4.2 e).

Medial aspect (fig. 6.4.1e): This aspect presents features (5), (6), (9), (11), (12, 12') and (13) as described above.

Characteristic features of the ulna: Compared to extant *Equus*, the Höwenegg hipparion has a more prominently developed ulna; the relationship of the processus coronoideus' (10–10') width versus caput radius maximum width indicates less reduction of the olecranon process; the corpus ulnae (12) is not reduced but coossified with the radius (12'); the distal limit (processus styloideus) has an open suture juxtaposed against the medial part of the trochlea carpi (9''' in radius); there is a narrow articular facet of the processus styloideus (radius: fig. 6.3.2: 9'''). These characteristics are believed to be plesiomorphic compared with *Equus* and geochronologically younger hipparions (so far as known).

Statistical Results

There were no significant correlations for the ulnae.

6.5 Scaphoideum (fig. 6.5.1a-f)

The scaphoideum is the medial element in the proximal carpal row. There are 23 Höwenegg hipparion scaphoidea mostly belonging to articulated skeletons. The scaphoideum is large, has a craniocaudally directed axis and a rectangular outline.

Cranial aspect (fig. 6.5.1a): The cranial aspect is dominated by its large, smooth surface, having been covered only by the joint capsule. On the proximolateral border the proximal facet for the radius (4) extends

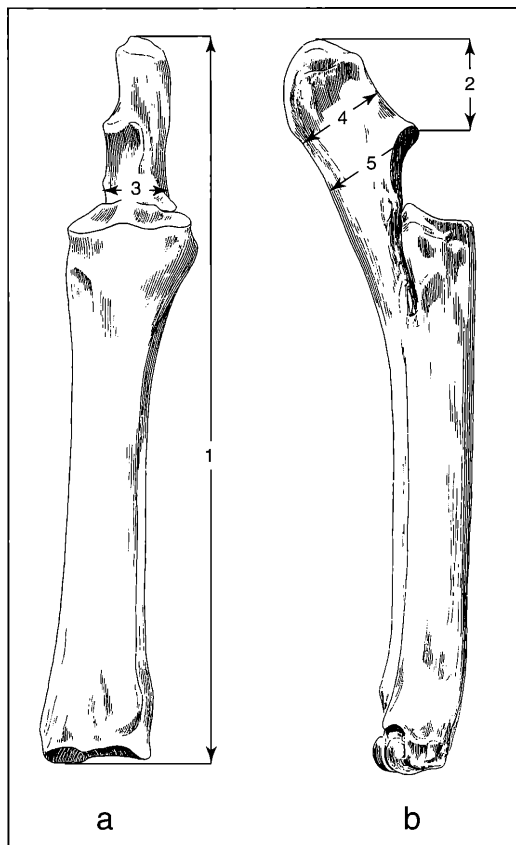


Figure 6.4.2. Measurements on the Ulna: a. cranial aspect; b. medial aspect.

somewhat onto the cranial aspect. On the lateral border there is a small scar for the ligamentum intercarpeum dorsale (=craniale) (1) which connects the scaphoideum with the lunatum (NICKEL et al. 1986: fig. 313-10). The laterodistal border is marked by the cranial border of the facet lunatum (2), which is more prominent than in *Equus*. The attachment site for the ligamentum collaterale medium proximale curtum (3) is prominent on the proximomedial border (see fig. 6.5.1f).

Table 6.4. Summary Statistics on Ulnae

Measurement	Sample size	Mean	Standard Deviation	Confidence Limits	Coefficient of Variation	Confidence Limits	Minimum	Maximum	Median
m1	5	362,20	20,47	343,30 381,10	5,65	1,95 9,35	342,40	391,60	365,30
m2	9	78,44	4,88	75,09 81,80	6,22	3,18 9,25	70,30	87,60	78,20
m3	8	39,19	3,80	36,41 41,96	9,70	4,65 14,75	34,00	45,00	39,40
m4	9	49,16	2,28	47,58 50,73	4,64	2,38 6,91	45,00	52,50	50,00
m5	8	57,14	2,96	54,98 59,30	5,18	2,50 7,86	52,00	60,40	56,95

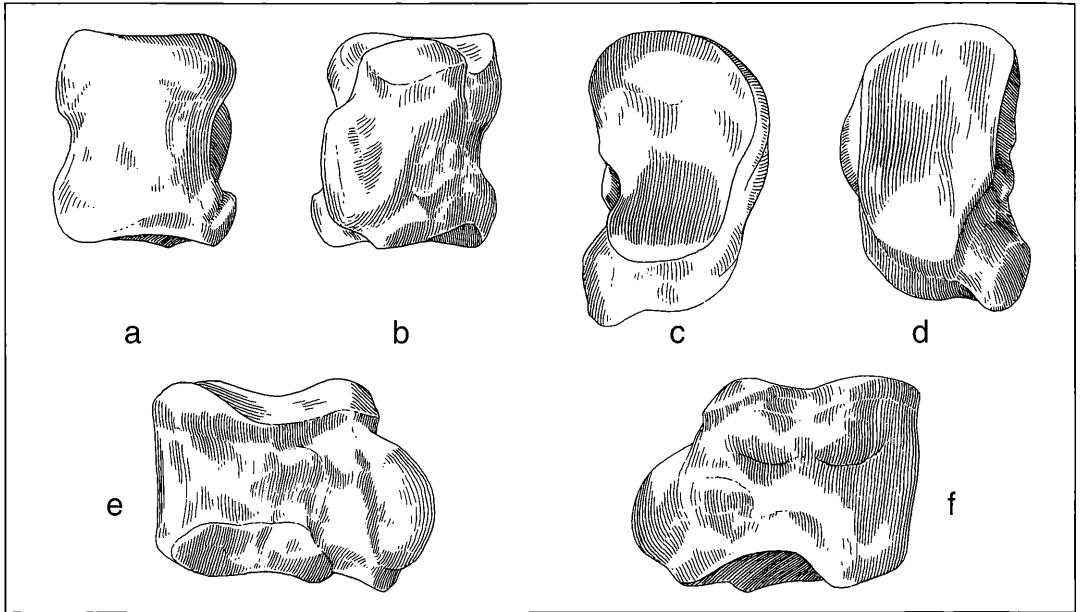


Figure 6.5.1. Scaphoideum: a. cranial aspect; b. caudal aspect; c. proximal aspect; d. distal aspect; e. lateral aspect; f. medial aspect (x 1,0).

Caudal aspect (fig. 6.5.1b): The dominant feature in this view is the strong, caudolaterally directed tubercle for attachment of the ligamentum obliquum volare (5), a portion of the ligamentum carpi volare profundum (ELLENBERGER & BAUM, 1977: 151). This ligament is connected with the crista transversa of the radius. The smaller protuberance for attachment of the ligamentum collaterale medium proximale curtum (3) can be seen in this view; this ligament attaches superiorly to the processus styloideus of the radius. On the distal border can be seen a portion of the distal facet (7) and a small articular facet for the trapezium (6; 14 x 5 mm). All undamaged Höwenegg hipparion scaphoidea have this small facet for the trapezium (6). The facet's craniocaudal length is always longer than the proximodistal length (no. 2), and varies considerably in its dimensions (7,0 mm x 4,2 mm to 15 mm x 6,2 mm). The smaller facets tend to be triangular shaped, with a distally-directed apex. The larger sized facets (of 6) have the first measurement being longer, and the cranial border is broader than the caudal one. GROMOVA (1955b: 91) has also found this small facet on all her sample of former U.S.S.R. scaphoidea. In those cases where the trapezium is vestigial, extant *Equus* has no facet. The caudal portion (4') of the proximal facet (4) extends more distally (than *Equus*) on the caudal side of the scaphoideum, enlarging the articular surface on the adjacent medial portion of the radius. The ligamentum collaterale medialis longus (3) and mediale distale cur-

tum (3'') are medially placed. The facet for the lunatum (2) is laterally placed.

Proximal aspect (fig. 6.5.1c): The proximal aspect is nearly completely dominated by the facet for the medial portion of the radius (4) (e.g. medial portion of the trochlea articularis carpea radius: fig. 10 f: 9'). The caudal portion is more restricted (4') than in *Equus* (GROMOVA, 1955b: 90), and is probably a plesiomorphic feature. On the lateral border there is a concave-shaped furrow (8) which corresponds to a similarly shaped structure on the lunatum; when in contact they form a proximodistally oriented synovial channel. Feature (5) is the laterocaudally extended tubercle for attachment of the ligamentum obliquum volare portion of the ligamentum carpi volari profundum. Features (3) and (3') represent the attachment sites for the ligamentum collaterale mediale proximale curtum, and ligamentum collaterale mediale longum, respectively.

Distal aspect (fig 6.5.1d): This aspect has an oval contour with the long axis directed craniomedially to caudolaterally. The distal facet (7) is large and bipartite; the cranial portion (7') is slightly convex and articulates with the magnum and the smaller mediocaudal component (7'') is concave and forms an angular-shaped facet for the trapezoideum. The facet for the trapezium (6) is located at the caudomedial corner and makes a sharply angled edge with the facet for the trapezoideum (7''). Laterally there is a bulbous tuberosity for attachment of the ligamentum carpi volare pro-

fundum (5), a variably developed sulcus for the musculus abductor pollicis longus (9) (ZHEGALLO, 1978: fig. 21G apl), and two distinct but small protuberances for attachment of the ligamentum interosseum (10).

Lateral aspect (fig. 6.5.1e) The lateral expression of the proximal facet (4,4') is long and sinuously curved in this view. A large elongated semi-oval shaped facet for the lunatum (12) can be seen on the cranioproximal border. On the distocranial border there is a smaller, trapezoidal-shaped facet for articulation with the lunatum (2), which meets a somewhat larger facet for the magnum (11), caudally. SONDAAR (1968: fig. 1 C-f, p. 13), GROMOVA (1955b: fig. 21-A1) and ZHEGALLO (1978: fig. 21-B) have erroneously characterized this facet as articulating with the lunatum. Facet (11) for the magnum is absent in extant horses and may well be reduced in later hipparions. The intervening area between the proximal (4) and distal (2, 11) facets is covered by remnant attachment sites for the ligamentum interosseum (10), and function to bind the scaphoideum and lunatum together (this is a very strong attachment in ZHEGALLO'S specimen, 1978: fig. 21-B).

Medial aspect (fig. 6.5.1f) The medial side of the scaphoideum has three principal, well developed collateral ligamentous attachments which are especially prominent in older individuals. Two are proximally located: the cranially placed attachment for the ligamentum collatoralia medium proximale curtum (3), and the caudally placed attachment for the ligamentum collatoralia medium longum (3'). The third is the distocranially situated rugosity (3'') for attachment of the ligamentum collatoralia medium distale curtum.

Characteristic features of the scaphoideum: The Höwenegg hipparion is characterized by its distinctly prominent distal lunatal facet (2); the absence of a large, distinct facet for articulation with the os magnum (11); a narrow posterior portion for articulation of the radius (4'); a strong prominent tuberosity (5) for attachment of the ligamentum carpi volare profundus with the ligamentum obliquum volare; a distinct presence of a distocranially placed facet for articulation with the trapezium (6); a facet for articulation with the trapezoideum (7'') being less extensive than the facet for magnum articulation (7'); a generally primitive morphology compared with modern *Equus* and probably later hipparions. GROMOVA (1955: 90) argued that *Hipparion* scaphoidea had a narrower cranial aspect than *Equus*.

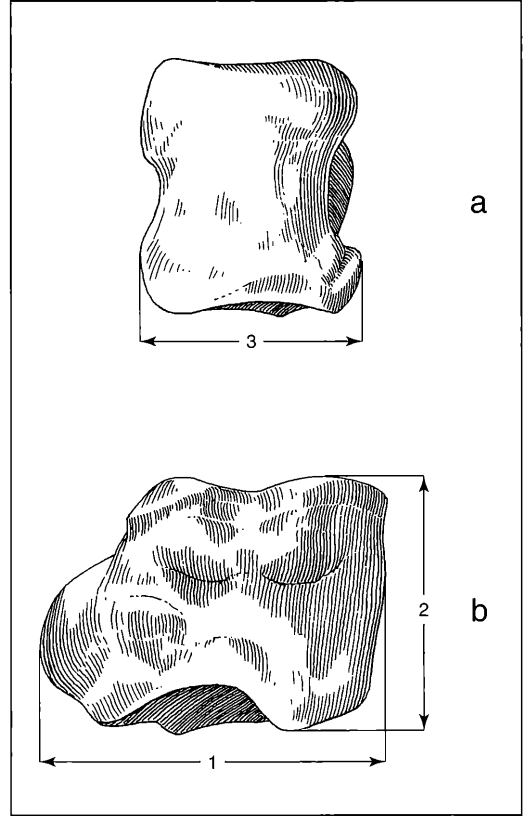


Figure 6.5.2. Measurements on the Scaphoideum: a. cranial aspect; b. medial aspect; m1 = greatest craniocaudal diameter; m2 = greatest proximodistal diameter; m3 = greatest mediolateral diameter.

Statistical Results

There were three variables measured on 22 scaphoidea, of which 15 were submitted for statistical analysis. The coefficient of variation was below 10 on all measurements. There were three significant correlations, all at or above the 99 % level: m1-m2, m1-m3 and m2-m3. These reflect the stability of these measurements and probable close relationship between the animal's body size and these dimensions.

Table 6.5. Summary Statistics on Scaphoidei (= Anterior Navicular)

Measurement	Sample size	Mean	Standard Deviation	Confidence Limits	Coefficient of Variation	Confidence Limits	Minimum	Maximum	Median
m1	15	38,84	1,72	37,92 39,76	4,43	2,76 6,11	36,70	43,10	38,80
m2	15	27,80	1,88	26,80 28,80	6,77	4,21 9,33	25,10	33,70	27,30
m3	14	23,57	1,94	22,50 24,64	8,22	4,99 11,45	21,60	29,40	22,80

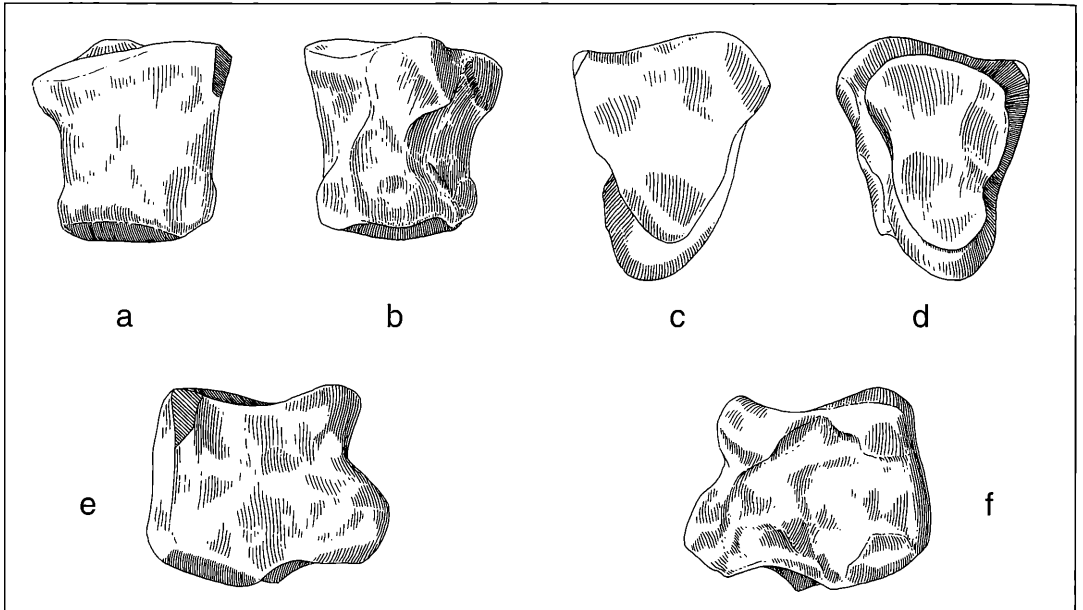


Figure 6.6.1. Lunatum: a. cranial aspect; b. caudal aspect; c. proximal aspect; d. distal aspect; e. medial aspect; f. lateral aspect (x 1,0).

6.6 Lunatum (fig. 6.6.1a-f)

The lunatum is the central element of the proximal carpal row. It is less massive than the scaphoideum, wedge shaped, wider cranially than caudally, and the apex is caudally directed.

Cranial aspect (fig. 6.6.1a): In this view the lunatum has a roughly square contour with a mediolaterally greater proximal than distal surface. The cranial surface is rough and has no articular facets. Along the proximal border is found a facet (1) for articulation of the radius. On the distal border is found a facet (2) for articulation of the magnum. There is a rugose scar (8) for attachment of the ligamentum intercarpum craniale on the cranial surface (NICKEL et al., 1986: fig. 313). While present on all specimens, this scar varies in size and often extends onto the medial wall. Its counterpart on the scaphoideum is feature (1; scaphoideum: fig. 6.5.1a). In the Höwenegg hipparion there is no scar for a ligamentous attachment of the ligamentum intercarpalae craniale between the lunatum and pyramidale (in cranial view); in extant *Equus* these scars are well developed (NICKEL et al., 1986: fig. 313). In more aged individuals (e.g. the Hö E skeleton), the cranial connection between these carpals seems to be weaker. The feature designated (a) represents a fracture, where the typical craniolateral border has been broken.

Caudal aspect (fig. 6.6.1b): The massive ligamentum carpi volare profundum (4) attaches to the distocentral aspect of this surface. This feature is comparable to a

similar feature found on the scaphoideum (fig. 6.5.1:5), and originates from the same ligamentous structure. Proximally is located the facet for the radius (1), and proximocentrally and medially is found the cranial and caudal portions of the facet for the scaphoideum (3). Facet (5) for the scaphoideum is found mediolaterally. There is a marked concavity of the medial border between facets (3) and (5).

Proximal aspect (fig. 6.6.1c): The radial facet (1) dominates this view. It presents a slight mediolateral depression between the broad cranial portion and the narrow pointed caudal portion. The intermediate depression corresponds to a transverse elevation in the medial aspect of the radial trochlea articularis carpea (radius: fig. 6.3.2, 9''). The caudal elevation of feature (1) extends somewhat distally (designated "x" in ZHEGALLO, 1979: fig. 22b), then contacting the intermediate portion of the facies articularis carpea radii. This is rare or absent in horses, and suggests an enlarged retroflexion of the articularis radiocarpea. Feature (4) is the attachment surface for the ligamentum carpi volare profundum; its lateral extension is distinct in all specimens.

Distal aspect (fig. 6.6.1d): There is a large distal facet with three component surfaces: facets (2) and (2'') articulate with the magnum, facet (2') with the unciforme. In the Höwenegg horse facets (2) and (2') form an angle of $140^\circ - 147^\circ$ at the cranial border (fig. 13a), whereas in extant *Equus* this angle is 150° and more. Facet (2') occupies about 1/3rd the distal articular sur-

face area; in extant *Equus* it is elevated (40 % or more). Facet (2'') is more concave in the Höwenegg horse than in extant *Equus*. The stronger inclination of features (2) and (2') produces a more pronounced relief of the whole distal facet in the Höwenegg horse than extant *Equus*. Facet (3) is the proximal facet for the scaphoideum (scaphoideum: fig. 6.5.2 f, 3; for feature (4) see figures 6.6.2 b, c, e and f).

Medial aspect (fig. 6.6.1f) The contour is rectangular with the caudally projecting ligamentum carpi volare profundum (4). The deepened central portion is covered by the rugose attachment site for the ligamentum interosseum (7); its corresponding placement on the scaphoideum is (10; fig. 6.5.1e). Proximally lies an elongated facet which narrows caudally (3). Distally two distinct facets are presented: the caudal (5) and cranial (6) facets for the scaphoideum. Facets (3), (5) and (6) articulate with facets (2) and (12) of the scaphoideum (fig. 6.5.1e). Facet (5) is lost in extant *Equus*, while facet (6) is a concave oval-shaped facet. The attachment site for the ligamentum intercarpeum dorsale (craniale) (8) is located on the distal aspect of the cranial surface (also see fig. 6.6.1a).

Lateral aspect (fig. 6.6.1e) The lunatum has a rectangular outline in this view. The central concave portion is covered by a rugose scar for attachment of the pyramidale's ligamentum interosseum (11). On the proximocranial surface is an elongated facet for the pyramidale (9) which has a broadened cranial portion. Distally there is a smaller semi-oval facet (10), also for the pyramidale. In extant *Equus* features (9) and (10) are caudally shortened, but proximally and distally enlarged. Facet (1) is the cranially elevated portion of the proximal facet, followed caudally by the transverse depression and the caudal elevation. Facet (12) articulates with a portion of the magnum facet. The hatched area (a) indicates the broken cranial edge.

Characteristic features of the lunatum: In comparison to extant *Equus* the Höwenegg horse lacks the ligamentum intercarpeum craniale between the lunatum and pyramidale; the articulatio radiocarpea has an increased retroflexion ability; the unciforme facet (2') is relatively small; the distal articular surface has a more pronounced relief (2, 2', 2''); the facets articulating with the pyramidale are elongated (9, 10, 11); 6) the facets articulating with the scaphoideum (5,6) are more completely developed. Most of the characters cited here

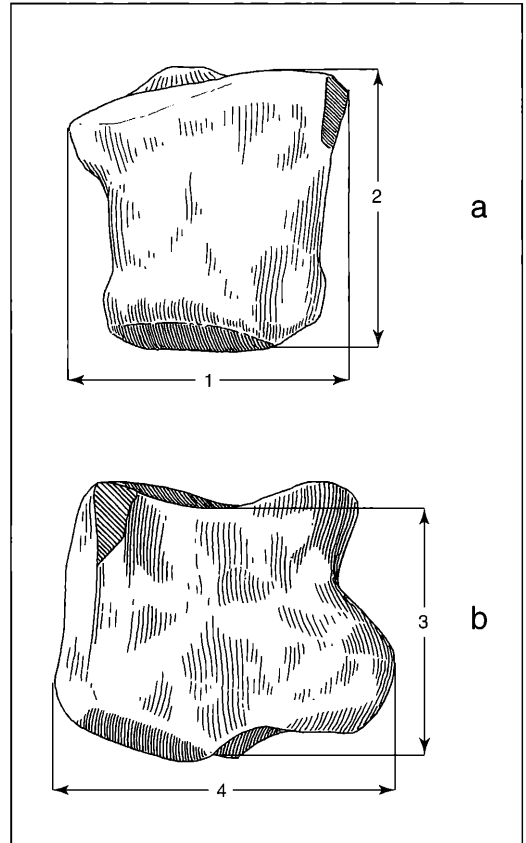


Figure 6.6.2. Measurements on the Lunatum: a. cranial aspect; b. lateral aspect.

may very well be plesiomorphic compared to the later hipparions and monodactyl horses.

Statistical Results

There were four variables measured on 19 lunata, of which 14 were statistically analysed. The coefficients of variation were below 10 on all measurements. There were three significant correlations, all at or above the 99 % level of significance: m1-m2, m2-m3 and m1-m3. The stability of these measurements and their meaning is the same as for variables m1-m3 of the scaphoidea.

Table 6.6. Summary Statistics on Lunata

Measurement	Sample size	Mean	Standard Deviation	Confidence Limits	Coefficient of Variation	Confidence Limits	Minimum	Maximum	Median
m1	14	27,48	1,88	26,44 28,51	6,83	4,15 9,51	25,20	32,80	27,25
m2	14	24,81	2,30	23,55 26,08	9,26	5,61 12,90	21,50	31,00	24,30
m3	13	27,21	1,89	26,13 28,29	6,93	4,11 9,75	25,00	32,20	26,80
m4	11	31,40	2,60	29,78 33,02	8,29	4,62 11,96	26,90	36,00	31,20

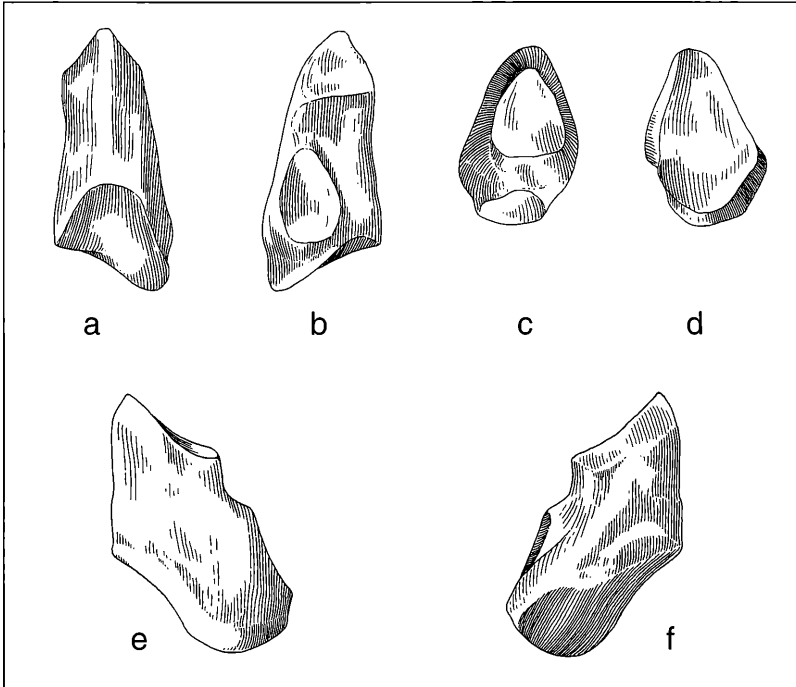


Figure 6.7 1. Pyramidale: a. cranial aspect; b. caudal aspect; c. proximal aspect; d. distal aspect; e. lateral aspect; f. medial aspect (x 1,0).

6.7 Pyramidale (fig. 6.7.1a-f)

The pyramidale is an elongated bone and the smallest in the proximal carpal row. In contrast to its lateral neighbor, the pisiforme, it is closely integrated within the forelimb basipodium. There are 18 pyramidales, mostly belonging to the articulated specimens.

Cranial aspect (fig. 6.7 1a): A central, proximodistally coursing bony crest (1), separates the medial (left) from the lateral (right) border. Atop the proximomedial border is the elongated craniocaudally oriented proximal facet for the lunatum (2). Distally, a crest meets the large distal facet for the unciforme (3). The smaller distal facet for the lunatum (4) contacts the unciforme facet (3) along its proximomedial border.

Caudal aspect (fig. 6.7 1b): Proximally is found the somewhat inclined, concave triangular-shaped facet (5) for the radius lateral trochlea. Distally is a small, irregularly shaped facet (5') which articulates with the pisiforme, and often connects facets (5) and (6). The larger ovoid-shaped facet for the pisiforme (6) is located distally and has its apex proximally directed, often contacting the small facet for the pisiforme (5').

Proximal aspect (fig. 6.7 1c): Presented in this aspect is the entire surface for the facet of the radius lateral trochlea (5) and the proximal portion of the pisiforme facet (6; in this view, nearly vertically directed). Facets (5) and (6) are separated by a keel separating the medial and lateral aspects of the bone.

Distal aspect (fig. 6.7 1d): This aspect is dominated by the elongated triangular-shaped facet for the unciforme (3). The facet can be characterized as being bipartite: the cranial portion (3') is concave and triangular-shaped with the apex oriented cranially (1); the caudal base (3'') is mediolaterally expanded and forms a 150° oblique angle to it (3'). In standing position the cranial portion (3') is in contact with the unciforme, while the caudal portion (3'') is not in permanent contact with its counterpart on the unciforme (GROMOVA, 1955b: fig. 23A, B). The proximal facet for the lunatum (2) is prominent along the medial border.

Lateral aspect (fig. 6.7 1e): This aspect is dominated by the rugose, rough lateral wall (7). Visible are the borders for the facet for the radius lateral trochlea (5), the pisiforme facet (6) and the distal facet for the unciforme (3), including its distal portion (3''). Facet (3'') is separated from the facet for the pisiforme (6) by a rugose narrow non-articular surface. The left vertical border on fig. 6.7.1e presents the cranial bony crest (1).

Medial aspect (fig. 6.7.1f): Proximally, this aspect presents a craniocaudally elongate facet (2) for the lunatum, which contacts facet (5) for the radius lateral trochlea at a 90° angle. Distally is found a semilunar-shaped facet for the lunatum (4). Facets (3) and (6) are found on the cranial and caudal surfaces, respectively. The bony portion between facets (2) and (4) is

Table 6.7 Summary Statistics on Pyramidale (= Triquetrum)

Measurement	Sample size	Mean	Standard Deviation	Confidence Limits		Coefficient of Variation	Confidence Limits		Minimum	Maximum	Median
m1	12	37,00	1,56	36,07	37,93	4,23	2,44	6,01	34,50	39,50	37,35
m2	12	21,38	1,11	20,71	22,04	5,21	3,01	7,41	19,20	23,10	21,45
m3	12	16,18	1,02	15,57	16,79	6,31	3,64	8,98	14,90	17,50	16,10
m4	11	15,70	1,61	14,70	16,71	10,29	5,71	14,86	12,50	17,60	15,80

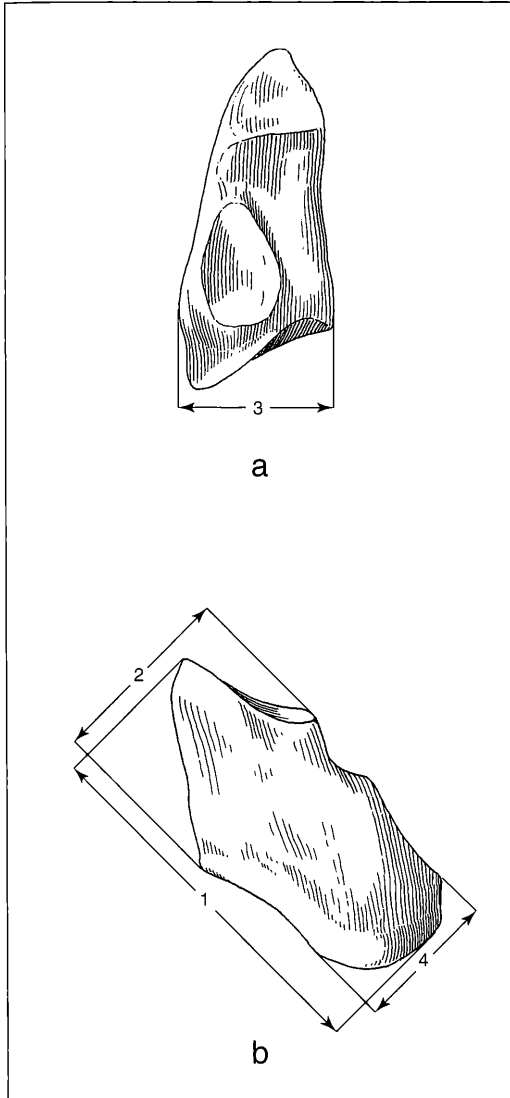


Figure 6.7.2. Measurements on the Pyramidale: a. caudal aspect; b. lateral aspect. m1 = maximum proximodistal distance; m2 = maximum craniocaudal distance; m3 = maximum medio-lateral distance; m4 = craniocaudal distance of distal heel.

sometimes very rugose (8) and most probably represents a strong ligamentous scar.

The larger facets such as the distal facet for the unciforme (3), the facet for the radius' lateral trochlea (5), and the larger facet for the pisiforme (6), show no significant variation within the Höwenegg sample. This is also true for the proximal facet for the lunatum (2). However, the distal facet for the lunatum (4) shows some variation and the small facet for the pisiforme (5') shows greater variation. In facet (5') 4 specimens (22 %) lack a facet, 6 (33 %) have an isolated facet, and 8 (45 %) have an elongated small facet, bridging the two facets for the pisiforme (5' and 6). The presence of facet (5') and its common junction with (6) gives a more developed articulation between the pyramidale and pisiforme bones as well as the lateral radial trochlea.

GROMOVA (1955b: 92, fig. 23V) described the small facet for the pisiforme (5') as a variable "isolated facies" in the Pavlodar "*Hipparion elegans*" sample. She also noted two variants in recent horses: isolated facies and joint facets (p. 92), suggesting a common degree of variation between at least these two equid lineages. The palaeontological collection of the Mainz Geoscience Institute preserves a domestic horse autopodium, having a pyramidale without the smaller facet for the pisiforme (5') (PIM-S-297). As the Höwenegg population demonstrates, a larger sample is needed to evaluate the variability and evolutionary significance of the pyramidale/pisiforme joint.

Characteristic features of the pyramidale: Compared to extant *Equus* the proximodistal length (measurement 1) is relatively greater; the entire bone is narrower (giving a more slender aspect), and appears to be more compact; the distal portion (3") of the unciforme distal facet (3) is longer in the Höwenegg hipparion, short and more parallel to the caudal (3') portion; this would appear to be related to the development of the MC IV.

Statistical Results

There were four variables measured on 21 pyramidale, of which 12 were statistically analysed. Coefficient of variation was below 10 on all measurements except m4 which was slightly elevated (CV = 10.29). There was only one significant correlation, m1-m2, at the 95-99 % level of significance. The lack of further significant correlations may be due both to the irregular shape and size variability of this bone.

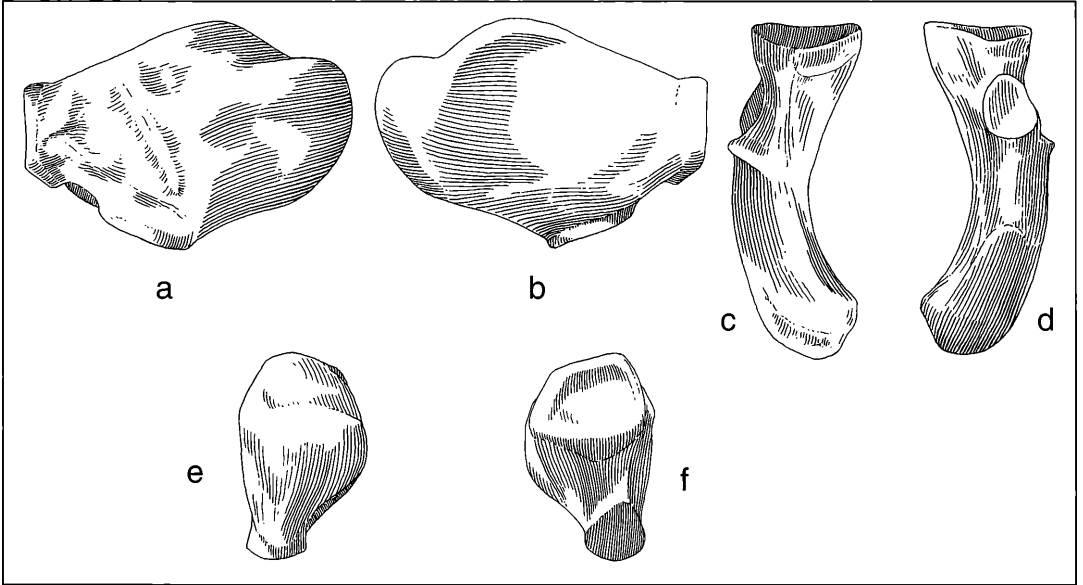


Figure 6.8.1. Pisiforme: a. cranial aspect; b. caudal aspect; c. proximal aspect; d. distal aspect; e. lateral aspect; f. medial aspect (x 1,0).

6.8 Pisiforme (fig. 6.8.1a-f)

The pisiforme bone is situated laterally in the proximal carpal row. It is a large, plate-like craniocaudally compressed bone, with the long axis horizontally oriented and having a convex cranially and concave caudally morphology. The pisiforme articulates with the lateral radius trochlea and the pyramidale by three large medially situated facets (1, 2 and 3 here). The free end of the pisiforme is the lateral aspect (GETTY, 1975: fig. 15-51-54; NICKEL et al., 1968: fig. 138e; ELLENBERGER & BAUM, 1977: fig. 273e). There are 25 Höwenegg pisiformes, mostly complete and belonging to skeletons.

Cranial aspect (fig. 6.8.1a): Most of the cranial wall (8) is rugose, but interrupted by a proximodistally oriented furrow (2-4 mm width, 1-2 mm depth) marking the tendinous insertion of the musculus extensor carpi ulnaris (5) (ELLENBERGER & BAUM, 1976: fig 273-7). This furrow is accompanied by two bony longitudinal crests, of which the medial crest (5') is thicker than the lateral crest (5''). The facet for the lateral (ulnar) radius trochlea (1) is located more medially than the larger facet for the pyramidale (2). Distal to, and making an approximately 60° angle with facet (1) is the smaller facet for the pyramidale (3). Facet (3) is present in all specimens; it never contacts with the larger pyramidale facet (2).

Caudal aspect (fig. 6.8.1b): The caudal surface (9) is smooth, concave, and elevated at the medial and lateral limits. The medial aspect presents a proximal facet for the lateral radius trochlea (1), a small facet for the proximal portion of the lateral radius trochlea (4), and

two facets for the pyramidale (3, smaller) and (2, larger). Facet (4) articulates with the proximal portion of the lateral radius trochlea (GETTY, 1975: fig. 15-54.4 and 15-43.4). The lateral facet for the pyramidale (2) is the counterpart of (6) in the pyramidale bone (fig. 6.7.2 b, c).

Proximal aspect (fig 6.8.1c): The proximal aspect is dominated by the pisiforme's longitudinal, rounded and angular margin (6). The medial aspect presents facets (1) and (4). Feature (5') represents the proximal end of the strongly protruding medial bony crest demarcating the attachment site for the musculus extensor carpi ulnaris.

Distal aspect (fig. 6.8.1d): The principal feature in this aspect is the distal rounded angular margin and the prominent facet for the pyramidale (2). Facet (3) for the pyramidale is opposed to, but does not contact facet (2). Directly lateral to (2) is situated the furrow for articulation of the extensor carpi ulnaris (5).

Lateral aspect (fig. 6.8.1e): This view shows the rough surface of the bone's lateral border, proximal margin (6), and distal margin (7).

Medial aspect (fig. 6.8.1f): The medial aspect presents the articular facets for the lateral radius trochlea (1) proximally, and the pyramidale (2), distally. The lateral aspect is termed the "free-end" by NICKEL et al. (1986). The junction of the rounded trapezoidal-shaped facet for the lateral (ulnar) radius trochlea (1), and smaller facet for the pyramidale (3) is marked. The larger facet for the pyramidale (2) is delimited at the distal limit. The caudal border of the pisiforme (9) is prominent.

Table 6.8. Summary Statistics on Pisiforme

Measurement	Sample size	Mean	Standard Deviation	Confidence Limits		Coefficient of Variation	Confidence Limits		Minimum	Maximum	Median
m1	14	43,79	1,65	42,88	44,70	3,77	2,30	5,24	40,30	46,20	43,90
m2	14	28,09	1,48	27,28	28,91	5,25	3,20	7,31	25,60	30,00	28,45
m3	14	16,37	1,23	15,69	17,05	7,53	4,58	10,48	14,30	18,50	16,30

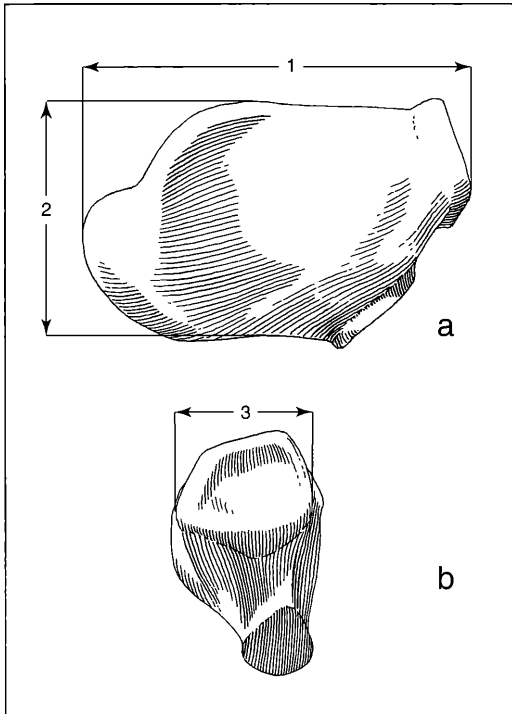


Figure 6.8.2. Measurements on the Pisiforme: a. caudal aspect; b. medial aspect. m1 = maximum mediolateral distance; m2 = maximum proximodistal distance; m3 = maximal craniocaudal distance.

The pisiforme is a sesamoid bone (GETTY, 1975: 288), and in contrast to the other carpals of the proximal row, it does not transmit weight from the stylo- and zeugopodium to the autopodium. The bone does have several important ligamentous attachments including: the accessorioulnar ligament (medially to the furrow, 5); the accessorio-metacarpal ligamentum, connecting the pisiforme with the ulnar portion of the radius, the pyramidale, the unciforme in *Hippotherium*, and the head of the MC IV (GETTY, 1975: fig. 16-7; NICKEL et al., 1986: 313). Also apparent is the attachment for a set of diverse muscles including: musculus extensor carpi ulnaris, musculus extensor carpi radialis, musculus flexor carpi ulnaris.

Characteristic features of the pisiforme: The pisiforme differs from that of extant *Equus* in its relatively longer mediolateral and narrow proximodistal dimensions (GROMOVA, 1955b: 92); the furrow for the musculus extensor carpi ulnaris is more distinct; the facets for the lateral ulnar radius trochlea (1) and the larger facet for the pyramidale (2) are not in contact with one another, but rather distant; the bone has an elongated lateral aspect (as in other hipparions) giving it an ovoid shape (fig. 6.8.1a, b; GROMOVA, 1955b: fig. 24A), presenting an overall square-shaped contour. The large facets (1) and (2) are of comparable size in the Höwenegg horse and *Equus*. However, the two small facets (3) and (4) adjacent to the radial facet (2), and the furrow for the extensor carpi ulnaris (5), do differ in their length and width.

Statistical Results

There were 3 variables measured on 24 pisiformes, of which 14 were subjected to analysis. The coefficients of variation were below 10 on all measurements. There was only one significant correlation, m2-m3, due largely to the irregular shape of this bone and resulting fluctuations in measurement variability.

6.9 Trapezium (fig. 6.9.1a-f)

The trapezium is the smallest element of the forelimb basipodium. Tridactyl horses (GROMOVA, 1952: 94, fig. 25), including the Höwenegg hipparion, contrast with extant *Equus* in having a more functional trapezium. Whereas the trapezium is absent in about 50% of *Equus* specimens, often being present on one side, it is present in all of the Höwenegg skeletons. In size it varies from being a pea-shaped structure to a discoidal or cylindrical mass, and is up to 15 mm in length. In exceptional cases the trapezium articulates with the trapezoideum and the MC II, but in the majority of specimens no articular facets are present. In many cases the trapezium is embedded in the distal portion of the ligamentum collatorale mediale carpi (GETTY 1975: 288).

The maximum proximodistal dimension of the Höwenegg trapezium ranges from 13.0 to 18.1 mm. It has a generally conical shape with the apex directed distally, and in lateral view (fig. 6.9.2e), one can discern the bone's curved long axis. The proximal head is broadened and contains a number of articular facets (fig. 6.9.2 a, b). The trapezium is generally craniocaudally oriented, and has articular facets with the trapezoideum and the head of MC II.

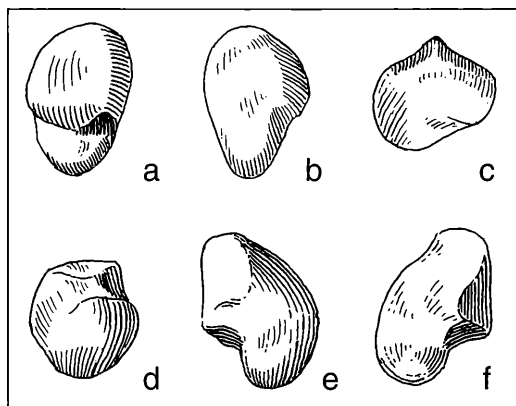


Figure 6.9.1. Trapezium: a. cranial aspect; b. caudal aspect; c. proximal aspect; d. distal aspect; e. lateral aspect; f. medial aspect (x 1,0).

Cranial aspect (fig. 6.9.1a): In this view the trapezium is placed posterior to the caudal aspect of the medial carpus. There is a larger facet (1) contacting the trapezoidium at an acute angle. A smaller facet articulating with MC II (2), strikes almost a 90° angle to facet (1). The distally curved aspect (3) is rugose, and the site for a ligamentous attachment surface. In some specimens (e.g. of the T-skeleton), the distal portion is very short).

Caudal aspect (fig. 6.9.1b): This aspect presents a strongly convex rugose surface (4) with a triangular outline for attachment of ligamentous fibers. The medial border often has a slight concave aspect (4') marking the distal border of facet (1).

Proximal aspect (fig. 6.9.1c): This aspect includes the trapezium's distal pointed apex (5), with its confluent medial and lateral borders.

Distal aspect (fig. 6.9.1d): The trapezoidium facet (1) is found proximally. Adjacent to facet (1), and placed at a 90° angle to it, is the small facet for the MC II (2). Distally, one finds the curved, non-articular portion of the trapezium (3).

Lateral aspect (fig. 6.9.1e): This aspect is dominated by the cranially inclined distal portion of the trapezium (3). On either side of this feature is the facet for the MC II (2) and the convex caudal facies (4).

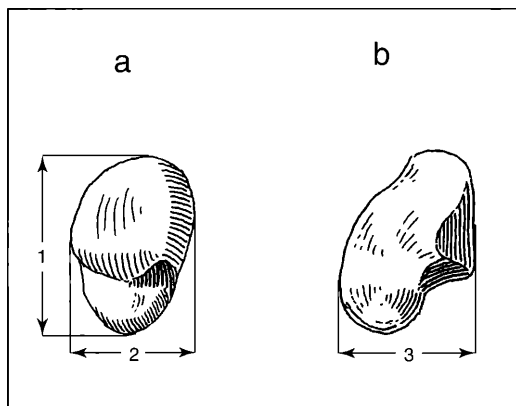


Figure 6.9.2. Measurements on the Trapezium: a. cranial aspect; b. medial aspect; m1 = maximum proximodistal distance; m2 = maximum mediolateral distance; m3 = maximum cranio-caudal distance.

Medial aspect (fig. 6.9.1f): This aspect presents the inclined distal non-articular portion of the bone (3), the distal end of the large trapezoidal facet (1) and the convex caudal facies (4). There is also a rugose notch for ligamentous attachment on the distal aspect of this view (6).

Characteristic features of the trapezium: Compared to extant *Equus*, the Höwenegg hipparion trapezium is morphologically more developed with articular facets for the trapezoidium and MC II, indicating movement capability at those joints.

Statistical Results

There were no significant correlations for the trapezium.

6.10 Trapezoidium (fig. 6.10.1a-f)

The trapezoidium has a wedge-like morphology with the keel directed cranially and the rectangular-shaped base directed caudally. Characteristic is a broad, convex articular surface which covers the proximal surface (1), extends somewhat cranially, and more extensively caudally. This facet articulates with the caudal portion of the proximal scaphoideum (fig. 6.5.2), thus assuming a biomechanical role as the medial cornerstone of the intercarpal articular system.

Cranial aspect (fig. 6.10.1a, with a certain medial component): The proximal border presents the main proximal articular facet with the scaphoideum (1) and

Table 6.9. Summary Statistics on Trapezia

Measurement	Sample size	Mean	Standard Deviation	Confidence Limits		Coefficient of Variation	Confidence Limits		Minimum	Maximum	Median
m1	11	20,35	1,33	19,52	21,17	6,52	3,64	9,40	18,60	23,40	20,00
m2	10	11,67	0,87	11,10	12,24	7,47	4,00	10,94	10,30	13,00	11,40
m3	11	10,05	0,74	9,59	10,52	7,37	4,11	10,63	8,80	11,20	10,20

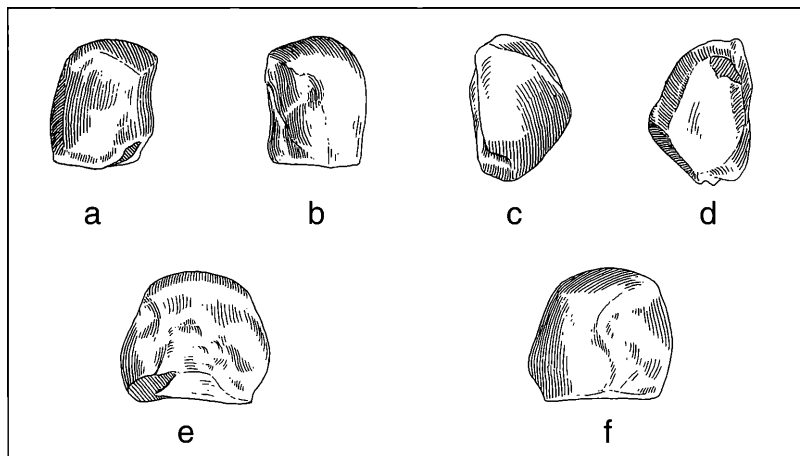


Figure 6.10.1. Trapezoideum: a. cranial aspect; b. caudal aspect; c. proximal aspect; d. distal aspect; e. lateral aspect; f. medial aspect (x 1,0).

its distalmost "beaked" extension (1'). Adjacent to (1') is the trapezoideum wedge's cranial keel (2), formed by the acute junction of the cranial border of the medial (3) and lateral walls (4). Feature (5) is a proximodistally oriented furrow accompanying the medial border of (1); probably the attachment site for the ligamente collaterale carpi medialis complex. This furrow is longer and deeper in extant *Equus*. Feature (6) represents the craniomedial border of the distal articular facet.

Caudal aspect (fig. 6.10.1b): This aspect is dominated by the facet for the scaphoideum (1), including its distalmost portion (1''). The border of the lateral aspect (4) is sharp. There is an elongate, curved furrow (4') for a ligamentous attachment, and a large tuberosity on the distal aspect of the laterocaudal border (4'') (or, alternatively, the groove and tuberosity appear as though they serve as a guide and attachment for a strong extensor tendon; e.g., extensor carpi ulnaris?). In the recent horse there is a well developed, but small articular facet for the magnum (SONDAAR, 1968: fig. 6B:d). It would appear that the large protuberance directed toward the magnum (4'') may be homologous to the magnum facet in extant *Equus*. At the distocaudal border of the main and convex articular facet is an oval flat-to-slightly concave surface (7): the contact facet with the scaphoideum (see also GROMOVA 1955: 95, fig. 25A:5c). This facet varies in size, i.e.: 7.8 x 5.6, 8.7 x 6.1, 8.8 x 5.7, 9.0 x 5.9, 9.9 x 6.6, 10.0 x 6.3. Feature 6 represents the caudal borders of the distal articular facet.

Proximal aspect (fig. 6.10.1c): This aspect is dominated by the convex main articular facet for the scaphoideum (1; including the cranial end, 1'). Cranially is also found a portion of the medial wall (3). Also depicted in this view is the lateral wall (4), a distinct ligamentous groove (4') and a large protuberance directed toward the magnum (4'').

Distal aspect (fig. 6.10.1d): This aspect is dominated by the facet for the MC II (6). The contour is irregularly triangular with the longest side being lateral (6'), the shortest mediocaudal (6''), and the intermediate side mediocranial (6'''). The MC II facet is slightly concave craniocaudally and convex mediolaterally. The border of another facet for the scaphoideum (7) is seen in close contact with the shortest side of the MC II facet (6''). Features (1'), (3), (4) and (4'') are as in fig. 17c; feature (x) is a postmortum fracture. In recent *Equus* and other monodactyl horses there is a facet for MC III (SONDAAR 1968: fig. 6B: e, 6C:e). There is no evidence for an MC III facet in the Höwenegg trapezoidea.

Lateral aspect (fig. 6.10.1e): In this view, the trapezoideum is square-to-rectangular shaped. It presents a convex profile for the main proximal articular facet (1). Adjacent to (1) is a rather large proximal and variably shaped facet for the magnum (8). At the distal limit is a smaller distal facet for the magnum (9); this facet is occasionally lacking. There is no evidence for posterior magnum facets, nor articulation with MC III.

Medial aspect (fig. 6.10.1f, with a caudal component): The center of this figure renders the sinous, proximodistally coursing border of the main articular facet. Features (1), (1') and (1'') are found proximally, cranially and caudally. The roughened non-articular surface of the medial wall (3) is separated from the facet for the scaphoideum (7) by a small furrow (5). The facet for the scaphoideum (7) is quite visible, as is its confluence with the main proximal articulation facet (1). The large protuberance directed to the magnum (4'') is found along the lateral border. As with the trapezium, the most prominent ligament is the ligamentum collaterale carpi mediale. This ligament is responsible for fixation and integration of the trapezoideum into its medial carpal position.

Characteristic features of the trapezoideum: There is a large proximal facet for the magnum and a small-

Table 6.10. Summary Statistics on Trapezoidea

Measurement	Sample size	Mean	Standard Deviation	Confidence Limits		Coefficient of Variation	Confidence Limits		Minimum	Maximum	Median
m1	13	16,80	0,71	16,40	17,20	4,21	2,50	5,92	15,50	18,00	16,70
m2	13	19,02	2,16	17,79	20,26	11,33	6,69	15,98	15,10	22,60	19,30
m3	13	14,15	2,06	12,97	15,32	14,55	8,54	20,56	12,70	20,60	13,50

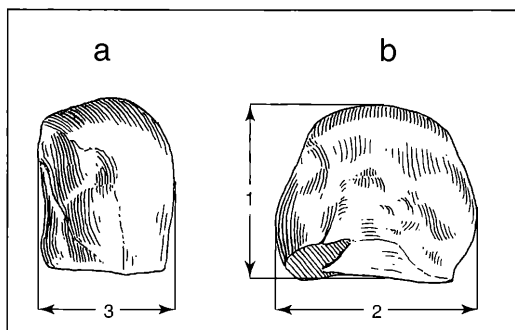


Figure 6.10.2. Measurements on the Trapezoideum: a. caudal aspect; b. lateral aspect; m1 = proximodistal distance; m2 = craniocaudal distance; m3 = mediolateral distance.

to-missing distal facet for the magnum; a large posterior protuberance; there is no articular facet for MC III; there is an articular facet for the scaphoideum.

Statistical Results

There were no significant correlations for the trapezoid-eum.

6.11 Magnum (fig. 6.11.1a-f)

The magnum is triangular-shaped in outline and is by far the largest bone in the distal carpal row. The magnum functions mainly for support of the monodactyl portion of the locomotor repertoire, and corresponds most closely in this regard with the cuneiform 3 of the hindlimb. The carpal proximal row differs from the tarsal row in having no tendency for proximodistal flattening of the lunatum, and reflects a different overall locomotor habitus from extant *Equus*.

Cranial aspect (fig. 6.11.1a): The magnum's cranial facies (1) is rugose, lacking articular facets. There is a strongly developed tuberosity on the medial aspect (1') which serves as the attachment site for the ligamentum collaterale carpi medialis. Two smaller ligaments attach distally (1'' and 1'''); these ligaments, the ligamenta carpometacarpea dorsalia, are directed distolaterally and attach to the proximal border of MC III. Along the lateral border is a small fossa (1^{iv}) for attachment of the ligamentum intercarpea which attaches the magnum and unciforme. This ligament is similar to the one in the proximal row which attaches the scaphoideum, lunatum and triquetrum. This morphology indicates that the magnum was firmly anchor-

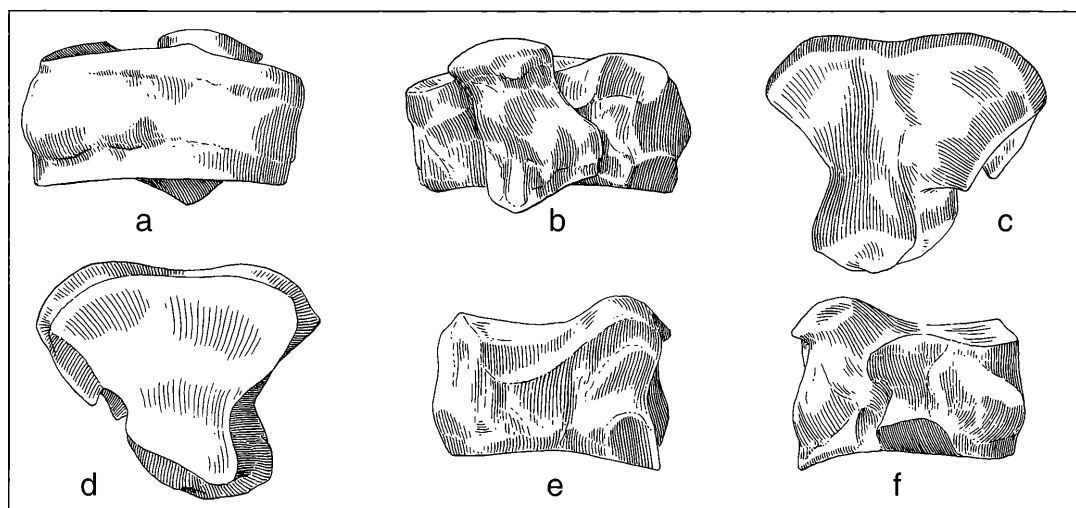


Figure 6.11.1. Magnum: a. cranial aspect; b. caudal aspect; c. proximal aspect; d. distal aspect; e. lateral aspect; f. medial aspect (x 1,0).

ed to the metacarpus, and permitted virtually no movement between these bones laterally. Feature (2) is the surface of the caudal articular head, (3) is the medial border of the proximal articular facet, and (4) is the caudalmost aspect of the distal articular facet.

Caudal aspect (fig. 6.11.1b): Feature (5) is a massive, rectangular shaped, proximolaterally to distomedially directed caudal projection of the magnum. Its proximal limit is the convex articular head (2) which articulates with the caudal portion of the lunatal distal facet (fig. 6.6.1d: 2"). Distal to the articular head lies a prominent tuberosity for the origin of the musculus interosseus (6). Feature (7') is the proximal facet and (7'') the distal facet for the trapezoideum. Distally is found the steeply inclined facet for MC II (8). Also distally situated are the proximal (9'), distal (9''), and caudal (9''') facets for articulation with the unciforme. The caudal articular head (2) rises above, and largely obscures the concave proximal articular facet (3).

Proximal aspect (fig. 6.11.1c): Most of the proximal facies is covered with articular facets. Caudally is the large ovoid lunatal facet (2). The cranial aspect includes two facets, separated by a craniocaudally oriented ridge (10). The medial facet (11) is concave and articulates with the cranial portion of the scaphoideum facet. The lateral facet (12) is also concave cranially and contacts the lateral surface of the lunatum facet (2).

Distal aspect (fig. 6.11.1d): This facies is nearly completely occupied by the gently undulating facet for the MC III (13). At the mediocranial border there is a small, obliquely disposed facet for the MC II (14). The medial tuberosity (1') bulges outward in this view.

Lateral aspect (fig. 6.11.1e): The central portion of this aspect is shallowly concave and roughened. There are three facets (15) for articulation with the unciforme: (15') is narrow and elongated craniodistally; (15'') is similarly narrow and extends proximodistally on the cranialward portion of the bone. Facets (15') and (15'') are mostly in contact with one another. A small facet (15''') is located at the caudodistal edge. Feature (1^{iv}) is the site of origin for the transverse ligament to the unciforme. Feature (12) is part of the lateral facet of the proximal facies.

Medial aspect (fig. 6.11.1f): This aspect combines the caudal aspect with the lateral portion of the cranial aspect. A prominent tuberosity for ligamentous attachment (1') occurs on the medial border. Proximally is found the caudal articular head (2), the proximal facet

for the trapezoideum (7') and the medial facet articulating with the scaphoideum (11). More distally is the attachment for the musculus interosseus (6) and the facet for MC II (8).

Characteristic features of the magnum: Included are this bone's: ovoid shape of the lunatal articular head; pronounced and bulbous tuberosity for attachment of the musculus interosseus (6); the small distal facet for the trapezoideum (7''); the caudal "pillar" supporting the articular head of the lunatal facet (2) is relatively elevated and oriented obliquely to the proximal articular surface.

Statistical Results

There were 3 variables measured on 22 magna, of which 14 analysed. The coefficients of variation were below 10 on all measurements. There was only one significant correlation, m1-m2, due largely to the irregular, generally triangular-shape, of this bone.

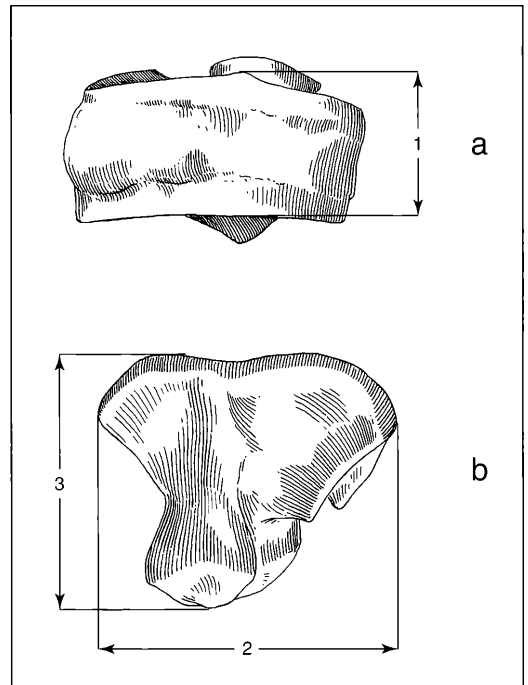


Figure 6.11.2. Measurements on the Magnum: a. cranial aspect; b. proximal aspect; m1 = proximodistal diameter; m2 = mediolateral diameter; m3 = craniocaudal diameter.

Table 6.11. Summary Statistics on Magna

Measurement	Sample size	Mean	Standard Deviation	Confidence Limits	Coefficient of Variation	Confidence Limits	Minimum	Maximum	Median
m1	14	17,85	0,75	17,44 18,26	4,18	2,55 5,81	16,50	19,00	17,80
m2	13	35,76	1,85	34,70 36,82	5,18	3,08 7,28	32,10	38,40	36,00
m3	9	31,57	2,43	29,89 33,24	7,71	3,94 11,48	29,20	36,50	30,40

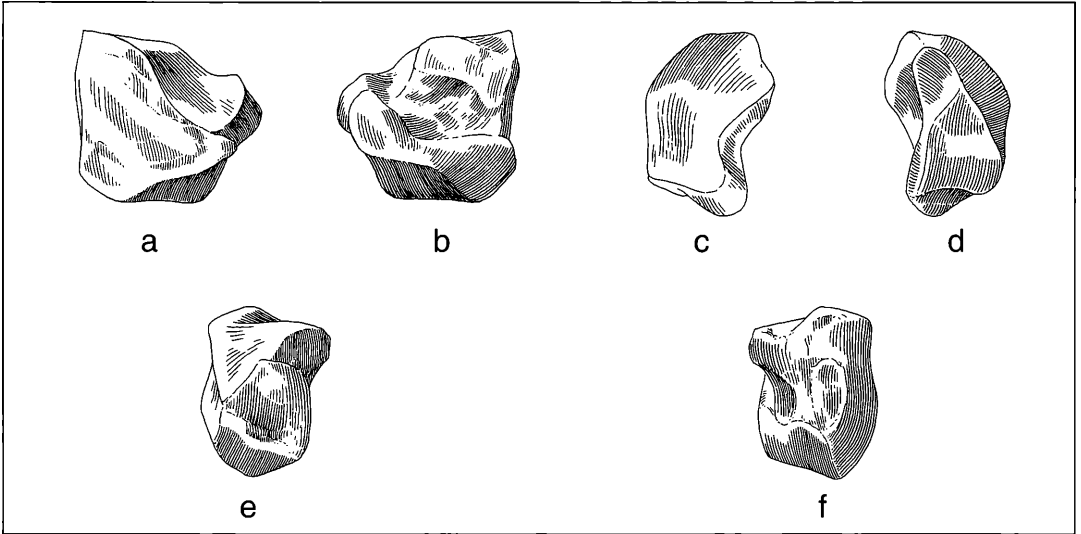


Figure 6.12.1. Unciforme: a. cranial aspect; b. caudal aspect; c. proximal aspect; d. distal aspect; e. lateral aspect; f. medial aspect (x 1,0).

6.12 Unciforme (fig. 6.12.1a-f)

The unciforme has a similar shape to the trapezoidum, but is larger and differs significantly in its possession of a caudal protuberance. The unciforme functions to transfer weight from the lunatum and triquetrum to the MC III and MC IV.

Cranial aspect (fig. 6.12.1a): This cranial facies (1) is convex, rough, and lacks articular facets. At the medial edge there is a small oval-shaped scar for the intercarpal ligament (2) which connects the unciforme with the lateral edge of the magnum. Proximally is found a large articular facet (3), and its laterally descending articular extension (3') for the triquetrum. Feature (4) is part of the distal facet for MC IV, and (5) represents the border of the medial MC III facet.

Caudal aspect (fig. 6.12.1b): The larger facet for the magnum (6) is found proximally and descends just short of the unciforme's central, deepened, non-articular surface (9) in this view. More distally placed is the medial facet for MC III (5), which is confluent with the lateral MC III facet (7). Proximal to facet (7) is the small facet for the magnum (8).

Proximal aspect (fig. 6.12.1c): This view is dominated by the large facet for the triquetrum (3) with its lateral

descending portion (3'). Feature (10) is a laterocaudal prominence. In other Höwenegg horses this prominence (10) is more developed as a strong tuberosity, probably for ligamentous attachment.

Distal aspect (fig. 6.12.1d): Centrally placed is the triangular-shaped distal facet for MC IV (4). This is separated from the medial facet for MC III (5) by a sharp, obliquely coursing ridge. Cranial to facets (4) and (5) is the prominent cranial wall (1), while caudally to facet (5) is a portion of the elongated larger facet for the magnum (6). The laterocaudal prominence (10) is also seen in this view.

Lateral aspect (fig. 6.12.1e): The tuberosity laterocaudal prominence (10) can be seen to clearly separate the descending portion of the triquetral facet (3') from the distal facet for the MC IV (4).

Medial aspect (fig. 6.12.1f): The central portion of this aspect has an oval-shaped scar for the intercarpal ligament (2). Proximally is located the border of the large facet for the triquetrum (3), and caudally is the larger facet for the magnum (6). Distally is located the deepened non-articular area (10), and facets (5) and (7) for MC III.

Characteristics features of the unciforme: There is a slight angle between the facet for MC III (5) and the

Table 6.12. Summary Statistics on Unciforme (= Hamata)

Measure- ment	Sample size	Mean	Standard Deviation	Confidence Limits		Coefficient of Variation	Confidence Limits		Minimum	Maximum	Median
m1	13	22,36	0,92	21,83	22,89	4,12	2,45	5,79	20,60	23,80	22,40
m2	12	13,49	0,81	13,01	13,98	6,02	3,47	8,56	12,10	15,20	13,55
m3	13	24,45	1,84	23,40	25,50	7,51	4,45	10,56	21,80	27,90	24,50

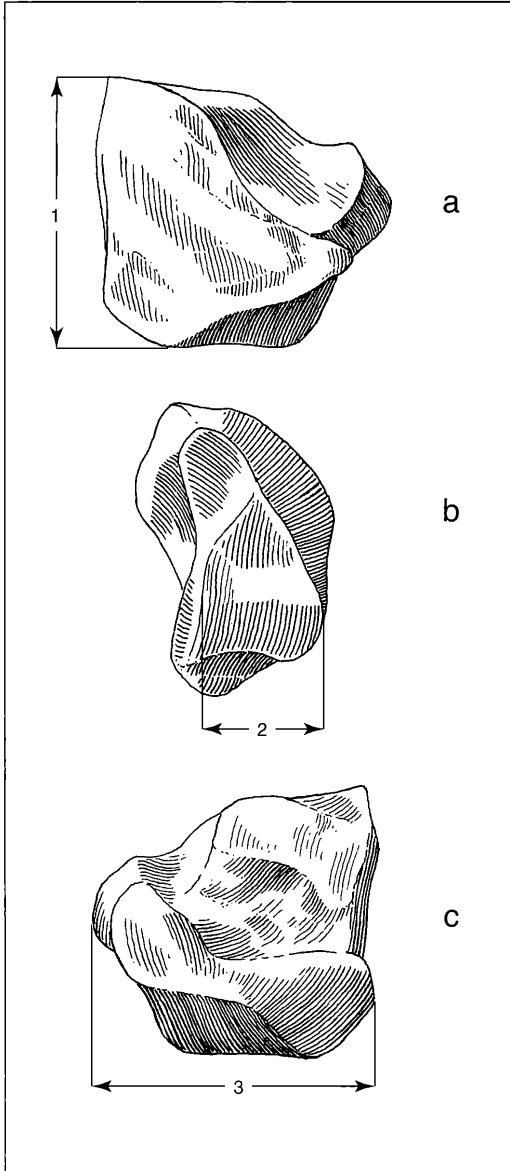


Figure 6.12.2. Measurements on the Unciform: a. cranial aspect; b. distal aspect; c. caudal aspect. m1 = proximodistal diameter; m2 = craniocaudal diameter; m3 = mediolateral diameter.

distal facet for MC IV (4); the facet for MC IV is relatively large, while the facet for MC V is indistinct, indicating this element's vestigial character. As a whole, the unciforme is narrow and proximodistally elongate.

Statistical Results

There were no significant correlations for the unciforme.

6.13. Summary of the Carpalia as a Functional Unit

The Höwenegg skeletons' completeness have allowed the first presentation of an articulated Old World hipparionine carpal skeleton (re: fig. 6.32.1 here). GROMOVA (1955: 98) described some characteristic features of the hipparion carpus based on a partially reconstructed specimens from Pavlodar. The Pavlodar horse had a carpus of greater length and slenderness than the Höwenegg hipparion. As noted by GROMOVA, body weight was transmitted principally through the carpus' cranial aspect; the caudal, lateral and medial aspects conducted a lesser proportion of the load. The lateral metapodials have complete articular contact with the overlying carpalia.

6.14 Metacarpale III (fig. 6.13.1a-f)

The Höwenegg sample has 31 metacarpale (MC) III's, mostly belonging to the articulated skeletons, and often including both right and left sides. Those MC III's not belonging to skeletons are mostly fragmentary. Because of the enormous load stress placed on the MC III's (weight bearing and movement at its articular surfaces), it is one of the strongest bones in the body (MT III perhaps being even stronger). As the broken fragments show, the compact layer in the semicylindrical shaft is especially thick cranially and medially. The medullary cavity extends far further towards the ends than in most of the other long bones, and there is little spongy substance.

Cranial aspect (fig. 6.13.1a): The diaphysial surface is smooth and mediolaterally convex. The proximal end presents the horizontal sharp edge of the facet for the magnum (1). Laterally is found the mediolaterally inclined edge of the facet for the unciforme (2), which together with facet (1) forms an angle of 130°; in extant *Equus* this angle is much greater (160°). Distally and on the medial aspect there are two rugose surfaces (3' and 3'') where the musculus extensor carpi radialis inserts. Distally are presented the cranial aspects of the medial (4) and lateral (4') trochlea metacarpi separated into two subequal portions by the crista sagittalis (5); these features articulate with the 1st phalanx III. Just proximal to the crista sagittalis (5) is a shallow, transverse, and sometimes triangular depression, the supratrochlear fossa (6), which articulates with the proximocranial border of the 1st phalanx III at the moment of its maximal extension during high speed locomotion. This depression is absent to vestigial in extant *Equus*. Yet more proximally placed are the medial (7) and lateral (7') protuberances which serve for ligamentous attachment (ligamentum collaterale laterale and mediale) for the fetlock joint. Whereas these protuberances are commonly found to be strongly built in Old World hipparionine horses, they are very weakly developed in extant *Equus*. The hypertrophied protuberances may result in MC III measurement 10 being as great or greater than measurement 11.

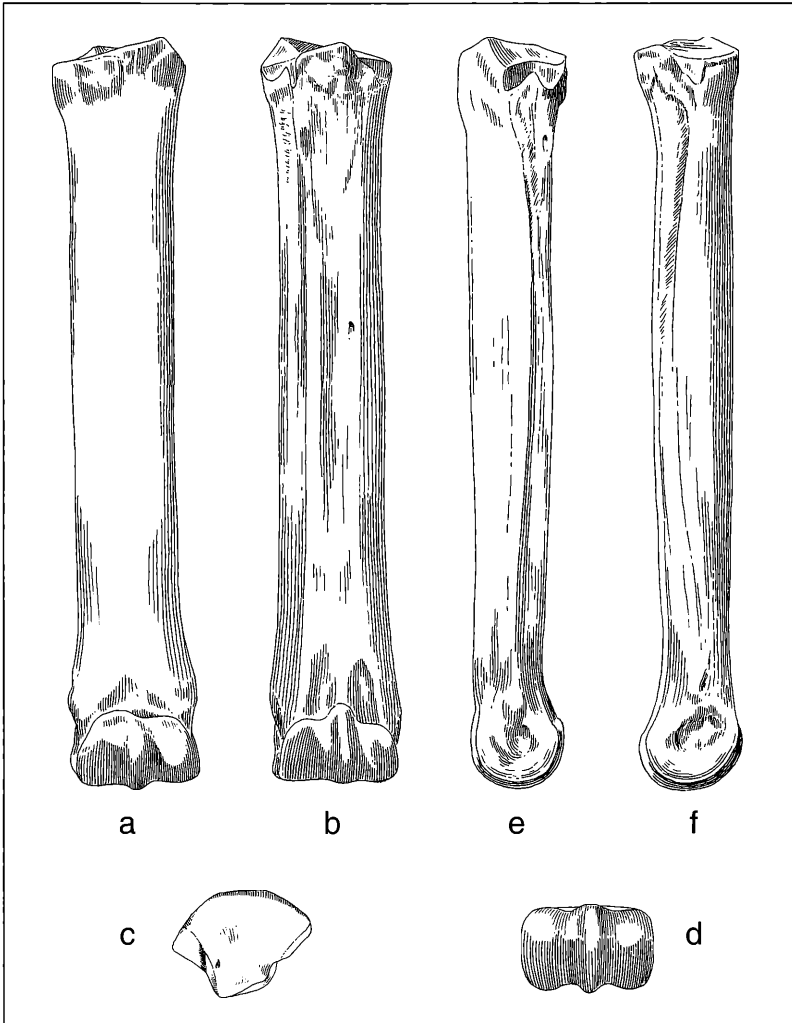


Figure 6.13.1. Metacarpale III: a. cranial aspect; b. caudal aspect; c. proximal aspect; d. distal aspect; e. lateral aspect; f. medial aspect (x 0,45).

Caudal aspect (fig. 6.13.1b): The central portion of the diaphysis has a rather depressed aspect intermediate between two parasagittally disposed long rugose ridges (11 and 11'). These rugose ridges attach MC III to MC II and IV respectively, nearly to, but not reaching the trochlea, leaving their trochlea free for independent articulation with their own phalanges. In extant *Equus* these rugose ridges are developed only half the distance on MC III, and are for the atrophied splint bones. Proximolaterally is found a small facet for the unci-forme (2) and its small, distally directed extension (2'), and more caudally directed facet (2''). Both facets (2') and (2'') articulate with MC IV, and vary in size amongst the Höwenegg horse sample, occasionally being absent. Centrally placed in craniocaudal view is a large prominent rugose swelling for the origin of the muscu-

lus interosseus (8). Medially is located the facet for articulation with MC II (9). A nutrient foramen (10), conducting vascular structures to and from the interior of the diaphysis, can commonly be observed at approximately mid-shaft (10). Proximal to the trochlea (4, 4'), and separated by an indistinct continuation of the crista sagittalis are two parasagittally placed deep depressions (12) for articulation of the proximal sesamoid bones and their insertion of the interosseus medius.

Proximal aspect (fig. 6.13.1c): The proximal surface is dominated by the articular surface for the magnum (1). On the medial border is the articular facet for MC II (9) and on the lateral border are the facets for the unci-forme (2) and MC IV (2').

Distal aspect (fig. 6.13.1d): The distal aspect presents centrally the crista sagittalis (5), and parasagit-

Table 6.13. Summary Statistics on Metacarpale III

Measurement	Sample size	Mean	Standard Deviation	Confidence Limits		Coefficient of Variation	Confidence Limits			Minimum	Maximum	Median
m1	10	212,82	5,70	209,10	216,54	2,68	1,44	3,92	203,00	220,20	212,60	
m2	10	207,39	5,90	203,54	211,24	2,84	1,53	4,16	197,90	215,30	207,30	
m3	15	31,74	1,67	30,85	32,63	5,27	3,28	7,26	28,90	34,80	31,50	
m4	15	22,47	0,76	22,06	22,87	3,39	2,11	4,67	20,90	23,80	22,40	
m5	16	39,92	1,05	39,37	40,46	2,64	1,68	3,61	37,70	41,90	40,00	
m6	15	27,88	1,31	27,18	28,58	4,69	2,92	6,46	25,70	29,70	28,10	
m7	15	34,62	1,13	34,02	35,22	3,26	2,03	4,49	32,80	36,70	34,30	
m8	16	11,69	1,22	11,06	12,32	10,45	6,60	14,31	9,50	14,50	12,00	
m9	14	7,50	2,83	5,94	9,06	37,69	21,03	54,36	5,20	14,10	6,00	
m10	13	39,52	1,49	38,66	40,37	3,77	2,24	5,30	37,00	42,20	39,60	
m11	12	37,09	1,60	36,14	38,05	4,33	2,50	6,15	33,70	39,90	36,85	
m12	13	28,32	1,25	27,60	29,03	4,42	2,63	6,22	27,20	30,60	28,00	
m13	13	24,78	1,13	24,13	25,42	4,56	2,71	6,41	23,40	27,60	24,50	
m14	13	26,37	1,23	25,67	27,07	4,65	2,76	6,53	24,40	28,60	26,50	

tally the trochlea metacarpi (4, 4'). The crista sagittalis is rounded cranially, is markedly sharper caudally, and is obliquely disposed so that the cranial extent is offset slightly laterally (see TOBIEN, 1968).

Lateral aspect (fig. 6.13.1e): This aspect presents the articular facet for the unciforme (2), the MC IV (2', 2''), more distally the lateral longitudinal ridge (11) and the lateral protuberance (7'), all described above. At the distal end is found a deep depression (13) for attachment of the ligamentum sesamoideum collaterale laterale (NICKEL et al., 1986; fig. 329:4).

Medial aspect (fig. 6.13.1f): This aspect presents proximally the articular facet for the magnum (1), protuberance for the musculus interosseus (8), and the facet for MC II (9). Located distally is the medial protuberance (7) and depression for the ligamentum sesamoideum collaterale mediale (13').

Characteristic features of the MC III: Included are: the steep inclination of the caudal portion for the unciforme facet (2); the shallow supratrochlear fossa (6); the strongly developed medial and lateral protuberances (7, 7') proximal to the trochlea; the caudal longitudinal rugose ridges for ligamentous attachment of MC II and MC IV (11 and 11'); the obliquely disposed, cranially flat, and caudally sharp crista sagittalis (5).

Statistical Results

The MC III had measurements on 14 variables for 27 specimens, of which 18 were analysed. We found measurements 15 and 16 of EISENMANN et al. (1988) to be useless for analysis due to their variability and lack of sufficient comparable data. Coefficients of variation were below 10 except for the proximal medial and lateral articular facets: m8 (CV = 10.45) and m9 (CV = 37.69). Measurement 9 was observed to be particularly variable in the Höwenegg population and virtually useless for descriptive statistical application.

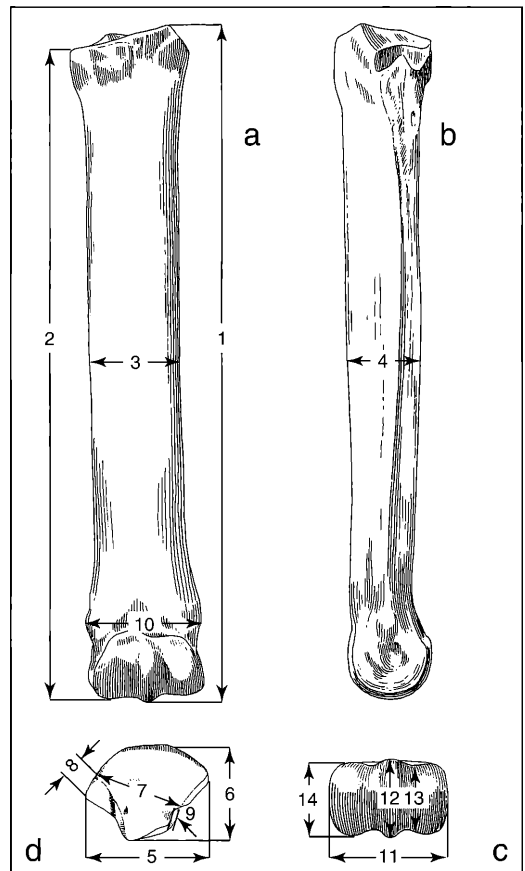


Figure 6.13.2. Measurements on the Metacarpale III: a. cranial aspect; b. lateral aspect; c. proximal aspect; d. distal aspect.

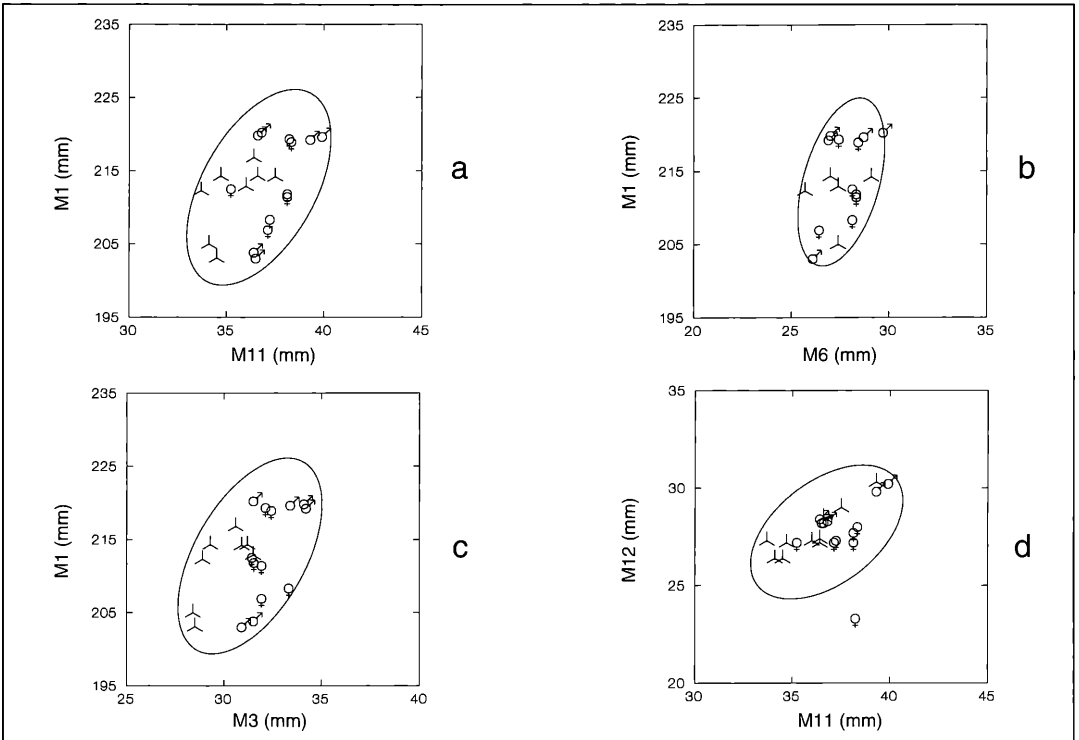


Figure 6.13.3. Bivariate Plots of Metacarpale III: a. M11 x M1; b. M6 x M1; c. M3 x M1; d. M11 x M12 (♂ = sex unknown).

There were 19 significant correlations, of which 9 were at or above the 99% level of significance. There were no negative correlations. Correlations with length measurements (m1 and m2) included four: m1-m2, m1-m6 (proximal articular depth), m2-m6 and m2-m7 (maximum diameter of the large proximal articular facet). Midshaft breadth (m3) proved to be more highly correlated, probably due to measurement consistency, than midshaft depth (m4), with the first having 5 significant correlations and the latter having none: m3-m11 (distal maximum articular breadth), m3-m10 (distal maximum supra-articular breadth), m3-m12 (distal maximum depth of the keel), m3-m6 (proximal articular breadth) and m3-m7 (maximum diameter of the large proximal articular facet). There were 8 correlations with measurements of the distal articular region (m10, m11, m12, m13 and m14) other than those listed above, including: m12-m13, m7-m12, m11-m12, m10-m12, m6-m12, m6-m10, m10-m11, m12-m14 and m7-m10. This high number of significant correlations reflects the high consistency of these variables' measurements. While both having elevated CV's, m8 (diameter of the anterior facet for the fourth carpal) and m9 (diameter of the articular facet for the second carpal) covaried with a significant probability. There is no immediate apparent functional reason for this, but it could be

related to the mediolateral limb movement at these joints. Finally, m6 (proximal articular depth) was found to correlate significantly with m7 (maximum diameter of the large proximal articular facet).

It is interesting to note that the most widely reported hipparionine metacarpal III measurements, and ones commonly used for interspecific bivariate comparisons, m1 (maximum length): m11 (distal articular width), were not significantly correlated! Nor were m1-m10 (distal maximum supraarticular breadth), m2 (medial length)-m10 nor m2-m11. This suggests sufficient independent variability in these bivariate measurements to raise caution in depending too heavily on such comparisons for species distinction. Another feature is that m4 (depth of the diaphysis at the level of m3) provided inferior statistical information compared to m3 (midshaft width), and therefore is deemed redundant for such analyses.

Figure 6.13.3a-d renders our results on bivariate measurements of MC III: a) M11 x M1 (maximum length x distal maximum articular breadth); b) M6 x M1 (proximal articular depth x maximum length); c) M3 x M1 (minimal [approximately mid-diaphyseal] width x medial length); and d) M11 x M12 (distal maximum articular breadth x distal maximal depth of mid-sagittal keel). There is no evidence of sexual dimorphism in these plots.

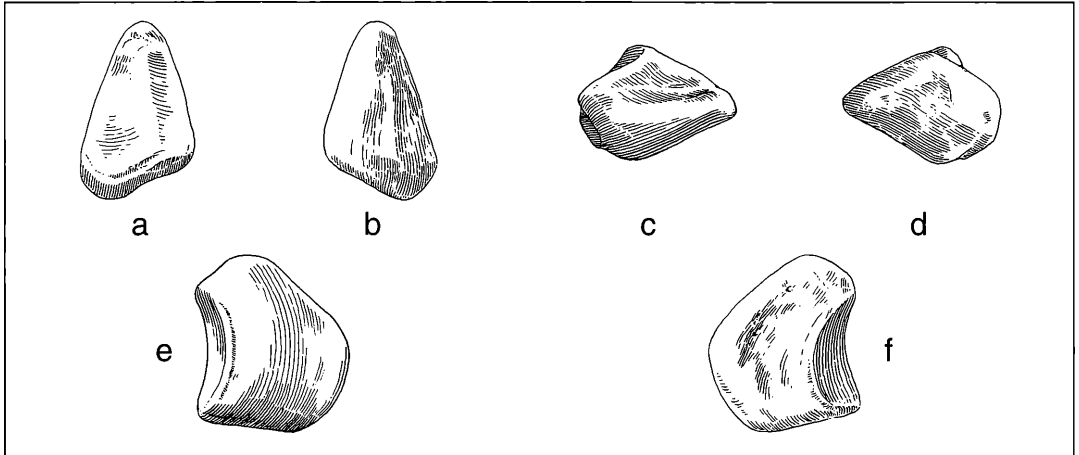


Figure 6.14.1.1. Medial Sesamoidea of Distal Metacarpale III: a. dorsal aspect; b. palmar aspect; c. proximal aspect; d. distal aspect; e. lateral aspect; f. medial aspect (x 1,0).

6.15 Sesamoidea of the Distal Metacarpale III (fig. 6.14.1.1 and 6.14.1.2)

There are several pairs (left and right foot) of sesamoidea mediale and laterale of distal metacarpale III. The paired, adjacently disposed, sesamoid bones form a portion of the fetlock joint, and articulate with the distal aspect of MC III and its crista sagittalis. One sesamoid has a medial position and is placed proximate to digit II (adaxial position). The other sesamoid resides laterally, placed adjacent to digit IV (abaxial position).

The sesamoidea have a three-sided pyramidal shape, with the apex directed proximally and the basis distally. One border is dominated by a large articular facet which contacts the distal MC III facet. The two other sides and the basis serve as the attachment site for the tendons and ligaments. The basis is particularly strongly attached by ligaments to the palmar border of phalanx 1 (ligamenta cruciata, ligamenta sesamoidea brevia, etc.; see also ZHEGALLO 1978: fig. 42).

6.15.1 Medial Sesamoid (fig. 6.14.1.1 a-g)

There are several examples of this element derived from the associated skeletons.

Dorsal aspect (fig. 6.14.1.1a): Feature (1) is the proximally directed rounded apex of the sesamoidei. Feature (2) is a large joint facet (nearly covering the entire surface here) which articulates with the distal end of MC III. This facet is subdivided into a narrower (5-6 mm) proximodistally elongated adaxial portion (2') contacting the medial wall of the crista sagittalis, and a larger abaxial portion (2'') which articulates with the medial portion of the trochlea metacarpi (note here that the axis we refer to is that of the MC III, not the vertebral column). Feature (2''') has a medio-distal ex-

tension also present in extant *Equus*. Both facets (2') and (2'') meet at a proximodistally coursing faint ridge (2'''). Ridge (2''') presents a flatter morphology in extant horses.

Palmar aspect (fig. 6.14.1.1b): A prominent medial longitudinal crest (4) separates the medial (abaxial) and lateral (adaxial) borders. The former border presents the facies musculi interossei (5; abaxial), providing attachment for the tendinous musculus interosseus medialis. The roughened border is concave over its entire proximodistal length, whereas in the extant horses only the proximal two third's of the border is deepened, with the distal third being even. The lateral (adaxial) wall is slightly convex and smooth (6), and slopes dorsally to the crista sagittalis. Together with this counterpart of the lateral sesamoid, it forms the facies flexoria through which the tendon of the musculus flexor profundus courses.

Proximal aspect (fig. 6.14.1.1c): Besides the apex (1), the smaller portion (2') of the articular facet (2) is visible as in the contralaterally placed broader one (2''). The medial crest (4) separates the totally concave facies for the musculus interosseus from the smooth, slightly convex medial portion of the musculus flexor profundus facies (6).

Distal aspect (fig. 6.14.1.1d): Feature (3) forms the bone's base and dominates this aspect. The outline of the basis takes the shape of an irregular quadrangle. Its sides are the brims of the articular facet (2', 2'', 2''') and the facies musculi interossea medialis (5) and facies musculi interossei lateralis (6). The angle between (5) and (6) at the palmar crest (4) is acute (about 50°), while in extant horses this angle is about 70°. This difference is due to the size-increase of the distal portion of the *Equus* sesamoid's abaxial surface.

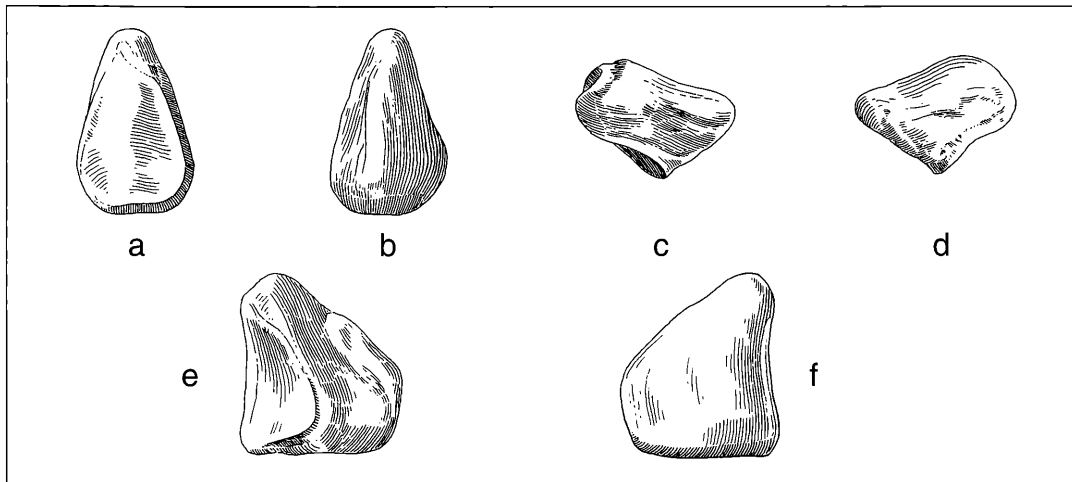


Figure 6.14.1.2. Lateral Sesamoid of Distal Metacarpale III: a. dorsal aspect; b. palmar aspect; c. proximal aspect; d. distal aspect; e. lateral aspect; f. medial aspect (x 1,0).

Lateral (adaxial) aspect (fig. 6.14.1.1e): This view is dominated by the lateral facies of the *musculus flexor profundus* (6). The surface is smooth, but at the palmar limit there is a flat, broad, proximo-distally coursing groove (6'). The crest (4) projects somewhat over this groove. This groove is absent, or replaced by a flatter feature of this facies (6) in *Equus*. GROMOVA (1955: 122, fig. 50v) described this distinction in her comparison of *Hipparion* (= *Cremohipparion* sensu BERNOR and TOBIEN, 1989) *moldavicum* from Taraklia and extant *Equus*. Feature (6'') is a long narrow furrow which may represent the attachment site for an extension of the joint cartilage, or perhaps for ligaments which connect the basis to the first phalanx III. This furrow is absent in *Equus*. Feature (2') represents the smaller lateral portion, and (2'') the larger medial portion of the articular facet (2).

Medial (abaxial) aspect (fig. 6.14.1.1f): Feature (5) presents the extensive rough, wrinkled and porous surface of the interosseus medialis facies, extending down to this aspect's basis (3). In *Equus*, the homologous rough surface covers only the middle and upper two thirds of the facies. Feature (2''') represents the larger, medial portion of the articular facet. Feature (2''') is a ridge separating (2'') from a smaller facet (2').

Characteristic features of the medial sesamoid of distal MC III: Included are: the well pronounced proximo-distal ridge (2''') on the dorsal surface separating the two articular facets for MC III (smoother and often nearly indistinct in extant *Equus*); in contrast to *Equus*, the interosseus facies (5) is well developed; the sesamoid's basis (3) is smaller in the Höwenegg horse than in *Equus* (massive here); facies (5) and (6) form an acute angle; crest (4) is inclined over the palmar extent of the flexor facies.

6.15.2 Lateral Sesamoid (fig. 6.14.1.2):

The paired sesamoid specimens are identical in most features. There are only some slight differences between them.

Dorsal aspect (fig. 6.14.1.2a): The laterodistal extension of (2'') is more reduced in this aspect than in the bone's counterpart.

Palmar aspect (fig. 6.14.1.2b): In this aspect the basis' border (3) is horizontal, not angular, as in Figure 6.15.1.2b. In other lateral sesamoids the basis' border is angular, and is taken as the morphological norm.

Proximal aspect (fig. 6.14.1.2c): This aspect is as in this bone's counterpart, although the bone is more irregularly shaped.

Distal aspect (fig. 6.14.1.2d): In this aspect the outlines of both specimen's bases are identical and quite different from those of *Equus*.

Lateral (abaxial) aspect (fig. 6.14.1.2e): The marginal bulge of the interosseus facies is somewhat more pronounced than this element's counterpart.

Medial (adaxial) aspect (fig. 6.14.1.2f): This aspect presents a relatively larger and deeper furrow (6'') than found in this sesamoid's counterpart.

The Hö A skeleton lacks sesama bina of the right forefoot. Based on the other Höwenegg-skeletons (e.g. M-55, G-54, T-56), we have observed no structural differences between the sesama bina of the left and right manus.

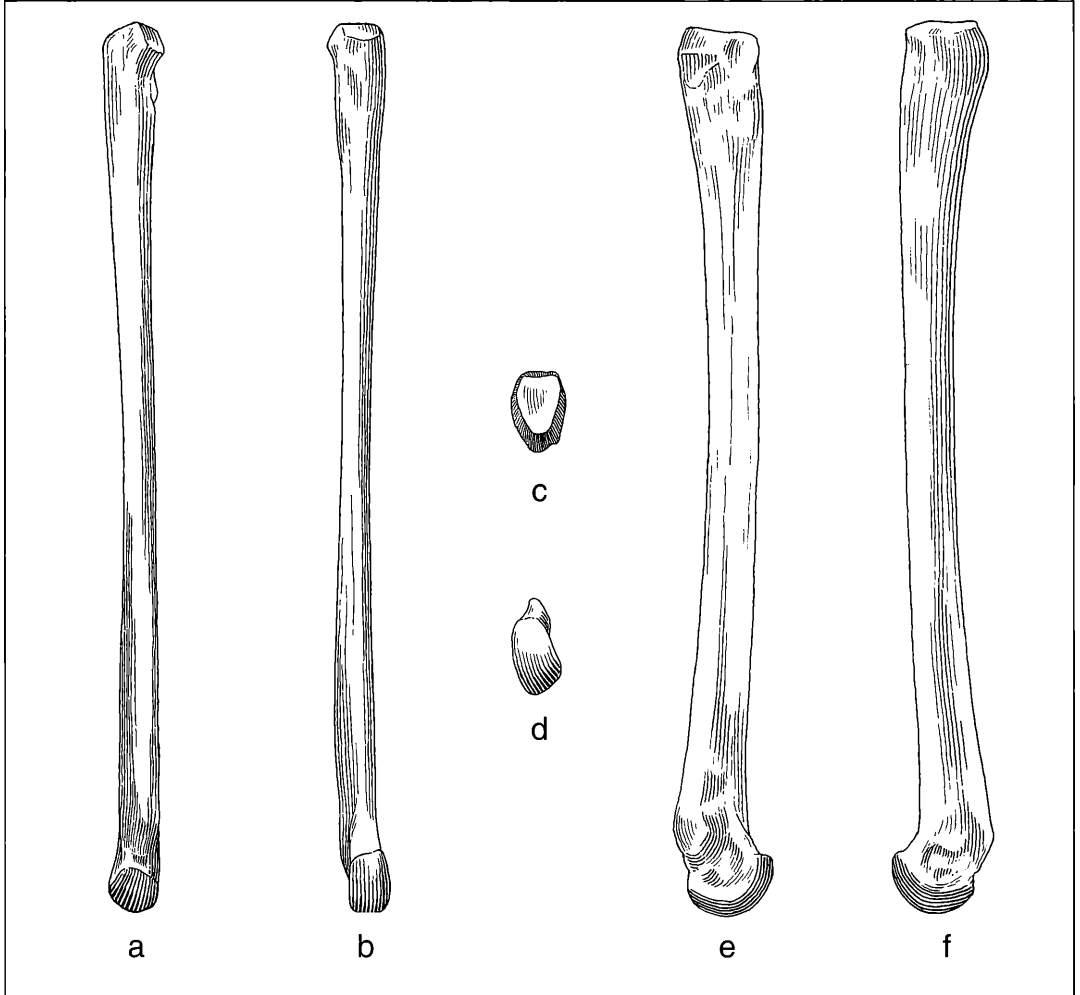


Figure 6.15.1. Metacarpale II: a. cranial aspect; b. caudal aspect; c. proximal aspect; d. distal aspect; e. lateral aspect; f. medial aspect (x 0,55).

6.16 Metacarpale II (figure 6.15.1a-f)

There are 20 Höwenegg MC II's, mostly belonging to the articulated skeletons. Often both right and left elements are found for single individuals. Many specimens have become mediolaterally bowed due to post-depositional diagenesis.

Cranial aspect (fig. 6.15.1a): A sharp longitudinal ridge (1) separates the smooth medial wall (2) from the roughened surface of the lateral wall (3). The proximally thickened end includes two articular facets, a larger articular facet for the magnum (4), and a smaller more distally situated facet for MC III (5). More laterally and distally placed is a broad roughened area (6) for ligamentous attachment of MC II with MC III. Feature

(6) is continuous with feature (3), which itself is continuous distally to a point somewhat proximal to the distal articular area (7). Distally is situated a depression for insertion of the ligamentum collaterale mediale.

Caudal aspect (fig. 6.15.1b): This aspect presents a small caudally extending portion of the proximal facet for the trapezoideum (8). The medial (2) and lateral (3) borders are separated by the rounded facies of this aspect. Just proximal to the distal articular surface (7) is a distinct fovea (7'') (proximodistal length: 11 mm; maximum width above articular border: 6.5 mm; maximal depth: 3 mm), accompanied by two proximally converging bony ridges (7'''). Feature (7'') is analogous to MC III feature (12), and is the site of attach-

Table 6.14. Summary Statistics on Metacarpale II

Measurement	Sample size	Mean	Standard Deviation	Confidence Limits	Coefficient of Variation	Confidence Limits	Minimum	Maximum	Median
m1	9	193,20	5,31	189,55 196,85	2,75	1,41 4,09	186,10	205,10	192,80
m2	11	11,09	1,17	10,37 11,82	10,51	5,83 15,19	9,60	13,70	10,90
m3	9	18,36	0,62	17,93 18,78	3,39	1,74 5,04	17,40	19,30	18,40
m4	9	13,39	0,68	12,92 13,86	5,09	2,61 7,57	12,20	14,70	13,30
m5	10	10,63	0,65	10,20 11,06	6,16	3,31 9,02	9,40	11,70	10,70
m6	11	19,99	0,56	19,64 20,34	2,82	1,58 4,07	19,20	21,20	20,00

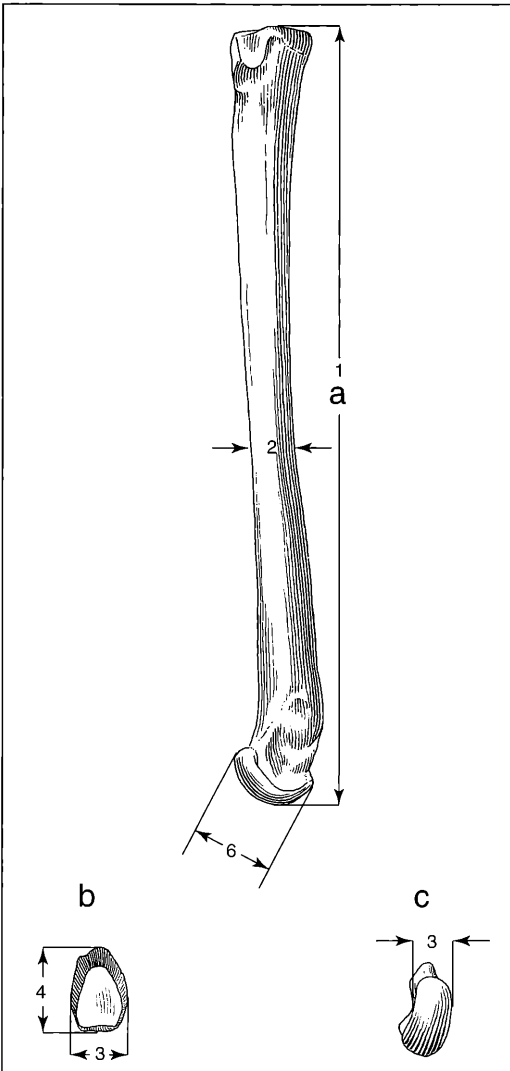


Figure 6.15.2. Measurements on the Metacarpale II: a. medial aspect; b. proximal aspect; c. distal aspect.

ment for the smallest sesamoids: sesamoidea articulationis MC II. Feature (7'') is particularly well developed on the left MC II of the T-skeleton (Hö T-29), whereas feature (7'') is rather reduced, and corresponds to the medial groove (12) on MC III (fig. 6.13.1).

Proximal aspect (fig. 6.15.1c): This aspect is dominated by the triangular shaped facet for the trapezoideum (8). The cranial ridge (1) is seen to be slightly rounded in this aspect.

Distal aspect (fig. 6.15.1d): The articular surface (7') is obliquely oriented in this aspect. The cranial process supraarticularis (9) has a distinctly pointed aspect in this view.

Lateral aspect (fig. 6.15.1e): Proximally, this aspect presents the facets for articulation with the magnum (4) and MC III (5). and the tuberosity for ligamentous connection with MC III (6). The lateral border (3) is dominated by its elongate raised ridge. The distal articular region (7) delimits the sesamoid fossa (7'') and more proximally situated lateral ridge. The processus supraarticularis (9) is prominent. Distally, the depression for attachment of the ligamentum collaterale laterale (10) and 1st phalanx II is marked.

Medial aspect (fig. 6.15.1f): The proximal aspect is rugose for ligamentous attachments. Distally, features (7), (7'') and (9) are as described above. The depression for the ligamentum collaterale mediale (11) is subequal in depth to the ligamentum collaterale laterale (10).

Characteristic features of the MC II: Included are: the deep fovea for the sesamoidea articulationis MC II (7''); a triangular outline for the proximal facet for the trapezoideum (8); a strong processus supraarticularis (9); strong retroflexion capability of the distal articular area (7); subequal deepening for collateral ligaments (10, 11) of the distal articular region (7).

Statistical Results

There were 6 variables measured on 20 specimens, 11 of which were statistically analysed. The coefficient of variation was below 10 for all measurements except m2 (CV = 10.51). There were only two significant correlations, both at the 95 %-99 % level of probability: m4-m6 and m5-m6. Measurement of this bone proved of limited value.

6.17 Sesamoidea of Distal Metacarpale II (fig. 6.16.1)

Not much has been reported concerning hipparion MC II and MC IV sesamoids, which correspond to the large sesamoids of the MC III (fig. 6.14.1&2.1: 2', 2'', 3', 3''). GROMOVA (1955: pl. 10, fig. 50g) published an articulated phalanx 1 of a lateral posterior digit, together with a digit III triangular-shaped sesamoid and two smaller rounded bones (X1, X2). The two rounded bones would appear to belong to the first phalanx and its unpreserved metatarsal.

The excellent preservation of the Höwenegg skeletons allows a more detailed study of these sesamoids. The presence of MC III sesama bina suggests the presence of sesamoids for digits II and IV. Paired sesamoids commonly occur in polydactyl ungulates and carnivora at the articular interface of the metapodial-1st phalanx (e.g. in rhinoceroses, HÜNERMANN 1989: fig. 80, 82; suids, bovids, *Canis* and *Felis*, BARON 1986: pl. 282-286 and other text-books). It is the normal condition to maintain sesamoidea for both the MC II and MC IV-Phalanx 1 joints (fig. 6.16.2). As the figure shows, these paired sesamoids are much smaller and differ morphologically from the distal MC III sesamoidea. Furthermore, these smaller sesamoidea exhibit size differences between themselves, with one counterpart always smaller than the other (re: fig. 6.31.1).

There are several pairs, as well as single specimens of the distal MC II sesamoidea in the Höwenegg collection. For the most part, these are derived from the articulated skeletal sample. The portion of the sesamoidea MC II which we describe below is the medial (abaxial) element.

Dorsal aspect (fig. 6.16.1a): Features (1) and (3) are, respectively, the homologues of the apex- and basis sesamoidei of the sesama bina. Facet (2'') corresponds to the main facet of the large sesamoids (2'' is in contact with the articular facet 7') of the MC II (fig. 6.15.1). Feature (2') is a very small, vertically oriented, proximodistally elongated facet (better seen in fig. 6.15.1: 2'). The facet is the homologue of the sesama bina's facet 2'. Feature (2''') marks the border of both facets, and forms a right angle (in contrast to the sesama bina facets with a larger angle). Feature (5) presents a shortened view of the facies musculi interossei medialis.

Palmar aspect (fig. 6.16.1b): Features (1) and (3) are the apex and basis, respectively. Feature (4) is the prominent process of the broad crest running from the apex to the basis. Features (5) and (6) are the expanded medial and lateral borders of the interosseus tendon and the flexoria facies, respectively.

Proximal aspect (fig. 6.16.1c): Feature (2'') is the proximal edge of the main articular facet. Feature (1) is the apex, from which a broad crest separates the large facies (5) and (6).

Distal aspect (fig. 6.16.1d): Feature (2'') represents the distal portion and limit of the articular facet. This fig-

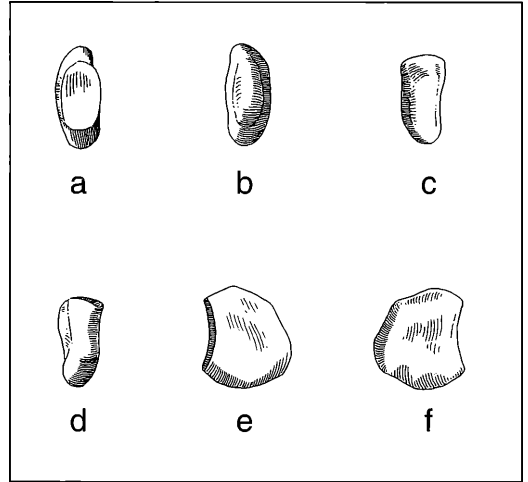


Figure 6.16.1. Sesamoidea of Distal Metacarpale II (Abaxial element): a. dorsal aspect; b. palmar aspect; c. proximal aspect; d. distal aspect; e. lateral aspect; f. medial aspect (x 1,0).

ure, as well as the three preceding ones, depict the plate-like morphology of the sesamoid, quite in contrast to the counterpart of the sesama bina contours.

Lateral aspect (fig. 6.16.1e): The slightly convex and smooth surface of the flexoria facies (6; similar to that of the central sesamoids) dominates this aspect. The small (2') facet is somewhat indistinct, but is separated from a large (2'') facet by a sharp crest.

Medial aspect (fig. 6.16.1f): Feature (5), the large interosseus facet, is slightly concave and finely roughened. This sesamoid would appear to be positioned to transfer energy through muscular, tendinous and ligamentous components along the medial (adaxial) border of MC II. By this means, the sesamoid's joint facet (2') covers only a portion of MC II's articular facet. There would appear to be no necessity for the lateral (adaxial) half to have a bony reinforcement. This implies the reduction of the respective portion of the musculus osseus and the lateral flexoria of MC II. Perhaps these elements were bound by fibrocartilage. One should expect a much smaller, still more reduced lateral (adaxial) element as known from other Höwenegg skeletons. But this bone is not preserved from this digit of the A-skeleton. Its absence may either be due to its evolutionary or postdepositional loss. If actually present, its size and morphology may be similar to the abaxial sesamoid of the MC IV (fig. 6.19.1a-f).

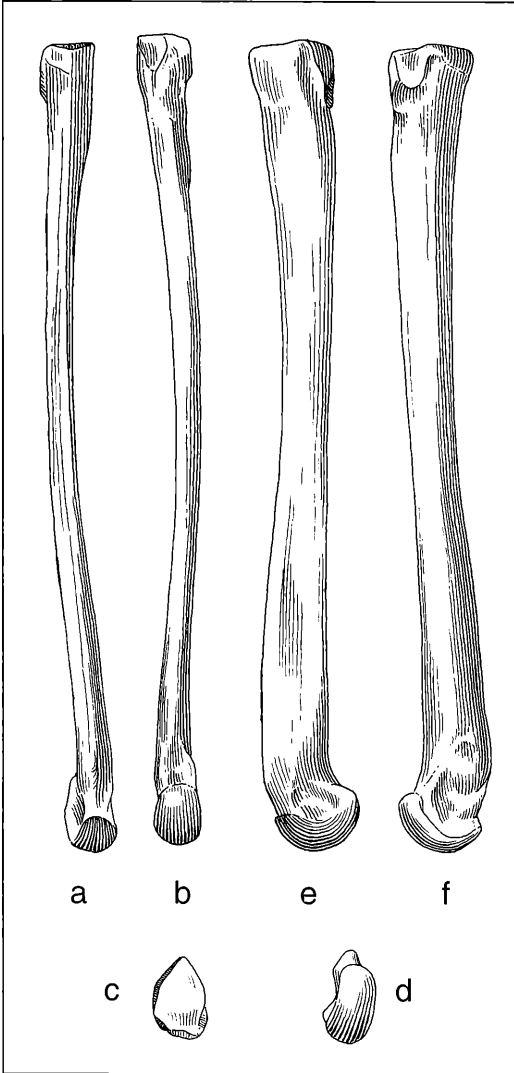


Figure 6.17.1. Metacarpale IV: a. cranial aspect; b. caudal aspect; c. proximal aspect; d. distal aspect; e. lateral aspect; f. medial aspect (x 0,55).

6.18 Metacarpale IV (fig. 6.17.1 a-f)

There are 21 MC IV's, mostly belonging to the articulated skeletons with both right and left elements present.

Cranial aspect (fig. 6.17.1a): This aspect is dominated by a sharp ridge coursing the length of the diaphysis (1). The proximal surface has three articular facets: the articular facet for the unciforme (4); the proximocranial (5) and proximomedial (6) articular facets for MC III. The distal articular area (7) presents the distal articular surface (7'), and the medial ligamentous depression (11). The lateral border (2) is smooth, with only the proximolateral aspect (12') having a roughened, convex surface for attachment of the ligamentum collaterale carpi laterale. The medial wall (3) is bipartite along the course of the diaphysis. One-third distally along the shaft is the roughened surface for interosseous articulation with MC III (3'). The caudal portion of the medial wall (3'') is smooth (fig. 6.17.1f).

Caudal aspect (fig. 6.17.1b): This aspect again presents the lateral (2) and medial (3) diaphyseal walls. A large triangular facet for articulation of MC V (10) is found proximally. This facet varies in size and outline within the Höwenegg sample, most having a transversely rectangular shape. The distal articular region (7) features the vestige of the crista sagittalis (7''), and the lateral (8) and medial (8') crests on either side of a distal fovea (7'''). Within the distal fovea (7''') there is a minute central ridge (9). Nearly all MC IV's presented broader distocaudal aspects and more faintly expressed crista than found in MC II's of the same individual. Note that features (7''') and (9) are not so well developed on this specimen as it is in other Höwenegg individuals. Features (7''), (7'''), (8), (8') and (9) are vestiges of the more primitive equid joint architecture as it is still represented in the distal MC III.

Proximal aspect (fig. 6.17.1c): This aspect is dominated by the articular facet for the unciforme (4). The cranial longitudinal ridge (1) is sharp. The borders for the proximocranial (5) and proximomedial (6) facets for articulation with MC III, as well as the articular facet with MC V (10) and the bulbous lateral ligamentous attachment (12') are present in this view. Whereas the proximal MC II has a triangular outline, the MC IV has a subpentangular outline.

Table 6.15. Summary Statistics on Metacarpale IV

Measurement	Sample size	Mean	Standard Deviation	Confidence Limits		Coefficient of Variation	Confidence Limits			Minimum	Maximum	Median
m1	6	189,80	3,55	186,81	192,79	1,87	0,76	2,99	183,40	193,00	190,90	
m2	10	11,06	0,70	10,60	11,52	6,37	3,42	9,32	10,10	12,50	11,05	
m3	12	18,98	1,12	18,32	19,65	5,87	3,39	8,36	16,50	20,50	19,30	
m4	12	14,51	1,20	13,79	15,23	8,29	4,78	11,81	12,30	16,30	14,20	
m5	9	11,16	0,25	10,99	11,32	2,20	1,13	3,27	10,80	11,60	11,20	
m6	9	19,82	0,44	19,52	20,13	2,22	1,14	3,31	19,10	20,40	19,90	

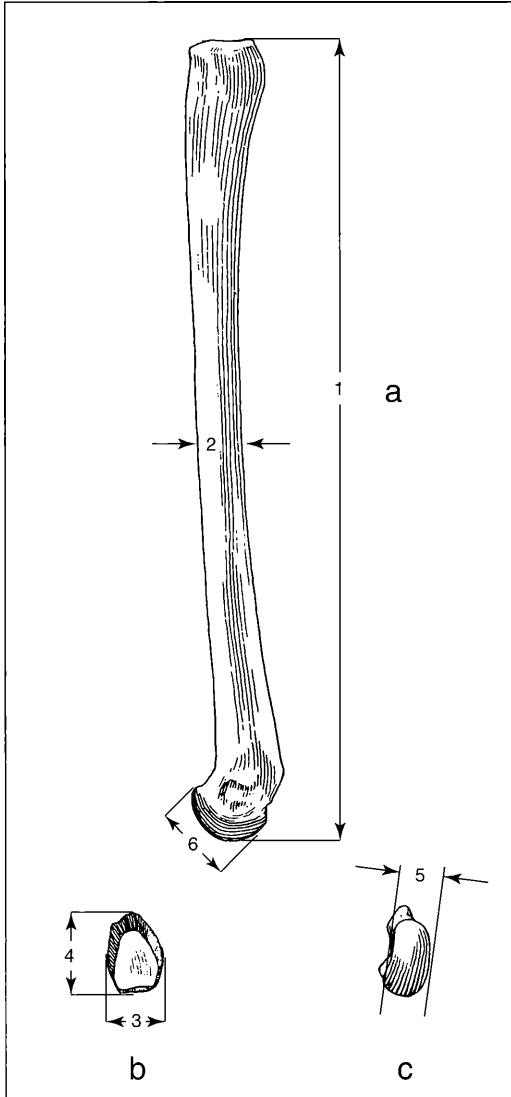


Figure 6.17.2. Measurements on the Metacarpale IV: a. medial aspect; b. proximal aspect; c. distal aspect.

Distal aspect (fig. 6.17.1d): The distal aspect is dominated by the joint articular surface (7'). Proximocranially is the processus supraarticularis (13). The remnant of the crista sagittalis (7''), the medial crest (8') and medial ligamentous depression can also be distinguished in this aspect.

Lateral aspect (fig. 6.17.1e): The proximal end of this aspect clearly distinguishes the bulbous ligamentous attachment (12'), the elongated area for ligamentous attachment (12''), and the crista (12''') separating fea-

tures (12') and (12''). Also apparent is the facet for articulation with MC V (10), and more distally, the smooth lateral wall (2). Distally, features (7), (7') and (13) are presented as discussed earlier. The distal articular limit is dominated by the circular lateral depression for the ligamentum collaterale (14).

Medial aspect (fig. 6.17.1f): Proximally this aspect clearly presents the proximocranial (5) and proximo-medial (6) articular surfaces for MC III. Both the roughened (3') and smooth (3'') surface of this aspect are clearly demonstrated. Features (7'), (11) and (13) of the distal articular region (7) are as described above.

Characteristic features of the MC IV: Included are: a large facet for MC V (10); the pentangular outline of the unciforme facet (4); the structure of the fossa with its medial ridge, proximal to the distal articular facet (features 7''', 8, 8', 9); the remnant crista sagittalis on the caudalmost limit of the distal facet (7''); the different habitus of the lateral and medial depressions (14, 11) for the collateral ligaments.

Statistical Results

There were 6 variables measured for 21 MC IV's, 12 of which were statistically analysed. The coefficient of variation was below 10 for all measurements. There were only two significant correlations, again both at the 95 %-99 % level of probability: m4-m5 and m1-m5. This bone is virtually identical in morphology to MC II so that differences in their statistical results is best considered to be random.

6.19 Sesamoidea of Distal Metacarpale IV (fig. 6.18.1)

There are two coosified sesamoids, a larger one (abaxial in reference to the MC III-axis) and a smaller one (adaxial) (fig. 6.18.2). In the following text both sesamoids are described together, whereby a'' indicates the abaxial (larger), and a''' the adaxial (smaller) sesamoid.

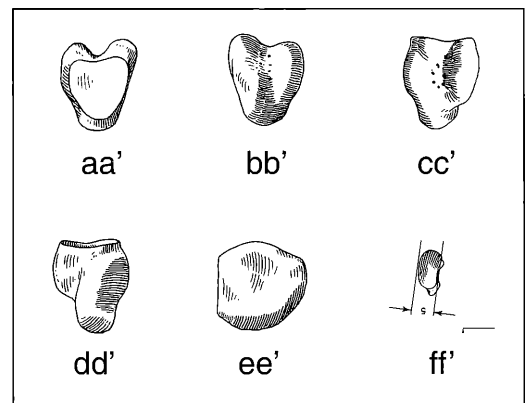


Figure 6.18.1. Sesamoidea of the Distal Metacarpale IV: aa'. dorsal aspect; bb'. palmar aspect; cc'. proximal aspect; dd'. distal aspect; ee'. lateral aspect; ff'. medial aspect (x 1,0).

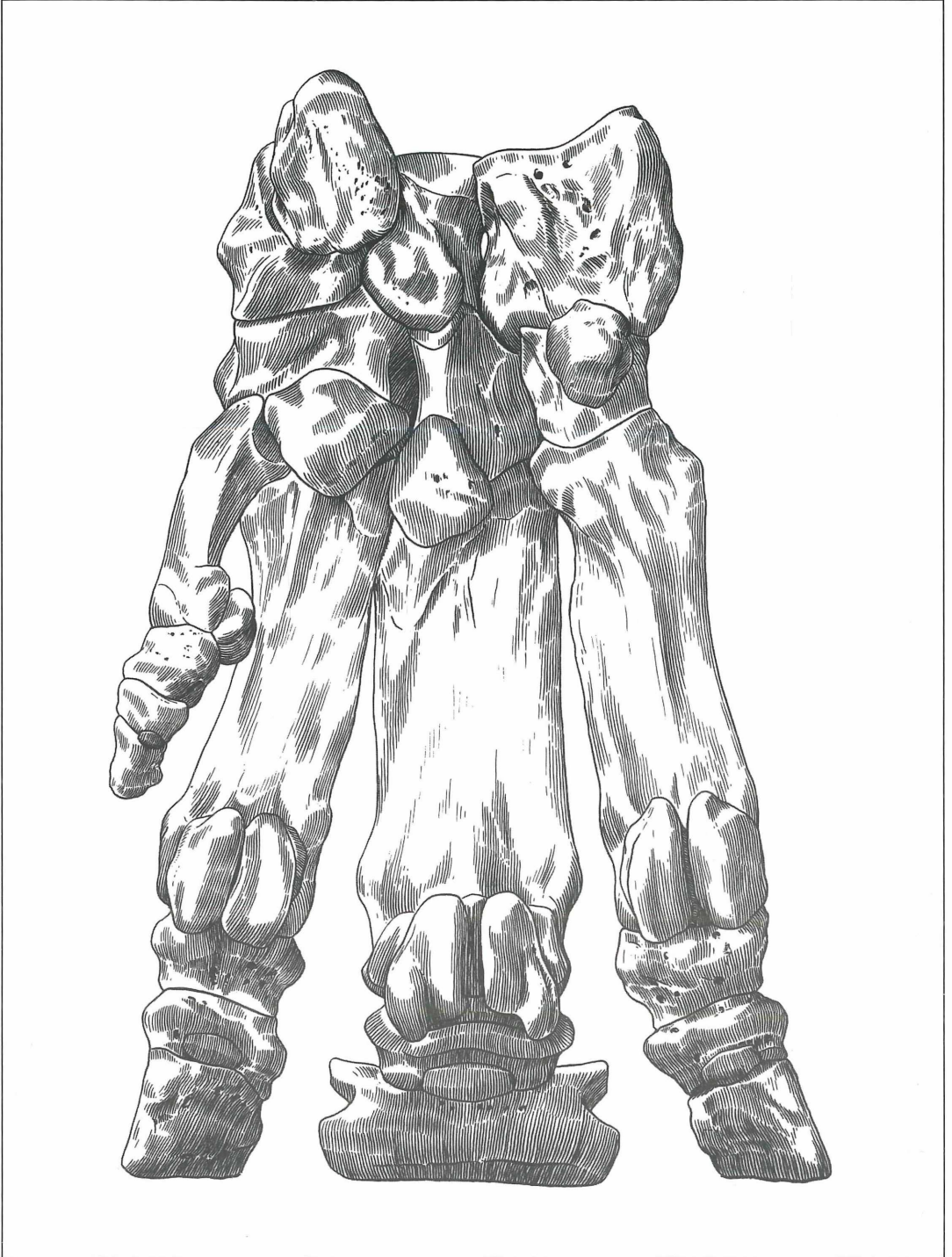


Figure 6.19.1. Manus, Plantar View of Höwenegg Rhinocerotid, *Aceratherium* (x 0,6837).

Dorsal aspect (fig. 16.18.1aa'): Feature (a1) is the apex of the abaxial sesamoid, and (a'1) is the apex of the adaxial sesamoid. The larger (a2) and the smaller (a'2) features are the joint facets shared between the two sesamoidea and the MC IV's distal joint. The dotted line (x) is the smooth coossification suture of the two sesamoidea. Feature (aba' = ab + a'b) represents the proximal suture. Its depression corresponds to a sulcus which separates the two sesamoidea. Feature (a3) represents the basis of the larger and (a'3) of the smaller sesamoidea. Feature (a'4) is the adaxial facies and (a5) abaxial facies for the interosseous tendon.

Palmar aspect (fig. 6.18.1bb'): This aspect is dominated by a central depression caused by the ossification structure (aba'). The darkened spots on either side of the suture are large pori which were produced during ossification. Features (a7) and (a'8) represent the walls of the sulcus: the former being the abaxial facies for the musculus flexorius, and the later (a'8) being the adaxial facies for the same. The sulcus itself housed a deep flexor tendon. Features (a5) and (a'4) are the corresponding facies of the interosseus tendons. The size difference between the two sesamoids is well demonstrated by their differing (a1-a3 versus shorter a'1-a'3) dimensions.

Proximal aspect (fig. 6.18.1cc'): Features (a2 and a'2) represent the proximal edge of the wear surface. Features (a7) and (a'8) are the walls of the facies for the musculi flexoria, which are subdivided by the ossified suture (aba'). Features (a3, a'3) represent the distal ends ("basis") of the two sesamoidea. They are very narrow, and contrast strikingly with the broad and massive basis of the central sesamoids.

Distal aspect (fig. 6.18.1dd'): This aspect presents many of the same morphological details as found in Figure 6.18.1c, c'. The abaxial facet for attachment of the large sesamoid's interosseus tendon is transected by the wear facet (a2). There is a bony swelling (a5') at the distal limit of the interosseus facet. This feature represents the homologous remnant of the prominent central facies interossea crest.

Abaxial and adaxial aspects (fig. 6.18.1ee', ff'): These aspects clearly present the size differences, outlines and plate habitus of the two MC IV sesamoidea.

Some differences are apparent between the MC II and MC IV sesamoids: the MC II specimens are larger, their interosseus facies are porous and slightly concave, the flexor facies are still somewhat bulbous and more similar to the central sesamoid structures. These details have nearly disappeared on the large MC IV sesamoid. A direct comparison of the smaller sesamoids is not possible.

The Höwenegg hipparion has been previously demonstrated to be, for the most part, a functionally monodactyl horse (TOBIEN, 1968). When comparing its sesamoid complex (2 central sesamoids plus 2 x 2 side sesamoids) with that of a functionally tridactyl perisso-

dactyl, such as the Höwenegg rhinocerotid, *Aceratherium*, (HÜNERMANN 1989: fig. 80, 82; here fig. 6.19.1), we observe that digit III of the Höwenegg hipparion (and later Old World hipparionine horses), have central sesamoids which hypertrophy. This hypertrophy was accompanied by the reduced function of digits II and IV. The evolution of this complex must be found in the ancestors of Old World hipparionines.

6.20 Proximal Sesamoid Bones of Metacarpale II and IV

The proximal MC II and MC IV each have a simple sesamoid bone. These both have a cranial facet. Each sesamoid has a flattened adaxial and a convex abaxial surface. Further description and illustration is unwarranted.

6.21 Metacarpal V (fig. 6.20.1a-f)

One of the rarest osteological elements found in hipparionine horses is the metacarpale V. The articulation of this small bone with the MC IV's and the carpus itself is very slight. During deposition and fossilisation this bone was undoubtedly very quickly disarticulated and lost. HENSEL (1860: 64, pl. 2, fig. 4, 8, 9) was the first to describe an articulated MC V from a Pikermi hipparion limb. GROMOVA (1955: 188, fig. 44g) figured an MC V complete with facets for articulation with the MC IV and the unciforme. SONDAAR (1968: fig. 5B) figured an MC V of the American hipparionine *Neohipparion floresi*, but this specimen lacked an unciforme facet. ZHEGALLO (1978: fig. 27) figured an unciforme of his Mongolian representatives of *Hippion theobaldi* which had a large articular facet for the MC V.

The general outline of the Höwenegg MC V is ovoid in both cranial and caudal aspects (fig. 6.20.1a, b). The proximal border is truncated, and the distolateral border is somewhat pointed. The bone exhibits considerable morphological variability, especially in its distal aspect, as would be expected in a vestigial element.

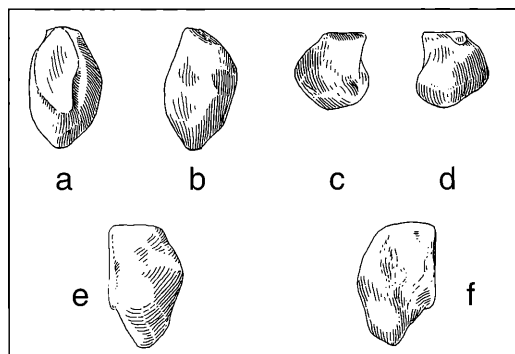


Figure 6.20.1. Metacarpale V: a. cranial aspect; b. caudal aspect; c. proximal aspect; d. distal aspect; e. lateral aspect; f. medial aspect (x 1,0).

The figured specimen (from the Hö A skeleton) is small and short, with the proximal articular facet for MC IV (1) occupying nearly 2/3rds the maximum length (16.7 mm). Other specimens, such as those belonging to the E-skeleton, have a greater length (21.5 mm) with an accentuated length distal to the facet.

Cranial aspect (fig. 6.20.1a): The MC IV facet (1) is proximodistally elongated here, and has an elongated oval contour. In other Höwenegg specimens this element has a shorter oval contour. The lateral wall (2) is bulbous, while the medial wall (3) is flatter. The caput (4) is flattened while the distal limit (5) is pointed.

Caudal aspect (fig. 6.20.1b): The caudal surface (6) is strongly vaulted and has an uneven contour. The caput (4) is inclined against a crest, which courses distally to the medial aspect of the bone.

Proximal aspect (fig. 6.20.1c): Features (2), (3) and (6) are as in figures 6.20.1a, b. Feature (1) represents the profile of the articular facet.

Distal aspect (fig. 6.20.1d): Feature (1') is the distal extension of the MC IV facet (1), which extends somewhat onto the lateral wall (2).

Lateral aspect (fig. 6.20.1e): This aspect depicts the dominance of the facet for the MC IV (1).

Medial aspect (fig. 6.20.1f): The medial wall (3) has a concavity surrounded by an irregular roughened surface (especially in the proximal part). Larger elements belonging to other skeletons (i.e. Hö T, E, III etc.) have a flatter depression. This depression would appear to be a site for ligamentous attachment.

Characteristic features of the MC V: Included are: The persistence of a large MC IV facet; the variable size and morphology of the bone.

As has been reported by earlier authors (GROMOVA, 1955, SONDAAR, 1967, ZHEGALLO, 1978), there sometimes exists an extra articular facet for the unciforme. A majority of the Höwenegg MC V's have this facet placed adjacent to the MC IV facet (1). The unciforme facet varies in size from being as little as a few square mm to more than 20 square mm (re: T-skeleton) in area. In the case where a pair of MC V's are known from a single individual, the unciforme facet is uniform in size and morphology. In the Höwenegg A skeleton the articular facet is missing in both the left and right elements.

6.22 Anterior 1st Phalanx III (fig. 6.21.1 a-f)

There are 19 specimens, left and right, all from the articulated skeletons. CAMP & SMITH'S (1942) work demonstrated that there are considerable differences between tridactyl horses (including hipparion) and *Equus* in the middle phalanges ligamentous and tendinous structures. In our description below, note that we replace cranial and caudal with dorsal and palmar, as is appropriate for the feet.

Dorsal aspect (fig. 6.21.1a): This aspect presents a smooth surface. Features (1) and (1') represent the

medial and lateral portions of the articular facet, respectively. There is a deep v-shaped groove at the palmar border (1'') for the articulation of the trochlea metacarpi's crista sagittalis. On the proximal border there is a narrow (2 mm), mediolaterally directed furrow (2), which marks the border of the dorsal attachment for the proximal articular cartilage (1, 1'). Just distally and along the sagittal plane, there is a distinct swelling with some delicate, vertically oriented furrows (3). ZHEGALLO (1978: fig. 39B) identified this feature (3) as the attachment site for the tendo extensor digitorum communis in extant *Equus*. In all actuality, the living horse has no direct attachment between this muscle and phalanx 1. However, the tendon is intimately united with the proximal 1st phalanx's joint capsular ligaments (NICHEL et al. fig. 453: 2, 2'; fig. 456: 3, and p. 386), and this we believe to be the function of this swelling. Distally are located the distal joint articular facet (4), and the attachment sites for the medial and lateral ligamenta collateralia (5). Superior to (5) are the tuberositas for attachment of the flexor digitalis superficialis (6; seu sublimis, seu perforatus = "perforatus scar" in CAMP & SMITH 1942: fig. 2, 3, 11).

Palmar aspect (fig. 6.21.1b): As with the previous aspect, (1) and (1') represent the medial and lateral aspects of the proximal articular facet. The palmar border has an incision for articulation of the crista sagittalis of the trochlea metacarpi (1''); it is presented here as a distinct V-shaped feature. The proximomedial and proximolateral surfaces have distinct attachment sites for the ligamentum collateralale of the fetlock joint (8). Feature (9) is the "V"-shaped attachment site for the ligamentum sesamoideum obliquum; the "V"-shaped feature (9') is the triangular-shaped groove immediately proximal to (9). The ligamentum sesamoideum centrale is connected proximally with (9), and distally with a somewhat roughened area (10). CAMP & SMITH (1942: figs. 24-28) have suggested that *Merychippus* does not have the ligamentum sesamoideum obliquum connected with the V-scar. Distally are located the distal joint facet (4), and a small (5 mm) elevated rugosity (4') situated along the sagittal plane. Attachment sites for the medial and lateral collateral ligaments (5) are clearly presented in this view, as are the profiles of the attachment sites for the tendon of the flexor digitalis superficialis (6). Proximal to (6) are located the scars for the ligamentum laterale volare (7). Note that features (5): (10) follow CAMP & SMITH (1942: figs. 24-29).

Proximal aspect (fig. 6.21.1c): This aspect demonstrates that the lateral outline (1') is larger than the medial one (1). The incision of the crista sagittalis groove (1'') is located just medial to the mid-palmar border, and the dorsopalmar groove for the MC III crista sagittalis (1''') is located just here. The profile of the deep internal V-scar (9') is situated on the palmar aspect of the mid-plane. Feature (3') represents one of the larger furrows of the dorsal proximal elevation (3 of fig. 6.21.1a).

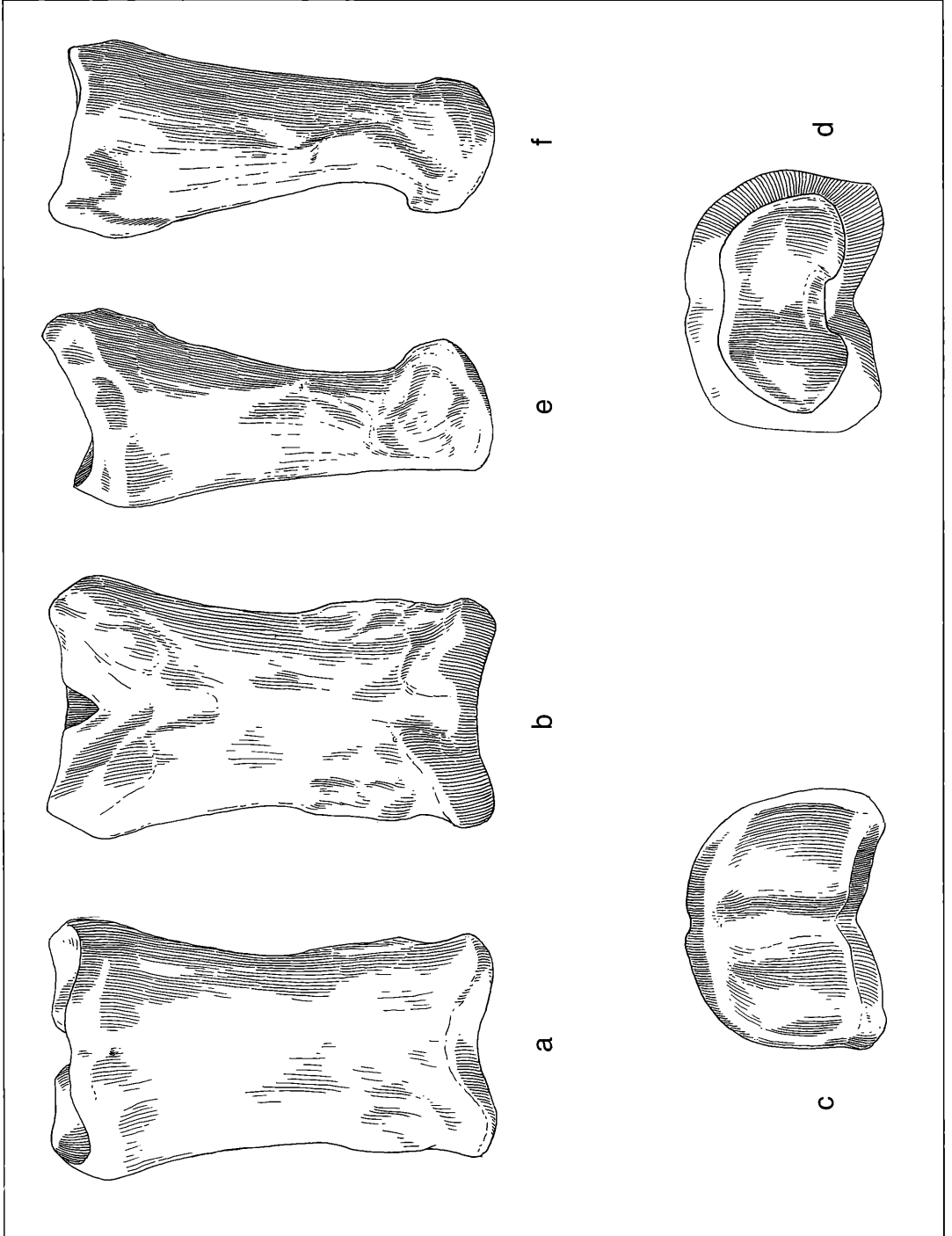


Figure 6.21.1. Anterior 1st Phalanx III: a. dorsal aspect; b. palmar aspect; c. proximal aspect; d. distal aspect; e. lateral aspect; f. medial aspect (x 1,0).

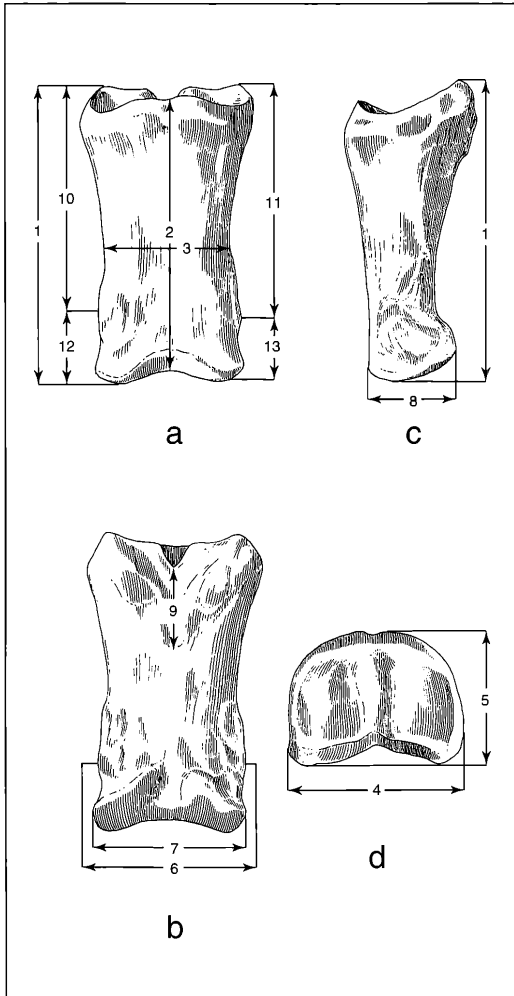


Figure 6.21.2. Measurements on Anterior 1st Phalanx III: a. dorsal aspect; b. palmar aspect; c. lateral aspect; d. proximal aspect (m10- m13 not given in table 6.16).

Distal aspect (fig. 6.21.1d): This aspect is dominated by the convex articular joint facet (4) which articulates with the 2nd phalanx III. The dorsopalmar groove (4'') separates the distal articular facet into medial and lateral elevations (4'''); see also fig. 6.22.1b: 4). A saddle-shaped joint (pastern) is formed at this articular surface (4) together with the inverse surface of the 2nd phalanx II. In extant *Equus*, this joint functions for flexion, extension and a slight degree of rotation and abduction/adduction. This contrasts sharply with the metacarpal III – 1st phalanx III (fetlock) joint which is a ginglymus (hinge joint), allowing only flexion and extension along the long axis. The metacarpal III's crista

sagittalis articulation with the 1st phalanx III's proximal incision functions as a locking mechanism for the ginglymus. Extant *Equus* has a more developed locking mechanism of the pastern joint than the Höwenegg horse, and can only slightly abduct at this joint surface during extreme flexion. As in other hipparion, the cranio-proximal end of the MC III crista sagittalis is distinctly flattened (fig. 6.14.2), and the corresponding groove of anterior 1st phalanx III is shallower than in extant *Equus*. This would imply a greater ability to abduct/adduct this joint. Feature (4') marks the rugosity in the incision between the medial and lateral elevations (4''') of the distal articular facet (4). The proximal bony swelling (3) and attachment surface for the ligamentum collaterale of the fetlock joint (8) are as in figures 6.22.1a and 6.22.1b, respectively.

Lateral aspect (fig. 6.21.1e): The lateral portion of the proximal articular facet (1'), the attachment surfaces for the lateral collateral ligament (5), for the tendo flexor digitalis superficialis (6), ligamentum laterale volare (7) and ligamentum collaterale of the fetlock joint (8) are as in figure 6.21.2. Proximal to (7) there is a 6 mm wide, 16 mm long furrow (11) which courses in an oblique proximodorsal to distopalmar direction. A similar, shorter and more weakly developed groove is found on the medial aspect (fig. 6.21.1f: 11'). Neither of these features have a roughened surface, and therefore are not likely scars either for ligamentous or tendinous attachment. They may mark the course of some larger neural or vascular structures.

Medial aspect (fig. 6.21.1f): Features (1) and (5) and (9) are as in figures 6.21.1b and 6.21.1e. Feature (4''') marks the proximal medial termination of the distal articular facet.

Characteristic features of the anterior 1st phalanx III: Included are: the subequal area and peripheral outline of the medial (1) and lateral (1') portions of the proximal articular surface; the proximal bulge on the dorsal wall (? attachment for the tendo extensor digitorum communis; the ligamentum sesamoideum centrale, 10), connected with the V-scar (9); compared to extant *Equus*, the relatively strong development of the perforatus scar (6) and the ligamentum laterale volare (7); the rugose surface within the palmar incision of the distal facet (4'); presence of a pair of flat, oblique grooves on the lateral and medial surfaces (11, 11').

Statistical Results

There were 9 variables measured for 19 specimens of anterior 1st phalanx III, 12 of which were statistically analysed. CV's were above 10 for 3 of the measurements: m7 (CV = 22.44), m8 (CV = 18.00) and m9 (CV = 25.83). There were 7 significant correlations, only one being at or above the 99 % level: m7-m9. Measurement 7 (distal articular breadth) was negatively correlated with m9 (minimal length of trigonum phalangis) suggesting that more gracile specimens had equally long, or perhaps even longer trigonum phalangis di-

Table 6.16. Summary Statistics on Anterior 1st Phalanges III

Measurement	Sample size	Mean	Standard Deviation	Confidence Limits	Coefficient of Variation	Confidence Limits	Minimum	Maximum	Median
m1	11	63,78	2,36	62,32 65,25	3,69	2,07 5,32	59,50	67,20	63,90
m2	12	60,18	1,89	59,06 61,31	3,13	1,81 4,45	57,50	63,40	60,25
m3	12	29,10	1,47	28,22 29,98	5,05	2,92 7,19	27,10	31,20	28,95
m4	11	40,85	1,86	39,69 42,00	4,54	2,54 6,55	36,40	43,20	41,20
m5	11	30,98	1,44	30,08 31,88	4,65	2,60 6,71	29,00	33,20	31,00
m6	12	33,75	1,62	32,79 34,71	4,79	2,77 6,81	31,60	36,40	33,60
m7	12	29,02	6,51	25,14 32,90	22,44	12,52 32,36	18,30	35,00	33,00
m8	10	22,77	4,10	20,09 25,45	18,00	9,43 26,58	19,00	31,20	21,00
m9	12	26,46	6,83	22,39 30,53	25,83	14,25 37,42	17,00	35,50	26,05

mensions. Measurement 7 was also negatively correlated with m4 (proximal breadth); the nature of this correlation is odd, but probably attributable to the same reason as the prior explanation given. Measurement 1 (maximum length) was correlated with anterior length (m2) and minimal (midshaft) breadth (m3). Anterior length (m2) and distal articular breadth (m8) were also found to be both correlated with m3.

6.23 Anterior 2nd Phalanx III (fig 6.22.1a-f):

There are 15 specimens, left and right, all from the articulated skeletons. In many features, the second phalanx resembles the first, but is only 1/2 the length. It is flattened dorsopalmarly, and the proximal width is nearly the same as the maximum length. In extant *Equus* these proportions are exaggerated to such an extent that the proximal mediolateral width is greater than the dorsopalmar length.

Dorsal aspect (fig. 6.22.1a): The bone's central aspect is convex and smooth in this view. It is broad proximally, becomes transversely constricted medially, and broadens again distally. The proximal articular facet (1) is inclined dorsally and divided into medial and lateral portions (1') by a rounded median ridge (1'') which articulates with the 1st phalanx III's trochlea (1''' of fig. 6.22.1c). The dorsal border is elevated (1''') to form the processus extensorius, which serves as the attachment site for a portion of the musculus extensor digitalis communis. Feature (2) represents the medial and lateral scars for attachment of the ligamentum collaterale of the phalanx 1/phalanx 2 digit III joint. The distal aspect presents the medial and lateral hollowed scars for attachment of the ligamentum collaterale (3) which binds the 2nd and 3rd phalanx III. The distal articular facet (4), as well as its proximal border (4'), are clearly seen in this aspect.

Palmar aspect (fig. 6.22.1b): Feature (2) is as in figure 6.22.1a. The distal articular facet's (4) palmar aspect is greater than its dorsal one (fig. 6.22.1a), and presents a shallow V-shaped distally directed depres-

sion (4''). Just proximal to this feature is a broad, rugose surface (5) which is the site of insertion for the tendo flexor digitorum profundus (perforans) (NICHEL et al., 1986: fig. 324: 6'). The transverse prominence for the "flexor tuberosity" (6; = "fibrocartilaginous plate" of CAMP & SMITH 1942: pl. 9, figs. D and I of *Merychippus*) includes an area for attachment of the ligamentum sesamoideum rectum (6'), a medial and lateral area for attachment of the tendo flexor digitorum profundus (6''), and a medial and lateral area for attachment of the ligamentum laterale volare (6''').

Proximal aspect (fig. 6.22.1c): This aspect is dominated by the proximal articular facet (1), its medial and lateral halves (1'), midsagittal ridge (1''), and dorsal border (1'''). Feature (6') represents the apex of the palmar border, and the attachment surface for the ligamentum sesamoideum rectum. Features (6''), (6''') and (2) are as in fig. 6.22.1b).

Distal aspect (fig. 6.22.1d): The distal articular facet (4), and its saddle-shape, dominates this view. The joint surface has subequally sized, and consistently different outlines of the medial and lateral elevations (4^{IV}), separated by a dorsopalmarly oriented depression (4'''). Feature (1) represents the peripheral outline of the broader proximal articular facet.

Lateral aspect (fig. 6.22.1e): The proximal aspect is dominated by the bulbous flexor tuberosity (6). Features (1'''), (2), (3), (4) and (6') are as in figs. 6.22.1a and b, in their lateral views. Feature (4') marks the proximal limit of (4).

Medial aspect (fig. 6.22.1f): The medial aspect is nearly the mirror-image of the lateral with regards to features (1'''), (2), (3), (4), (6) and (6').

Characteristic features of the anterior 2nd phalanx III: Included are: the proximal mediolateral width is nearly the same as the dorsopalmar length, whereas in extant *Equus* the width dimension is greater; the flexor tuberosity (6) is prominent; the different outlines of the distal articular surface's medial and lateral elevations (4^{IV}).

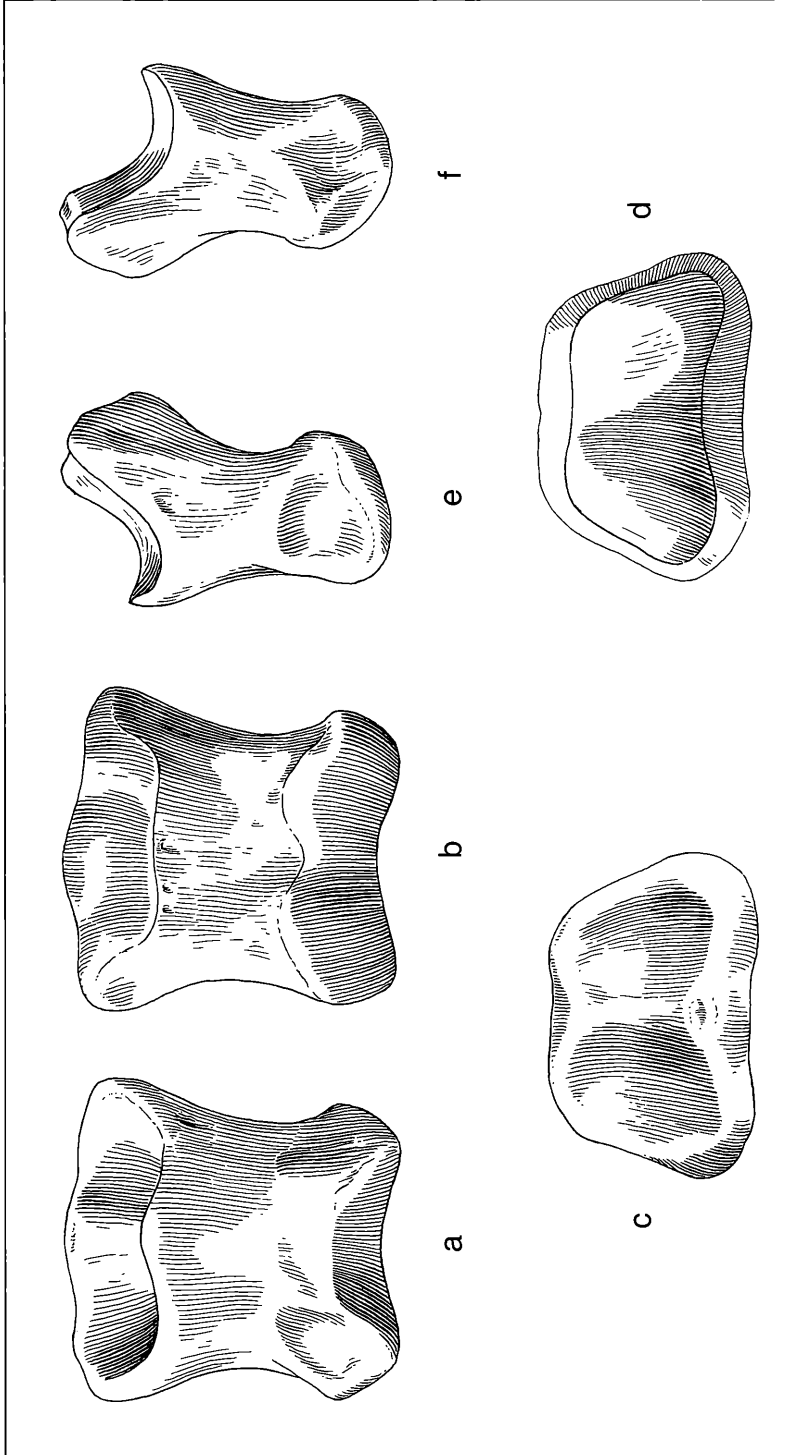


Figure 6.22.1. Anterior 2nd Phalanx III: a. dorsal aspect; b. palmar aspect; c. proximal aspect; d. distal aspect; e. lateral aspect; f. medial aspect (x 1,0).

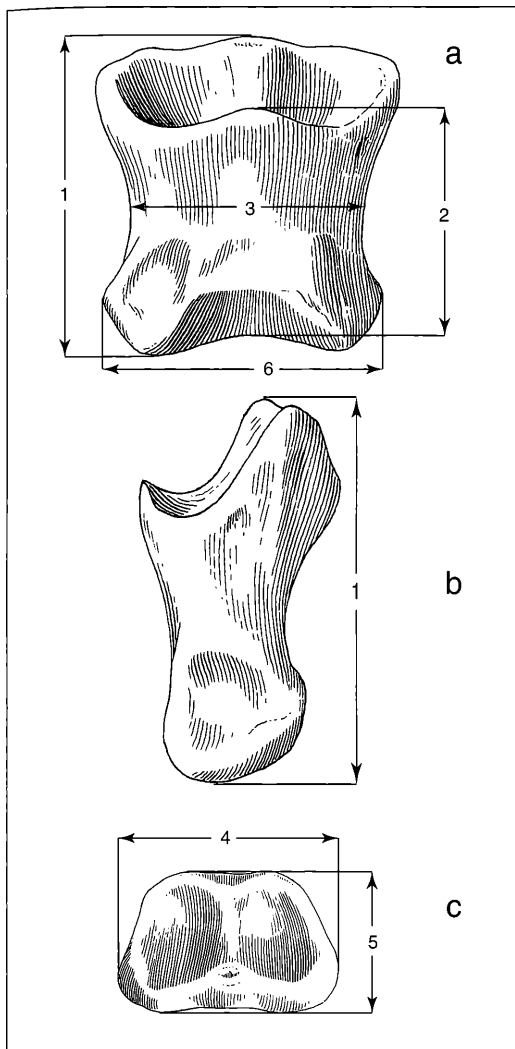


Figure 6.22.2. Measurements on Anterior 2nd Phalanx III: a. dorsal aspect; b. lateral aspect; c. proximal aspect.

Statistical Results

There were 6 variables measured for 15 specimens of anterior 2nd phalanx III, 11 of which were analysed. The coefficients of variation were below 10 for all measurements. There were 10 significant correlations, two being at the 99%+ level of correlation. The two length measurements m1 (maximum length) and m2 (anterior length) accounted for four of the correlations: m1-m2, m1-m4 (proximal maximal breadth), m2-m4 and m2-m3 (minimum midshaft breadth). Midshaft width (m3) was further correlated with m5 (proximal maximum depth), m4 (proximal maximum breadth) and m6 (distal articular maximum breadth). Proximal maximum depth (m5) was correlated with m4 and m6. Measurement 6 was further correlated with m4. The fact that all measurements significantly correlated with all other measurements reflects the metric stability of this bone.

6.24 Anterior 3rd Phalanx III (fig. 6.23.1a-f):

The bony anterior third phalanx III is tightly bound within a ligamentous and cartilaginous hoof capsule. In the living horse, as most probably in hipparionine horses, a plate of cartilage attaches to the distal angles of the bone on each side, and resides superiorly and anteriorly to the lower sesamoid. There are 13 anterior 3rd phalanges, from both the left and right sides. These elements are quite similar to the posterior 3rd phalanges III; their identification is made secure by virtue of their articulation with the complete skeletal sample.

Dorsal aspect (fig. 6.23.1a): In veterinarian anatomy the "parietal surface" (1) consists of not only the dorsal portion, but also the medial (1') and lateral (1'') surfaces. As in extant *Equus*, the dorsal surface is strongly convex, while the medial surface (1') is slightly steeper than the lateral one (1'') (see also the outline of the articular facet in proximal view; fig. 6.23.1c: 1'). The distal portion of (1) is strongly roughened and wrinkled (2) indicating attachment of the subcutaneous layer, which supports the third phalanx within the hoof capsule. Numerous foramina perforate the bone in this region, permitting the passage of blood vessels to the hoof. Adjacent and proximal to the wrinkled surface there is a sharp transition to a smoother parietal surface surface (2'). This boundary is more striking than found in extant *Equus*.

Table 6.17. Summary Statistics on Anterior 2nd Phalanges III

Measurement	Sample size	Mean	Standard Deviation	Confidence Limits		Coefficient of Variation	Confidence Limits		Minimum	Maximum	Median
m1	15	41,47	1,40	40,72	42,21	3,37	2,10	4,64	39,40	44,00	41,70
m2	15	32,85	1,24	32,19	33,51	3,78	2,35	5,20	30,50	35,20	32,60
m3	15	31,85	1,17	31,23	32,48	3,67	2,28	5,05	30,00	34,50	31,80
m4	14	42,04	1,54	41,19	42,89	3,67	2,24	5,11	39,50	44,50	41,75
m5	15	27,37	2,69	25,93	28,80	9,84	6,10	13,58	20,00	33,70	27,70
m6	14	36,49	2,45	35,13	37,84	6,73	4,09	9,36	30,20	41,00	36,55

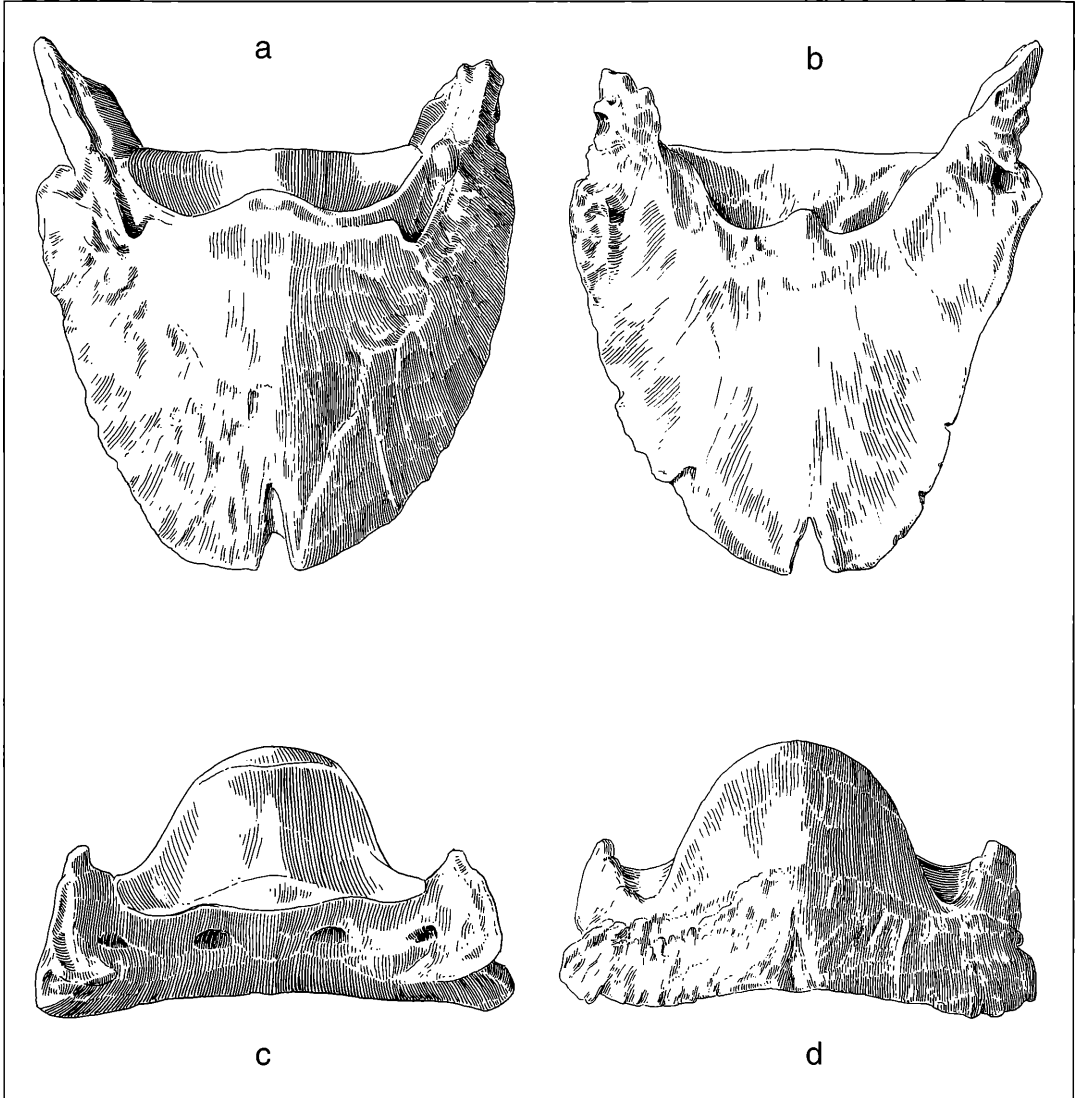


Figure 6.23.1. Anterior 3rd Phalanx III: a. dorsal aspect; b. palmar aspect; c. proximal aspect; d. distal aspect.

The parietal and articular surfaces (3) meet at the coronary border (3'). The latter is axially elevated to the extensor process (3''), on which inserts the *tendo extensor digitalis communis*. Distal to the coronary border (3') there is a medial and a lateral deep groove for attachment of the *ligamentum collaterale* binding phalanx 2 to phalanx 3 (3'''). Posterior to the articular facet, both medially and laterally, are the flat processes: *palmaris medialis* and *palmaris lateralis* (4). In extant *Equus* these processes are occasionally divided into proximal distal angles. The Höwenegg hipparion has a deep mid-

dorsal notch at the distal extent of the parietal surface, the *crena marginis solearis* (5). This structure is vestigial to absent in the extant horse, but common in fossil and some recent perissodactyls. The dorsal surface meets the palmar surface (or sole surface in veterinarian terminology) at a sharp angle, the *margo solearis* (6). **Palmar aspect** (fig. 6.23.1b): The sole surface is divided by the *linea semilunaris* (7) into the larger distal *planum cutaneum* (8), and the smaller proximal *facies flexoria* (9). The latter is dominated by a prominent central protuberance (9') for attachment of the

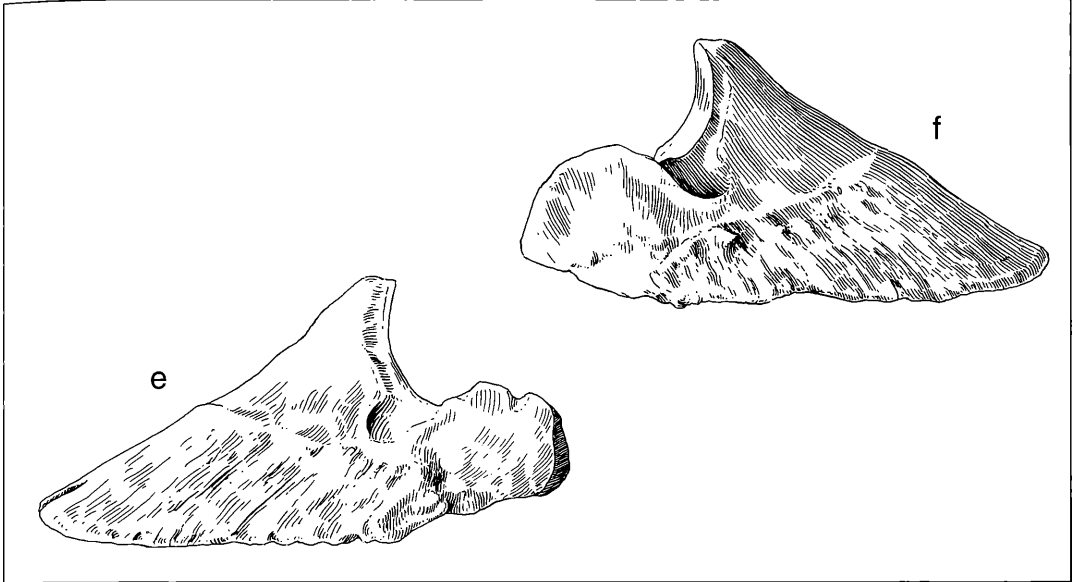


Figure 6.23.1. Anterior 3rd Phalanx III: e. lateral aspect; f. medial aspect (x 1,0).

flexor digitalis profundus tendon (= tendo perforans of CAMP & SMITH 1942: fig. 8, as well as earlier authors). The area of the deep flexor tendon is accompanied abaxially by two corresponding grooves: the sulcus solearis medialis and lateralis (10). Both continue into the foramen soleare mediale and laterale (11): most conspicuous features in proximal view (fig. 6.23.1c: 11). Both are openings of the internal canalis solearis. This branching canal system serves as the passage for neuro-vascular structures which supply the marginal portions of the parietal and sole surfaces.

Proximal aspect (fig. 6.23.1c): The articular facet (3) presents a median sagittal ridge (3), accompanied by a lateral and a medial fossa (3^v) and (3^w), respectively. This saddle-shaped feature makes the facet confluent with the trochlea of the second phalanx. The lateral fossa (3^v) is somewhat larger than the medial one (3^w). The lateral wall's (1^u) lower inclination than the medial wall (1^v; re: figs. 6.23.1a and c) reveals a certain asymmetry of the third phalanx: the lateral half being slightly larger than the medial one. The inverse can be seen for the first and second phalanx, whereby the medial portions are more strongly built than the lateral ones: phalanx 1 – 1 and 4^u medial; phalanx 2 – 1^v medial, 4^v medial. The same situation recurs also in the recent horse (ELLENBERGER-BAUM 1977: 138). Feature (12) is a small, transversely elongated articular facet for the distal sesamoid bone. Contralaterally are found the foramina solearia (11). Peripheral to these are two contralaterally disposed smaller openings, the foramina processus palmaris mediale et laterale (13). The fora-

mina open near the medial and lateral borders as well as the peripheral border of the sole, and continue as an open furrow, the sulcus parietalis medialis and lateralis (13'). The sulcus is rather indistinct in the Höwenegg hipparion, but well developed in the living horse (NICHEL et al., 1986: fig. 140: 23). The foramina and sulci serve for the passage of blood vessels. Feature (14) includes the medial and lateral furrows for the ligamentous attachment of the hoof cartilage (ligamenta chondrangularia collateralis medialis et lateralia).

Distal aspect (fig. 6.23.1d): The difference between the strongly wrinkled, slightly elevated portions (2) of the parietal surface against its smooth proximal portion (2') is particularly apparent in this aspect. For features (1', 1'', 3'', 3''', 4 and 5) see sections 6.23.1a, b above.

Lateral aspect (fig. 6.23.1e): Feature (13) is the foramen processus palmaris lateralis which is continuous anteriorly with the sulcus parietalis lateralis (13'). Features (1, 2', 3, 3'' and 3''') are as in figures 6.23.1a and b.

Medial aspect: (fig. 6.23.1f): Features (3, 3'', 3''', 4, 13 and 13') are as in the lateral aspect (fig. 6.23.1e). The processus palmaris medialis (4) supports a furrow for the medial portion of the cartilaginous plate.

Characteristic features of the anterior 3rd phalanx III: Included are: the sharp boundary between the wrinkled (2) and smooth (2') portion of the parietal surface; the well developed crena marginalis solearis (5); the pronounced mediolateral asymmetry (1'' versus 1'); the indistinct sulcus parietalis (13') on the lateral and medial walls.

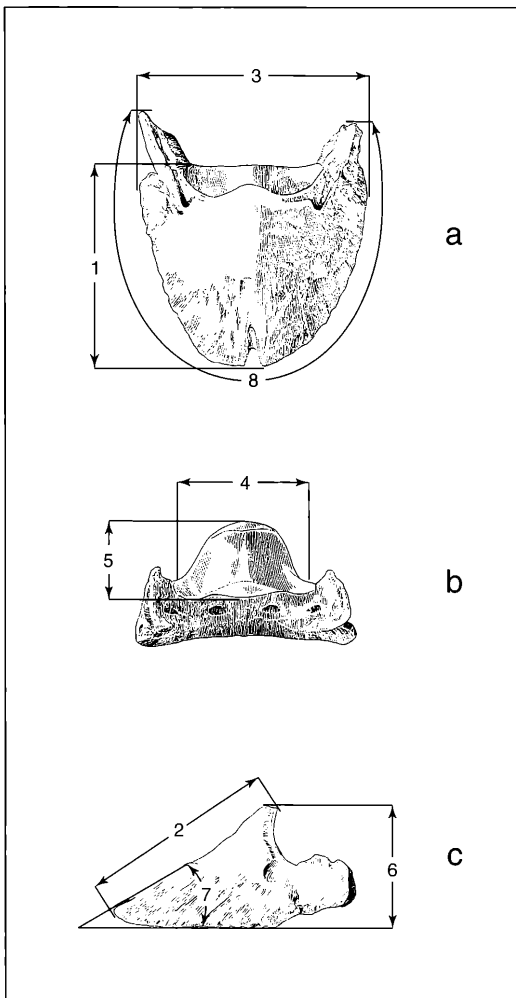


Figure 6.23.2. Measurements on Anterior 3rd Phalanx III: a. dorsal aspect; b. proximal aspect; c. lateral aspect.

Statistical Results

The phalanx for the hoof had 8 variables measured for 13 specimens, 10 of which were analysed. The coefficients of variation were below 10 for all measurements. There were 2 significant correlations, both at the 95 % level of significance: m5-m6 and m5-m7.

6.25 Distal Sesamoidea of Anterior Phalanx III (fig. 6.24.1)

The sesamoid (os sesamoideum distale) is articulated between phalanx 2 and 3 of digit III (re: fig. 6.31.1; see also NICKEL et al. 1986: fig. 140, 141). The sesamoid are elongate and transmit forces of the fetlock joint.

Dorsal aspect (fig. 6.24.1a): Feature (1) is the facies articularis with the second phalanx. It is transversely extended, has a central elevation (1') which articulates with the depression (4'') of the 2nd phalanx (fig. 6.22.2b). This facet (1) enlarges the articular surface of the third phalanx. The sesamoid and third phalanx articulate with a palmar facet (2) in figure 6.24.1d. Features (2) and (1) make a right angle with one another.

Palmar aspect (fig. 6.24.1b): Feature (5) includes the medially and laterally disposed attachment sites for the ligamenta sesamoidea collateralia medialis and lateralis. Feature (6) is the facies flexoria, occupying the whole palmar surface, and providing a gliding surface for the tendon of the deep flexor muscle ("scutum distale"). The facies flexoria is indistinctly subdivided by a proximodistally oriented central elevation (6'). Feature (7) is the straight border of the proximal side (= margo proximalis). Feature (8) is the convex border of the distal side (= margo distalis). It is united with the third phalanx by the strong ligamentum sesamoideum distale impar.

Proximal aspect (fig. 6.24.1c): The surface is slightly roughened and has a field of pori (fig. 6.24.1a: 4) near the margin and adjacent to the facies articularis (1) and the central elevation (1'). The pori are larger and deeper than in extant horses. The margo distalis (8) borders the facies flexoria with its central elevation (6). A limb of the deep digital flexor tendon inserts on the proximal facies (NICKEL et al. 1989: fig. 324: 6'; fig.456: 2').

Table 6.18. Summary Statistics on Anterior 3rd Phalanges III

Measurement	Sample size	Mean	Standard Deviation	Confidence Limits	Coefficient of Variation	Confidence Limits	Minimum	Maximum	Median
m1	6	57,38	1,84	55,84 58,93	3,20	1,29 5,11	55,50	60,10	56,85
m2	5	71,98	2,43	69,74 74,22	3,38	1,17 5,59	69,30	75,50	72,50
m3	0								
m4	5	61,34	5,96	55,83 66,85	9,72	3,32 16,13	54,00	70,00	62,00
m5	10	23,27	1,00	22,62 23,92	4,29	2,31 6,28	21,70	25,00	23,40
m6	8	41,05	2,52	39,21 42,89	6,15	2,96 9,33	38,00	45,00	40,65
m7	6	51,78	2,62	49,58 53,99	5,06	2,04 8,08	47,80	54,20	52,45
m8	2	165,00	7,07		4,29		160,00	170,00	165,00

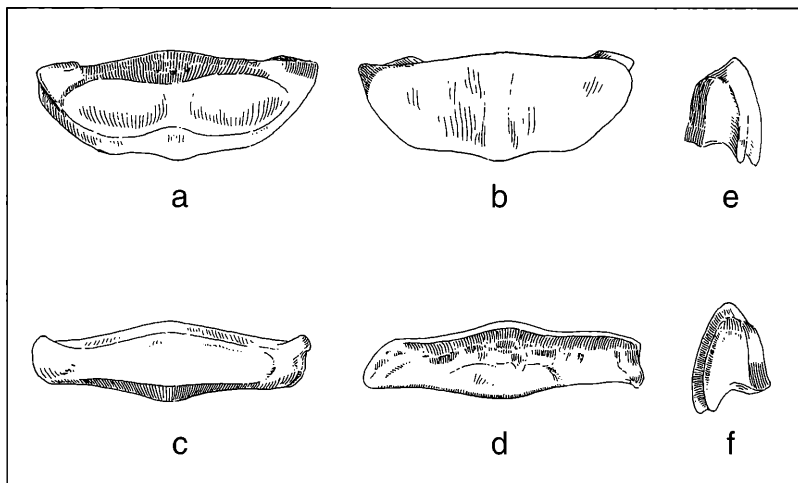


Figure 6.24.1. Distal Sesamoida of Anterior Phalanx III: a. dorsal aspect; b. palmar aspect; c. proximal aspect; d. distal aspect; e. lateral aspect; f. medial aspect (x 1,0).

Distal aspect (fig. 6.24.1d): Feature (2) is the articular facet for the distal phalanx. The facet has an ovoid outline, and contrasts with extant horses which have a narrower, more elongate facet. The resting surface (3) is roughened and has some flat, small pits. In extant horses there are instead deeper pits separated by dorsopalmarly oriented pillars (canales sesamoidales), which are in part filled by the interphalangeal joint's synovial fluid (HERTSCH & STEFFEN 1986: 353). Feature (8) is the margo distalis of the facies flexoria.

Lateral aspect (fig. 6.24.1e): This aspect presents a number of remarkable features: the margo distalis (8); the pitted distal surface (3); the facies articularis for the 2nd phalanx; the central elevation (1') of (1).

Medial aspect (fig. 6.24.1f): Feature (3) is as in fig. 6.24.1. The medial limit of this facies is broader than the lateral one (fig. 6.24.1e: 3). Feature (6) is the palmar facies flexoria and feature (1) is the facies articularis for the 2nd phalanx.

Characteristic features of the sesamoidum distale anterior: Included are: 1) the small ovoid joint facet for the 3rd phalanx, (2; compare the measurement of *Hippotherium* and *Equus*); 2) the absence of the canales sesamoidales on the distal bony surface.

GROMOVA (1955: 125) described the morphology and function of the Taraklia "*Hipparion*" moldavicum distal sesamoids. GABUNJA (1961: 122, 123) cited, but did not describe a number of hipparion sesama bina (28) and distal sesamoids (4) of a large hipparion from Kujalnik near Odessa. ZHEGALLO (1978: fig. 42) figured a distal sesamoid in dorsal and proximal aspects of "*Hipparion*" theobaldi mogoicum from the "Turolian" locality of Kirgis-Nur II, Outer Mongolia.

6.26 Anterior 1st Phalanx II (fig. 6.25.1a-f):

There are 15 1st phalanges of digit II, both the left and right sides, from the articulated skeletons. The first phalanx is elongate and transversely compressed. The abaxial wall is somewhat convex, while the adaxial wall is concave, and in marked contrast to the bilaterally symmetrical first phalanx III.

Dorsal aspect (fig. 6.25.1a): Feature (1) is the proximal joint facet for articulation with the distal facet of MC II. On the dorsal border there is a small prominence (1'), which is the site of insertion for an extensor tendon (TOBIEN 1953: pl. 3, fig. 1), most probably the tendo musculi extensor digitalis lateralis. This feature may be similar to that found on the main digit (III), where the tendon inserts on the dorsolateral side (NICKEL et al. 1986: fig. 453: 3'). Halfway along the bone's axis there is a marked constriction; distally the bone again enlarges mediolaterally. Feature (2) is the distal articular surface, revealing its characteristically rugose dorsal border.

Palmar aspect (fig. 6.25.1b): Similar to the V-scar on the 1st phalanx digit III (fig. 6.21.1b) is a comparable, but much more weakly developed feature, the trigonum phalangis proximalis (3). This feature is characterized as having two lightly-built V-shaped crests, separated by a shallow sulcus (3') for insertion of the ligamenta sesamoida obliqua (lateral and medial; see also TOBIEN 1953, pl. 3, fig. 3: Fbd.). There are no traces of a ligamentum sesamoidum rectum, which in extant *Equus* partially covers the two oblique sesamoidan ligaments. Halfway along the palmar wall is a small (5 mm), elongated and elevated scar (4), which may be as in the 1st phalanx III, the attachment site for the ligamentum sesamoidum centrale (re: reconstruction of CAMP & SMITH 1942: fig. 28, pl. 8, fig. O and P for *Merychippus* and *Pliohippus*, and fig. 29 for *Hippari-*

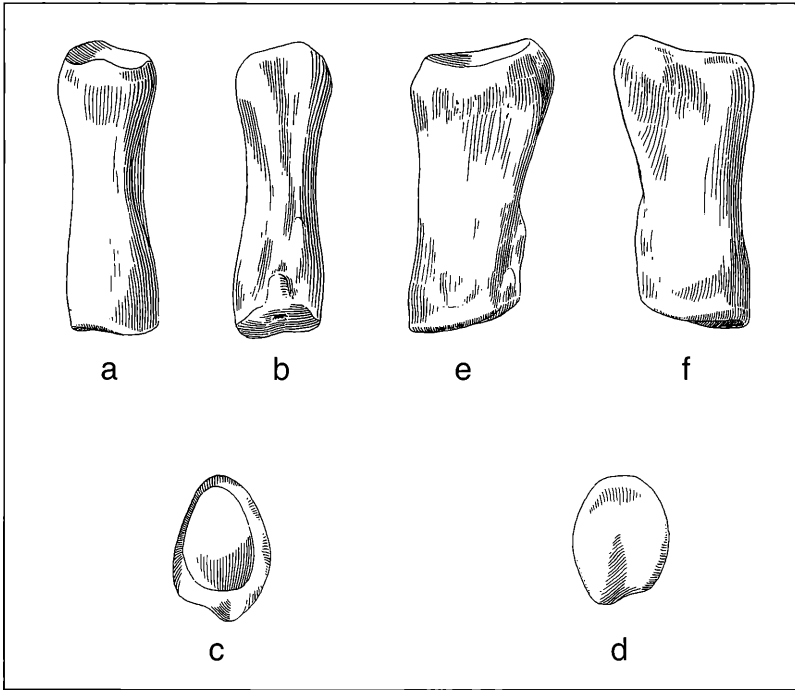


Figure 6.25.1. Anterior 1st Phalanx II: a. dorsal aspect; b. palmar aspect; c. proximal aspect; d. distal aspect; e. lateral aspect; f. medial aspect (x 1,0).

on). On the distal portion of the abaxial border there is a thick, proximodistally oriented tuberosity (5). In correspondence to the digit III phalanx, this tuberosity represents the insertion of the tendo flexor digitalis superficialis (seu musculus flexor digitorum sublimis, TOBIEN 1953: pl. 3, fig. 2; seu perforatus, CAMP & SMITH 1942: fig. 28), which is apparently united dorsally with the abaxial ligamentum laterale palmare (in CAMP & SMITH 1942: fig. 28: lateral volar ligament). The corresponding structure on the adaxial side (5') is shorter and reduced to a smaller crest. Just proximal to the distal articular facet (2), and in the depression between the two crests (5 and 5') is a small, but distinct tuberosity (4 x 5 mm; feature 6), which seems to have no correlative structure on the adjacent surface of 1st phalanx of digit III (fig. 6.21.1b).

Proximal aspect (fig. 6.25.1c): The dominant feature in this view is the ovoid triangular outline and concave hollowing of the proximal articular surface for MC II (1). On the palmar aspect, the abaxial border has a distinct prominence (3) for attachment of the ligamentum sesamoideum obliquum abaxiale (laterale). Feature (3') is the deepened recurved adaxial palmar surface. The ligamentum sesamoideum obliquum is reduced in this aspect. Feature (1') is as in figure 6.25.1a.

Distal aspect (fig. 6.26.1d): The distal articular surface (2) has a broad ovoid outline, which extends further on the abaxial (5) than the adaxial (5') side. Both ab-

axial (5) and adaxial (5') flexor superficialis prominences are separated by a longitudinal sulcus distalis (2') which fades dorsally. This is the counterpart for the longitudinal crest (fig. 6.26.1c) on the 2nd phalanx II.

Lateral aspect (fig. 6.25.1e): Feature (9) is a broadly rugose surface for attachment of the ligamentum collaterale mediale (adaxiale); there is a corresponding attachment surface on MC II (11, fig. 6.15.1f). Feature (10) is a smaller rugose surface for attachment of the ligamentum collaterale mediale (adaxiale) with phalanx 2. Features (1', 3, 3', 5 and 6) are as in figure 6.25.1b.

Medial aspect (fig. 6.25.1f): The main portion of this surface is smooth. On the proximopalmar edge there is an elevation for the ligamentum collaterale laterale (7), which connects with feature (10) on the MC II (fig. 6.15.1e). Distally, feature (8) is a weakly rugose surface for attachment of the collateral ligament with phalanx 2. Feature (5) is as described above (see also TOBIEN 1953: pl. 3, fig. 1: subl.).

Characteristic features of the 1st anterior phalanx digit II: Included are: the reduced, weak trigonum phalangis proximalis (3) and the intermediate sulcus (3'); the distinct scarred ridge for the ligamentum sesamoideum centrale (4); the different size attachment scars for the flexor digitalis superficialis tendons (5 versus 5'); the tiny bony tuberosity (6), the distinct sulcus distalis on the distal facet (2').

Table 6.19. Summary Statistics on Anterior 1st Phalanges II

Measurement	Sample size	Mean	Standard Deviation	Confidence Limits	Coefficient of Variation	Confidence Limits	Minimum	Maximum	Median		
m1	8	36,10	0,83	35,50	36,70	2,29	1,11	3,48	35,20	37,70	36,10
m2	8	20,84	0,84	20,23	21,45	4,02	1,94	6,10	19,20	21,90	20,75
m3	8	14,43	0,66	13,94	14,91	4,56	2,20	6,93	13,60	15,40	14,30
m4	8	10,00	0,57	9,58	10,42	5,71	2,75	8,66	9,00	11,10	10,00
m5	7	14,54	1,01	13,75	15,33	6,98	3,11	10,84	13,60	16,00	14,10
m6	7	12,70	0,64	12,20	13,20	5,00	2,24	7,77	11,70	13,50	12,80

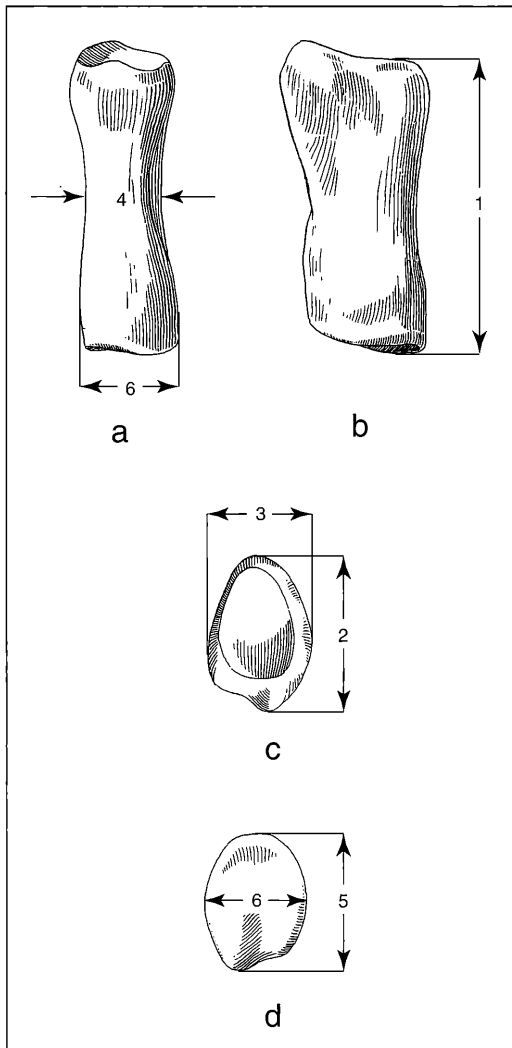


Figure 6.25.2. Measurements on Anterior 1st Phalanx II: a. dorsal aspect; b. medial aspect; c. proximal aspect; d. distal aspect.

Statistical Results

There were 6 variables measured for 15 specimens of anterior 1st phalanx II, 8 of which were analysed. The coefficient of variation was below 10 for each of the measurements. There were 6 significant correlations, two at or above the 99 % level of significance: m1 (maximum length along dorsal border)-m3 (proximal mediolateral width) and m3-m5 (distal anteroposterior length). Measurement 1 further correlated with m5 and m6 (distal mediolateral width). Measurement 3 further correlated with m6. The final correlation was between m2 (proximal anteroposterior length) and m5. For bivariate comparisons, m1-m5 or m1-m6 would be the most suitable.

6.27 Anterior 2nd Phalanx II (fig. 6.26.1a-f):

There are 13 specimens, left and right, all from articulated skeletons. As in the toes of the main digit, the 2nd phalanx of digit II is the smallest. However, the degree of reduction found in the medial (adaxial) portion of the bone is greater than found in the 1st phalanx of the series, and reduction is even greater when compared to the 1st and 2nd phalanges of digit III (figs. 6.22.1 and 6.23.1).

Dorsal aspect (fig. 6.26.1a): Feature (1) is the proximal articular facet for the 1st phalanx II. The median longitudinal ridge (1') separates the medial (1'') from the lateral (1''') concave portions of the proximal articular facet. The median ridge itself is rather crest-like, and clearly contrasts with the rounded tuberosity on the corresponding 2nd phalanx of digit III. There are several specimens with the median ridge (1') intact, and whose compacta layer is removed in the middle portion, leaving the underlying spongiosa layer free. The damage is very small: 1 mm length, but it enlarges to several millimeters in other specimens. The median ridge is in narrow contact with, and fits into the sulcus digitalis (2') of the first phalanx II (fig. 6.25.2d). In those 2nd phalanx specimens which have spongiosa exposed on the median ridge (1'), the corresponding surface on the 1st phalanx sulcus digitalis (2'; fig. 6.25.2d) shares this same condition. The corollary, when 2nd phalanges II specimens have median ridges

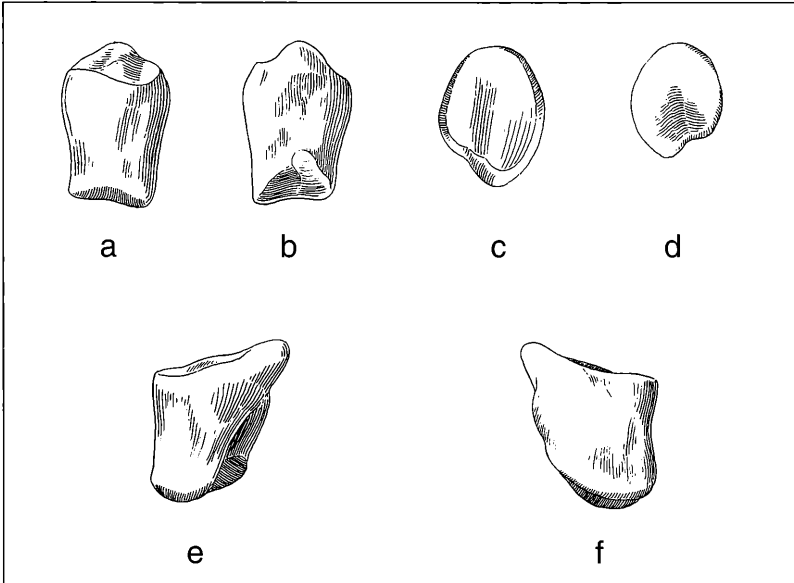


Figure 6.26.1. Anterior 2nd Phalanx II: a. dorsal aspect; b. palmar aspect; c. proximal aspect; d. distal aspect; e. lateral aspect; f. medial aspect (x 1.0).

(1') without opened spongiosa (e.g. with intact compacta), their counterpart on the sulcus distalis of phalanx 1 likewise has an intact compacta. The contact of spongiosa portions is typical for diarthritic joints (e.g. fossae nudatae, = fossae synoviales; TOBIEN 1991). We believe it likely that these features reflect the actual in vivo condition, and are not taphonomic or post-collection artifacts, and as such reflect wear of the joint surface. Feature (2) in this view reveals the slightly proximally extended dorsal border of the distal facet.

Palmar aspect (fig. 6.26.1b): Feature (3) is a large, laterally situated process for insertion of the adaxial flexor digitalis sublimis (= superficialis; = perforatus) tendon (see also TOBIEN 1952: 143, pl. 3, fig. 4, 5). The adaxial portion, and the rest of the flexor tuberosity, are reduced. Feature (4) is a distinct bulbous tuberosity for attachment of collateral ligaments, and is similar to feature (8) on the 1st phalanx II (fig. 6.25.1d). Feature (2) is the distal joint facet for phalanx 3, separated by a sulcus distalis (2') in a lateral and medial part, similar to the joint facet of phalanx 2, digit III (fig. 6.23.1b: 4''). The medial portion is shortened and reduced (2''), whereas the lateral part is elongated distally (2'''), thus preserving the former original status of the facet.

Proximal aspect (fig. 6.26.1c): This view is dominated by the oval outline of the proximal joint surface (1). The median ridge (1') subdivides the facet into lateral (1'''), and medial (1'') portions. Palmarward is located the insertion of the flexor digitalis sublimis. Lateral to (3) is a slight, lateropalmarly situated notch of the facet (5), which is presented in all specimens and always resides lateral to the central ridge.

Distal aspect (fig. 6.26.1d): This view is dominated by the oval-shaped distal joint facet (2). The medial border (2'') is recurved (re: fig. 6.26.1b), while the lateral border (2''') is comparatively reduced. The reduced adaxial halves of both the proximal and distal facets reveal the principal mode for reduction of the bone as a whole, and compares strikingly with the bilateral symmetry of the anterior 2nd phalanx digit III (fig. 6.22.1). A similar, although less developed tendency can be seen in anterior phalanx 2 digit II (and also anterior phalanx 1 digit 2) of the Höwenegg *Aceratherium* (a rhinoceros; HÜNERMANN 1989: fig. 39b, e and fig. 36b, e). Feature (2') is a deeply developed longitudinal sulcus distalis which fades near the center of the facet. The compacta is removed, and the spongiosa is laid bare at the inferiormost portion of some phalanx 2 specimens.

Lateral aspect (fig. 6.26.1e): This view highlights the reduction of the adaxial surface (2''), and contrasts strikingly with the larger abaxial surface in the background (2''). Particularly notable is the dorsally-shifted adaxial border and the prominent lateropalmar edge of the phalanx (6). Feature (3) is as in previous views.

Medial aspect (fig. 6.26.1f): This surface is smooth except for the rugose tuberosity (4) at the lateropalmar border. The proximal border has a distinct process for insertion of the flexor digitalis sublimis tendon (3). Most distally is located the medial portion (2'') of the distal articular facet, while somewhat more proximally on the palmomedial border is located the lateral aspect (2''') of the distal articular surface.

Table 6.20. Summary Statistics on Anterior 2nd Phalanges II

Measure-ment	Sample size	Mean	Standard Deviation	Confidence Limits	Coefficient of Variation	Confidence Limits	Minimum	Maximum	Median
m1	13	16,02	0,56	15,70 16,34	3,49	2,07 4,90	15,10	17,20	16,00
m2	13	19,78	1,28	19,04 20,51	6,47	3,84 9,09	17,20	21,30	20,20
m3	12	15,08	0,71	14,66 15,50	4,69	2,71 6,67	14,10	16,30	15,00
m4	12	13,85	0,72	13,42 14,28	5,20	3,00 7,40	13,00	15,40	13,75
m5	11	12,63	1,09	11,95 13,30	8,60	4,79 12,41	11,00	13,90	13,00
m6	12	12,34	0,58	11,99 12,69	4,72	2,73 6,71	11,10	13,40	12,35

Characteristic features of the 2nd anterior phalanx digit II:

Included are: the process for insertion of the flexor digitalis sublimis tendon (3); the well developed midsagittal longitudinal ridge (1') on the proximal joint facet (1); the prominent sulcus distalis (2') of the distal joint surface (2); the lateropalmar rugosity for attachment of ligaments (4); the mediopalmar refraction (5) of the proximal joint facet (1).

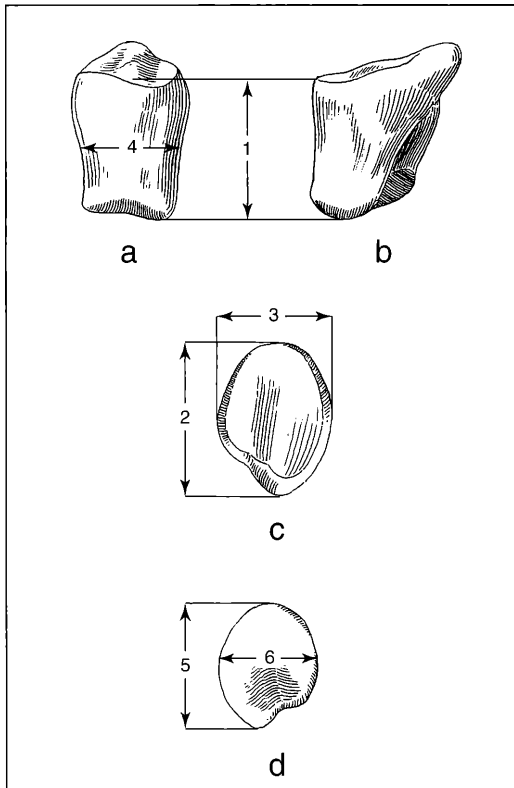


Figure 6.26.2. Measurements on Anterior 2nd Phalanx II: a. dorsal aspect; b. lateral aspect; c. proximal aspect; d. distal aspect.

Statistical Results

There were 6 variables measured for 13 specimens of anterior 2nd phalanx II. Coefficient of variation was below 10 for all measurements. There were 10 significant correlations, 3 being at or above the 99 % level of significance: m2 (proximal anteroposterior length)-m5 (distal anteroposterior length), m2-m3 (proximal mediolateral length) and m4 (midshaft width)-m5 (distal anteroposterior length). Measurement 3 correlated further with m6 (distal mediolateral width), m4 and m5. Measurement 1 (maximum length along dorsal border) correlated with m2 and m4 correlated with m6.

6.28 Anterior 3rd Phalanx II (fig. 6.27.1a-f):

There are 15 specimens, left and right, all from the articulated skeletons. Compared with the terminal phalanx of the middle toe, the third phalanges of the side toes show the most extreme morphological transformation.

Dorsal aspect (fig. 6.27.1a): The proximal joint facet (1) is subdivided into a smaller adaxial (1') and larger abaxial (1'') portions by parasagittal, dorsopalmarly oriented longitudinal ridge (1''). The dorsal surface is morphologically sharply subdivided into a smooth proximal (2) surface, and a perforated and rugose distal (2') surface as is characteristically found on all hooves (fig. 6.27.1a: 1,2). Feature (3) is a bulbous tuberosity for attachment of the extensor digitalis communis tendon, and shows a marked similarity to the homologous feature on 3rd phalanx III's (re: TOBIEN 1952, pl. 3, fig. 5: Hba = Hufbeinast" in ELLENBERGER-BAUM's terminology: fig. 279, 283: v). However, compared to the 3rd phalanx III's (fig. 6.23.1a-f: 4), it is strongly reduced.

Palmar aspect (fig. 6.27.1b): Feature (4) is the processus palmaris lateralis. On its palmar side there begins a long, slightly undulating edge, which ends at the distal "margo solearis" (6) of the phalanx. Feature (7) is a bulbous prominence on the adaxial border (5) for attachment of the flexor digitalis profundus tendon (= facies flexoria). Feature (8) is the foramen soleare laterale.

Proximal aspect (fig. 6.27.1c): The proximal articular facet (1) is found in this view to be asymmetrical, extended palmarward, and directed toward the proces-

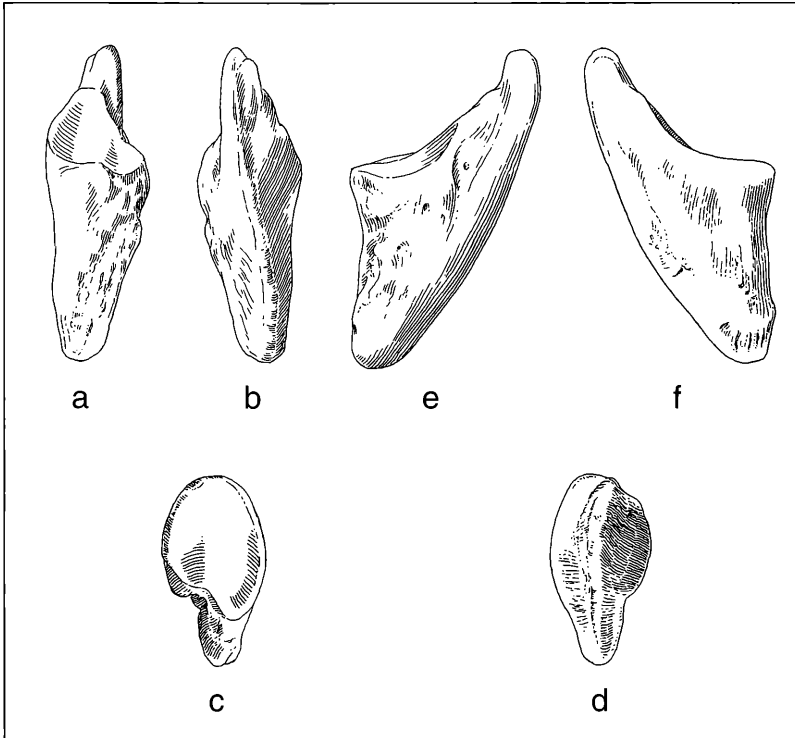


Figure 6.27.1. Anterior 3rd Phalanx II: a. dorsal aspect; b. palmar aspect; c. proximal aspect; d. distal aspect; e. lateral aspect; f. medial aspect (x 1,0).

sus palmaris lateralis (4). The mediopalmar incisure (9) is stronger than that found on the 2nd phalanx (fig. 6.26.1c: 5), and the longitudinal ridge (1'') separates the still more weakly developed adaxial portion (1') from the larger abaxial portion (1''') of the joint surface. TOBIEN has not observed any feature indicative of a fossa synovialis. Feature (3) is the extensor processus, (7) is the facies flexoria, and feature (8) is the foramen soleare laterale (see medial aspect: fig. 6.27.1f).

Distal aspect (fig. 6.27.1d): The parietal surface includes the smooth (2) and perforated rugose (2') portions. Feature (6) is the margo solearis, ending at the terminus of the processus palmaris lateralis (4), which itself is turned slightly laterally. Feature (7) is the adaxial border extension of facies flexoria for the flexor digitalis profundus tendon.

Lateral aspect (fig. 6.27.1e): Distovolarly to the processus palmaris (4) there begins a deep furrow, the sulcus solearis lateralis (8'), which enters into the foramen soleare laterale (8). Both features are likewise present on the anterior 3rd phalanx III (figs. 6.23.1b, c: 11 and 10, respectively). The medial equivalents of these features are completely reduced as other ones during the transformation procedure of this phalanx. As for the terminal middle phalanx, the sulcus and the

foramen solearis of the 3rd phalanx II apparently conducted vascular structures for the nutrition of the cartilaginous hoof capsule and its related subcutaneous layers.

The sulcus (8') and the foramen solearis (8) are located laterally to the longitudinal ridge of the joint articular surface (1''; figs. 6.27.2 b, c, f). On anterior phalanx 3 of digit III, the position of the two features (8 and 8') is lateral to the saddle-like elevation (3 between the deepening for 3^{IV} and 3^V: fig. 6.23.1e) of the joint facet (11: fig. 6.23.1c; 10: fig. 6.23.1b). Therefore, it seems that the two articular ridges (3 on the main toe, 1'' on the side toe) and therefore the joint surfaces themselves, are not completely identical (homologous in a comparative sense). A further discussion of this matter is beyond the scope of this description. Feature (10) is a lateral remnant of the linea semilunaris, which palmarly borders the sulcus solearis (8') much as feature (7) does on the medial side of the anterior 3rd phalanx III (fig. 6.23.1c). Feature (1') is the smaller portion of the articular facet. Features (3), (5), (6) and (7) are as in figs. 6.28.1a-d.

Characteristic features of the 3rd anterior phalanx II: Included are: the longitudinal ridge of the joint facet (1''); the smooth and perforated rugose portions of the parietal surface (2, 2'); processus tendo extensor digi-

Table 6.21. Summary Statistics on Anterior 3rd Phalanges II

Measurement	Sample size	Mean	Standard Deviation	Confidence Limits		Coefficient of Variation			Minimum	Maximum	Median
m1	4	26,65	2,54	24,03	29,27	9,52	2,51	16,53	23,40	29,60	26,80
m2	2	38,10	2,12			5,57			36,60	39,60	38,10
m3	4	21,53	1,86	19,60	23,45	8,64	2,29	15,00	19,00	23,20	21,95
m4	6	15,37	1,08	14,46	16,28	7,04	2,83	11,26	14,00	16,50	15,50

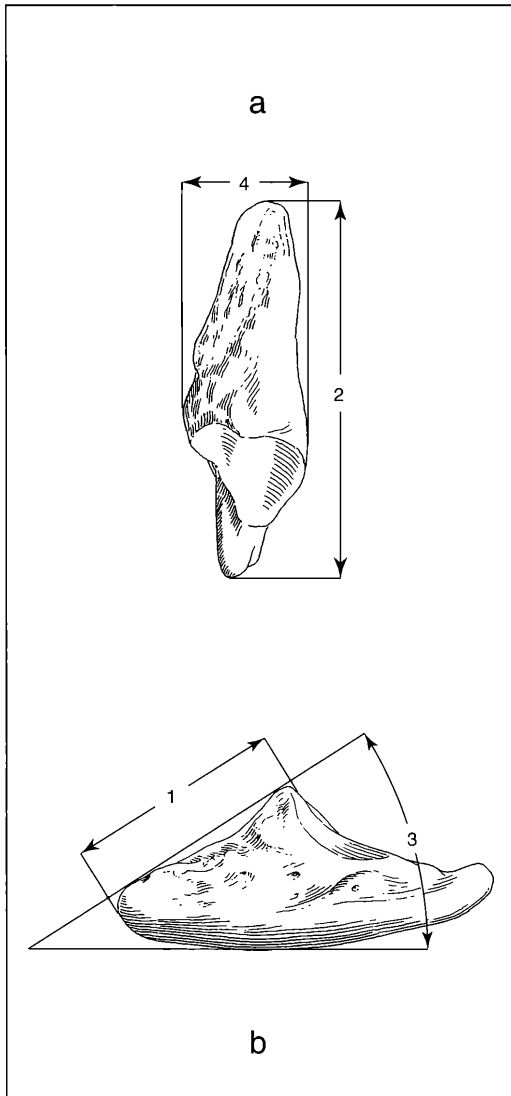


Figure 6.27.2. Measurements on Anterior 3rd Phalanx II: a. dorsal aspect; b. lateral aspect.

talis communis (3); processus palmaris lateralis (4); facies flexoria for the flexor digitalis profundus tendon (7); foramen soleare laterale (8); sulcus solearis lateralis (8'); remnant of the linea semilunaris (10).

Medial aspect (fig. 6.27.1f): The numbered osteological details are as in the foregoing figures. In the rugose portion of the lateral border (2') there is often a narrow sulcus (1-2mm wide), coursing parallel to the margo solearis, which might be homologous to the sulcus parietalis lateralis of the 3rd phalanx of recent horses (NICKEL et al. 1986: fig. 14D: 23) which conducts vascular structures. This parietal sulcus is not apparent on the 3rd phalanges III.

Statistical Results

There were no significant correlations for the anterior 3rd phalanx II.

6.29 Anterior 1st Phalanx IV (fig. 6.28.1a-f):

There are 17 specimens, left and right, all from the articulated skeletons. No morphological difference can be detected between this element, and the corresponding one of the anterior 1st phalanx digit II (fig. 6.25.1a-f).

Dorsal aspect (fig. 6.28.1a): In comparison to the 1st phalanx digit II, the dorsal aspect (fig. 6.25.1a) has a slightly stronger prominence (1').

Palmar aspect (fig. 6.28.1b): Feature (4) of the 1st phalanx digit II is absent on the palmar aspect here, but both the proximodistally elongated swelling (5) and triangular bony elevation (6) are well developed.

Proximal aspect (fig. 6.28.1c): This element is similar to that of the 1st phalanx digit II in its proximal outline. However, this element's palmar edge is somewhat straighter, and the fossa indicated by (3') is virtually indiscernible. To a certain degree these slight differences reflect the differences in MC II and MC IV distal facet morphology.

Distal aspect (fig. 6.28.1d): In this aspect the adaxial edge (5') of the articular facet (2) is more constricted than found on the 1st phalanx digit II.

Lateral aspect (fig. 6.28.1e): There are no obvious differences in this aspect with the 1st phalanx digit II. However, the collateral scars (7-10) are slightly stronger on this bone.

Medial aspect (fig. 6.28.1f): The morphology and comparison of this aspect compared to the 1st phalanx digit II is as described above for the lateral aspect.

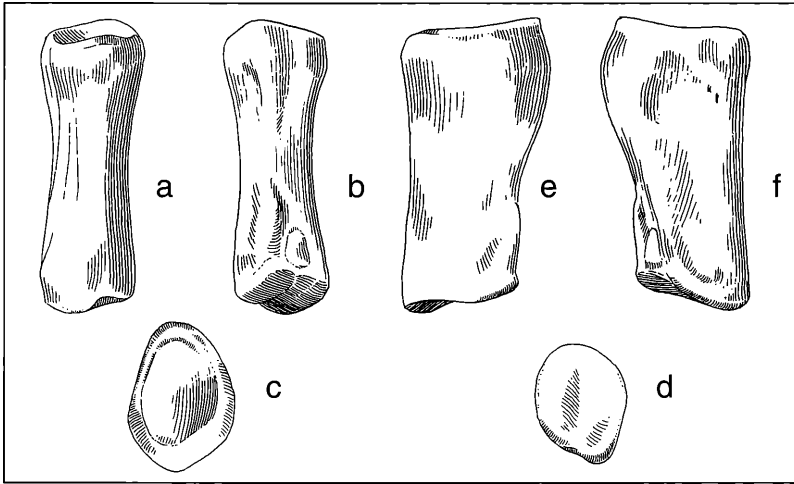


Figure 6.28.1. Anterior 1st Phalanx IV: a. dorsal aspect; b. palmar aspect; c. proximal aspect; d. distal aspect; e. lateral aspect; f. medial aspect (x 1,0).

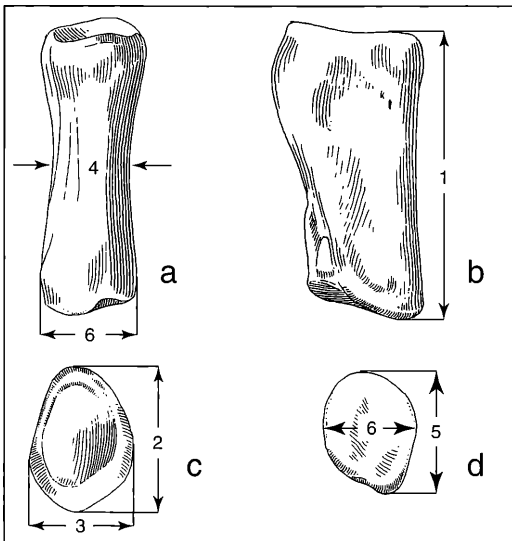


Figure 6.28.2. Measurements on Anterior 1st Phalanx IV: a. dorsal; b. medial; c. proximal; d. distal aspect.

Characteristic features of the 1st phalanx IV: Included are slight differences with the 1st phalanx II: absence of the scar for attachment of the ligamentum sesamoideum centrale (4); stronger collateral scars; more rounded outlines of the articular facets in this element. Moreover, comparing all the figures of the two bones (figs. 6.25.1a-e and 6.28.1a-e), the 1st phalanx of digit IV would appear to be slightly more massive than those of the 2nd digit. This observation is not obvious from the measurements at hand, but are still suggestive that digit IV could have been more weight bearing than digit II.

Statistical Results

There were no significant correlations for the anterior 1st phalanx IV.

6.30 Anterior 2nd Phalanx IV (fig. 6.29.1a-f)

There are 17 2nd phalanx IV specimens, left and right, all from the articulated skeletons. As with the first phalanges of digits II and IV, the second phalanges II and IV have few morphological differences.

Dorsal aspect (fig. 6.29.1a): Features (1', 1'', 1''') and (3) at the proximal end are as in fig. 6.26.2 a of the

Table 6.22. Summary Statistics on Anterior 1st Phalanges IV

Measure-ment	Sample size	Mean	Standard Deviation	Confidence Limits	Coefficient of Variation	Confidence Limits	Minimum	Maximum	Median
m1	8	36,44	1,57	35,29 37,58	4,30	2,08 6,53	34,40	39,50	36,15
m2	8	21,34	0,98	20,62 22,05	4,59	2,22 6,97	20,30	23,20	20,90
m3	8	14,53	1,06	13,75 15,30	7,28	3,51 11,06	13,00	16,50	14,20
m4	8	10,15	0,70	9,64 10,66	6,89	3,32 10,46	9,10	11,20	10,15
m5	8	14,71	0,92	14,04 15,39	6,29	3,03 9,54	13,20	16,40	14,60
m6	8	13,01	0,72	12,49 13,54	5,53	2,67 8,40	12,30	14,30	12,80

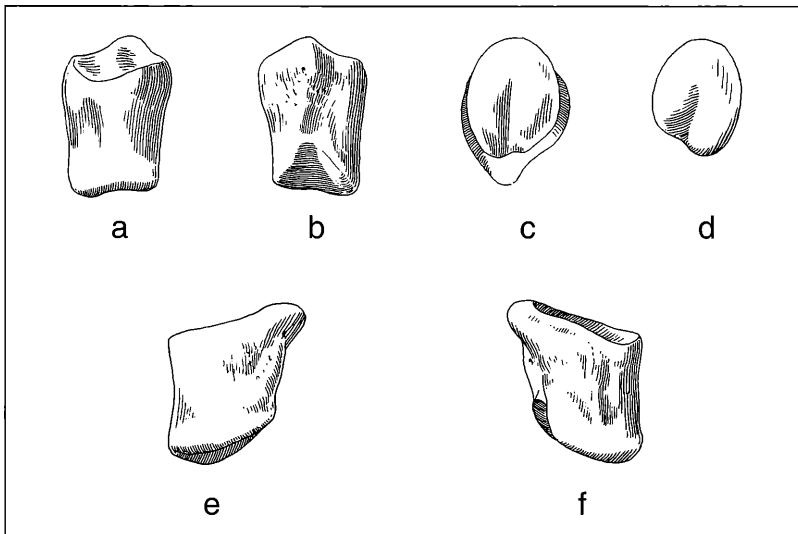


Figure 6.29.1. Anterior 2nd Phalanx IV: a. dorsal aspect; b. palmar aspect; c. proximal aspect; d. distal aspect; e. lateral aspect; f. medial aspect (x 1,0).

2nd phalanx digit II. The same holds true for the dorsal border of the distal joint facet (2).

Palmar aspect (fig. 6.29.1b): This aspect shows a somewhat more strongly developed rugose surface for the attachment of ligaments (4) and a broader corresponding groove laterally than found in digit II. The sulcus distalis (2') of the distal facet (2) is open on the palmar surface of this phalanx, while being closed on digit II's. However, this character shows some variability.

Proximal aspect (fig. 6.29.1c): This aspect reveals a facet (1) which is somewhat mediolaterally broader

than the corresponding facet of digit II (fig. 6.26.1c). Also, the mediopalmar-incision (5) is slighter. However, phalanx 2 digit IV has a larger, better developed processus for the tendo flexor digitalis sublimis (3).

Distal aspect (fig. 6.29.1d): The lateral border (2'') of the distal facet (2) is broader than found in the 2nd phalanx digit II.

Lateral aspect (fig. 6.29.1e): This aspect reveals a more strongly developed rugose surface for the attachment of ligaments (4), and a more bulky processus (3) than seen in digit II. Also the sulcus distalis (2') longitudinally separates the two portions of the distal facet (2) in this element.

Medial aspect (fig. 6.29.1f): The medial aspect shows the palmar extension of feature (2'''), followed by the strongly rugose feature (4) and feature (6).

Characteristic features of the 2nd phalanx IV: Included are: the more strongly expressed rugose surface (4) and broader corresponding groove laterally than found in digit II; the open sulcus distalis (2'); the broader facet (1); the fainter mediopalmar incision (5); the better developed processus for the tendo flexor digitalis sublimis (3); the broader lateral border (2''); the longitudinally separated sulcus distalis (2'); the palmar extension of (2''') and strong (4)-rugosity.

Statistical Results

There were 6 variables measured for 14 specimens, 9 of which were analysed. The coefficient of variation was below 10 for all measurements. There were 2 significant correlations, one at or above the 99% level: m3 (proximal mediolateral length)-m4 (midshaft width). The other significant correlation was m2 (proximal anteroposterior length)-m5 (distal anteroposterior length).

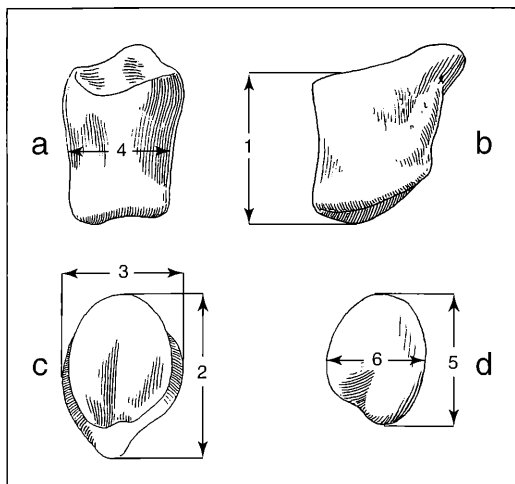


Figure 6.29.2. Measurements on Anterior 2nd Phalanx IV: a. dorsal aspect; b. lateral aspect; c. proximal aspect; d. distal aspect.

Table 6.23. Summary Statistics on Anterior 2nd Phalanges IV

Measure-ment	Sample size	Mean	Standard Deviation	Confidence Limits		Coefficient of Variation	Confidence Limits		Minimum	Maximum	Median
m1	9	15,84	0,32	15,63	16,06	2,00	1,03	2,97	15,30	16,20	15,90
m2	8	20,25	0,81	19,66	20,84	4,01	1,94	6,09	18,80	21,30	20,50
m3	9	15,21	0,75	14,69	15,73	4,94	2,53	7,34	14,20	16,80	15,10
m4	9	13,88	0,80	13,33	14,43	5,78	2,96	8,61	12,90	15,70	13,80
m5	9	12,50	0,62	12,08	12,92	4,93	2,53	7,34	11,40	13,50	12,50
m6	9	12,42	0,62	12,00	12,85	4,96	2,54	7,38	11,90	13,50	12,30

6.31 Anterior 3rd Phalanx IV (fig. 6.30.1a-f)

There are 16 specimens, left and right, all from articulated skeletons. The illustrations for this figure have been made from a specimen which had lost the processus palmaris lateralis (4) after initial preparation. However, there exists a cast which was made while the bone was still complete. The missing portions of the bone have been illustrated from the cast material. As with phalanges 1 and 2 of digits II and IV, the 3rd phalanx of digit IV differs little with its counterpart of digit II.

Dorsal aspect (fig. 6.30.1a): This aspect's smooth portion (2) is well separated from the adjacent wrinkled portion (2'), which is itself subdivided by the proximodistally coursing sulcus parietalis (2''). Feature (2''') is distinctly smaller on the lateral phalanx. The sulcus parietalis carries a blood vessel (NICHEL et al. 1986: 75), which is larger on the lateral phalanx, and reveals the increased blood supply of the hoof cartilage. The

details of the articular facet (1, 1', 1'', 1''' and 1^{iv}) are as on digit II. The extensor process (3) is more accentuated here than on the corresponding digit of phalanx II.

Palmar aspect (fig. 6.30.1b): Compared with phalanx 3 of digit II (fig. 6.27.2b), the sulcus solearis, its foramen (8') and the facies flexoria (7) are here more robust. Feature (x) demarcates the post-preparation fracture.

Proximal aspect (fig. 6.30.1c): The joint facet (with 1', 1'' and 1''') is mediolaterally broader, and the extensor processus (3) is more voluminous than seen on its counterpart. Feature (4) is the broken basis of the palmar process with the fracture (x).

Distal aspect (fig. 6.30.1d): The facies flexoria (7) on the medial wall (5) is somewhat emphasized on this figure, as is the broken base of the palmar process (4).

Lateral aspect (fig. 6.30.1e): This aspect reveals the more massive construction of this element than its counterpart in digit II.

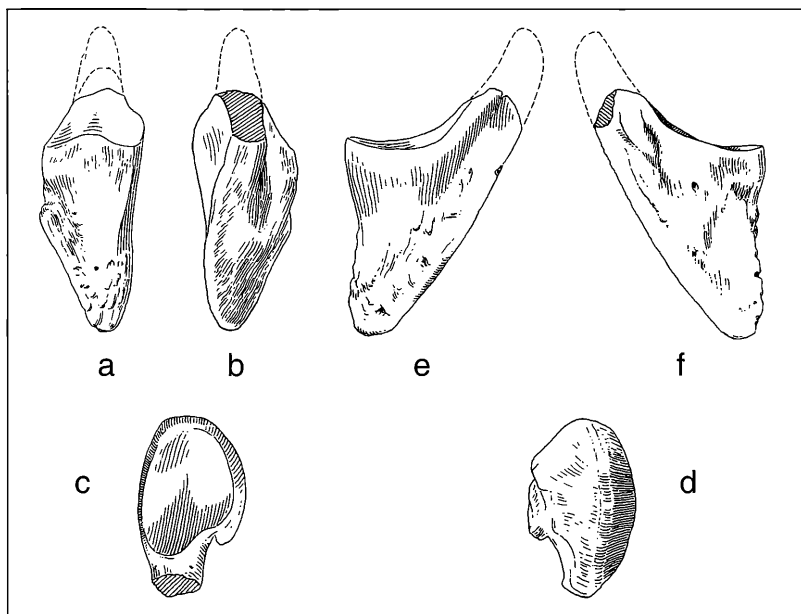


Figure 6.30.1. Anterior 3rd Phalanx IV: a. dorsal aspect; b. palmar aspect; c. proximal aspect; d. distal aspect; e. lateral aspect; f. medial aspect (x 1,0).

Table 6.24. Summary Statistics on Anterior 3rd Phalanges IV

Measurement	Sample size	Mean	Standard Deviation	Confidence Limits	Coefficient of Variation	Confidence Limits	Minimum	Maximum	Median
m1	6	27,75	1,70	26,31 29,19	6,14	2,47 9,82	25,50	29,60	28,00
m2	6	39,58	3,12	36,96 42,21	7,87	3,15 12,59	34,70	43,70	40,25
m3	8	21,13	1,91	19,73 22,52	9,04	4,34 13,74	17,50	23,70	21,25
m4	7	15,27	1,10	14,41 16,13	7,21	3,21 11,21	13,80	16,40	15,50

Medial aspect (fig. 6.30.1f): This aspect compares to the corresponding one for digit II as described for the lateral aspect.

Characteristic features of the 3rd phalanx IV: Included are: the separation of features (2) and (2''); the smaller (2''); the larger impression for a blood vessel; the more accentuated extensor process (3); the more robust development of the sulcus solearis (8'), its foramen (8) and the facies flexoria for attachment of the flexor digitalis profundus (7); the broader proximal joint facet; generally more robust build than found in its digit II counterpart.

Statistical Results

There were 4 variables measured for 15 specimens, 8 of which were analysed. Coefficient of variation was below 10 for all measurements. There was 1 significant correlation being at or above the 95 % level of significance: m1 maximum length along dorsal border)-m4 (proximal mediolateral width).

6.32 Summary of the Osteological Contrasts between Phalanges 1, 2 and 3 of digit's II and IV

The corresponding phalanges of digits II and IV are not anatomical mirror images: digit IV is more robust (TOBIEN 1982: 1048). On the first phalanx this is seen by: the prominence (1'); the outlines of the proximal articular facets; the stronger collateral scars (7-10). On the second phalanx this includes: the attachment of ligaments (4) and the corresponding groove; the medio-laterally broader proximal articular facet (1); the process for the tendo flexor digitalis sublimis (3); the lateral portions (2''') of the distal facet. On the third phalanx this is reflected in: the larger sulcus parietalis (2''); the process for the tendon extensor digitalis communis (3); the sulcus solearis and its foramen (8', 8); the facies flexoria (7); the broader proximal articular facet (1).

Also, there are differences in the corresponding metacarpals: MC IV is larger and retains vestiges of the crista sagittalis (see also TOBIEN 1982: 1048). Moreover, digit IV has a greater overall length than digit II (TOBIEN 1982: 1048, 1049). The more heavily built digit IV suggests that there was a functional weight-bearing shift away from the paraxonic midline of MC III and toward digit IV. This may be due to the greater load sustained by digit IV when the horse turned abaxially while moving (fig. 6.31.1).

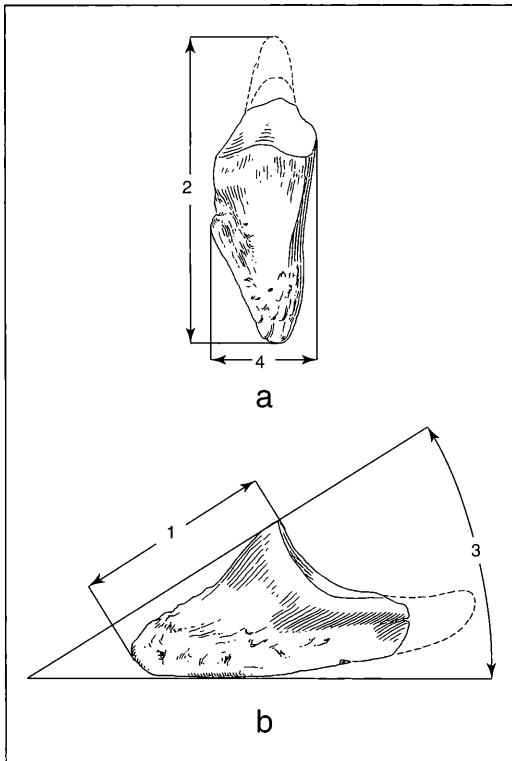


Figure 6.30.2. Measurements on the Anterior 3rd Phalanx IV: a. dorsal aspect; b. lateral aspect.

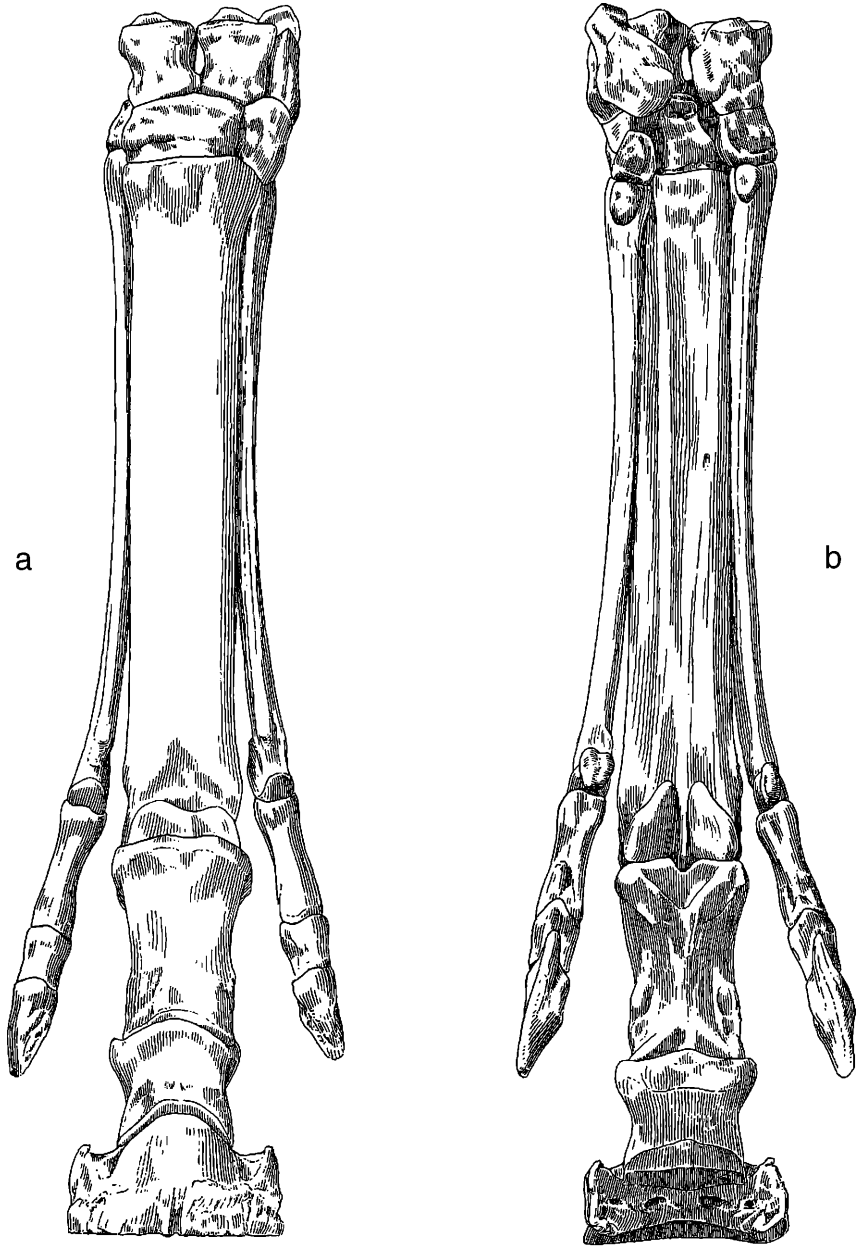
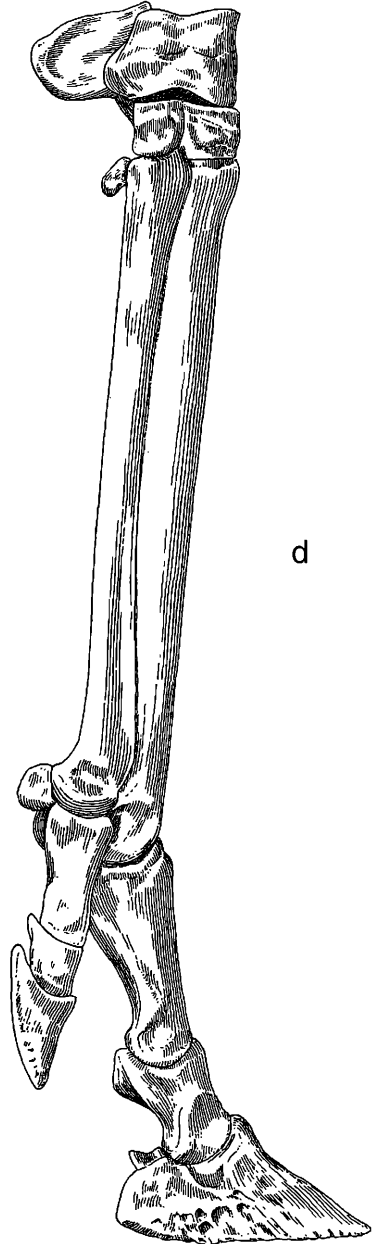
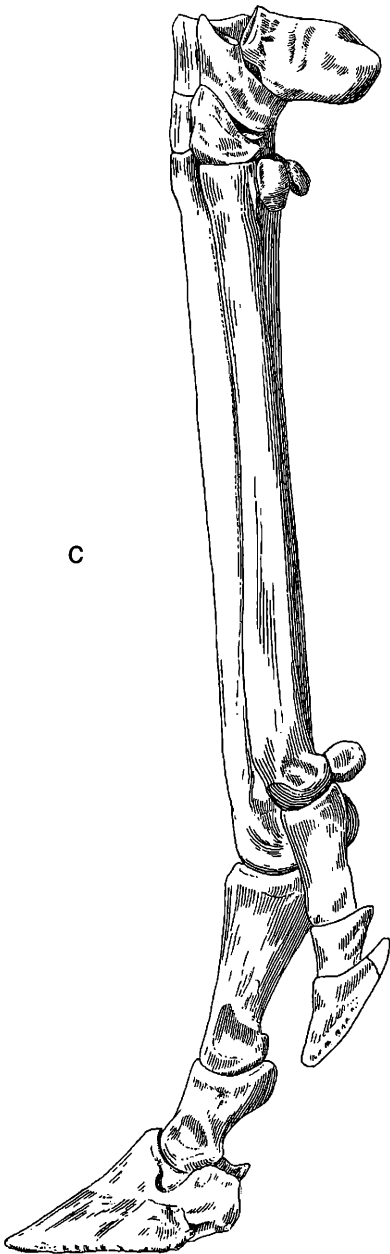


Figure 6.31.1. Reconstruction of the Höwenegg A-Skeleton Forelimb Basipodium, Metapodium and Acropodium: a. dorsal view; b. ventral view; c. lateral view; d. medial view.



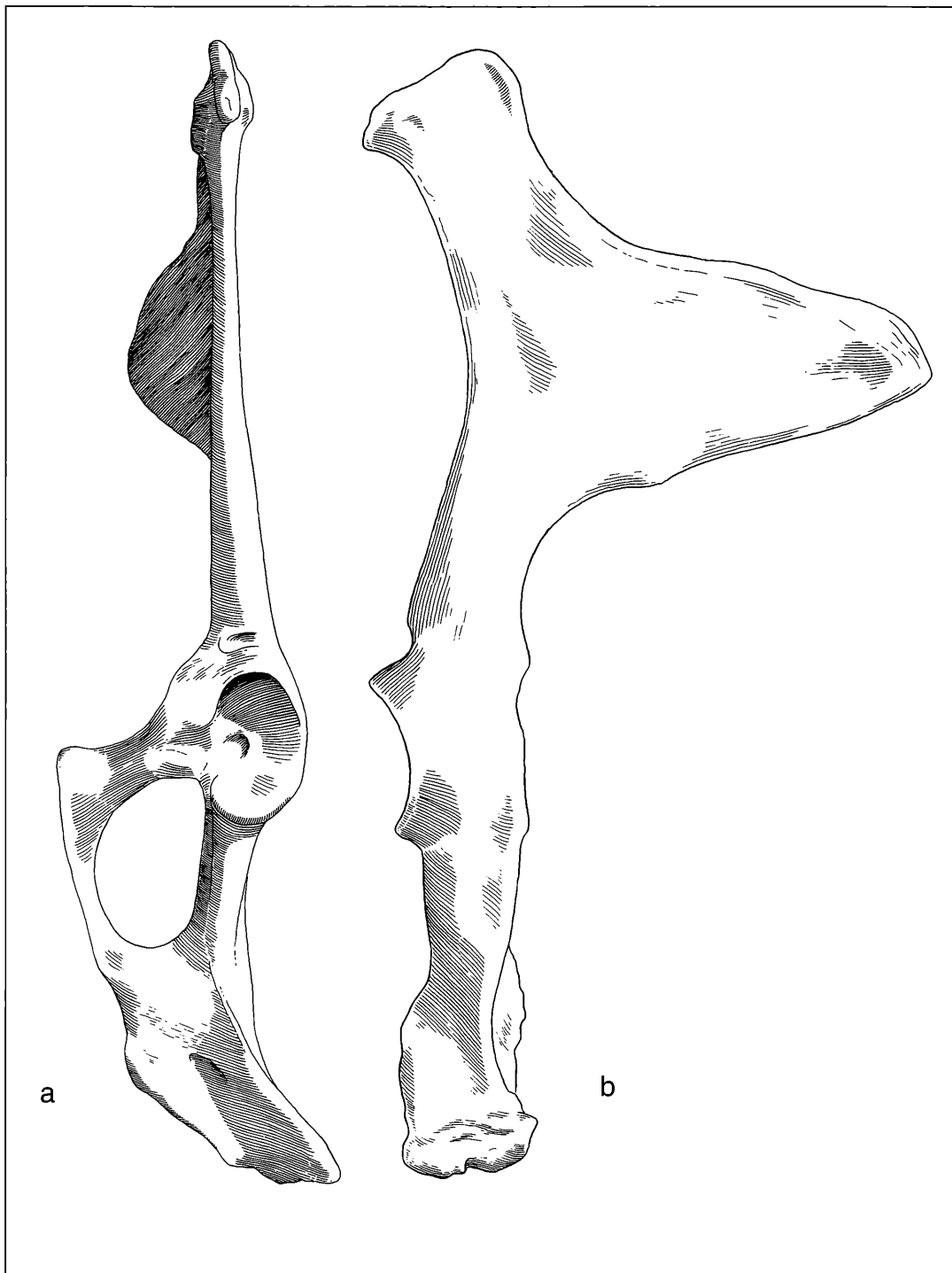


Figure 7.1.1.1. Pelvic Bone: a. ventral aspect; b. dorsolateral aspect (x 0,36).

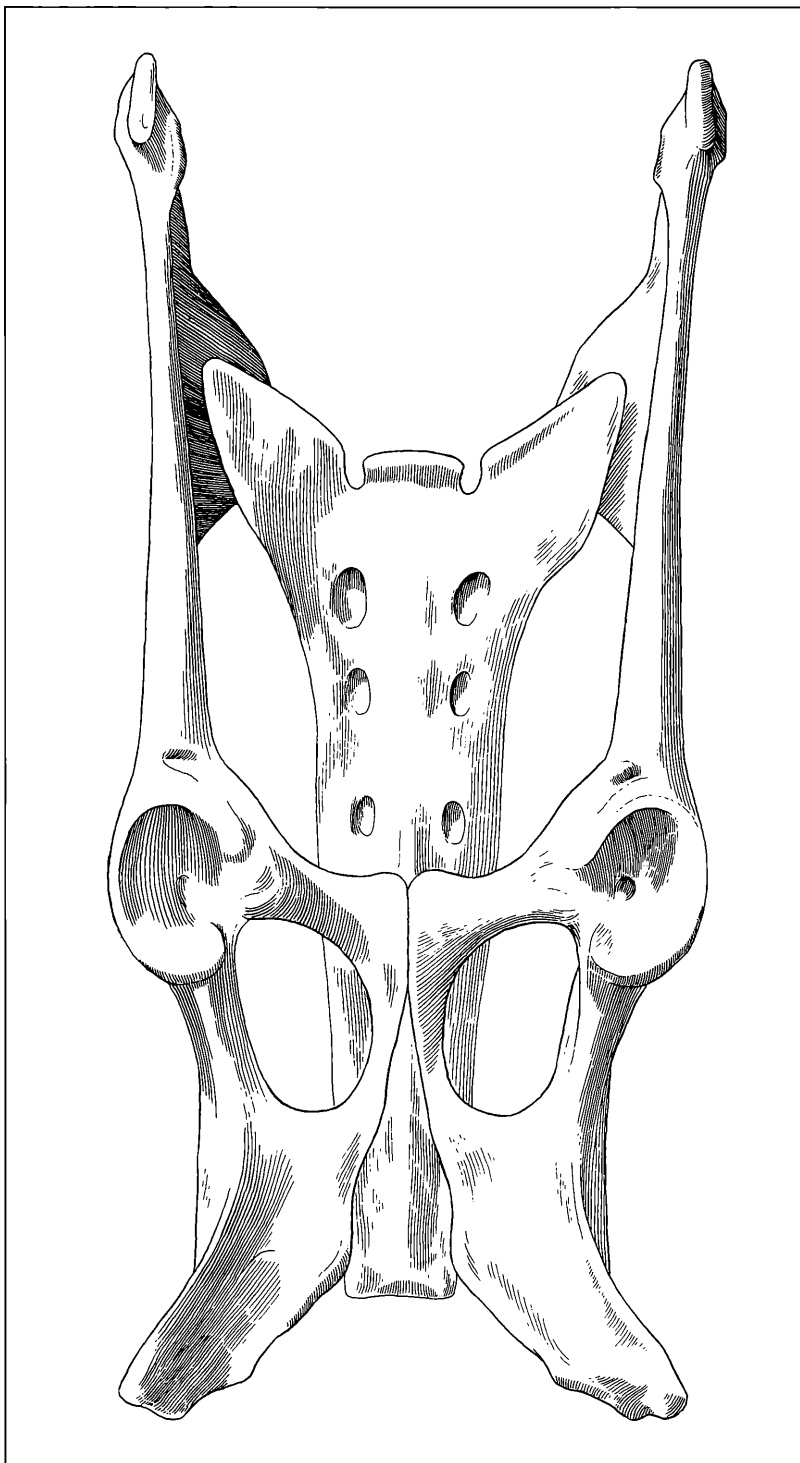


Figure 7 1.1.2. Pelvic Girdle: sacrum, right and left pelvis reconstructed in articulation (x 0,38).

7. The Pelvic Limb: Anatomy and Statistics of the Osteological Elements

7.1. Pelvic Girdle (fig. 7.1.1)

The pelvis, as represented by Hö 35/62 has an expanded iliac blade which includes the site for the dorsal attachment of the gluteus medius. The iliac shaft is long and narrow, yet not as much so as in *Equus* or *Pliohippus* (i.e. see HUSSAIN, 1975, and fig. 7.1.1.1 and 7.1.1.2, here). The obturator foramen, as preserved in Hö 54/B2, is elongate and egg-shaped in its peripheral contour, being somewhat pointed posteriorly. The width/length index is 55. Referral to HUSSAIN (1975:188) places this *Hipparion* species index in the middle of the range for *Merychippus* (48-63), distinctly below the ranges of *Pseudhipparion* (66), *Pliohippus* (74-76) and *Equus* (72-74). It is distinctly above the range for *Mesohippus* (43-50) and very close to a value reported for *Hipparion* (58) by Gromova (1952:87). Figure 7.1.1.2 is a reconstruction of the Pelvic Girdle.

Statistical Results

There were no significant correlations for the pelvis.

7.2 Femur (fig. 7.2.1.2a-f)

There are 15 femora found mostly in association with the articulated skeletons.

Cranial aspect (fig. 7.2.1.2a): Proximally, the articular head (1; caput femoris) is only moderately convex on its dorsal surface. The fovea capitis (1') is deep, triangular shaped, with the dorsal border elongated caudodistally, in marked contrast to *Asinus somaliensis* (= *Equus africanus*) (NMB 10858), *Hippotigris* (= *Equus grevyi*) (10876) and *Equus przewalsky* (NMB 10881). The trochanter major (3) is massive, proportionally more so than in extant *Equus*, and is subdivided by the trochanteric notch (3'') into a pars cranialis (3'), which is on a level with the caput, and a pars caudalis (3''), which projects considerably above the head of the femur. The Höwenegg hipparion has a deeper trochanteric notch (3'') than is found in extant horses. Distally, the collum femoris (2) is very short. Laterally, there is a prominent trochanter tertius (4), which is located nearer to the trochanter major (3) than in extant *Equus*. Medially is located the trochanter minor (9). The distal articular surface includes the trochlea ossis femoris (8) and the prominent tuberos epicondylis medialis (14) and lateralis (14'). While the epicondylus medialis is usually strongly developed in

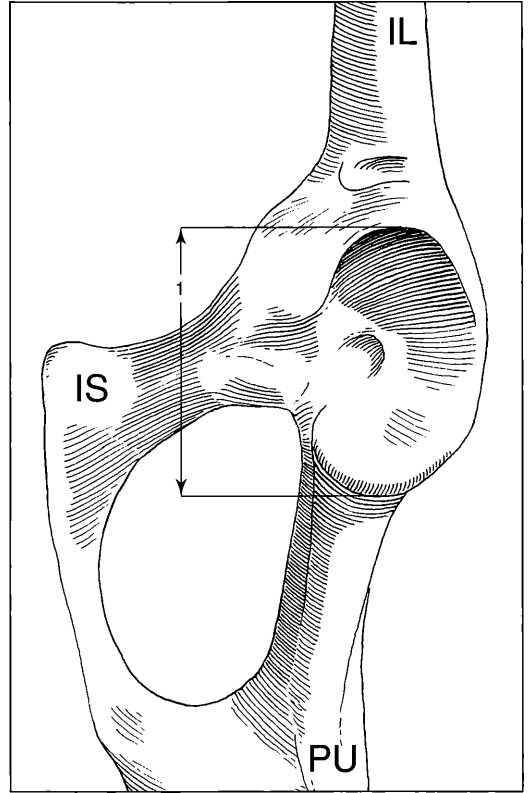


Figure 7.1.2. Measurements on the pelvis, oblique view: PU = pubis; IL ileum; IS = Ischium (m2 and m3 are maximum length and width of the pelvis, respectively).

extant horses, it is flat and weakly developed in the Höwenegg horse. The fossa extensoria (11) is a deeply excavated feature on the distolateral aspect of the femur; extant *Equus* tends to have a shallower fossa.

Caudal aspect (fig. 7.2.1.2b): Proximally are found the medially located caput femoris (1), and the prominent laterally placed trochanter major (3) with its pars cranialis (3'). Intervening between features (1) and (3) is the deeply excavated trochanteric fossa (10) and the laterally situated, deeply excavated, intertrochanteric crest (10'). The intertrochanteric crest is usually rounded in hipparion, and more crest-like or sharpened in extant

Table 7.1. Summary Statistics on the Pelvic Girdle

Measurement	Sample size	Mean	Standard Deviation	Confidence Limits	Coefficient of Variation	Confidence Limits	Minimum	Maximum	Median
m1	4	61,45		56,83 66,07	7,28	1,94 12,62	57,50	66,30	61,00
m2	1	445,00	4,47				445,00	445,00	445,00
m3	1	255,00					255,00	255,00	255,00

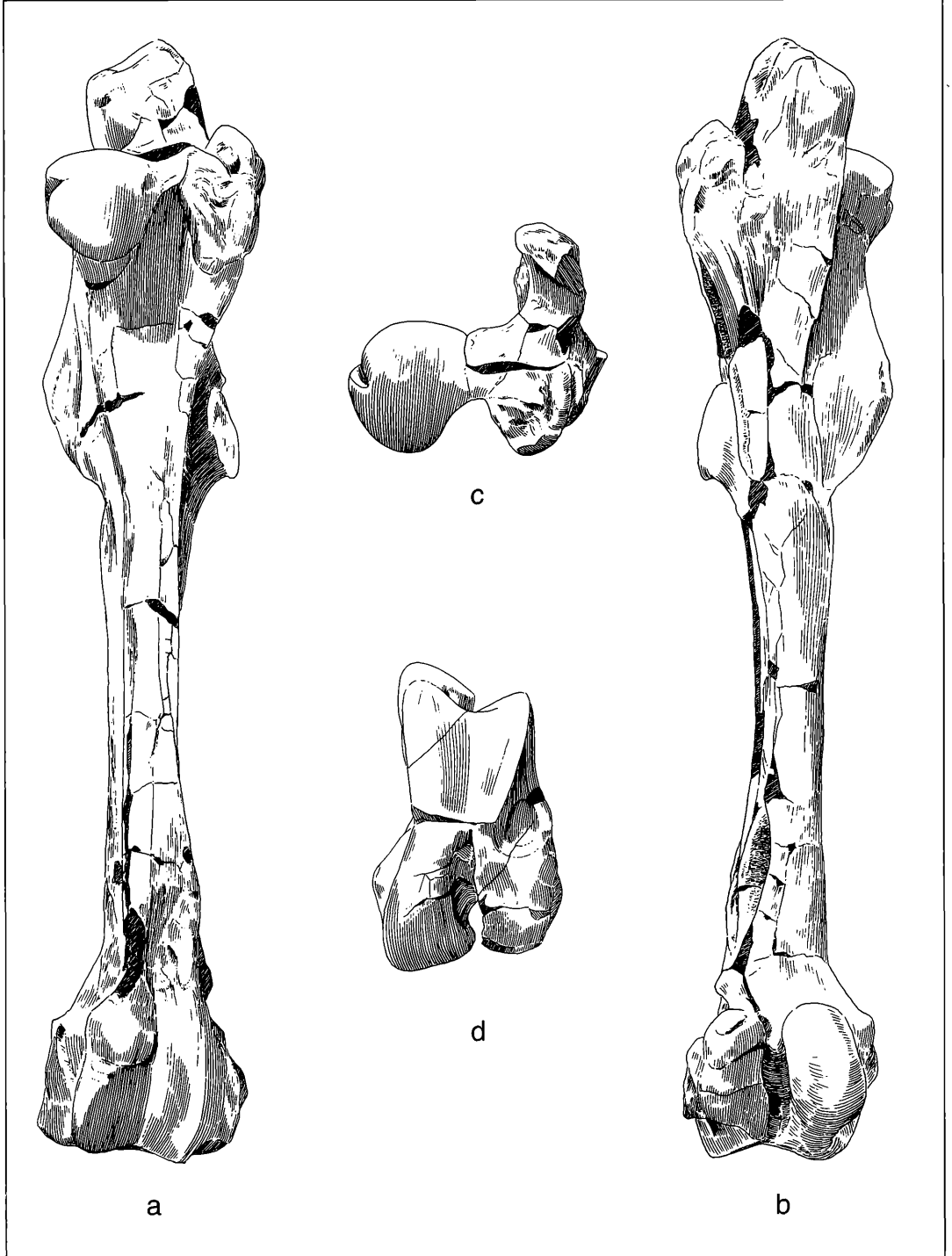


Figure 7.2.1.1. Unreconstructed Femur: a. cranial aspect; b. caudal aspect; c. proximal aspect; d. distal aspect (x 0,40).



Figure 7.2.1.1. Unreconstructed Femur: e. lateral aspect; f. medial aspect (x 0,40).

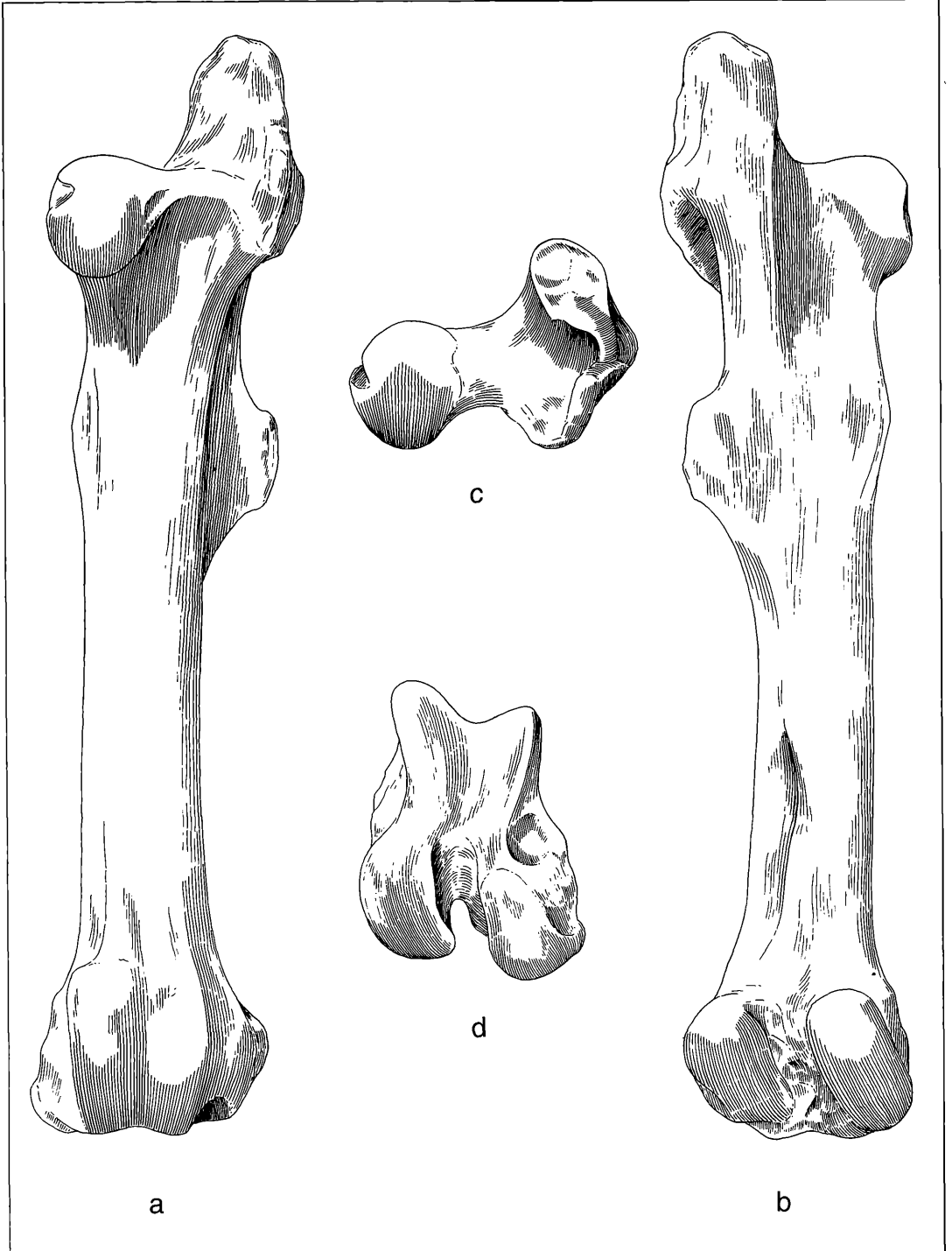


Figure 7.2.1.2. Reconstructed Femur: a. cranial aspect; b. caudal aspect; c. proximal aspect; d. distal aspect (x 0,40).

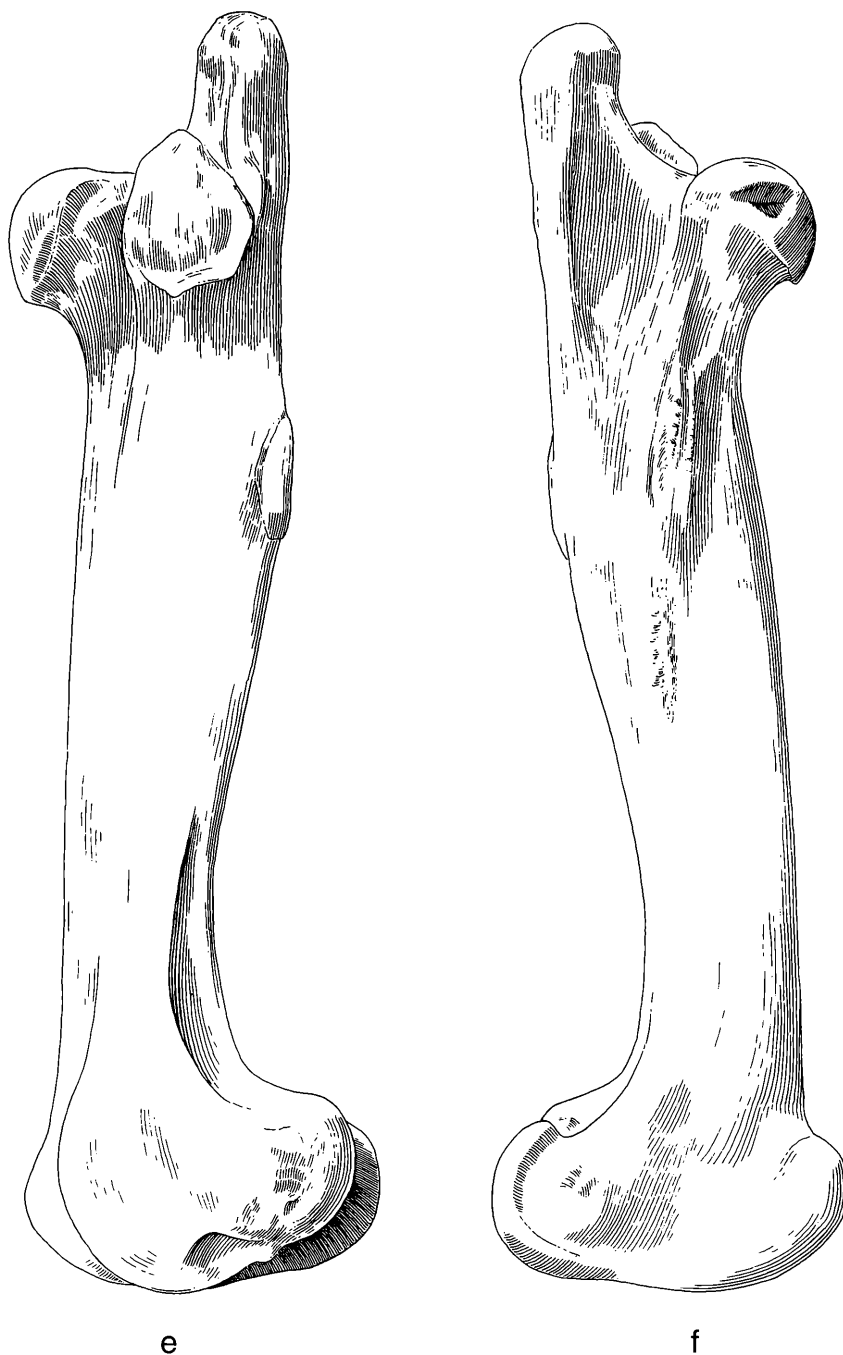


Figure 7.2.1.2. Reconstructed Femur: e. lateral aspect; f. medial aspect (x 0,40).

horses. Distally, on the shaft, is found a deep fossa condylaris (5). The distalmost extent of feature (5) is flattened in the Höwenegg horse, whereas in extant horses there is usually a sharp edge at the distal limit. GROMOVA (1955: 87) has cited a small crista in western U.S.S.R. hipparions which arises dorsally to the medial condyle of the trochlea; this feature is not present in the Höwenegg femora (but is in the Eppelsheim femur of *Hippotherium primigenium*). Distomedially, the furrow for the musculus poplitea (13) is well developed, having far more prominent borders than seen in extant horses. The distal articular surface includes the prominent condyli lateralis (6) and medialis (7), with the intervening fossa intercondylaris medialis (6').

Proximal aspect (fig. 7.2.1.2c): This aspect presents the prominent caput femoris (1), its fovea capitis (1') and the femoral neck (1''). Laterally, the arcuate shaped trochanter major (3) and its pars cranialis (3'), pars caudalis (3'') and trochanteric notch (3''') are apparent.

Distal aspect (fig. 7.2.1.2d): This aspect is dominated by the outward flare of the trochlea ossis femoris (8), medialis (8') and lateralis (8'') portions. Caudally and more proximally are situated the epicondylus medialis (14) and lateralis (14'). Situated on the lateral surface is the deeply excavated, rounded fossa extensoria (11). Most distally are the condyli lateralis (6), medialis (7), and fossa intercondylaris medialis (6').

Lateral aspect (fig. 7.2.1.2e): Proximally, this aspect presents the caput femoris (1) and trochanter major (3, 3', 3'', 3''') discussed above. Just distal to the pars caudalis of the trochanter major (3'') is found the trochanter tertius (4). At the distal extent of the diaphysis one can discern the elongate-oval shaped deep depression of the fossa condylaris (5). The distocranial articular area presents the condylus lateralis (8''; foreground) and the condylus medialis (8'; background). Distocaudally is rendered the condylus lateralis (6), fossa musculus poplitei (12), condylus medialis (7) and epicondylus lateralis (14').

Medial aspect (fig. 7.2.1.2f): Proximally, the medial view presents the caput femoris (1), trochanter major (3, 3', 3'', 3'''), and trochanteric fossa (10) and intertrochanteric crest (10') discussed earlier. Distal to the caput femoris (1) is the prominent trochanter minor (9). The distal extremity presents the prominent condylus medialis trochlea osseus femoris (8') cranially, and the condylus medialis (7) and epicondylus medialis (14) caudally.

Characteristic features of the femur: Included are its: very short collum femoris (2); massive trochanter major (3); fossa condylaris (5) not closed distally; well developed intertrochanteric crest (10'); fossa extensoria (11) deep; epicondylus medialis (14) weak and flat.

Statistical Results

There were 10 variables measured for 16 specimens, 12 of which were analysed. The coefficient of variation was below 10 for each of the measurements except

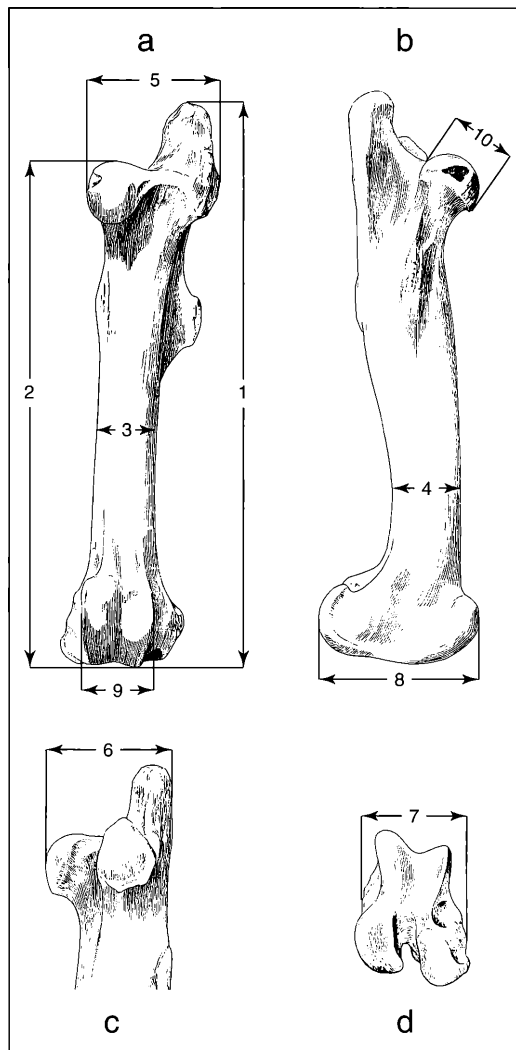


Figure 7.2.2. Measurements on the Femur: a. cranial aspect; b. medial aspect; c. proximal aspect; d. distal aspect.

m3 (CV = 14.62; minimal breadth) and m6 (CV = 12.59; proximal maximum depth). These high coefficients of variation are most likely attributable to the difficulty in measuring these points; we find them of little use for statistical analysis because there appears to be no reasonable method of reducing measurement error.

There was only 1 significant correlation: m1 (maximum length)-m2 (length from caput femoris to lateral condyle); these are two parallel length measurements. Our analysis suggests that the hipparion femur is not a particularly good limb bone for quantitative prediction.

Table 7.2. Summary Statistics on Femora

Measurement	Sample size	Mean	Standard Deviation	Confidence Limits		Coefficient of Variation	Confidence Limits		Minimum	Maximum	Median
m1	7	399,51	23,29	381,34	417,68	5,83	2,60	9,06	365,00	422,60	405,00
m2	6	367,00	19,08	350,92	383,08	5,20	2,09	8,30	345,00	400,00	367,50
m3	3	41,07	6,01	33,91	48,22	14,62	2,04	27,21	37,50	48,00	37,70
m4	3	55,43	4,81	49,70	61,17	8,68	1,31	16,05	51,50	60,80	54,00
m5	8	108,36	9,25	101,61	115,11	8,54	4,10	12,97	96,80	123,10	110,55
m6	3	108,33	13,64	92,07	124,59	12,59	1,82	23,37	98,00	123,80	103,20
m7	6	91,42	4,37	87,74	95,10	4,78	1,92	7,63	86,20	97,50	92,70
m8	9	106,82	8,32	101,10	112,54	7,79	3,98	11,60	92,60	119,00	110,20
m9	7	56,57	4,17	53,32	59,82	7,37	3,28	11,45	52,00	61,10	57,00
m10	12	55,48	2,52	53,97	56,98	4,54	2,62	6,45	50,50	59,20	55,00

7.3 Patella (fig. 7.3.1)

The patella is the largest sesamoid bone of the equine skeleton. It is embedded in the musculus quadricipitis femoris tendon anteriorly, and articulates with the femoral trochlea posteriorly (fig. 7.2.1).

Cranial aspect (fig. 7.3.1a): The outline is irregularly quadrilateral. The cranial surface is roughened, except one smoother large facet for attachment of the ligamentum patellae intermedium (5). This facet is elongated in a medioproximal to laterodistal direction (length: 30 mm), and has a subrectangular outline (width = 15 mm). Lateral to facet (5) is an expanded, diffusely bordered area for the attachment of the ligamentum patellae laterale (6). The proximal border (1) is the basis patellae, serving as the insertion for the quadriceps tendon. The apex patellae (2) is located distally. The lateral border (3) is rounded and has distinct proximo-lateral (3') and distolateral (3'') portions. The medial border is expanded to the processus cartilagineus (4).

In recent horses this bony processus continues in an elongated pointed cartilaginous structure, the fibrocartilago parapatellaris medialis (NICKEL et al. 1986: fig. 185:3). The ligamentum patellae mediale attaches to this cartilage as well as to the tibia. This fibrocartilage probably existed in the Höwenegg horse.

Caudal aspect (fig. 7.3.1b): The proximal 1/3rd of this surface presents the triangular-shaped basis (1). Features (1') and (1'') are the rounded lateral and medial rounded ridges of the triangle. Features (2)–(4) follow Figure 7.3.1a. The majority of the caudal surface is occupied by the trochlea femoris' (7) articular facet. The facet is bipartite: the larger medial portion (7') has a shallow-concave aspect and articulates with the larger medial condylus of the trochlea femoris (fig. 7.2.1a: 8'); laterally is a smaller shallow fossa (7'') which articulates with the lateral trochlea femoris (fig. 7.2.1a: 8''). Both facets are separated by a broad, proximodistally and obliquely coursing convex ridge which termi-

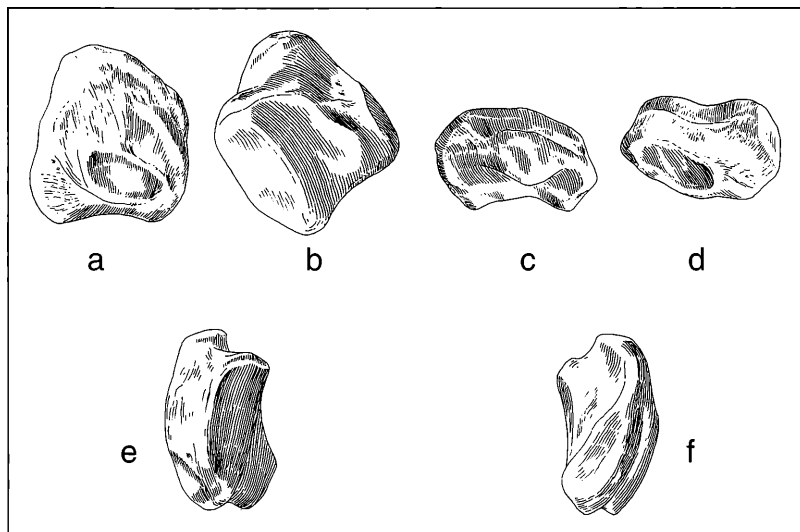


Figure 7.3.1. Patella: a. cranial aspect; b. caudal aspect; c. proximal aspect; d. distal aspect; e. lateral aspect; f. medial aspect (x 0,40).

Table 7.3. Summary Statistics on Patellae

Measurement	Sample size	Mean	Standard Deviation	Confidence Limits	Coefficient of Variation	Confidence Limits	Minimum	Maximum	Median
m1	13	69,78	2,88	68,14 71,43	4,13	2,45 5,80	64,40	73,50	70,40
m2	13	61,99	2,58	60,52 63,47	4,16	2,47 5,85	57,60	65,50	61,30
m3	14	33,32	2,64	31,86 34,78	7,93	4,82 11,05	30,00	39,00	33,65

nates at the apex patellae (7^{'''}). This ridge courses into the trochlea femoris (fig. 7.2.1: 8).

Proximal aspect (fig. 7.3.1c): The basis patellae (1) is a caudally inclined eminence with laterally (1') and medially (1'') coursing ridges. The basis is marked by the proximal border (7^{''}) of the trochlea femoris articular facet. The cranial border includes the proximal attachment borders for the ligamentum patellae intermedium (5) and laterale (6). Feature (4) is the bony basis of the processus fibrocartilagineus medialis.

Distal aspect (fig. 7.3.1d): This view includes the apex patellae (2), the attachment surface for the ligamentum patellae intermedium (5), the basis (damag-

ed) for the processus fibrocartilagineus medialis (4) and the distomedial border of the articular facies for the trochlea femoris (7' of 7).

Lateral aspect (fig. 7.3.1e): Both the basis (1) and apex (2) are visible, as are the three parts of the trochlea femoris articular facet (7', 7'' and 7''' of 7), the basis of the processus fibrocartilagineus (4), and the distolateral portion of feature (5).

Medial aspect (fig. 7.3.1f): The numbered characteristics need no further explanation. They can be interpreted by combination with the other aspects of the patella.

Characteristic features of the patella: Compared to *Equus* the Höwenegg hipparion patella has: a more quadrangular outline; a more pointed basis (1); a shorter processus fibrocartilagineus medialis (4); and a relatively larger lateral portion of the facies articularis.

Statistical Results

There were 3 variables measured for 20 specimens of patella, 14 of which were analysed. The coefficients of variation were below 10 for all measurements. There was 1 significant correlation at the 95 % level of significance: m2 (mediolateral width)-m3 (anteroposterior depth).

7.4 Tibia (fig. 7.4.1.2a-f)

There are 16 tibiae in a relatively good state of preservation. The Höwenegg hipparion tibia is a robustly built long bone which has a triangular-shaped cross-section proximally, and a rectangular-shaped cross-section distally.

Cranial aspect (fig. 7.4.1.2a): In this view the proximal end of the tibia presents the tuberculum intercondylare laterale (4) and mediale (4'). Cranially, and slightly inferiorly, are the tuberositas tibiae (5, 5'), which include both a sharp lateral border (5; larger) and medial (5'; smaller) border. In contrast to the Höwenegg hipparion, GROMOVA (1955:88) has reported that extant *Equus* has a higher medial than lateral crest. The tuberositae are separated by an intervening sulcus tuberositas tibiae (5'') for insertion of the ligamentum patellae intermedium. The margo cranialis (5''') of the tuberositas tibiae (5) exhibits a rugose surface (7) for insertion of the musculus semitendinosus. Distally are found the malleolus mediale (9) and a strongly rugose feature (9') which is notably weaker in *Equus*. At the distal limit are also found the malleolus lateralis (12) and the articular grooves for the astragalus (14-14).

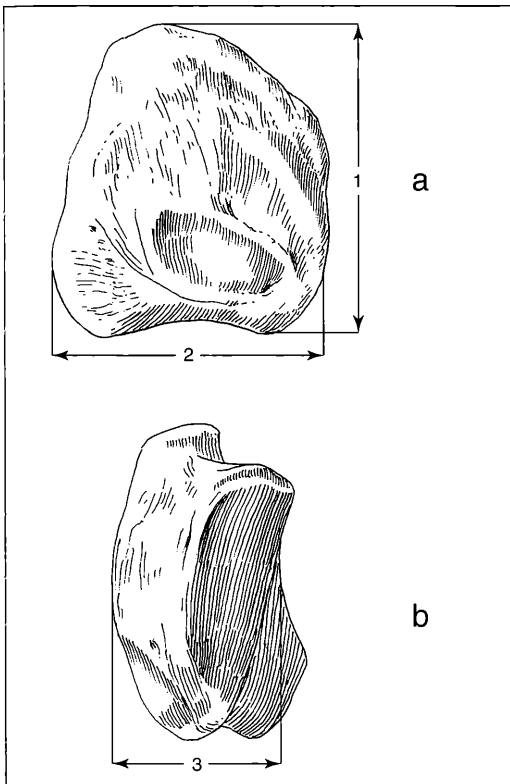
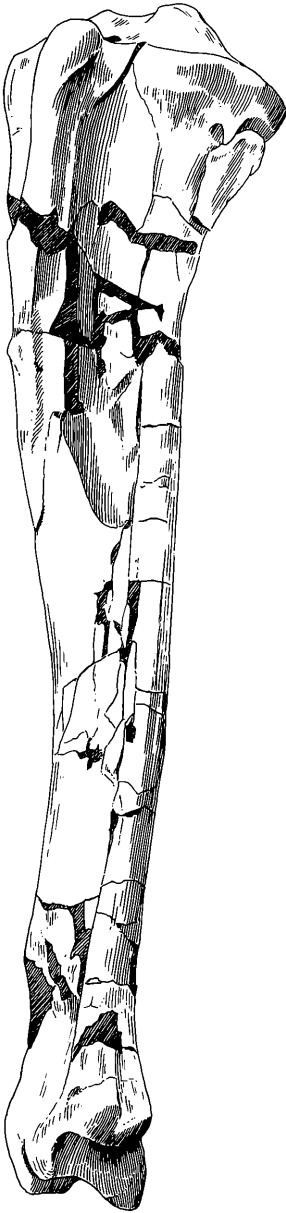


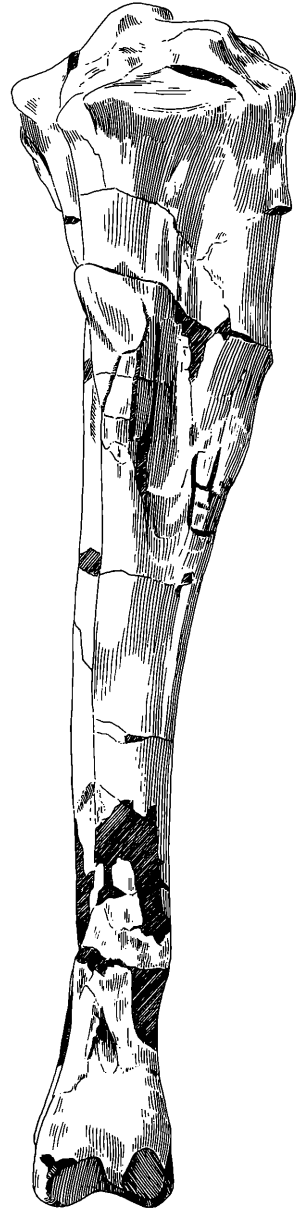
Figure 7.3.2. Measurements on the Patella: a. cranial aspect; b. lateral aspect; m1 = proximodistal diameter; m2 = mediolateral diameter; m3 = craniocaudal diameter.



Figure 7.4.1.1. Unreconstructed Tibia: a. cranial aspect; b. caudal aspect; c. lateral aspect; d. medial aspect (x 0,40).



c



d

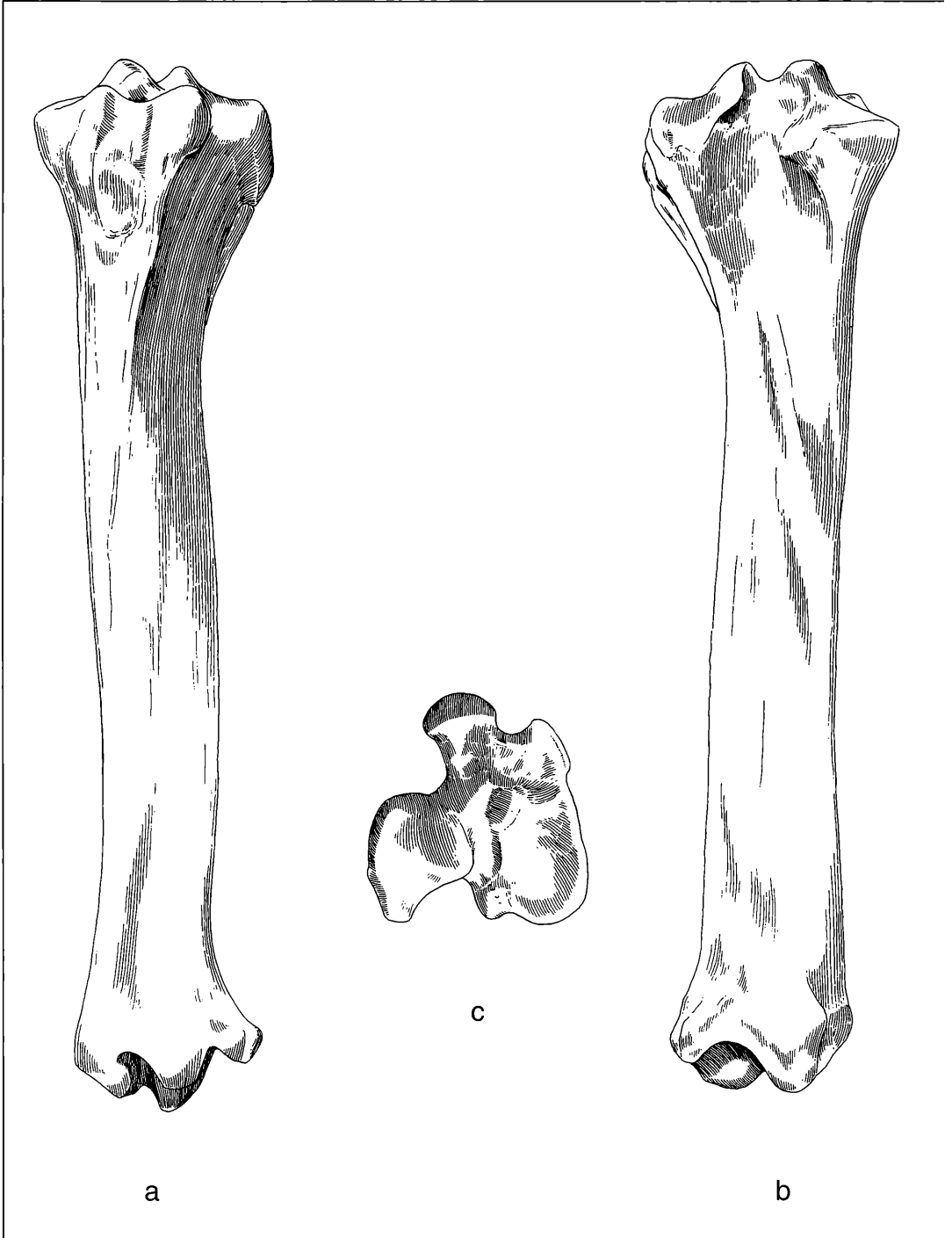
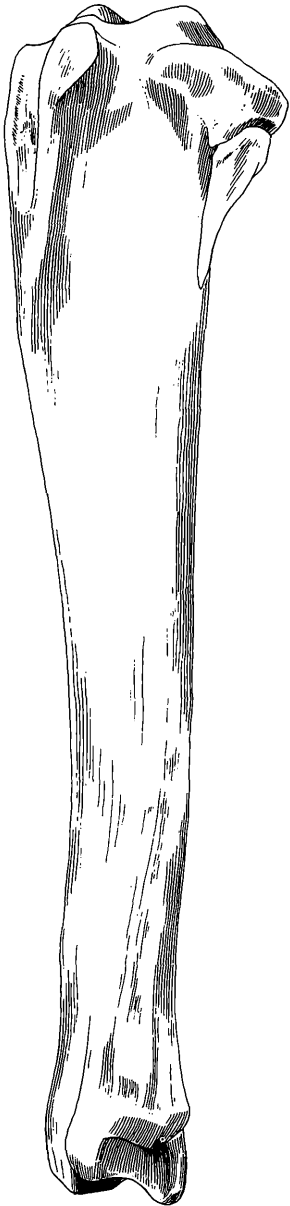
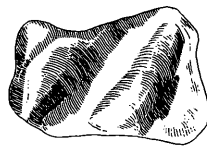


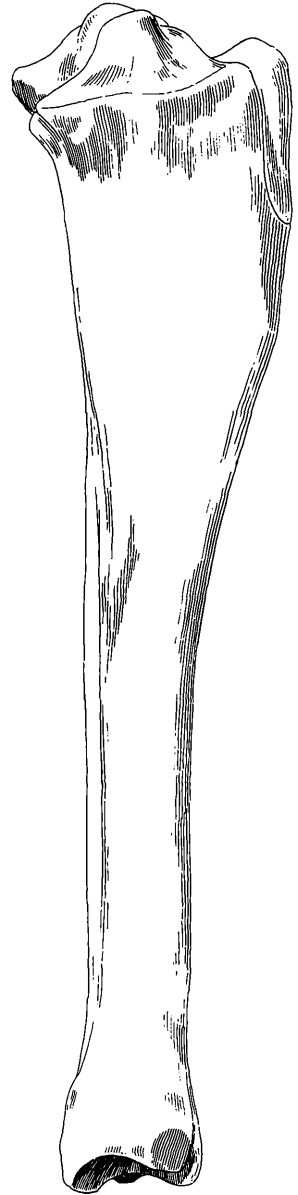
Figure 7.4.1.2. Reconstructed Tibia: a. cranial aspect; b. caudal aspect; c. proximal aspect; d. distal aspect; e. lateral aspect; f. medial aspect (x 0,40).



e



d



f

Caudal aspect (fig. 7.4.1.2b): Proximally are found the medial (4) and laterale (4') tuberculi intercondylare and the medial tuberositas tibia (5') described above. On the proximocaudal surface there is also the caudalmost extension of the lateral (2') and medial (3') condyle articular surface. Between these two features there is a deep fossa for the origin of the musculus gastrocnemius (10''), typical for Old World hipparion (GROMOVA 1955: 89). Just distal to this fossa is a broad flattened area, the incisura poplitea (10'''), for attachment of the popliteus muscle. The caudal tibial shaft is dominated by a series of slightly transversely oriented longitudinal ridges, the lineae musculares (10). Medially, the lineae musculares are bordered by the lineae musculi poplitei (10'). The distal limit to the tibia presents the medial (9) and lateral (12) malleoli, and the distally direct lateral articular groove for the astragalus (14). The distolateral aspect also presents the sulcus malleolaris (13) which dissects the lateral (12) and medial (12') aspects of the malleolus lateralis. The sulcus (13) is typical of Old World hipparion and indicates a bony guide for a tendon of the musculus extensor digitorum lateralis; this muscle slip would have dorsiflexed the fourth digit.

Proximal aspect (fig. 7.4.1.2c): This aspect is dominated by the prominent condylus laterale (2), condylus mediale (3), intervening tuberculum intercondylare (4, 4') and sulcus intercondyloideus (6). There is no distinct transverse crest in the sulcus intercondyloideus (6; = area intercondylaris in NICKEL et al. 1986: fig. 197), separating the two grooves for the fasciae of the ligamentum cruciatum (6, area centralis of sulcus intercondylaris; 8, area caudalis of sulcus intercondylaris) as in extant horses. Also, in contrast to other Old World hipparions and *Equus*, the medial tuberculum intercondylare (4') is higher than the lateral tuberculum (4) (GROMOVA 1955: 89). At the cranialmost extent one can discern the larger lateral (5), than medial (5') crest of the tuberositas tibia, as well as the distinct concave sulcus tuberositas tibiae (5''). Finally, a deeply excavated sulcus extensoris (5'') is located between features (5) and (5').

Distal aspect (fig. 7.4.1.2d): The distal end of the tibia has the two transverse articular grooves (14, 14') for the astragalus, separated by an articular ridge (15). The fossa synovialis found in association with these features would appear to be better developed in living horses (NICKEL et al. 1986: fig. 210: 5') than the Höwenegg hipparion. The very strongly developed malleolus mediale (9) is apparent here. The malleolus lateralis (12, 12') is more weakly developed, and as cited above, is clearly dissected by the sulcus malleolaris (13). The knob-like caudal portion of the malleolus lateralis (12') is present here as in all known hipparions, and absent in extant *Equus*. GROMOVA (1955: 90, fig. 20-81: z, y) has argued that this feature (12') is undoubtedly the distalmost vestige of the fibula.

Lateral aspect (fig. 7.4.1.2e): The proximal extent presents the prominent tuberositas tibiae (5) and its various structures (5, 5', 5'', 5'''), the insertion for the musculus semitendinosus (7), and the sulcus extensoris (2'') described above. One can also clearly discern the facies articularis fibulae (1), the caput fibulae (11) and the vestigial fibula (fi). Distally the malleoli mediale (9), lateralis (12, 12'), sulcus malleolaris (13) and lateral articular groove for the astragalus (14) are clearly seen.

Medial aspect (fig. 7.4.1.2f): The proximal end presents the tuberculi intercondylari (4, 4'), various features of the tuberositas tibiae (5, 5', 5'') and insertion of the musculus semitendinosus described earlier. Distally is presented the medial malleolus (9).

Characteristic features of the tibia: Compared with recent *Equus*, the Höwenegg hipparion exhibits: a deeply excavated caudal facies of the articularis fibulae (2') and facies articularis of the condylus mediale (3'); differing proximal height of the laterale (4) and mediale (4') components of the tuberculum intercondylare; more subequal height of the lateral (5) and medial (5') tuberositas tibia; no transverse crest between the sulcus intercondyloideus centralis (6) and caudalis (8); the strongly rugose surface of the malleolus mediale (9') and laterale (12); the lack of a fossa synovialis on the articular ridge between the astragalus articular ridges; the knob-like distocaudal vestige of the fibula (12').

Statistical Results

There were 9 variables measured for 26 specimens of tibia, 19 of which were analysed. The coefficients of variation were below 10 for all measurements except m3 (CV = 13.18; minimum shaft breadth) and m4 (CV = 14.96; minimum depth of the diaphysis taken at the level of m3). The high CV's can be directly accounted for as being measurement error of these points, since the attribute "minimum" is a subjective criterion for these "anatomical points"

There were 4 significant correlations, two being at the 99 %+ level of correlations: m1 (maximum length)-m2 (medial length) and m3-m4. The first of these correlations is high due to their parallel measurement; we believe it unnecessary to take these parallel measurements in that their duplication adds no essential biological or statistical information. Measurements 3 and 4 are taken perpendicular to one another. In this case these measurements were highly negatively correlated, suggesting that as one measurement declines the other raises. The implication is that this point of the tibia, being oblong in shape, enjoys some functional accommodation: as one aspect becomes larger the other accommodates by a corresponding decline in its dimension.

The two other significant correlations both have probabilities of 0.027: m1-m8 (distal maximum depth) and m2-m8. These correlations signify that maximum length and distal maximum depth would appear to be very useful measurements for judging size and proportion of the hipparion hind limb.

Table 7.4. Summary Statistics on Tibiae

Measurement	Sample size	Mean	Standard Deviation	Confidence Limits		Coefficient of Variation	Confidence Limits			Minimum	Maximum	Median
m1	12	364,58	13,09	356,78	372,37	3,59	2,08	5,11	347,00	390,00	360,00	
m2	12	342,80	11,66	335,85	349,75	3,40	1,97	4,84	330,60	360,00	336,50	
m3	13	42,60	5,61	39,39	45,81	13,18	7,75	18,61	32,40	49,20	44,60	
m4	13	38,71	5,79	35,39	42,02	14,96	8,77	21,15	32,00	46,40	35,50	
m5	10	93,18	7,78	88,10	98,26	8,35	4,47	12,23	83,70	102,00	93,80	
m6	10	85,09	3,35	82,91	87,27	3,93	2,12	5,75	80,00	91,00	84,70	
m7	19	70,14	1,86	69,26	71,02	2,65	1,76	3,54	66,70	73,40	70,40	
m8	18	45,04	2,51	43,82	46,26	5,57	3,65	7,49	41,20	50,50	44,90	
m9	10	53,66	4,29	50,86	56,46	7,99	4,28	11,70	46,30	60,00	53,00	

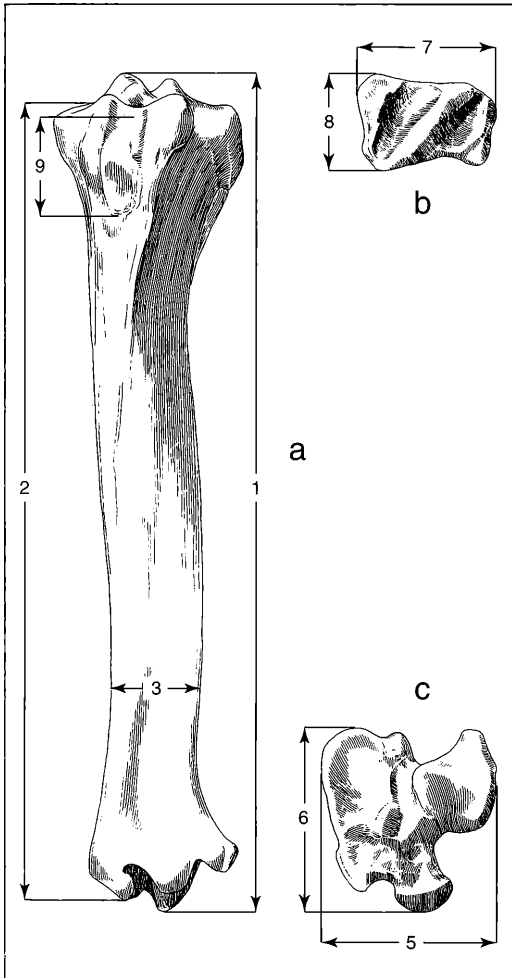


Figure 7.4.2. Measurements on the Tibia: a. cranial aspect; b. proximal aspect; c. distal aspect (m4 measured perpendicular to m3).

7.5 Fibula (fig. 7.5.1a-d):

Three Höwenegg hipparion skeletons have yielded the following fibulae:

- 1) The Hö A-54 proximal left fibula fragment (head = caput fibulae) in situ on the tibia (fig. 7.5.1a, b: 1, 2, 3). The head has a lateral orientation, as the facies articularis (11 in fig. 7.4.1b, e), the proximal part of which is free, because of a slight distal shift of the caput fibulae during fossilization. Its measurements are as follows: craniocaudal dimension of the facies articularis fibulae = 22.4 mm; proximodistal dimension ("height") of facies articularis fibulae = 20.8 mm; mediolateral dimension of the caput fibulae = 21.1 mm; craniocaudal dimension of the caput fibulae = 12 mm; proximodistal dimension of the whole fragment = 38 mm;
- 2) Hö T skeleton has both left and right fibulae (Hö T-76, left; Hö T-75, right). The length of Hö T-76 is 167.5 mm and the distal end is complete. The length of T-75 is 165 mm (with distal end broken; estimated original length = 168 mm).
- 3) Hö E skeleton, with both left and right fibulae (Hö E-107, left; Hö E-103, right). The left fibula is rather complete, except the distal end of about 30 mm length. The right fibula is fragmentary without the caput and distal end (length of fragment: 120 mm).

The morphological description given below is based on the Hö T 76 left fibula (proximal and distal aspects omitted due to lack of morphological details).

Cranial aspect (fig. 7.5.1a): The corpus fibulae (1) is a long slender rod-like structure with a triangular contour. It has a craniocaudally expanded, mediolaterally flattened proximal head (2) which tapers to a rod-like shaft distally (1) with a pointed, distal apex. This aspect also presents the facies medialis capitis fibulae (6) for articulation with the tibia and, contralaterally, a proximodistally oriented ridge on the lateral facies (8).

Caudal aspect (fig. 7.5.1b): This aspect presents all the features described in the cranial aspect (1), (2), (6), (7) and (8).

Lateral aspect (fig. 7.5.1c): The head presents a number of salient features. Most proximally are the cranial

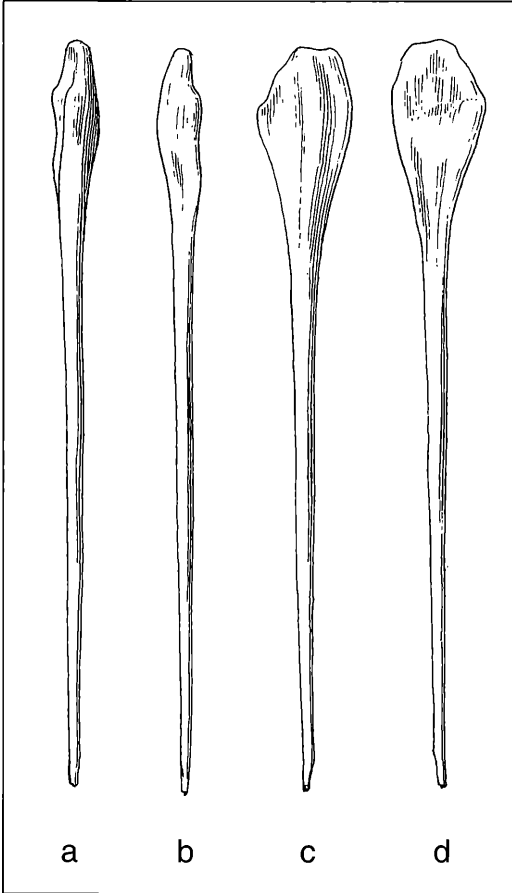


Figure 7.5.1. Fibula: a. cranial aspect; b. caudal aspect; c. lateral aspect; d. medial aspect (x 0,60).

(4) and caudal (3) margins of the caput. Along the head's midline there is a proximodistal ridge (8) flanked cranialward by a broad furrow (9) and caudalward by a deep fossa (10). The distal portion of the caudal margin of the capitis fibulae (5) is also seen in this view.

Medial aspect (fig. 7.5.1d): This aspect presents the facies medialis capitis fibulae (6) and proximally (7), the rugose surface of (6) for contact with the tibial facies articularis. Features (2), (3), (4) and (5) are as in previous views.

Characteristic features of the fibula: Compared to extant *Equus* (e.g. *Equus (Hippotigris)*, MB 9827 right fibula inverted) the Höwenegg hipparion has: a smaller caput fibulae (2); a more rounded outline; weaker lineae; a mediolaterally convex facies; a flat medial facies. DE CHRISTOL (1852) and HENSEL (1860: 34-35) discussed the presence of a fibula in hipparion, but offered no morphological details. RÜTMEYER (1862) followed

these earlier authors with a more detailed description of the fibula from a Pikermi hipparion. KOVALESKY (1873: 18) recognized the interruption in the middle part of the bone, as in the living horse, and in contrast to *Anchitherium*, where the fibula is complete. In every case the distal end of the tibia corresponds to the malleolus lateralis of the distal articulation facet of the tibia (fig. 44d, e: 12, 12'). GROMOVA (1955:90) described only the details of the malleolus lateralis. Proximal portions of the bone were not at her disposal. GABUNJA (1961) did not encounter any proximal portions of the fibula in his investigations of the hipparions from Moldavia, the Ukraine and Georgia. HUSSAIN (1975: 192) noticed that in anchitheriine and equine horses the proximal end of the fibula is expanded, and only the distal end is fused with the tibia. This is in fact the case with the Höwenegg hipparion.

7.6 Astragalus (fig. 7.6.1a-f)

The astragalus is the medial element of the proximal tarsal row. There are 29 astragali, mostly belonging to the articulated skeletons.

Cranial aspect (fig. 7.6.1a): The dominant feature in this view is the large trochlea astragalus (1) with its obliquely disposed medial (2) and lateral (3) ridges, and trochlear groove (4). The trochlea forms an angle with the sagittal plane of about 15° – 20°. Its lateral ridge (3) is more massive than the medial (2) one. Distomedially is found the attachment site for the ligamentum collatorale medium curtum: the tuberculum mediale tali (5). Intermediate between features (2) and (5) there is a deep ovoid shaped cavity (6) which provides further attachment surface for this ligament. The ligamentum tarsi dorsalis would have attached distal to the tuberculum tali (5) and fanned-out to attach to the proximal surfaces of MT II and MT III, and the dorsal borders of the naviculare and cuneiforme 3 (ELLENBERGER-BAUM 1977: 188). Feature (7) represents a pointed aspect of the facet for the naviculare (14).

Caudal aspect (fig. 7.6.1b): There are four facets for articulation with the calcaneum seen in this view: 1) the transversely concave facet (8) and its tongue-shaped distal extension (8') which contacts the lateral wall of the calcaneum, distal to the processus coracoideus; 2) the large rectangular-shaped facet for the sustentaculum tali (9); 3) distolaterally a bipartite angular facet for the distal wall of the calcaneum (10); 4) adjacent to facet (10), and making an acute angle to it, is the astragalar facet for the cuneiforme 3 (11). The protuberance for the ligamentum colli medialis brevis (12) is found proximomedially and is substantially smaller than the tuberculum mediale tali (5). Lateral to the tongue-shaped (8') extension is a swelling, which marks the origin of the ligamentum talocalcaneum laterale (13).

Proximal aspect (fig. 7.6.1c): Features (1), (2), (3), (4), (5), (8) and (13) are as in fig. 7.6.1a, b.; no additional information is added here.

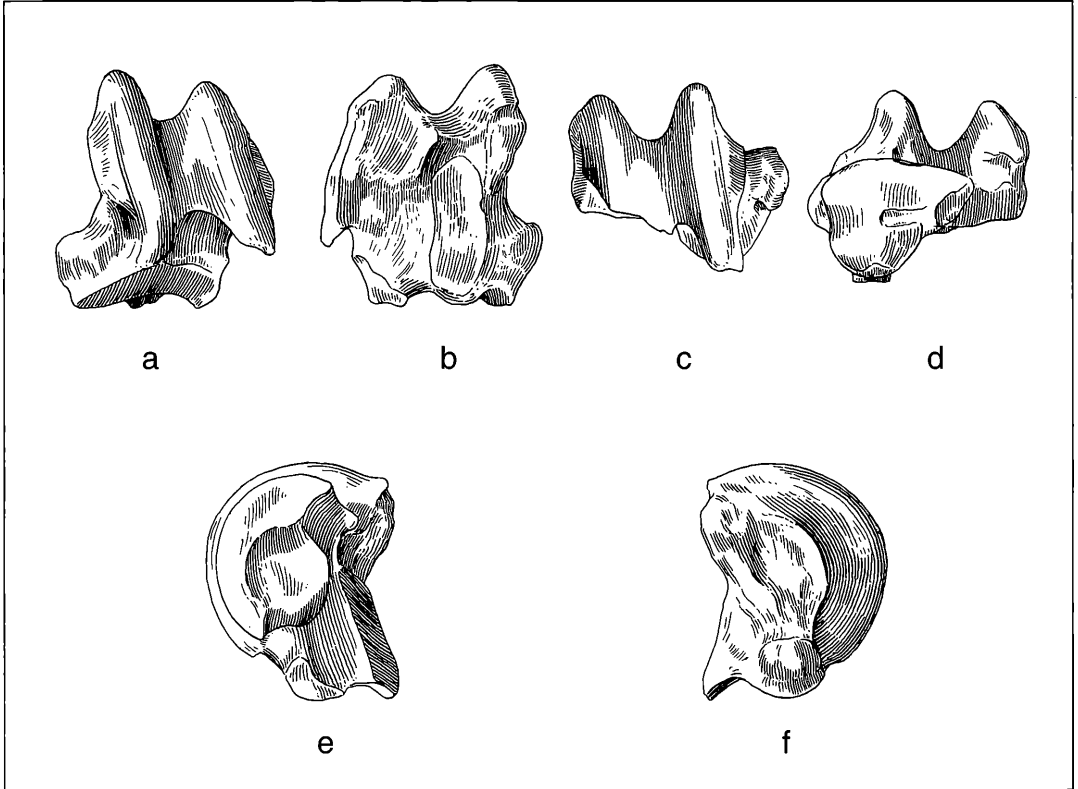


Figure 7.6.1. Astragalus: a. cranial aspect; b. caudal aspect; c. proximal aspect; d. distal aspect; e. lateral aspect; f. medial aspect (x 0,50).

Distal aspect (fig. 7.6.1d): This aspect is dominated by the craniocaudally convex facet for the naviculare (14). Caudally, the pointed aspect (7) of the facet for the naviculare (14) is clearly seen. A non articular U-shaped furrow for a fossa synovialis (15) is present from its opening on the lateral border into the central aspect of the naviculare facet where it ends (14). The exact counterpart is found on the proximal facet of the extant *Equus naviculare* (TOBIEN 1991).

Lateral aspect (fig. 7.6.1e): This aspect renders the larger medial trochlear ridge in the background (2) and subequally-sized lateral trochlear ridge in the foreground (3). Centrally located are the facet for the calcaneum (8) and the attachment site for the ligamentum talocalcaneum laterale (13). Located distally is the facet for the calcaneal distal wall (10). Located caudally is the calcaneal sustentaculum tali facet (9) and the protuberance for the ligamentum colli medialis brevis (12).

Medial aspect (fig. 7.6.1f): The medial aspect is dominated cranially by the trochlear medial ridge (2). Located caudally is the protuberance for the ligamentum colli medialis brevis (12) and the caudalmost point of

the naviculare facet (7). Distally one can clearly discern the oval-shaped tuberculum mediale tali (5) and the medial aspect of the ovoid cavity (6).

Characteristic features of the astragalus: Compared to recent wild *Equus* the Höwenegg hipparion have: very deep and sharp contours of the ovoid cavity (6); the naviculare facet (14) has a rounded and shortened medial border (re: GROMOVA 1955: 94); the tuberculum mediale tali (5), the protuberance for the ligamentum colli medialis brevis (12) and the attachment for the ligamentum talocalcaneum laterale (13) are more prominent (especially in comparison to similarly sized recent *Hippotigris*); the facet for cuneiforme 3 (11) is more prominent distally (= no. 7 in GROMOVA 1955: 99); the facet for the sustentaculum tali of the calcaneum (9) is relatively broader mediolaterally; the surface between the lateral trochlear ridge (3) and the calcaneal facet (8) is sharp (also fig. 7.6.1c: 8), whereas in horses it is rounded and separated from the proximal and lateral borders of (8) by a narrow rim of non-articular, rugose bone (EISENMANN's discrimination: 1988: 56, 57D).

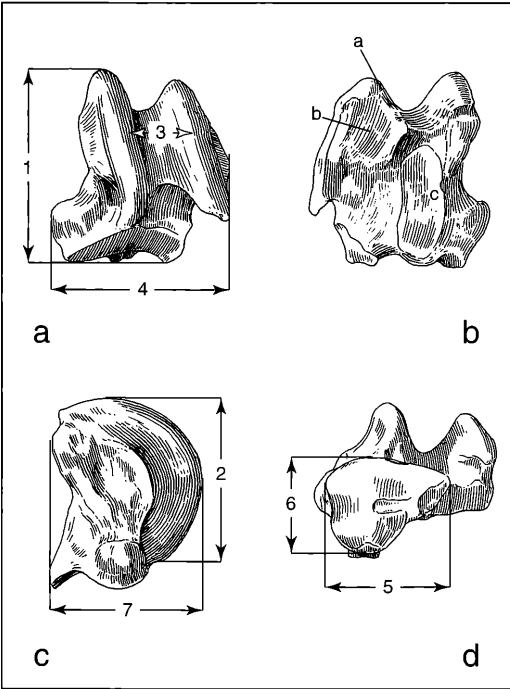


Figure 7.6.2. Measurements on the Astragalus: a. cranial aspect; b. caudal aspect; c. medial aspect; d. distal aspect.

Statistical Results

There were 7 variables measured for 30 specimens of astragalus, 23 of which were analysed. The coefficients of variation were below 10 for all measurements. There were 13 significant correlations; of these, all but three were at or above the 99 % level of significance: m1 (maximum length)-m3 (trochlear articular breadth); m2 (maximum diameter of the medial condyle)-m3 (breadth at the trochlea); m3-m5 (distal articular breadth). Measurement 1 further correlated at or above the 99 % level with m2, m6 (distal articular depth) and m7 (maximum medial depth). Measurement 6 correlated at or above the 99 % level with 4 further measurements: m7, m5, m2 and m3. Measurement 7 correlated with three further measurements at or above the 99 % level: m2, m4 (maximum breadth) and m3.

The hipparion astragalus is a commonly occurring bone in Neogene assemblages. Common bivariate measurements are m1 versus m5 or m2 versus m7. The results of this investigation would suggest that m1-m6, m1-m7, m2-m7 or m2-m6 are more statistically stable for estimations of size and body weight. We provide plots below then that are a mix of commonly reported as well as statistically stable bivariate measurements: a) M7 x M1 (maximum medial depth x maximum length); b) M7 x M2 (maximum medial depth x

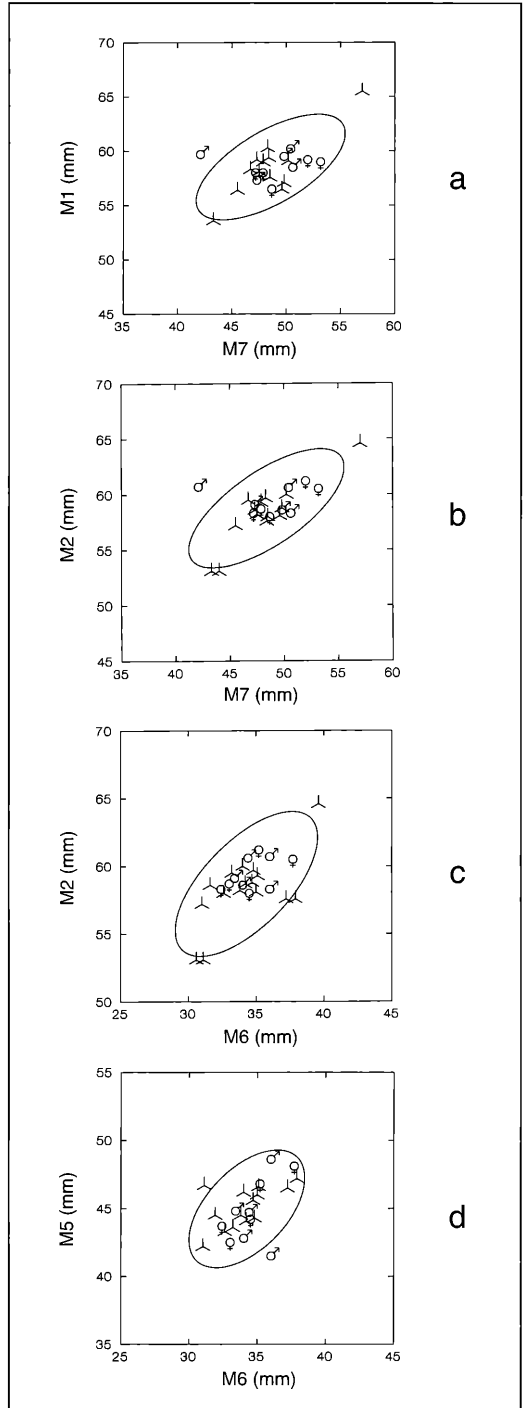


Figure 7.6.3. Bivariate Plots of Astragalus: a. M7 x M1; b. M7 x M2; c. M6 x M2; d. M6 x M5.

Table 7.5. Summary Statistics on Astragali

Measurement	Sample size	Mean	Standard Deviation	Confidence Limits		Coefficient of Variation	Confidence Limits		Minimum	Maximum	Median
m1	22	58,10	2,46	57,02	59,18	4,24	2,92	5,56	53,60	65,50	57,80
m2	21	58,50	2,20	57,50	59,49	3,76	2,56	4,96	53,10	64,60	58,30
m3	23	28,77	2,08	27,88	29,67	7,23	5,02	9,45	25,00	33,00	28,40
m4	18	59,76	2,18	58,69	60,82	3,65	2,39	4,91	56,30	63,80	59,95
m5	21	44,78	1,81	43,97	45,59	4,03	2,75	5,32	40,50	48,10	44,50
m6	20	34,42	2,25	33,38	35,46	6,54	4,40	8,68	31,00	39,60	34,20
m7	17	48,91	2,97	47,42	50,39	6,07	3,91	8,22	43,30	57,00	48,40

maximum diameter of the medial condyle); c) M6 x M2 (distal articular depth x maximum diameter of the medial condyle); d) M6 x M5 (distal articular depth x distal articular breadth). There is no apparent sexual dimorphism revealed in these plots.

7.7 Calcaneum (fig. 7.7.1a-f)

The calcaneum is the largest tarsal element. In most regards its morphology is much like extant *Equus*.

Cranial aspect (fig. 7.7.1a): In this view the calcaneum is elongated proximodistally and flattened mediolaterally (2; also 7.7.1e, f). The proximal end is a thickened bulbous tuber calcanei (2'). The tendon of the musculus gastrocnemius attaches at the proximomedial extent of the tuber calcis (2'') and the ligamentum plantare longum (2''') attaches to its caudal aspect. Distally, the calcaneum has a medially expanded sustentaculum tali for articulation with the astragalus (3)

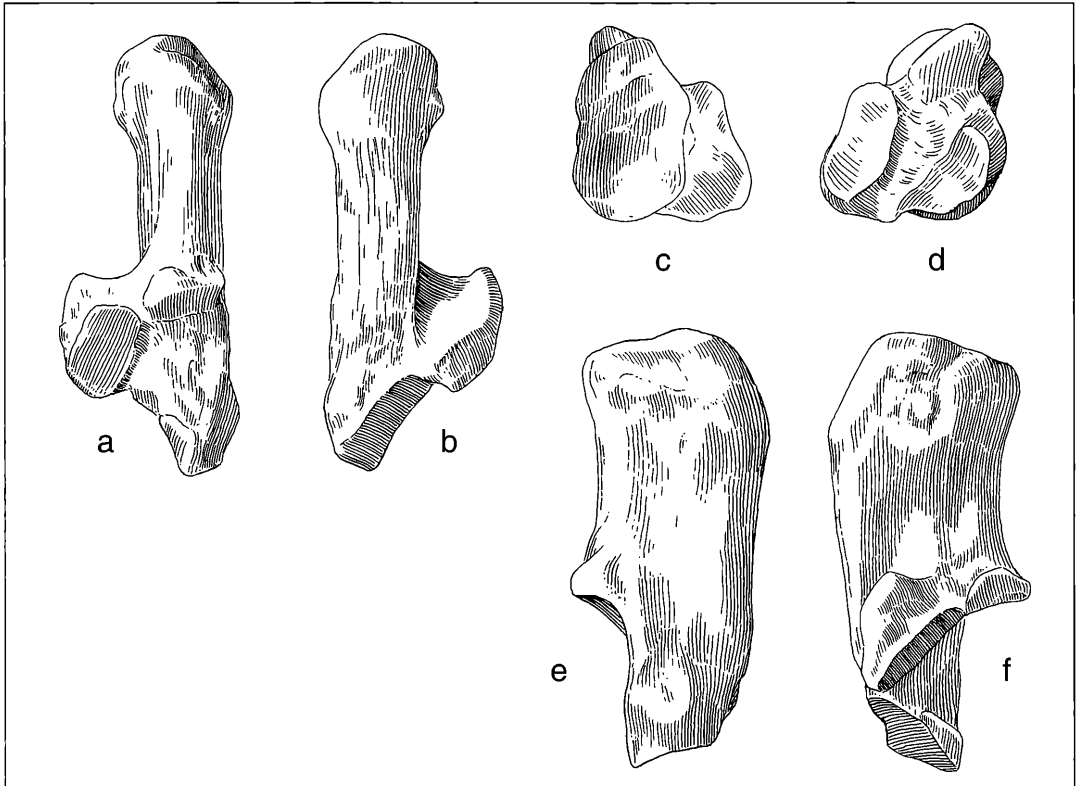


Figure 7.7.1. Calcaneum: a. cranial aspect; b. caudal aspect; c. proximal aspect; d. distal aspect; e. lateral aspect; f. medial aspect (x 0,50).

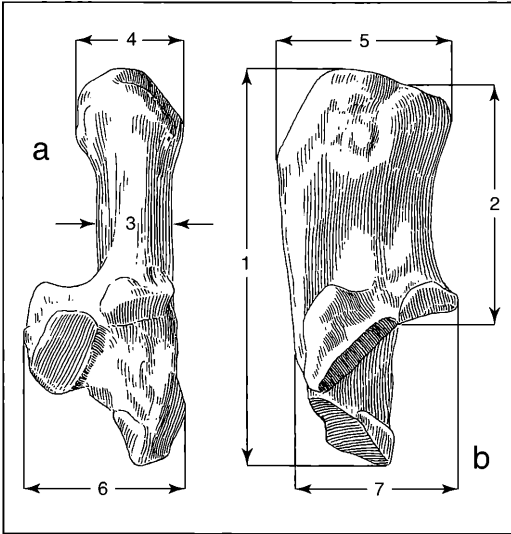


Figure 7.7.2. Measurements on the Calcaneum: a. cranial aspect; b. medial aspect.

(fig. 7.6.1a, b, c). There are four distally located articular facets. Facet (4) is for articulation with facet (8) of the astragalus. Facet (4) has a distally-directed, tongue-like elongation (4') which articulates with facet (8') of the astragalus. Medially there is a slightly concave ovoid facet (5) which articulates with facet (9) of the astragalus. Most distally there is a half-oval shaped, steeply inclined facet (6) which articulates with facet (11) of the astragalus (re: fig. 7.6.1a).

Caudal aspect (fig. 7.7.1b): Features (2), (2'), (2'') and (3) are depicted here from the caudal aspect. The sulcus tendinosus musculi flexor hallucis longus (7) is found intervening the space between features (2) and (3) (for comparison with extant *Equus* see NICKEL et al. 1986: fig. 482: 3, 3'). The mediolaterally oriented, rectangular-shaped facet for the naviculare is found most distally (8).

Proximal aspect (fig. 7.7.1c): Features (2'), (2''), (2'''), (3) and (7) have been cited earlier here. Most superiorly located is the processus coracoideus (9).

Distal aspect (fig. 7.7.1d): This aspect presents the wedge-shaped facet for articulation with the astragalus (4), and distalmost facets (5) for the astragalus and (8) for the naviculare in the foreground. The bulbous medial and lateral curvatures of the tuber calcanei (2') are found in the background.

Lateral aspect (fig. 7.7.1e): This view is dominated centrally by the proximal portion of the calcaneum (2). Most proximally is found the tuber calcanei (2') and the attachment for the tendo musculi gastrocnemii (2''). A rugose scar for tendinous attachment (11) is found between these features of the tuber calcanei. Located distally are the processus coracoideum (9), the rugose surface for an undefined ligamentous attachment (10) and the lateral border of the facet for the naviculare (8).

Medial aspect (fig. 7.7.1f): Features (2), (2'), (2''), (2'''), (3), (4, with edge of the wedge), (5), (6), (8), (9) can all be identified from the previous figures. An additional tendinous attachment (12) is found on the medial side of the tendo calcanei (probably corresponds to the tendo accessorius: NICKEL et al. 1986: fig. 479: 14).

Characteristic features of the calcaneum: Compared with several recent wild "*Equus*" specimens the most remarkable differences are: the broader facet for the naviculare (8); the abbreviated processus coracoideus (9); the medial border of the sustentaculum tali is more horizontal than in *Equus*, giving a more massive effect for feature (3); in *Equus* this border is inclined more mediolaterally (after GROMOVA 1955: 103).

Statistical Results

There were 7 variables measured for 31 specimens, 24 of which were analysed. The coefficients of variation were below 10 for all measurements except m3 (CV = 11.43; minimum breadth), undoubtedly due to the difficulty of accurately measuring this point. Of these, four were at the 95 % level of significance: m4 (proximal maximum breadth)-m7 (distal maximum depth); m3-m4; m4-m5 (proximal maximum depth); m3-m7. At the 95 % level of significance m7 correlated with m5 and m6 (distal maximum depth) while m3 correlated with m5.

The hipparion calcaneum is a commonly preserved bone in Holarctic and Ethiopian Neogene horizons, and therefore widely used for bivariate comparison.

Table 7.6. Summary Statistics on Calcanea

Measurement	Sample size	Mean	Standard Deviation	Confidence Limits	Coefficient of Variation	Confidence Limits	Minimum	Maximum	Median
m1	18	112,66	2,28	111,55 113,77	2,02	1,33 2,72	110,00	117,80	111,75
m2	19	73,12	2,22	72,06 74,17	3,04	2,02 4,05	69,00	78,00	72,80
m3	22	23,39	2,67	22,21 24,56	11,43	7,83 15,04	19,60	30,20	22,95
m4	24	34,26	2,81	33,08 35,44	8,19	5,73 10,65	30,10	43,50	33,95
m5	24	49,39	3,07	48,09 50,68	6,22	4,36 8,08	45,70	57,60	48,55
m6	18	49,24	2,75	47,90 50,58	5,59	3,66 7,53	42,60	54,10	49,15
m7	20	50,66	3,01	49,27 52,04	5,94	4,00 7,89	45,90	60,00	50,45

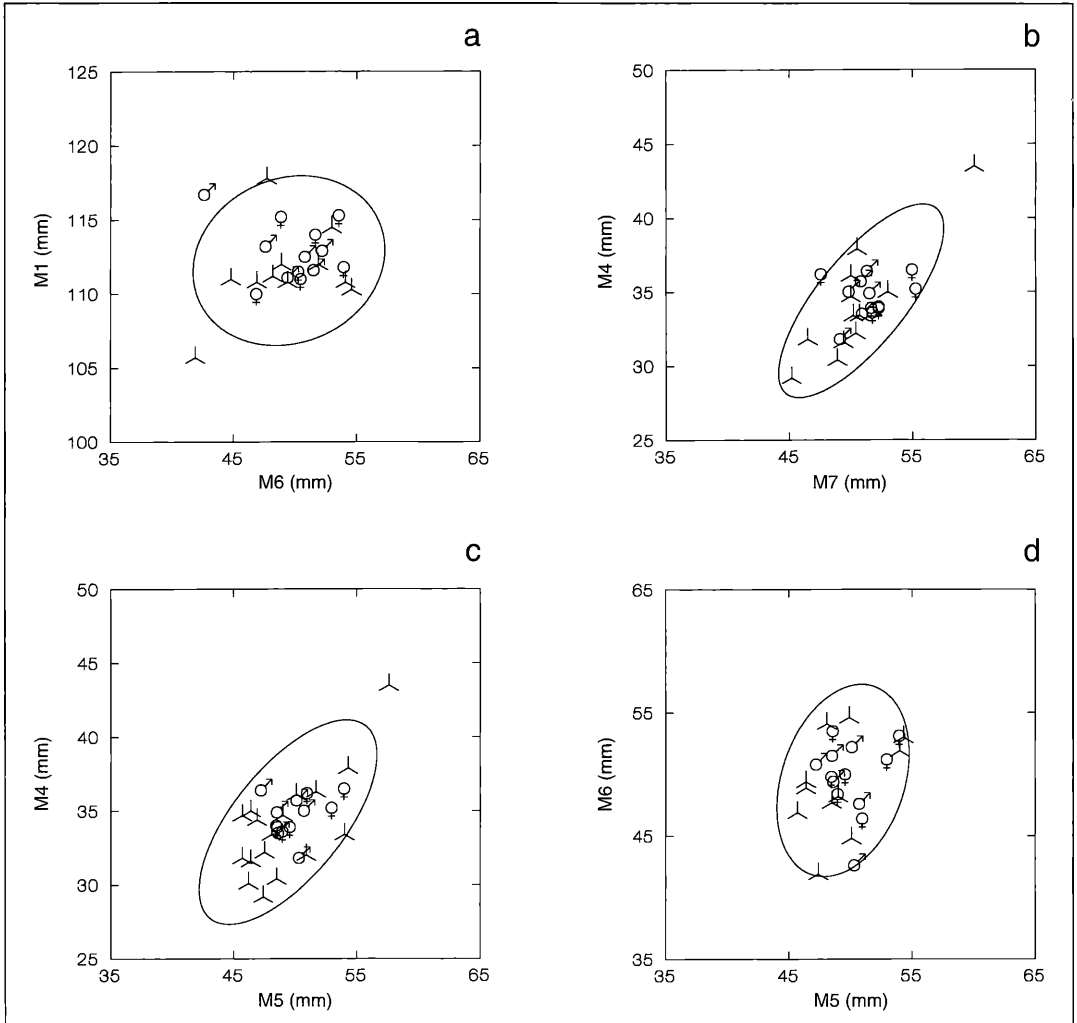


Figure 7.7.3. Bivariate Plots of the Calcaneum: a. M6 x M1; b. M7 x M4; c. M5 x M4; d. M5 x M6.

Dimensions commonly used are maximum length (m1) versus m6 (distal maximal breadth) or m7 (distal maximum depth). Since m1 was not highly correlated with either of these measurements, some caution should be given to the use of this bone for such comparisons. However, we do use it as one of our variables here because it is commonly used by equid researchers and is a useful size estimator: a) M6 x M1 (distal maximum breadth x maximum length); b) M7 x M4 (distal maximum depth x proximal maximum breadth); c) M5 x M4 (proximal maximum depth x proximal maximum breadth); d) M5 x M6 (proximal maximum depth x distal maximum breadth). There is no evidence of sexual dimorphism in these comparisons.

7.8 Naviculare (fig. 7.8.1a-f)

There are 22 naviculares, mostly belonging to skeletons, and including many left-right pairs. The naviculare, along with the astragalus and the calcaneum, belongs to the proximal tarsal row. It is a plate-like, trapezoidally-shaped bone similar to the cuneiforme 3 (fig. 7.10.1), and the magnum in the carpus (fig. 6.11.1).

Cranial aspect (fig. 7.8.1a): There is no articular facet on this surface and the surface itself is rugose. On the medial side there is a strongly developed tuberosity for ligamentous attachment (1); it is a branch of the ligamentous tarsi dorsale, which also attaches to the tuberculum tali (feature (5) of fig. 7.6.1). A distally placed sharp rim (1') separates the tuberosity from the medio-

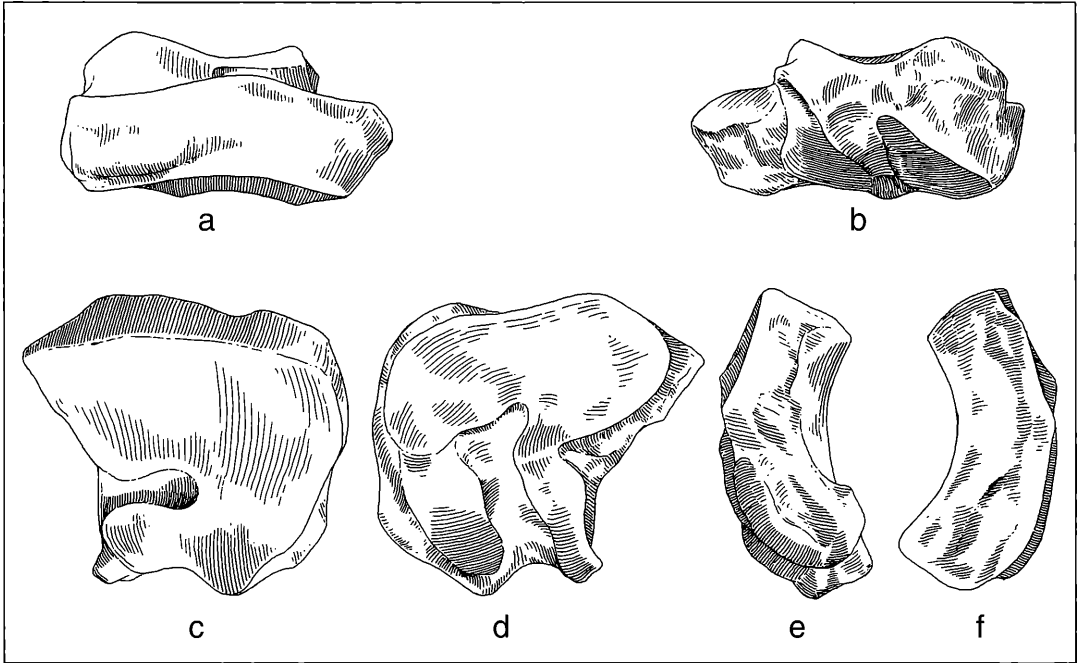


Figure 7.8.1. Naviculare: a. cranial aspect; b. caudal aspect; c. proximal aspect; d. distal aspect; e. lateral aspect; f. medial aspect (x 1,0).

distal border of the distal facet. In some Höwenegg naviculares the lateral portion of the cranial facies is slightly smoothed, most likely for the attachment of a flexor muscle tendon. Feature (7) is the caudal border of the proximal fossa synovialis (fig. 7.8.1c: 7). For description of features (2), (3) and (4) see Figures 7.8.1b and c.

Caudal aspect (fig. 7.8.1b): The caudal aspect includes two proximally directed elevations: the processus lateralis naviculare (2) and processus medialis naviculare (3). Feature (3) is more massive than (2) having a strong prominence on the medial facies for tendinous insertion (fig. 7.8.1e: (10)). Feature (2) occasionally has a small articular facet (2'); approximately 4 X 6 mm) on its anteriormost aspect which contacts features (9) of the astragalus (fig. 7.6.1b), and (5) of the calcaneum (fig. 7.7.1a) (= c12 in GROMOVA 1955: fig. 33B, p. 104). Between the processes (3) and (2) is the sulcus caudalis naviculare (4). Feature (1'') represents the cranio-medial border of the caudal facies. Feature (5) is a non-articular area for the fossa synovialis distalis.

Proximal aspect (fig. 7.8.1c): This view is virtually entirely dominated by the large proximal facet (6) which articulates with the astragalus facet (14; fig. 7.6.1d). Naviculare facet (6) is slightly concave medio-laterally, and the posterior portion has a median de-

pression which is confluent with the sulcus caudalis naviculare (4). Facet (6) is invaded distolaterally by the medially directed U-shaped incision for the proximal fossa synovialis (7).

Distal aspect (fig. 7.8.1d): A large articular facet (8) covers most of the distal facies, and in turn is invaded caudocranially by a long, broad, Y-shaped incision for the fossa synovialis distale (5). In extant horses this fossa continues through to the medial border (HUSSAIN 1975: fig. 7a; TOBIEN 1991). The large cranial portion (8) and its laterocaudal lanceolate process (8') are the counterparts of the proximal facet of the cuneiforme 3 (fig. 7.10.1c: (1)). The mediocaudal facets for cuneiforme 1 + 2, (9) and (9'), are sharply separated from one another by a transverse crest, with facet (9') being more inclined than facet (9). The caudal facet for the cuboideum (10) is located at the laterocaudal border, distal to the laterocaudal lanceolate process (8').

Lateral aspect (fig. 7.8.1e): This aspect presents the proximodistally elongated caudal facet for the cuboideum (10) and a craniocaudally oriented narrow, cranial facet for the cuboideum (11). Also apparent in the background is the processus medialis naviculare (3).

Medial aspect (fig. 7.8.1f): The medial wall has a bulbous tuberosity (12) which increases in size caudally. This prominence is separated from the mediocaudal facets of the cuneiforme (9 and 9') by a 3 mm broad

Table 7.7. Summary Statistics on Naviculare (= Posterior Naviculare)

Measure-ment	Sample size	Mean	Standard Deviation	Confidence Limits		Coefficient of Variation	Confidence Limits		Minimum	Maximum	Median
m1	13	13,35	0,71	12,95	13,76	5,28	3,14	7,43	12,30	14,50	13,60
m2	13	43,28	2,01	42,13	44,43	4,64	2,76	6,52	39,10	46,50	43,20
m3	13	39,45	1,34	38,69	40,22	3,39	2,02	4,76	37,90	41,50	39,10

rim (12'). The prominence (12) is the attachment site for a branch of the ligamentum tarsi dorsale. Feature (x) intervenes between features (8) and (9).

Characteristic features of the naviculare: Included are: the proximal surface is not flat, having its medial and lateral cranial portions inclined away from one another along a craniocaudal axis; the processus lateralis naviculare (2) is smaller and more weakly developed than the processus medialis naviculare (3); the cranial facet for the cuboideum (11) is mostly very small and sometimes missing.

Statistical Results

There were no significant correlations for the naviculare.

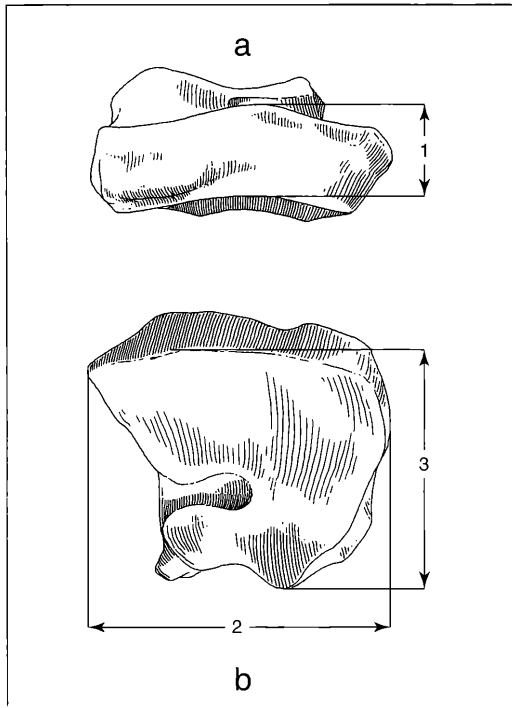


Figure 7.8.2. Measurements on the Naviculare: a. cranial aspect; b. proximal aspect. m1 = proximodistal diameter; m2 = mediolateral diameter; m3 = craniocaudal diameter.

7.9 Cuneiforme 1 + 2 (fig. 7.9.1a', b', c, d).

The cuneiforme 1 + 2 develops by the fusion of the entocuneiforme (= cuneiforme mediale = tarsale 1) and the mesocuneiforme (= cuneiforme intermedium = tarsale 2). Along with the cuneiforme 3 and cuboideum it forms the distal tarsal row. Mediolaterally it is elongated, while craniocaudally it is shorter and has a rather irregular surface. In standing position the cuneiforme 1 + 2 (= small cuneiforme) occupies a mediocaudal position in the tarsal group. It contacts the MT II and MT III distally, the cuneiforme 3 cranially and the naviculare proximally. Functionally, the cuneiforme 1 + 2 acts as the structural cornerstone along the caudomedial border of the tarsus. Because of the irregular shape of this bone, we describe it only in four aspects.

Craniomedial aspect (fig. 7.9.1a'): Proximally is the concave-shaped facet for the naviculare (1). Feature (2) is a proximodistally coursing furrow representing the site of fusion between the cuneiforme 1 (3) and cuneiforme 2 (4). Distally are located the facet for the caudal edge of cuneiforme 3 (5) and the facet for the MT II (6). The lateral border (at point 3) of the cuneiforme 1 + 2 is thickened by rugose ligamentous attachment.

Caudomedial aspect (fig. 7.9.1b'): This aspect has no articular facet, only the border for the naviculare facet (1) and the MT III facet (7). Surface (8) demarks the attachment site for a portion of the ligamentum tarsi dorsale (= ligamentum talocentrodismetatarseum). This scar is similarly developed in extant species of *Equus*.

Proximal aspect (fig. 7.9.1c): This aspect is dominated by the large irregular-ovoid facet for the naviculare (1). This facet bridges the furrow (2) between cuneiforme 1 and 2.

Distal aspect (fig. 7.9.1d): This aspect presents a number of facet surfaces: cuneiforme 1 (3) bears a facet (6) for the MT II; cuneiforme 2 (4) bears a facet for MT III (7) and a facet for the caudal border of the cuneiforme 3 (5). As in a majority of the Höwenegg horses, this individual's facets (6) and (7) are completely isolated from one another. However, Hö 219/54 shows a slight contact of these facets along their caudal borders. None of the Höwenegg skeletons includes specimens with completely separated cuneiformes 1 and 2, which has been found in some speci-

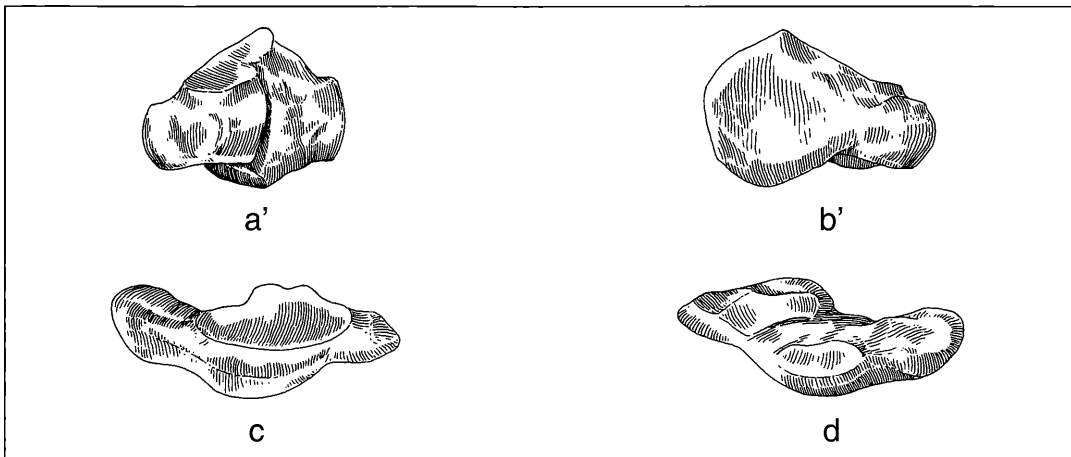


Figure 7.9.1. Cuneiforme 1+2: a'. craniomedial aspect; b'. caudomedial aspect; c. proximal aspect; d. distal aspect (x 1,0).

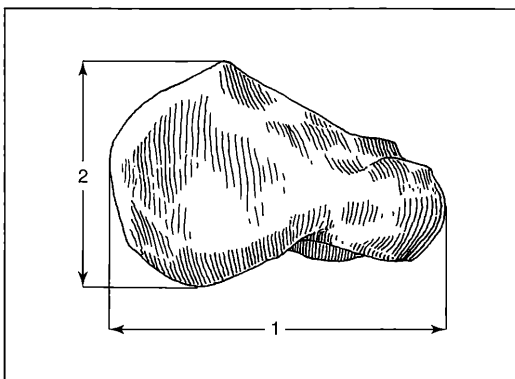


Figure 7.9.2. Measurements on the Cuneiforme 1+2; caudo-medial aspect. m1 = maximum mediolateral diameter; m2 = maximum proximodistal diameter.

mens of living horses and in one case of the fossil horse *Dolichohippus* (HUSSAIN 1975: 202).

Characteristic features of the cuneiforme 1+2: The reader is referred to GROMOVA (1955: 105 – 106) and HUSSAIN (1975: 202) for comparisons between *Equus* and the Höwenegg horse.

Statistical Results:

There were no significant correlations for the small cuneiforme.

Table 7.8. Summary Statistics on Cuneiforme 1+2

Measure- ment	Sample size	Mean	Standard Deviation	Confidence Limits	Coefficient of Variation	Confidence Limits	Minimum	Maximum	Median
m1	10	37,70	1,62	36,65 38,75	4,29	2,30 6,27	35,30	40,40	37,60
m2	11	21,33	1,13	20,62 22,03	5,29	2,96 7,63	19,90	23,00	20,90

7.10 Cuneiforme 3 (fig. 7.10.1a-f)

The cuneiforme 3 has a plate-like morphology, as does its proximal neighbor the naviculare and the magnum in the carpus. All three of these bones are positioned centrally within the central axis and function as weight-bearing bones. The cuneiforme 3 has a semi-circular restricted outline in its cranial half and a medio-laterally restricted shape in its caudal half.

Cranial aspect (fig. 7.10.1a): This aspect is dominated by a mediolaterally expansive tuberosity spanning the medial 2/3rds of this facies (1; fig. 7.10.1a, c, d). As seen in the naviculare (fig. 7.8.1a), this ligamentous scar is proximally and distally accompanied by narrow proximal and distal borders of their respective proximal and distal surface (1' and 1''); fig. 7.10.1a, e, f). This prominent tuberosity and the similar naviculare tuberosity are attachment sites for the ligamentum tarsi dorsale obliquum (= ligamentum talocentrodisto-metatarseum). This ligament extends cranially to the distal surface of the astragalar tuberculum mediale tali (5; fig. 7.6.1; NICKEL et al 1986: 212). This large ligament securely binds the naviculare/cuneiforme 3 joint, and is an amphiarthrosis; according to NICKEL et al. (1986: 172, 211) it "is a joint in which the contact surfaces on the adjacent bones are congruent, more or less flat. No extension movements are possible." TOBIEN (1991) has noted that the "non-articular surfaces" (his quotes) of the astragalar naviculare facet (fig. 7.8.1d: 15), the proxi-

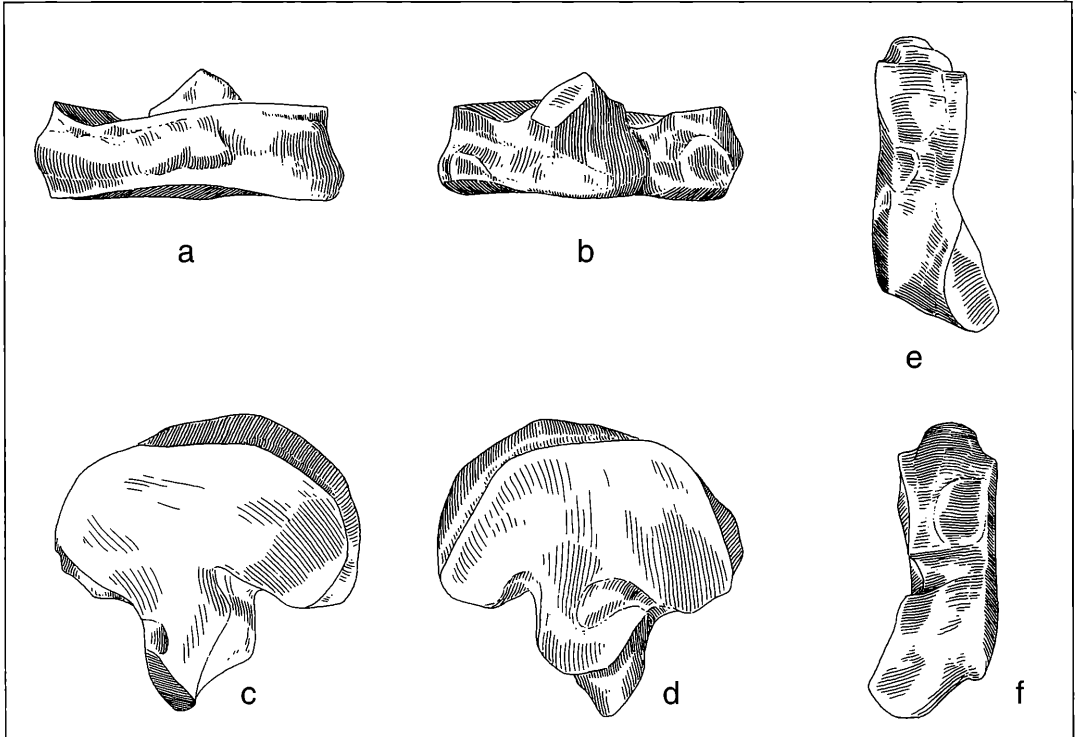


Figure 7.10.1. Cuneiforme 3: a. cranial aspect; b. caudal aspect; c. proximal aspect; d. distal aspect; e. lateral aspect; f. medial aspect (x 1,0).

mal and distal facets of the naviculare (fig. 7.8.1c, d: 7, 5), the cuneiforme 3 (fig. 7.10.1c, d: 7, 10), and the head of MT III (fig. 7.12.1c: 2), are not attachment sites for ligaments, rather, they are fossae synoviales. Feature (4') is the apex of cuneiforme 3's caudal protuberance, with the posterior facet for the cuboideum.

Caudal aspect (fig. 7.10.1b): Centrally in this view is located the posterior facet for the cuboideum (4). Laterally there is a small anterior facet for the cuboideum (5), and medially a larger anterior facet for the cuneiforme 1+2 (6). Figures 7.10.1a and b render the somewhat inclined proximal facet for the naviculare (2) and the more horizontal facet for the distal articulation of the MT III (3).

Proximal aspect (fig. 7.10.1c): This aspect is dominated by the proximal articular facet for the naviculare (2). On the medial side is a deep, craniolaterally protruding non-articular incision (7) for a fossa synovialis (there is a corresponding portion found on the naviculare). Together, these form a short *channel synovialis* with its inlet on the medial side. In monodactyl horses this structure is more extensive, and extends to the lateral border (TOBIEN, 1991). Feature (8) is the border of a lateral fossa synovialis; this feature is more developed on other Höwenegg specimens (e.g. T-56 skele-

ton, left side). Cranially and just adjacent to the posterior facet for the cuboideum (4) is a very small rugose fossa (9) for ligamentous attachment.

Distal aspect (fig. 7.10.1d): The distal facet for the MT III (3) is truncated on the lateral side by a short, oval-shaped fossa synovialis (10). On the medial side there is a reflected surface, termed here the medial incision (11).

Lateral aspect (fig. 7.10.1e): Feature (1) represents a protuberance for the ligamentum tarsi dorsale obliquum with its accompanying peripheral rims (1', 1''). Feature (1''') is part of the lateral cranial facies which lacks a rugose surface. Features (2) and (3) are the proximal and distal facets, respectively. Features (4) and (5) are posterior and anterior facets for the cuboideum, respectively. Feature (10) is the incision for the lateral fossa synovialis.

Medial aspect (fig. 7.10.1f): This aspect finds the separation between the medial entrance of the proximal fossa synovialis (7) and the remainder of the medial incision (11). Also prominent in this view are features for the massive ligamentous attachment cited above (1, 1', 1''), the proximal articular facet for the naviculare (2), the distal articular facet for the MT III (3), anterior facet for the cuneiforme 1+2 (6).

Table 7.9. Summary Statistics on Cuneiforme 3

Measurement	Sample size	Mean	Standard Deviation	Confidence Limits		Coefficient of Variation		Confidence Limits		Minimum	Maximum	Median
m1	12	12,03	0,65	11,65	12,42	5,40	3,12	7,68	11,00	13,00	11,95	
m2	12	38,88	1,61	37,93	39,84	4,14	2,39	5,88	36,30	41,30	38,85	
m3	12	34,50	2,33	33,11	35,89	6,74	3,89	9,60	31,30	38,80	33,90	

Characteristic features of the cuneiforme 3: Compared to recent *Equus*, the Höwenegg hipparion has more weakly developed cranial ligamentous attachments and shorter fossae synoviales. There is no evidence in the Höwenegg sample for the presence of two small facets (for cuneiforme 1+2 and MT II respectively, distal to facet (4) in lateral view), as found by GROMOVA (1955: fig. 35 A 1, p. 107) in some other hipparionine horses.

Statistical Results

There were 3 variables measured for 18 specimens of cuneiform 3, 12 of which were analysed. The coefficient of variation was below 10 for each measurement. There was one significant correlation at the 95 % level: m2 (maximum mediolateral width)-m3 (maximum dorsoventral depth).

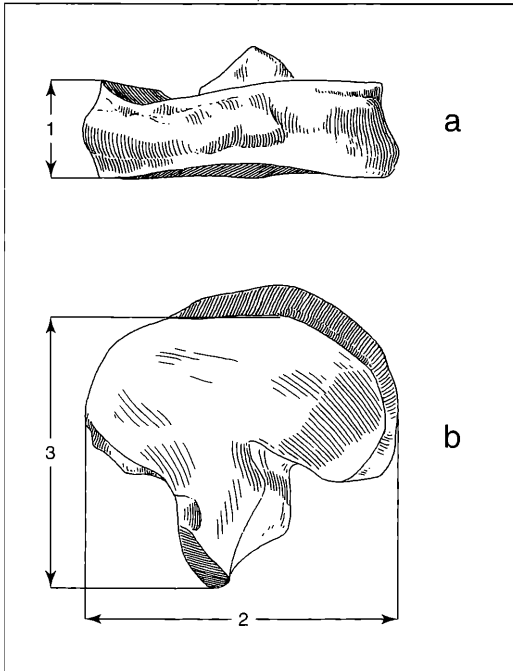


Figure 7.10.2. Measurements on the Cuneiforme 3: a. cranial aspect; b. proximal aspect: m1 = proximodistal diameter; m2 = maximum mediolateral diameter; m3 = maximum craniocaudal diameter.

7.11 Cuboideum (fig. 7.11.1a-f)

The cuboideum is the lateral bone of the distal tarsal row, and is approximately equal in its proximodistal dimension to the combined length of the naviculare and cuneiforme 3. In this way, the bone bridges the space between the first tarsal row and the metatarsus. The bone is quadrangular shaped with a craniocaudally long axis (fig. 7.11.1d, e and f). Of its six aspects, three (cranial, caudal and lateral) surfaces are continuously rugose and are the sites for extensive ligamentous attachments (fig. 7.11.1a, b, e).

Cranial aspect (fig. 7.11.1a): The lateral half of this aspect is more rugose than the medial one, with the ligamentous scar of the lateral surface extending somewhat onto the cranial surface. Features (1) and (1') are the cranial and caudal borders of the large proximal calcaneal facet. On the medial side are found the anterior facet for the cuneiforme 3 (2) and the facet for the MT III (3). On the lateral side are found the smaller cranial (5) and larger caudal (6) ligamentous tuberosities for attachment of the ligamentum collaterale tarsi longum laterale and plantare, respectively. Feature (7) is an obliquely oriented smooth furrow, which when in articulation with the adjacent bones, forms a canal for the passage of the proximal perforating vascular structures.

Caudal aspect (fig. 7.11.1b): The cranial (1; background) and caudal (1'; foreground) portions for the calcaneal facet are found proximally. Medially and closely adjacent to one another are found: the posterior facet for the naviculare (9), the posterior facet for the cuneiforme 3 (8), the furrow for vascular structures of the tarsus (7) and the facet for MT IV (4). Caudally is found a thicker ligamentous tuberosity.

Proximal aspect (fig. 7.11.1c): This aspect is dominated by the large facet for the calcaneum (1), together with its caudally directed process (1') and the medially located astragaloid oval facet (10). Craniomedially, is the anterior facet for the cuneiforme 3 (2). Medially, is the posterior facet for the naviculare (9). Features (5) and (6) are the two lateral ligamentous tuberosities of the lateral wall.

Distal aspect (fig. 7.11.1d): This aspect is dominated by the articular surfaces for MT III (3) and MT IV (4). Feature (8) is the posterior facet for the cuneiforme 3 and feature (7) is the caudal portion of the canalis tarsi. Features (5) and (6) are of the lateral aspect.

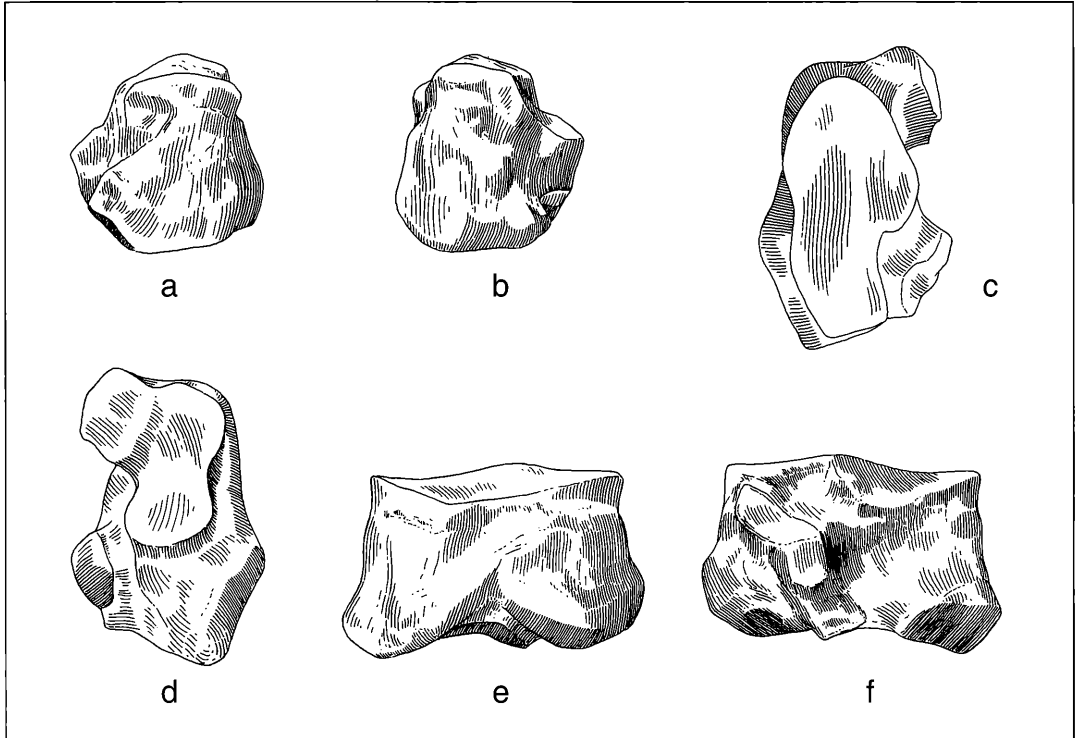


Figure 7.11.1. Cuboideum: a. cranial aspect; b. caudal aspect; c. proximal aspect; d. distal aspect; e. lateral aspect; f. medial aspect (x 1,0).

Lateral aspect (fig. 7.11.1e): Proximally are found the calcaneal facet (1) and (1'), while distally is found the MT IV facet (4). The lateral surface is dominated by two ligamentous tuberosities, (5) and (6). The larger caudal tuberosity (6) is the attachment surface for the ligamentum collaterale tarsi longum plantare, while the smaller (5) is the attachment surface for the ligamentum collaterale tarsi longum laterale (ZHEGALLO 1978: fig. 32, p. 50).

Medial aspect (fig. 7.11.1f): This aspect has a variegated topography with several facets, grooves and eminences. Proximally is found the caudal portion of the facet for the calcaneum (1'), the facet for the astragalus (10), and somewhat more caudally, the anterior facet for the naviculare (11). Distally are located the

caudal ligamentous tuberosity (6), the facet for MT IV (4), the facet the cuneiforme 3 (2) and the facet for MT III (3). Caudally, the medial surface has the posterior facet for the naviculare (9) coursing obliquely and distally to join the posterior facet for the cuneiforme 3 (8); these facets are themselves separated by a faint ridge. Cranial to facets (8) and (9) is the perpendicularly coursing furrow for the tarsal vascular canal (7).

Characteristic features of the cuboideum: Comparisons of the Höwenegg hipparion cuboideum with recent *Equus* can be made referring to GROMOVA (1955: pp. 107-109) and HUSSAIN (1975: 203).

Statistical Results

There were 3 variables measured for 20 specimens of cuboideum, 14 of which were analysed. Coefficient of

Table 7 10. Summary Statistics on Cuboidea

Measurement	Sample size	Mean	Standard Deviation	Confidence Limits		Coefficient of Variation	Confidence Limits		Minimum	Maximum	Median
m1	14	27,14	2,14	25,96	28,32	7,88	4,79	10,97	21,50	29,40	27,80
m2	14	39,53	1,88	38,49	40,56	4,75	2,89	6,60	37,00	43,50	39,25
m3	13	25,07	2,53	23,62	26,52	10,08	5,96	14,20	21,80	30,40	23,60

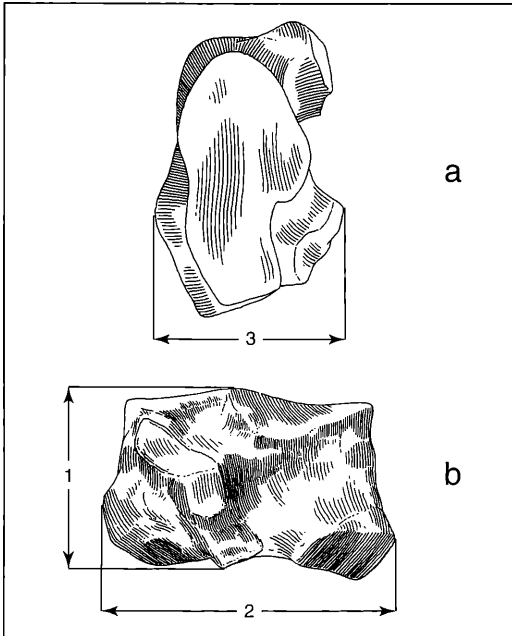


Figure 7.11.2. Measurements on the Cuboideum: a. proximal aspect; b. medial aspect. m1 = maximum craniocaudal diameter; m2 = maximum proximodistal diameter; m3 = maximum mediolateral diameter.

variation was below 10 for all measurements except m3, which was only slightly elevated (CV = 10.08). There was one significant correlation at the 95 % level: m2 (maximum craniocaudal length)-m3 (maximum mediolateral breadth).

7.12 Metatarsale III (fig. 7.12.1a-f)

There are 32 metatarsal III's (MT III's) in the Höwenegg sample, mostly belonging to the articulated skeletons. Often, the MT III's come as pairs of a single skeleton. The MT III's are consistently more massive, elongate and more strongly built than the MC III's. Along with the astragali, calcanea and MC III's, the MT III's are the most common element in the Höwenegg assemblage.

Cranial aspect (fig. 7.12.1a): In this aspect, the diaphyseal surface is smooth and the shaft has a rounded cross section (not semicylindrical as at the MC III). The proximal border reveals the slightly concave surface of the proximal facet (1). Just distally there is a well developed tuerositas metatarsi (2) for partial ligamentous attachment of the ligamentum tarsi dorsale and insertion of the musculus tibialis cranialis. Laterally feature (3) includes the superior and inferior facets for the cuboid. Distally are found the crista sagittalis (4), medial (4') and lateral (4'') trochleae for articula-

tion with the 1st phalanx. Just proximal to the distal articular surface is a triangular depression, the fossa supertrochlearis metatarsi (6). This feature is similar, but more deeply and broadly developed (mediolateral = 30 mm; proximodistal = 20 mm) than its counterpart on the MC III (fig. 6.13.1a: 6). It permitted hyperextension (dorsiflexion) of the MT III – 1st phalangeal joint.

Caudal aspect (fig. 7.12.1b): The proximal margin bears several joint facets. On the lateral border there is a larger triangular facet (7') for articulation with MC IV. This feature is separated by a 3 mm wide furrow from a smaller, circular facet (7''), also for articulation with MC IV. Both facets (7') and (7'') articulate with the MT IV. Medially, there is a rugose surface for a ligamentous attachment (8). Medially there are two larger facets for articulation with MT II: one more laterally (9'), the other on the medial border (9''). Distally, along a lateral parasagittal plane is found a flat rugose linear feature (10) which was the attachment site for the interosseous ligament attaching the MT IV to the MT III. This ligamentous depression fades at about 60 mm above the trochlea, where the distal end of the MT IV becomes free from a ligamentous connection with the MC III. A similar flat rugose depression (11) is found for interosseous attachment of the MT II and MT III. Feature (11) courses distally in a medial parasagittal plane to about 50 mm above the trochlea. Both MT II and MT IV would have been unbound to MT III by interosseous membranes from this point distally. Proximal to the trochlea are the supertrochlear grooves (12), separated by a continuation of the crista sagittalis (in fig. 7.12.1b damaged). They are shallower than the corresponding MC III grooves. Distally, the medial trochlea (4') is larger than the lateral one (4''). The distal sagittal crista (4), although damaged, is a sharp keel.

Proximal aspect (fig. 7.12.1c): The proximal surface is dominated by a facet for the cuneiform 3 (13). On the distolateral border is the facet for the cuboid (14). A small furrow (15) separates (14) from the small lateral facet for MT IV (7''). The furrow (15) has a counterpart on the distal facet of cuneiforme 3 (fig. 7.10.1c:10). This furrow (and others in the hipparion foot) functioned as a channel for synovial fluid (TOBIEN 1991, see also p. 22 of ms). Caudosagittally is found a ligament attachment surface (8). Medially are found the two articular facets for MT IV (9' and 9'').

Distal aspect (fig. 7.12.1d): This aspect presents the crista sagittalis (4) medially, the medial trochlea (4') and lateral trochlea (4''). As in extant *Equus* the medial trochlea is broader than its lateral counterpart. In contrast to *Equus* however is the cranial aspect of the crista sagittalis (4). While as in *Equus* the caudal profile is sharp and narrow (see graphs fig. 7.12.2 and text below), the cranial aspect is relatively flattened. Feature (6) is the prominent proximal border of the fossa supratrochlearis and feature (5) is the medial protuberance for the ligamentum collaterale.

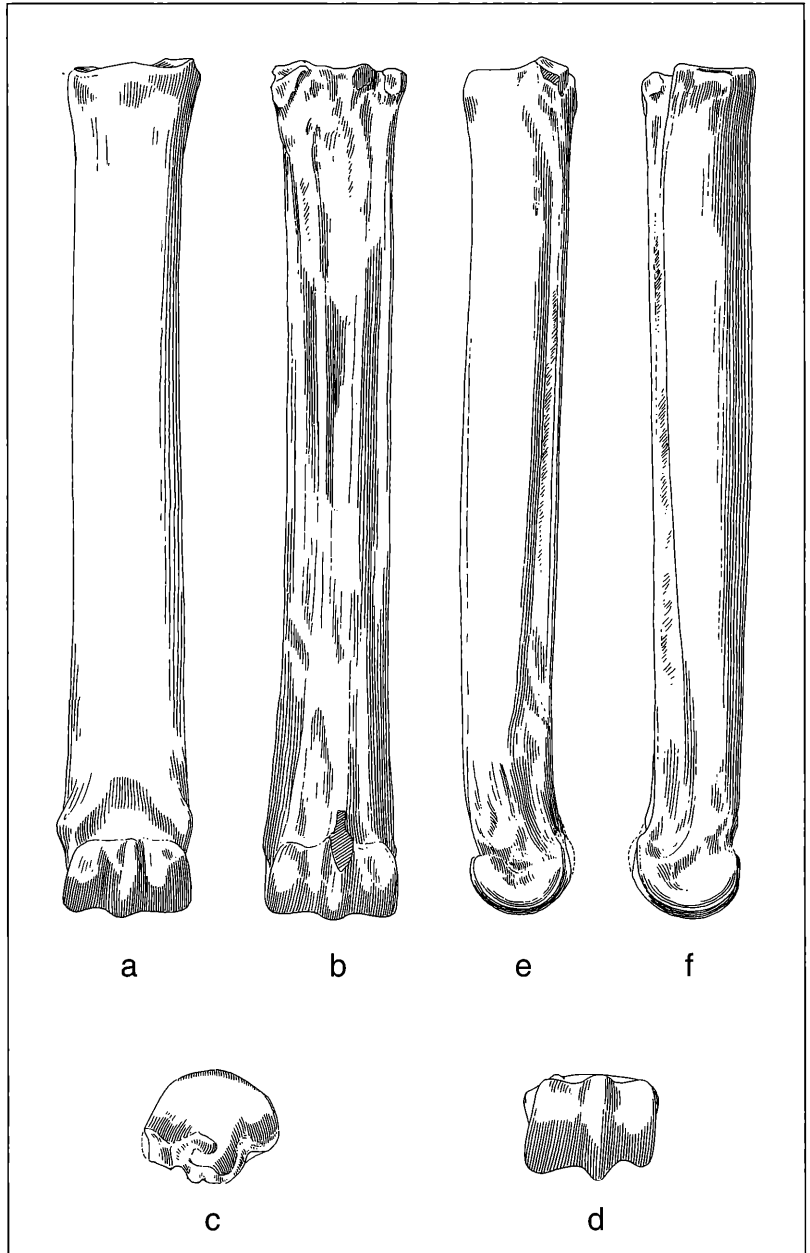


Figure 7.12.1. Metatarsale III: a. cranial aspect; b. caudal aspect; c. proximal aspect; d. distal aspect; e. lateral aspect; f. medial aspect (x 0,45).

Lateral aspect (fig. 7 12.1e): The cranial border is dominated by the tuberositas metatarsi (2). The cuboid facet (3) is caudally placed, and has clearly depicted the sharp ridge (14) dividing its superior, and more medial and inferior portions. Caudally is a rugose surface for ligamentous attachment (8). Feature

(16) is a groove for the laterally coursing dorsal metatarsal artery, common in extant *Equus*. There is another similar depression more distally (17), adjacent to feature (10), which would appear to be yet another vascular groove. We have not observed feature (17) either on the other Höwenegg MT III, nor recent

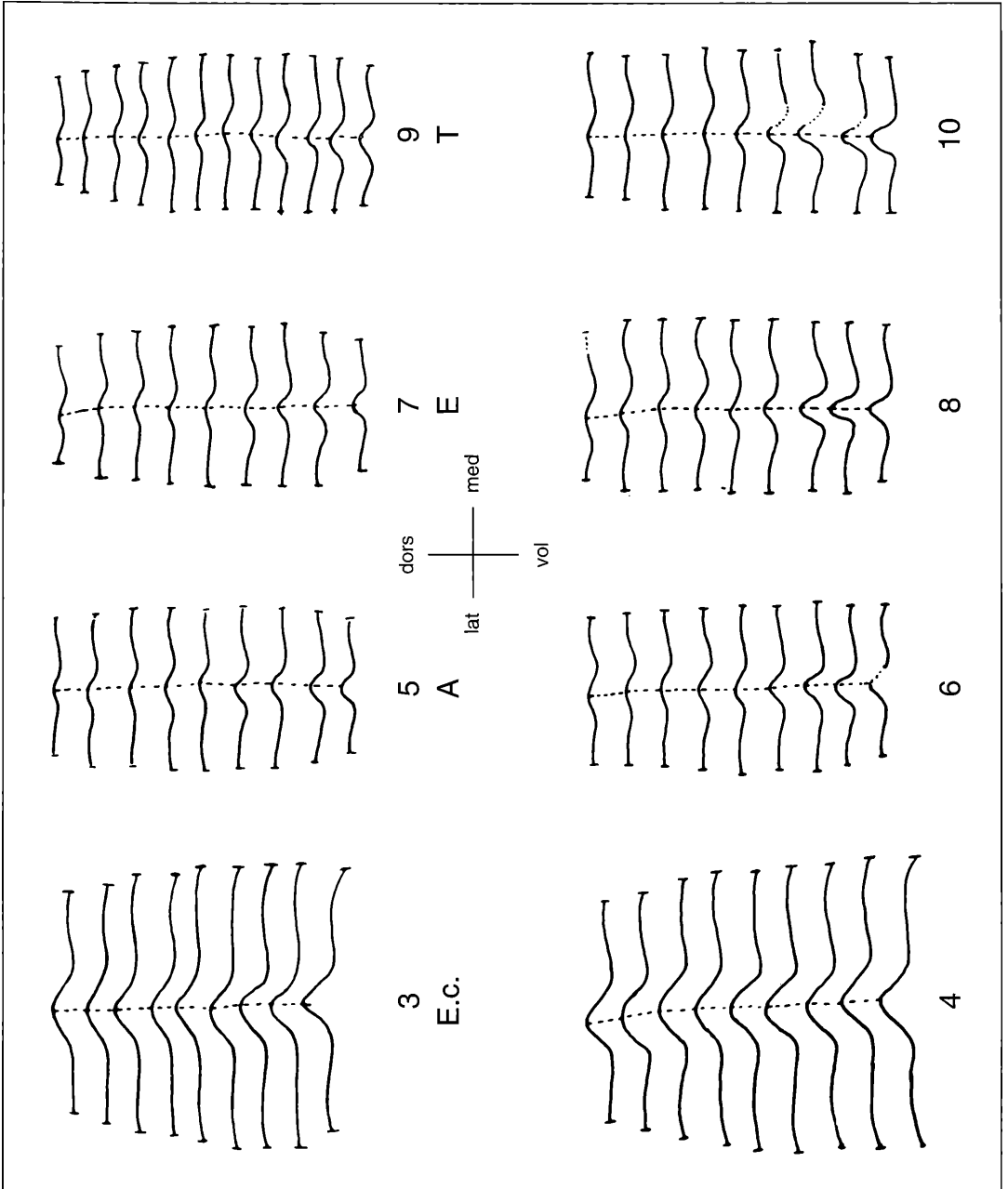


Figure 7.12.2. Profiles of Metatarsale III Distal Sagittal Keel Morphology

Equus. Perhaps this is an individual variant (see STEBLIN 1929; in TOBIEN 1982). Feature (18) is a lateral depression for attachment of the ligamentum sesamoideum.

Medial aspect (fig. 7.12.1f): In this aspect the proximal end presents the lateral facet for MT II (9') and the medial tuberositas metatarsi (2) for ligamentous attachment. Feature (11) is the long, rugose ridge for

interosseous attachment of the MT II. As with the lateral counterpart (10), the ridge for the interosseous attachment of MT II and MT III (11) terminates well before the articular condyles of MT III. Feature (18) represents the lateral depression for attachment of the ligamentum sesamoideum (CAMP & SMITH 1942: fig. 7). Feature (4) and (4') are as described above.

Characteristic features of the Höwenegg MT III: Included are: 1) the large fossa supratrochlearis (6); 2) primitive, caudally flattened, crista sagittalis (4); 3) weak articular connection between proximal ends of MT III and MT IV (7''); 4) the lack of interosseous ligamentous connections distally between MT III and both MT II and MT IV; 5) presence of a broader medial trochlea (4') than lateral trochlea (4''); 6) presence of a well developed groove (15) for the fossa nudata (synovialis); 7) functional capability for hyperextension of the MT III – 1st phalangeal joint; 8) free distal ends of MT II (11) and MT IV (10), enabling some independent movement of these digits.

Some other comments on the function of the MT III – 1st phalangeal joint should be mentioned. It is apparent that the 1st phalanx contacted the dorsal border of the MT III during hyper-extension (dorsiflexion) of the joint (GROMOVA 1955: 110, fig. 40, A2:x). The depression for the fossa supratrochlearis (6) is strongly developed in the Höwenegg hipparion and contrasts sharply with the homologous shallow or absent depression in extant *Equus*. The function of this feature was previously discussed by GROMOVA (1955:111), HUSSAIN (1975:207) and TOBIEN (1982:1047) and believed to have allowed greater dorsiflexion of the 1st phalanx, which in turn resulted in bringing the fetlock joint closer to the ground. In *Equus* and other monodactyl equids, the absence of this groove depression sharply limits dorsiflexion, but may contribute to a greater springing capability in the extant horse.

The flexion directing the crista sagittalis (4) remains low dorsally in the Höwenegg horse, which is an archaic feature. Using a perigraph (used by physical anthropologists; TOBIEN 1962), a series of transverse sections were drawn every 10 mm, proximo-distally, for the MT III (including Höwenegg skeletons A, E & T; fig. 7.12.2: 5-10). The palmar (volar) drawings show the large and sharp peaks corresponding to a prominent crista sagittalis (fig. 7.12.1b, c, d). In the dorsal section, where the maximum metatarsal III – 1st phalangeal dorsiflexion takes place, the sagittal-peaks decrease in height (fig. 7.12.2a: 5-10: upper (dorsal) parts in the figures). There would appear to be no strong functional correlation between the extreme dorsiflexion capability at the 1st phalanx – MT III joint and the development of a prominent sharp "guiding" crista (4). However, when true functional monodactyly was achieved in *Equus*, the crista sagittalis did acquire its actual uniform sharp development.

Statistical Results

There were 14 variables measured for 36 specimens of MT III, 24 of which were analysed. The coefficient of variation was below 10 for each measurement except m8 (CV = 19.42; diameter of the articular facet for fourth tarsal) and m9 (CV = 30.95; diameter of the articular facet for the second tarsal). These facets are analogous to those on the metacarpal III which also showed similarly elevated CV's. There were 26 significant correlations, 10 of which were at the 99 % level of significance.

The two length measurements, m1 and m2, correlated the most highly ($r = 0.988$), but this was due strictly to the parallel nature of these measurements; interestingly enough neither correlated highly with any other variable. The two medial-shaft measurements m3 (mediolateral) and m4 (depth) were the next most highly correlated, again due to their nearly identical defini-

Table 7.11. Summary Statistics on Metatarsale III

Measurement	Sample size	Mean	Standard Deviation	Confidence Limits	Coefficient of Variation	Confidence Limits	Minimum	Maximum	Median
m1	18	242,52	7,76	238,74 246,29	3,20	2,10 4,30	223,90	252,10	242,25
m2	19	237,19	7,28	233,75 240,64	3,07	2,04 4,10	218,90	247,90	236,00
m3	24	31,39	2,25	30,44 32,33	7,15	5,01 9,30	24,80	35,00	31,65
m4	24	28,62	1,63	27,93 29,30	5,68	3,99 7,38	23,70	32,00	28,60
m5	18	41,77	2,09	40,75 42,79	5,01	3,28 6,74	37,30	46,50	41,80
m6	19	34,29	2,29	33,20 35,37	6,68	4,43 8,93	30,60	40,20	34,60
m7	16	39,46	1,44	38,72 40,21	3,66	2,32 4,99	37,10	43,10	39,35
m8	17	9,89	1,92	8,93 10,85	19,42	12,29 26,55	6,10	14,00	9,90
m9	16	6,53	2,02	5,49 7,57	30,95	18,62 43,27	3,10	9,00	7,10
m10	22	39,65	2,77	38,44 40,87	6,98	4,79 9,16	30,40	43,40	39,45
m11	23	37,77	1,89	36,96 38,58	4,99	3,47 6,52	34,90	42,00	37,70
m12	22	30,70	1,21	30,17 31,23	3,94	2,71 5,17	28,60	34,30	30,65
m13	23	25,33	1,29	24,78 25,88	5,08	3,53 6,63	22,80	28,80	25,20
m14	23	27,27	1,72	26,53 28,01	6,29	4,37 8,21	23,40	29,90	27,20

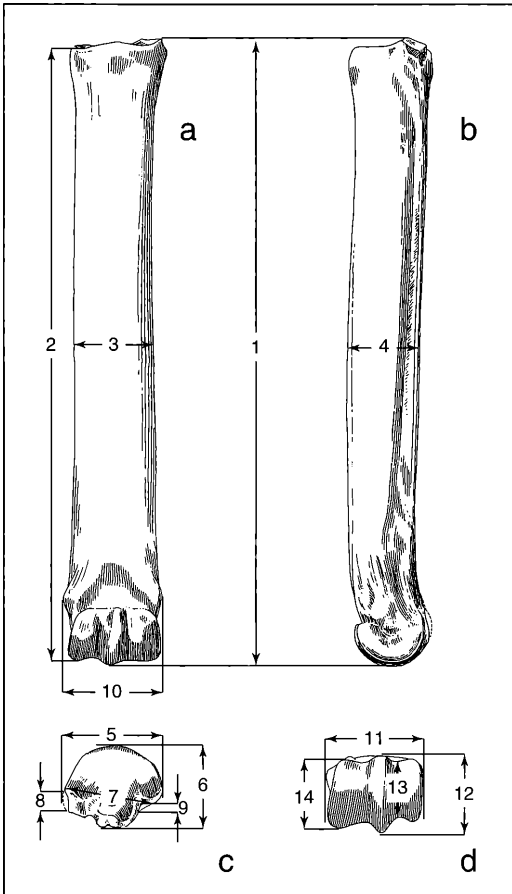


Figure 7.12.3. Measurements on the Metatarsale III: a. cranial aspect; b. lateral aspect; c. proximal aspect; d. distal aspect.

tions. Measurement 3 was further significantly correlated with m11 (distal maximum articular breadth), m7 (maximum diameter of the articular facet for the third tarsal), m5 (proximal articular breadth) and m12 (distal maximum depth of the keel). Measurement 4 was significantly correlated with m14 (distal maximum depth of the medial condyle), m11, m7, m12 and m13 (distal maximum depth of the lateral condyle).

There were five standard measurements taken of the proximal articular surface: m5 (proximal articular breadth); m6 (proximal articular depth); m7 (maximum diameter of the articular facet for the third tarsal); m8 (diameter of the articular facet for the fourth tarsal); m9 (diameter of the articular facet for the second tarsal). Interestingly, only m6 showed no significant correlation. Measurement 5 showed a significant negative correlation with m9 suggesting that as proximal articular breadth increased, the facet diameter decreased. A

plausible explanation may be that as more weight is directed through metatarsal III itself, there is less load borne on the surface articulating with the second tarsal, and hence less articular facet diameter. Measurement 5 showed further significant correlations with m7, m10, m11 and m12. Measurement 7 showed significant correlations with distal articular measurements m13, m12, m10 and m11. Measurement 8 correlated with distal articular measurements m11 and m14.

There were five distal articular measurements taken (note that we omitted recommended m15 because of intrinsic variability in this measurement and its dubious value for biological explanation): m10 (distal maximum supra-articular breadth), m11 (distal maximum articular breadth), m12 (distal maximum depth of the keel), m13 (distal minimum depth of the lateral condyle) and m14 (distal maximum depth of the medial condyle). Other than those correlations cited above, the following correlations were found: m12-m13, m11-m13, m13-m14.

Figure 7.12.4a-d renders our results on bivariate measurements of MT III: a) M11 x M1 (distal maximum articular breadth x maximum length); b) M6 x M1 (proximal articular depth x maximum length); c) M3 x M1 (minimal [approximately mid-diaphyseal] width x medial length); and d) M11 x M12 (distal maximum articular breadth x distal maximal depth of mid-sagittal keel). There is no evidence of sexual dimorphism found in these plots.

7.13 Sesamoidea of Distal Metatarsale III (fig. 7.13.1a-f)

There are several pairs of sesamoidea of distal MT III posterior (ossa sesamoidea proximalia digiti III posterioris or sesama bina of veterinarianian nomenclature). These include both left and right elements from the articulated skeletons. Their anatomical position is identical to those articulating with MC III (fig. 6.14.1.1&2 'g), and articulate with the MT III at its crista sagittalis. Morphologically they are virtually identical to the anterior sesama bina, and we limit our discussion to their most distinguishing features.

The medial sesamoid (fig. 7.13.1.1a-f):

Dorsal aspect (fig. 7.13.1.1a): The most distinctive feature of this aspect is the shortened distomedial border of articular facet (2''). The anterior sesamoid counterpart has this border distomedially extended (fig. 6.14.1.1a), giving it a transversely broader base.

Palmar aspect (fig. 7.13.1.1b): The abbreviated distomedial border (2'') gives a narrower basis angle (3) between the interosseus facies (5) and the facies flexoria (6). The contrast between the roughened facies (5) and the smooth facies (6) is ubiquitous for all anterior and posterior sesama bina.

Proximal aspect (fig. 7.13.1.1c): There are no differences in this aspect with the counterpart in the anterior limb.

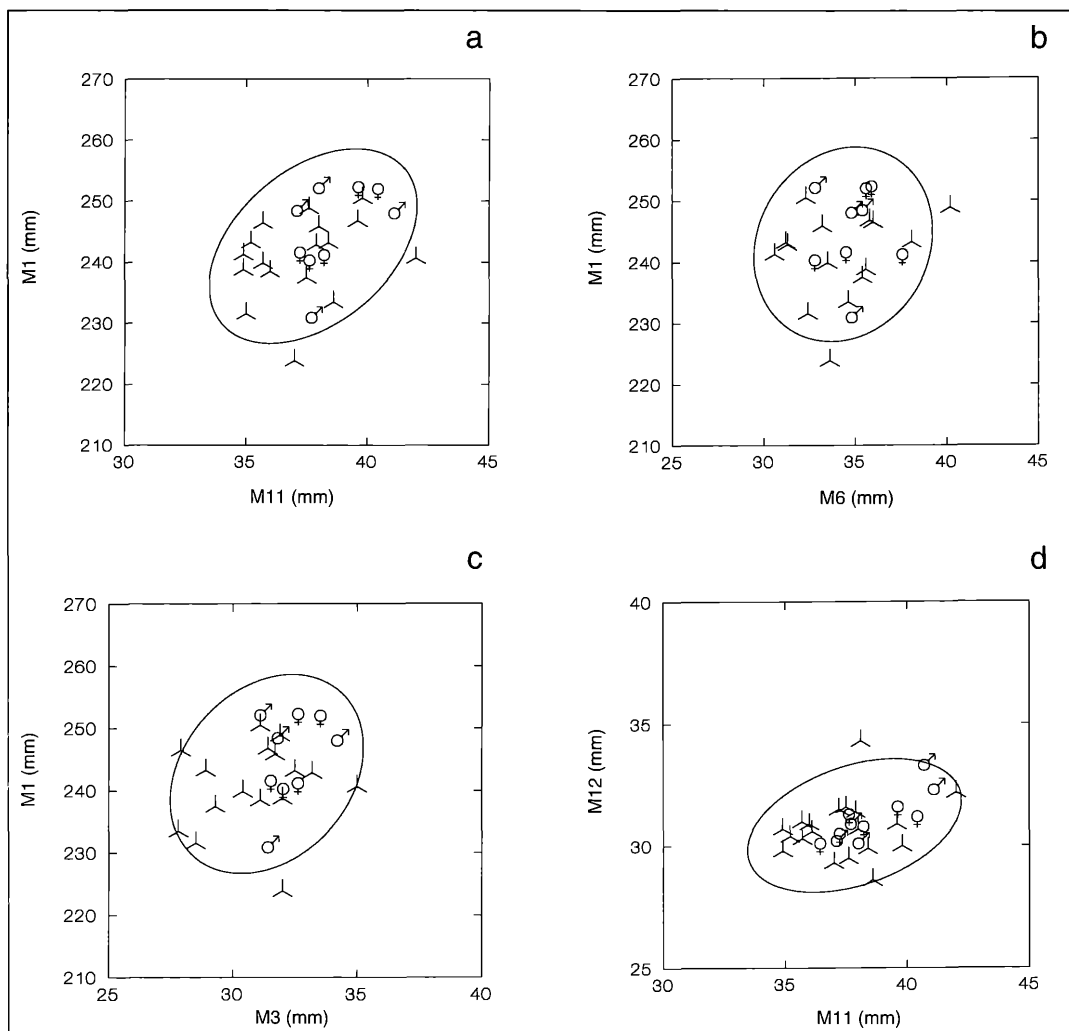


Figure 7 12.4. Bivariate Plots on the Metatarsale III: a. M11 x M1; b. M6 x M1; c. M3 x M1; d. M11 x M12.

Distal aspect (fig. 7.13.1.1d): This aspect is dominated by the basis (3), which has at its dorsomedial border two well defined rugose surfaces: an elongated tuberosity (3') and a rounded eminence (3''), both for ligamentous attachment.

Lateral aspect (fig. 7.13.1.1e): As exemplified in this specimen, there is often a flat, proximodistally coursing groove (6') just dorsalward of the palmar middle crest (4). Another rather constant feature is the narrow groove (6'') which courses parallel to the peripheral facet rim (1').

Medial aspect (fig. 7.13.1.1f): There are no differences in this aspect with the counterpart in the anterior limb.

Characteristic features of the medial sesamoid of distal MT III: Included are: 1) the shortened disto-medial border of the articular facet (2'') giving the narrower basis angle (3) than found in the anterior limb's counterpart sesamoid; 2) the roughened facies (5); 3) the smooth facies (6); 4) the proximodistally coursing groove (6'); 5) the narrow groove (6'') coursing parallel to the peripheral facet rim (1').

The lateral sesamoid (fig. 7.13.1.2a-f):

In comparison to the anterior counterpart of this bone, we find only slight, and inconsistent differences in the morphology of the tendinous attachments at the basis (3) which elude characterization.

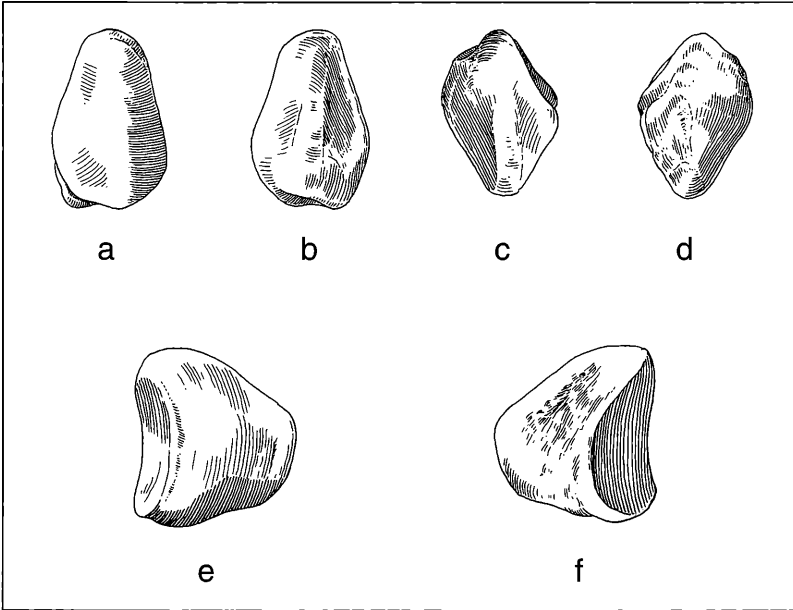


Figure 7.13.1.1. Medial Sesamoidea of the Distal Metatarsale III: a. dorsal aspect; b. palmar aspect; c. proximal aspect; d. distal aspect; e. lateral aspect; f. medial aspect (x 1,0).

Based on material from Taraklia (Moldavia), GROMOVA (1955: 122, fig. 50 V, V') noted that there are two groups of sesama bina: one proximally elongated and tapered (fig. 50 V'), the other shortened (fig. 50V). Based on our observations here, it is most likely that the the former morphology characterizes the hindfoot sesamoids, while

the latter characterizes the forefoot sesamoids. The Höwenegg sesamoidea exhibit a somewhat different morphological pattern: the relatively slender, proximally-pointed sesamoids belong to the forefoot, and the shorter, proximally abridged bones are elements of the hind foot. This pattern is found in some extant *Equus*.

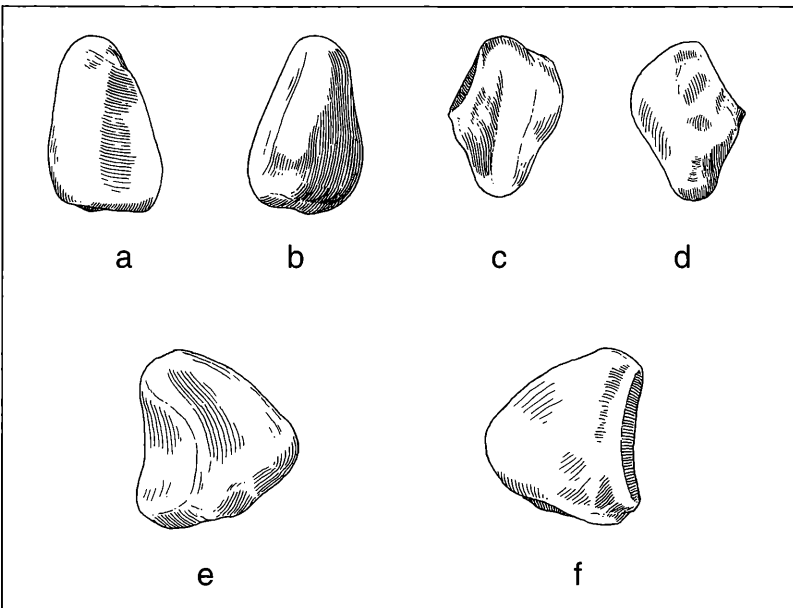


Figure 7.13.1.2. Lateral Sesamoidea of the Distal Metatarsale III: a. dorsal aspect; b. palmar aspect; c. proximal aspect; d. distal aspect; e. lateral aspect; f. medial aspect (x 1,0).

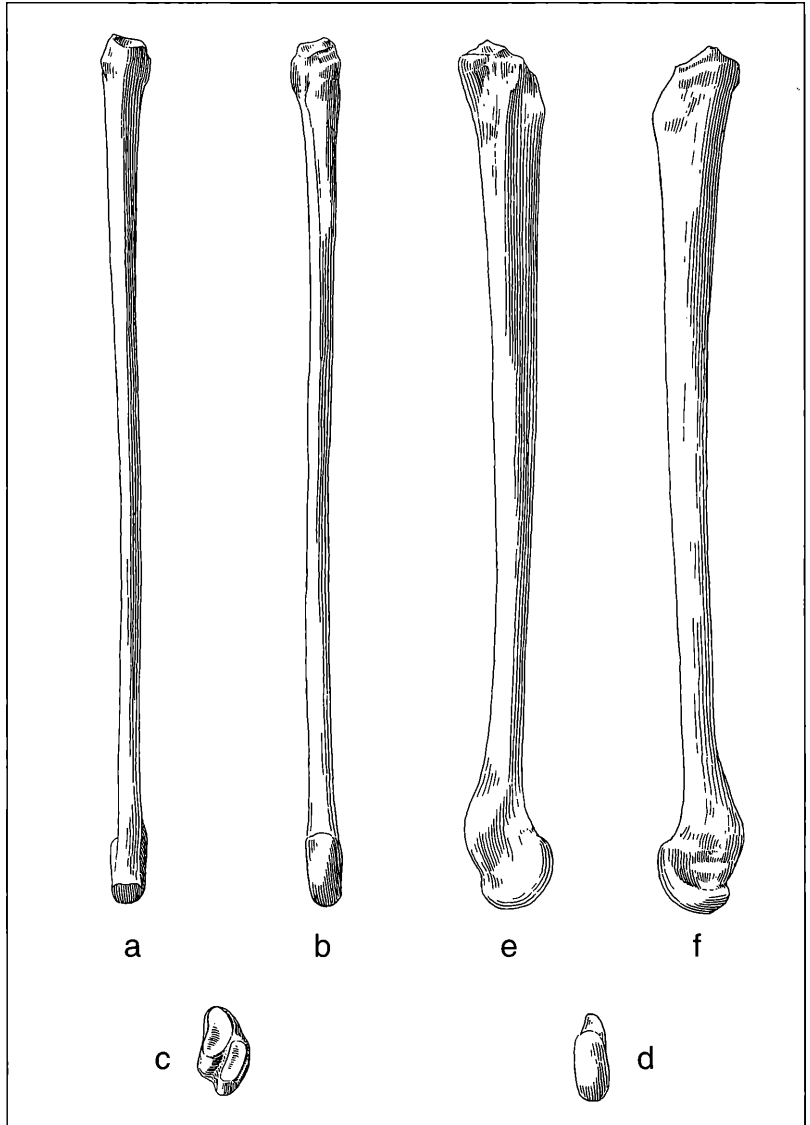


Figure 7.14.1. Metatarsale II: a. cranial aspect; b. caudal aspect; c. proximal aspect; d. distal aspect; e. lateral aspect; f. medial aspect (x 0,50).

7.14 Metatarsale II (fig. 7.14.1a-f)

There are 18 mostly complete MT II's derived from the articulated skeletons. As the MT III's vary in size, so do the MT II's: length range = 211.9 – 235.9 mm. The MT II diaphyses are more slender than those of the MC II's, but the proximal epiphyses are more robustly built than in the MC II.

Cranial aspect (fig. 7.14.1a): Proximally, this aspect presents the facet for the cuneiform 1 (1), laterally the border of the caudal facet for articulation with the MT III (3), and medially a protuberance for ligamentous

attachment (4). Feature (6) represents the smooth medial surface of the bone. A sharp, proximodistally coursing edge (5), separates (6) from the lateral wall, the cranial portion of which is roughened for the ligamentum metatarsum (7; for connection of MT II with MT III). The roughness, however, disappears distally after 2/3rds the length of the bone, marking its terminus. At the terminus, the shaft becomes rhomboidal shaped. Feature (8) is the short end of the articular facet; it projects much further distally.

Caudal aspect (fig. 7.14.1b): Proximally, this aspect presents the smaller facet for articulation with the cuneiforme 2 (2). Medially there is a massive ligamentous protuberance (9). Distally on the diaphysis is the upper portion of a slightly broadened, proximodistally coursing, caudal keel (10). This keel (10) separates the smoother portions of the lateral wall (7') from the overall smoother and convex medial wall (6). Located distally is the proximally extended articular facet (8) with a very faint keel. Just proximal to the facet is a flat fovea (8'), which contrasts in its greater shallowness with feature (7'') of the MC II (fig. 7.14.1b).

Proximal aspect (fig. 7.14.1c): This aspect presents a larger lateral facet for the cuneiforme 1 (1) and smaller medial facet for the cuneiforme 2 (2). These two features are separated by a distinct, rather deep furrow (14). Feature (6) represents the bone's medial border.

Distal aspect (fig. 7.14.1d): This aspect is dominated by the distal articular facet (8) for the digit's 1st phalanx. Feature (8)'s proximodistal axis is depicted here as being obliquely oriented with respect to the diaphysial axis (represented here by the processus supraarticularis 12). In the MC II the angle that the articular facet makes with the diaphysis is actually greater.

Lateral aspect (fig. 7.14.1e): This aspect again presents a portion of the articular facet for the cuneiforme 1 (1). The border of the caudal facet for the MT III (3) is well presented here. Feature (11) is the cranial facet for this same contact. Both facets (3) and (11) are rather small and lack contour, suggesting a limited functional connection with the MT III. Distally, feature (12) is the prominent processus supraarticularis. The hypertrophy of this structure emphasizes the strong retroversion of the distal articular head. Feature (13) is a broad, but flat depression for the ligamentum collaterale laterale. Features (7) (7') (8) and (8') are as in figures 7.14.1a, b.

Medial aspect (fig. 7.14.1f): This aspect presents the entire smooth medial wall of MT II (6). The smooth wall is bounded by sharp cranial (5) and caudal (15) keels. The caudal keel (15) descends beginning just inferior to the protuberance (4), distally, approximately 2/3rds of the diaphysis' length. Along this length it makes a right angle with the MT II lateral wall, and a smoother, convex border with the medial wall. Distally, the caudal keel (15) dissipates as a low rugose ridge. Features (1), (2) and (11) are as in figures fig. 7.14.2c and e, features (8), (8') and (12) as in figures 7.14.1a, b, d and e.

Characteristic features of the Metatarsale II: Included are: 1) the proximal heads of the MT II are structurally very similar to those of *Equus*; 2) the slenderness of MT II is not only expressed in the cranial and caudal views but also in the medial and lateral aspects; 3) there is a very faint crista sagittalis on the caudal portion of joint facet (8); retroflexion of the distal portion of feature (8) is strong, emphasized by the processus supraarticularis (12). The torsion of the distal epiphysis on the diaphysis is low.

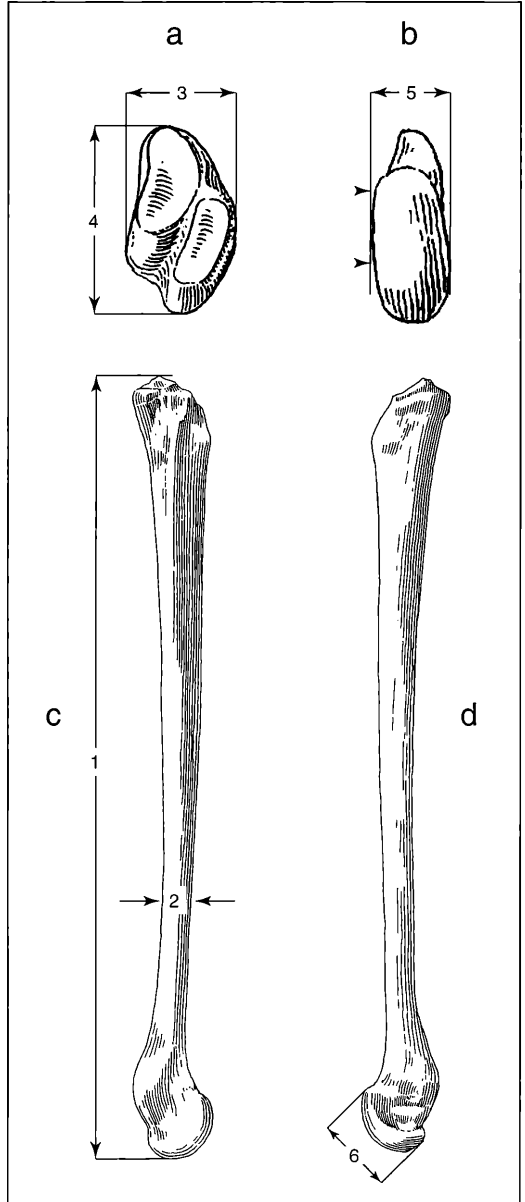


Figure 7.14.2. Measurements on the Metatarsale II: a. proximal aspect; b. distal aspect; c. lateral aspect; d. medial aspect.

Statistical Results

There were 6 variables measured for 16 specimens, 9 of which were analysed. The coefficients of variation were below 10 for all measurements. There was one significant correlation at the 95 % level: m5 (distal articular breadth); m6 (distal articular depth).

Table 7.12. Summary Statistics on Metatarsale II

Measure- ment	Sample size	Mean	Standard Deviation	Confidence Limits	Coefficient of Variation	Confidence Limits	Minimum	Maximum	Median
m1	8	223,09	5,86	218,81 227,36	2,63	1,27 3,98	211,90	229,40	224,00
m2	9	11,19	0,94	10,54 11,84	8,40	4,29 12,52	10,00	12,50	11,10
m3	8	21,85	1,55	20,72 22,98	7,11	3,42 10,79	19,60	23,80	22,10
m4	8	15,38	0,88	14,73 16,02	5,75	2,77 8,73	13,90	16,50	15,50
m5	9	10,48	0,59	10,07 10,88	5,64	2,89 8,40	9,70	11,50	10,60
m6	9	21,87	0,91	21,24 22,49	4,17	2,14 6,21	20,80	23,70	21,60

7.15 Sesamoidea of the Distal Metatarsale II (fig. 7.15.1a, a'-f, f')

The metatarsale II sesamoidea includes a larger abaxial (= medial) element, and a smaller adaxial (= lateral) element fused together along their sagittal contact (fig. 7.15.1a-f: the larger sesamoid, fig. 7.15.2a'-f': the smaller sesamoid). As explained below, the MT II sesamoid is a virtual mirror-image of the MT IV sesamoid.

Dorsal aspect (fig. 7.15.1a, a'): The articular facet is smooth and has sharply delineated borders. The abaxial portion has a flat surface, while the adaxial surface rises abruptly as it approaches the adaxial border. The apex (a1) and basis (a3) protrude palmarward. Features (a'1) and (a'3) are the corresponding portions of the small (adaxial) element.

Palmar aspect (fig. 7.15.1b, b'): This aspect presents the maximal dorsopalmar extension of both the large and small sesamoids (a1-a3, a'1-a'3, respectively) and the adaxial (a'4) and abaxial (a5) facies. Feature (a7) is the abaxial facies for the flexorius, and adaxially (aba') is found the coossification suture for the two sesamoidea.

Proximal aspect (fig. 7.15.1c, c'): Proximally, the suture (aba') forms a furrow, which is bordered by the facies (a7) of the flexorius of the large (abaxial) sesamoid, and by the facies (a'8) of the small element. This furrow houses a tendon of the flexorius profundus, which inserts at the procesus palmaris lateralis of the posterior 3rd phalanx of digit III (fig. 7.20.1).

Distal aspect (fig. 7.15.1d, d'): In this aspect feature (aba') has a rather broad, and somewhat shallower coossification contact than found in the proximal view. Features (a2), (a'2), (a3), (a'3) (a'4), (a5), (a7) (a'8) are as in the previously described views.

Adaxial (lateral) aspect (fig. 7.15.1e, e'): The aspect reveals the striking size contrasts between the small (adaxial) and large (abaxial) sesamoids. The numbered features are as on the previous figures.

Abaxial (medial) aspect (fig. 7.15.1f, f'): This aspect is dominated by the facies for the abaxial branch of the interosseus medius (a5). The surface of (a5) is roughened and in parts provided with fine pori. The large sesamoid's apex (a1) is a characteristic feature found in most Höwenegg individuals.

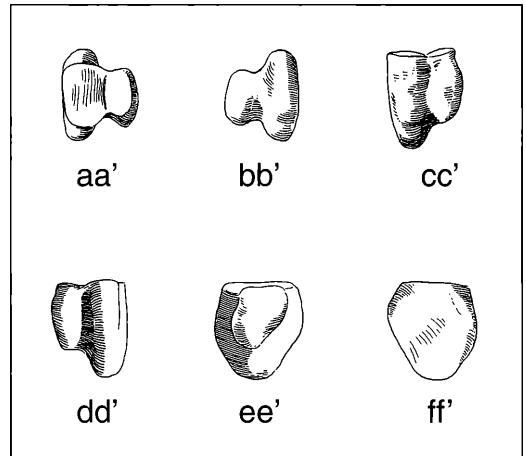


Figure 7.15.1. Sesamoidea of the Distal Metatarsale II: aa' dorsal aspect; bb' palmar aspect; cc' proximal aspect; dd' distal aspect; ee' adaxial aspect; ff' abaxial aspect (x 1,0).

Characteristic features of the metatarsal II sesamoid: Included are: 1) the presence of a coossified pair with the adaxial portion being sharply subequal in size to the abaxial one; 2) presence of a large dorsal facet; 3) lack of any morphological difference between the right and left MT II sesamoid.

7.16 Metatarsale IV (fig. 7.16.1a-f)

There are 18 mostly complete left and right MT IV's derived from the articulated skeletons. The size differences between MC IV and MT IV are of a similar magnitude to those found between the MC II's and MT IV's. Maximum length measurement ranges are: MC IV – 183.4 – 193.0; MT IV: 215.8 – 237.6. In the Hö A skeleton MT IV is 14.7 % longer than the MT II, and the MT III is 12.7 % longer than the MC III.

Cranial aspect (fig. 7.16.1a): Proximally this aspect presents the articular facet for the cuboid (1). Distally, is located the mediocranial facet for MT III (2). Medially, is the MT III articular facet (3). Distal to the epiphysis

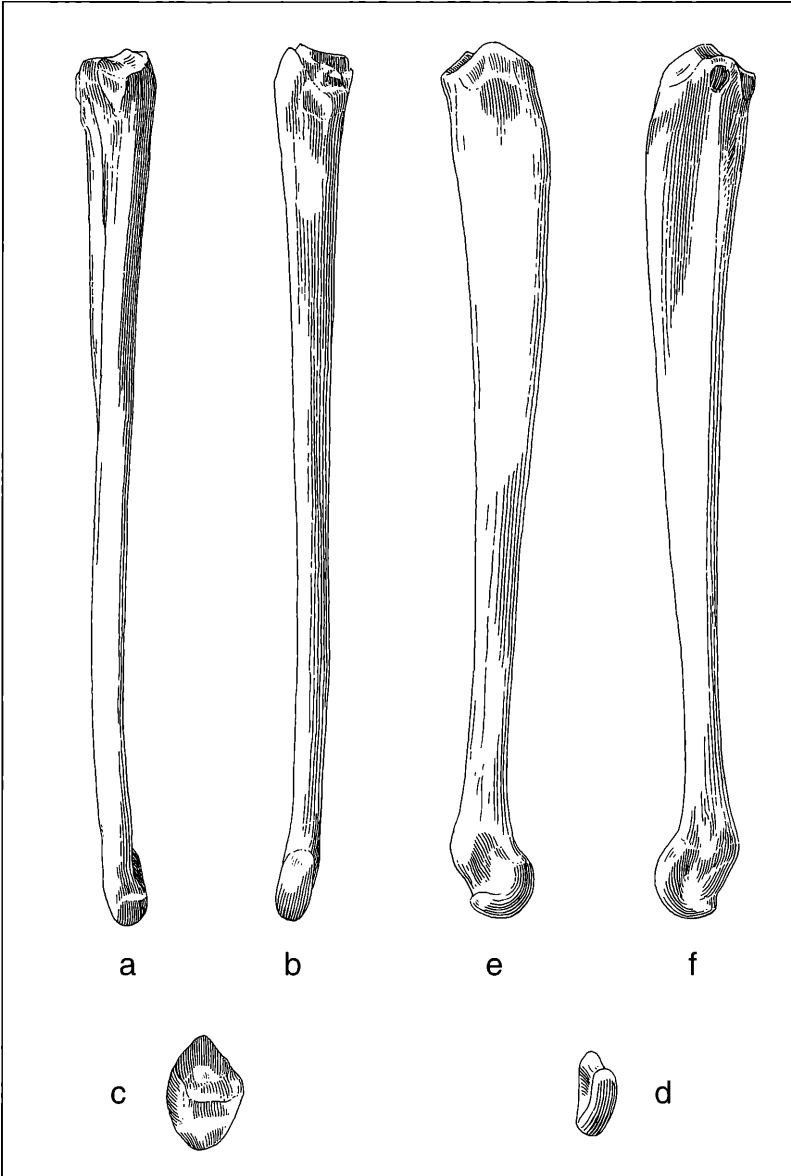


Figure 7.16.1. Metatarsale IV: a. cranial aspect; b. caudal aspect; c. proximal aspect; d. distal aspect; e. lateral aspect; f. medial aspect (x 0,50).

there is a roughened, proximodistally extended insertion for the ligamentum metatarsium (4), which connects the MT IV with its counterpart on the MT III. Feature (4) narrows distally and its rough texture dissipates approximately at the limit of the medial and distal 1/3rd of the bone. It forms, together with feature (5), the rounded cranial border of the MT IV (6). Feature (8) is the cranial portion of the distal joint, and feature (9) is the prominent beak-like processus supraarticularis.

Caudal aspect (fig. 7 16.1b): In this aspect feature (1) is presented as a slightly inclined, flat structure. Just distally is a large protuberance for ligamentous attachment (10). Further distally is the rounded caudal edge (11) separating the medial (5) and lateral diaphysial walls (7). Feature (11) is the rounded caudal edge, coursing distally to the articular facet (8) which rises further proximally on this side than on the cranial side.

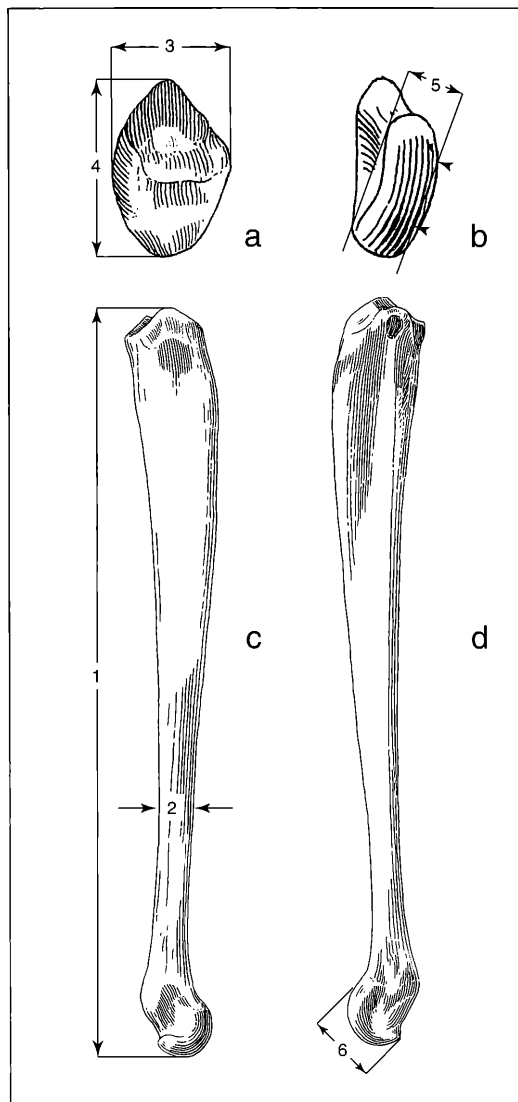


Figure 7.16.2. Measurements on Metatarsale IV: a. proximal aspect; b. distal aspect; c. lateral aspect; d. medial aspect.

Proximal aspect (fig. 7.16.1c): In this aspect the cranial portion is dominated by the large, angular articular facet for the cuboid (1). In the center of this facet is a "non-articular" area measuring 5 x 6 mm. A similar "non-articular" area exists adjacent to the cuboid's MT IV facet (5 x 4,4 mm). TOBIEN (1991) has interpreted these as being fossae nudatae. The MT IV facets of the other cuboids have similar fossae nudatae, but these are smaller and less developed (II-53 right, 77/56 right, 979/62 right, B-119 left, J-38 right), and would appear to be a consistent feature of the MT IV's. It is not known whether they are present in extant *Equus*. Feature (10) is the proximal view of the ligamentous protuberance.

Distal aspect (fig. 7.16.1d): This aspect clearly depicts the torsion of the distal articular facet (8) on the diaphysal axis. Feature (9) is the prominent processus supraarticularis, and feature (12) is a depression for the ligamentum collaterale laterale.

Lateral aspect (fig. 7.16.1e): Proximally, this aspect depicts the cranially-directed inclination of the cuboid facet (1). The broad lateral wall (7) is clearly seen, and bounded cranially by the attachment surface for the ligamentum metatarsium (4). Features (8), (8'), (9) and (12) are as cited previously. The contrast in cranial- and caudalward extensions of the distal articular facet (8) is clearly seen here.

Medial aspect (fig. 7.16.1f): This aspect reveals yet a different perspective on feature (1)'s orientation, and its bipartite morphology. Features (1), (3), (6) and (10) are as in figs. 7.16.1a and b. The roughened portion for the ligamentum metatarsium (4) dissipates distally, indicating a discontinuation of its interosseous connection with the MT III. Features (5), (8), (9) are as in fig. 7.16.1e. Feature (13) is the depression for the medial collateral ligament.

Characteristic features of metatarsale IV: Included are: 1) the consistently greater length (per individual) than MC IV; 2) the bipartite, inclined articular facet for the cuboid (1); 3) presence of a fossa nudata proximally (1a); 4) the heavily-built proximal epiphysis; 5) otherwise overall great morphological similarity to MC IV.

Statistical Results

There were 6 variables measured for 16 specimens, 10 of which were analysed. The coefficient of variation

Table 7.13. Summary Statistics on Metatarsale IV

Measurement	Sample size	Mean	Standard Deviation	Confidence Limits	Coefficient of Variation	Confidence Limits	Minimum	Maximum	Median
m1	7	225,59	6,55	220,47 230,70	2,90	1,30 4,51	216,50	237,60	225,40
m2	8	11,64	1,13	10,81 12,46	9,71	4,65 14,77	10,20	13,10	11,90
m3	9	30,23	1,47	29,22 31,24	4,86	2,49 7,23	28,70	33,10	29,60
m4	9	21,21	1,46	20,21 22,22	6,89	3,52 10,26	19,20	24,30	21,00
m5	10	9,81	0,57	9,44 10,18	5,78	3,10 8,45	9,10	10,90	9,95
m6	9	20,60	1,24	19,75 21,45	6,01	3,08 8,94	18,60	22,50	20,20

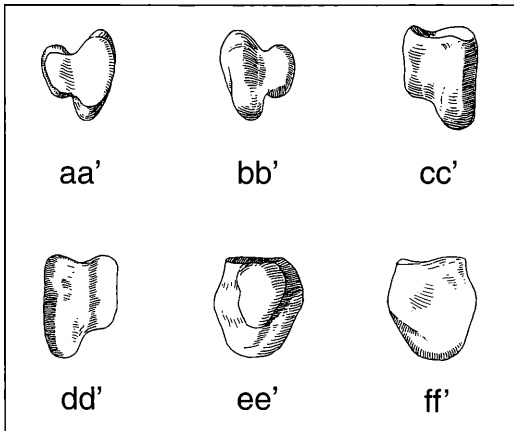


Figure 7.17.1. Sesamoides of the Distal Metatarsale IV: aa' dorsal aspect; bb' palmar aspect; cc' proximal aspect; dd' distal aspect; ee' adaxial aspect; ff' abaxial aspect (x 1,0).

was below 10 for each of the measurements. There was one significant correlation at the 95 % level: m1 (maximum length): m3 (proximal maximum breadth). Metatarsale IV is morphologically virtually identical to MT II, so their differences in significant correlations should be viewed as most likely being random.

7.17 Sesamoides of Distal Metatarsale IV (fig. 7.17.1a, a'-f, f')

The MT IV sesamoids are a virtual mirror image of the MT II's with a smaller adaxial and larger abaxial portion coosified along their combined midline. Slight differences can be discerned when comparing Figures 7.15.1 and 7.17.1, but these are either due to the artist's perspective or individual variability.

7.18 Posterior 1st Phalanx III (fig. 7.18.1a-f)

There are 21 1st phalanges III, often left and right and belonging to the articulated skeletons. There are also eight isolated specimens. There are very few differences between these phalanges and their counterparts in the manus. Their size is similar, with the maximum length ranges for the anterior 1st phalanges III being: anterior (n=11): 59.5-67.2, mean: 63.8; posterior (n=12): 59.0-67.6, mean: 63.8. The close size and morphology of the first phalanges is essentially the same in extant *Equus*. Therefore, we have abbreviated our description of these elements here and refer the reader to the anterior 1st Phalanx III for a more complete description.

Dorsal aspect (fig. 7.18.1a): The tuberos attachment site for the ligamentum laterale volare (7) is comparatively strong and proximally elongated.

Palmar aspect (fig. 7.18.1b): In this aspect, the incision of the crista sagittalis (1'') is deeper than the

counterpart on the forelimb. The attachment of the ligamentum sesamoideum centrale (10) varies in size and thickness both with an individual's age and between individuals. The dorsopalmar groove (4') is distally broadened.

Proximal aspect (fig. 7.18.1c): In contrast to the anterior 1st phalanx III, the lateral portion of the proximal facet (1') is smaller than its medial (1) counterpart. However, there may be exceptions (re: ELLENBERGER & BAUM 1977: 138: "Während am (Mt3) und der Ph.I und II die medialen Knochenhälften etwas stärker sind als die lateralen, ist es beim Hufbein "(Ph.III)" umgekehrt").

Distal aspect (fig. 7.18.1d): The saddle-shaped distal articular joint has a greater topographic profile because of the deeper incision of the midsagittal groove (4''). It is likely that there was less extension and abduction/adduction allowed at this joint than its counterpart in the manus.

Lateral aspect (fig. 7.18.1e): None of the posterior 1st phalanx III specimens have the proximodistally to palmardistally smooth vascular groove (11) present on the anterior 1st phalanx III. Most of the Höwenegg skeletons have more pronounced features (5), (6), (7), (8) and (9) than the A-skeleton depicted here.

Medial aspect (fig. 7.18.1f): This aspect preserves more pronounced features (5), (6), (7), (8) and (9) than found in the anterior 1st phalanx III.

Characteristic features of the 1st phalanx III posterior: Included are: 1) the deeper incision of the dorso-palmar groove of the crista sagittalis (1''); 2) differences in size of the medial (1) and lateral (1') facets of the proximal joint; the distal articular surface (4'' and 4''') has a steeper profile due to the deeper depression of (4''); the distopalmar incision (4) is broader at its base.

Statistical Results

There were 9 variables measured for 20 specimens, 12 of which were analysed. The coefficients of variation were below 10 for all measurements except m9 (minimum length of the trigonum phalange; CV = 13.10). There were 16 significant correlations, 11 of which were at or above the 99 % level of significance. The most highly correlated measurements were m3 (minimum, or midshaft, breadth) and m5 (proximal depth); these measurements likely reflect body mass of the individual. Measurement 3 was further significantly correlated with m4 (proximal breadth) and m7 (distal articular breadth). Measurement 1 (maximum length) correlated with several dimensions: m2 (anterior length, a parallel length measurement), m5 (proximal depth), m3, m8 (distal articular depth), m7 and m4. Measurement 2 further correlated with m5, m7 and m3. Measurement 4 correlated with m7, m5, and m6. The remaining correlation was between m5 and m7.

Measurements 10, 11, 12 and 13 proved to have no significant correlations. These four dimensions essentially duplicate m1 to give some accounting of dimen-

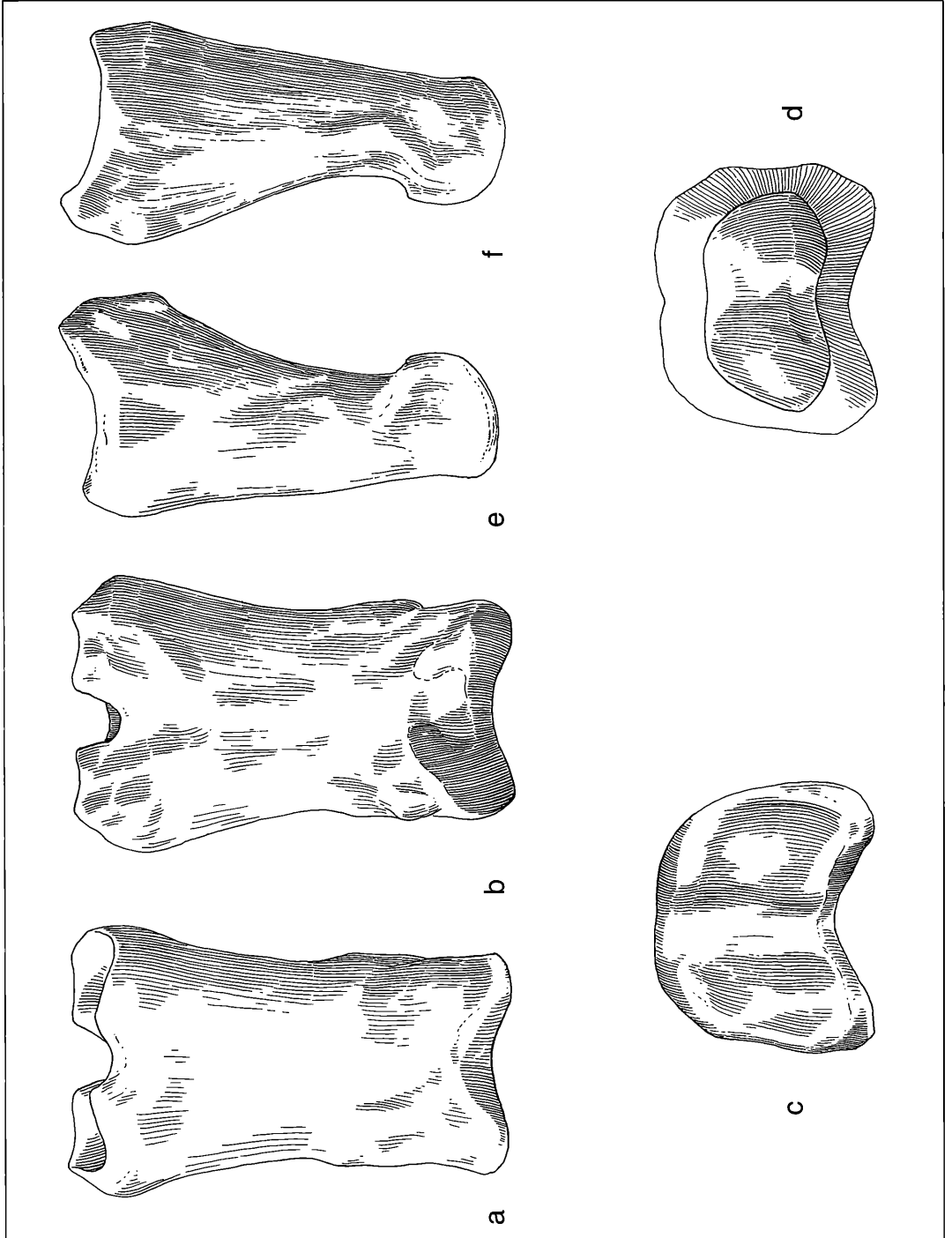


Figure 7.18.1. Posterior 1st Phalanx III: a. dorsal aspect; b. palmar aspect; c. proximal aspect; d. distal aspect; e. lateral aspect; f. medial aspect (x 1,0).

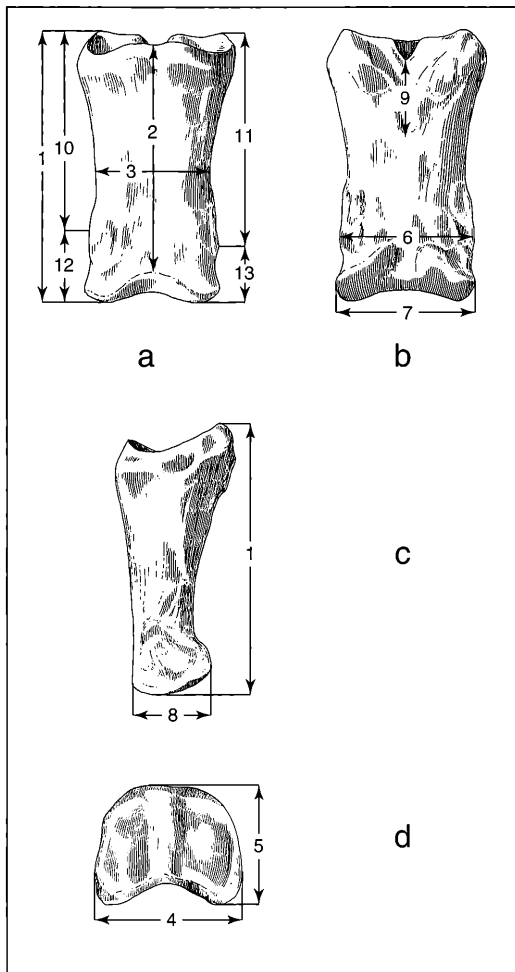


Figure 7.18.2. Measurements on the Posterior 1st Phalanx III: a. dorsal aspect; b. palmar aspect; c. lateral aspect; d. proximal aspect (m10- m13 not given in table 7.14).

Table 7.14. Summary Statistics on Posterior 1st Phalanges III

Measurement	Sample size	Mean	Standard Deviation	Confidence Limits	Coefficient of Variation	Confidence Limits	Minimum	Maximum	Median
m1	12	63,58	2,33	62,20 64,97	3,66	2,12 5,21	59,00	67,60	63,45
m2	12	58,76	2,42	57,32 60,20	4,12	2,38 5,86	55,60	62,80	58,90
m3	12	30,87	1,47	29,99 31,74	4,77	2,76 6,79	28,10	33,00	30,50
m4	12	43,09	2,10	41,84 44,34	4,86	2,81 6,92	40,20	47,50	42,55
m5	12	33,15	1,58	32,21 34,09	4,75	2,75 6,76	30,60	35,60	33,10
m6	12	34,53	1,30	33,75 35,30	3,76	2,17 5,34	32,80	36,90	34,60
m7	12	33,30	1,19	32,59 34,01	3,56	2,06 5,06	31,30	35,30	33,45
m8	12	20,86	1,10	20,20 21,51	5,27	3,04 7,49	19,00	22,80	21,05
m9	12	27,95	3,66	25,77 30,13	13,10	7,49 18,71	21,20	34,00	28,30

sions m12 and m13. The failure of these measurements to correlate with any others, and their essential net duplication of m1 suggest that they have little biological relevance.

7.19 Posterior 2nd Phalanx III (fig. 7.19.1a-f)

There are 17 posterior 2nd phalanx III's, nearly all belonging to the articulated skeletons. There are a further 9 isolated posterior 2nd phalanx III's. There are no principal morphological differences between this element and its counterpart in the manus. Maximum length measurements of the anterior and posterior 2nd phalanx III's are as follows: anterior (n=15) range = 39.4–44.0 mm, mean = 41.5 mm; posterior (n=16) range = 40.2–45.3 mm, mean = 42.8 mm. The size differences are negligible. Our following description is meant to highlight any remarkable differences between the posterior and anterior 2nd phalanges III's.

Dorsal aspect (fig. 7.19.1a): No significant osteological difference is noted from this aspect.

Palmar aspect (fig. 7.19.1b): The distally directed intercondylar furrow (4^{''}) is usually deeper and broader than in the manus' counterpart. The flexor tuberosity (6, including structures 6', 6'' and 6''' ; for the fibrocartilaginous plate) has a slight variation in its contour.

Proximal aspect (fig. 7.19.1c): There are no size and/or contour differences in the medial and lateral (1') portions of the proximal articular facet (1) which characterized the 1st phalanx.

Distal aspect (fig. 7.19.1d): The distal articular facet (4) has a more restricted (= smaller) peripheral contour because of its deeper midsagittal groove (4''') and the more pronounced medial and lateral condyles (4^{IV}).

Lateral aspect (fig. 7.19.1e): The midsagittal ridge (1'') of the proximal facet (1) is somewhat more pronounced. It terminates as a prominence at the dorsal border (1''') of the proximal articular facet (1). This is the site for a tendinous insertion of the common digital extensor (NICKEL et al. 1986, fig. 324: 4'). The prominence (1''') is more developed in this element than the anterior 2nd phalanx III.

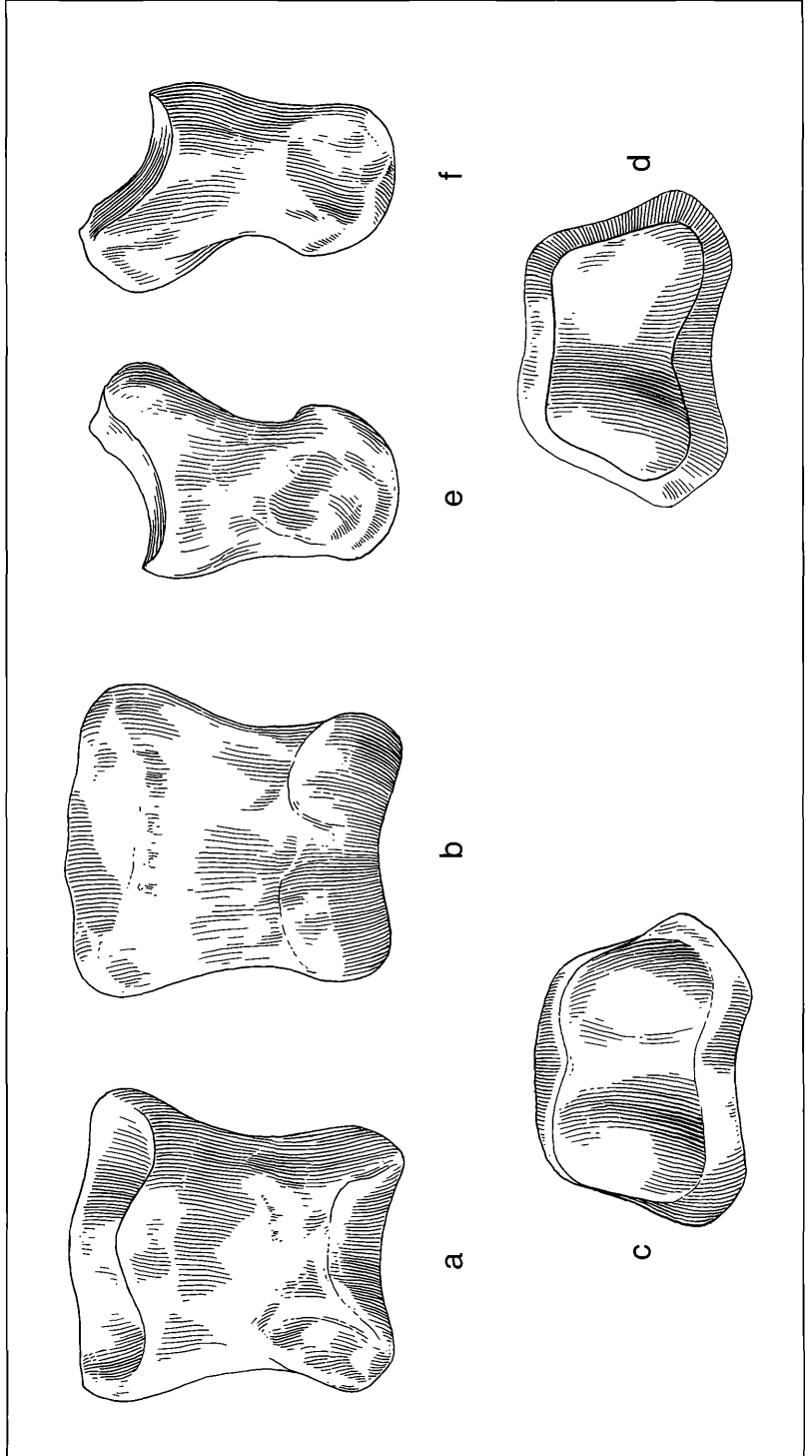


Figure 7 19.1. Posterior 2nd Phalanx III: a. dorsal aspect; b. palmar aspect; c. proximal aspect; d. distal aspect; e. lateral aspect; f. medial aspect (x 1,0).

Table 7.15. Summary Statistics on Posterior 2nd Phalanges III

Measurement	Sample size	Mean	Standard Deviation	Confidence Limits	Coefficient of Variation	Confidence Limits	Minimum	Maximum	Median
m1	11	42,76	1,54	41,81 43,72	3,60	2,01 5,18	40,20	45,30	42,70
m2	11	32,30	1,38	31,44 33,16	4,27	2,39 6,16	30,00	34,00	32,90
m3	11	31,34	1,07	30,67 32,00	3,43	1,92 4,94	29,20	33,00	31,30
m4	11	43,13	1,74	42,05 44,21	4,02	2,25 5,80	41,00	46,20	42,50
m5	11	29,83	1,81	28,70 30,95	6,07	3,39 8,75	27,70	34,00	29,40
m6	11	34,98	1,18	34,25 35,72	3,37	1,89 4,85	32,50	36,90	35,00

Medial aspect (fig. 7.19.1f): There are no additional features found in this aspect.

Characteristic features of the 2nd phalanx III, posterior: Included are: the distally directed intercondylar furrow (4^{''}) is mostly broader and deeper than the manus' counterpart; the distal medial and lateral condyles (4^{iv}) are more pronounced; the proximodorsal tuberos prominence (1^{''}) is relatively hypertrophied. The actual differences are so slight, that it would be difficult to distinguish anterior versus posterior 2nd phalanges III if we did not have the articulated skeletons.

Statistical Results

There were 6 variables measured for 15 specimens, 11 of which were analysed. The coefficients of variation were below 10 for each of the measurements. There were 6 significant correlations, 3 of which were at or above the 99 % level of significance. The length measurements m1 (maximum) and m2 (anterior surface) accounted for the majority of correlations: m2–m3 (minimum breadth), m1–m4 (proximal maximum breadth), m1–m2 and m1–m3. The two remaining correlations were: m3–m4 and m4–m6 (distal articular maximum breadth). Measurement 5 showed no significant correlation, and incidentally had the highest CV (=6.07). The most likely bivariate combinations would normally be m1-m4 or m1-m6. Given that the former showed a significant correlation here, and the latter did not, we provisionally recommend m1-m4 for bivariate comparisons. Alternatively, m1-m3 would be recommended.

7.20 Posterior 3rd Phalanx III (fig. 7.20.1a-f)

There are 12 specimens of this element, left and right, and all derived from the articulated skeletons. As with the posterior 1st and 2nd phalanges III, there are very few differences between this element and its counterpart in the manus.

Dorsal aspect (fig. 7.20.1a): A feature, long known from extant *Equus*, is the narrower outline of the hind hoof than the fore hoof. This narrowness is seen when comparing the dorsal and palmar views (fig. 7.20.1a and b) with the manus' counterpart (figs. 6.24.1a and b). Also, the articular facets are transversely narrower in the posterior 3rd phalanx III. In this aspect, features (1), (1') and (1'') present a more convex contour. The processus palmares laterales and mediales (4) are more inwardly (palmarwardly) directed in the hind phalanx (fig. 7.20.1a, b). The rugose distal portion of the parietal surface (2) is less sharply demarcated than on the manus' counterpart, and the crena marginis solearis (5) is deeper and wider in the hind phalanx.

Palmar aspect (fig. 7.20.1b): The borders of the linea semilunaris (7) are steeper in the hind hoof (in relation to the stronger transverse constriction of the whole

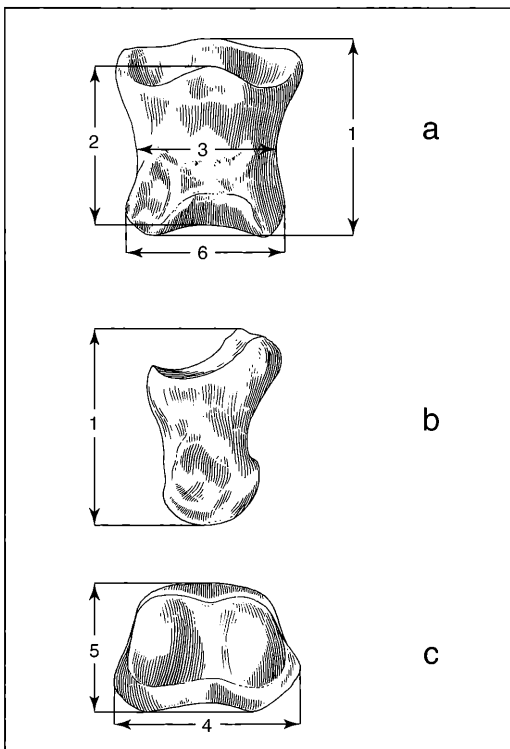


Figure 7.19.2. Measurements on the Posterior 2nd Phalanx III: a. dorsal aspect; b. lateral aspect; c. proximal aspect.

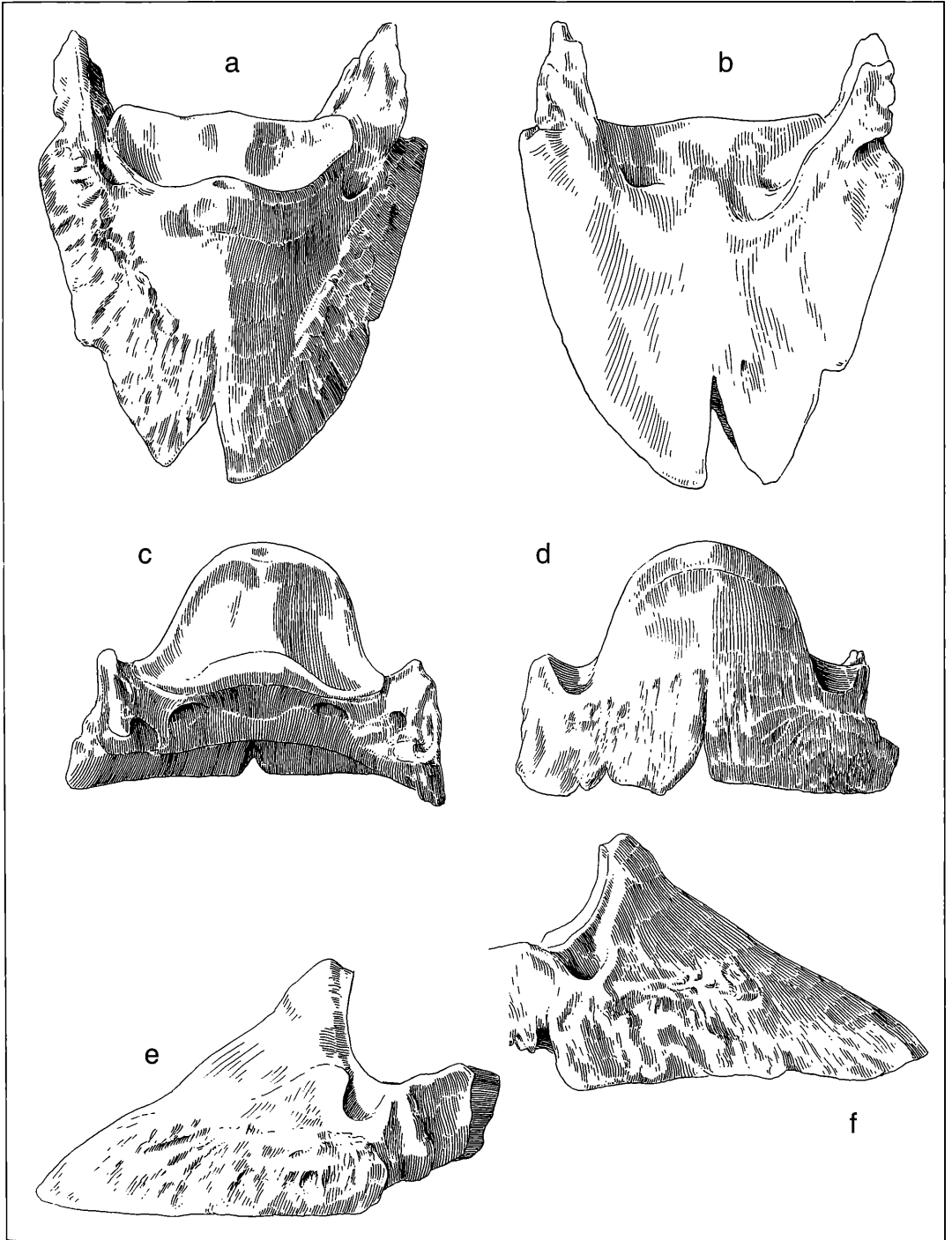


Figure 7.20.1. Posterior 3rd Phalanx III: a. dorsal aspect; b. palmar aspect; c. proximal aspect; d. distal aspect; e. lateral aspect; f. medial aspect (x 1,0).

Table 7.16. Summary Statistics on Posterior 3rd Phalanges III

Measure-ment	Sample size	Mean	Standard Deviation	Confidence Limits		Coefficient of Variation	Confidence Limits		Minimum	Maximum	Median
m1	6	57,68	2,95	55,20	60,17	5,12	2,06	8,17	52,20	61,20	58,10
m2	3	65,83	9,67	54,31	77,36	14,69	2,05	27,33	60,10	77,00	60,40
m3	0										
m4	5	57,60	2,58	55,22	59,98	4,49	1,55	7,42	54,00	61,00	58,00
m5	6	20,93	1,27	19,86	22,00	6,07	2,44	9,70	19,00	23,00	20,95
m6	4	36,43	1,34	35,04	37,81	3,67	0,99	6,36	35,00	38,20	36,25
m7	6	47,28	3,66	44,20	50,37	7,74	3,10	12,38	40,00	50,10	48,40
m8	1	165,00							165,00	165,00	165,00

bone), and the peripheral outline of the anterior hoof is relatively expanded transversely. The attachment area for the tendon of the flexor digitalis profundus (9') is large, invested with furrows, and covers a larger part of the facies flexoria (9; = sole of foot).

Proximal aspect (fig. 7.20.1c): There are no marked size differences between the lateral (3^{IV}) and medial (3^V) articular surfaces of feature (3). Moreover, the inclinations of the medial (1') and lateral (1'') portions of the parietal surface are identical. The articular facet for the distal sesamoid bone is transversely broader and proximodistally higher than in the manus' counterpart.

Distal aspect (fig. 7.20.1d): The large crena (5) is marked, as is the transition between the rugose (2) and smooth portion (2') of the parietal surface.

Lateral aspect (fig. 7.20.1e): There are no remarkable differences in this aspect.

Medial aspect (fig. 7.20.1f): In some specimens the foramen processus palmaris (13) is visible. The sulcus parietalis medialis and lateralis (13'), known in *Equus*, is absent.

Characteristic features of the 3rd phalanx III: Included here are: the narrow peripheral outline of the hoof (fig. 7.20.1a,b); the shortness of the proximal articular facet (3); the stronger convexity of the parietal surface (1, 1', 1''); the straight, palmarward-directed processus palmaris laterales et mediales (4); the deeper and wider crena marginis solearis (5); the narrow arc formed by the linea solearis; the prominent attachment for the tendon of the flexor digitalis profundus (9 = the "perforatus scar"); the identical inclination of the lateral

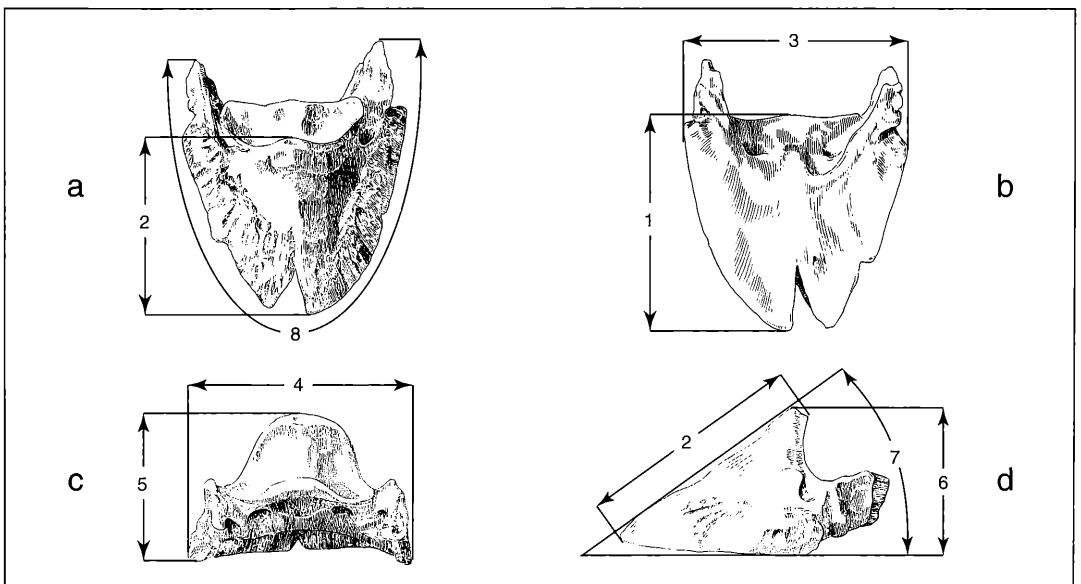


Figure 7.20.2. Measurements on the Posterior 3rd Phalanx III: a. dorsal; b. palmar; c. proximal; d. lateral.

and medial walls (1',1''); the large facet (12) for the distal sesamoid.

GROMOVA (1955:124) recognized this very difference in hipparion material from Taraklia and Pavlodar and referred them accordingly to the fore- and hind feet of these horses. She further described a set of characters which she used to discriminate these elements. The Höwenegg skeletons confirm her observations.

Statistical Results

There were 8 variables measured for 11 specimens of posterior 3rd phalanx III, 6 of which were analysed. The coefficients of variation were below 10 for all measurements except m2 (anterior length; CV = 14.69). There was 1 significant correlation at the 95 %–99 %+ level of significance, m5 (articular depth)-m7 (angle between sole and the dorsal line).

7.21 Distal Sesamoidea of Posterior Phalanx III (fig. 7.21.1a-f)

As with the sesama bina, there are no basic differences between anterior and posterior distal sesamoids (re: fig. 6.24.1a-f). There are however some features worthy of description.

Dorsal aspect (fig. 7.21.1a): This aspect reveals a somewhat more symmetrical contour than found in the anterior foot's counterpart. The margo proximalis (7) and margo distalis (8) are relatively reduced compared to the anterior sesamoid (fig. 6.24.1a). Also, the attachment sites for the collateral ligaments are less prominent. The central elevation (1') between the two

articular facets (1'',1''') is variable in both this and the anterior sesamoidea: in some individuals it is elevated and well separated, in others there is a continuous transition between the two facets.

Palmar aspect (fig. 7.21.1b): In this aspect, the posterior sesamoid is more elongate than its anterior counterpart. The facies flexoria (6) is smooth in both.

Proximal aspect (fig. 7.21.1c): This aspect illustrates the rugose surface for ligamentous attachment and contained pori.

Distal aspect (fig. 7.21.1d): This aspect reveals no remarkable difference with the anterior limb's sesamoid counterpart.

Lateral and medial aspects (fig. 7.21.1e, f): The illustrations would appear to show striking contrasts between this bone and its anterior limb counterpart (fig. 6.24.1e,f). However, this is an artifact of the artist's perception.

Characteristic features of the Höwenegg distal sesamoidea of posterior phalanx III: Included are: the more ovoid outline in dorsal and palmar aspect (fig. 7.21.1a,b) due to the margo distalis' (8) shortening; the less prominent attachment sites for the ligamenta collateralia (5).

Both the Höwenegg anterior and posterior sesamoidea distale differ from those found in wild extant *Equus* by their more slender outline and the larger facet for the 3rd phalanx III. Also, the Höwenegg posterior distal sesamoid has a somewhat concave margo proximalis.

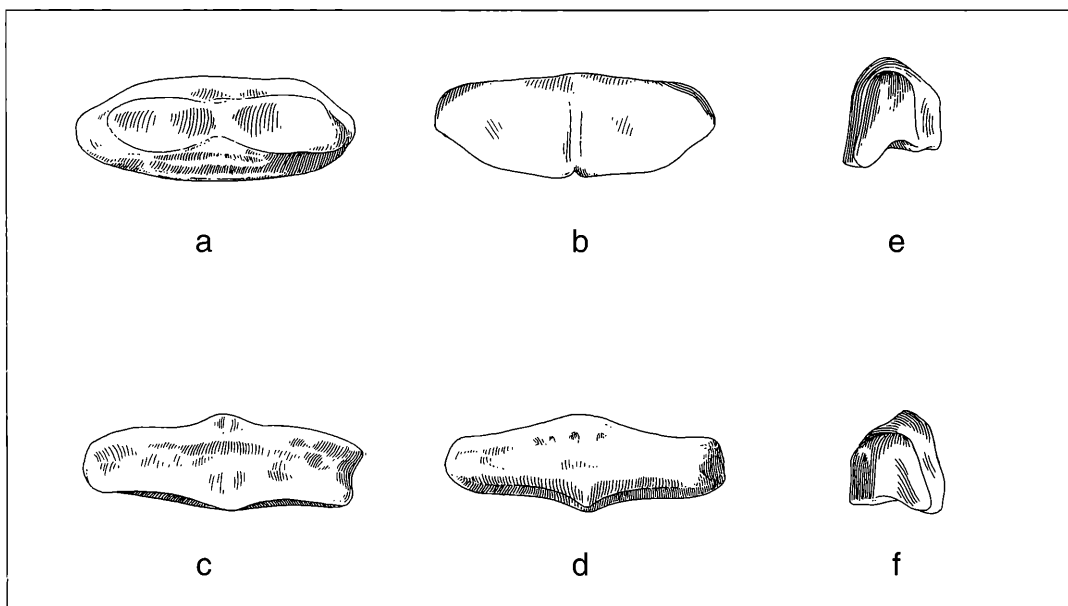


Figure 7.21.1. Distal Sesamoidea of Posterior Phalanx III: a. dorsal aspect; b. palmar aspect; c. proximal aspect; d. distal aspect; e. lateral aspect; f. medial aspect (x 1,0).

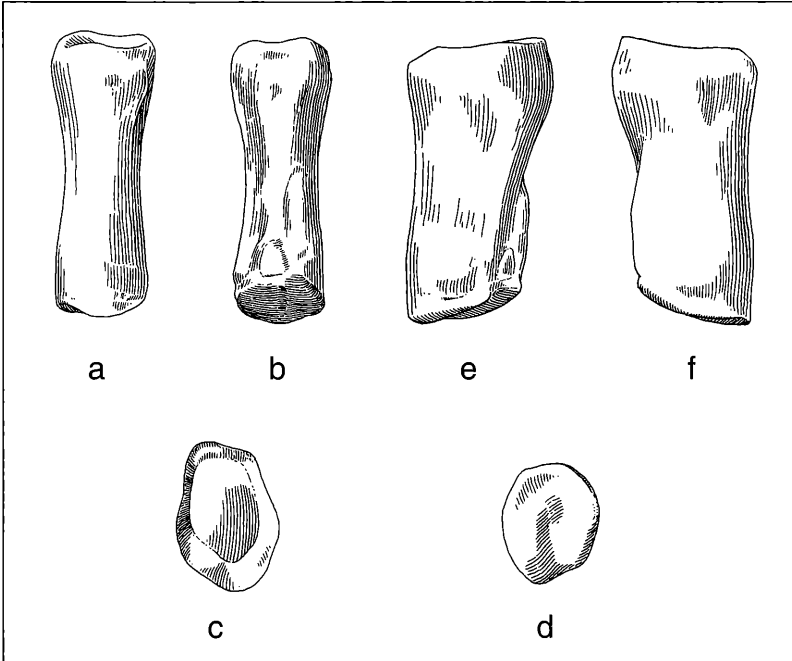


Figure 7.22.1. Posterior 1st Phalanx II: a. dorsal aspect; b. palmar aspect; c. proximal aspect; d. distal aspect; e. lateral aspect; f. medial aspect (x 1,0).

7.22 Posterior 1st Phalanx II (fig. 7.22.1a-f)

There are 17 specimens of posterior 1st phalanx II, left and right, all belonging to articulated skeletons. These phalanges are quite similar to their counterparts in the manus. Once again, we will only comment here on differences which we find between these and the 1st phalanx digit II, anterior.

Dorsal aspect (fig. 7.22.1a): In this aspect the 1st phalanx digit II is seen as being more massively built than its counterpart in the anterior limb.

Palmar aspect (fig. 7.22.1b): The "V-scar" of the ligamentum sesamoideum centrale is present (4), but is not as elongate as in the manus 1st phalanx digit II. The abaxial (5) and adaxial (5') insertion of the tendo flexor digitalis superficialis are well developed.

Proximal aspect (fig. 7.22.1c): The articular facet for the MT II (1) is voluminous and has a more rounded outline than its counterpart in the manus.

Distal aspect (fig. 7.22.1d): The distal articular facet (2) has a deeper and cranio-caudally longer sulcus (2') than found in the manus' counterpart.

Lateral aspect (fig. 7.22.1e): The scar for the ligamentum collaterale laterale (abaxiale) (8) is stronger and larger than in the manus' counterpart.

Medial aspect (fig. 7.22.1f): The tuberosity for the ligamentum collaterale mediale (adaxiale) (10) is more elaborated. This suggests a stronger tendinous attachment than found in the manus' counterpart.

Characteristic features of the posterior 1st phalanx II: Included are: the greater massivity of the bone than its anterior counterpart; the proximal facet (1) is

Table 7.17. Summary Statistics on Posterior 1st Phalanges II

Measure-ment	Sample size	Mean	Standard Deviation	Confidence Limits	Coefficient of Variation	Confidence Limits	Minimum	Maximum	Median
m1	9	35,28	1,57	34,20 36,36	4,44	2,28 6,60	32,00	36,90	35,60
m2	9	22,30	1,03	21,59 23,01	4,60	2,36 6,84	21,00	24,60	22,00
m3	10	15,15	1,06	14,46 15,84	6,98	3,74 10,22	13,80	17,10	14,85
m4	10	11,38	1,03	10,71 12,05	9,06	4,85 13,28	9,80	13,30	11,20
m5	10	15,02	0,85	14,46 15,58	5,67	3,05 8,30	14,10	17,10	14,90
m6	10	13,14	0,55	12,78 13,50	4,16	2,23 6,08	12,40	13,90	13,00

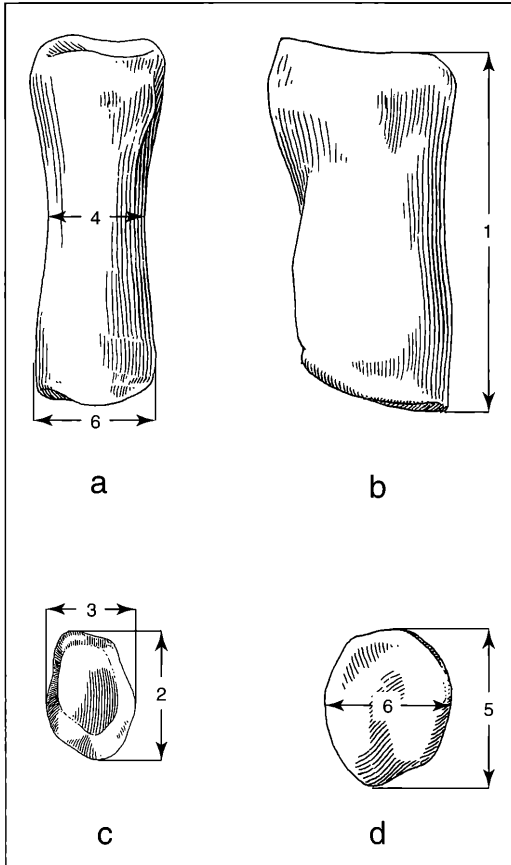


Figure 7.22.2. Measurements on the Posterior 1st Phalanx II: a. dorsal; b. medial; c. proximal; d. distal aspects.

larger; the distal articular facet's central sulcus (2') is deeper and more elongate.

Statistical Results

There were 6 variables measured for 17 specimens, 10 of which were analysed. The coefficients of variation were below 10 for each measurement. There were 4 significant correlations, one of which was at the 99 % level of significance: m3 (proximal mediolateral width)- m6 (distal mediolateral width). Measurement 3 further correlated with m1 (maximum length along dorsal border) and m5 (distal anteroposterior length). Measurement 6 further correlated with m2 (proximal anteroposterior length). If bivariate measurements are reported, the best ones would be m2-m6, due to their significant correlation. While m1 shows more variability, it is a logical choice for comparison also.

7.23 Posterior 2nd Phalanx II (fig. 7.23.1a-f)

There are 18 posterior 2nd phalanges II, left and right, all derived from articulated skeletons. As with the posterior 1st phalanges II, there are few differences between these and the 2nd phalanges II of the manus.

Dorsal aspect (fig. 7.23.1a): Unlike the anterior 2nd phalanges II, the proximal articular surface's median longitudinal ridge (1') shows no sign of compacta removal.

Palmar aspect (fig. 7.23.1b): There are no differences with the manus' counterpart.

Proximal aspect (fig. 7.23.1c): There are no differences with the manus' counterpart.

Distal aspect (fig. 7.23.1d): In this aspect the sulcus distalis (2') is longer and deeper, and the compacta at the distopalmar border is not removed.

Lateral aspect (fig. 7.23.1e): There are no differences with the manus' counterpart.

Medial aspect (fig. 7.23.1f): There are no differences with the manus' counterpart.

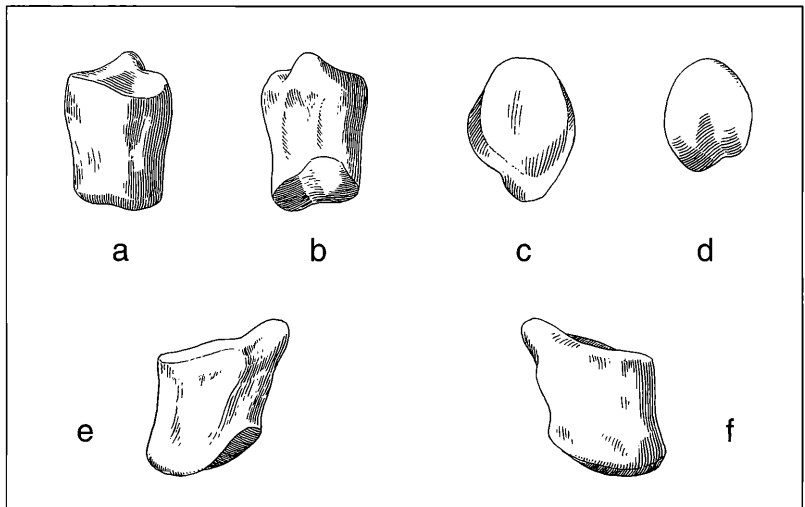


Figure 7.23.1. Posterior 2nd Phalanx II: a. dorsal aspect; b. palmar aspect; c. proximal aspect; d. distal aspect; e. lateral aspect; f. medial aspect (x 1,0).

Table 7.18. Summary Statistics on Posterior 2nd Phalanges II

Measurement	Sample size	Mean	Standard Deviation	Confidence Limits	Coefficient of Variation	Confidence Limits	Minimum	Maximum	Median
m1	10	15,28	1,37	14,39 16,17	8,95	4,79 13,12	11,80	17,00	15,65
m2	10	20,94	0,85	20,39 21,49	4,06	2,18 5,94	20,10	22,90	20,65
m3	10	15,63	0,92	15,03 16,23	5,86	3,14 8,57	14,60	17,40	15,40
m4	10	14,68	0,95	14,06 15,30	6,47	3,47 9,47	13,10	16,30	14,35
m5	9	12,70	1,03	11,99 13,41	8,08	4,12 12,03	11,30	14,70	12,50
m6	9	12,26	0,56	11,87 12,64	4,58	2,35 6,82	11,40	13,00	12,40

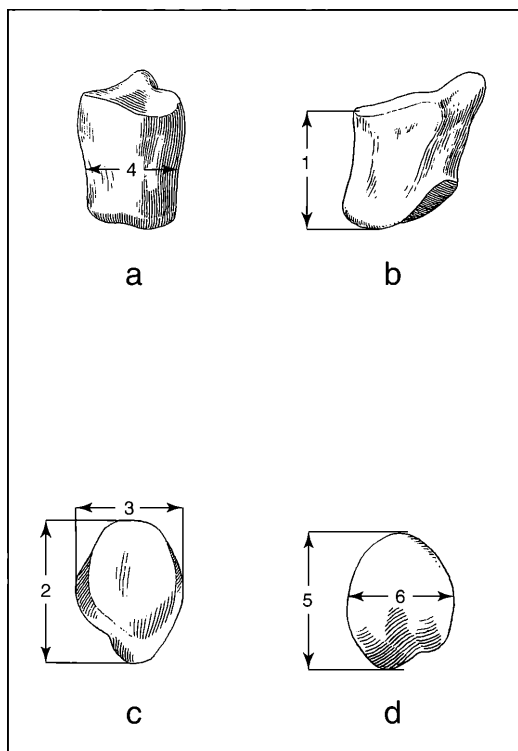


Figure 7.23.2. Measurements on the Posterior 2nd Phalanx II: a. dorsal aspect; b. medial aspect; c. proximal aspect; d. distal aspect.

Characteristic features of the posterior 2nd phalanx II: Included are: no substantial differences with the anterior counterpart; there is a lack of compacta removal on the medial longitudinal ridge (1') of the proximal articular surface and the sulcus distalis (2') of the distal articular surface.

In general the entire bone appears to be slightly more heavily built than the anterior counterpart.

Statistical Results

There were 6 variables measured for 16 specimens of posterior 2nd phalanx II, 10 of which were analysed. The coefficients of variation were below 10 for each of the measurements. There were three significant correlations, one of which was at or above the 99 % level: m3 (proximal mediolateral length)-m4 (midshaft mediolateral width). Measurement 3 and m4 individually correlated with m6 (distal mediolateral width).

7.24 Posterior 3rd Phalanx II (fig. 7.24.1a-f)

There are 12 specimens, left and right, all from articulated skeletons. Many of these specimens are damaged. This element is quite similar to its counterpart in the manus; we highlight only the differences.

Dorsal aspect (fig. 7.24.1a): The rugose dorsal surface (2') variably has a sulcus parietalis (2'') as found in the 3rd phalanx of digit III.

Palmar aspect (fig. 7.24.1b): The morphological details figured in this aspect are virtually identical with the manus' counterpart.

Proximal aspect (fig. 7.24.1c): The processus palmaris lateralis (4) has a small dorsopalmar furrow near its terminus. This structure corresponds to the incisura

Table 7.19. Summary Statistics on Posterior 3rd Phalanges II

Measurement	Sample size	Mean	Standard Deviation	Confidence Limits	Coefficient of Variation	Confidence Limits	Minimum	Maximum	Median
m1	9	27,59	1,41	26,62 28,56	5,12	2,62 7,62	25,50	30,20	27,90
m2	9	39,38	2,37	37,75 41,01	6,01	3,08 8,95	36,20	44,30	38,80
m3	10	21,79	2,54	20,13 23,45	11,68	6,22 17,14	16,80	24,30	22,90
m4	10	15,50	0,78	14,99 16,01	5,01	2,69 7,32	14,60	17,10	15,45

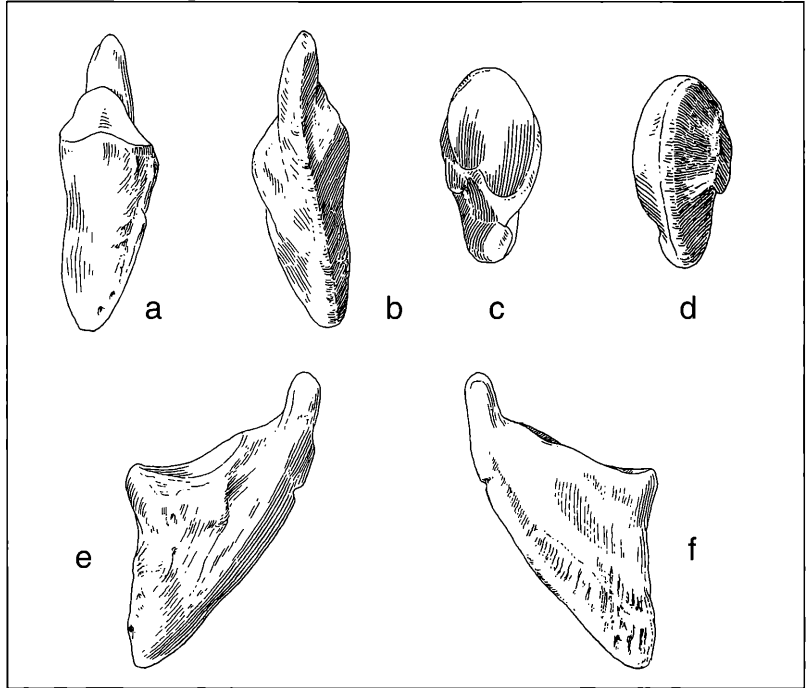


Figure 7.24.1. Posterior 3rd Phalanx II: a. dorsal aspect; b. palmar aspect; c. proximal aspect; d. distal aspect; e. medial aspect; f. lateral aspect (x 1,0).

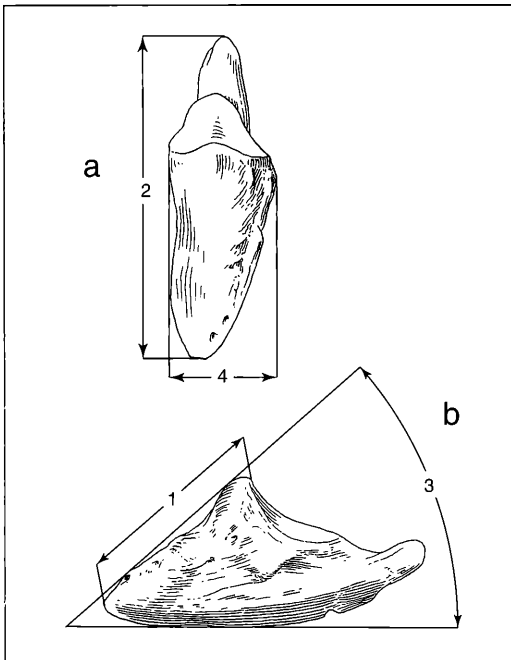


Figure 7.24.2. Measurements on the Posterior 3rd Phalanx II: a. dorsal aspect; b. medial aspect.

processus palmaris of NICKEL et al. (1986: figs. 140, 141: 25' and 25''): an "archaic variant" of the normal single processus palmaris.

Distal aspect (fig. 7.24.1d): The facies flexoria for attachment of the flexor digitalis profundus (7) is more prominent than the manus' counterpart.

Medial aspect (fig. 7.24.1f): The processus palmaris lateralis (4) is prominent in this view. A low-lying, flat furrow (2'') separates the smooth dorsoparietal surface (2) from the rugose, more ventrally placed parietal surface.

Lateral aspect (fig. 7.24.1e): There are no significant differences in this aspect with the manus' counterpart.

Characteristic features of the posterior 3rd phalanx II: Included are: 1) doubling of the palmar processus palmaris lateralis (4), an archaic feature; 2) general overall great similarity with the 3rd phalanx digit II, anterior.

Statistical Results

There were no significant correlations for the posterior 3rd phalanx II.

7.25 Posterior 1st Phalanx IV (fig. 7.25.1a-f)

There are 17 1st phalanges IV, left and right, all from the articulated skeletons. A comparison with the anterior 1st phalanx IV shows no significant differences. We discuss only some slight differences here.

Dorsal aspect (fig. 7.25.1a): The ligamentous scar just proximal to the distal articular facet (2) is stronger than its counterpart in the manus.

Palmar aspect (fig. 7.25.1b): The ligamentous attachments for the flexor digitalis superficialis (5, abaxial; 5' adaxial) and the distal midsagittal bulge (6) are more prominent than in the manus. Also, the trigonum (3) is slightly more developed.

Proximal aspect (fig. 7.25.1c): The articular facet for the MC IV is relatively smaller, and the dorsal prominence (1') is more weakly developed.

Distal aspect (fig. 7.25.1d): There are no significant differences with the manus' counterpart.

Lateral aspect (fig. 7.25.1e): There are no significant differences with the manus' counterpart.

Medial aspect (fig. 7.25.1f): The small fossa (11) just distal to the proximal articular surface is more weakly developed than its counterpart in the manus.

Characteristic features of the posterior 1st phalanx IV: There are no significant differences with the anterior 1st phalanx digit IV.

Statistical Results

There were 6 variables measured for 17 specimens, 11 of which were analysed. The coefficients of variation were below 10 for all measurements except m5

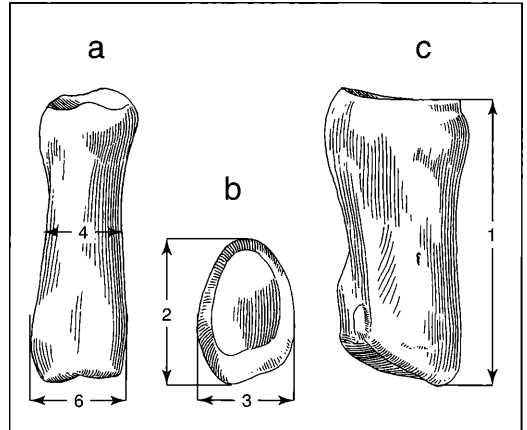


Figure 7.25.2. Measurements on the Posterior 1st Phalanx IV: a. dorsal aspect; b. medial aspect; c. proximal aspect (m5 taken perpendicular to m6; re: fig. 7.22.2).

(distal anteroposterior length; CV = 11.89). There were 5 significant correlations, one at the 99%+ level of significance: m2 (proximal anteroposterior length)-m5 (distal anteroposterior length). Measurement 2 also correlated with m6 (distal mediolateral width) and m3 (proximal mediolateral width). Measurement 6 further correlated with m1 (maximum length along dorsal border) and m3.

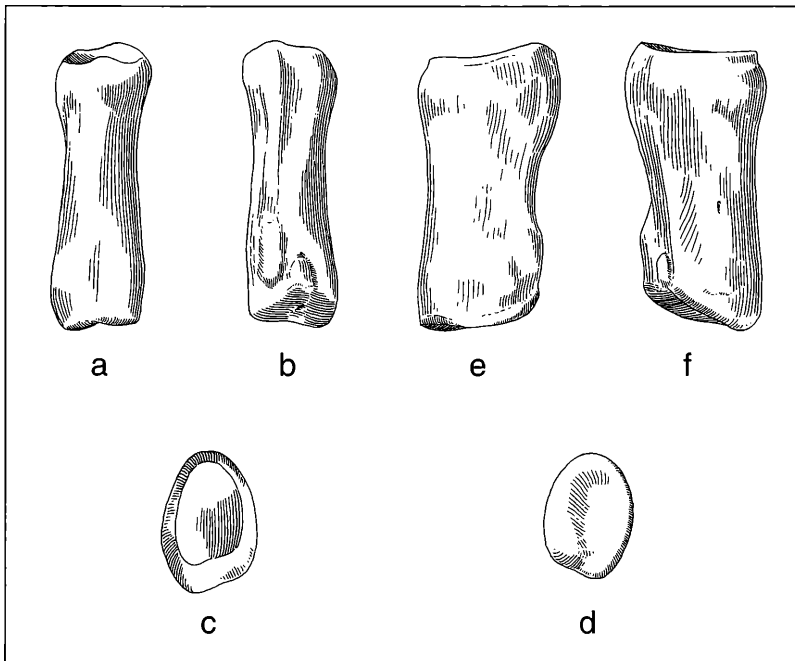


Figure 7.25.1. Posterior 1st Phalanx IV: a. dorsal aspect; b. palmar aspect; c. proximal aspect; d. distal aspect; e. lateral aspect; f. medial aspect (x 1,0).

Table 7.20. Summary Statistics on Posterior 1st Phalanges IV

Measurement	Sample size	Mean	Standard Deviation	Confidence Limits		Coefficient of Variation	Confidence Limits		Minimum	Maximum	Median
m1	8	35,05	1,20	34,17	35,93	3,43	1,66	5,20	33,80	36,80	34,55
m2	9	21,53	1,58	20,45	22,62	7,34	3,75	10,93	19,80	24,80	21,20
m3	11	14,69	1,34	13,86	15,52	9,12	5,07	13,17	12,30	16,90	14,40
m4	10	10,66	0,84	10,11	11,21	7,88	4,22	11,53	9,50	12,00	10,40
m5	11	15,17	1,80	14,05	16,30	11,89	6,58	17,19	13,50	19,60	14,30
m6	11	13,18	0,69	12,75	13,61	5,23	2,92	7,54	12,30	14,60	13,20

7.26 Posterior 2nd Phalanx IV (fig. 7.26.1a-f)

There are 18 2nd phalanx IV specimens, left and right, derived from the articulated skeletons. There is also a single isolated bone also referred to this element.

Dorsal aspect (fig. 7.26.1a): In this aspect, the incision between the median longitudinal ridge (1') and the process for insertion of the tendo flexor digitalis sublimis (3) is deeper and is transversely somewhat broader distally than its counterpart in the manus.

Palmar aspect (fig. 7.26.1b): The process for flexor digitalis sublimis tendon (3) is more accentuated than in the manus' counterpart.

Proximal aspect (fig. 7.26.1c): The mediopalmar incision (5) of the proximal articular surface is deeper than its counterpart in the manus.

Distal aspect (fig. 7.26.1d): There are no morphological differences with the manus' counterpart.

Lateral aspect (fig. 7.26.1e): The rugose surface (4) for ligamentous attachment is more weakly developed here.

Medial aspect (fig. 7.26.1f): There are no morphological differences with the manus' counterpart.

Characteristic features of the posterior 2nd phalanx IV: Included are: there are no significant features with its counterpart in the manus.

Statistical Results

There were 6 variables measured for 16 specimens, 11 of which were analysed. The coefficients of variation were below 10 for all measurements. This bone, essentially indistinguishable in morphology from posterior 2nd phalanx II had six significant correlations, all at or above the 99 % level. The difference in levels of significance between these bones must be seen as being random. Variables m2 (proximal dorsopalmar length) and m6 (distal mediolateral width) formed the basis for most of

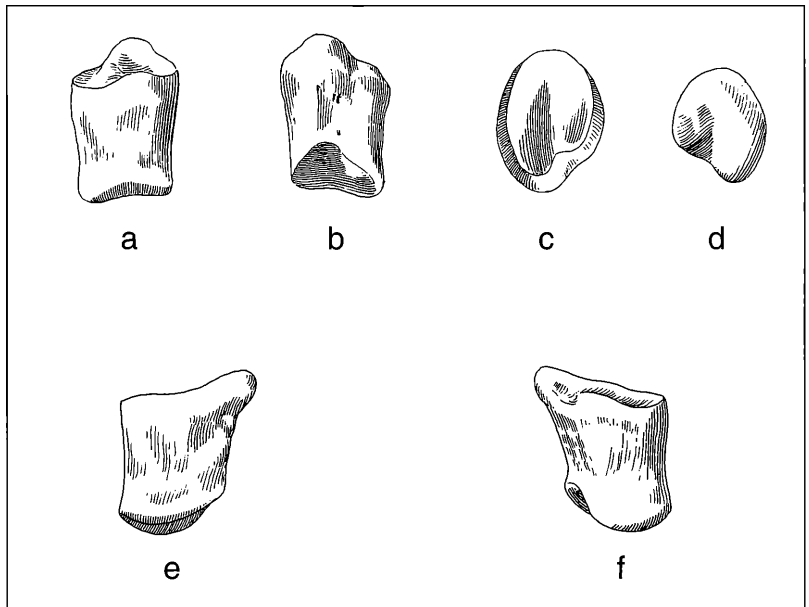


Figure 7.26.1. Posterior 2nd Phalanx IV: a. dorsal aspect; b. palmar aspect; c. proximal aspect; d. distal aspect; e. lateral aspect; f. medial aspect (x 1,0).

Table 7.21. Summary Statistics on Posterior 2nd Phalanges IV

Measure-ment	Sample size	Mean	Standard Deviation	Confidence Limits	Coefficient of Variation	Confidence Limits	Minimum	Maximum	Median
m1	12	15,10	0,60	14,74 15,46	3,96	2,29 5,64	14,20	16,40	15,05
m2	12	20,91	0,92	20,36 21,46	4,40	2,54 6,25	19,90	22,80	20,45
m3	11	15,34	1,06	14,68 16,00	6,92	3,86 9,98	13,60	16,50	15,30
m4	12	14,45	1,19	13,74 15,16	8,21	4,73 11,70	12,90	16,10	14,35
m5	11	12,29	0,61	11,91 12,67	4,94	2,76 7,12	11,10	12,90	12,50
m6	12	12,04	0,46	11,77 12,32	3,82	2,21 5,43	11,40	12,70	11,80

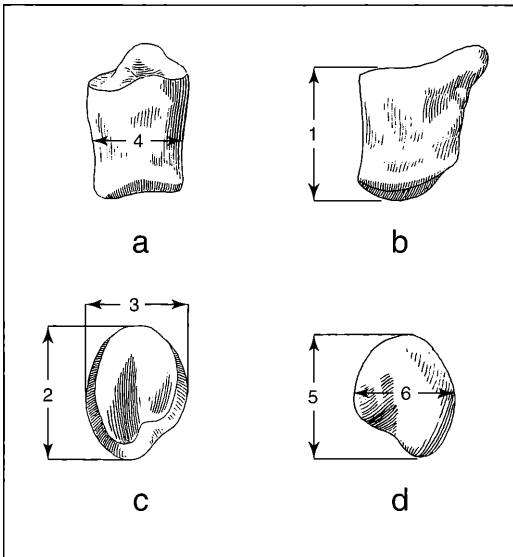


Figure 7.26.2. Measurements on the Posterior 2nd Phalanx IV: a. dorsal aspect; b. medial aspect; c. proximal aspect; d. distal aspect.

the correlation pattern found: m2-m4 (mid-shaft width), m2-m3 (proximal mediolateral width), m2-m6 (distal mediolateral width), m3-m6, m4 -m6. In addition m3 and m4 were also significantly correlated with one another.

Table 7.22. Summary Statistics on Posterior 3rd Phalanges IV

Measure-ment	Sample size	Mean	Standard Deviation	Confidence Limits	Coefficient of Variation	Confidence Limits	Minimum	Maximum	Median
m1	10	26,65	2,60	24,95 28,35	9,75	5,21 14,30	23,50	30,40	25,55
m2	7	38,23	3,21	35,72 40,74	8,41	3,74 13,08	34,10	43,20	37,60
m3	9	22,14	2,05	20,73 23,56	9,26	4,72 13,80	20,10	25,50	21,80
m4	10	14,96	1,41	14,04 15,88	9,41	5,03 13,79	13,00	17,00	14,80

7.27 Posterior 3rd Phalanx IV (fig. 7.27.1a-f)

There are 14 posterior 3rd phalanges IV, left and right, derived exclusively from the articulated skeletons. There are only very minor differences between this bone and its counterpart in the manus.

Dorsal aspect (fig. 7.27.1a): The smooth portion (2) of the facies parietalis is distinct from the rugose surface (2'). There is a prominent sulcus parietalis (2'').

Palmar aspect (fig. 7.27.1b): There are no significant differences with the manus' counterpart.

Proximal aspect (fig. 7.27.1c): The articular facet (1) is transversely broader and larger overall than the manus' counterpart.

Distal aspect (fig. 7.27.1d): There are no significant differences with the manus' counterpart.

Lateral aspect (fig. 7.27.1e): There are no significant differences with the manus' counterpart.

Medial aspect (fig. 7.27.1f): On the distal end of the facies flexoria for the tendon of the flexor digitalis profundus (7), there is an oblique furrow (7') which is virtually absent in the manus' counterpart. Its function is unknown.

Characteristic features of the Posterior 3rd phalanx digit IV: Included are: the lack of any significant differences with the manus' counterpart.

Statistical Results

There were 4 variables measured for 14 specimens, 10 of which were analysed. The coefficients of variation were below 10 for all measurements. There were two significant correlations, one of which was at or above the 99 %+ level: m2 (maximum length along anterior border)-m3 (proximal dorsopalmar height).

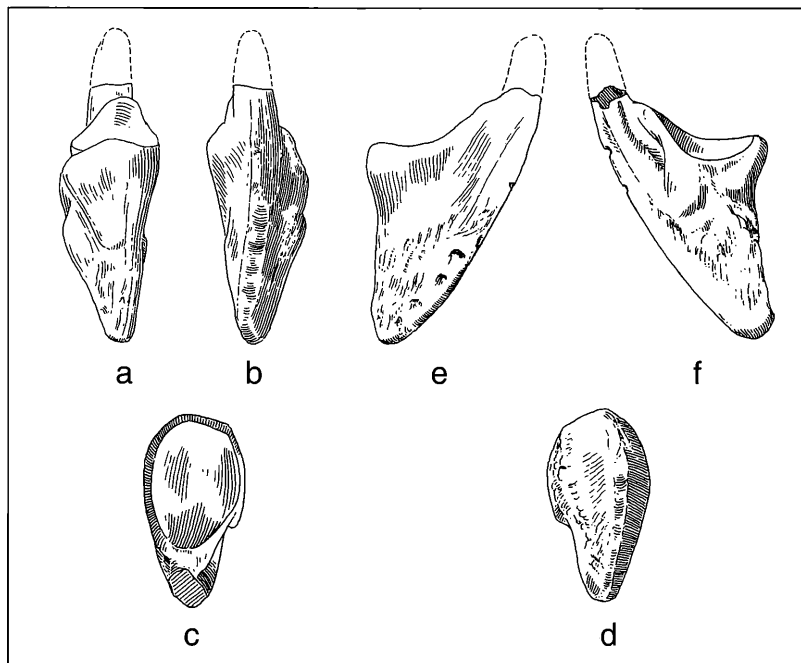


Figure 7.27.1. Posterior 3rd Phalanx IV: a. dorsal aspect; b. palmar aspect; c. proximal aspect; d. distal aspect; e. lateral aspect; f. medial aspect (x 1,0).

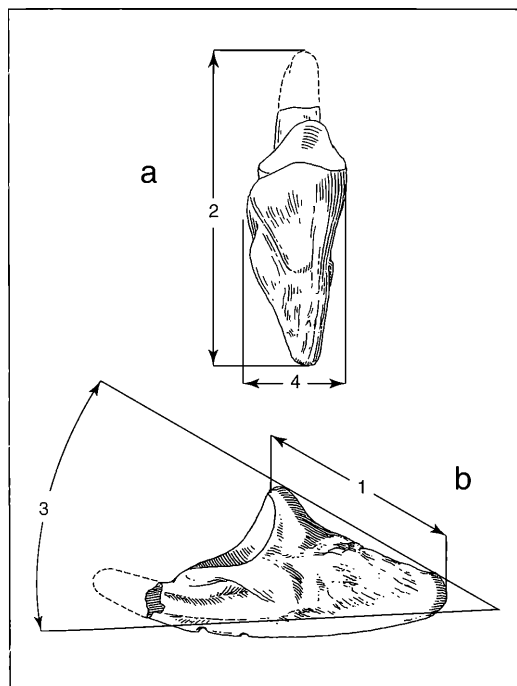


Figure 7.27.2. Measurements on the Posterior 3rd Phalanx IV: a. dorsal aspect; b. medial aspect.

The other significant correlation was m1 (maximum length along dorsal border)-m4 (proximal mediolateral width).

7.28 Summary of the Osteological Characteristics of the Abaxial and Adaxial Phalanges of the Hind Foot:

The phalanges of the posterior digits II and IV are nearly identical to their counterparts in the anterior limb. The slight differences in their lengths are not statistically significant (for details see TOBIEN 1982: 1049). There is a tendency however for the 1st phalanges of the fore foot to be somewhat longer and more slender than their hindfoot counterparts.

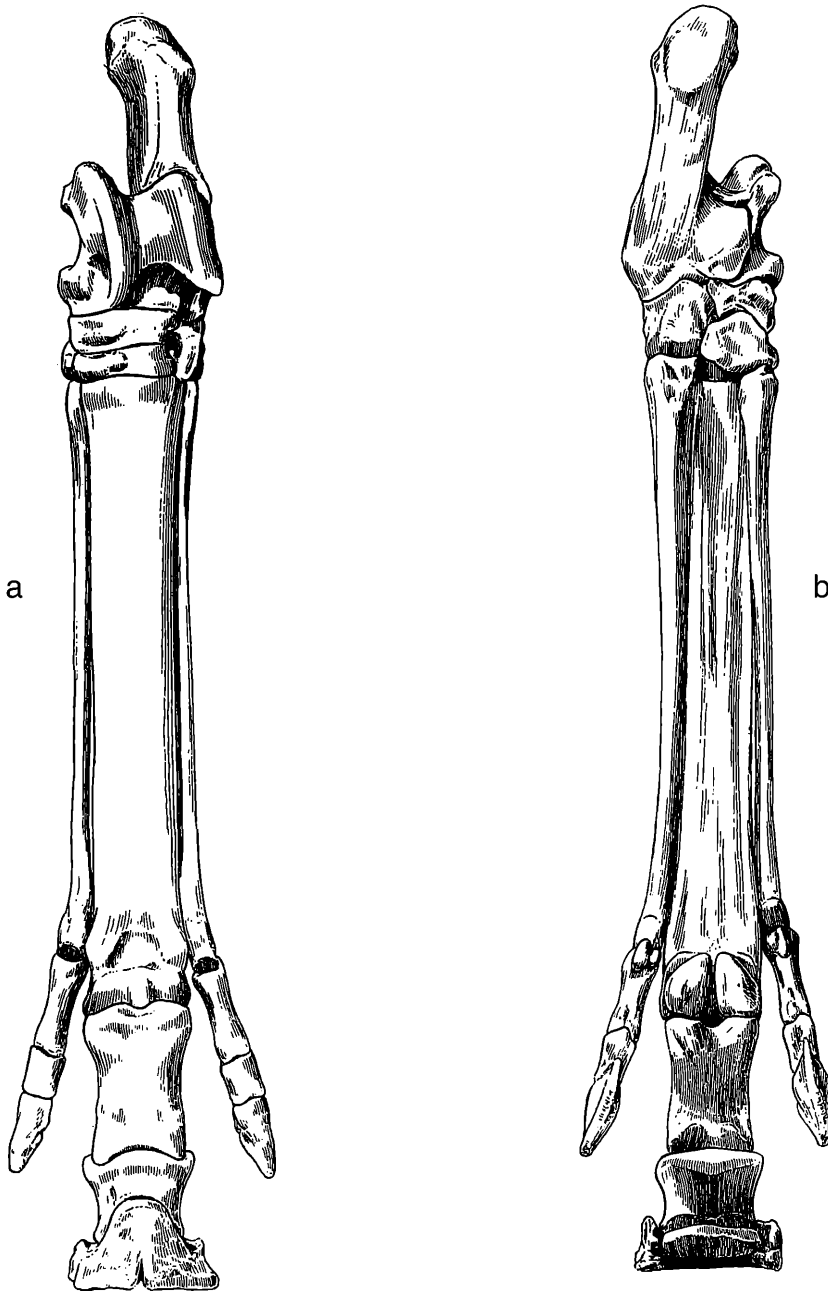
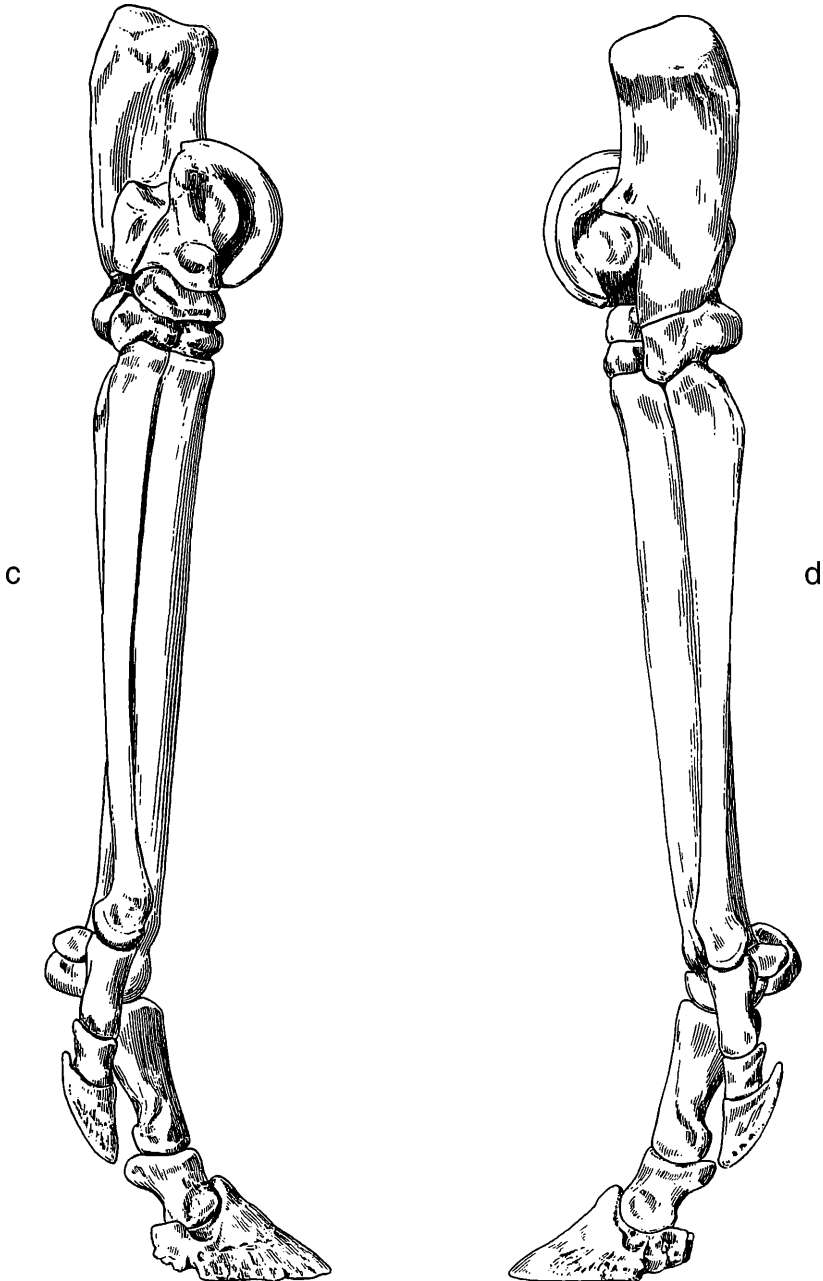


Figure 7.28.1 Posterior tarsus, metatarsus and phalanges as a whole: a. cranial; b. caudal; c. medial; d. lateral (x 0,40).



8. Discussion

The Höwenegg hipparion is remarkable from a number of standpoints. First and foremost the assemblage is unequalled in its preservation of several complete skeletons which remain articulated. Recent work by JÖRG & ROTHAUSEN (1991) and WOODBURNE et al. (1996) has strengthened the interpretation that this assemblage was accumulated over a very short duration, and as such it closely approximates an actual biological population. We can then, with a degree of confidence, establish the "expected" range of variation in anatomical features, morphologic character states and metric variables used by paleoecological researchers for taxonomic assignment and phylogenetic reconstruction. This represents the central theme of our investigation and has been the basis from which we have pursued a number of investigations on Old World hipparions over the last two decades (re: BERNOR, TOBIEN & WOODBURNE, 1989).

The Höwenegg horse, *Hippotherium primigenium* stands near the base of the Old World hipparion radiation, and as would be expected, it retained many primitive skeletal characters. The skull closely resembles that of *Cormohipparion "occidentale"* s.l. in the retention of a shallowly incised nasal notch, a large preorbital fossa which is deep medially and posteriorly and placed well anterior to the lacrimal bone. The cheek tooth dentition is typically *H. primigenium* in the high complexity of occlusal enamel bands, relatively low maximum crown height (ca. 50 mm for P⁴ and M¹), and the mediolateral cross grooving of the cheek teeth thought to be indicative of a browse component in their dietary intake (BERNOR & ARMOUR-CHELU, in press). The canines are sexually dimorphic with males exhibiting a large, robustly developed morphology while the females have a reduced peg-like form. The postcranium also is typically *H. primigenium*-like in the morphology and proportions of the metapodials and phalanges (BERNOR, TOBIEN & WOODBURNE, 1989; BERNOR, MITTMANN & RÖGL, 1993; BERNOR et al. 1993; BERNOR & FRANZEN, 1997) and exhibits some primitive features such as the retention of a somewhat more distinct ulna (although fully fused to the radius). The carpalia and tarsalia are remarkable for their extensive articular surfaces and existence of fossae nudatae, or synovial channels, which suggest extensive intercarpal and intertarsal joint mobility, and mobility between these and articulating metapodials and phalanges. However, the lack of suitable hipparion comparative material prohibits our understanding of locomotor diversity within the group. The spine is typically equine except for the remarkable discovery that *H. primigenium* had very long spinous processes for T₁-T₁₃, with T₁₄-T₁₈ being lumbarized as in extant *Equus*.

The Höwenegg hipparion has been central to several recent Old World hipparion investigations. Establishing

this population's variability in skull, dental and postcranial characters has allowed us to pursue detailed comparisons of several Central European assemblages of *Hippotherium "primigenium"* s.l. Indeed, *H. primigenium* was the only hipparion in Central Europe for much of the Vallesian. Recent work would suggest that there was a late MN 9 divergence of Austrian and Hungarian members of this lineage (BERNOR, MITTMANN & RÖGL, 1993; BERNOR et al., 1993; RÖGL et al., 1993;) from more westerly populations characterized by the MN 11 locality of Dorn Dürkheim (BERNOR & FRANZEN, 1997).

Anatomically then, *Hippotherium primigenium* s.l. is a plausible "ancestor" for Old World hipparionine horses. Earliest hipparion occurrences in the Potwar Plateau of Pakistan (PILBEAM et al., 1996), Sinap Turkey (KAPPELMAN et al., 1996), Chor'ora Ethiopia and Spain all share the morphologic hallmarks of this primitive taxon (BERNOR, TOBIEN & WOODBURNE, 1989; BERNOR et al., 1996; WOODBURNE, BERNOR & SWISHER, 1996). While hipparion evolution was remarkably conservative through the Vallesian of Central Europe and perhaps equivalent aged horizons in Pakistan and East Africa, Southeast Europe and Southwest Asia record an early explosive radiation of hipparionine horses (BERNOR et al., 1996; FORTELIUS et al., 1996). A number of independent lineages arose in the later Miocene, some being monospecific such as "*Hipparion" dermatorhinum* (China), others being members of species diverse lineages such as *Hipparion* s.s. (Eurasia), *Cremohipparion* (Eastern Europe, Southwest Asia and China), and early members of the "*Sivalhippus*" Complex. These lineages all show distinct distributions in time and space, but the pattern is one of episodic biogeographic extension followed by long provincial isolation. Some geographic areas such as Central Europe, Spain, the Indian Subcontinent and Sub-Saharan Africa evidently had prolonged periods of isolation where new and innovative functional anatomical complexes arose resulting in some of the more derived hipparion lineages such as *Proboscicdipparion* in China and *Eurygnathohippus* in Africa.

However, hipparion systematics is not without its problems, perhaps foremost being the group's penchant for homoplasy. It appears as though no part of the hipparion horse's skeleton was entirely immune to convergence: not the snout proportions, facial morphology, dental morphology or postcranial morphology. This makes dependence on a particular bone or functional complex hazardous for evolutionary reconstructions. Securing evolutionary lineages requires both character state and morphometric analyses and the establishment of character congruence to support any given phylogenetic interpretation (BERNOR & LIPSCOMB, 1995). Homoplasy has nearly always been found in

lineages that were distinct for a long duration, such as the loss of the preorbital fossa in *Hipparion*, advanced members of the "Sivalhippus" Complex and the dwarf radicle of *Cremohipparion*, and is readily identifiable as such because distinct synapomorphies ally these individual species with other members of their own group. In more limited cases, such as *Hipparion* s.s., it may be that characters of the face and snout evolved convergently between species of this group and require more detailed analyses for fully understanding their evolutionary relationships (BERNOR & ARMOUR-CHELU, in press).

The Höwenegg hipparion, and indeed Central European *Hippotherium primigenium* lived in highly equable, warm temperate to subtropical woodlands and forests (BERNOR et al., 1988). TOBIEN (1952) has shown that *Hippotherium primigenium* was capable of functional monodactyly during running, but also enjoyed the capability of walking on all three toes during slower, more deliberate locomotion. The spine is another indication of a locomotor repertoire which differs from *Equus*: the long spinous processes of the thoracic and lumbar vertebrae suggest a strongly developed musculature for rotation and mediolateral movement of the spine which would have been advantageous when the animal made repeated quick "darting" turns at high speed. Therefore, both the anatomy and biotic context of this species is one of a woodland/forest setting rather than a "steppe" or savanna environment.

In a recent review of the ecomorphology of Old World hipparions, BERNOR & ARMOUR-CHELU (in press) have reported a vast range of morphologies and likely dietary preferences. Some lineages became more committed browsers evolving highly retracted nasals (such as "*Hipparion*" *dermatorhinum*, *Cremohipparion proboscideum* and *Cremohipparion licenti* and *Proboscidipparion pater* and *Proboscidipparion sinense*) while others became more committed grazers (such as members of *Hipparion* s.s., the small radicle of *Cremohipparion* [*macedonicum*, *matthewi*, *periafricanum*] and members of the African hipparion lineage, *Eurygnathohippus*). The latest Pliocene/early Pleistocene horse *Eurygnathohippus* became the most extreme grazer developing a broad mandibular symphysis, hypertrophied and procumbent 1st and 2nd lower incisors with accompanying atrophied 3rd incisors, and cheek teeth that approached crown heights of nearly 90 mm. Clearly, hipparionine horses enjoyed a remarkable adaptive success across all of the Old World. Their evolutionary diversity has proven invaluable for provincial-to-intercontinental scale correlation and biogeographic reconstruction. BERNOR & LIPSCOMB (1995) found that hipparion intercontinental dispersion closely tracked global sea-lowering events: times of glacio-eustatic sea lowering appeared to correspond to long range biogeographic extensions between Europe and Asia and Eurasia and Africa. Old World hipparionines

likewise seem to have responded to heightened seasonality in the late Miocene by aggressively radiating into multiple species-rich lineages. Later in the Pliocene, the group became progressively more restricted to East Asia and Africa where they evolved the most derived and unique morphologies known: the hyper-browser *Proboscidipparion* in China and the hyper-grazer *Eurygnathohippus* in Africa. The group would appear to have become extinct in the middle Pleistocene, ca. 0.7 m.y.

Hippotherium primigenium was a remarkably adaptable equid. Initially favoring warm temperate to tropical conditions it invaded virtually every region of the Old World and readily evolved new and frequently novel morphologies. The Höwenegg hipparion is particularly important because it has given us an important insight into the anatomy and behavior of the stem species of the Old World hipparion radiation.

9. Summary

We present here a detailed anatomical description, character state attribution and morphometric characterization of the Höwenegg hipparion assemblage. This assemblage is significant from three particular standpoints: it is one of the oldest known, and at the same time precisely dated Old World hipparions (ca. 10.3 m.y.; SWISHER, 1996); it is morphologically primitive representing a plausible ancestor for all Old World hipparionines (BERNOR, TOBIEN & WOODBURNE, 1989; WOODBURNE, BERNOR & SWISHER, 1996); it closely resembles an actual biological population in that the assemblage was accumulated over a short duration (JÖRG & ROTHAUSEN, 1991; WOODBURNE et al., 1996). Of the 14 partial-to-complete skeletons we report here on the 12 adult individuals; the fetus and foal will be the subject of a separate study.

We have defined our methods so as to account for variability in discrete morphologic character states as well as continuous variables. The discrete characters are restricted to morphologic states of the skull, maxillary dentition and mandibular dentition following previous work (BERNOR, TOBIEN & WOODBURNE, 1989; BERNOR & LIPSCOMB, 1991, 1995). Facial morphology was found to be stable in this assemblage, while dental characters generally showed more variability. Despite this variability however we feel confident that dental characters can be useful for species identification and evolutionary reconstruction when the middle stage-of-wear is used for comparison and analysis (re: BERNOR & FRANZEN, 1997). We have further found that there is no evident sexual dimorphism in any skull or dental character except the size of the canine: males have larger canines than females.

We have provided a detailed anatomy of the thoracic and pelvic limbs. We have correlated all visible fea-

tures of the various limb bones to corresponding features in extant *Equus* and derived their specific function. In the case of digits II and IV which have no homologue in *Equus*, we have made reasoned interpretations of osteologic features with reference to digit III whenever possible. When viewed in detail there are several features in which *Hippotherium* and *Equus* differ, mostly being related to one's tridactyl and the other's monodactyl anatomy. We have further studied postcranial anatomy by pursuing a detailed morphometric analysis of virtually every bone. We follow EISENMANN et al. (1988) closely, and advance additional measurements in the cases of the carpalia and tarsalia in order to characterize the population more completely. We have found no sexual dimorphism in the bones, and in fact most measurements on most bones exhibit relatively low coefficients of variation. Use of bivariate comparisons have thus far proven useful for taxonomic identifications and assignment (re: BERNOR & ARMOUR-CHELU, in press).

Our description of the vertebral column is brief. The Höwenegg hipparion vertebral column is particularly remarkable for the long spinous processes on thoracic vertebrae T1-T14. We relate this morphology to the development of the dorsal axial musculature for mediolateral movement of the spine which enabled this equid to make sharp turns while running. The Höwenegg hipparion also exhibited the ability to assume functional tridactyly during slow locomotion or monodactyly during cursorial locomotion (TOBIEN, 1952).

Recent work on the phylogenetic relationships of the Höwenegg hipparion (BERNOR, TOBIEN & WOODBURNE, 1989; BERNOR & LIPSCOMB, 1991, 1995; WOODBURNE, BERNOR & SWISHER, 1996) has verified previous assertions (BERGGREN & VAN COUVERING, 1974; FORSTÉN, 1968) that *Hippotherium primigenium* is a plausible stem species of the Old World hipparion radiation. Environmental reconstruction of first appearing Central European hipparions (BERNOR et al., 1988, 1991) further confirms that this horse was adapted to forest and woodland environments (FORSTÉN, 1968), not savannas.

Our work here has been aimed more at describing and characterizing the skeletal anatomy of the Höwenegg hipparion than further pursuing evolutionary, biogeographic and paleoecological work. We intend it to be useful as a guide for identification and comparison with other hipparion assemblages, setting discrete and morphometric parameters for alpha taxonomy and to foster further diverse paleobiological study of this fascinating and diverse group of fossil equids.

10. Literature

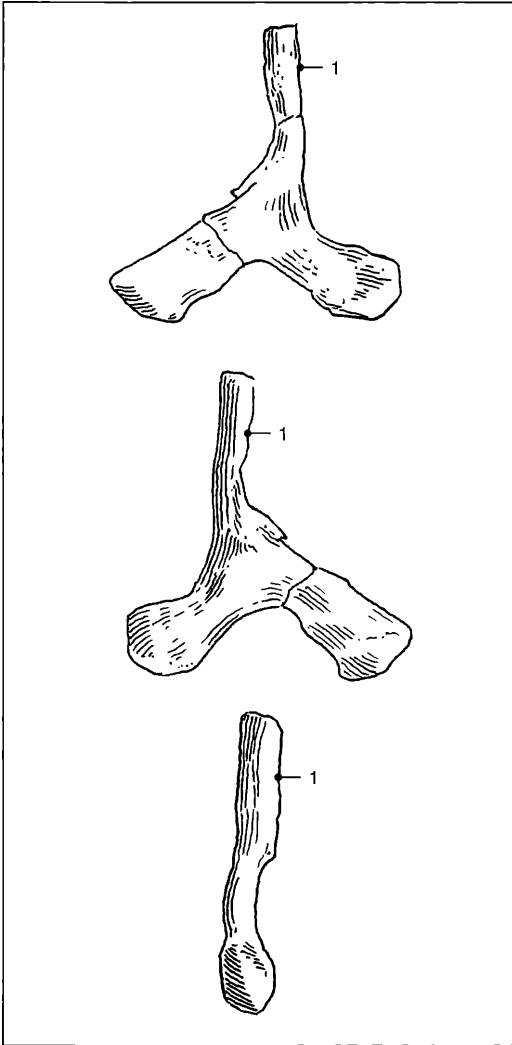
- BARANYI, J., & LIPPOLT H.J. & TODT, W. (1976): Kalium-Argon Alterbestimmungen an tertiären Vulkaniten des Oberrhein-graben-Gebietes. II. Die Alterstraverse vom Hegau nach Lothringen. – Oberrhein. Geol. Abh., **25**, 41–62, 6 Abb., 1 Tab.; Karlsruhe.
- BARRY, J.C., LINDSAY, E.H. & JACOBS, L.L. (1982): A biostratigraphic zonation of the middle and upper Siwaliks of the Potwar Plateau of Northern Pakistan. – Palaeogeog., Palaeoclimat., Palaeoeco., **37**, 95–130; Amsterdam.
- BEAUMONT, G. DE (1986): Les carnivores (Mammifères du Néogène de Höwenegg (Hegau, Baden-Württemberg). – Carolina, **44**, 35–43; Karlsruhe.
- BECKER-PLATEN, J. D., BENDA, L. & STEFFENS, P. (1977): Litho- und biostratigraphische Deutung radiometrischer Altersbestimmungen aus dem Jungtertiär der Türkei. Geol. Jb., **B 25**, 139–167; Hannover.
- BERG, D.E. (1970): Die jungtertiäre "Antilope" *Miotragocerus* (ein Beispiel für die Problematik paläontologischer Analyse fossiler Tragoceren/Bovidae, Mammalia). Habil.-Schrift Univ. Mainz, 198 pp.; Mainz (unveröff.).
- BERGGREN, W.A., KENT, D.V., SWISHER, C.C. III & AUBRY, M.-P. (1995): A revised Cenozoic geochronology and chronostratigraphy. – In: BERGGREN, W.A., KENT, D.V. & HARDENBOL, J. (eds.): Geochronology, Time Scales, and Global Stratigraphic Correlations: A Unified Temporal Framework for an Historical Geology. Society of Economic Paleontologists and Mineralogists Special Publication No. **54**: 129–212; Tulsa.
- BERGGREN, W.A., KENT, D.V. & VAN COUVERING, J.A. (1985): Neogene geochronology and chronostratigraphy. – In: N.J. SNELLING (ed.): The Chronology of the Geological Record. Geological Society of London., Mem. **5**, 211–260; London.
- BERGGREN, W.A. & VAN COUVERING, J.A. (1974): The late Neogene: Biostratigraphy, geochronology and paleoclimatology of the last 15 million years in marine and continental sequences. – Palaeogeog. Paleoclim. Paleoeco., **16** (1/2), 1–216, 15 Fig., 12 Tab., 1 App.; Amsterdam.
- BERNOR, R.L. (1983): Geochronology and zoogeographic relationships of Miocene Hominoidea. – In: CIOCHON, R.L. & CORRUCINI, R.S. (Eds): New Interpretations of Ape and Human Ancestry, 21–64; New York.
- BERNOR, R.L. (1984): A zoogeographic theater and biochronologic play: the time/biofacies phenomena of Eurasian and African Miocene mammal provinces. – Paléobiol. Contin., **14**, 121–142; Montpellier.
- BERNOR, R.L. (1985): Systematic and evolutionary relationships of the hipparionine horses from Maragheh, Iran (Late Miocene, Turolian age). – Palaeovert., **15** (4): 173–269, 19 Abb., 2 Tab.; Montpellier.
- BERNOR, R.L. & ARMOUR-CHELU, M.J. (1997): Later Neogene Hipparions from the Manonga Valley, Tanzania. – In: T. HARRISON (ed.): Neogene Paleontology of the Manonga Valley, Tanzania, Topics in Geobiology Series; ff. New York.
- BERNOR, R.L. & ARMOUR-CHELU, M.J. (in press): Toward an Evolutionary History of African Hipparionine Horses. In: T. BROMMAGE & SCHRENK, F. (eds.): African Biogeography, Climate Change and Early Hominid Evolution, Wenner-Gren Foundation Conference Livingstonia Beach Hotel, Salima, Malawi; Oxford.
- BERNOR, R.L. & HUSSAIN, S.T. (1985): An assessment of the systematic, phylogenetic and biogeographic relationships of Siwalik hipparionine horses. – J. Vert. Paleo., **5** (1): 32–87, 22 Abb., 7 Tab.; Norman.

- BERNOR, R.L., KOVAR-EDER, J., LIPSCOMB, D., RÖGL, F., SEN, S. & TOBIEN, H. (1988): Systematics, stratigraphic and paleo-environmental contexts of first-appearing hipparion in the Vienna Basin, Austria. – *J. Vert. Paleo.*, **8** (4): 427–452, 11 Abb., 9 Tab.; Norman.
- BERNOR, R.L., KOVAR-EDER, J., SUC, P. & TOBIEN, H. (1990): A contribution to the evolutionary history of European late Miocene age hipparionines (Mammalia: Equidae). – *Paléobio. continent.*, **XVII**: 291–309, 3 fig.; Montpellier.
- BERNOR, R.L. & LIPSCOMB, D. (1991): The systematic position of "*Plesiohipparion*" aff. *huangheense* (Equidae, Hipparionini) from Gülyazi, Turkey. *Mitt. Bayer. Staatslg. Paläont. hist. Geol.*, **31**: 107–123, 3 Fig, 2 Tab.; München
- BERNOR, R.L. & LIPSCOMB, D. (1995): A consideration of Old World hipparionine horse phylogeny and global abiotic processes. – In: VRBA, E., DENTON, G. PARTRIDGE, T. & BURCKLE, L. (eds.): *Paleoclimate and Evolution, With Emphasis on Human Origins*, 163–177; Yale: New Haven.
- BERNOR, R.L., MITTMANN, H.-W., KRETZOI, M. & TOBIEN, H. (1993): A preliminary systematic assessment of the Rudabánya hipparions. – *Mitt. Bayer. Staatslg. Paläont. hist. Geol.*, **33**: 1–20; München.
- BERNOR, R.L., MITTMANN, H.-W. & RÖGL, F. (1993): The Götzenendorf hipparion. *Ann. Nat. Mus. Wien*. **95A**: 101–120; Wien.
- BERNOR, R.L., QIU, Z. & HAYEK, L.-A. (1990): Systematic revision of Chinese hipparion species described by Sefve, 1927. – *Amer. Mus. Novit.*, **2984**: 1–60, 18 Abb., 5 Tab., 2 App.; New York.
- BERNOR, R.L., & QIU, Z. & TOBIEN, H. (1987): Phylogenetic and biogeographic bases for an Old World hipparionine horse geochronology. – *Ann. Inst. Geol. Hung. Proc. VIIIth Internat. Cong. R.C.M.N.S.*, pp. 43–53, 6 Abb.; Budapest.
- BERNOR, R.L. & TOBIEN, H. (1989): Two small species of *Cremochiparion* (Equidae, Mamm.) from Samos, Greece. – *Mitt. Bayer. Staatslg. Paläont. hist. Geol.*, **29**: 207–226, 3 Fig, 9 Tab.; München.
- BERNOR, R.L., TOBIEN, H. & WOODBURN, M.O. (1989): Patterns of Old World hipparionine evolutionary diversification and biogeographic extension. – In: LINDSAY, E. H., FAHLBUSCH, V. & MEIN, P. (eds.): *European Neogene Mammalian Chronology – NATO ASI series. Series 180*: 263–319, 8 Fig., 2 Tab.; New York.
- BERNOR, R.L., WOODBURN, M.O. & VAN COUVERING, J.A. (1980): A contribution to the chronology of some Old World faunas based on hipparionine horses. – *Géobios*, **13** (5): 35–59; 9 Fig., 2 Tab.; Lyon.
- CAMP, C.L. & SMITH, N. (1942): Phylogeny and functions of the digital ligaments of the horse. – *Mem. Univ. Calif.*, **13**: IV+69+124, 39 figs., 4 pls.; Berkeley.
- CANDE, S.C. & KENT, V. (1992): A new geomagnetic polarity time scale for the late Cretaceous and Cenozoic. – *J. Geophys. Res.*, **97** (B10): 13917–13951; Baltimore.
- CHRISTOL, J. DE (1852): *Lettre sur l'Hipparion*. *Bull. Soc. géol. France*, **9** (2): 255–256; Paris.
- DEEKE, W. (1917): *Geologie von Baden*. – 782 pp; Berlin.
- EISENMANN, V., ALBERDI, M.-T. GIULI, C. DE & STAESCHE, U. (1988): *Studying fossil horses*. Vol. 1: Methodology. – In: WOODBURN, M. & SONDAAR, P. (eds.): *Coll. papers "New York Intern. Hipparion Conference, 1981, VIII + 71, 29 Fig.; Leiden*.
- ELLENBERGER, W. & BAUM, H. (1977): *Handbuch der vergleichenden Anatomie der Haustiere*. – 18. Ed.: 1155 pp., 1689 figs.; Berlin.
- ESTES, R. D. (1991): *The Behavior Guide to African Mammals*. – Univ. Calif. Press, California.: 611 pp. 29 chapters with figures and tables.
- FORSTÉN, A.M. (1968): Revision of Palearctic *Hipparion*. – *Acta Zool. Fenn.*, **119**: 1–134, 42 Fig., 27 Tab., 4 Pl.; Helsinki.
- FORSTÉN, A.M. (1985): *Hipparion primigenium* from Höwenegg/Hegau, FRG. – *Ann. Zool. Fennici*, **22**: 417–422, 4 Fig., 3 Tab.; Helsinki.
- GABUNJA, L.K. (1959): *Histoire du genre Hipparion*. – Ed. Acad. Sci. USSR, Moscou, traduction en français B.R.G.M., 69 Fig., 151 Tab., 23 Pl.; Paris.
- GETTY, R. (1982): *The Anatomy of the Domestic Animals*. – 1211 + xiv pp.; Philadelphia.
- GREGOR, H.J. (1982): Die jungtertiären Floren Süddeutschlands. *Paläökarpologie, Phytostratigraphie, Paläoökologie, Paläoklimatologie*. – 278 S; Stuttgart.
- GROMOVA, V. (1952): Le genre *Hipparion*. – *Inst. Paleontol. Acad. Sci. l'USSR* 36. 12: 1–473, 54 Abb., 18 Tab., 13 Taf.; Paris (Translated from Russian by St. Aubin. *Bur. Rech. Min. Geol.*, Ann. C.E.D.P.).
- HAQ, B.U., & HARDENBOL, J. & VAIL, P.R. (1987): Chronology of fluctuating sea levels since the Triassic. – *Science*, **235**: 1156–1167; Washington, D.C..
- HENSEL, R.F. (1860): *Über Hipparion mediterraneum*. – *Abf. Akad. Wiss. Berlin*, 27–121, 4 pls.; Berlin.
- HULBERT, R.C. (1988): *Cormohipparion* and *Hipparion* (Mammalia, Perissodactyla, Equidae) from the late Neogene of Florida. *Bull. – Florida State Mus. Bio. Sci.*, **33** (5): 229–338, 26 Fig., 10 Tab.; Gainesville.
- HULBERT, R.C. & MACFADDEN, B.J. (1991): Morphological transformation and cladogenesis at the base of the adaptive radiation of Miocene hypsodont horses. – *Novitates*, **3000**: 1–61, 17 Fig., 9 Tab., New York.
- HÜNERMANN, K. A. (1982): Rekonstruktion des *Aceratherium* (Mammalia, Perissodactyla, Rhinocerotidae) aus dem Jungtertiär vom Höwenegg (Hegau) (Baden-Württemberg, BRD). – *Z. geol. Wiss. Berlin*, **10** (7): 929–942; Berlin.
- HÜNERMANN, K. A. (1989): Die Nashornskellette (*Aceratherium incisivum* KAUP 1832) aus dem Jungtertiäre vom Höwenegg im Hegau (Südwestdeutschland, Vallesium, Obermiozän). – *Andrias*, **8**: 13–64; Karlsruhe.
- JÖRG, E. (1951): Über einige Beobachtungen in den Öhninger Schichten am Höwenegg. – *Mitt.-Bl. bad. geol. Landesanstalt*, **1950**: 75–77; Freiburg.
- JÖRG, E. (1954): Die Schichtfolge der Fossilfundstelle Höwenegg (Hegau) (pontische Mergel und Tuffite der oberen Süßwassermolasse). *Jber. Mitt. oberhein. geol. Ver.*, **n. F. 35**: 67–87; Stuttgart.
- JÖRG, E., (1956): Geologische und biostratonomische Beobachtungen an der unterpliozänen Fossilfundstätte Höwenegg (Hegau). – *Schr. Ver. Gesch. u. Naturgesch. d. Baar*, **24**: 198–207; Donaueschingen.
- JÖRG, E., (1957): Tierwelt und Landschaft am Höwenegg (Hegau) zur Unterpliozänzeit. – *Hegau, Z. f. Gesch. Volkskde., Naturgesch.*, **2** (4): 117–125; Singen.
- JÖRG, E., & REST, H., & TOBIEN, H. (1955): Die Ausgrabungen an der jungtertiären Fossilfundstätte Höwenegg/Hegau 1950–54. – *Beitr. naturkdl. Forsch. Südwestdeutschl.*, **14**: 3–21; Karlsruhe.
- JÖRG, E., & ROTHHAUSEN, K. (1991): Zur Schichtfolge und Biostratonomie der Wirbeltierfundstelle Höwenegg (Hegau, Südwestdeutschland, Vallesium, Obermiozän). – *Andrias*, **8**: 13–64; Karlsruhe.
- KALB, J., JOLLY, C.J., TEBEDGE, S., MEHRATE, A., SMART, C., OSWALD, E.B., WHITEHEAD, P.F., ADEFRIS, T. & SCHATZINGER,

- V.R. (1982): Vertebrate faunas from the Awash Group, Middle Awash Valley, Afar, Ethiopia. – *J. Vert. Paleol.*, **2** (2): 37–258; Norman.
- KAPPELMAN, J., SEN, S., FORTÉLIUS, M., DUNCAN, A., ALPAGUT, B., CRABAUGH, A., GENTRY, A., LUNKKA, J.P., McDOWELL, F., SOLUNIAS, N., VIRANTA, S. & WERDELLIN, L. (1996): Chronology and biostratigraphy of the Miocene Sinap Formation of central Turkey. – In: BERNOR, R.L., FAHLBUSCH, V. & MITTMANN, H.-W. (eds.): *The Evolution of Western Eurasian Neogene Mammal Faunas*, 78–95, 10 Fig., 2 Tab.; New York.
- KOWALEWSKI, V. (1873): *Sur l'Anchitherium aurelianense* Cuv. et sur l'histoire paléontologique des cheveaux. – *Mém. Acad. Sci. St. Petersburg*, **20** (7), IV+73; St. Petersburg.
- LIPPOLT, H.J., GENTNER, W. & WIMMENAUER, W. (1963): Altersbestimmungen nach der Kalium-Argon-Methode an tertiären Eruptivgesteinen Südwestdeutschlands – *Jh. geol. Landesamt Baden-Württ.*, **6**: 507–538; Freiburg.
- LUTZ, A. (1965): Jungtertiäre Süßwasserstracoden aus Süddeutschland. – *Geol. Jb.*, **82**: 271–330; Hannover.
- MACFADDEN, B.J. (1980): The Miocene horse *Hipparion* from North America and from the type locality in Southern France. – *Palaeo.*, **23** (3): 617–635, 15 Fig.; London.
- MACFADDEN, B.J. (1984): Systematics and phylogeny of *Hipparion*, *Neohipparion*, *Nannippus*, and *Cormohipparion* (Mammalia, Equidae) from the Miocene and Pliocene of the New World. – *Amer. Mus. Nat. Hist. Bull.*, **179** (1): 1–196, 151 Fig., 45 Tab.; New York.
- MACFADDEN, B.J. & WOODBURN, M.O. (1982): Systematics of the Neogene Siwalik hipparions (Mammalia, Equidae) based on cranial and dental morphology. – *J. Vert. Paleol.*, **2** (2): 185–218, 19 Fig., 3 Tab.; Norman.
- MATTHEW, W.W. (1929): Critical observations upon Siwalik mammals. – *Bull. Am. Mus. Nat. Hist.*, **61**: 437–560, 55 Fig.; New York.
- MÄUSNEST (1976): Über die Anomalien des erdmagnetischen Feldes im Gebiet einiger Hegauvulkanitvorkommen. – *Oberrhein. geol. Abh.* **25**: 63–74; Karlsruhe.
- MÄUSNEST, O. & SCHREINER, A. (1982): Karte der Vorkommen von Vulkangesteinen im Hegau. – *Abh. Geol. Landesamt Baden-Württemberg*, **10**: 1–48.
- MEIN, P. (1989): European mammal correlations. – In: LINDSAY, E. H., FAHLBUSCH, V. & MEIN, P. (eds.): *European Neogene Mammal Chronology* – NATO ASI series. Series **180**: 73–90; New York.
- MEYER, H. VON (1833): Beiträge zur Petrefactenkunde, Fossile Säugethiere. – *Nova acta Academie caesarensis Leopoldino-Carolinae germanicae naturae curiosum*, **16**: 423–516; Halle.
- NICKEL, R., SCHUMMER, A. & SEIFERLE, E. (1986): The anatomy of the domestic animals 1. The locomotor system of the domestic animals. – 499 pp.; Berlin & Hamburg.
- PETERS, J. (1987): Cuboscaphoids, naviclo-cuboids, langauge barriers and the use of standardised nomenclatures in archeozoological studies. – *Archaeozoologica*, **12**: 43–46; Berlin.
- PILBEAM, D., MORGAN, M., BARRY, L.C. & FLYNN, L. (1996): European MN units and the Siwalik faunal sequence of Pakistan. – In: BERNOR, R.L., FAHLBUSCH, V. & MITTMANN, H.-W. (eds.): *The Evolution of Western Eurasian Neogene Mammal Faunas*, 96–105, 3 Fig., 1 Tab.; New York.
- QIU, Z., WEILONG, H., & ZHIHUI, G. (1988): The Chinese hipparionine fossils. – *Palaeo. Sin.*, Ser. C., **175**, 25: 1–250, 70 Fig., 22 Tab., 47 Pl.; Beijing.
- RIETSCHEL, S., TRUNKO, L. & WEISSBRODT, W. (1985): Südbadische Fossilfunde. Fundstätten Öhringen und Höwenegg. – Führer zu Ausstellungen, Museum am Friedrichsplatz, **6**: 1–46, 74 figs.; Karlsruhe.
- RÖGL, F. & DAXNER-HÖCK, G. (1996): Late Miocene Paratethys correlations. – In: BERNOR, R.L., FAHLBUSCH, V. & MITTMANN, H.-W. (eds.): *The Evolution of Western Eurasian Neogene Mammal Faunas*, 47–55, 3 Fig.; New York.
- RÜTMEYER, L. (1861): Beiträge zur Kenntnis der fossilen Pferde und zur vergleichenden Odontographie der Huftiere überhaupt. *Verh. Naturforsch. Ges. Basel*, **3** (1): 558–693, 45 pls.; Basel.
- RUTTE, E. (1962): Schlundzähne von Süßwasserfischen – *Palaeontographica*, **A120**: 165–212; Stuttgart.
- SCHLEICH, H.H. (1986): Vorläufige Mitteilung zur Bearbeitung der fossilen Schildkröten der Fundstelle Höwenegg. *Carolina*, **44**: 47–56; Karlsruhe.
- SCHREINER, A. (1963): Geologische Untersuchungen am Höwenegg (Hegau). – *Jh. geol. Landesamt Baden-Württemberg*, **6**: 395–420; Freiburg.
- SCHREINER, A. (1966): Geologische Karte von Baden-Württemberg 1: 25000. – *Geol. Landesamt Baden-Württemberg, Erläuterungen zu Blatt 8118 Engen*: 190 pp; Freiburg.
- SCHREINER, A. (1970): Erläuterungen zur Geologischen Karte des Landkreises Konstanz mit Umgebung 1: 50 000. – Herausgeb. *Geol. Landesamt Baden-Württemberg*, 286; Freiburg.
- SCHREINER, A. (1976): Hegau und westlicher Bodensee. *Sammlg. geol. Führer*, **62**: 93 pp; Stuttgart.
- SEN, S. (1986): Contribution à la magnétostratigraphie et à la paléontologie des formations continentales Néogènes du pourtour méditerranéen. Implication biochronologiques et paleobiologiques. – *Thèse d'Etat, Univ. Paris 6*, No. **86.19** 209 pp; Paris.
- SEN, S. (1989): *Hipparion* Datum and its chronologic evidence in the Mediterranean area. – In: LINDSAY, E. H., FAHLBUSCH, V. & MEIN, P. (eds.): *European Neogene Mammal Chronology* – NATO ASI series. Series **180**: 495–505, 4 Fig.; New York.
- SEN, S. (1996): Present state of magnétostratigraphic studies in the continental Neogene of Europe and Anatolia. – In: BERNOR, R.L., FAHLBUSCH, V. & MITTMANN, H.-W. (eds.): *The Evolution of Western Eurasian Neogene Mammal Faunas*, 56–63, 2 Fig.; New York.
- SKINNER, M. & MACFADDEN, B.J. (1977): *Cormohipparion* n. gen. (Mammalia, Equidae) from the North American Miocene (Barstovian-Clarendonian). – *J. Paleont.* **51** (5): 912–926, 7 Fig.; Tulsa.
- SOKAL, R.R. & ROLF, F.J. (1969): *Biometry*. 1–776, 3 App.; San Francisco.
- SONDAAR, P.Y (1968): The osteology of the manus of fossil and recent *Equus*, with special reference to phylogeny and function. – *Verh. Koninkl. Nederl. Akad. Wetenschappen, afd. Natuurkunde*, **25** (1): 1–76; Amsterdam.
- STEININGER, F.F., & BERNOR, R.L. & FAHLBUSCH, V. (1989): European Neogene marine/continental chronologic correlations. – In LINDSAY, E. H., FAHLBUSCH, V. & MEIN, P. (eds.): *European Neogene Mammalian Chronology* – NATO ASI series. Series **180**: 15–46; New York.
- STEININGER, F.F., BERRGGREN, W.A., KENT, D.V., BERNOR, R.L., SEN, S. & J. AGUSTI (1996): Circum-Mediterranean Neogene (Miocene and Pliocene) marine-continental chronologic correlations of European mammal units. – In: BERNOR, R.L., FAHLBUSCH, V. & MITTMANN, H.-W. (eds.): *The Evolution of Western Eurasian Neogene Mammal Faunas*, 7–46, 3 Fig., 1 App.; New York.

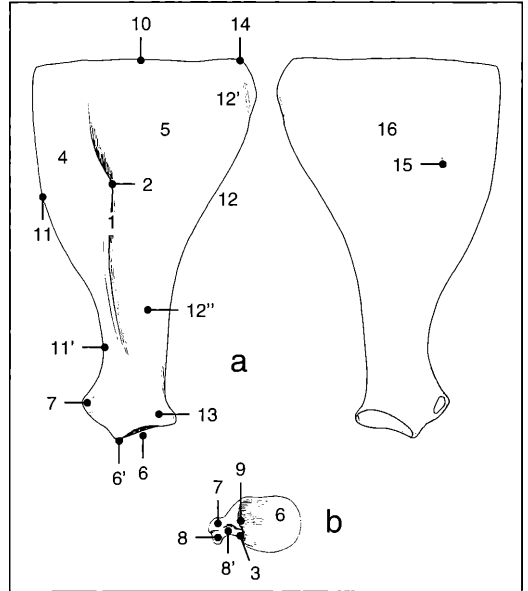
- SWISHER, C.C. III (1996): New $^{40}\text{Ar}/^{39}\text{Ar}$ dates and their contribution toward a revised chronology for the late Miocene nonmarine of Europe and West Asia. – In: BERNOR, R.L., FAHLBUSCH, V. & MITTMANN, H.-W. (eds.): The Evolution of Western Eurasian Neogene Mammal Faunas, 64–77, 1 Fig., 5 Tab.; New York.
- TOBIEN, H. (1938): Über *Hipparion*-Reste aus der obermiozänen Süswassermolasse Südwestdeutschlands. Z. deutsch. geol. Ges., **90**: 177–192; Hannover.
- TOBIEN, H. (1951): Über die Grabungen in der oberen Süswassermolasse des Höwenegg (Hegau). – Mitt. Bl. bad. geol. Landesanstalt, **1950**: 72–74; Freiburg.
- TOBIEN, H. (1952): Über die Funktion der Seitenzehen tridactyl-er Equiden. – N. Jb. Geol. Paläont. Abh., **96**: 137–172.; Stuttgart.
- TOBIEN, H. (1954): Jungtertiäre Wirbeltiere vom Höwenegg/Hegau. – Umschau, **54**: 559–581; Frankfurt.
- TOBIEN, H. (1956): Zur Ökologie der jungtertiären Säugetiere vom Höwenegg (Hegau) und zur Biostratigraphie der europäischen *Hipparion*-Fauna. – Schr. Ver. Gesch. Naturgesch. Baar, **24**: 208–223; Donaueschingen.
- TOBIEN, H. (1957a): Sobre la Bioestratigrafía de la Fauna de *Hipparion*. – Cursillos Conf. Inst. "Lucas Malladá, **4**: 121–126; Madrid.
- TOBIEN, H. (1957b): Die Bedeutung der unterpliozänen Fossilfundstelle Höwenegg für die Geologie des Hegaus. – Jh. geol. Landesamt Baden-Württemberg, **2**: 193–208; Freiburg.
- TOBIEN, H. (1958): Die Ausgrabungen an der unterpliozänen Fossilfundstätte Höwenegg (Hegau). – Z. deutsch. geol. Ges., **110**: 617–618; Hannover.
- TOBIEN, H. (1959a): Die Ausgrabungen an der pontischen Fossilfundstätte Höwenegg (Hegau). – Cursillos Conf. Inst. "Lucas Malladá, **6**: 59–62; Madrid.
- TOBIEN, H. (1959b): *Hipparion*-Funde aus dem Jungtertiär des Höwenegg (Hegau). – Heimat, **67**: 121–140; Öhringen.
- TOBIEN, H. (1962): Über Carpus und Tarsus von *Deinotherium giganteum* KAUP (Mamm., Proboscidea). – Paläont. Z. (H. SCHMIDT-Festband): 231–238; Stuttgart.
- TOBIEN, H. (1970): Subdivision of Pontian Mammalian Faunas. – Comm. mediterr. neogene Stratigr. Proc. IV. Session Bologna 1967. Gior. Geol., **35**: 1–5; Bologna.
- TOBIEN, H. (1982): Osteologische Bemerkungen zum Fussbau von *Hipparion* (Equidae, Mammalia) aus der jungtertiären Wirbeltier-Fundstätte Höwenegg/Hegau. – Z. geol. Wiss., **10**: 1043–1057; Berlin.
- TOBIEN, H. & JÖRG, E. (1959): Die Ausgrabungen an der jungtertiären Fossilfundstätte Höwenegg (Hegau) 1955–1959. – Beitr. naturkd. Forsch. SüdwDtl., **18**: 175–191; Karlsruhe.
- TOBIEN, H. (1986): Die jungtertiäre Fossilgrabungsstätte Höwenegg im Hegau (Südwestdeutschland). Ein Statusbericht. – Caroloinea, **44**: 9–34; 11 Fig., 2 Tab., 1 Pl.; Karlsruhe.
- TOBIEN, H. (1992): On the fossae nudatae in the basipodia of *Equus* and of some fossil tridactyl horses (Equidae, Mammalia). – Ann. Zool. Fennici, **8**, 381–400, 35 figs., 2 tabs.; Helsinki.
- VAN COUVERING, J.A. (1972): Radiometric calibration of the European Neogene. – In: W.W. BISHOP & J.A. MILLER (eds.): Calibration of Hominoid Evolution, 247–71, 2 Fig., 2 Tab.; Edinburgh.
- VIDALENCE, D.A.CH. (1979): La ceinture et les membres pelviens d'un Equidé miocène *Anchitherium aurelianense* (Cuv. 1823). – Ecole Nat. Vet. Toulouse, Thèse (Dipl d'Etat) Année 1979, **34**: 1–290; Toulouse.
- WAGNER, J.J., & DELALOYE, M. & HEDLEY, I. (1975): Données géochronométriques et paléomagnétiques sur l'extension du volcanisme du Hegau en Suisse (Ramsen, Schaffhouse). – C. R. des Séances, SPHN, Genève, N.S. **10** (1): 46–57; Genf.
- WEBB, S.D. & HULBERT, R.C. 1986. Systematics and evolution of *Pseudhipparion* (Mammalia, Equidae) from the late Neogene of the Gulf Coastal Plain and the Great Plains. Contrib. Geol., Univ. Wyoming, Spec. Pap., **3**: 237–272, 15 Fig., 5 Tab.; Laramie.
- WEISKIRCHNER, W. (1975): Vulkanismus und Magmenentwicklung im Hegau. – Ueber. Mitt. oberrhein. Geol. Ver. N.F., **57**: 117–134; Stuttgart.
- WITTMANN, O. (1937): Deckentuff und Molasse am Höwenegg. Ein Beitrag zur Entwicklungsgeschichte eines Hegauvulkanes. – Jber. Mitt. oberrhein. Geol. Ver. N.F., **26**: 1–32; Stuttgart.
- WOODBURNE, M.O. & BERNOR, R.L. 1980 On superspecific groups of some Old World hipparionine horses. – J. Paleoo., **8** (4): 315–327, 9 Fig., 2 Tab.; Norman.
- WOODBURNE, M.O., BERNOR, R.L. & SWISHER, C.C. III (1996): An appraisal of the stratigraphic and phylogenetic bases for the "Hipparion" Datum in the Old World. – In: BERNOR, R.L., FAHLBUSCH, V. & MITTMANN, H.-W. (eds.): The Evolution of Western Eurasian Neogene Mammal Faunas, 124–136, 4 Fig., 1 Tab.; New York.
- WOODBURNE, M.O., MACFADDEN, B.J. & SKINNER, M.J. (1981): The North American "*Hipparion*" datum and implications for the Neogene of the Old World. – Géobios, **14** (4): 493–524, 10 Abb., 2 Tab.; Lyon.
- WOODBURNE, M.O., THEOBALD, G., BERNOR, R.L., SWISHER, C.C. III, KÖNIG, H. & TOBIEN, H. (1996): Advances in the geology and stratigraphy at Höwenegg, southwestern Germany. – In: BERNOR, R.L., FAHLBUSCH, V. & MITTMANN, H.-W. (eds.): The Evolution of Western Eurasian Neogene Mammal Faunas, 106–123, 10 Fig., 1 Tab.; New York.
- ZAPPE, H. (1989): *Chalicotherium goldfussi* KAUP aus dem Vallesium vom Höwenegg im Hegau (Südwestdeutschland). – Andrias, **6**: 117–128; Karlsruhe.
- ZHEGALLO, V.I. (1978): The Hipparions of Central Asia. (in Russian) – Joint Soviet Mongolian Palaeontol. Exp. Trans., **7**: 1–Moscow.

Appendix: Legends for those figures which indicate morphological features



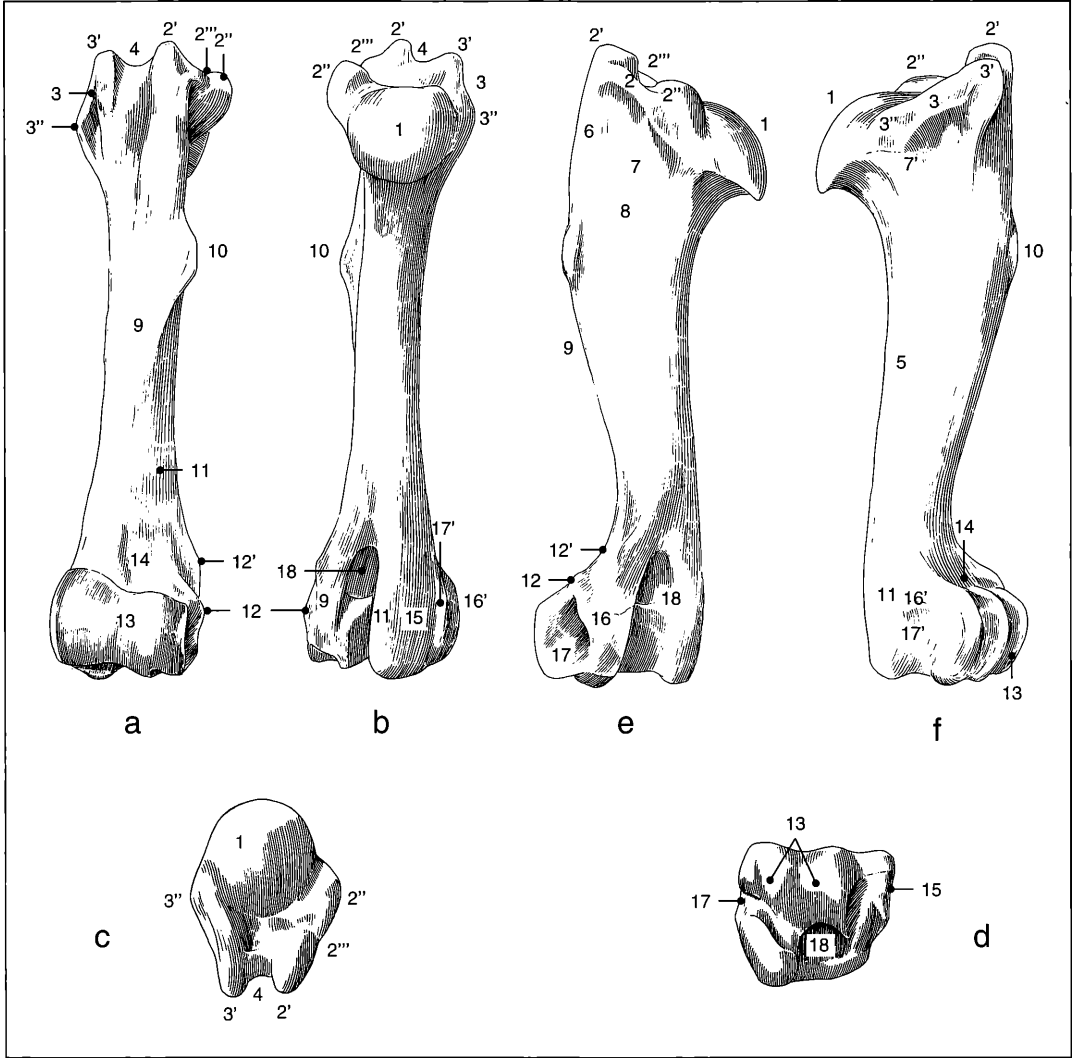
Hyoid (fig. 4.7)

- 1 processus lingualis



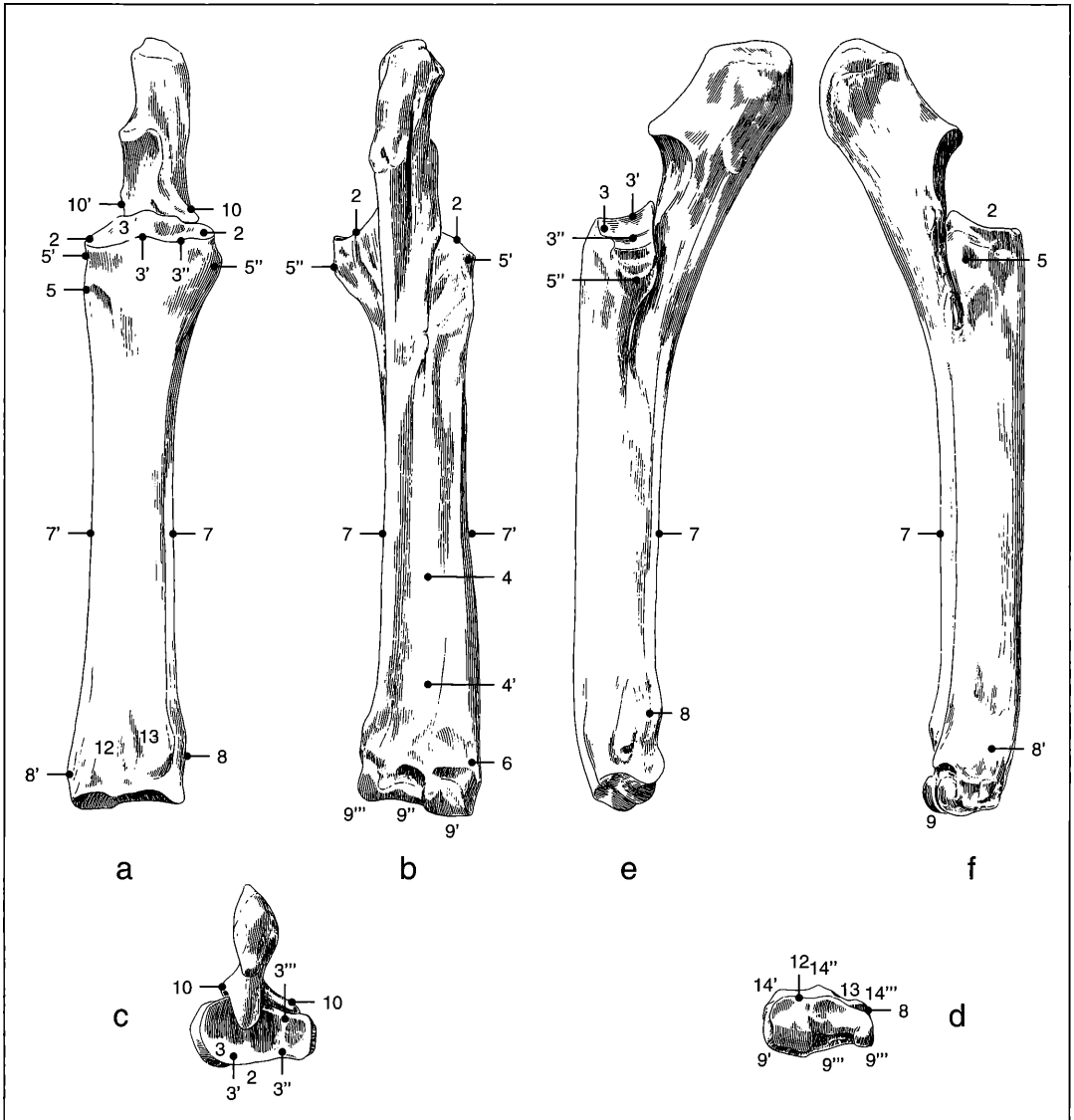
Scapula (fig. 6.1.1)

- 1 spina scapulae
- 2 tuber spinae scapulae
- 3 incisura glenoidalis
- 4 fossa supraspinata
- 5 fossa infraspinata
- 6 cavitas glenoidalis
- 6' cavitas glenoidalis, lateral border
- 7 tuberculum supraglenoidale (=collum scapulae)
- 8 processus coracoideus
- 8' incisura coracoidea
- 9 cavitas glenoidalis, cranial border
- 10 bony margo dorsalis
- 11 margo cranialis
- 11' incisura scapulae
- 12 margo caudalis
- 12' attachment site for musculus infraspinatus
- 12'' lineae musculares
- 13 tuberosity for attachment of the musculus teres minor
- 14 angulus caudalis
- 15 linea serrata
- 16 fossa subscapularis



Humerus (fig. 6.2.1)

- | | |
|---|---|
| <p>1 caput humeri
 2 tuberculum majus
 2' pars cranialis of (2)
 2'' pars caudalis of (2)
 2''' intervening depression between tuberculi 2' and 2''
 3 tuberculum minus
 3' pars cranialis of (3)
 3'' pars caudalis
 4 sulcus intertubularis
 5 tuberculum intermedium between 2'' and 3''; missing in hipparion
 6 fascies musculus infraspinati
 7 tuberositas musculus teres minor
 7' tuberositas musculus teres major
 8 linea musculus tricipitis
 9 crista humeri
 10 tuberositas deltoidea</p> | <p>11 sulcus musculus brachialis
 12 epicondylus lateralis
 12' crista epicondylus lateralis
 13 condylus humeri
 14 fossa radialis
 15 epicondylus medialis
 16 lateral distocaudal protuberance for ligamentous attachment
 16' medial distocaudal protuberance for ligamentous attachment
 17 lateral distocaudal depression for ligamentous attachment
 17' medial distocaudal depression for ligamentous attachment
 18 fossa olecrani
 19 accessory fossa for the musculus extensor digitorum</p> |
|---|---|



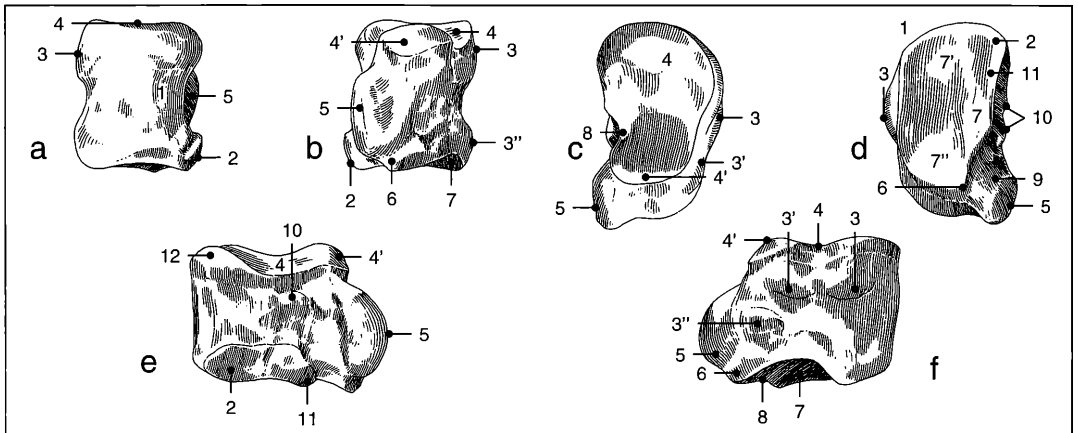
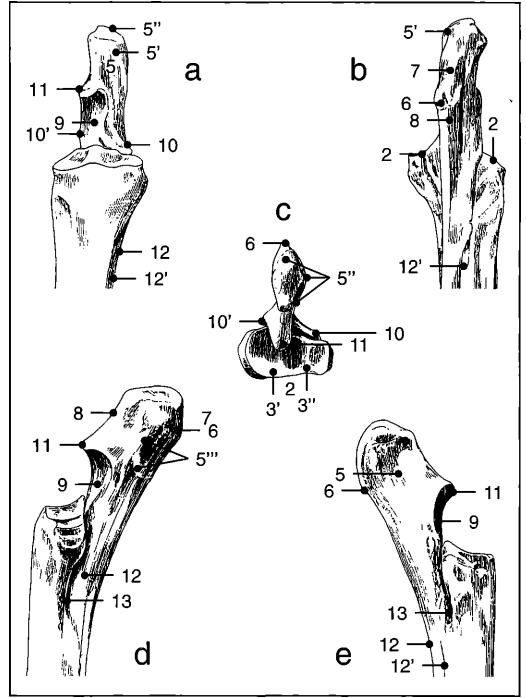
Radius (fig. 6.3.1.2)

- 2 caput radii
- 3 fovea capitis radii
- 3' medial ridge of the fovea capitis radii
- 3'' lateral ridge of the fovea capitis radii
- 3''' no incisure on the caudal border of the fovea capitis radii
- 4 caudal face of the radius
- 4' distal portion of the caudal face
- 5 tuberositas radii + ligamente collaterale medialis
- 5' sulcus proximal of the tuberositas radii
- 5'' ligamentum collaterale laterale
- 6 crista transversa
- 7 lateral border of the corpus radii
- 7' medial border of the corpus radii
- 8 processus styloideus lateralis (= distal limit of the ulna)

- 8' processus styloideus medialis
- 9 trochlea carpi
- 9' medial facies trochlea articularis carpea
- 9'' intermediate portion of the trochlea carpi
- 9''' lateral facies trochlea articularis carpea
- 10 processus coronoideus ulnae lateralis
- 10' processus coronoideus ulnae medialis
- 12 tendonous groove for the musculus extensor digitorum communis
- 13 tendonous groove for the musculus extensor digitorum lateralis
- 14' crista medialis
- 14'' crista intermedia
- 14''' crista lateralis

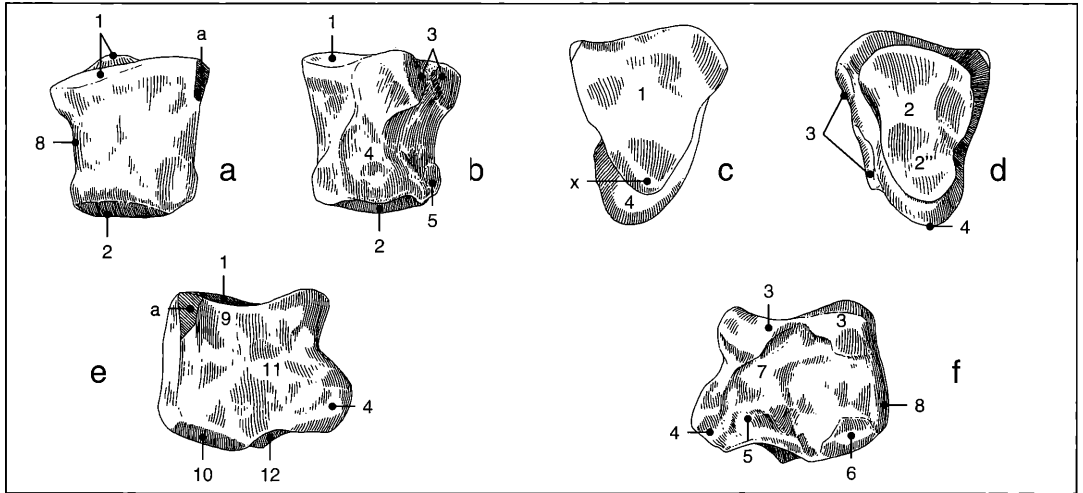
Ulna (fig. 6.4.1)

- 5 olecranon
- 5' tuber olecrani
- 5'' caput laterale musculus tricipitis
- 5''' attachment scar for musculus anconaeus
- 6 attachment scar for musculus flexor carpi ulnaris
- 7 attachment scar for musculus tensor fasciae antebrachii
- 8 attachment scar for musculus flexor digiti profundus
- 9 incisura trochlearis (=semilunaris)
- 10 processus coronoideus lateralis
- 10' processus coronoideus medialis
- 11 processus anconaeus
- 12 corpus ulnae
- 12' suture line of corpus ulnae coossification
- 13 spatium interosseum



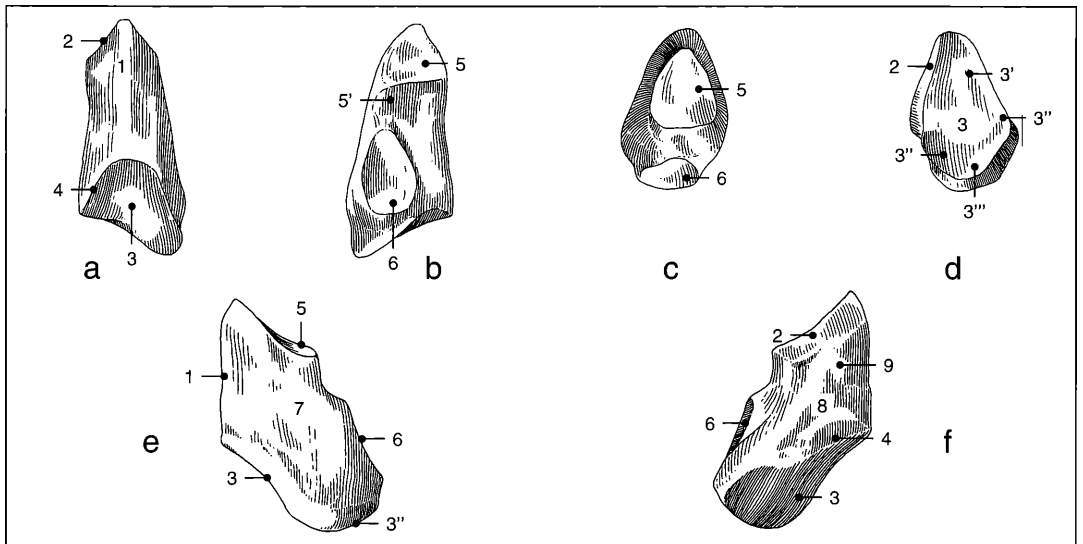
Scaphoideum (fig. 6.5.1)

- 1 attachment site for ligamentum intercarpeum dorsale (=craniale)
- 2 cranial border of lunatum facet
- 3 attachment site for ligamentum collaterale mediale proximale curtum
- 3' attachment site for ligamentum collaterale mediale longum
- 3'' attachment site for ligamentum collaterale mediale distale curtum
- 4 proximal articular facet for medial portion of the radius
- 4' caudal portion of (4)
- 5 tubercle for attachment of ligamentum obliquum volare
- 6 facet for articulation of the trapezium
- 7 distal facet, medial part
- 7' distal facet, cranial part for the magnum
- 7'' distal facet, caudal part for the trapezoideum
- 8 furrow cranial to (5); forms a vertical channel with the medial wall of the lunatum
- 9 sulcus for the musculus abductore pollicis longus
- 10 attachment site for ligamentum interosseum
- 11 facet for the magnum in extant *Equus* (absent here)
- 12 proximal facet for the lunatum



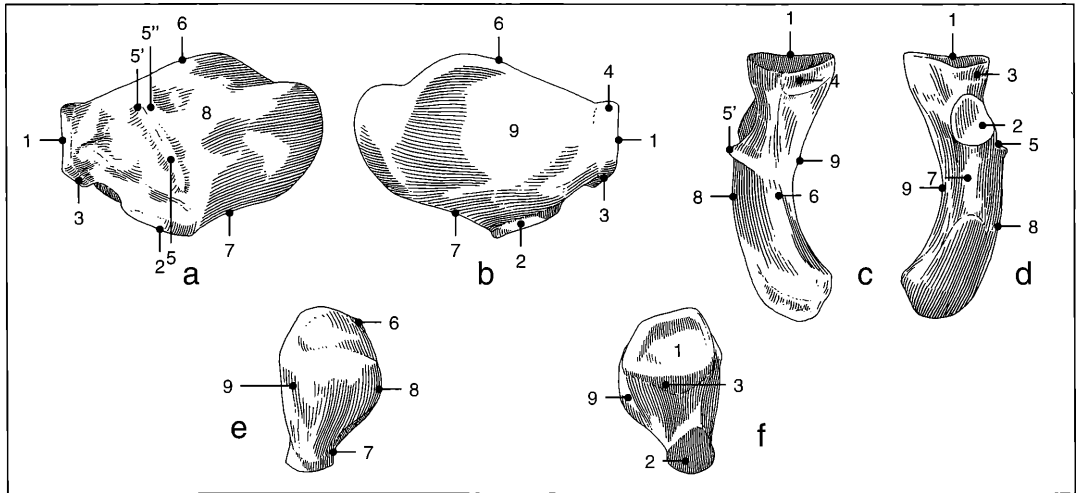
Lunatum (fig. 6.6.1)

- | | |
|---|---|
| <p>1 facet for the radius
 2 distal facet 2 and 2' for the magnum, 2' for the unciforme
 3 facet for the scaphoideum (cranial and caudal portions)
 4 attachment site for ligamentum carpi volare (craniale) profundum
 5 caudal facet for the scaphoideum
 6 cranial facet for the scaphoideum
 7 attachment site for the ligamentum interosseum (for the scaphoideum)</p> | <p>8 attachment site for the ligamentum intercarpeum dorsale (craniale)
 9 proximal facet for the pyramidale
 10 distal facet for the pyramidale
 11 attachment site for the ligamentum interosseum of the pyramidale
 12 facet for the magnum
 x caudal elevation designated by ZHEGALLO 1979, and us here</p> |
|---|---|



Pyramidale (fig. 6.7.1)

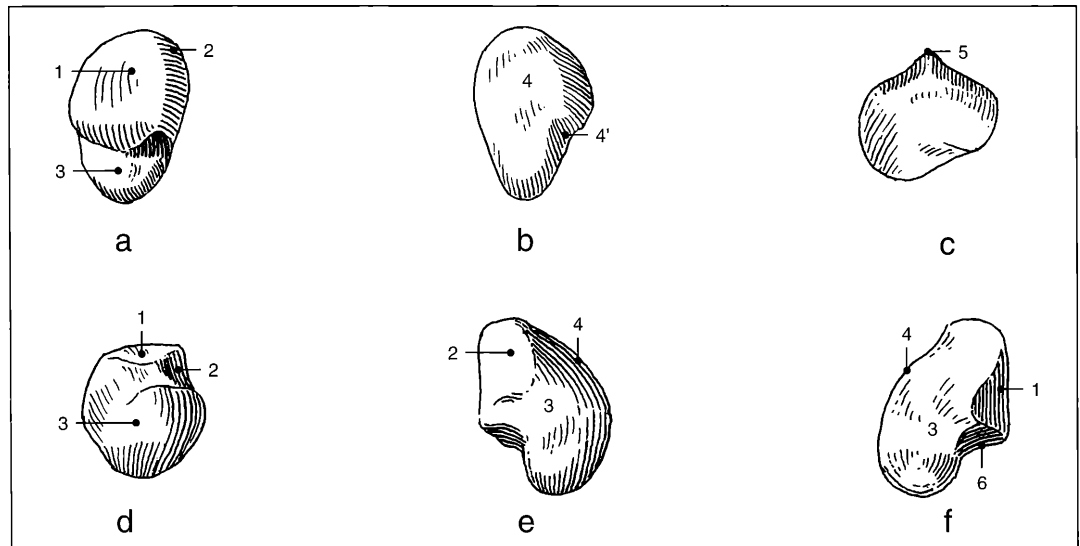
- | | |
|---|--|
| <p>1 bony crest
 2 proximal facet for the lunatum
 3 distal facet for the unciforme
 3' cranial portion of (3)
 3'' distal portion of (3)
 4 distal facet for the lunatum</p> | <p>5 facet for the radius lateral trochlea
 5' small facet for the pisiforme
 6 facet for the pisiforme
 7 lateral wall
 8 medial wall</p> |
|---|--|



Pisiforme (fig. 6.8.1)

- 1 facet for the lateral (ulnar) radius trochlea
- 2 larger facet for the pyramidale
- 3 smaller facet for the pyramidale
- 4 small facet for the proximal portion of the lateral (ulnar) radius trochlea
- 5 furrow for the tendonous insertion of the musculus extensor carpi ulnaris
- 5' medial crest of (5) demarking the attachment site for the musculus extensor carpi ulnaris

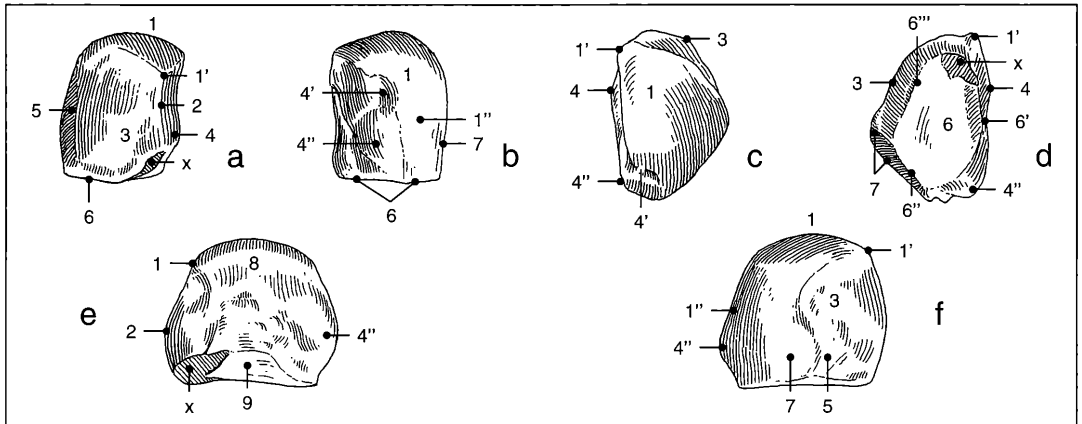
- 5'' lateral crest of (5)
- 5''' proximal end of the strongly protruding median bony crest for attachment of the musculus extensor carpi ulnaris
- 6 proximal margin of the pisiforme
- 7 distal margin of the pisiforme
- 8 cranial wall of the pisiforme
- 9 the caudal wall of the pisiforme



Trapezium (fig. 6.9.1)

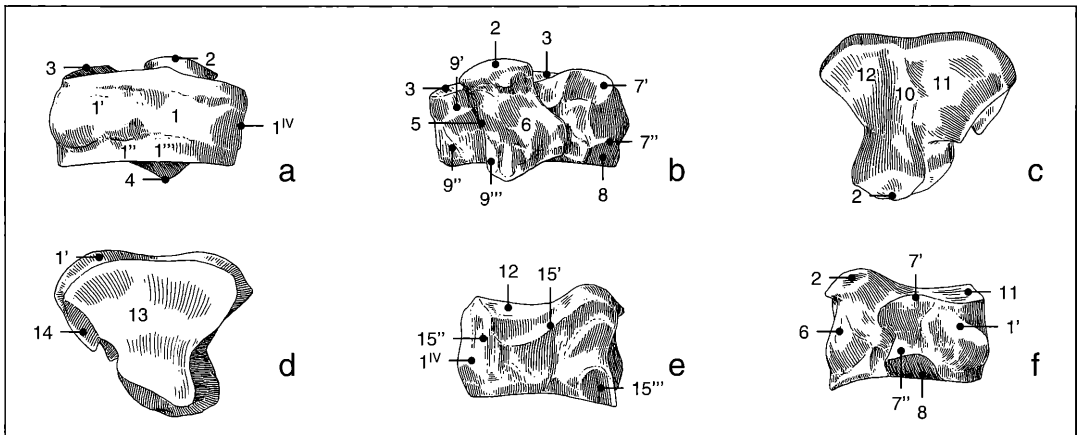
- 1 large facet for the trapezoideum
- 2 small facet for the MC II
- 3 distally reflected portion
- 4 convex caudal facies

- 4' indentation on the medial border of (4)
- 5 distal apex of the trapezium
- 6 rugose notch for ligamentous attachment



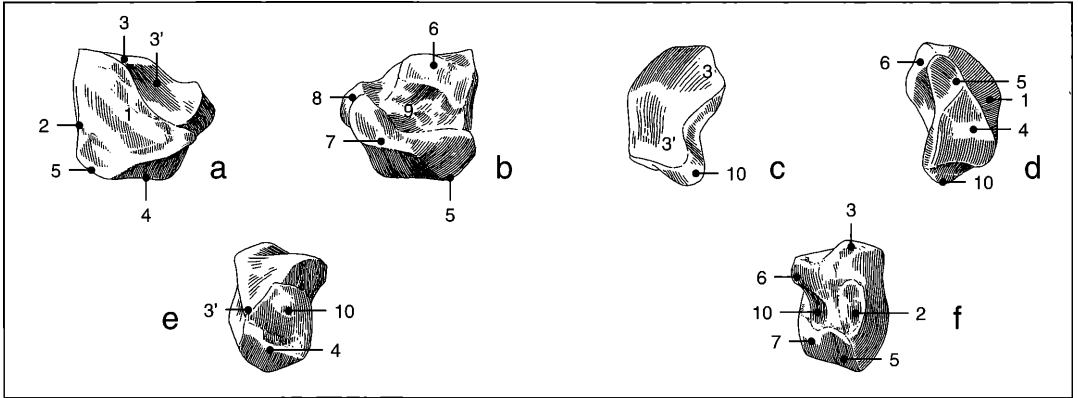
Trapezoidium (fig. 6.10.1)

- | | |
|--|--|
| <p>1 main proximal articular facet for the scaphoideum
 1' cranial continuation terminating at the apex of (1)
 1'' distal portion of (1)
 2 cranial keel of the trapezoidium wedge
 3 rugose non-articular facies of the medial wall
 4 lateral wall
 4' groove for ligamentous attachment
 4'' tuberosity on distal aspect of laterocaudal border (directed toward the magnum)</p> | <p>5 non-articular shallow furrow accompanying the medial border of (1)
 6 distal articular facet for MC II
 6' longest border of the triangular MC II facet
 6'' shortest border of the MC II facet
 6''' intermediate side of MC II facet
 7 facet for contacting the scaphoideum
 8 proximal facet for the magnum
 9 distal facet for the magnum
 x postmortem fracture</p> |
|--|--|



Magnum (fig. 6.11.1)

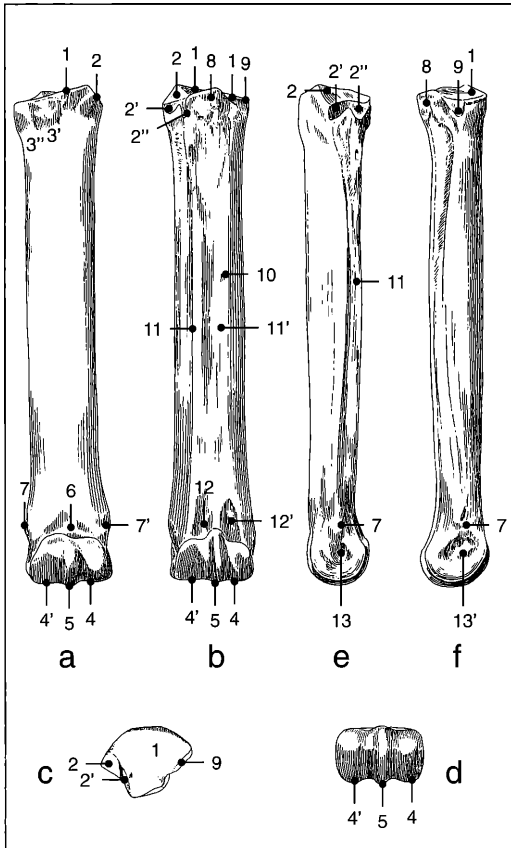
- | | |
|---|---|
| <p>1 cranial facies of magnum
 1' medial tuberosity for attachment of the ligamentum collaterale carpi medialis
 1''+1''' ligamentous attachment site at the distal border of (1)
 1IV attachment site for the ligamentum intercarpea attaching the magnum and the unciforme
 2 caudal articular head for the lunatum
 3 proximal articular surface
 4 distal articular facet
 5 caudal projection of the magnum
 6 attachment of the musculus interosseus
 7' proximal facet for the trapezoidium
 7'' distal facet for the trapezoidium</p> | <p>8 facet for the MC II
 9 facets for the unciforme
 9' proximal facet for the unciforme
 9'' distal facet for the unciforme
 9''' caudal facet for the unciforme
 10 craniocaudal ridge separating facets (11) and (12)
 11 medial facet articulating with the scaphoideum
 12 lateral facet articulating with the lunatum
 13 articular facet for MC III
 14 articular facet for MC II
 15 lateral facets for articulation with the unciforme (15', 15'', 15''')</p> |
|---|---|



Unciforme (fig. 6.12.1)

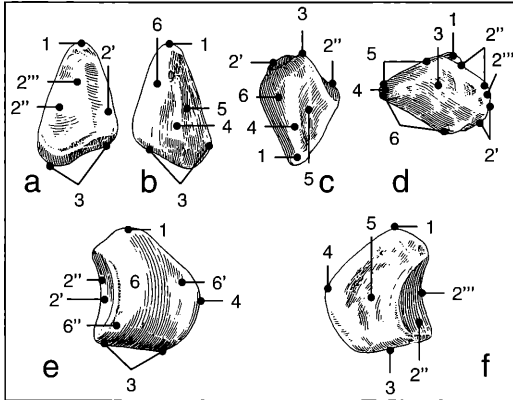
- 1 cranial facies
- 2 oval-shaped scar for articulation of intercarpal ligament
- 3 large facet for articulation of triquetrum (proximal portion)
- 3' lateral descending extension of (3)
- 4 distal facet for MC IV
- 5 medial facet for MC III

- 6 larger facet for the magnum
- 7 lateral MC III facet
- 8 small facet for the magnum
- 9 non-articular internal area of caudal facies
- 10 laterocaudal prominence (often a strong tuberosity)



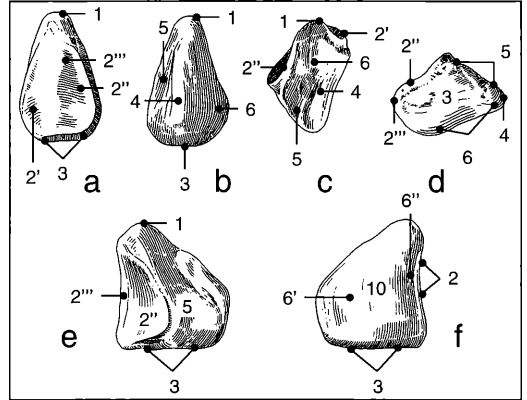
Metacarpale III (fig. 6.13.1)

- 1 articular facet for the magnum
- 2 articular facet for the unciforme
- 2' proximocranial articular facet for MC IV
- 2'' distocranial articular facet for MC IV
- 3, 3' rugose surfaces for insertion of the musculus extensor carpi radialis
- 4 medial trochlea metacarpi
- 4' lateral trochlea metacarpi
- 5 crista sagittalis (separating features 4 and 4')
- 6 supratrochlear fossa
- 7 medial protuberance
- 7' lateral protuberance
- 8 protuberance for the musculus interosseus
- 9 facet for articulation with MC II
- 10 nutrient foramen
- 11+11' longitudinal rugose surfaces for ligamentous attachments to MC II and MC IV
- 12+12' supratrochlear depressions
- 13 depression for the ligamentum sesamoideum collaterale laterale
- 13' depression for the ligamentum sesamoideum collaterale mediale



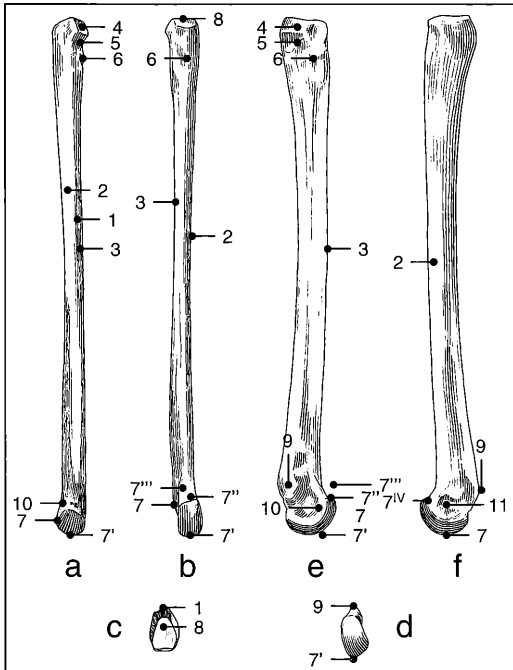
Medial Sesamoidea of the Distal Metacarpale III (fig. 6.14.1.1)

- 1 apex sesamoidei
- 2 joint facet for MC III
- 2' lateral portion of joint facet (2)
- 2'' medial portion of joint facet (2)
- 2''' proximodistal ridge of joint facet (2)
- 3 basis sesamoidei
- 4 medial proximodistally coursing palmar crest
- 5 facies musculi interossei medialis (abaxiale)
- 6 lateral facies of the musculus flexor profundus (adaxiale)
- 6' palmar proximodistally coursing groove
- 6'' long narrow furrow for attachment of joint cartilage



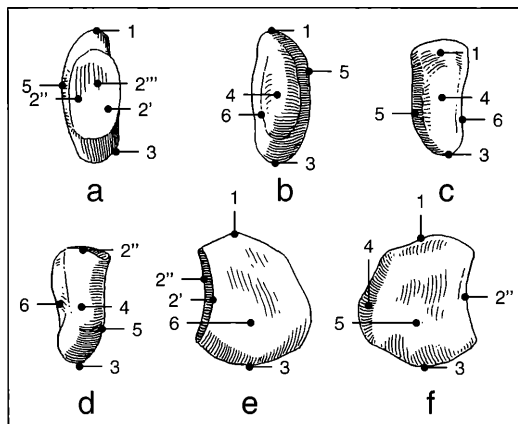
Lateral Sesamoidea of the Distal Metacarpale III (fig. 6.14.1.2)

- 1 apex sesamoidei
- 2 joint facet for MC III
- 2' medial portion of joint facet (2)
- 2'' lateral portion of joint facet (2)
- 2''' proximodistal ridge of joint facet (2)
- 3 basis sesamoidei
- 4 medial proximodistally coursing palmar crest
- 5 facies musculi interossei lateralis
- 6 facies musculi interossei medialis
- 6' palmar proximodistally coursing groove
- 6'' long narrow furrow for attachment of joint cartilage



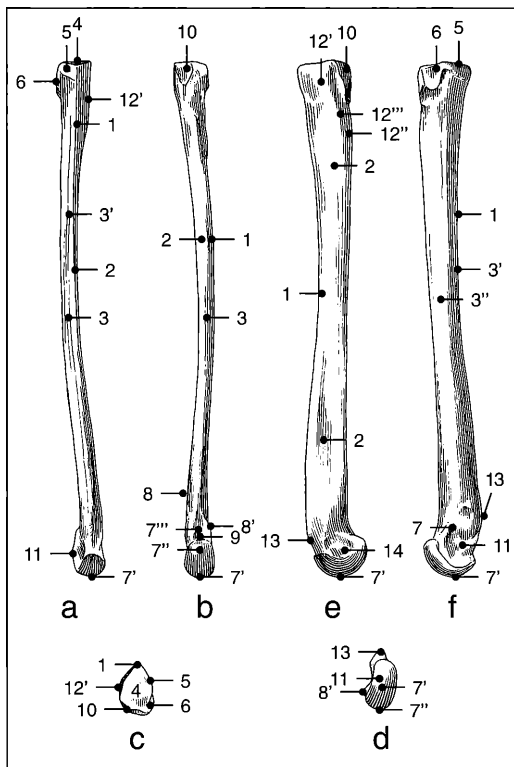
Metacarpale II (fig. 6.15.1)

- 1 cranial longitudinal ridge
- 2 medial wall
- 3 lateral wall
- 4 facet for articulation of magnum
- 5 facet for articulation with MC III
- 6 tuberosity for fibrous contact with MC III
- 7 distal articular region
- 7' articular facet for 1st phalanx II
- 7'' fossa for articulation of the sesamoidea articulationis MC II
- 7''' lateral ridge delimiting 7''
- 7'''' medial ridge delimiting 7''
- 8 proximal facet for the trapezoideum
- 9 processus suparticularis
- 10 depression for the ligamentum collaterale laterale
- 11 depression for the ligamentum collaterale mediale



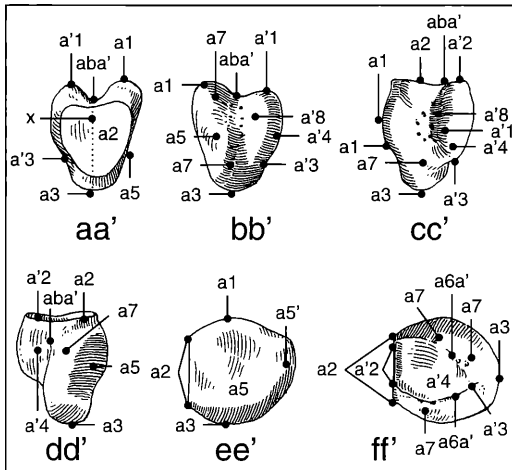
Sesamoidea of the Distal Metacarpale II, Abaxial Element (fig. 6.16.1)

- 1 apex sesamoidei
- 2' small adaxial (lateral) facet for contact with the MC II rudimentary crista (not seen in figure)
- 2'' large abaxial (medial) facet for contact with the trochlea of MC II
- 2''' proximodistal ridge of the 2'-2'' facet
- 3 basis sesamoidei
- 4 medial crest of the palmar side
- 5 facies musculi interossei medialis
- 6 facies flexoria of the medial sesamoid



Metacarpale IV (fig. 6.17.1)

- 1 cranial longitudinal ridge
- 2 lateral border
- 3 medial border
- 3' sharply delimited ridge for interosseous attachment with MC III (feature 11) - roughened surface;
- 3'' smooth surface of 3'
- 4 articular facet for unciforme
- 5 proximocranial articular facet for MC III
- 6 proximomedial articular facet for MC III
- 7 distal articular region
- 7' articular facet for 1st phalanx IV
- 7'' vestige of crista sagittalis
- 7''' small distal fovea proximal to border of 7'
- 8 lateral crest, outlining 7'''
- 8' medial crest outlining 7'''
- 9 central minute ridge in 7'''
- 10 articular facet for MC V
- 11 medial ligamentous depression
- 12' bulbous tuberosity for ligamentous attachment
- 12'' elongated area for ligamentous attachment
- 12''' crista separating 12' and 12''
- 13 processus supraarticularis
- 14 circular lateral depression for ligamentum collaterale



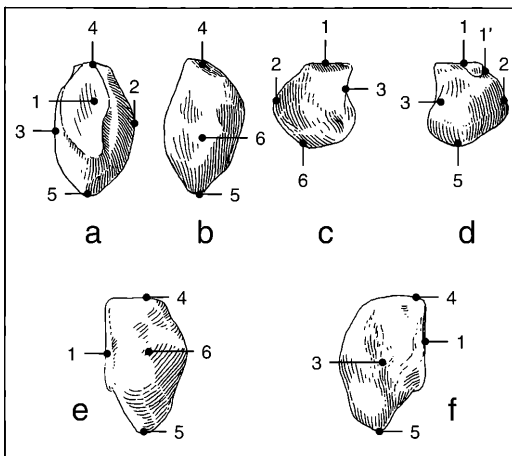
Sesamoidea of the Distal Metacarpale IV
(fig. 6.18.1 large (= abaxial) sesamoidea a-f;
small (= adaxial) sesamoidea a'-f')

Abaxial (large) sesamoid:

- a1 apex sesamoidea
- a2 joint facet for MC IV
- a3 basis sesamoidea
- a5 abaxial facies for the interosseus tendon
- a6 coossification suture of both sesamoidea
- a7 abaxial facies for the musculus flexorius
- x coossification suture
- aba' juncture of the abaxial and adaxial pair
- a2 wear facet

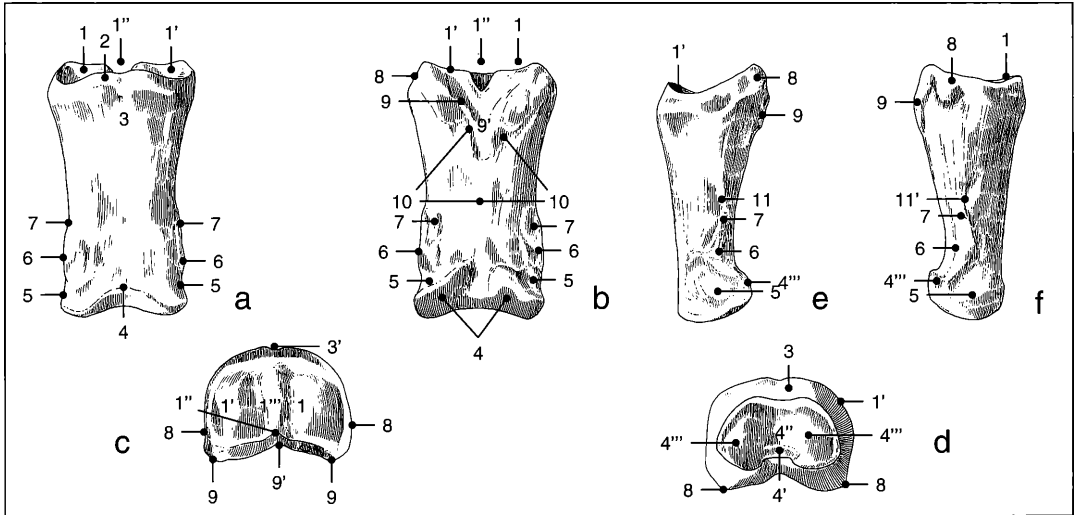
Adaxial (small) sesamoid:

- a'1 apex sesamoidea
- a'2 facet for MC IV
- a'3 basis sesamoidea
- a'4 adaxial facies for the interosseus tendon
- a'5 bony protuberance of the a'5's distal border
- a'6 coossification suture of both sesamoidea
- a'8 adaxial facies for the musculus flexorius



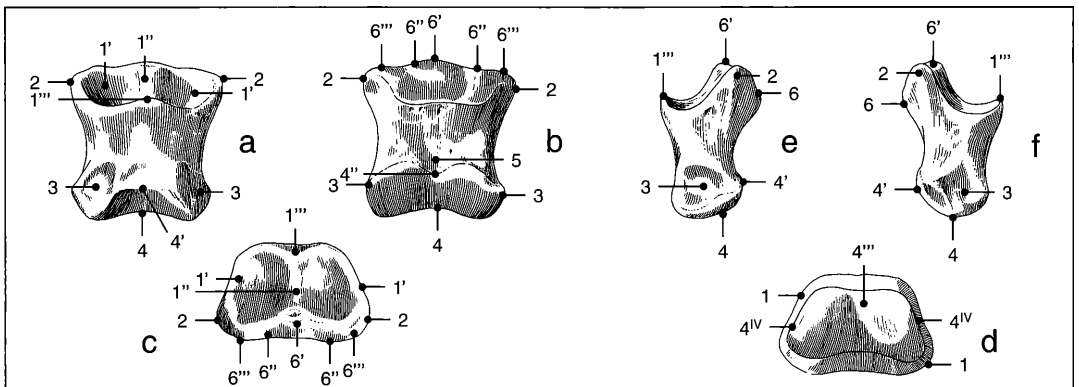
Metacarpale V (fig. 6.20.1)

- 1 facet for the MC IV
- 1' distal end of facet (1)
- 2 lateral wall
- 3 medial wall
- 4 caput
- 5 distal limit
- 6 caudal surface



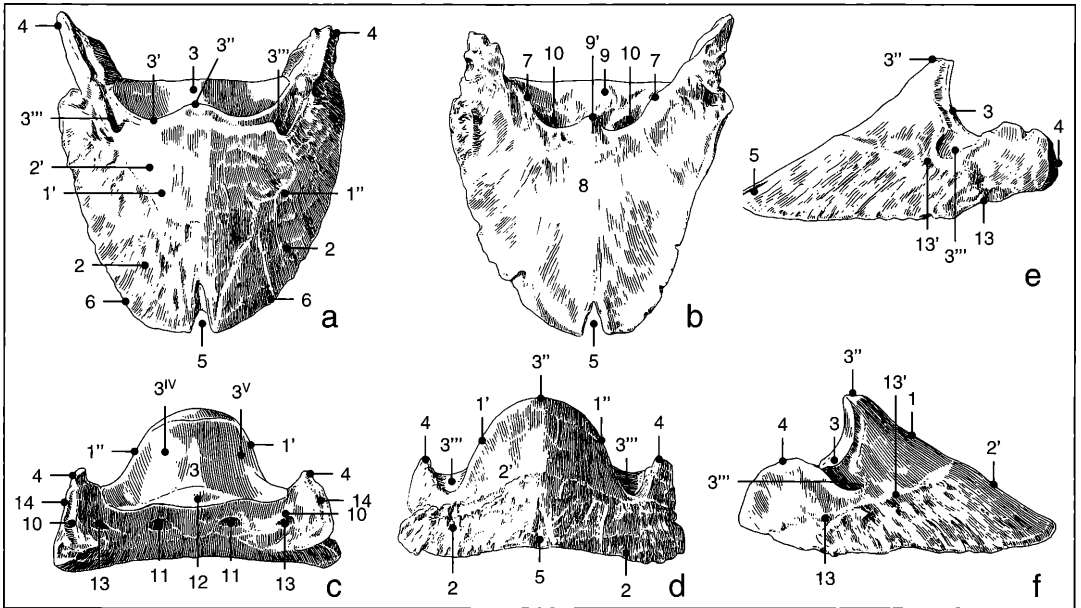
Anterior 1st Phalanx III (fig. 6.21.1)

- | | |
|---|---|
| <p>1 articular facet, and its medial portion
 1' lateral portion of (1)
 1'' palmar V-shaped groove for the crista sagittalis
 1''' dorsopalmar groove for the crista sagittalis of MC III
 2 narrow furrow for attachment of the (1) articular cartilage
 3 proximodorsal bony swelling with vertically oriented furrows; 3', a large furrow
 4 distal joint facet
 4' rugose surface on the palmar incision of the distal facet
 4'' dorsopalmar groove on (4)
 4''' medial and lateral elevations of (4)</p> | <p>5 attachment of medial and lateral collateral ligaments
 6 attachment of the flexor digitalis superficialis („perforatus scar“)
 7 attachment for ligamentum laterale volare
 8 attachment for ligamentum collaterale of the fetlock joint
 9 attachment for ligamentum sesamoideum obliquum („V-shaped scar“)
 9' triangular groove in the „V-scar“
 10 attachment of ligamentum sesamoideum centrale
 11 furrow on the lateral surface
 11' furrow on the medial surface</p> |
|---|---|



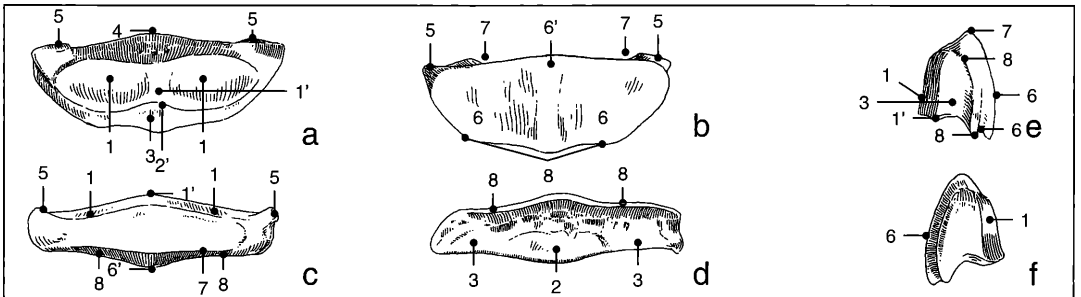
Anterior 2nd Phalanx Digit III (fig. 6.22.1)

- | | |
|--|--|
| <p>1 proximal articular facet
 1' medial and lateral portions of (1)
 1'' midsagittal ridge of (1)
 1''' dorsal border of (1)
 2 medial and lateral scar for the ligamentum collaterale of phalanx 1/ phalanx 2 digit III articulation
 3 medial and lateral scar of the ligamentum collaterale for phalanx 2/ phalanx 3 digit III articulation
 4 distal articular facet
 4' proximal border of (4)</p> | <p>4'' distally directed depression of (4)
 4''' volopalmar oriented depression of the saddle structure
 4'''' medial and lateral elevations of the saddle structure
 5 rugose surface for insertion of the flexor digitorum profundus
 6 flexor tuberosity
 6' area for ligamentum sesamoideum rectum of (6)
 6'' medial and lateral area for the tendo flexor digitorum profundus
 6''' medial and lateral area for the ligamentum laterale volare</p> |
|--|--|



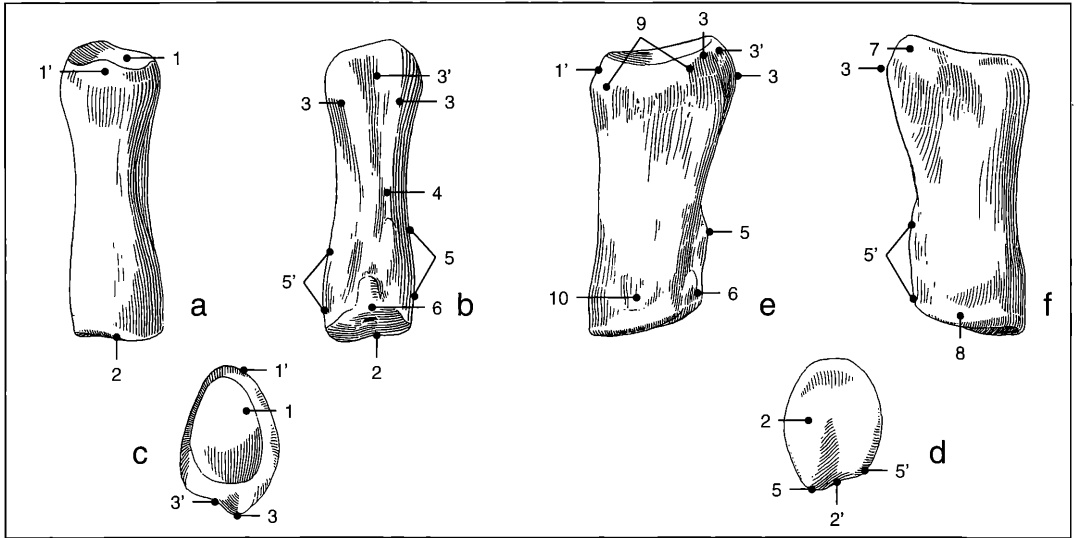
Anterior 3rd Phalanx III (fig. 6.23.1a-f)

- | | |
|--|---|
| <p>1 dorsal portion of the parietal surface
 1' medial portion of the parietal surface
 1'' lateral portion of the parietal surface
 2 distal roughened and wrinkled parietal surface
 2' smooth proximal portion of the parietal surface
 3 articular surface of the phalanx
 3' coronary border of the articular surface
 3'' extensor process for the insertion of the extensor digitalis communis
 3''' medial and lateral groove for ligamentous attachment of the ligamentum collaterale
 3^{iv} lateral fossa of proximal articular surface
 3^v medial fossa of proximal articular surface
 4 processus palmaris lateralis and medialis
 5 crena marginis solearis</p> | <p>6 margo solearis
 7 linea semilunaris
 8 planum cutaneum of the sole surface
 9 facies flexoria of the sole surface
 9' protuberant attachment area of the flexor digitalis profundus tendon („tendo perforans“)
 10 sulcus solearis medialis et lateralis
 11 foramen soleare mediale et laterale
 12 articular facet for the distal sesamoid bone
 13 foramina processus palmaris mediale et laterale
 13' sulcus parietalis medialis and lateralis
 14 medial and lateral furrows for the attachment of the ligaments of the hoof cartilage (ligamenta chondrungiaria collateralis medialis et lateralis)</p> |
|--|---|



Distal Sesamoidea of Anterior Phalanx III (fig. 6.24.1)

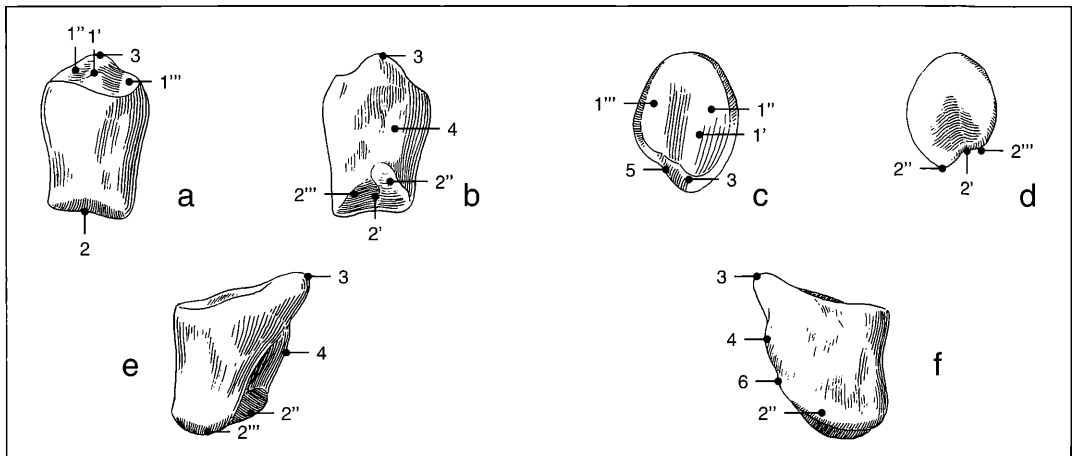
- | | |
|--|---|
| <p>1 facies articularis for the 2nd phalanx
 1' central elevation of (1)
 2 palmar articular facet for the 3rd phalanx
 2' border with (1)
 3 bony surface with indistinct pits
 4 proximal side of the bone</p> | <p>5 attachment for ligamenta sesamoidea collateralia medialis et lateralis
 6 facies flexoria
 6' central elevation of (6)
 7 margo proximalis
 8 margo distalis</p> |
|--|---|



Anterior 1st Phalanx II (fig. 6.25.1)

- 1 proximal joint facet to the MC II
- 1' prominence at the dorsal border of (1)
- 2 distal articular surface for the 2nd phalanx II
- 2' sulcus distalis on the distal facet (2)
- 3 trigonum phalangis proximalis for attachment of the ligamentum sesamoideum obliquum
- 3' shallow sulcus intermediate to feature 3
- 4 scar demarcating the attachment site for the ligamentum sesamoideum centrale
- 5 abaxial insertion of the tendo flexor digitalis superficialis

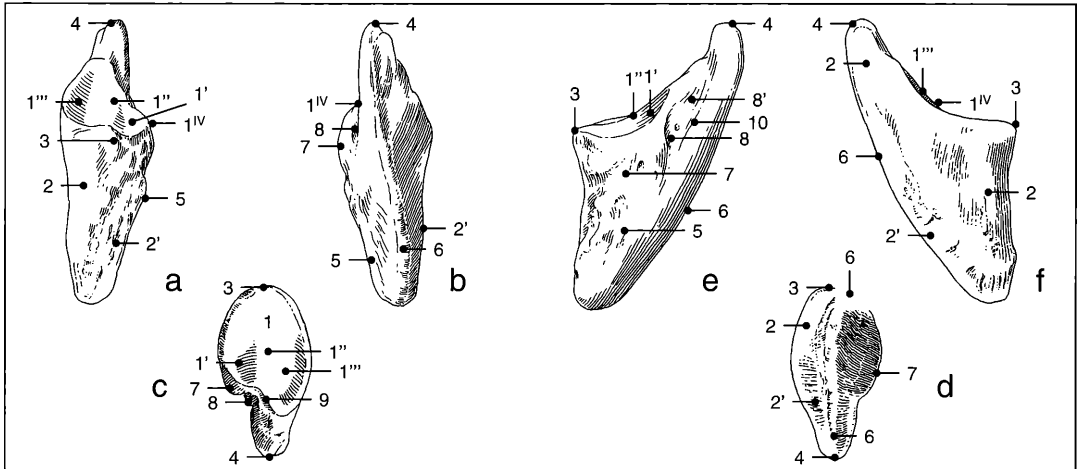
- 5' adaxial insertion of the tendo flexor digitalis superficialis
- 6 tiny tuberosity
- 7 scar of the ligamentum collaterale laterale (abaxiale) with the MC II
- 8 scar for attachment of the ligamentum collaterale laterale (abaxiale) with the 2nd phalanx
- 9 rugose surface for the ligamentum collaterale mediale (adaxiale)
- 10 rugose surface for attachment of the ligamentum collaterale mediale (adaxiale) with the phalanx 2



Anterior 2nd Phalanx II (fig. 6.26.1)

- 1 proximal surface for articulation with 1st phalanx digit II
- 1' midsagittal longitudinal ridge of (1)
- 1'' medial portion of (1)
- 1''' lateral portion of (1)
- 2 distal joint facet for articulation with 3rd phalanx digit II
- 2' sulcus distalis of (2)

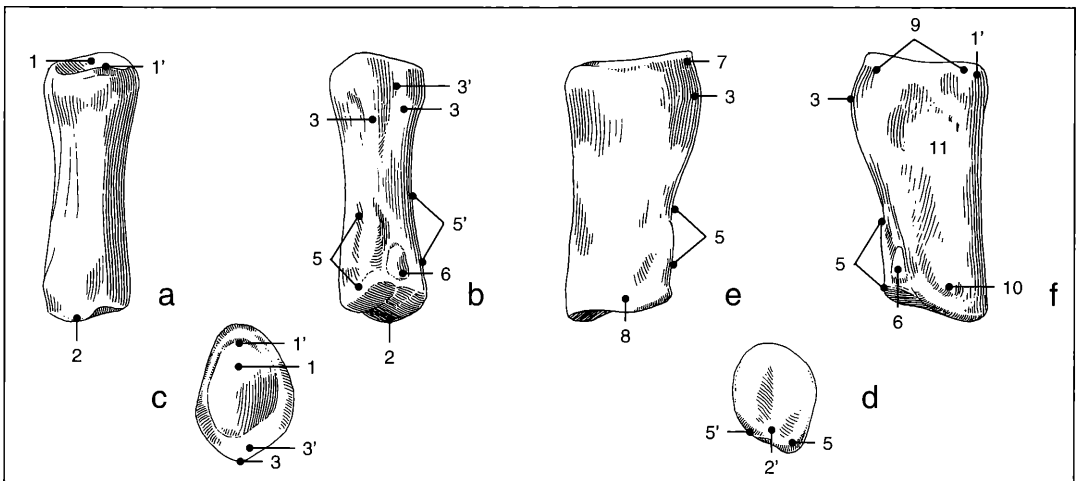
- 2'' medial portion of (2)
- 2''' lateral portion of (2)
- 3 process for insertion of the flexor digitalis sublimis
- 4 rugose tuberosity for ligamentous attachments
- 5 lateropalmar reflection of proximal peripheral border
- 6 mediopalmar border



Anterior 3rd Phalanx II (fig. 6.27.1)

- 1 proximal joint facet for articulation with the 2nd phalanx
- 1' lateral portion of (1)
- 1'' longitudinal ridge of (1)
- 1''' medial portion of (1)
- 1^{IV} lateral (= abaxial) coronary border of (1)
- 2 smooth dorsal portion of the parietal surface
- 2' dorsal perforated rugose portion of the parietal surface
- 3 tuberosity for attachment of the extensor digitalis communis

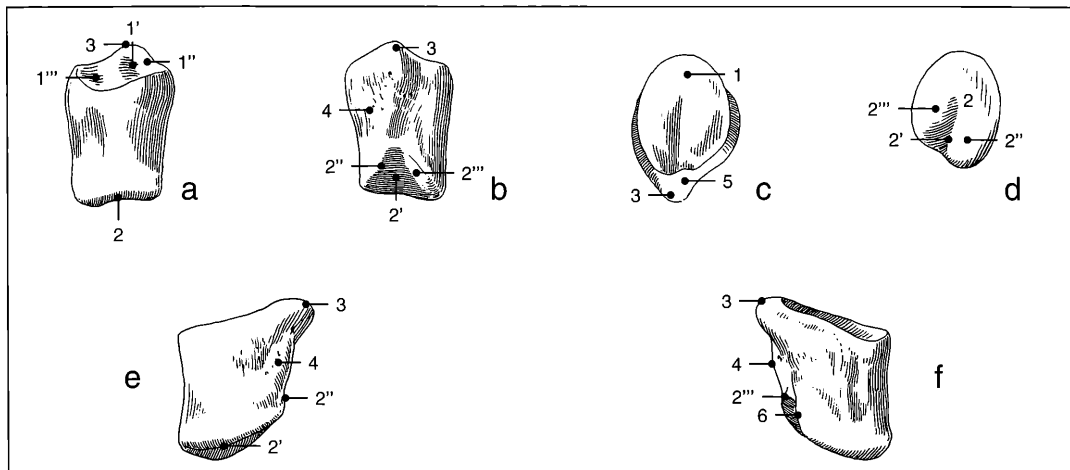
- 4 processus palmaris lateralis
- 5 adaxial border of the phalanx
- 6 margo solearis
- 7 facies flexoria for attachment of the flexor digitalis profundus tendon
- 8 foramen soleare laterale
- 8' sulcus solearis lateralis
- 9 lateropalmar incisure of (1)
- 10 linea semilunaris



Anterior 1st Phalanx IV (fig. 6.28.1)

- 1 proximal joint facet with the MC IV
- 1' prominence at the dorsal border of (1)
- 2 distal joint facet for articulation with the 2nd phalanx IV
- 2' sulcus distalis on the distal facet (2)
- 3 weak trigonum phalangis proximalis
- 3' deepening of the trigonum
- 4 scar for attachment of the ligamentum sesamoideum centrale
- 5 abaxial insertion for flexor digitalis superficialis
- 5' adaxial insertion of (5)

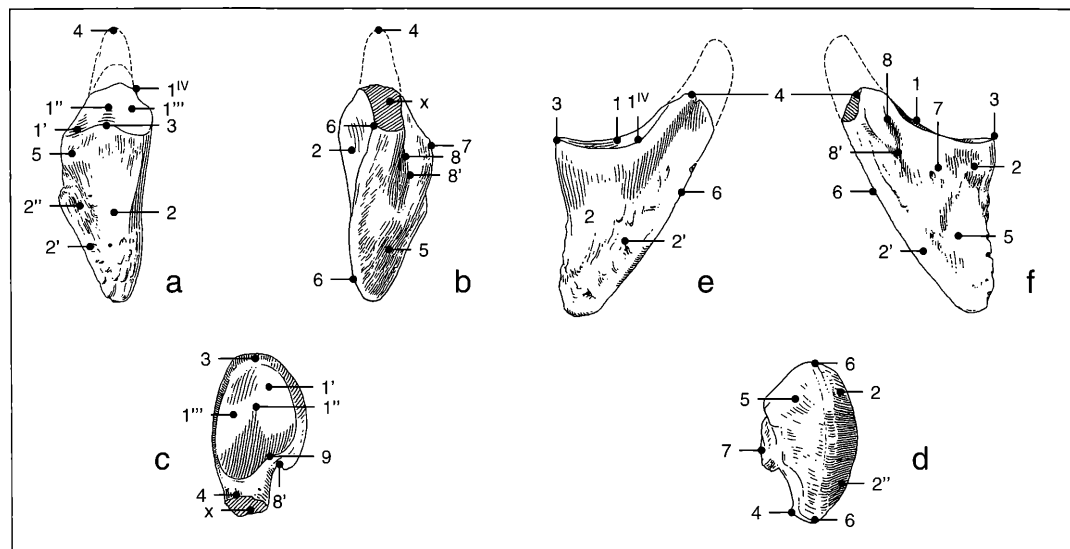
- 6 miniscule bony tuberosity
- 7 scar for the attachment of the ligamentum collaterale laterale (abaxiale) with the MC II
- 8 scar for attachment of the ligamentum collaterale laterale (abaxiale) connecting this element with the 2nd phalanx
- 9 surface for attachment of the ligamentum collaterale mediale (adaxiale) attaching the 1st phalanx with MC IV
- 10 rugose surface for the ligamentum collaterale mediale (adaxiale) with the 2nd phalanx
- 11 flat depression palmo-distalward of the proximal border (9)



Anterior 2nd Phalanx IV (fig. 6.29.1)

- 1 proximal joint facet
- 1' median longitudinal ridge of (1)
- 1'' lateral portion of (1)
- 1''' medial portion of (1)
- 2 distal joint facet
- 2' sulcus distalis of (2)

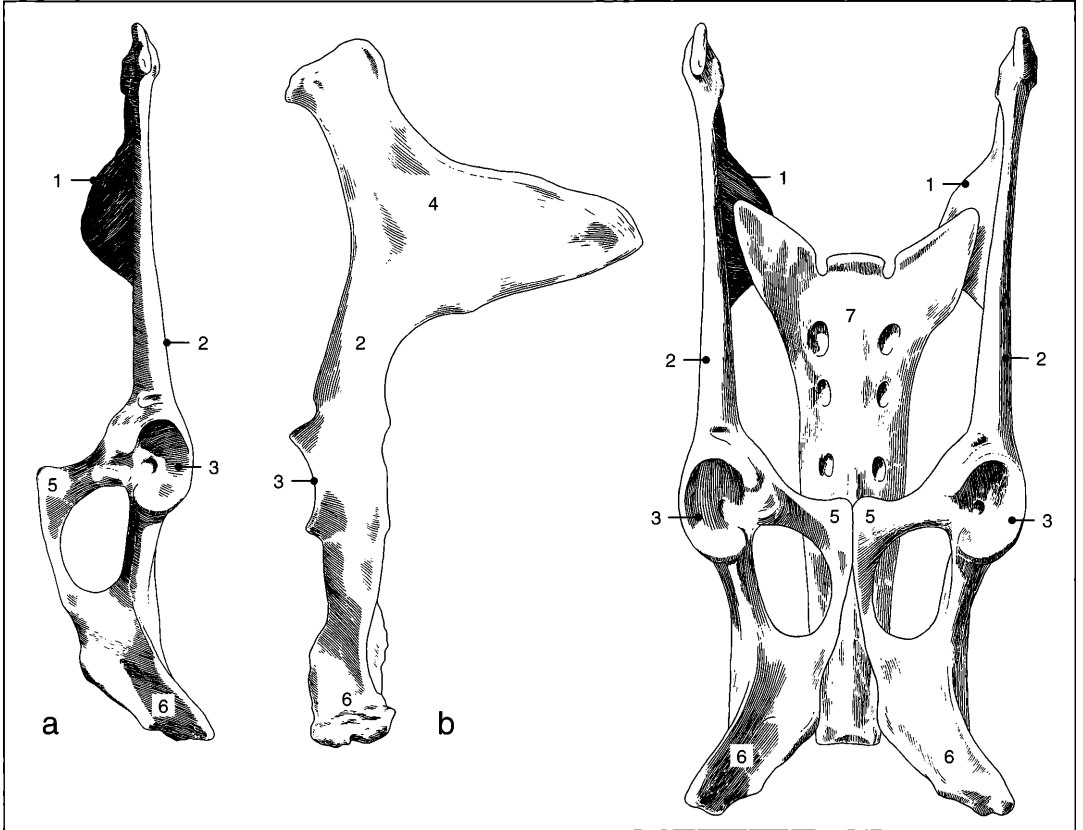
- 2'' lateral portion of (2)
- 2''' medial portion of (2)
- 3 process for insertion of the flexor digitalis sublimis
- 4 rugose surface for attachment of ligaments
- 5 mediopalmar incision of (1)
- 6 mediopalmar edge of the phalanx



Anterior 3rd Phalanx IV (fig. 6.30.1)

- 1 proximal joint facet for distal phalanx 2 digit IV
- 1' medial portion of (1)
- 1'' longitudinal ridge of (1)
- 1''' lateral portion of (1)
- 1^{IV} lateral coronary border of (1)
- 2 smooth portion of the parietal surface
- 2' wrinkled portion of the parietal surface
- 2'' sulcus parietalis
- 3 processus for attachment of the extensor digitalis communis

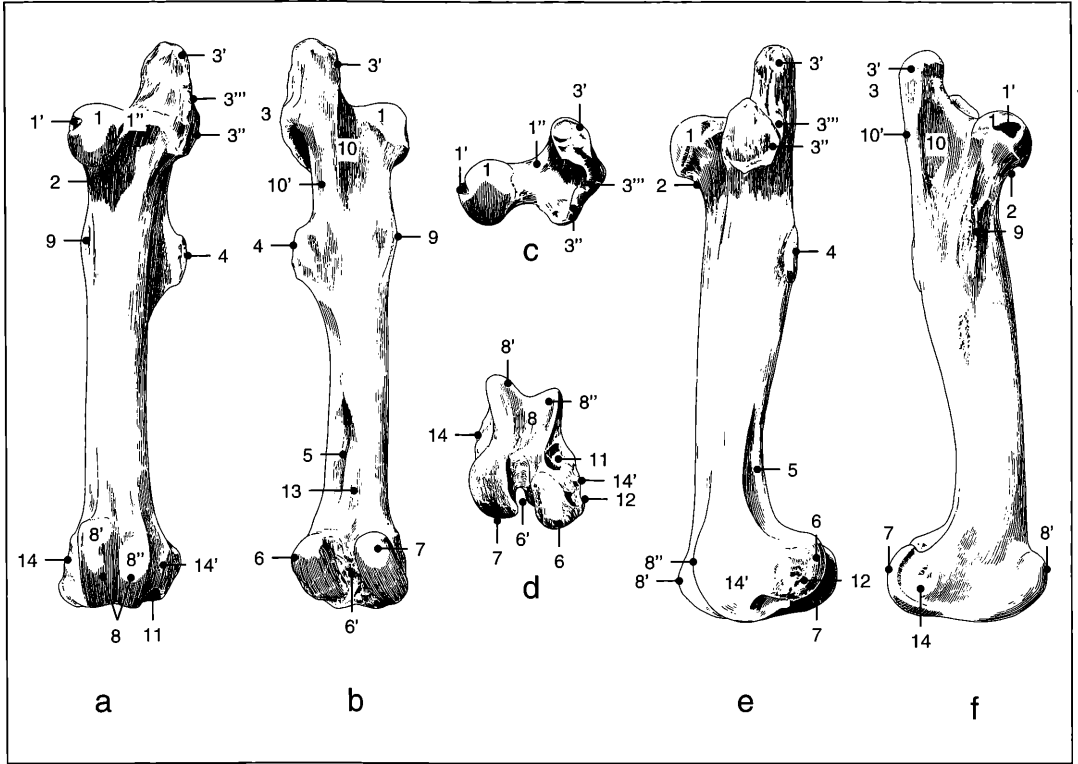
- 4 processus palmaris lateralis
- 5 medial border
- 6 margo solearis
- 7 facies flexoria for attachment of the flexor digitalis profundus
- 8 foramen solearis
- 8' sulcus solearis
- 9 mediopalmar incision of (1)
- x broken area



Pelvic girdle (fig. 7.1.1.1 and fig. 7.1.1.2)

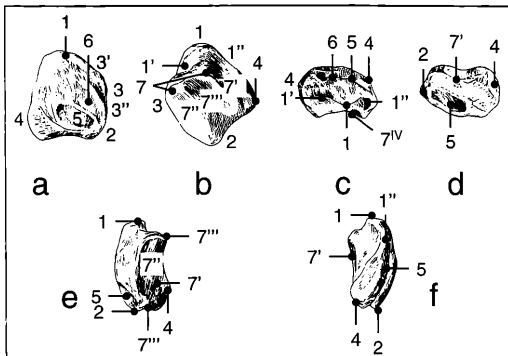
- 1 Iliac blade
- 2 Iliac shaft
- 3 Obturator foramen
- 4 Iliac fossa

- 5 Pubis
- 6 Ischium
- 7 Sacrum



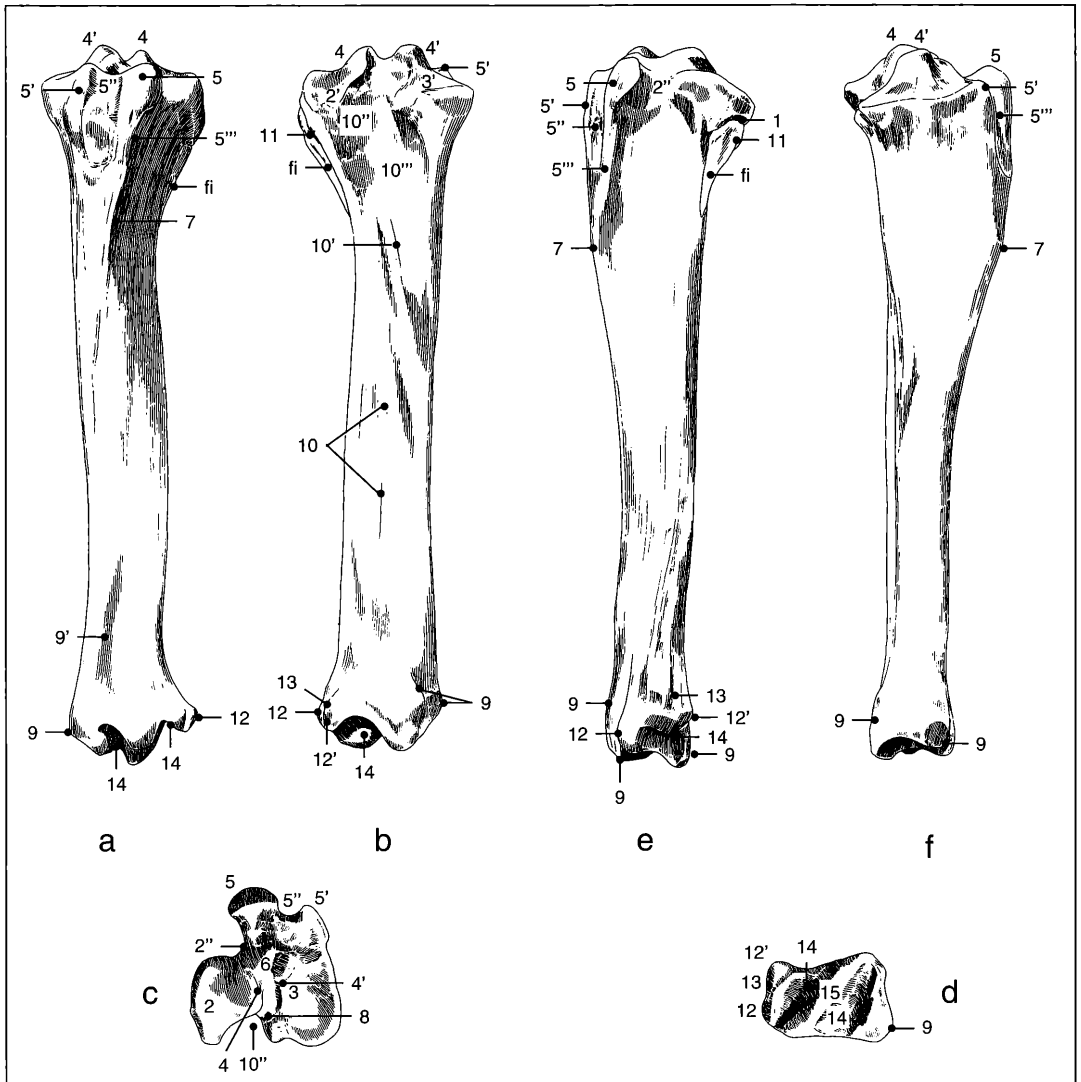
Femur (fig. 7.2.1.2)

- | | | | |
|------|----------------------------------|-----|--|
| 1 | caput femoris | 7 | condylus medialis |
| 1' | fovea capitis | 8 | trochlea ossis femoris |
| 1'' | femoral neck | 8' | condylus medialis trochlea osseus femoris |
| 2 | collum femoris | 8'' | condylus lateralis trochlea osseus femoris |
| 3 | trochanter major | 9 | trochanter minor |
| 3' | trochanter major, pars cranialis | 10 | trochanteric fossa |
| 3'' | trochanter major, pars caudalis | 10' | intertrochanteric crest |
| 3''' | trochanteric notch | 11 | fossa extensoria |
| 4 | trochanter tertius | 12 | fossa musculus poplitei |
| 5 | fossa condylaris | 13 | furrow for attachment of the musculus poplitei |
| 6 | condylus lateralis | 14 | epicondylus medialis |
| 6' | fossa intercondylaris medialis | 14' | epicondylus lateralis |



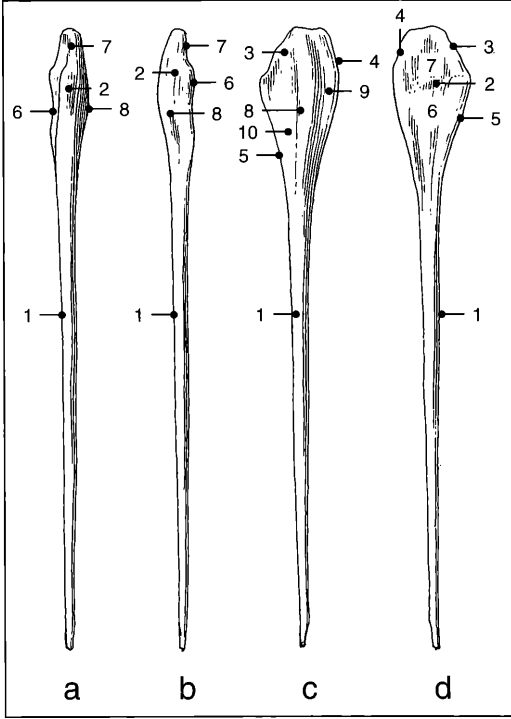
Patella (fig. 7.3.1)

- | | |
|-------|---|
| 1 | basis patellae |
| 1' | lateral ridge of (1) |
| 1'' | medial ridge of (1) |
| 2 | apex patellae |
| 3 | lateral border |
| 3' | proximolateral portion of (3) |
| 3'' | distolateral portion of (3'') |
| 4 | processus fibrocartilagineus medialis |
| 5 | attachment site for the ligamentum patellae intermedium |
| 6 | attachment site for the ligamentum patellae laterale |
| 7 | articular facet for the trochlea femoris |
| 7' | medial portion of (7) |
| 7'' | lateral portion of (7) |
| 7''' | rounded ridge separating (7') and (7'') |
| 7'''' | proximal border of (7) |



Tibia (fig. 7.4.1.2)

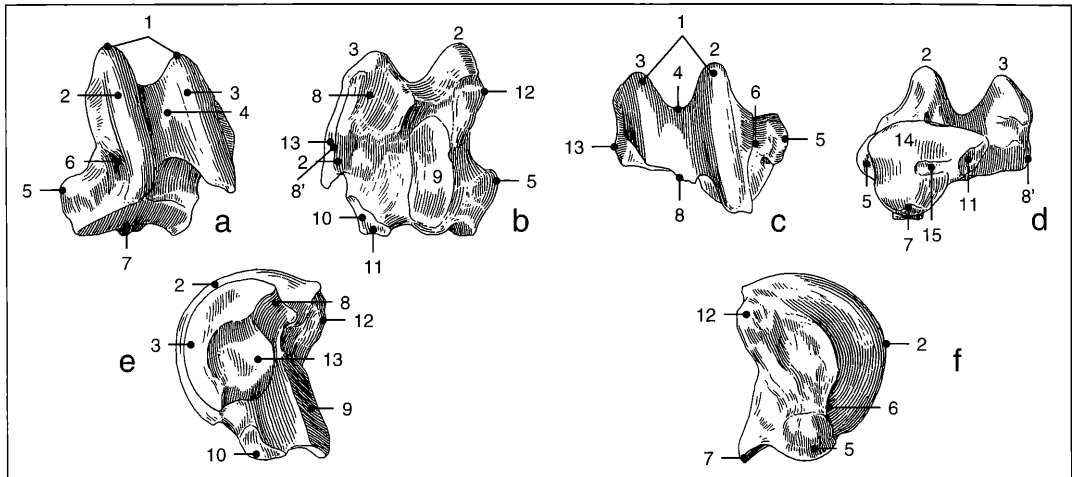
- | | | | |
|------|---|-------|---|
| 1 | facies articularis fibulae | 8 | sulcus intercondyloideus: area caudalis |
| 2 | condylus laterale | 9 | malleolus mediale |
| 2' | caudal facies of (2) | 9' | rugose feature of (9) |
| 2'' | sulcus extensoris of (2) | 10 | lineae musculares |
| 3 | condylus mediale | 10' | linea musculus poplitei |
| 3' | facies articularis of (3) | 10'' | fossa for the origin of the musculus gastrocnemius |
| 4 | tuberculum intercondylare laterale of eminentia intercondylaris | 10''' | incisura poplitea |
| 4' | tuberculum intercondylare mediale of eminentia intercondylaris | 11 | caput fibulae |
| 5 | tuberositas tibiae, lateral crest | 12 | cranial aspect of the malleolus lateralis |
| 5' | tuberositas tibiae, medial crest | 12' | caudal aspect of the malleolus lateralis (distalmost vestige of the fibula) |
| 5'' | sulcus tuberositas tibiae | 13 | sulcus malleolaris |
| 5''' | margo cranialis | 14-14 | articular grooves for the astragalus |
| 6 | sulcus intercondyloideus: area centralis | 15 | articular ridge between 14-14 |
| 7 | insertion of the musculus semitendinosus | fi | vestige fibula |



Fibula (fig. 7.5.1)

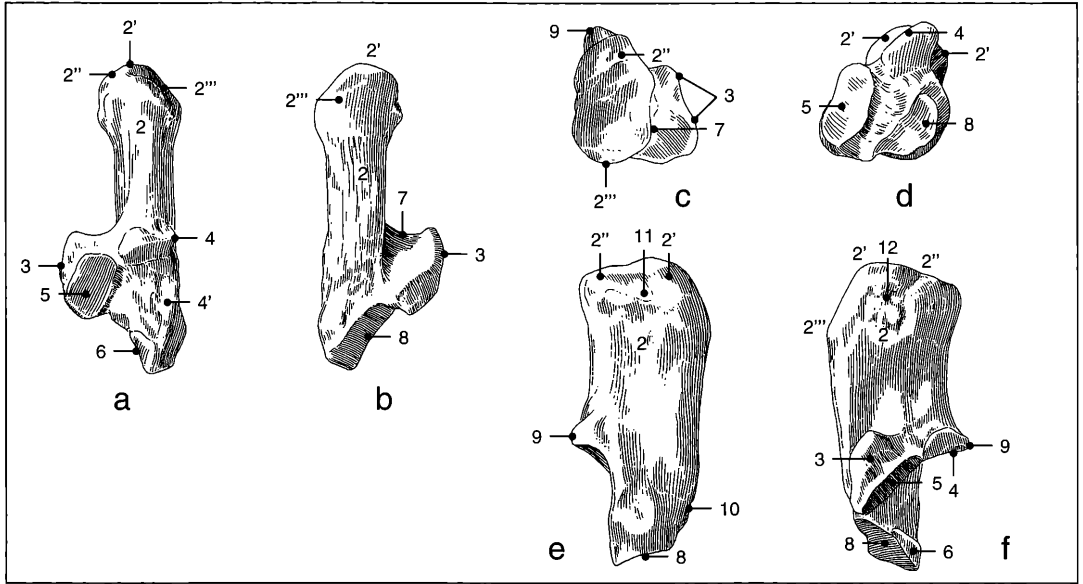
1+2 fibula

- 1 corpus fibulae
- 2 caput fibulae
- 3 caudal margin capitis fibulae
- 4 cranial margin capitis fibulae
- 5 distal portion of (3)
- 6 facies medialis capitis fibulae
- 7 rugose surface of (6) for contact with the tibial facies articularis)
- 8 proximodistal ridge on the caput's lateral facies
- 9 broad furrow cranial to (8)
- 10 deep fossa caudal to (8)



Astragalus (fig. 7.6.1)

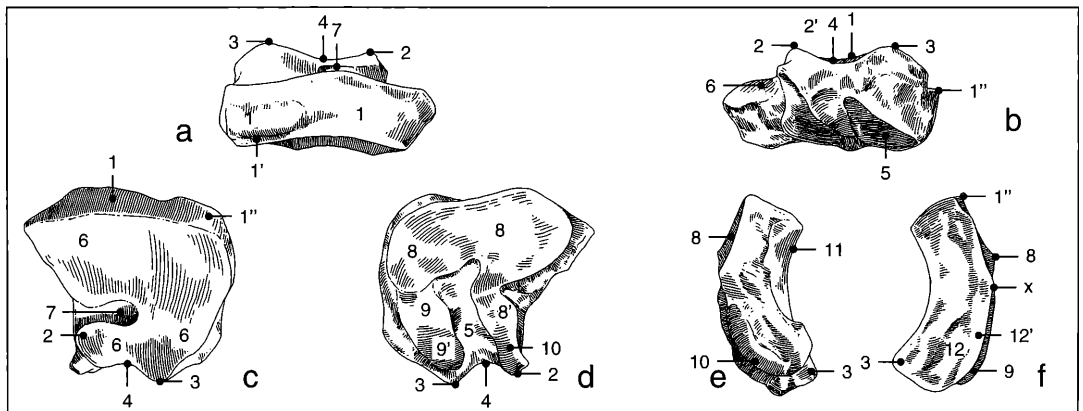
- 1 trochlea astragalus
- 2 medial ridge of trochlea
- 3 lateral ridge of trochlea
- 4 trochlear groove
- 5 tuberculum mediale tali; attachment site for ligamentum collatorale medium curtum
- 6 ovoid cavity between (2) and (5)
- 7 pointed aspect of the facet for the naviculare
- 8 facet for the calcaneum
- 8' tongue-like distal extension of (8)
- 9 facet for the sustaculum tali of the calcaneum
- 10 facet for the distal wall of the calcaneum
- 11 facet for the cuneiforme 3
- 12 protuberance for the ligamentum colli medialis brevis
- 13 attachment site for the ligamentum talocalcaneum laterale
- 14 facet for the naviculare
- 15 fossa synovialis of the navicular facet



Calcaneus (fig. 7.7.1)

- 2 calcaneus, proximal portion
- 2' tuber calcanei
- 2'' attachment site for tendo musculus gastrocnemii
- 2''' attachment site for ligamentum plantare longum
- 3 sustentaculum tali
- 4 articulation facet for (8) of the astragalus
- 4' lateral lanceolate extension for (8') of the astragalus
- 5 ovoid facet for (9) of the astragalus

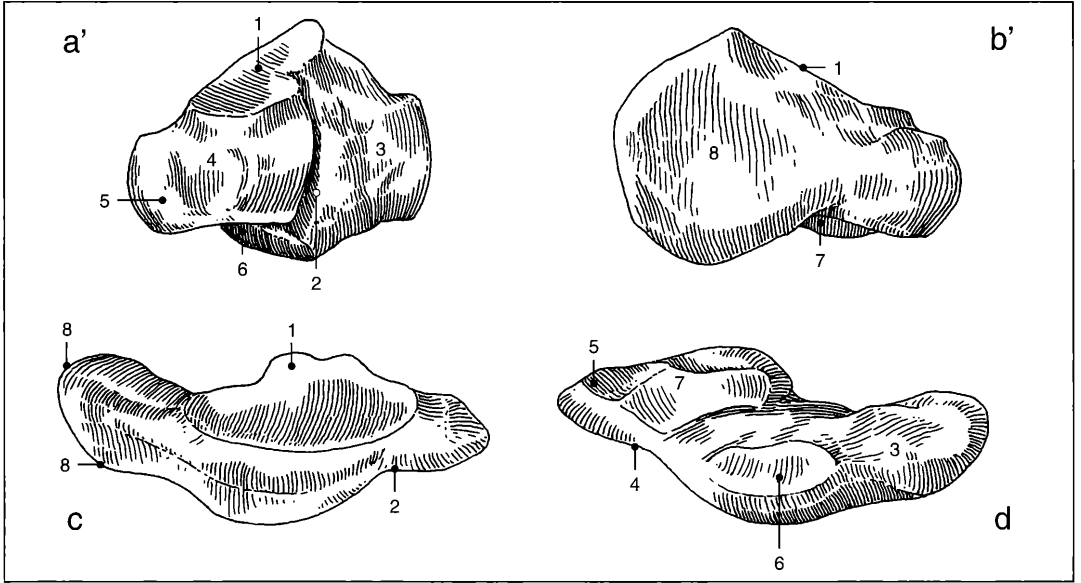
- 6 half-oval facet for articulation with facet (11) of the astragalus
- 7 sulcus tendinosus musculus flexor hallucis longus
- 8 facet for the naviculare
- 9 processus coracoideus
- 10 rugose surface for ligamentous attachment
- 11 rugose surface for muscular attachment
- 12 rugose surface for tendonous attachment



Naviculare (fig. 7.8.1)

- 1 tuberosity for ligamentous attachment
- 1' distal sharp rim of (1)
- 1'' craniomedial border of the naviculare
- 2 processus lateralis naviculare
- 2' small articular facet
- 3 processus medialis naviculare
- 4 sulcus caudalis naviculare
- 5 fossa synovialis distale
- 6 proximal facet for articulation with the astragalus

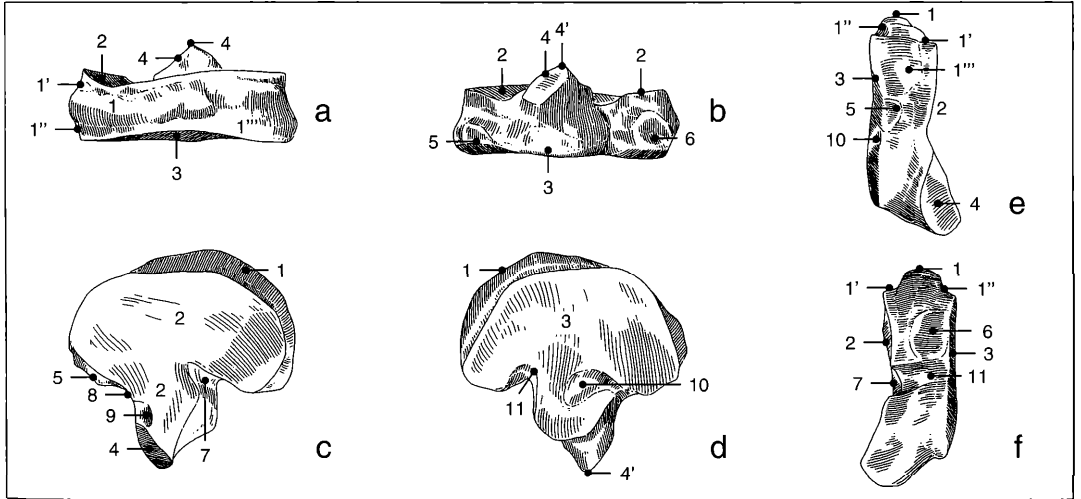
- 7 fossa synovialis proximale
- 8 cranial portion of the distal articular facet
- 8' latero-caudal-lanceolate process of (8)
- 9+9' medio-caudal facets for the cuneiforme 1+2
- 10 caudal facet for the cuboideum
- 11 cranial facet for the cuboideum
- 12 medial tuberosity for ligamentous attachment
- 12' elongated rim distal to (12)
- x feature between 8 and 9



Cuneiforme 1+2 (fig. 7.9.1)

- 1 facet for the naviculare
- 2 furrow demarcating the fusion of cuneiforme 1+2
- 3 cuneiforme 1
- 4 cuneiforme 2
- 5 facet for the caudal border of cuneiforme 3

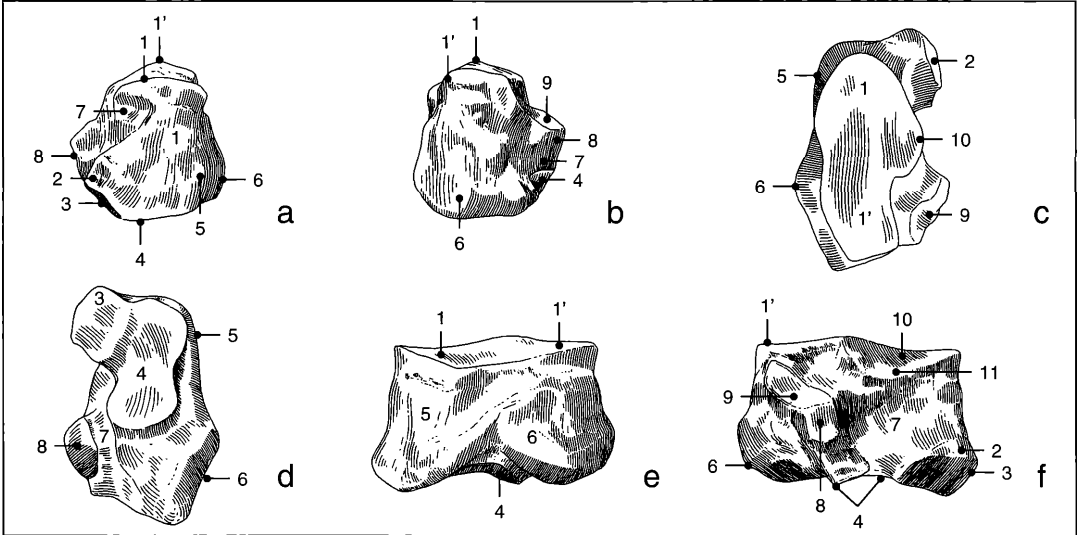
- 6 facet for the metatarsale II
- 7 facet for the metatarsale III
- 8 large scar for attachment of a portion of the ligamentum tarsi dorsale



Cuneiforme 3 (fig. 7.10.1)

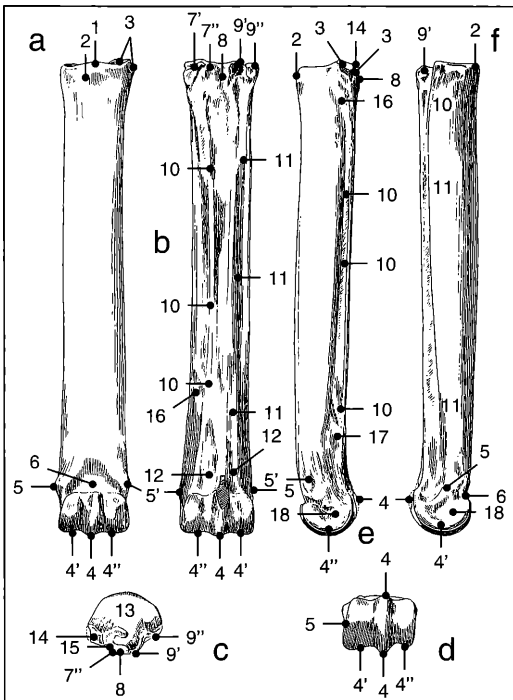
- 1 mediolaterally expansive tuberosity for attachment of the ligamentum tarsi dorsale obliquum
- 1' proximal rim of (1)
- 1'' distal rim of (1)
- 1''' smooth lateral portion of (1)
- 2 proximal articular facet for the naviculare
- 3 distal articular facet for MT III
- 4 posterior facet for the cuboideum

- 4' apex of 4
- 5 anterior facet for the cuboideum
- 6 anterior facet for the cuneiforme 1+2
- 7 incision of medial fossa synovialis on the proximal facet
- 8 incision for lateral fossa synovialis on the proximal facet
- 9 small rugose fossa for ligamentous attachment
- 10 incision for distolateral fossa synovialis
- 11 medial incision



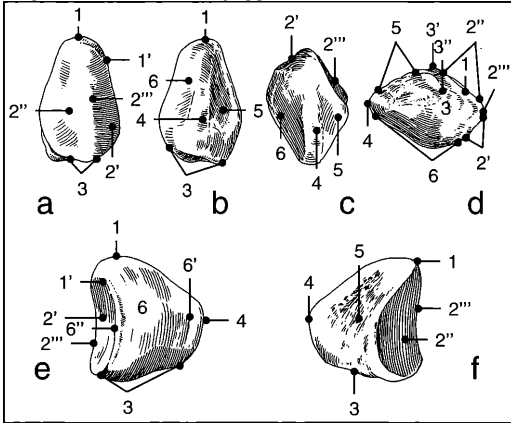
Cuboideum (fig. 7.11.1)

- 1 cranial border of the calcaneal facet
- 1' caudal border of the calcaneal facet
- 2 anterior facet for cuneiforme 3
- 3 facet for MT III
- 4 facet for MT IV
- 5 smaller cranial tuberosity for the attachment of the ligamentum collaterale tarsi longum laterale
- 6 larger caudal tuberosity for attachment of the ligamentum collaterale tarsi longum plantare
- 7 furrow for passage of vascular structures
- 8 posterior facet for the cuneiforme 3
- 9 posterior facet for the naviculare
- 10 facet for the astragalus
- 11 anterior facet for the naviculare



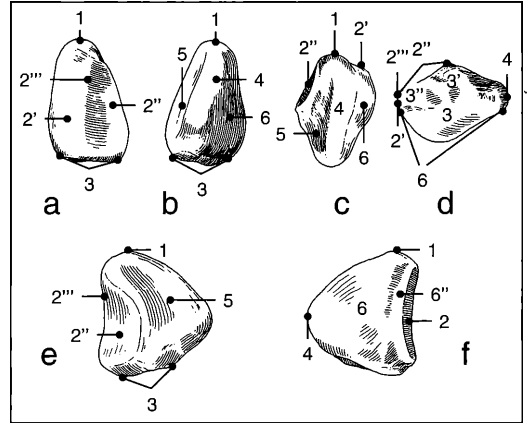
Metatarsale III (fig. 7.12.1)

- 1 border of the proximal facet
- 2 tuberositas metatarsi
- 3 proximal and distal facets for the cuboid facet (re: #14 above)
- 4 crista sagittalis
- 4' medial trochlea metatarsi
- 4'' lateral trochlea metatarsi
- 5 medial protuberance
- 5' lateral protuberance
- 6 depression of the fossa supratrochlearis
- 7 facets for articulation with MT IV
- 7' large lateral joint facet for MT IV
- 7'' small lateral facet for MT IV
- 8 caudal rugose surface for ligamentous attachment
- 9 facets for articulation with MT II
- 9' lateral facet for MT II
- 9'' medial facet for MT II
- 10 long rugose linea for attachment of the interosseus ligament [membranous] connecting MT IV to the MT III
- 11 long rugose linea for attachment of the interosseus membrane connecting MT II to the MT III
- 12 caudal supratrochlear grooves
- 13 facet for cuneiforme 3
- 14 facet for the cuboid
- 15 groove for the fossa nudata (synovialis)
- 16 arterial vascular groove
- 17 arterial vascular groove
- 18 lateral depression for attachment of the ligamentum sesamoideum



Medial Sesamoidea of the Distal Metatarsale III
(fig. 7.13.1.1)

- 1 apex sesamoidei
- 1' peripheral facet rim
- 2 dorsal facet
- 2' lateral portion of (2) for articulation with MT III
- 2'' medial portion of (2) for articulation with MT III
- 2''' proximodistal ridge of the joint facet (2)
- 3 basis sesamoidei
- 3' elongated tuberosus portion of (3)
- 3'' rounded eminence (3)
- 4 palmar side middle crest
- 5 facies musculi interossei medialis
- 6 facies flexoria
- 6' proximodistally coursing groove
- 6'' narrow groove on the surface of (6) running proximodistally parallel to the peripheral facet (1')

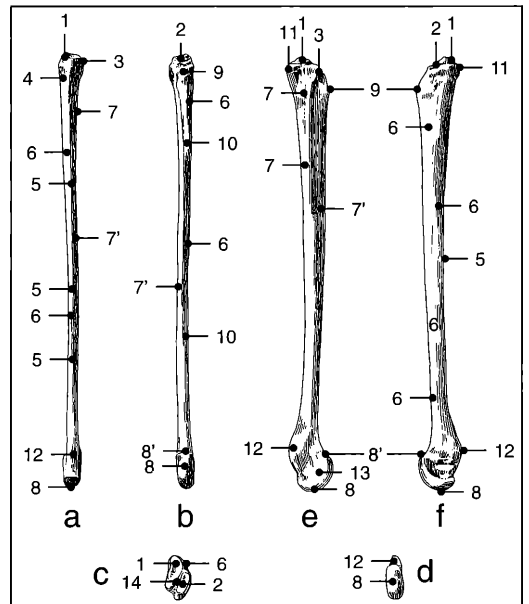


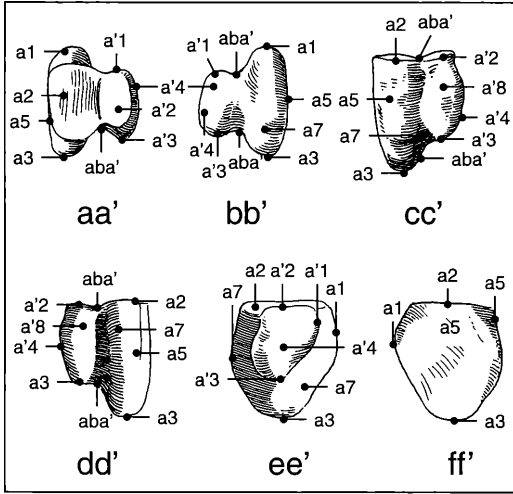
Lateral Sesamoidea of the Distal Metatarsale III
(fig. 7.13.1.2)

- 1 apex sesamoidei
- 2 joint facet for MT III
- 2' medial portion of joint facet (2)
- 2'' lateral portion of joint facet (2)
- 2''' proximodistal ridge of joint facet (2)
- 3 basis sesamoidei
- 4 medial proximodistally coursing palmar crest
- 5 facies musculi interossei medialis
- 6 facies flexoria of the lateral sesamoid

Metatarsale II (fig. 7.14.1)

- 1 lateral articular facet for the cuneiforme 1
- 2 medial articular facet cuneiforme 2
- 3 border of the caudal facet for articulation with MT III
- 4 protuberance for ligamentous attachment
- 5 sharp cranial keel separating features (6) and (7)
- 6 smooth medial wall
- 7 roughened portion of the lateral wall for attachment of the ligamentum metatarsium
- 7' smoother portion of the lateral wall
- 8 distal articular surface for 1st phalanx II showing the broader portion of the joint on the caudal border
- 8' flat fovea proximal to (8)
- 9 ligamentous protuberance
- 10 caudal keel
- 11 cranial facet for articulation with the MT III
- 12 processus supraarticularis
- 13 depression for the ligamentum collaterale laterale
- 14 furrow separating features (1) and (2)
- 15 caudal keel





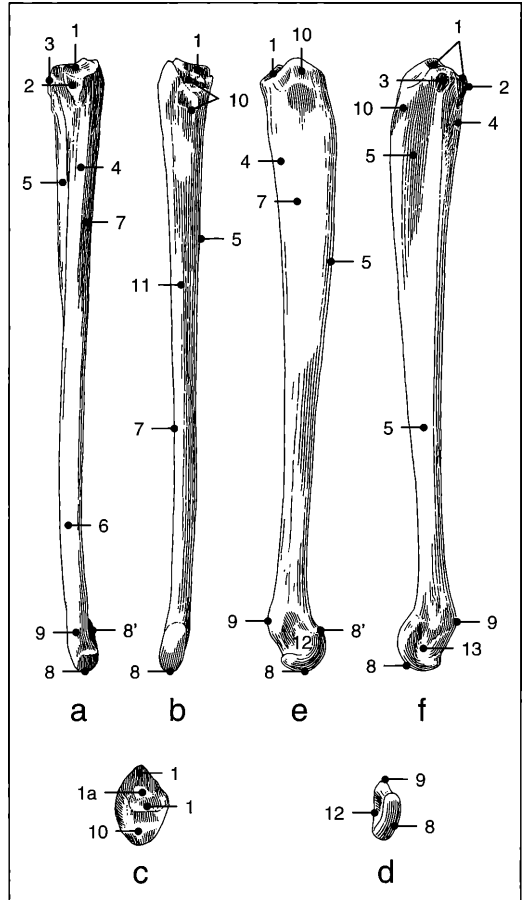
Sesamoidea of the Distal Metatarsale II (fig. 7.15.1)

Abaxial (large) sesamoid (fig. 7.15.1a-f)

- a1 apex sesamoidei
- a2 joint facet for the MT II
- a3 basis sesamoidei
- a5 abaxial facies for attachment of the interosseous medius
- a7 abaxial facies for the flexorius
- aba' coosification suture for both sesamoidea

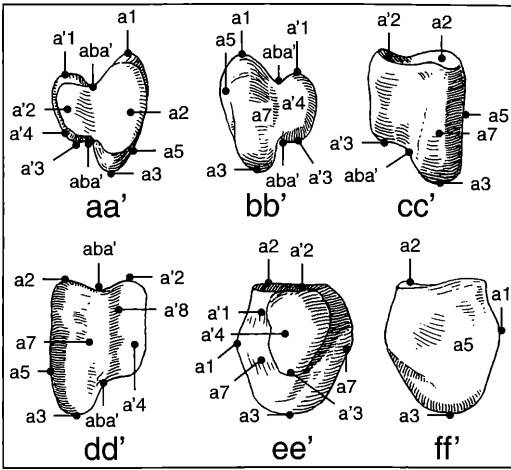
Adaxial (small) sesamoid (fig. 7.15.1a'-f')

- a'1 apex sesamoidei
- a'2 joint facet for the MT II
- a'3 basis sesamoidea
- a'4 adaxial facies
- a'8 adaxial facies for the flexorius
- aba' coosification suture for both sesamoidea



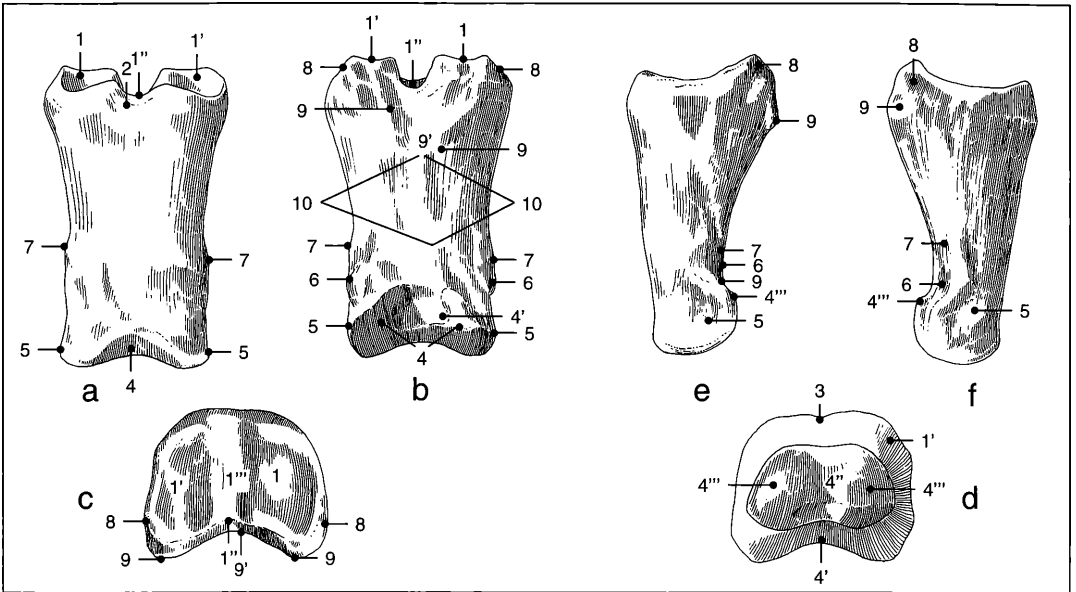
Metatarsale IV (fig. 7.16.1)

- 1 articular facet for the cuboid
- 1a „non-articular“ area for fossa nudatae
- 2 mediocranial facet for the MT III
- 3 medial facet for the MT III small caudal facet
- 4 roughened portion of the medial wall for attachment of the ligamentum metatarsaeum
- 5 smooth, slightly concave medial diaphysal border
- 6 distal rounded cranial ridge
- 7 slightly convex lateral wall
- 8 distal articular facet for the 1st phalanx
- 8' caudal projection of feature (8)
- 9 processus supraarticularis
- 10 large ligamentous tuberosity
- 11 rounded caudal linea separating features (5) and (7)
- 12 depression for the ligamentum collaterale laterale
- 13 depression for the ligamentum collaterale mediale



Sesamioidea of Distal Metatarsale IV (fig. 7.17.1)

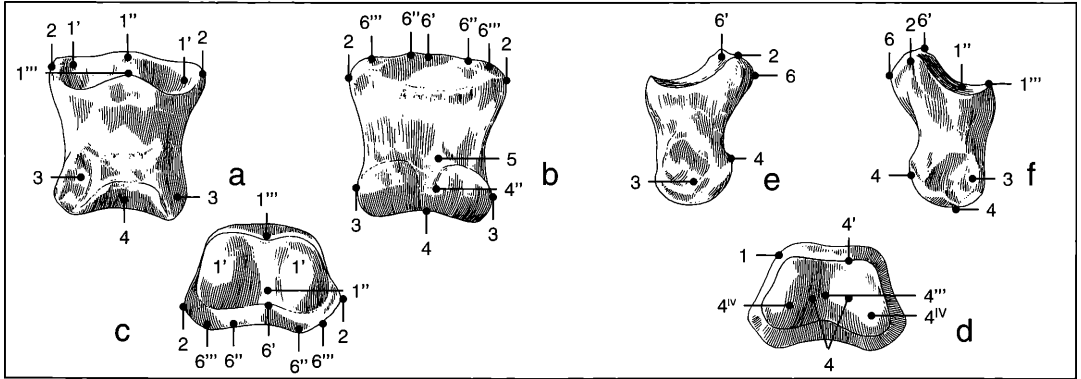
The MT IV sesamoids are a virtual mirror image to those of MT II. Refer to the figure legends for figures 7.15.1a, a'-f, f' for the osteological details.



Posterior 1st Phalanx III (fig. 7.18.1)

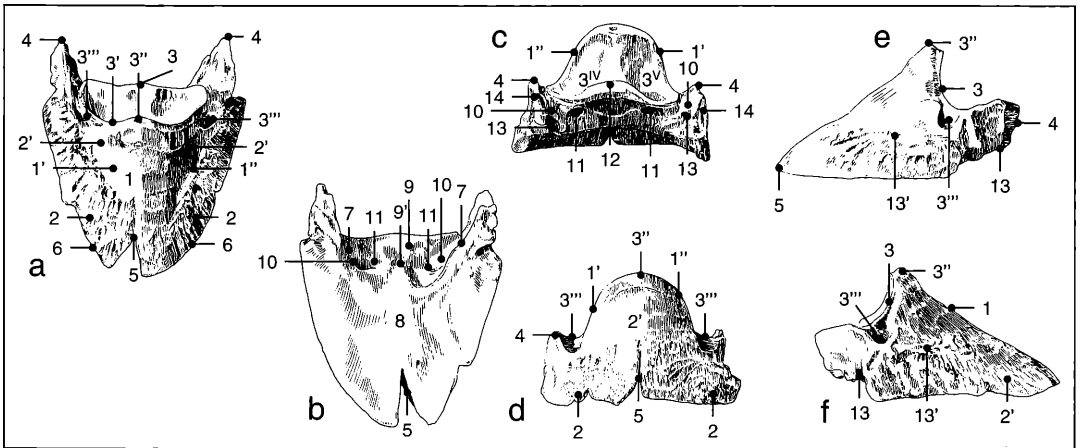
- 1 medial portion of proximal articular facet
- 1' lateral portion of (1)
- 1'' palmar border incision of the crista sagittalis
- 1''' dorsopalmar groove for the crista sagittalis of MT III
- 2 impression for attachment of the proximal articular cartilage
- 3 proximal bony swelling with furrows on the dorsal wall
- 4 distal articular surface
- 4' rugose feature on the distal articular surface
- 4'' midsagittal groove of (4)
- 4''' medial and lateral elevations of (4)

- 5 attachment of medial and lateral collateral ligaments
- 6 attachment of the flexor digitalis superficialis („perforatus scar“)
- 7 attachment for the ligamentum laterale volare
- 8 attachment for the ligamentum collaterale of the fetlock joint
- 9 attachment for the ligamentum sesamoideum obliquum („V-scar“)
- 9' triangular groove of the „V-scar“
- 10 attachment for the ligamentum sesamoideum centrale
- 11 no vascular groove here



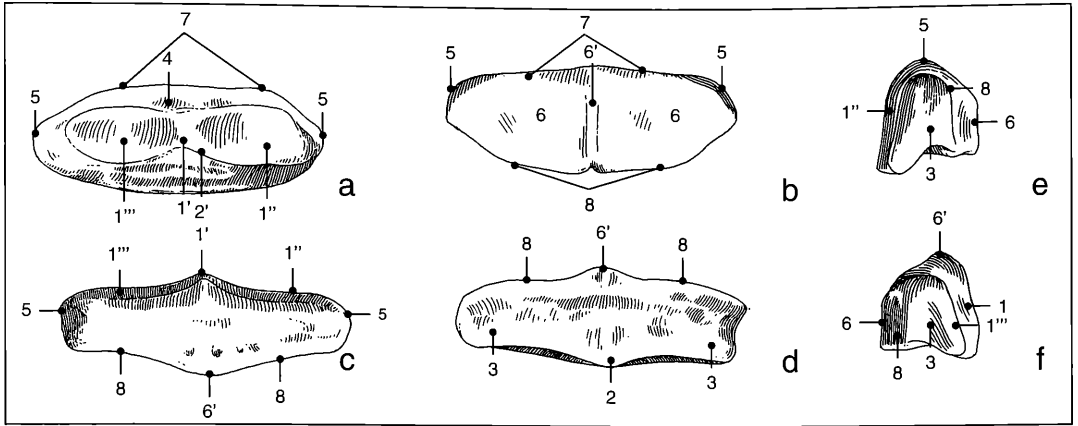
Posterior 2nd Phalanx III (fig. 7.19.1)

- | | |
|--|---|
| <p>1 proximal articular facet
 1' medial and lateral portions of (1)
 1'' midsagittal ridge of (1)
 1''' proximodorsal tuberos prominence of (1)
 2 medial and lateral attachment scar of the ligamentum collaterale of phalanx 1/phalanx 2 digit III articulation
 3 medial and lateral scar of the ligamentum collaterale for articulation with the 3rd phalanx
 4 distal articular facet
 4' cranial border of (4)
 4'' distally directed intercondylar furrow of (4)</p> | <p>4''' distal midsagittal groove of (4)
 4'''' medial and lateral condyles of (4)
 5 rugose surface for the insertion of the flexor digitorum sublimis
 6 flexor tuberosity
 6' area for attachment of the ligamentum sesamoideum rectum of (6)
 6'' medial and lateral sites for attachment of the flexor digitorum sublimis (22.3.92)*
 6''' medial and lateral sites for attachment of the ligamentum laterale volare</p> |
|--|---|



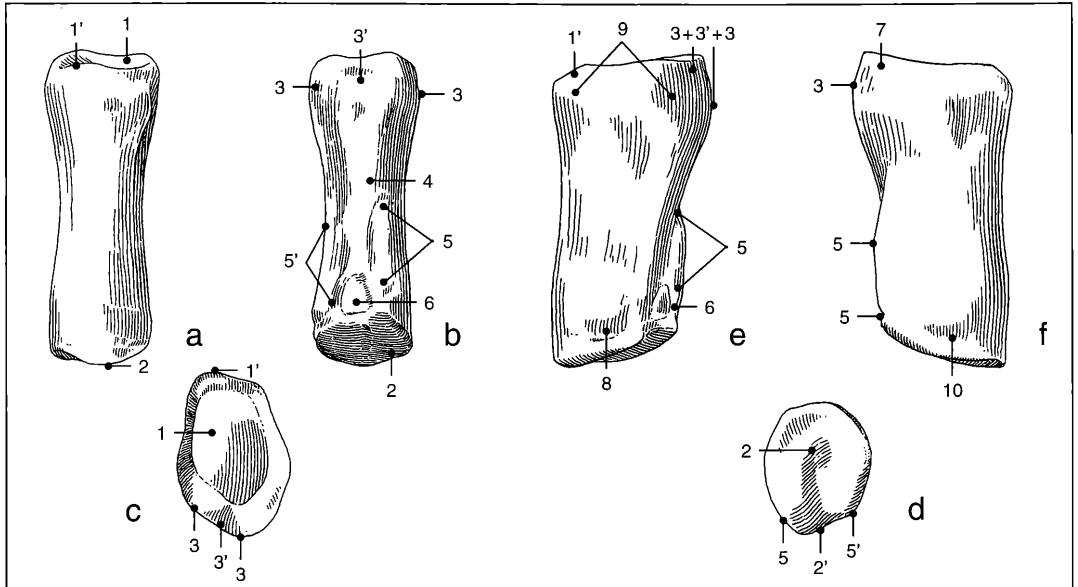
Posterior 3rd Phalanx III (fig. 7.20.1)

- | | |
|---|---|
| <p>1 dorsal portion of the parietal surface
 1' medial portion of the parietal surface
 1'' border between (1) and (2)
 2 rugose distal portion of the parietal surface
 2' smooth proximal portion of the parietal surface
 3 proximal articular surface
 3' coronary border of the articular surface
 3'' extensor process of the coronary border
 3''' medial and lateral groove for attachment of the ligamentum collaterale
 3'''+3'''' lateral and medial articular surfaces of feature (3)
 4 processus palmaris lateralis and medialis
 5 crena marginis solearis</p> | <p>6 border of the sole (= margo solearis)
 7 linea semilunaris
 8 planum cutaneum of the sole surface
 9 facies flexoria of the sole surface
 9' attachment site for the flexor digitalis profundus („tendo perforans“)
 10 sulcus solearis medialis et lateralis
 11 foramen soleare mediale and laterale
 12 articular facet for the distal sesamoid bone
 13 foramen processus palmaris mediale and laterale
 13' sulcus parietalis medialis and lateralis
 14 medial and lateral furrows for attachment of the ligaments of the hoof cartilage</p> |
|---|---|



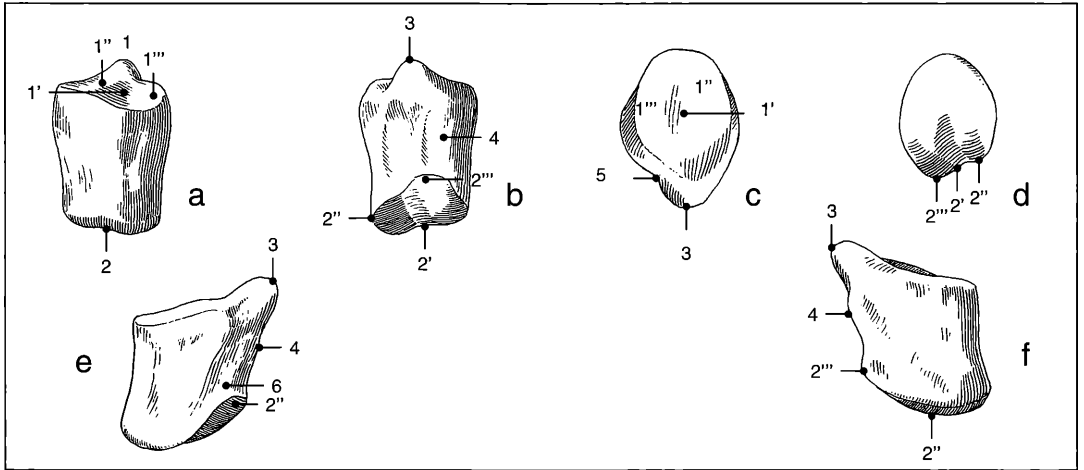
Distal Sesamoidea of the Posterior Phalanx III (fig. 7.21.1)

- | | | | |
|------|---|----|---|
| 1 | facies articularis for phalanx 2 | 4 | proximal surface |
| 1' | central elevation of (1) | 5 | attachment sites for the ligamenta collateralia |
| 1'' | medial portion of the facies articularis | 6 | facies flexoria |
| 1''' | lateral portion of the facies articularis | 6' | central elevation of (6) |
| 2 | dorsodistal facet for articulation with the 3rd phalanx | 7 | margo proximalis |
| 2' | border of (2) against (1') | 8 | margo distalis |
| 3 | rugose surface with irregular discontinuous fossae | | |



Posterior 1st Phalanx II (Fig. 7.22.1)

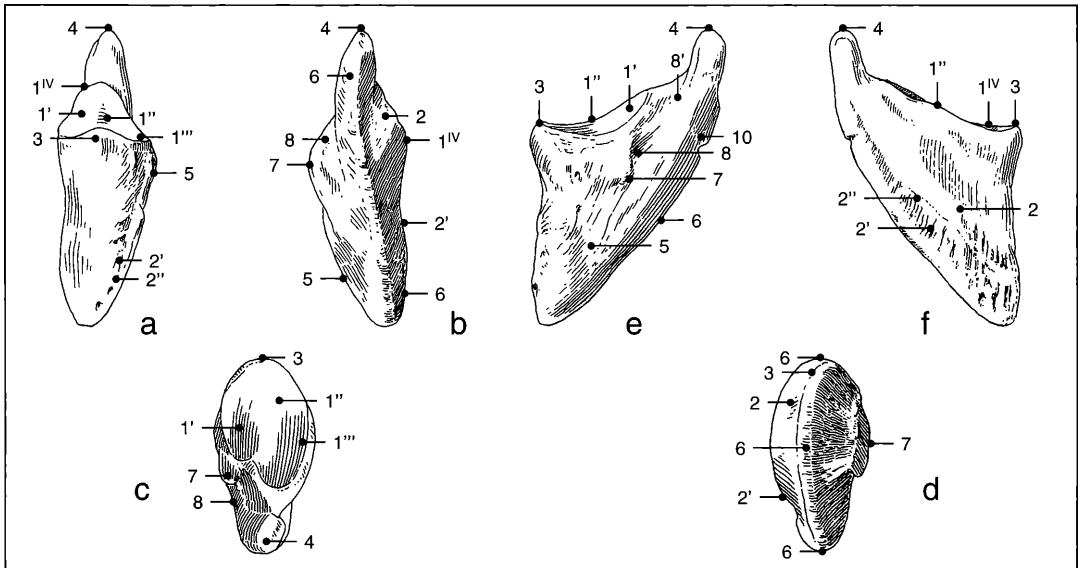
- | | | | |
|----|--|----|--|
| 1 | proximal articular facet for MC II | 6 | small bony tuberosity |
| 1' | proximodorsal prominence (1) | 7 | insertion scar for the ligamentum collaterale laterale (abaxiale) attaching the 1st phalanx with MC II |
| 2 | distal surface for articulation with the 2nd phalanx II | 8 | insertion scar for the ligamentum collaterale laterale (adaxiale) attaching the 1st and 2nd phalanges |
| 2' | sulcus distalis on the distal facet (2) | 9 | tuberosity for the ligamentum collaterale laterale (adaxiale) attaching the 1st phalanx with MC II |
| 3 | weak trigonum phalangis proximalis | 10 | tuberosity for the ligamentum collaterale mediale (abaxiale) attaching the 1st and 2nd phalanges II |
| 3' | deepening of the trigonum | | |
| 4 | „V-scar“ of the ligamentum sesamoideum centrale | | |
| 5 | abaxial site for insertion of the flexor digitalis superficialis | | |
| 5' | adaxial site for insertion of the flexor digitalis superficialis | | |



Posterior 2nd Phalanx II (fig. 7.23.1)

- 1 proximal joint facet for 1st phalanx digit II
- 1' medial longitudinal ridge of (1)
- 1'' medial portion of (1)
- 1''' lateral portion of (1)
- 2 distal joint facet for 3rd phalanx II
- 2' sulcus distalis of (2)

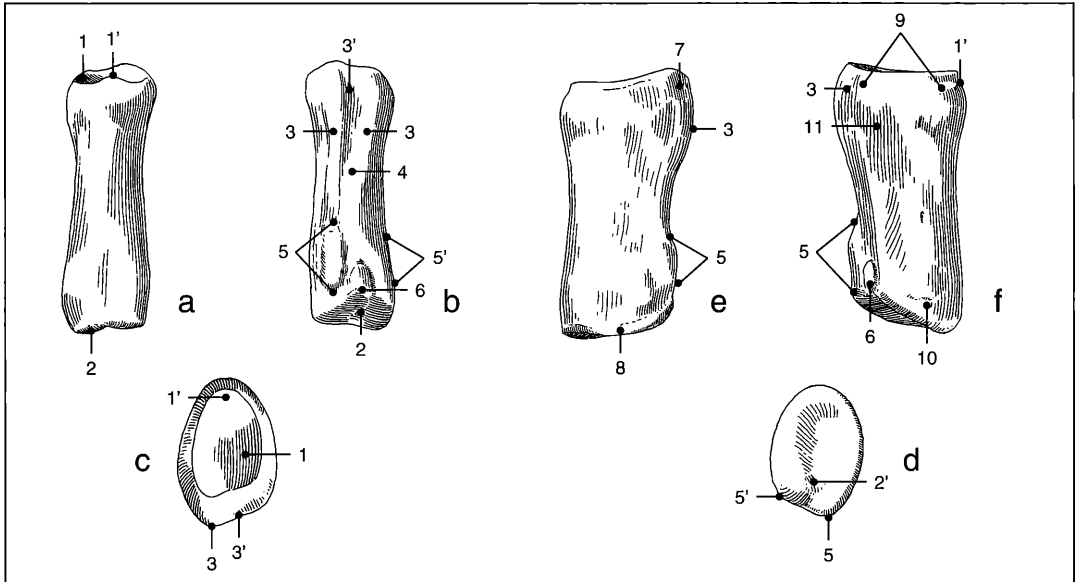
- 2'' lateral portion of (2)
- 2''' medial portion of (2)
- 3 process for insertion of the tendo flexor digitalis sublimis
- 4 tuberosity for attachment of ligaments
- 5 mediopalmar indentation of (1)
- 6 mediopalmar border of the phalanx



Posterior 3rd Phalanx II (fig. 7.24.1)

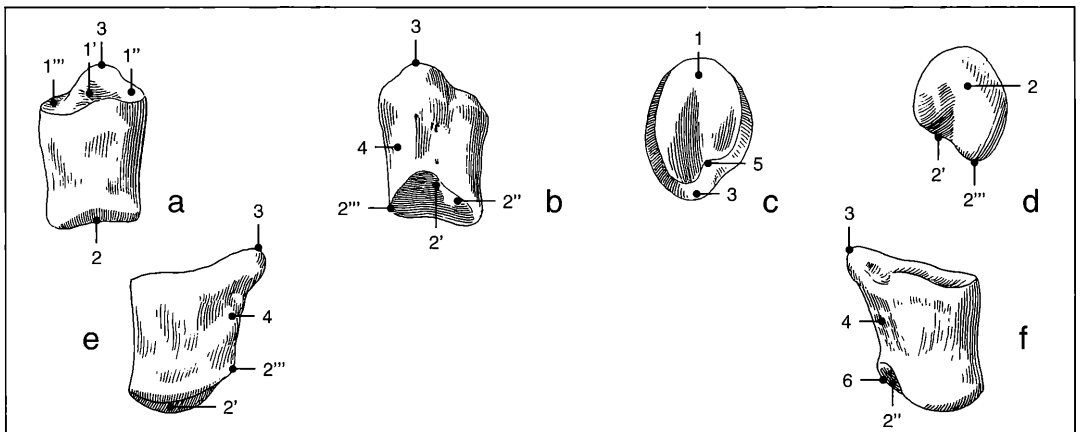
- 1 proximal articular surface for the 2nd phalanx
- 1' medial portion of (1)
- 1'' longitudinal ridge of (1)
- 1''' lateral portion of (1)
- 1IV lateral coronary border of (1)
- 2 smooth dorsal portion of the parietal surface
- 2' wrinkled dorsal portion of the parietal surface
- 2'' sulcus parietalis (variable)
- 3 processus for attachment of the extensor digitalis communis

- 4 processus palmaris lateralis
- 5 medial wall of the phalanx
- 6 margo solearis
- 7 facies flexoria for attachment of the flexor digitalis profundus
- 8 foramen soleare laterale
- 8' sulcus solearis lateralis
- 9 mediopalmar incision of (1)
- 10 linea semilunaris



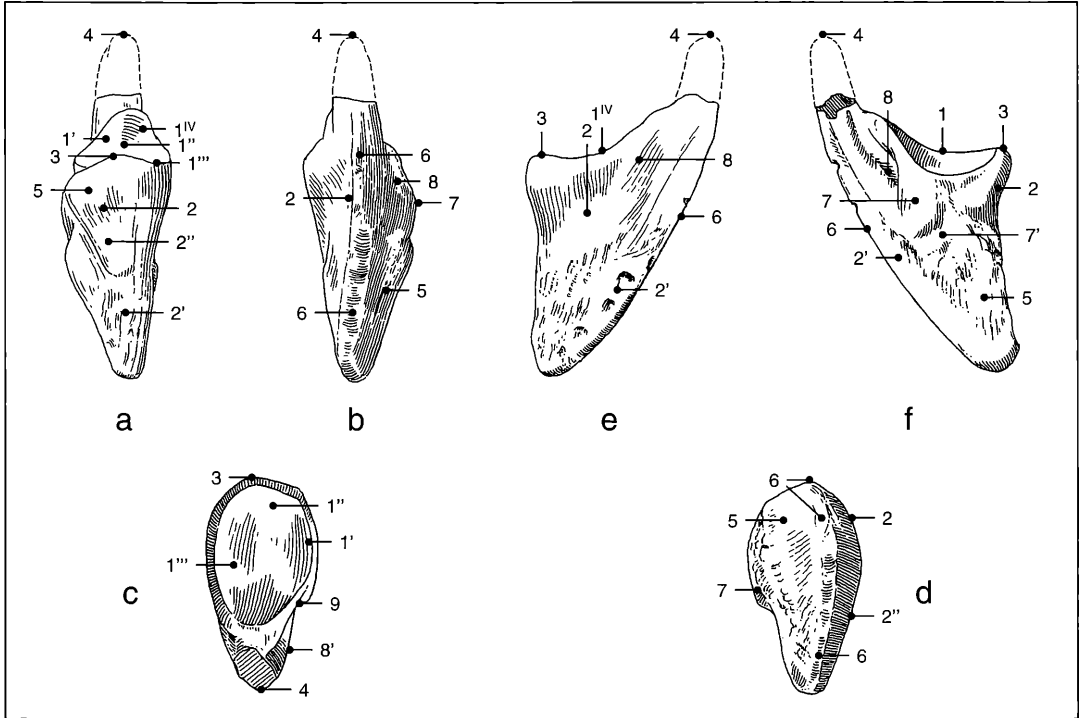
Posterior 1st Phalanx IV (fig. 7.25.1)

- | | |
|---|---|
| <p>1 proximal articular surface for the MT IV
 1' prominence at the dorsal border of (1)
 2 distal articular surface for the 2nd phalanx digit IV
 2' sulcus distalis on the distal facet (2)
 3 weak trigonum phalangis proximalls
 3' deepening of the trigonum
 4 scar for attachment of the ligamentum sesamoideum centrale
 5 abaxial insertion of the tendo flexor digitalis superficialis
 5' adaxial insertion of (5)</p> | <p>6 distal midsagittal bony tuberosity
 7 scar for attachment of the ligamentum collaterale laterale (abaxiale) with MT IV
 8 scar for attachment of the ligamentum collaterale laterale (abaxiale) with the phalanx 2, IV
 9 rugose surface for attachment of the ligamentum collaterale mediale (adaxiale) with MT IV
 10 rugose surface for attachment of the ligamentum collaterale mediale (adaxiale) with the 2nd phalanx
 11 small fossa distal to the proximal articular surface (9)</p> |
|---|---|



Posterior 2nd Phalanx IV (fig. 7.26.1)

- | | |
|---|---|
| <p>1 proximal joint facet for the 1st phalanx digit IV
 1' median longitudinal ridge of (1)
 1'' lateral portion of (1)
 1''' medial portion of (1)
 2 distal joint facet for 3rd phalanx IV
 2' sulcus distalis of (2)</p> | <p>2'' medial portion of (2)
 2''' lateral portion of (2)
 3 process for insertion of the tendo flexor digitalis sublimis
 4 rugose surface for the attachment of ligaments
 5 mediopalmar incision of (1)
 6 mediopalmar border of the phalanx</p> |
|---|---|



Posterior 3rd Phalanx IV (Fig. 7.27.1)

- 1 proximal articular surface with the 2nd phalanx
- 1' medial portion of (1)
- 1'' longitudinal ridge of (1)
- 1''' lateral portion of (1)
- 1'''' lateral coronary border of (1)
- 2 smooth dorsal portion of the parietal surface
- 2' rugose dorsal portion of the parietal surface
- 2'' sulcus parietalis of (2)
- 3 processus for attachment of the tendo extensor digitalis communis

- 4 processus palmaris lateralis
- 5 medial wall of the phalanx
- 6 margo solearis
- 7 facies flexoria for the tendon of the flexor digitalis profundus
- 7' oblique furrow on (7)
- 8 foramen solearis laterale
- 8' sulcus solearis lateralis
- 9 mediopalmar incision of (1)

Excavation site Höwenegg

(Upper Miocene, Vallesian, Hegau area, SW-Germany)

Publications on Geology and Palaeontology by the State Museum of Natural History Karlsruhe, Germany

andrias 6, 8, 10

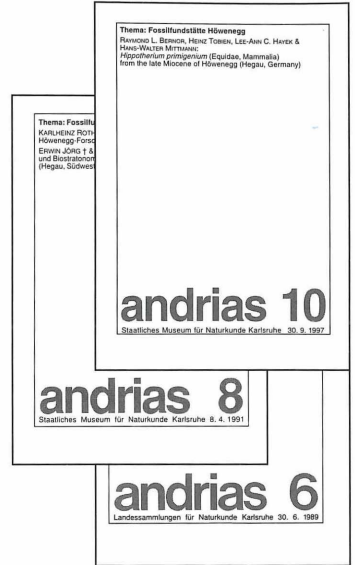
HÜNERMANN, K. A. (1989): Die Nashornskelette (*Aceratherium incisivum* Kaup, 1832) aus dem Jungtertiär vom Höwenegg im Hegau (Südwestdeutschland). – *Andrias*, **6**: 1–116.

ZAPFE, H. (1989): *Chalicotherium goldfussi* Kaup aus dem Vallesien vom Höwenegg im Hegau (Südwestdeutschland). – *Andrias*, **6**: 117–128.

ROTHAUSEN, K. (1991): Heinz Tobien 80 Jahre - Höwenegg Forschung 53 Jahre. – *Andrias*, **8**: 5–12.

JÖRG, E. & ROTHAUSEN, K. (1991): Zur Schichtfolge und Biostratonomie der Wirbeltierfundstelle Höwenegg (Hegau, Südwestdeutschland, Vallesium, Obermiozän). – *Andrias*, **8**: 13–64.

RAYMOND L. BERNOR, HEINZ TOBIEN, LEE-ANN C. HAYEK & HANS-WALTER MITTMANN: *Hippotherium primigenium* (Equidae, Mammalia) from the late Miocene of Höwenegg (Hegau, Germany). – *Andrias*, **10**: 230 pp.



Beiträge zur naturkundlichen Forschung in Südwestdeutschland 14, 18, 24

JÖRG, E., REST, H. & TOBIEN, H. (1955): Die Ausgrabungen an der jungtertiären Fossilfundstätte Höwenegg/Hegau 1950–54. – *Beitr. naturkd. Forsch. SüdwDtl.*, **14**: 3–21.

TOBIEN, H. & JÖRG, E. (1959): Die Ausgrabungen an der jungtertiären Fossilfundstätte Höwenegg/Hegau 1955–59. – *Beitr. naturkd. Forsch. SüdwDtl.*, **18**: 175–181.

JÖRG, E. (1965): *Ophisaurus acuminatus* nov. spec. (Anguidae, Rept.) von der pontischen Wirbeltier-Fundstätte Höwenegg/Hegau. – *Beitr. naturkd. Forsch. SüdwDtl.*, **24**: 23–30.



carolinea 44

TOBIEN, H. (1986): Die jungtertiäre Fossilgrabungsstätte Höwenegg im Hegau (Südwestdeutschland). Ein Statusbericht. – *Carolinea*, **44**: 9–34.

BEAUMONT, G. DE (1986): Les Carnivores (Mammifères) du Néogène de Höwenegg/Hegau, Baden-Württemberg. – *Carolinea*, **44**: 35–46.

SCHLEICH, H.H. (1986): Vorläufige Mitteilungen zur Bearbeitung der fossilen Schildkröten der Fundstelle Höwenegg. – *Carolinea*, **44**: 47–50.

TRUNKÓ, L. (1986): Geologische Aufschlußgrabung am Höwenegg. – *Carolinea*, **44**: 179–181.

